UNIVERSITY OF SOUTHAMPTON

FACULTY OF MEDICINE

Cancer Sciences Unit

Modelling chronic lymphocytic leukaemia (CLL) cell:microenvironment interactions in two- and three-dimensional culture systems

by

Elizabeth Anne Lemm

Thesis for the degree of Doctor of Philosophy

July 2016

UNIVERSITY OF SOUTHAMPTON

ABSTRACT

FACULTY OF MEDICINE

Cancer Sciences Unit

Thesis for the degree of Doctor of Philosophy

MODELLING CHRONIC LYMPHOCYTIC LEUKAEMIA (CLL) CELL:MICROENVIRONMENT INTERACTIONS IN TWO- AND THREE-DIMENSIONAL CULTURE SYSTEMS

By Elizabeth Anne Lemm

Chronic lymphocytic leukaemia (CLL) is a common B-cell malignancy characterised by the accumulation of malignant B cells in the blood, bone marrow and secondary lymphoid organs. CLL cells rapidly undergo apoptosis when cultured *in vitro*, highlighting the importance of supporting tissue microenvironments for pathogenesis. The survival of CLL cells depends on a complex interplay of distinct cell types, the extracellular matrix and soluble factors within the microenvironment and as such modelling the CLL microenvironment has been an area under intense investigation. This study investigated the use of a novel method, 'acoustic trapping' to model the CLL microenvironment. The overarching hypothesis is that acoustic trapping devices can be used to 'levitate' CLL cells away from artificial surfaces and, with the use of the HFFF2 fibroblast cell line, a three dimension (3D) model of the CLL:stromal microenvironment can be created to probe molecular interactions between the two cell types *in vitro*.

The first experiments characterised the use of the HFFF2 cell line for its suitability for use in this project. Results indicated that co-culture with the cell line promoted CLL cell survival in all samples studied and further experiments demonstrated that CLL cell survival occurred in a contact-independent manner. Optimisation of 'acoustic trapping devices' designed and manufactured by Dr Peter Glynne-Jones (Faculty of Engineering and the Environment, University of Southampton), demonstrated that both CLL and HFFF2 cells could be co-levitated to form agglomerates that contracted over a 48 hour period to form 3D structures. However further investigations revealed that there was a significant loss of viability of both cell types in the devices and this led to the conclusion that at present, acoustic trapping devices have not been optimised enough to allow for modelling of the CLL microenvironment.

Further experiments concentrated on the characterisation of the HFFF2 co-culture model using gene expression profiling (GEP) to determine CLL:fibroblast interactions *in vitro*. Results indicating that there was a distinct gene expression profile in CLL cells that had been co-cultured with HFFF2 cells or HFFF2-derived conditioned media (CM) resulting in the enrichment of a number of different cytokines and chemokines. Analysis of four specific cytokines/chemokines revealed that culture with HFFF2 CM resulted in the upregulation of IL-6, IL-8, CXCL2 and CCL2. Purification of CLL cells lead to the discovery that some were directly induced following culture with HFFF2-CM while the induction of others required a third intermediate cell type. Overall results demonstrate that the HFFF2 cell line is a suitable model for investigating CLL/microenvironment interactions and in this model HFFF2 cells, accessory cells and soluble factors are working together to provide pro-survival signals to the CLL cells.

Table of Contents

Table of Contents ..... **i**
List of Tables ..... **v**
List of Figures ..... **vii**
DECLARATION OF AUTHORSHIP ..... **xi**
Acknowledgements ..... **xiii**
Definitions and Abbreviations ..... **xv**
Chapter 1: Introduction **3**

1.1 Overview 3
1.2 Chronic lymphocytic leukaemia 3

1.2.1 Staging systems and prognostic markers 4
1.2.2 Current treatment strategies 12

1.3 The microenvironment 16

1.3.1 The tissue stroma 19
1.3.2 The microenvironment in haematological malignancies 24

1.4 The microenvironment in CLL 31

1.4.1 Cellular players in the CLL cell microenvironment 36
1.4.2 Microenvironment-associated signalling pathways 42
1.4.3 BCR crosstalk to the microenvironment 44
1.4.4 Chemokines and cytokines secreted by stromal cells 49
1.4.5 Chemokines and cytokines secreted by CLL cells 51
1.4.6 Chemokines and cytokines and the pathogenesis of CLL 52
1.4.7 Adhesion molecules 52
1.4.8 TNF family receptors 53
1.4.9 Modelling the CLL microenvironment 57

1.5 Cell culture methods 58

1.5.1 Two dimensional cell culture 58
1.5.2 *In vivo* models 59
1.5.3 Three dimensional tissue culture 59
1.5.4 3D culture methods 62
1.5.5 Novel 3D models 69

1.6 Particle manipulation in an acoustic field 71

1.6.1 Acoustic forces 71
1.6.2 Applications of acoustic trapping 75
1.6.3 The acoustic trapping device 76
1.6.4 The use of acoustic trapping devices to model the CLL microenvironment 79

1.7 Hypothesis and Aims 80

1.7.1 Hypothesis 80
1.7.2 Aims 80

Chapter 2: Materials and Methods **83**

2.1 Cell culture techniques 83

2.1.1 Materials 83
2.1.2 Primary CLL samples 83
2.1.3 CLL cell purification 84
2.1.4 Cell lines 85
2.1.5 CLL and HFFF2 co-culture experiments 85

2.2 Protein techniques 87

2.2.1 Materials 87
2.2.2 α-SMA immunofluorescence 87
2.2.3 CXCL12 enzyme-linked immunosorbent assay (ELISA) 88

2.2.4 Western blotting 88
2.3 Flow cytometry techniques 91
2.3.1 Materials 91
2.3.2 Annexin-V/propidium iodide staining for the analysis of CLL cell viability 91
2.3.3 CXCR4 expression on CLL cells 95
2.3.4 IgM and CXCR4 phenotype and signalling experiments 95
2.3.5 CLL cell migration assay 97
2.3.6 CCL2 intracellular expression 97
2.4 Molecular biology techniques 99
2.4.1 CLL cell RNA extraction 99
2.4.2 RNA clean up 99
2.4.3 Determining RNA integrity 100
2.4.4 First strand complementary DNA synthesis 102
2.4.5 Quantitative polymerase chain reaction 102
2.5 Gene expression profiling experiments 106
2.5.1 Gene expression profiling experiments outline 106
2.5.2 Analysis of raw GEP experiment data performed by Cambridge Genomic Services 106
2.5.3 Multiple comparisons of GEP data 107
2.5.4 Gene set enrichment analysis using GSEA software 107
2.6 Acoustic trapping device techniques 109
2.6.1 Acoustic trapping device 109
2.6.2 Set up of acoustic trapping devices and injection of cells 113
2.6.3 Cell labelling 119
2.6.4 Measurement of the minimum voltage required to levitate cells in acoustic trapping device 120
2.7 Statistics 122

Chapter 3: Investigating the HFFF2 cell line as a model system for studying CLL microenvironment interactions 125

3.1 Introduction 125
3.2 Hypothesis 126
3.3 Aims and objectives 126
3.4 The HFFF2 fibroblast cell line protects CLL cells from spontaneous apoptosis 127
3.4.1 Differences in levels of spontaneous apoptosis of CLL samples 128
3.4.2 Ability of the HFFF2 cell line to protect CLL cells from spontaneous apoptosis 131
3.4.3 Heterogeneity in levels of cytoprotection from the HFFF2 cell line 131
3.5 Primary lymph node fibroblasts protect CLL cells in a similar way to the HFFF2 cell line 136
3.6 HFFF2-cytoprotection occurs in a contact-independent manner 140
3.6.1 Generation of HFFF2-derived CM 140
3.6.2 Ability of HFFF2-derived CM to protect CLL cells from spontaneous apoptosis 142
3.6.3 Direct comparison between direct co-culture and CM 142
3.6.4 HFFF2 cells protect CLL cells from spontaneous apoptosis through a microporous membrane 147
3.7 Summary of survival data 148
3.8 Characterisation of the HFFF2 cell line 152
3.9 Key Findings 157
3.10 Discussion 157
3.10.1 HFFF2 cells protect CLL cells from spontaneous apoptosis 157
3.10.2 Suitability of the HFFF2 cell line as a model system for investigating CLL/microenvironment interactions 158
3.10.3 HFFF2 cells protect CLL cells in a non-contact dependent manner 159
3.10.4 Ability of HFFF2 cell line to transdifferentiate into myofibroblasts 160

3.10.5 Final Comments 161

Chapter 4: Optimisation of acoustic trapping devices for modelling CLL/microenvironmental interactions in three dimensions 165

4.1 Introduction 165
4.2 Hypothesis 166
4.3 Aims and objectives 166
4.4 Initial assessment of CLL and HFFF2 cell levitation in acoustic trapping devices 166
4.5 Co-levitation of CLL and HFFF2 cells 168
4.5.1 Optimisation of cell numbers injected into acoustic trapping devices 168
4.5.2 Co-levitation of CLL and HFFF2 cells using different fluorescent dyes 174
4.5.3 Co-levitation of CLL and HFFF2 cells at later time points 174
4.6 Effect of extended levitation on CLL and HFFF2 cells 179
4.7 Analysis of CLL and HFFF2 cell viability using propidium iodide exclusion 188
4.8 Analysis of caspase 3/7 activation in CLL cells following levitation in acoustic trapping devices 201
4.9 Analysis of caspase 3/7 activation in HFFF2 cells in acoustic trapping devices 207
4.10 Exploration of physical stimuli 215
4.11 Key findings 218
4.12 Discussion 218
4.12.1 Ability of CLL and HFFF2 cells to levitate in acoustic trapping device 218
4.12.2 Morphology of agglomerates following levitation in acoustic trapping devices for longer period of time 219
4.12.3 Viability of CLL and HFFF2 cells in acoustic trapping device 220
4.12.4 Final comments 222

Chapter 5: Role of the chemokine receptor CXCR4 and its ligand CXCL12 in HFFF2-cytoprotection 227

5.1 Introduction 227
5.2 Hypothesis 228
5.3 Aims and objectives 229
5.4 Separation of HFFF2-CM to determine approximate molecular weight of candidate molecules responsible for HFFF2-mediated cytoprotection 229 231
5.5 Ability of the HFFF2 cell line to secrete CXCL12 233
5.6 The effect of HFFF2 cell co-culture on CXCR4 expression on CLL cells 236
5.7 Effect of HFFF2-derived CM on CXCR4 expression on CLL cells 239
5.8 Effect of neutralising antibodies to CXCR4 and CXCL12 on HFFF2-mediated CLL cell survival 243
5.9 Key findings 248
5.10 Discussion 248
5.10.1 The potential role of a HMW molecule in HFFF2-derived CM-mediated protection of CLL cells 248
5.10.2 The HFFF2 cell line secretes the chemokine CXCL12 250
5.10.3 Co-culture with HFFF2 cells prevents recovery of CXCR4 while HFFF2-CM increases CXCR4 expression 250
5.10.4 Neutralising antibodies to CXCL12 and CXCR4 prevent CXCL12-mediated migration but are unable to block HFFF2-mediated protection to CLL cells 251
5.10.5 Final comments 252

Chapter 6: Candidate molecules involved in HFFF2-mediated cytoprotection to CLL cells 255

6.1 Introduction 255
6.2 Hypothesis 255
6.3 Aims and objectives 256
6.4 GEP experiment outline 256
6.5 Analysis of raw GEP data performed by Cambridge Genomic services 257

6.6 Multiple comparisons of GEP data 263
6.7 Transcriptional differences between CLL cells cultured alone and in the presence of the HFFF2 cell line 265
6.7.1 Assessment of HFFF2 cell contamination 269
6.8 Transcriptional differences between CLL cells cultured alone and in the presence of HFFF2-CM 271
6.9 Transcriptional responses to anti-IgM stimulation 280
6.9.1 Modulation of transcriptional responses 280
6.9.2 Gene set enrichment analysis using GSEA software 285
6.10 Effect of co-culture of CLL cells with HFFF2 cells on surface IgM expression and signal capacity 289
6.11 Analysis of *IL6, IL8, CCL2* and *CXCL2* mRNA expression following co-culture of CLL cells with HFFF2-derived CM 296
6.11.1 Comparison of responses between CLL PBMC and purified CLL cells 298
6.12 Quantitation of intracellular levels of CCL2 by flow cytometry 302
6.13 Viability of purified CLL cells compared to CLL PBMC cultures 305
6.14 Key Findings 307
6.15 Discussion 307
6.15.1 Data quality from GEP experiment 307
6.15.2 HFFF2 cell contamination in CLL cell RNA 308
6.15.3 Transcriptional differences following survival-inducing culture with HFFF2 cells and HFFF2-derived CM 308
6.15.4 Modulation of transcriptional responses to antigen by microenvironmental co-stimulation 309
6.15.5 Surface IgM expression and CLL signal capacity following co-culture with HFFF2 cells 309
6.15.6 Enrichment of chemokines and cytokines following culture with HFFF2 cells or HFFF2-derived CM 310
6.15.7 Viability of purified CLL cells 312
6.15.8 Final comments 313

Chapter 7: Final discussion 317

7.1 Overview of findings 317
7.2 Use of acoustic trapping devices to model the CLL microenvironment 319
7.3 Suggestions for future work to investigate the use of acoustic trapping devices to model the CLL microenvironment 321
7.4 The role of chemokine and cytokines in HFFF2-mediated cytoprotection using the HFFF2 cell line model 322
7.5 Suggestions for future work to investigate the role of chemokine and cytokines in HFFF2-mediated cytoprotection using the HFFF2 cell line model 324

Chapter 8: List of References 329
Appendix A 361
CLL patient data 361

Appendix B 365
Acoustic trapping device videos 365

Appendix C 369
Purification data 369

Appendix D 379
RNA integrity results 379

Appendix E 389
GEP supplementary data 389

List of Tables

Table 1.1: : Prognostic subgroups and associated risk genetic factors in CLL at point of diagnosis (adapted from (Puiggros et al., 2013)). 11

Table 1.2: Novel strategies in the treatment of CLL 14

Table 1.3: Potential molecular interactions of the CLL microenvironment 55

Table 1.4: The main advantages and disadvantages of 2D and 3D cultures and *in vivo* animal experiments 60

Table 1.5: Main methods currently used for the generation of 3D cultures and their application in the current literature 65

Table 2.1: Dilutions and suppliers of the primary and secondary antibodies utilised for western blotting 90

Table 2.2: Concentrations and suppliers of the neutralising antibodies utilised in viability experiments....93

Table 2.3: Names, dilutions and suppliers of the cell trace and fluorescent dyes used to label cells in acoustic trapping device experiments....119

Table 4.1: Summary of morphology of agglomerates formed in the ultrasound devices using different initial cell concentrations....173

Table 4.2: Measurement of temperature changes over 8 hour period in the acoustic trapping devices 216

Table 4.3: Determination of the minimum voltage required for levitation of fluorescent beads....217

Table 5.1: Levels of CXCL12 secreted from various stromal cell types in the literature 235

Table 6.1: Characteristics of patients selected for GEP experiments 259

Table 6.2: Results of multiple comparisons carried out by Cambridge Genomic Service....264

Table 6.3: Top 50 differentially expressed genes following comparison between CLL cells cultured alone and CLL cells cultured in the presence of HFFF2 cells 267

Table 6.4: HFFF2 cell contamination 270

Table 6.5: Top 50 differentially expressed genes following comparison between CLL cells cultured alone and CLL cells cultured in the presence of HFFF2-derived CM....274

Table 6.6: Fold changes of the top 50 regulated genes in CLL cells in the presence of HFFF2-derived CM in comparison to the fold changes following direct culture with HFFF2 cells....276

Table 6.7: Chemokine and cytokines upregulated following co-culture with HFFF2 cells or HFFF2-derived CM and their function in CLL cell biology....277

Table 6.8: Top 50 differentially expressed genes following comparison between CLL cells cultured alone and CLL cells stimulated αIgM beads....282

Table 6.9: Effect of HFFF2 co-culture on CLL cell response to anti-IgM stimulation 284

Table 6.10: Characteristics of patients used in HFFF2/IgM experiments....290

List of Figures

Figure 1-1: Pathogenesis of CLL subsets 7

Figure 1-2: Kaplan-Meier survival curve comparing CLL patients with mutated and unmutated *IGVH* genes. Taken from (Hamblin et al., 1999). 8

Figure 1-3: Main genetic aberrations in CLL and their clinical significance....9

Figure 1-4: Main genetic aberrations in CLL and their clinical significance....10

Figure 1-5: The tumour microenvironment in solid tumours....17

Figure 1-6: The tumour microenvironment shapes the hallmarks of cancer (Taken from (Hanahan and Coussens, 2012) 18

Figure 1-7: Mesenchymal stem cells....22

Figure 1-8: Model of myofibroblast transdifferentiation 23

Figure 1-9: Structure of a lymph node....29

Figure 1-10: CLL cell proliferation centres 33

Figure 1-11: Homing of CLL cells to the tissue microenvironment....35

Figure 1-12: Cellular and molecular interactions in the CLL microenvironment (adapted from (Burger et al., 2009a) 41

Figure 1-13: The BCR signalosome 46

Figure 1-14: Different BCR signalling responses and variable clinical outcome in CLL (adapted from (Packham et al., 2014)).....47

Figure 1-15: BCR crosstalk with microenvironment receptors 48

Figure 1-16: Overview of the common methods used for 3D cell culture (Breslin and O'Driscoll, 2013)....64

Figure 1-17: Ultrasound standing wave....73

Figure 1-18: Acoustic forces acting in a half wavelength field....74

Figure 1-19: Acoustic trapping device 78

Figure 2-1: Amicon Ultra-15 centrifugal filter units (Merck Millipore)....86

Figure 2-2: Transwell chamber plates 94

Figure 2-3: Preparation of Bioanlyzer chips 101

Figure 2-4: First strand complementary DNA synthesis....103

Figure 2-5: TaqMan quantitative PCR method....104

Figure 2-6: Typical amplification plot from qPCR experiments 105

Figure 2-7: Acoustic trapping device in a 6 well plate format....111

Figure 2-8: Set up of acoustic trapping devices 115

Figure 2-9: Injection of cells into acoustic trapping devices 117

Figure 2-10: Calculation of approximate height beads will no longer levitate in the acoustic trapping device....121

Figure 3-1: Gating strategy for Annexin-V/PI experiments 129

Figure 3-2: Comparison of spontaneous apoptosis levels between the different CLL prognostic subgroups 130

Figure 3-3: Effect of HFFF2 co-culture on CLL cell survival 132

Figure 3-4: Effect of HFFF2 co-culture on CLL cell survival 133

Figure 3-5: Comparison of HFFF2-cytoprotection levels between different CLL prognostic subgroups 134

Figure 3-6: Correlation between spontaneous apoptosis and HFFF2-cell-mediated cytoprotection at 24 and 48 hours 135

Figure 3-7: Characterisation of lymph node fibroblasts 137

Figure 3-8: Effect of primary lymph node fibroblast co-culture on CLL cell survival 139

Figure 3-9: Comparison of different HFFF2 culture periods used to generate HFFF2-derived CM 141

Figure 3-10: Effect of HFFF2-derived CM on CLL cell survival 143

Figure 3-11: Effect of HFFF2-derived CM on CLL cell survival 144

Figure 3-12: Comparison of HFFF2-derived CM protection levels between different CLL disease subsets 145

Figure 3-13: Comparison of protection to CLL cells between HFFF2 direct co-culture and HFFF2-derived CM 146

Figure 3-14: Effect of HFFF2-cytoprotection following separation of both cell types by a microporous membrane 149

Figure 3-15: Effect of HFFF2-cytoprotection following separation of both cell types by a microporous membrane 150

Figure 3-16: Comparison of the ability of different culture methods using the HFFF2 cell line to provide protection from spontaneous apoptosis to CLL cells 151

Figure 3-17: Characterisation of the HFFF2 cell line 153

Figure 3-18: Characterisation of the HFFF2 cell line 155

Figure 4-1: Short-term levitation of CLL cells in acoustic trapping device 169

Figure 4-2: Short term levitation of HFFF2 cells in acoustic trapping device 171

Figure 4-3: Co-levitation of CLL and HFFF2 cells in acoustic trapping devices 175

Figure 4-4: Levitation of CLL cells in the acoustic trapping device; 4 hour analysis 177

Figure 4-5: Co-levitation of CLL and HFFF2 cells for 48 hours; parallel analysis in multiple in acoustic trapping devices. 181

Figure 4-6: Levitation of HFFF2 cells for 48 hours; parallel analysis in multiple in acoustic trapping devices. 183

Figure 4-7: Direct comparison of CLL, HFFF2 and mixed agglomerate morphology after 48 hours levitation in devices. 185

Figure 4-8: Summary of levitation findings comparing agglomerates containing CLL cells alone, HFFF2 cells alone and CLL and HFFF2 cells 187

Figure 4-9: Analysis of CLL cell viability using propidium iodide following levitation in acoustic trapping devices 191

Figure 4-10: Viability of CLL cells following 8 hours levitation in acoustic trapping devices 193

Figure 4-11: Viability of CLL cells following 8 hours levitation in acoustic trapping device 195

Figure 4-12: Viability of HFFF2 cells following 8 hours levitation in acoustic trapping device... 197

Figure 4-13: Viability of HFFF2 cells following 8 hours levitation in acoustic trapping device... 199

Figure 4-14: Optimisation of caspase 3/7 reagent staining 203

Figure 4-15: Viability of CLL cells following 8 hours levitation in acoustic trapping device using CellEvent caspase 3/7 reagent 205

Figure 4-16: Viability of HFFF2 cells following 8 hours levitation in acoustic trapping device using CellEvent caspase 3/7 reagent 209

Figure 4-17: Viability of CLL cells following culture on conventional tissue culture plastic versus non-treated petri dishes 211

Figure 4-18: Viability of HFFF2 cells following culture on conventional tissue culture plastic versus non-treated petri dishes 213

Figure 5-1: Separation of HFFF2-CM using Millipore separation columns with a 3kDa cut-off 231

Figure 5-2: Effect of low and high molecular weight fractions of HFFF2-CM on CLL cell survival 232

Figure 5-3: Quantification of CXCL12 levels in HFFF2 cell culture supernatant 234

Figure 5-4: Effect of HFFF2 cell culture on CXCR4 expression on CLL cells 237

Figure 5-5: Effect of HFFF2 cell co-culture on CXCR4 expression on CLL cells 238

Figure 5-6: Effect of HFFF2-derived CM on CXCR4 expression on CLL cells 240

Figure 5-7: Comparison of HFFF2 direct co-culture and HFFF2-derived CM on CXCR4 expression on CLL cells 241

Figure 5-8: Comparison of HFFF2 direct co-culture and HFFF2-derived CM on CXCR4 expression on CLL cells 242

Figure 5-9: Effect of neutralising antibodies to CXCR4 and CXCL12 on CLL cell migration 245

Figure 5-10: Effect of a CXCR4-specific neutralising antibody on the cytoprotective effects of HFFF2 cells on CLL cells 246

Figure 5-11: Effect of a neutralising antibody to CXCL12 on the protection provided by the HFFF2 cell line 247

Figure 6-1: Hierarchical clustering of RNA samples for GEP analysis 260

Figure 6-2: Hierarchical clustering of all RNA samples 261

Figure 6-3: Multi-dimensional scaling plot of all RNA samples 262

Figure 6-4: Comparison of CLL cells cultured alone and CLL cells cultured in the presence of the HFFF2 cell line 266

Figure 6-5: Comparison of CLL cells cultured alone and CLL cells cultured in the presence of HFFF2-derived CM 273

Figure 6-6: Comparison of CLL cells cultured alone and CLL cells cultured in the presence of αIgM beads 281

Figure 6-7: Schematic representing the GSEA results using the Cannonical Pathways data set....287

Figure 6-8: Schematic representing the GSEA results using the Cannonical Pathways data set....288

Figure 6-9: Surface IgM expression following co-culture with the HFFF2 cell line....291

Figure 6-10: Surface IgM expression following co-culture with the HFFF2 cell line....292

Figure 6-11: Surface IgM expression following co-culture with the HFFF2 cell line....293

Figure 6-12: Calcium flux analysis for two representative patients (CLL 635a and CLL 695) following co-culture with the HFFF2 cell line....294

Figure 6-13: Calcium flux analysis following co-culture with HFFF2 cells....295

Figure 6-14: Abundance of *IL6, IL8, CCL2* and *CXCL2* mRNA expression in CLL cells following co-culture with HFFF2-derived CM 297

Figure 6-15: Abundance of *IL6, IL8, CCL2* and *CXCL2* mRNA expression in CLL cells following co-culture with HFFF2-derived CM 299

Figure 6-16: Abundance of *IL6, IL8, CCL2* and *CXCL2* mRNA expression in CLL cells following co-culture with HFFF2-derived CM 300

Figure 6-17: Relationship between percentage non-CD5/CD19 cells and fold change of *IL6, IL8, CCL2* and *CXCL2* abundance following culture with HFFF2-derived CM....301

Figure 6-18: Intracellular staining of CCL2 in CLL cells 303

Figure 6-19: Level of CCL2 expression in CLL cells via intracellular staining using flow cytometry....304

Figure 6-20: Comparison of viability and HFFF2 protection levels in CLL PBMC and purified CLL cultures 306

Figure 6-21: Proposed model for a pro-survival mechanism involving HFFF2 cells, accessory cells and chemokines/cytokines....314

DECLARATION OF AUTHORSHIP

I, Elizabeth Anne Lemm

declare that this thesis entitled

MODELLING CHRONIC LYMPHOCYTIC LEUKAEMIA (CLL) CELL:MICROENVIRONMENT INTERACTIONS IN TWO- AND THREE-DIMENSIONAL CULTURE SYSTEMS

and the work presented in it are my own and has been generated by me as the result of my own original research.

I confirm that:

1. This work was done wholly or mainly while in candidature for a research degree at this University;
2. Where any part of this thesis has previously been submitted for a degree or any other qualification at this University or any other institution, this has been clearly stated;
3. Where I have consulted the published work of others, this is always clearly attributed;
4. Where I have quoted from the work of others, the source is always given. With the exception of such quotations, this thesis is entirely my own work;
5. I have acknowledged all main sources of help;
6. Where the thesis is based on work done by myself jointly with others, I have made clear exactly what was done by others and what I have contributed myself;
7. [Delete as appropriate] None of this work has been published before submission [or] ~~Parts of this work have been published as~~: [please list references below]:

Signed: .....

Date: .....

Acknowledgements

Firstly, I would like to thank my supervisor Professor Graham Packham for giving me the opportunity to carry out this research in his laboratory and his support and guidance throughout my PhD. I would also like to thank my second supervisor Professor Martyn Hill for his knowledge and guidance.

All the acoustic trapping devices used within this project were created by Dr Peter Glynne-Jones who played a pivotal part in this PhD. He was always available to explain the physics behind the ultrasonic levitation and to help with any problems that arose with the devices. Without his help and advice I could not have completed a proportion of the work in this thesis.

I am also grateful to the members of the CLL lab group for their support and encouragement during my PhD. Particularly to Dr Samantha Dias and Dr Alison Yeomans for mentoring me in the lab and to Dr Samantha Drennan and Dr Lindsay Smith for always providing a pleasant work environment.

I would especially like to thank my parents and family for their continued encouragement and moral support in every venture I undertake. Particular thanks must go to my partner Adam, for his patience and support, for his proof reading and computer help, and always listening to me moan about the stressful periods of the PhD. Without these people I would not have been able to achieve completing my PhD.

Finally I would like to acknowledge and thank the Cancer Research UK Centre and the University of Southampton for providing me with a scholarship to pursue my studies.

Definitions and Abbreviations

2D	Two dimension
3D	Three dimension
α-SMA	Alpha-smooth muscle actin
ALL	Acute lymphoblastic leukaemia
APRIL	Apoptosis-inducing ligand
BAFF	B-cell activating factor
BCA	Bicinchoninic acid
BCMA	B-cell maturation antigen
BCR	B-cell receptor
BM	Bone marrow
BMSC	Bone marrow stromal cell
BSA	Bovine serum albumin
CAF	Cancer associated fibroblast
cAMP	Cyclic adenosine monophosphate
CAR	Chimeric antigen receptor
CFSE	Carboxyfluorescein succinimidyl ester
CLL	Chronic lymphocytic leukaemia
CM	Conditioned media
CMV	Cytomegalovirus
CR	Complete remission
CpG-ODN	CpG oligodeoxynucleotides
DC	Dendritic cell
DMEM	Dulbecco's Modified Eagle Medium
DMSO	Dimethyl sulfoxide
DTT	Dithiothreitol
ECM	Extracellular matrix
EDTA	Ethylenediaminetetraacetic acid
EGFR	Epidermal growth factor receptor
EMT	Epithelial-mesenchymal transition
FACS	Fluorescent activated cell sorting

FC	Fold change
FCS	Foetal calf serum
FDC	Follicular dendritic cell
FISH	Fluorescence in situ hybridization
Fn	Fibronectin
FRET	Fluorescence resonance energy transfer
FSC	Forward scatter
GC	Germinal centre
GDP	Guanosine diphosphate
GEA	Gene expression analysis
GEP	Gene expression profiling
GPCR	G-protein coupled receptor
GSEA	Gene set enrichment analysis
GSH	Glutathione
GTP	Guanosine triphosphate
HEV	High endothelial venule
HFFF2	Human Caucasian foetal foreskin fibroblast
HMW	High molecular weight
HNSCC	Head and neck squamous cell carcinoma
HSC	Haematopoietic stem cell
HSC70	Heat shock cognate protein 70
IC	Isotype control
ICAM-1	Intercellular adhesion molecule 1
Ig	Immunoglobulin
IGHV	Immunoglobulin heavy chain variable region
IGLV	Immunoglobulin light chain variable region
IgV	Immunoglobulin variable
ITAM	Immunoreceptor tyrosine-based activation motif
LFA-1	Lymphocyte function-associated antigen 1
LMW	Low molecular weight
LN	Lymph node
M-CLL	*IGHV* mutated CLL

MDR	Minimal deleted region
MDS	Multi-dimensional scaling
MDSC	Myeloid derived suppressor cell
MMP	Matrix metalloproteinases
MRD	Minimal residual disease
mRNA	Messenger RNA
MSC	Mesenchymal stromal cell
MZ	Marginal zone
NFκB	Nuclear factor kappa B
NGS	Next generation sequencing
NK cell	Natural killer cell
NLC	Nurse-like cell
NZB	New Zealand black
ORR	Overall response rate
OS	Overall survival
PB	Peripheral blood
PBMC	Peripheral blood mononuclear cell
PBS	Phosphate buffered saline
PC	Proliferation centre
PDMS	Polydimethylsiloxane
PFA	Paraformaldehyde
PFS	Progression free survival
PI	Propidium iodide
PI3K	Phosphoinositide 3-kinase
PR	Partial response
PRF	Primary radiation force
PS	Phosphatidylserine
RT	RT
S1PR1	Sphingosine-1-phosphate receptor 1
SD	Standard deviation
SDF-1	Stromal cell-derived factor 1
SDS	Sodium dodecyl sulfate

SHM	Somatic hypermutation
sIg	Surface immunoglobulin
sIgM	Surface IgM
SLO	Secondary lymphoid organ
SSC	Side scatter
TACI	Transmembrane activator and calcium modulator and cyclophilin ligand interactor
TAM	Tumour-associated macrophage
TBS	Tris-buffered saline
TCL-1	T-cell leukemia/lymphoma 1
TME	Tumour miroenvironment
TGF- β	Transforming growth factor beta
U-CLL	*IGHV* unmutated CLL
UPR	Unfolded protein response
US	Ultrasound
USW	Ultrasound standing wave
USWT	Ultrasound standing wave trap
VCAM-1	Vascular cell adhesion protein 1
VEGF	Vascular endothelial growth factor
VLA-4	Very late antigen-4
ZAP70	Zeta-chain-associated protein kinase 70

Chapter One

Introduction

Chapter 1: Introduction

1.1 Overview

The overall goal of the experiments described in this thesis was to assess the potential utilisation of a novel three-dimensional (3D) cell culture method using ultrasound standing waves to investigate the role of the microenvironment in chronic lymphocytic leukaemia (CLL). Studies were performed using the HFFF2 fibroblast cell line as a model of the CLL microenvironment and this project focuses on the optimisation of 'acoustic trapping devices' to further understand CLL/fibroblast molecular interactions that promote CLL cell survival *in vitro*. The introduction will therefore provide the key background to the four main elements of the project; (i) CLL, (ii) the role of the microenvironment in CLL, (iii) 3D cell culture methods and (iv) acoustic trapping as a novel method for cell culture.

1.2 Chronic lymphocytic leukaemia

CLL is a B-cell malignancy and is the most common leukaemia in the Western World with just under 3000 people diagnosed annually in the UK (CRUK website, www.cancerresearchuk.org). CLL is characterised by the accumulation of malignant B cells in the blood, bone marrow (BM) and secondary lymphoid organs (SLOs) (most commonly the lymph nodes (LN) and spleen). Often classified as a disease of the elderly, CLL mainly affects people over the age of 60 with only around 10-15% of patients diagnosed under the age of 50 (Rozman and Montserrat, 1995). Men are affected more than women, with a 2:1 dominance (Rozman and Montserrat, 1995), and have a less favourable clinical course (Catovsky et al., 1989). CLL is a highly heterogeneous disorder with varied outcomes; some patients live for many years with the disease while others have a more rapidly progressing disease despite receiving aggressive treatment. The symptoms of CLL can also vary between patients, however many are asymptomatic and approximately 50% of cases are diagnosed by routine blood tests for other reasons (CRUK website, www.cancerresearchuk.org). If symptoms are present they are often mild at first and slowly worsen through progression of the disease. The symptoms are vague and similar to that of flu, including swollen lymph glands, weight loss, fever and tiredness caused by anaemia. Some patients also have recurrent infections.

1.2.1 Staging systems and prognostic markers

Staging systems for CLL were devised by Rai and colleagues in 1975 (Rai et al., 1975) and Binet and colleagues in 1981 (Binet et al., 1981) and these staging systems still form the foundations on which diagnosis and decisions regarding treatments are made. However due to the great heterogeneity between CLL patients, these staging systems often fail to predict the clinical course. Due to this heterogeneity and the importance of identifying patients with aggressive disease, research has focused on the identification of potential prognostic markers. Current prognostic markers include the presence or absence of somatic mutations of *IGHV* genes (Damle et al., 1999, Hamblin et al., 1999), the surface expression of a number of molecules including CD38 (Matrai, 2001, Damle et al., 1999), the integrin subunit CD49d (Gattei et al., 2008, Rossi et al., 2008, Shanafelt et al., 2008, Bulian et al., 2014, Majid et al., 2011), the chemokine receptor CXCR4 (Pepper et al., 2015, Ganghammer et al., 2016) and intracellular expression of ZAP70 (Crespo et al., 2003, Wiestner et al., 2003a, Dürig et al., 2003). Some of these are discussed in more detail later in this chapter. The clinical value of many of these markers still remains unclear and currently *TP53* mutation is the only biomarker that drives treatment decisions in CLL (Zenz et al., 2008, Stilgenbauer et al., 2002, Oscier et al., 2002). This is due to the fact that loss of function of p53-mediated DNA-damage response is associated with resistance to chemotherapy. Genetic aberrations are well known for their pathogenic and prognostic relevance in CLL. As such, Dohner et al*.,* outlined that patients could be stratified into a hierarchy of five main prognostic subgroups. Finally, soluble serum markers have also been associated with prognostic value including increased serum thymidine kinase (Kallander et al., 1984, Hallek et al., 1999) and serum β2-microglobulin (Gentile et al., 2009, Di Giovanni et al., 1989).

In addition to the above, novel classes of biomarkers have started to be identified in CLL. Firstly the activity of microRNAs (miRNAs); miRNA profiling revealed a unique miRNA signature that was differentially expressed in U-CLL and M-CLL patients and ZAP70 positive and ZAP70 negative patients (Calin et al., 2005) indicating that prognosis could be determined independent of *IGHV* gene mutation and ZAP70 status. Two of these miRNAs are miR-15a and miR16-1. miR-15a and miR16-1 have been described as tumour supressors in CLL (Calin et al., 2002, Cimmino et al., 2005, Calin et al., 2005) by directly repressing the expression of the anti-apoptotic gene BCL2 in CLL cells (Cimmino et al., 2005). miR-34a is another miRNA shown to have prognostic value in CLL. miR-34a is transcriptionally induced by p53 (He et al., 2007) and deletion of p53 is associated with the downregulation of the miRNA (Dijkstra et al., 2009). Wei et al., demonstrated that miR-34a was able to induce cell cycle arrest and caspase-dependent apoptosis via BCL2 (Wei

et al., 2008). Secondly, epigenetic abberrations such as DNA methylation have emerged as a novel class of biomarker (Kulis et al., 2012). Epigenetics, particularly DNA methylation is emerging as a useful method to track cellular origin (Queiros et al., 2015) and several epigenetic biomarkers are currently being assessed in the clinic (Heyn et al., 2013). Quieros et al., were able to classify CLL patients into three subgroups namely naive B-cell-like, intermediate and memory B-cell-like CLL using five epigenetic markers. They suggested that epigenetics was the strongest predictor for time to first treatment (TTFT); they demonstrated that the three subgroups based on epigenetic biomarkers predicted prognosis more accurately than *IGHV* mutation status (Queiros et al., 2015).

1.2.1.1 IGHV gene mutations

Mutations of *IGHV* genes are naturally acquired in normal B cells by somatic hypermutation (SHM) in response to antigen. As mentioned previously, CLL derives from B lymphocytes whose main role in normal biology is to elicit an antibody-directed immune response including against infections. This immune response is mediated by the B-cell receptor (BCR). The extracellular domain of the BCR consists of two heavy and two light chain immunoglobulins (Ig) which together form two pockets where antigens bind. Variation of this surface immunoglobulin (sIg) is important for diversity to enable the synthesis of specific antibodies. This diversity is in part a consequence of error-prone genetic recombination of different Ig genes and as a result humans can synthesise antibodies against virtually any foreign determinant. Further variation of the variable regions of the sIg occurs via SHM in the germinal centres (GC). GC form in peripheral lymphoid organs in response to antigen (MacLennan, 1994) and it is within these GC that B cells differentiate into the antibody producing plasma cells and memory cells. Within GC B cells proliferate and diversify by SHM in the immunoglobulin variable genes (IgV) to produce high affinity B cells.

It was found that CLL patients fall into two main subsets based upon the somatic mutation status of the variable regions of the expressed sIg heavy chain (Schroeder and Dighiero, 1994, Hamblin et al., 1999, Damle et al., 1999). Cells with *IGHV* mutations are classified as mutated (M-CLL) whereas those with ≥98% sequence homology with the nearest germline *IGVH* gene are classified as unmutated (U-CLL) (Figure 1-1). These two subsets are characterised by very different clinical behaviour. U-CLL is generally a more aggressive disease with a median survival of only 95 months compared to a median survival of 293 months for patients with M-CLL (Figure 1-2) (Hamblin et al., 1999). It is believed that U-CLL and M-CLL have different B cells of origin; U-CLL is thought to derive from a naive B cell that has not gone through affinity maturation in lymphoid organs (Stevenson and Caligaris-Cappio, 2004). In comparison, M-CLL derives from a memory B

cell which has a high affinity for antigen and have previously undergone affinity maturation (Stevenson and Caligaris-Cappio, 2004, Forconi et al., 2010).

1.2.1.2 Genetic aberrations in CLL

Genetic aberrations have provided a helpful insight into determining patients with rapidly progressing disease and have started to help overcome the problems with the heterogeneous nature of the disease. Chromosomal abnormalities are detected in up to 80% of CLL patients (Stilgenbauer et al., 2000, Dohner et al., 2000, Malek, 2013) and many now have a known prognostic value and play an important role in CLL pathogenesis. Fluorescence *in situ* hybridisation (FISH) has been used as the gold standard in detecting chromosomal abnormalities in CLL, however over recent years, next generation sequencing (NGS) methods have revealed a wide range of gene mutations in CLL which has allowed for the refining of prognostic subgroups. As described in Section1.2.1, genetic aberrations have been used to predict prognosis and following studies by Dohner et al., 2000, patients can be split into prognostic subgroups (Figure 1-3, Figure 1-4 and Table 1.1). Table 1.1 outlines these prognostic subgroups and associated genetic factors. Aberrations with a very high risk are del17p, *TP53* mutations and/or *BIRC3* mutation (Rossi et al., 2013). High risk are del11q, *ATM* mutation and/or *NOTCH* mutation and/or *SF3B1* mutations (Tsimberidou et al., 2009). Trisomy 12 is associated with an intermediate risk (Dohner et al., 2000), and does not significantly affect survival compared to normal karyotype and low risk aberrations are isolated del13q (Parker et al., 2011).

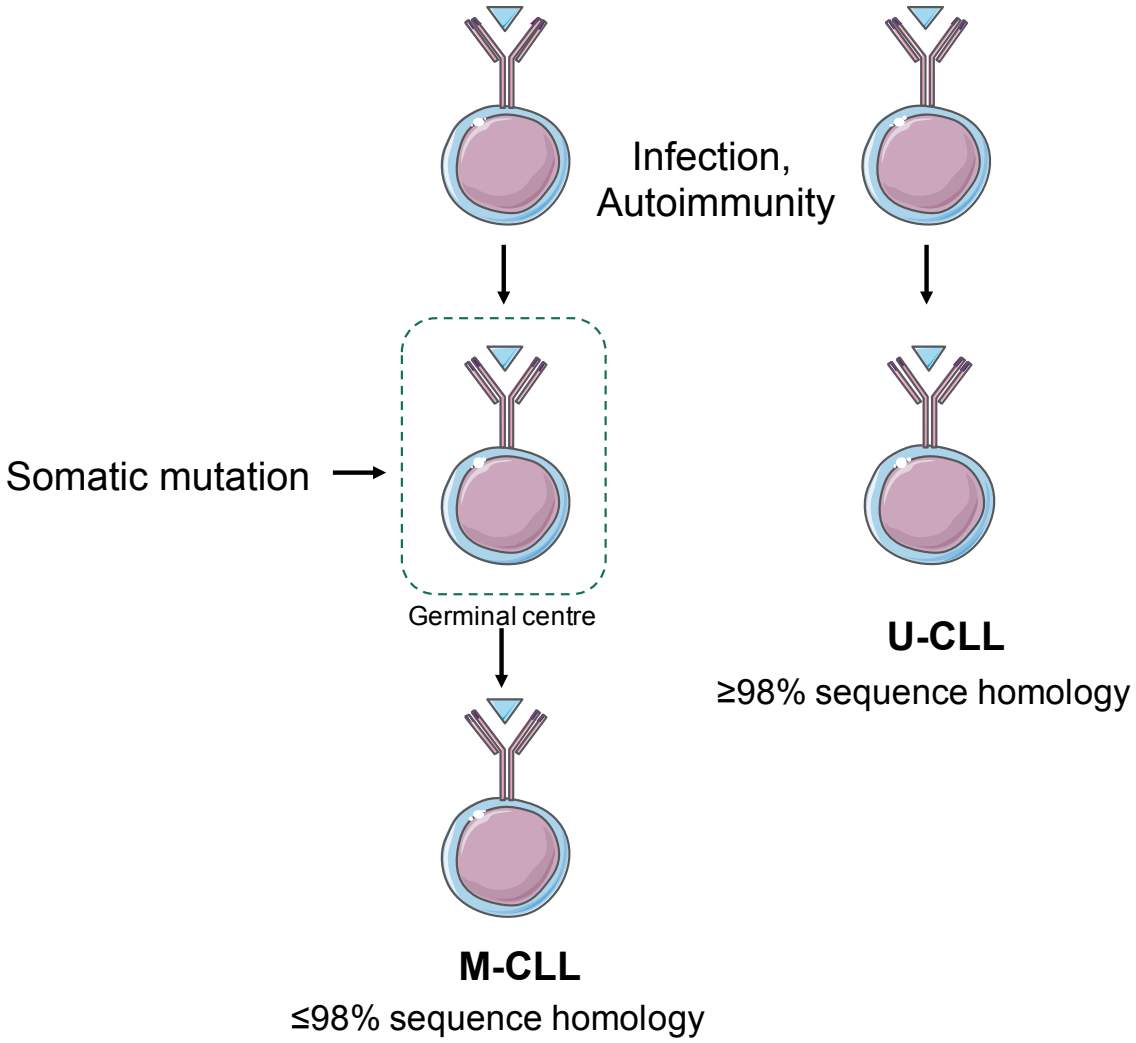

FIGURE 1-1: PATHOGENESIS OF CLL SUBSETS

Pathogenesis of the 2 major subsets mutated and unmutated CLL (M-CLL and U-CLL respectively). Infection or autoimmunity are likely initial drivers, with transformation to U-CLL occurring before initiation of somatic mutation while M-CLL is believed to develop from more mature B cells presumed to have undergone antigen selection in the germinal centre (Adapted from (Stevenson et al., 2011)).

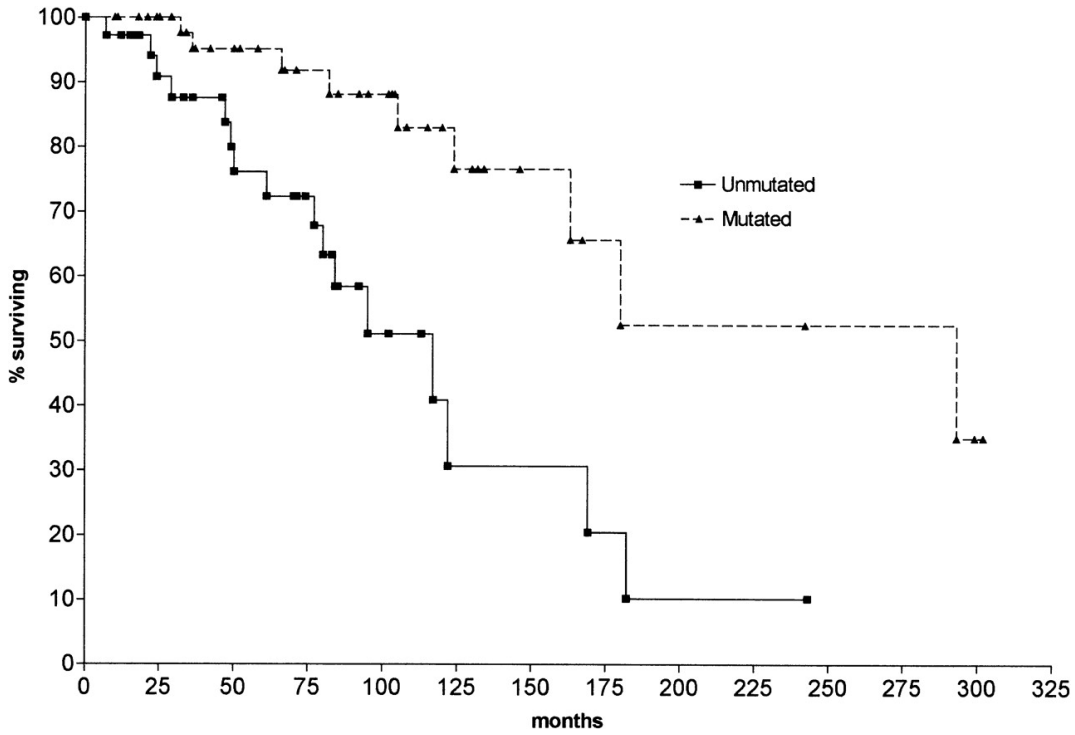

FIGURE 1-2: KAPLAN-MEIER SURVIVAL CURVE COMPARING CLL PATIENTS WITH MUTATED AND UNMUTATED *IGVH* GENES. TAKEN FROM (HAMBLIN ET AL., 1999).

Kaplan-Meier survival curve comparing CLL patients with mutated and unmutated *IGHV* genes. Median survival for unmutated CLL: 117 months; median survival for mutated CLL: 293 months. The difference is significant at the P = .001 level (log rank test).

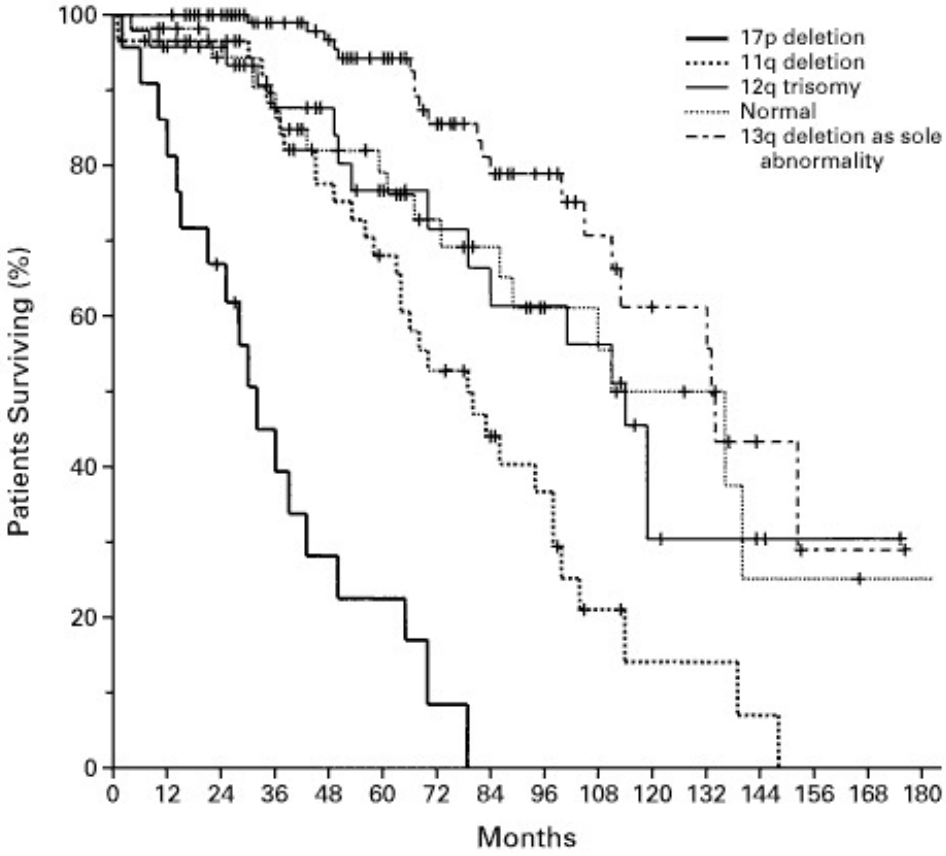

No. at Risk																
17p deletion	23	18	13	8	5	4	1	0	0	0	0	0	0	0	0	0
11q deletion	56	53	47	43	33	27	20	15	10	4	2	2	1	0	0	0
12q trisomy	47	44	41	29	24	17	14	13	12	11	4	3	2	1	1	0
Normal	57	51	45	37	30	27	20	17	12	11	6	5	2	2	1	1
13q deletion as sole abnormality	117	117	106	91	80	63	45	36	24	16	12	11	3	1	1	0

FIGURE 1-3: MAIN GENETIC ABERRATIONS IN CLL AND THEIR CLINICAL SIGNIFICANCE

Kaplan-Meier curve demonstrating the probability of survival among patients in the five genetic categories (Taken from (Dohner et al., 2000)). Number of patients per catergory is displayed in the table before the curve.

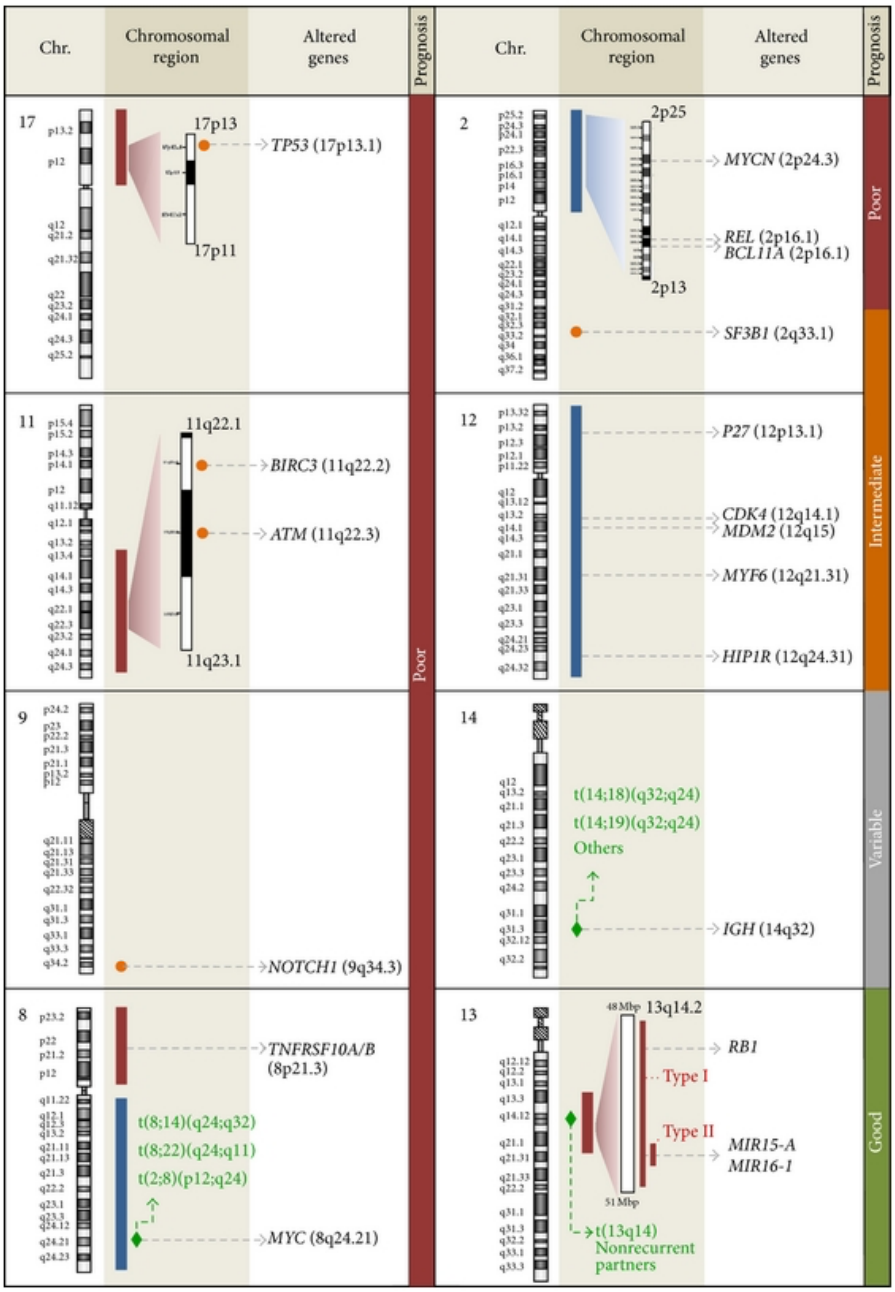

FIGURE 1-4: MAIN GENETIC ABERRATIONS IN CLL AND THEIR CLINICAL SIGNIFICANCE

Genetic abnormalities grouped by chromosome. Loses and gains are represented in black and blue bars respectively, breakpoints for translocations are depicted as green diamonds and loci where recurrently mutated genes are located are shown in orange circles. (Image taken from (Puiggros et al., 2013)).

TABLE 1.1: : PROGNOSTIC SUBGROUPS AND ASSOCIATED RISK GENETIC FACTORS IN CLL AT POINT OF DIAGNOSIS (ADAPTED FROM (PUIGGROS ET AL., 2013)).

Category	Associated genetic factors	
Very high risk	del(17p) *TP53* mutation *BIRC3* mutation	Deletion of 17p is found in approximately 2-8% of CLL patients at diagnosis (Delgado et al., 2012, Wawrzyniak et al., 2014, Dohner et al., 2000). Deletion of 17p is found in 30% of patients that have refractory CLL following treatment and is therefore considered one of the most frequently acquired aberration following cytotoxic therapy (Wawrzyniak et al., 2014, Stilgenbauer et al., 2009). Patients with 17p deletions show the shortest overall survival (OS) and progression free survival (PFS). This is probably explained by the loss of *TP53* causing cell-cycle deregulation. *BIRC3* disrupting mutations and deletions have been rarely detected in CLL at diagnosis (4%) but detected in 24% of fludarabine-refractory CLL patients (Rossi et al., 2012).
High risk	del(11q) *ATM* mutation *NOTCH1* mutation *SF3B1* mutation	5-20% of CLL patients have deletion of the long arm of chromosome 11 (Dohner et al., 2000, Marasca et al., 2013, Zenz et al., 2010). The minimal deleted region (MDR) of chromosome 11 harbours the *ATM* gene in almost all cases.
Intermediate risk	Trisomy 12 Normal karyotype and FISH	Trisomy 12 is the third most common aberration and is detected in 10–20% of CLL cases. Trisomy 12 is unique as it often appears as a unique cytogenetic alteration (40–60% of cases).
Low risk	Isolated del(13q)	Deletion of 13q14 region, is the most common cytogenetic abnormality found in CLL patients and is detected in approximately 50% of patients (Dohner 2000). 13q deletions include MiR-15a and MiR16-1 which have been shown to have a tumour suppressor function in CLL (Calin et al., 2002, Klein et al., 2010). Loss of 13q14 can lead to BCL2 overexpression (Cimmino 2006).

1.2.2 Current treatment strategies

Treatment of CLL is usually based on multiple factors including (i) stage of disease, (ii) severity of symptoms, (iii) blood counts and (iv) disease progression. For indolent disease, a "watch and wait" approach is normally employed with studies showing that suitable patients who follow this approach have similar outcomes to those treated early in the course of their disease. There are many treatment options for patients with more aggressive disease including radiation, combination drug regimens, surgery and stem cell transplants. In general, patients who are older or frail are typically treated with less aggressive regimens than those who are younger and healthier. The most favoured treatment approach for newly diagnosed patients is fludarabine-based treatments and more commonly fludarabine-based combination therapies such as FCR (fludarabine, cyclophosphamide and rituximab, an (anti-CD20 antibody)). Although FCR is an established standard-of-care for physically fit patients with CLL requiring therapy (Hallek et al., 2010) there is the need for the accurate identification of patients likely to achieve long PFS given the toxicity of such compounds. There is a small subset of M-CLL patients which achieve long-term PFS on an FCR treatment regime. In this subset of patients with mutated *IGHV* genes a plateau was seen on the PFS curve, with no relapses beyond 10.4 years in 42 patients (Thompson et al., 2016). These data indicate that in this small subset, FCR has the possibility to cure the disease. However, for the majority CLL is still an incurable disease with many patients relapsing from minimal residual disease (MRD).

1.2.2.1 New treatment strategies

It has become increasingly apparent that successful treatment of CLL must target the proliferative compartment of the disease. This proliferative compartment resides within the tissues, particularly the LN (Herishanu et al., 2011), See Section1.4). Increased appreciation of the importance of BCR signalling in CLL has also provided new opportunities for drug therapy. BCR pathways are important drivers of the survival and proliferation of CLL cells (see Section1.4.2.1) and recent work has focussed on inhibiting specific pathways acting downstream of this receptor. In particular, two lead compounds have emerged from clinical trials that target signalling kinases downstream of the BCR, namely ibrutinib which inhibits Bruton's tyrosine kinase (BTK) and idelalisib which inhibits the delta isoform of phosphoinositol-3 kinase (PI3Kδ). Both of these compounds have shown extremely promising results. Ibrutinib is now FDA approved for the treatment of CLL (Advani et al., 2013, Byrd et al., 2013, Byrd et al., 2012) and idelalisib has also been used as a treatment strategy of CLL and can be used a single therapy with modest response rates (Brown et al., 2013), or in combination with rituximab where improved

response rates have been seen (Brown et al., 2014b, Furman et al., 2014). Idelalisib is also approved by the FDA for the treatment of several types of blood cancer including CLL, however recently some severe toxicity issues have emerged and as a result the US prescribing information contains a black box warning for fatal and/or severe diarrhea or colitis, hepatotoxicity, pneumonitis and intestinal perforation (ZYDELIG (idelalisib tablets) Full prescribing information, Gilead Sciences, Inc., Foster City, CA, 2014).

A remarkable feature of both of these drugs is that clinical response is associated with a profound lymphocytosis whereby cells redistribute from the disease tissues compartments into the blood stream (Woyach et al., 2014, Brown et al., 2014a, Herman et al., 2014). It is not clear whether this is due to blockage of pathways mediating CLL cell entry into tissues, inhibition of cell retention, or both. The effects of both ibrutinb and idelalisib have been studied *in vitro* and demonstrated that inhibition of BTK and PI3K had effect on migration and adhesion. Ibrutinib inhibits CLL cell chemoktaxis to CXCL12 and CXCL13 *in vitro* (Ponader et al., 2012, de Rooij et al., 2012) and strongly inhibited integrin α4β1-mediated adhesion to fibronectin and VCAM-1 (de Rooij et al., 2012). Herman et al., tested the ability of *ex vivo* patient samples to migrate and adhere following treatment of ibrutinib in a phase II clinical trial. They compared the ability of cells taken pre-treatment to cells taken following 28 days of ibrutinib therapy to adhere. After 28 days on ibrutinib, CLL cells displayed a severely reduced adhesion ability. They also demonstrated that ibrutinib could interfere with adhesion by causing cells to detach from a confluent stromal layer (Herman et al., 2014). These data suggest that ibrutinib can not only prevent CLL cell adhesion but can release adhered cells from the microenvironment, consistent with the lymphocytosis from the LN into the PB seen within hours of starting treatment (Herman et al., 2014). Idelalisib also inhibits CLL cell chemotaxis towards CXCL12 and CXCL13 and migration beneath stromal cells (pseudoemperipolesis) (Hoellenriegel et al., 2011) as well as CLL cell adhesion to endothelial cells and bone marrow stromal cells (BMSC) *in vitro* (Fiorcari et al., 2015a). The underlying molecular mechanisms of these reductions in migration and adhesion are likely to be complex, and may involve effects on both BCR-mediated signalling, or 'off-target effects' via signalling through other receptors which may also utilise BTK and/or PI3K for signal transduction. Regardless, the striking lymphocytosis highlights the importance of CLL cell recirculation and microenvironmental interactions *in vivo*.

Other promising targets include BCL2 inhibitors or BH3 mimics such as ABT-199, immunodulatory drugs such as lenalidomide or chimeric antigen receptor (CAR) T cell therap. Details of current novel treatment strategies are outlined in Table 1.2.

TABLE 1.2: NOVEL STRATEGIES IN THE TREATMENT OF CLL

Category of novel treatment strategy	Examples	Mechanism of action	Use in CLL
BCR inhibitors	BTK inhibitors (Ibrutinib)	Ibrutinib is an oral, selective and irreversible inhibitor of BTK (Pan et al., 2007). *In vitro* studies have demonstrated the ability of ibrutinib to induce apoptosis in CLL cells cultured in media alone or with microenvironment stimulation such as CD40L, BAFF or IL-4 (Herman et al., 2011). Ibrutinib interferes with CLL-cell adhesion and migration. (de Rooij et al., 2012, Ponader et al., 2012).	Phase II studies demonstrated an overall response rate (ORR) of 90% with a 7% having complete remission (CR) and 65% showing partial remission (PR). The estimated PFS from these studies at 30 months was 69% (Byrd et al., 2015, Byrd et al., 2013). These trials led to the phase III trial (RESONATE trial) comparing ibrutinib to ofatumumab. The ibrutinib arm had a higher ORR, PFS and OS compared to the ofatumumab arm (Byrd et al., 2014). Based on this trial, ibrutinib was approved for use by the FDA for patients with refractory CLL.
	PI3K inhibitors (Idelalisib)	Idelalisib is a selective and reversible inhibitor of PI3K-δ (Herman et al., 2010). *In vitro* studies have demonstrated the ability of idelalisib to induce apoptosis in CLL cells cultured alone or with microenvironment stimulations (CD40L or TNF-α) (Herman et al., 2010, Hoellenriegel et al., 2011).	In a Phase II study with CLL patients the ORR was 72% with 39% demonstrating PR. The median PFS from this study was 15.8 months (Brown 2014). The subsequent phase III trial evaluated the activity of rituximab plus idelalisib (Furman 2014). This trial demonstrated superiority for the combination of idelalisib and rituximab over rituximab standalone therapy.
	SYK inhibitors (Fostamatinib and Entospletinib)	Fostamatinib (R406) is a potent and selective inhibitor of SYK (Braselmann et al., 2006). Entospletinib is an oral selective inhibitor of SYK and is more selective than R406 (Currie et al., 2014). The SYK inhibitor fostamatinib inhibits downstream signalling of the BCR and has been shown to increase survival in the Eμ-TCL1 transgenic mice. (Suljagic et al., 2010).	In a phase I/II study 55% achieved PR (Friedberg et al., 2010). In a CLL phase II study for Entospletinib the ORR was 61% all of which were PR and there was a PFS of 14 months (Sharman et al., 2015).

BCL2 inhibitors	ABT-199	ABT-199 is a BH3 mimetic. BH3 is the binding domain common to the BH3 family of proteins which play a key role in apoptosis. CLL-cell survival and proliferation relies on the over-expression of the anti-apoptotic protein BCL2 (Hanada et al., 1993).	A Phase I clinical trial demonstrated that ABT-199 was highly active against relapsed/refractory disease. The OR rate was 84%, of which 20% achieved a CR (Seymour et al., 2013).
Immunomodulatory drugs	Lenalidomide	Lenalidomide is an immunomodulatory drug which has multiple effects on the tumor microenvironment and immune system. The precise mechanism of action of lenalidomide is not yet completely defined. Effects in CLL include: antiangiogenic effect, blockade of pro-tumour cytokines, inhibition of pro-survival interactions between BMSC and CLL cells, and enhancement of T cell function (Chanan-Khan et al., 2006).	In a phase II study of CLL patients with relapsed or refractory CLL observed OR and CR rates were 47% and 9% respectively (Chanan-Khan et al., 2006). Lenalidomide has been used recently as a frontline therapy in combination with rituximab (James et al., 2014, Thompson et al., 2014, Thompson et al., 2016).
Cellular therapy	Chimeric antigen receptor (CAR) T cell therapy	CAR T cell therapy is the *ex vivo* manipulation of T cells to produce T cells that have a chimeric antigen. CAR T cell therapy overcomes the defect seen in T cell surveillance in CLL (Kalos et al., 2011).	In CLL, trials of CAR T-cells expressing a receptor to the CD19 antigen have been successful in the treatment of relapsed/refractory CLL. 29% achieved a CR, 29% a PR and there was an OR rate of 57% (Porter et al., 2015).
CXCR4 antagonists	Plerixafor	Plerixafor, a bicyclam molecule is a specific, small molecule antagonist of CXCR4 which is licenced for stem cell mobilisation and is currently in clinical trials for CLL. Plerixafor inhibits chemotaxis to CXCR4 and therefore effectively blocks the ability of CLL cells to home to the tumour microenvironment. Plerixafor also overcomes the protective effect of microenvironment models *in vitro* (Stamatopoulos et al., 2012).	In a phase I dose-escalation trial plerixafor was given in combination with rituximab. Plerixafor was well tolerated there was an associated increase in lymphocyte count, suggesting successful mobilization of CLL cells from the LN and marrow (Andritsos et al., 2010). A phase I clinical trial of plerixafor used incombination rituximab showed a plerixafor dose-dependent mobilization of CLL cells into the peripheral blood.

1.3 The microenvironment

The microenvironment is a compilation of accessory cells that work together through cell-cell contact and soluble factors to provide a supportive environment for the functioning cells within the organ or tissue in which they reside. In terms of cancer, interactions between tumour cells and the non-malignant cells form what is termed the tumour microenvironment. The tumour microenvironment is defined as all non-cancerous cells present in the tumour; this can include fibroblasts, immune cells, cells comprising the blood vessels as well as the extracellular matrix (ECM) and any soluble factors produced by these cells. Intercellular communication within the tumour microenvironment is driven by a complex network of chemokines, cytokines and growth factors. The tumour microenvironment is essential for tumour cell proliferation, angiogenesis, invasion, and metastasis and the non-malignant cells in the tumour microenvironment often play a tumour-promoting role.

The components of the tumour microenvironment can be broadly split into three main groups: cells of haematopoietic origin, cells of mesenchymal origin and the non-cellular component (Figure 1-5). Different tumours as well tumours in different stages of progression contain differing proportions of these components. Haematopoietic cells arise in the bone marrow and can be subdivided into cells of the lymphoid lineage, consisting of T cells, B cells and natural killer (NK) cells, and those of the myeloid lineage, which includes macrophages, neutrophils and myeloid-derived suppressor cells (MDSCs). Cells of mesenchymal origin are derived from the mesenchyme and include fibroblasts, myofibroblasts, mesenchymal stem cells (MSCs), adipocytes and endothelial cells. The non-cellular component of the tumour microenvrionment consists of many distinct components, the major player being the ECM.

Many cell types comprising the tumour microenvironment have been implicated in tumour survival and progression. Tumour microenvironment niches support tumour cell survival by contributing to all of Hanahan and Weinburgs ‘Hallmarks of cancer’ (Hanahan and Coussens, 2012, Hanahan and Weinberg, 2011, Hanahan and Weinberg, 2000, Shain et al., 2015) (Figure 1-6). Virtually every stromal cell type has been demonstrated to have the ability of support the proliferation of cancer cells. Further to proliferation support, stromal cells in the tumour microenvironment are also able to help cancer cells evade growth suppression. The tumour microenvironment can fuel the growth of tumour cells, contribute to metastatic potential and shield malignant cells from cytotoxic agents, thus, direct targeting of the tumour stroma has become an attractive strategy for the development of new therapeutic agents.

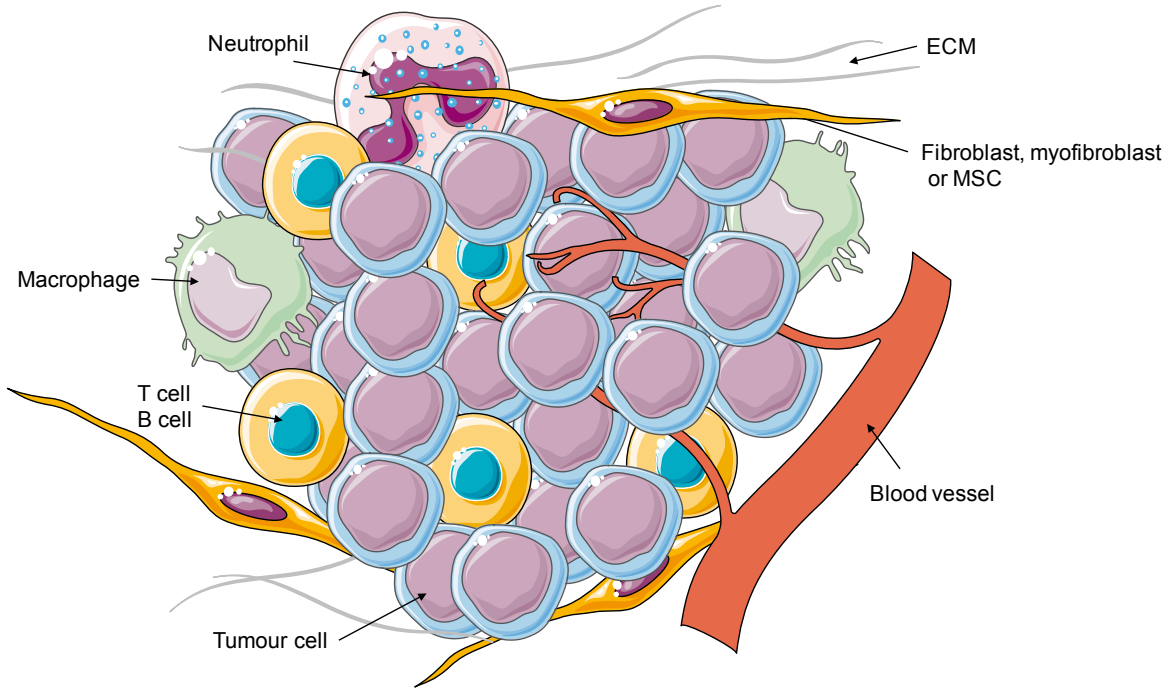

FIGURE 1-5: THE TUMOUR MICROENVIRONMENT IN SOLID TUMOURS

Tumour cells in solid tumours are surrounded by a complex microenvironment consisting of a number of different cellular players including stromal cells, blood vessels and infiltrating inflammatory cells. The tissue stroma composes of cells including fibroblasts, myofibroblasts and mesenchymal stromal cells. Most stromal cells participate in tumour cell growth, angiogenesis, extracellular matrix remodelling and epithelial mesenchymal transition. Fibroblasts support tumour cell growth by secreting a plethora of cytokines and growth factors. Immune cells include both B and T lymphocytes as well as neutrophils and macrophages. M2-like polarised macrophages, also known as tumour associated macrophages (TAMs) also contribute to tumour cell growth. Image made using Servier medical art.

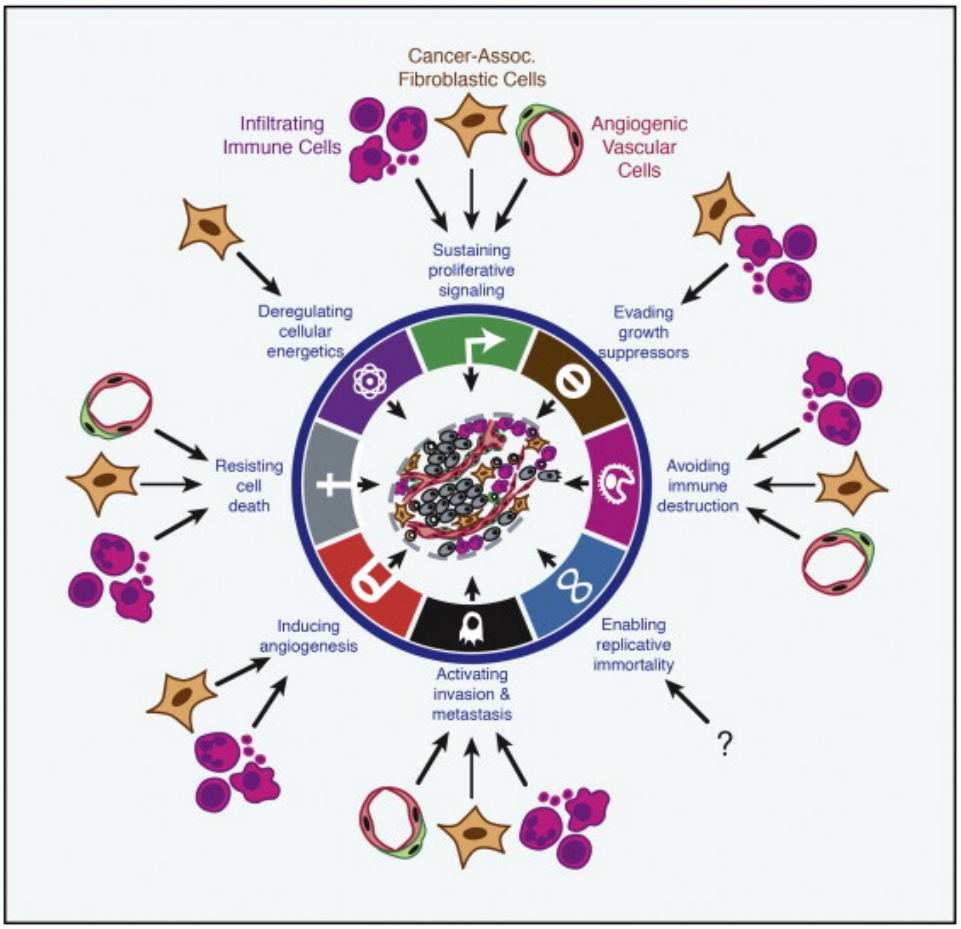

FIGURE 1-6: THE TUMOUR MICROENVIRONMENT SHAPES THE HALLMARKS OF CANCER (TAKEN FROM (HANAHAN AND COUSSENS, 2012)

The tissue microenvironment has the ability to support tumour development by fostering the key hallmarks of malignancy (six core and two new emerging): resistance to cell death, cell homing and invasion, sustained proliferation, avoiding immune destruction, self-renewal and stemness, angiogenesis deregulating cellular energetics, and evading growth suppressors. The relationship between malignant cells and microenvironment stromal cells enables and sustains malignant cell growth.

1.3.1 The tissue stroma

One of the major and most researched part of the tumour microenvironment is the tissue stroma. The 'stroma' is the collective term for the supportive tissue consisting of a number of cells including fibroblasts, myofibroblasts, epithelial, vascular, smooth muscle and immune cells along with their ECM and extracellular molecules. In cancer, tumour cells and their stroma have been shown to co-evolve and the nature of the interaction between stromal cells and tumour cells is often bidirectional (Li et al., 2007). Interactions between stromal and malignant cells leads to altered growth factor and chemokine production by fibroblasts, which ultimately provide growth and survival signals and drug resistance. Tumour cells also attract stromal cells into the tumour microenvironment where these cells then in turn affect tumour cell survival by fostering many of the hallmarks as discussed in Figure 1-6

1.3.1.1 Mesenchymal stromal cells

The term MSC is a term used to define a heterogeneous subset of multipluripotent stem cells. These cells have the ability for self-renewal and, upon exposure to the appropriate signals can differentiate into various cell types including osteoblasts, adipocytes and chondrocytes which subsequently give rise to multiple mesenchymal tissues including bone, fat and cartilage respectively (Figure 1-7). The differentiation of MSC into lineage specific cells is controlled by a number of factors including cell:cell and cell:ECM interactions, cytokines, chemokines as well as growth factors (Pittenger et al., 1999, Wagner and Ho, 2007). The term MSC itself is ill-defined and covers not only the original mesenchymal stem cell that was defined by Caplan in 1994 but now includes stromal stem cells, multipotent stromal cells, mesenchymal stromal cells and also multipotent adult progenitor cells (Caplan, 1994). This makes the interpretation of their role in the progression of malignancies more complex. However, MSCs have been implicated in a number of pathological conditions such as tissue repair, inflammation as well as cancer.

MSCs display homing to sites of injury and inflammation in a number of pathological conditions including cancer (Wu and Zhao, 2012). The mechanism involved in the recruitment of MSC into tumour sites occurs through a number of chemoattractants such as vascular endothelial cell growth factor (VEGF) (Schichor et al., 2006), tumour produced IL-8 (Birnbaum et al., 2007), and chemokines such as CCL2 (Dwyer et al., 2007) and CXCL12 (Spaeth et al., 2008, Xu et al., 2009, Hara et al., 2008, Wynn et al., 2004). Once within the tumour site, *in vivo* tracking has shown that MSCs differentiate into fibroblasts, pericytes and myofibroblasts (Kidd et al., 2008) to create an environment that is similar to a chronic wound (Dvorak, 1986). Once within the tumour microenvironment, MSC are an

important source of several inflammatory cytokines including IL-6, IL-10, CCL5 and VEGF (Bergfeld and DeClerck, 2010). MSC have four main effects on tumour cells. (i) they affect cell survival having both a pro-and anti-apoptotic effect on tumour cells demonstrated by studies using a number of different tumours (ii) they contribute to the tumour vasculature by producing angiogenic factors (Feng and Chen, 2009), (iii) they promote tumour cell motility and metastasis through the production of CCL5 (Xu et al., 2009) and finally (iv) they have a immunomodulatory role by inhibiting T helper lymphocytes, dendritic cells, B cells and NK cells (Sotiropoulou and Papamichail, 2007).

1.3.1.1 Fibroblasts

The most predominant cell type in the tissue stroma is the fibroblast (Brouty-Boyé, 2005). These spindle shaped, metabolically active cells play a critical role in the structural framework of the stroma by regulating the ECM and tissue fluid and pressure levels. Fibroblasts are the primary producers of ECM components and also regulate the degradation of the ECM through the secretion of matrix metalloproteinases (MMPs) (Kalluri and Zeisberg, 2006). Fibroblasts exhibit several phenotypes, but under normal conditions they are present in a non-contractile, 'inactive' state. During wound healing and pathological conditions that requires tissue remodelling, under the appropriate signals, fibroblasts transdifferentiate into their 'active' counterpart the myofibroblast (Figure 1-8). These activated fibroblasts, myofibroblasts, were originally described by Giulio Gabbiani in 1971 (Gabbiani et al., 1971) and differ morphologically and functionally from quiescent fibroblasts. In response to mechanical stress, myofibroblasts acquire stress fibres (Hinz et al., 2007) and express α-smooth muscle actin (α-SMA) both of which are specific to the activated phenotype. During wound healing, these transdifferentiated and activated myofibroblasts serve as a scaffold structure for cell growth and secrete a number of different growth and chemotactic factors which leads to an influx in immune and vascular cells to help tissue repair (Hinz, 2007).

It has been demonstrated that transforming growth factor beta (TGF-β) coordinates myofibroblast transdifferentiation both *in vivo* and *in vitro* (Abe et al., 2001, Yang and Liu, 2001, Serini et al., 1998, Vaughan et al., 2000). A number of studies have demonstrated the importance of TGF-β in myofibroblast transdifferentiation. Studies have shown that treatment with TGF-β to a number of different cell types induces α-SMA expression, the accumulation of spindle shaped cells and promotes the generation of a contractile force (Vaughan et al., 2000). Additional cytokines have been tested, yet none where able to produce the responses seen by TGF-β (Ronnov-Jessen and Petersen, 1993). As such treatment of TGF-β is now used routinely to cause myofibroblast differentiation *in vitro*.

1.3.1.1.1 Fibroblasts in cancer

As in normal tissue homeostasis, fibroblasts are the main cellular components of the tumour stroma. Myofibroblasts are present in the stroma of many types of solid tumours and in some cancers, fibroblasts even constitute a larger proportion of cells in the tumour than cancer cells themselves (Li et al., 2007). Tumours have often been described as wounds that do not heal and therefore within solid tumours fibroblasts are mainly present in their activated phenotype and known as 'cancer associated fibroblasts' (CAFs). CAFs secrete a variety of soluble factors which not only affect tumour cells but also other cells in the microenvironment. Through the secretion of these soluble factors, CAFs promote tumour growth and invasion and enhance angiogenesis.

Many groups have studied the impact of myofibroblasts on disease progression. and α-SMA expression has been linked to metastasis and disease progression in a number of different cancer types including breast cancer, pancreatic cancer, prostate cancer and lung cancer (Yamashita et al., 2012, Hwang et al., 2008, Olumi et al., 1999). CAFs can also directly be used a prognostic marker in a number of solid tumours and often correlate with histopathological grade (Paulsson and Micke, 2014, Nakao et al., 2009, Chuaysri et al., 2009, Underwood et al., 2015).

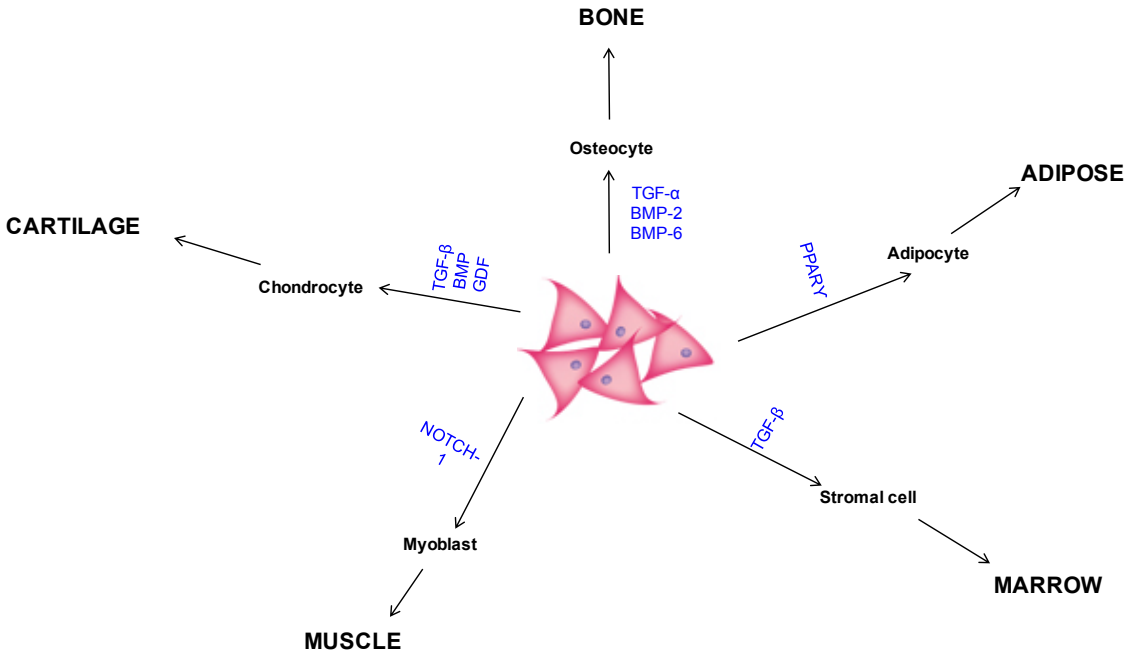

FIGURE 1-7: MESENCHYMAL STEM CELLS

MSCs are a heterogeneous subset of multipluripotent stem cells. These cells have the ability for self-renewal and, upon exposure to the appropriate signals they can differentiate into various cell types. The differentiation of MSC into lineage specific cells is controlled by a number of factors including cell:cell and cell:ECM interactions, cytokines, chemokines as well as growth factors (Pittenger et al., 1999, Wagner and Ho, 2007).

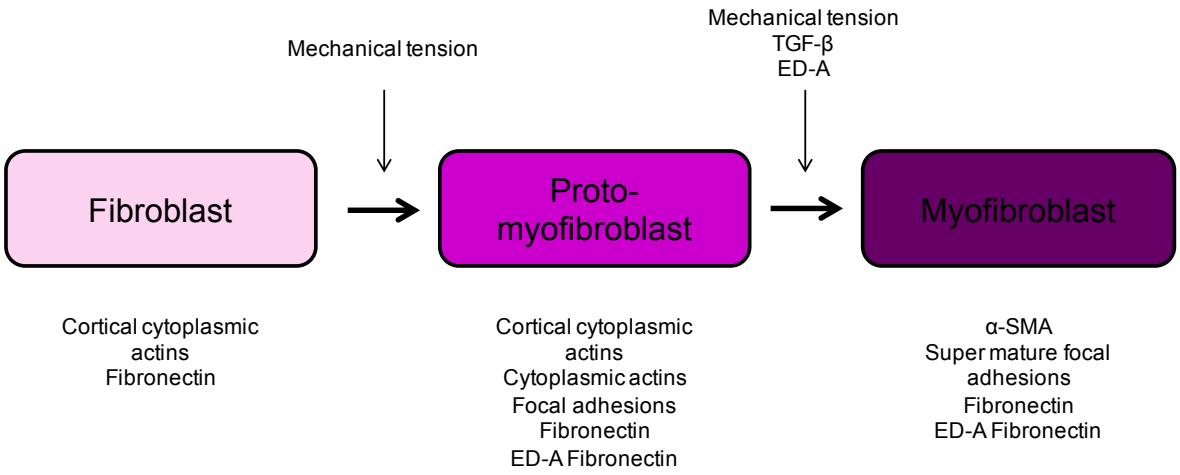

FIGURE 1-8: MODEL OF MYOFIBROBLAST TRANSDIFFERENTIATION

Fibroblasts in their resting 'inactive' state have been shown to contain actin but do not express stress fibres or form adhesion complexes to the ECM. Under mechanical stress fibroblasts will differentiate into the intermediary counterpart the proto-myofibroblast. In comparison to fibroblasts, proto-myofibroblasts start to form cytoplasmic actin which contain stress fibres which are attached to focal adhesions. Proto-myofibroblasts also express and organise cellular fibronectin, including the ED-A splice variant at their cell surface. Presence or treatment ofTGF-β further increases the expression of ED-A fibronection. Both of these factors in the presence of further mechanical stress cause the cell to differentiate into the active counterpart, the myofibroblast. Myofibroblasts are characterised by the expression of α-SMA which forms extensive contractile stress fibres to supermature focal adhesions.

1.3.2 The microenvironment in haematological malignancies

The role of the microenvironment has been most widely researched in terms of solid tumours however, the microenvironment also plays an important role in haematological malignancies. Although mainly present in the peripheral blood, haematological cancers develop in specialised tumour microenvironments that contain different populations of accessory cells. These cells interact with malignant cells and promote tumour growth and survival (Caligaris-Cappio, 2003). In haematological malignancies the BM and SLO most often form the tumour microenvironment compartments. Like solid tumours, the haematological tumour microenvironment consists of accessory stromal cells and immune cells.

The microenvironment of haematological malignancies, as with solid tumours often mirrors the environment of the tissue in a normal physiological state. The microenvironment in haematological malignancies can differ to that in solid tumours, because of specific features of lymphocytes such as antigen stimulation. The BM and SLO have entirely different microenvironments, due to the fact that each is finely tuned to support different aspects of lymphocyte maturation and differentiation and therefore there are also differences between the two sites in terms of supporting malignant cells.

1.3.2.1 The bone marrow microenvironment

The BM resides within the central compartment of long and axial bones and hosts the development of mature B cells from committed progenitors leading to the production of B cells which are equipped with a functional antigen receptor. It is also the main site of haematopoiesis and it serves as a reservoir for the pluripotent haematopoietic stem cells (HSCs) which generate all haematopoietic lineages including erythrocytes, granulocytes, monocytes, lymphocytes and platelets. HSCs are maintained in specialised niches by accessory cells and the development of B cells from these early progenitors requires intimate contact with the stroma (Nagasawa, 2006). There are two distinct microenvironmental niches in the BM, the ‘osteoblastic’ and ‘vascular’ niches. Key components of the BM microenvironment involved in normal haematopoiesis is critical for leukaemia/microenvironment interactions. These niches contain a number of accessory cells, such as osteoblasts and osteoclasts, MSC, endothelial stromal cells and immune cells and all these cells work together to regulate the process of haematopoiesis. As with normal cells, leukaemia cells are also dependent on signals from these cells (Dührsen and Hossfeld, 1996).

1.3.2.2 The secondary lymphoid organ microenvironment

SLOs function to form a filtration and surveillance system to capture pathogens and their antigens, to allow for presentation to cells of the immune system. The SLOs are supported by a network of endothelial and mesenchymal stromal cells. The LNs and spleen are the main two SLO affected in CLL.

The LNs are encapsulated aggregates of lymphoid tissue which are located along the lymphatic channels throughout the body. The LNs receive extracellular fluid filtrate, known as lymph from all epithelia, connective tissue and most organs. As lymph empties into the LN it contains a collection of molecules including antigens, microorganisms and immune cells. LN have three main compartments, the cortex, the paracortex and medulla. Once inside the LN T and B lymphocytes home to separate areas known as the B- and T-cell zones. The T-cell zones in the LN contain both CD4+ and CD8+ T cells as well as subsets of dendritic cells. In the B -cell zone lymphocytes are organised into structures called follicles (Figure 1-9). B cells are supported by a network of follicular dendritic cells (FDCs). If the B cells in the follicle have responded to antigen then the follicle will contain a GC (Figure 1-9b).

The spleen is an abdominal organ and is one of the main filters of blood in the body and serves the same role in immune responses to blood-borne antigens as that of LN in response to lymph-borne antigens. The spleen contains cells from both the innate and adaptive immune system which are able to respond to any blood-borne antigens. Blood vessels enter the spleen and branch into arterioles. The arterioles are surrounded by organised lymphoid compartments which are organised in a similar fashion as the LNs. This area containing lymphoid compartments is known as the white pulp.

1.3.2.1 Homing of cells to the SLO tissue microenvironment

Lymphocyte homing to and within the SLOs is not static, but a highly dynamic process with lymphocytes being constantly on the move. Malignant B cells exploit the physiologic mechanisms of normal lymphocyte migration and homing to the SLOs to access supportive microenvironmental niches. After lymphocytes enter the SLO from the blood they organise themselves into the B-cell follicles and T-cell zones. Within their respective compartments B and T cells continue to migrate searching for antigen. This homing and migration of lymphocytes is largely due to members of the chemokine family. Chemokines are small, mostly secreted, chemoattractive proteins that function through G protein-coupled receptors (GPCR).

Lymphocytes enter the SLO across the endothelium via high endothelial venules (HEV). This entry process involves selectin or integrin supported rolling, chemokine-mediated

integrin activation and integrin-mediated adhesion (Cyster, 1999). The most prominent chemokine expressed by HEV and involved in lymphocyte entry is CCL21 (Gunn et al., 1998, Nagira et al., 1998). The chemokines CXCL12 and CXCL13 have also been shown to contribute to lymphocyte entry into the SLO (Miyasaka and Tanaka, 2004, Cyster, 2005). Once through the endothelium and into the SLO, chemokines direct the lymphocytes to their respective zones. Homing of B cells into follicles is dependent on the chemokine CXCR5 expressed on the surface of B lymphocytes and its ligand CXCL13 which is expressed by stromal cells within the follicles (Gunn et al., 1998, Cyster et al., 2000, Allen and Cyster, 2008). T cell migration to T-cell zones is dependent on the chemokine CCR7 and its two ligands CCL19 and CCL21 (Forster et al., 1999, Gunn et al., 1999). Naive T cells express abundant amounts of CCR7 while CCL19 and CCL21 are produced by stromal cells in the T-cell zone. Once into their respective zones, chemokines further function to help the lymphocyte screen antigen presenting cells for antigen and bring them in close contact with other cells.

Upon activation with antigen, T and B cells undergo changes in their positioning within their respective zones. These changes allow T-B cell interactions at the T cell area-B cell follicle border to occur (Cyster, 2005, Cyster, 1999, von Andrian and Mackay, 2000, Jenkins et al., 2001). Following antigen receptor engagement, B cells upregulate CCR7 while the levels of CXCR5 remains the same (Reif et al., 2002). This increase in CCR7 causes B cells to relocalise to the B/T-zone boundary (Reif et al., 2002). Upon antigen encounter T cells transiently increase CXCR5. This balanced increase results in antigen-specific B-T cell interactions at the borders.

It is clear that lymphocytes are also constantly exiting the SLO and recirculating through the peripheral blood (PB). Sphingosine-1-phosphate (S1P) has been shown to be involved in lymphocyte egress from the SLO (Cyster, 2005). There is an increasing concentration gradient that exists between the interior of the lymphoid tissue and the adjacent blood or lymph. S1P concentrations are high in blood and lymph, and low in tissues, presumably due to the higher activity of S1P degrading enzymes in tissue (Maceyka and Spiegel, 2014). The receptor S1PR1 is required for egress and B cells upregulate this receptor when ready to leave the tissue. When B cells are ready to exit the SLO and enter the blood, S1PR1 is re-expressed so that B cells can respond to the chemotactic effect of high S1P levels in circulation. When B cells re-enter the blood, S1P downregulates S1PR1.

Retention of B cells in the SLO is largely dependent on the presence of antigen. Antigen engagement in lymphoid tissues downregulates the S1PR1 ensuring that the B cell receives the necessary activation to undergo clonal expansion and be released as effector

cells (Cyster and Schwab, 2012). If B cells do not encounter antigen, they quickly upregulate S1PR1 and exit the tissue.

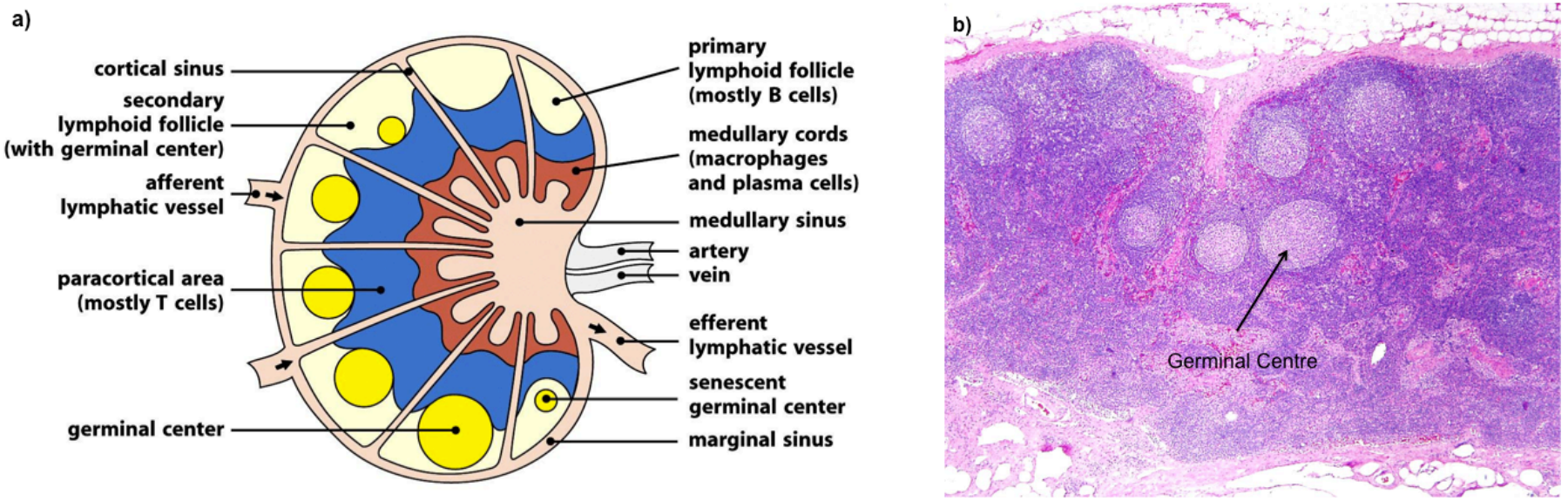

FIGURE 1-9: STRUCTURE OF A LYMPH NODE

(a) Diagram of lymph node architecture (Taken from Immunobiology (Janeway CA Jr, 2001)). (b) Histology of a lymph node displaying germinal centres denoted by the arrow.

1.4 The microenvironment in CLL

The microenvironment has long been recognised to play an important role in the pathogenesis of CLL. This is first indicated by the fact that CLL cells readily accumulate *in vivo* however they rapidly undergo spontaneous apoptosis when cultured *in vitro*, implying that their apoptosis resistance *in vivo* relies on external survival factors rather than being an intrinsic factor of the CLL cell itself (Burger et al., 2000, Kurtova et al., 2009, Collins et al., 1989). These observations indicate that signals from the microenvironment are important for the prolonged survival of CLL cells *in vivo*. Secondly, many cells of the CLL microenvironment have been shown to confer a protective effect against chemotherapeutic agents. Thirdly, despite major improvements in the treatment, CLL still remains an incurable disease with many patients relapsing from MRD and there is growing evidence that the microenvironment harbours malignant cells acting as a shield from the cytotoxic effects of chemotherapy, thus serving as a reservoir from which relapse may occur. Finally, the role of the microenvironment is further exemplified by the lymphocytosis which is seen in patients following the BCR kinase inhibitors ibrutinib and idelalisib (Woyach et al., 2014, Brown et al., 2014b). This striking lymphocytosis and effects of ibrutinib and idelalisib on migration and adhesion *in vitro* highlights the importance of the microenvironment in CLL cell recirculation through the PB and tissue microenvironment.

The majority of circulating CLL cells are in the G0/early G1 phase of the cell cycle, and therefore it was long thought that CLL was due to failed apoptosis rather than a disease of proliferation. However, since those early views, several data have demonstrated that the proliferative rates of CLL cells are higher than previously first thought and CLL cells, in fact, have a dynamic kinetic behaviour (Messmer et al., 2005, Calissano et al., 2009). Further to this patients with higher proliferation rates have been shown to have a more active and progressive disease (Messmer et al., 2005). Due to the fact that CLL cells retain the ability to respond to stimuli from stromal cells, T cells and antigen all of which favour cell proliferation it is believed that the microenvironment at least in part accounts for this dynamic behaviour (Caligaris-Cappio and Ghia, 2008). CLL cell proliferation occurs in specialised compartments known as proliferation centres or pseudofollicles (Schmid and Isaacson, 1994) and these compartments are represented by focal aggregates of proliferating cells (Figure 1-10). The proliferative capacity of cells within these centres is confirmed by immunohistochemistry studies demonstrating that these proliferation centres are clusters of CD19+, Ki67+ cells (Figure 1-10b). Proliferation centres are a major hallmark and histopathological characteristic of the CLL microenvironment and are observed mainly in the LNs. Interestingly, proliferation centres

are not visualised in any other B cell-malignancies, indicating that proliferation centres are a hallmark of CLL (Caligaris-Cappio and Ghia, 2008). The role of the microenvironment in CLL cell proliferation is further demonstrated by the fact that proliferation centres not only contain tumour cells, but also other bystander cells and proliferation centres act as an area for interactions between different populations of cells.

The key cellular players in the CLL microenvironment, discussed in more detail below (Section1.4.1) are stromal cells, monocyte-derived nurse-like cells (NLC) and T cells. These accessory cells contribute to the CLL microenvironment through direct cell contact and a number of different soluble factors including cytokines, chemokines and adhesion molecules. CLL cells themselves are able to shape their microenvironment via the secretion of chemokines which attract these protective accessory cells into the microenvironment. The interaction of CLL cells with these accessory cells in the CLL microenvironment is likely to be complex involving several pathways, cell types and soluble factors.

Experiments have shown that CLL cells respond to their microenvironment by demonstrating the activation of signalling pathways resulting in the change of expression of genes involved in cellular activation and proliferation (Herishanu et al., 2011). Herishanu et al., found in a genome wide microarray that CLL cells isolated from different tissue compartments showed gene expression profiles that reflected differential activation of signalling pathways in the different compartments. CLL cells from the LN upregulated a number of genes involved in BCR signalling (Herishanu et al., 2011).

CLL cells are able to manipulate their homing mechanisms in order to enter this protective microenvironment. CLL cells are constantly circulating throughout the body in the PB. Chemotactic signals are sent from the tissue stromal cells in the BM and SLOs which attract CLL cells into the microenvironment in a similar fashion as described in Section1.3.2.1. Like healthy B cells, CLL cells express the chemokine receptors CXCR4 and CXCR5 which bind to the chemokines CXCL12 and CXCL13 respectively (Burger et al., 2009a, Burger et al., 1999, Burkle et al., 2007), both of which are released by a variety of stromal cells within the microenvironment. CLL cells migrate down chemokine gradients and together these chemokines and their receptors, drive B cells to migrate out of the PB and into the protective microenvironment (Figure 1-11).

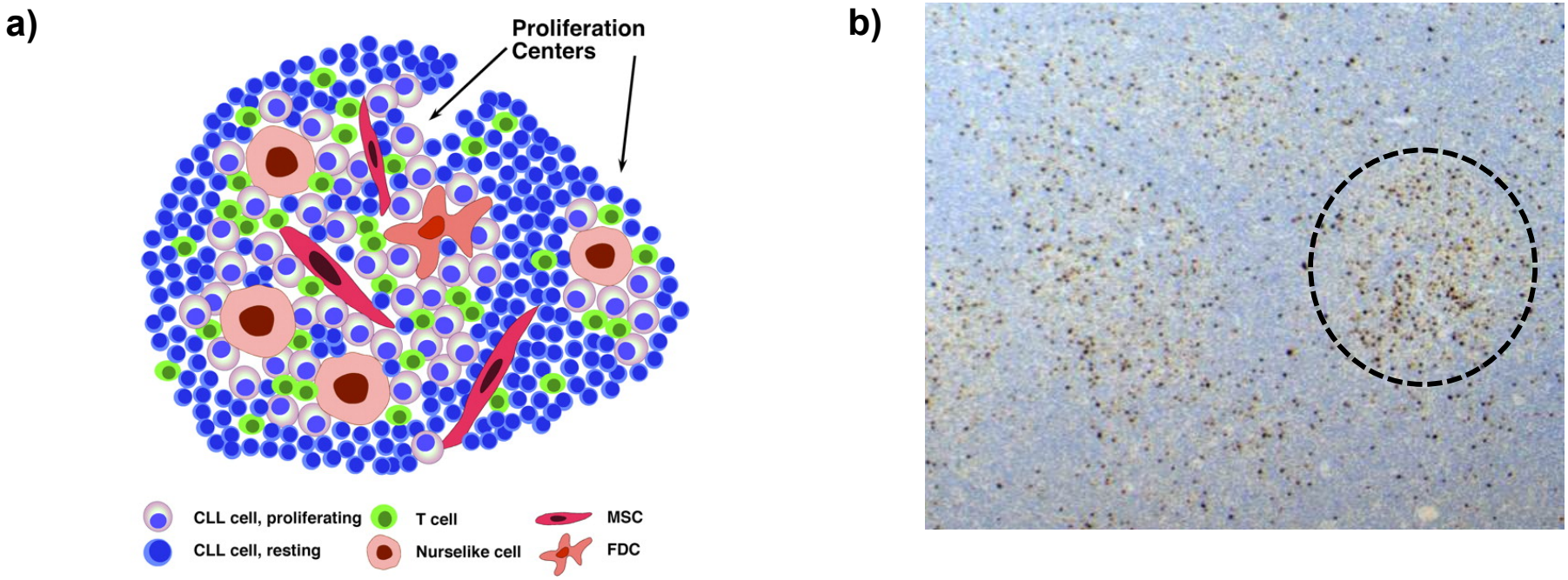

FIGURE 1-10: CLL CELL PROLIFERATION CENTRES

In secondary lymphoid tissues, CLL cells interact with a variety of accessory cells, such as mesenchymal stromal cells (MSCs), nurse-like cells (NLCs), T cells and also follicular dendritic cells (FDCs). The formation of proliferation centre is a major hallmark of CLL histopathology. The interactions between CLL cells and the accessory cells within these proliferation centres are critical for providing growth and survival signals to the CLL cells inducing their proliferations. (a) Graphical representation of proliferation centres in CLL (Image taken from (Burger et al., 2009a)). (b) Immunohistochemistry image. Staining indicates Ki67+ cells. Dotted line encircles proliferation centres.

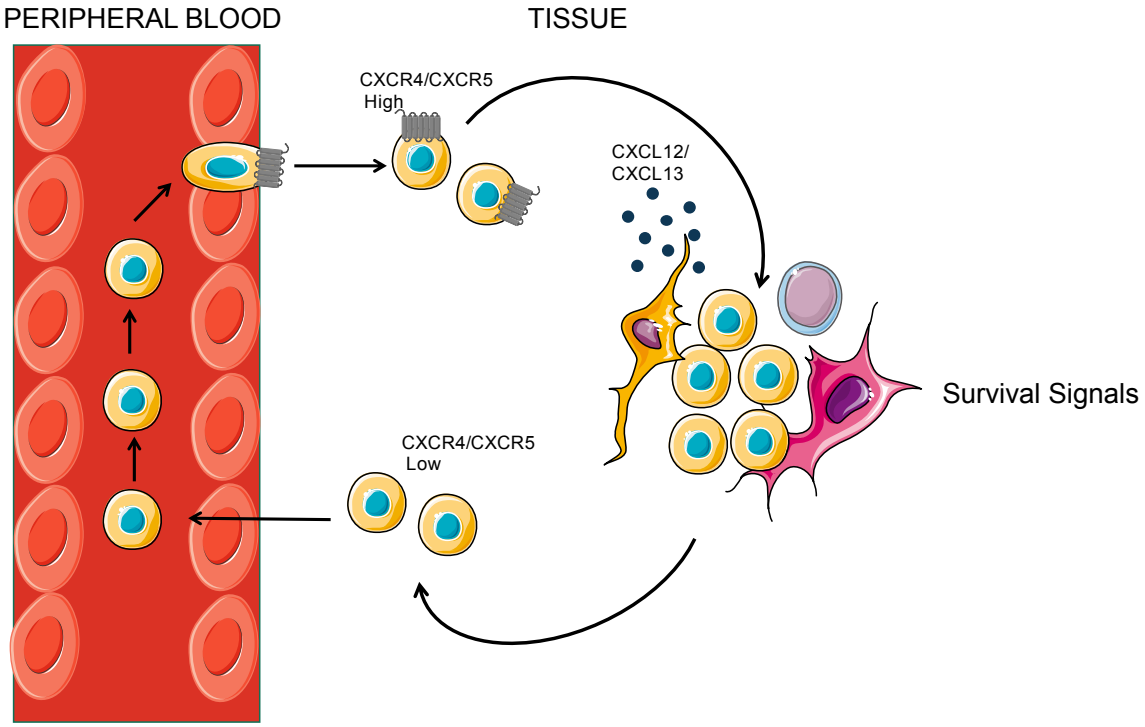

FIGURE 1-11: HOMING OF CLL CELLS TO THE TISSUE MICROENVIRONMENT

CLL cells circulate freely in the PB, however they are attracted to tissue microenvironments like the BM and LN by chemokine gradients established by stromal cells. The chemokines CXCL12 and CXCL13 are secreted by cells within the tissue such as MSCs and NLCs. These chemokines have chemoattractant activity and bind to the chemokine receptors CXCR4 and CXCR5 on CLL cells respectively. This results in transmigration of CLL cells into tissue where they are protected by a variety of anti-apoptotic and pro-survival signals. Binding of the chemokines to their respective receptor causes down modulation and therefore CLL cells leaving the tissue microenvironments have low expression of the receptors. Circulating CLL cells in the PB characteristically express variable levels of surface CXCR4, while CLL cells resident in the tissue microenvironments and in close contact to CXCL12 secreting cells have lower levels of surface CXCR4 (Ghobrial et al., 2004). Peripheral blood CLL cells express variable levels of CXCR4 depending on whether they have recently left the CXCL12-expressing tissues or have recovered receptor expression and are preparing to re-enter with CLL cells in the blood (Coelho et al., 2013, Calissano et al., 2009).

1.4.1 Cellular players in the CLL cell microenvironment

Many cellular players have been shown to promote CLL cell survival, proliferation, tissue homing and retention acting via a wide range of molecular interactions. The most researched to date are MSC, NLC and T cells (Figure 1-12).

1.4.1.1 Stromal cells

BMSC were the first cells characterised to support CLL cells (Lagneaux et al., 1999). BMSC form protective niches within the BM similar to those seen in normal B cell biology and nourish CLL in a similar fashion to what is observed during normal haematopoiesis. When co-cultured *in vitro* CLL cells migrate towards BMSCs and the importance of BMSC interactions is demonstrated by the fact that CLL cells have high binding affinity for BMSC and *in vitro* CLL cells spontaneously migrate beneath the BMSC monolayers, a phenomenon termed pseudoemperipolesis (Burger et al., 1999). When in close proximity the stromal counterparts protect CLL cells from spontaneous and drug induced apoptosis (Lagneaux et al., 1999, Kurtova et al., 2009, Burger et al., 2000). BMSC also play a role in the homing of CLL cells into the tissue microenvironment through the secretion of the homing chemokine CXCL12 (Burger et al., 1999).

Many reports to date have focussed on the effects of stromal cells on the behaviour and phenotype of CLL cells however emerging literature is demonstrating the ability of CLL cells to affect the behaviour of the supporting cells within the CLL microenvironment. Ding *et al.,* demonstrated the ability of CLL cells to induce a rapid (within 30 minutes) phosphorylation or ERK and AKT in MSC. This activation occurred when the two cell types were separated by a microporous membrane indicating the activation of MSC was mediated by soluble factors released by CLL cells (Ding et al., 2009). This activation of MSC by CLL cells was hypothesized as a key step for the proliferation, migration and differentiation of MSC ultimately promoting the survival of malignant CLL cells. Lutzny *et al.,* further demonstrated a bi-directional cross talk between CLL cells and the stromal microenvironment by showing the ability of CLL cells to induce the expression of protein kinase C (PKC)-βII in BM stromal cells which lead to the activation of NF-κB in the stromal cells. The expression of PKC-βII and the subsequent activation of NF-κB in bone marrow stromal cells are prerequisites to support the survival of CLL cells (Lutzny et al., 2013). These studies by Lutzny et al*.,* and Ding et al*.,* demonstrate important survival signalling pathways which involve a bi-directional cross talk between CLL cells and stromal cells.

Cell communication has typically been understood to consist of secreted soluble factors along with direct cell contact. However new literature is beginning to outline the importance of an additional layer of intercellular communication involving the secretion

and uptake of extracellular vesicles. Exosomes are small (50-100nm diameter) extracellular vesicles. CLL cells have been shown to secrete exosomes and that they are readily taken up by stromal cells (Ghosh et al., 2010, Paggetti et al., 2015, Farahani et al., 2015). The uptake of exosomes by stromal cells have been shown to alter the behavior of recipient cells in a number of different ways. Firstly, the uptake of CLL exosomes was shown to activate the AKT signaling pathway in BMSC leading to the modulation of the β-catenin pathway and increased expression of cyclin D1 and c-myc in BMSCs (Ghosh et al., 2010). Secondly exosomes secreted by CLL cells have been shown to alter the transcriptome of HS-5 stromal cells inducing the expression of genes such as c-fos and ATM (Farahani et al., 2015). Finally, the transfer of exosomal protein and microRNA by CLL exosomes induces an inflammatory phenotype in MSC resembling that of CAFs (Paggetti et al., 2015).

The understanding of the cross talk between CLL and stromal cells helps with better understanding of signaling pathways involved in the survival of CLL cells ultimately leading to better therapeutic targeting of the protective microenvironment.

1.4.1.2 Nurse-like cells

NLC differentiate *in vitro* when blood mononuclear cells from CLL patients are cultured at high density for approximately 7-14 days (Burger et al., 2000). NLCs are large, round adherent cells and were originally named after thymic nurse cells that nurture developing thymocytes due to the cells sharing a number of the same features (Burger et al., 2000).

NLC can be found in the spleen and lymphoid tissue of CLL patients (Burkle et al., 2007, Tsukada et al., 2002). NLCs promote the migration of CLL cells into the tissue microenvironment through the secretion of the chemokines CXCL12 (Burger et al., 2000) and CXCL13 (Burkle et al., 2007). NLC also protect CLL cells from undergoing spontaneous or drug-induced apoptosis (Burger et al., 2000a, Nishio et al., 2005, Burger et al., 2009). NLCs have been shown to protect CLL cells through a number of different molecules including the chemokine CXCL12 (Burger et al., 2000, Nishio et al., 2005), the TNF family receptors BAFF and APRIL (Nishio et al., 2005), the chemokines CCL3 and CCL4 (Hoellenriegel et al., 2011), CD31 and CD100/Plexin B1 (Deaglio et al., 2005) and through activation of the BCR-associated signalling cascade (Burger et al., 2009b). The interactions between CLL and NLCs is bidirectional and as well as NLCs attracting CLL cells into the microenvironment, CLL cells are also able to actively recruit NLC to the microenvironment through the secretion of the chemokines CCL3/CCL4 (Burger et al., 2009b).

CLL-NLC are characterised by a high level of expression of CD68 (Tsukada et al., 2002, Boissard et al., 2015) and CD163 (Boissard et al., 2015, Ysebaert and Fournie, 2011) and by a gene expression pattern resembling that of tumour associated macrophages (TAMS) (Ysebaert and Fournie, 2011). NLC belong to the M2 macrophage subset also known as the wound-healing subset and have potent immunosuppressive functions through the secretion of a number of cytokines (Fiorcari et al., 2015b). NLCs have been shown to share several features with TAMS in solid tumours through the secretion of IL-10, IL-8, and high surface expression of CD11b, HLA-DR, CD163 and CD206 (Fiorcari et al., 2015b). TAMs have many roles in cancer progression including recruitment of accessory cells to the microenvironment or anatomical sites, angiogenesis, metastasis and immune evasion. There is a correlation between the number of TAMs in solid tumours and poor prognosis.

1.4.1.3 Follicular dendritic cells

In normal B cell biology, FDCs play an active role and are found to cluster in the centre of B cell follicles in SLOs forming a dense network of cells. Evidence for FDC involvement in CLL biology *in vivo* lacks solid evidence however, when CLL cells are cultured *in vitro* with FDCs they are protected from apoptosis. This protection occurs via direct cell contact and is dependent on ligation of CD44 and up-regulation of the anti-apoptotic protein MCL1 (Pedersen et al., 2002). FDCs have also been shown to be involved in the homing of CLL cells into the microenvironment by the production the chemokine CXCL13 (Nagira et al., 1998).

1.4.1.4 T cells

T cells are shown to play different roles in the progression of CLL and as such T cells have become a bit of a controversial topic in CLL research. One thing that is known is that the overall number of circulating T cells, both $CD4^+$ and $CD8^+$ in untreated CLL patients is increased (Serrano et al., 1997). The reason for this increase however is not known. It could possibly be due to immune reactivity with the CLL clone, or could be due to interactions with microbial reactions or virus reactivation, both of which are more prevalent in CLL patients. However, it has been shown that although the absolute number is increased there are abnormalities in the phenotype of CD4 and CD8 T cells including inversion of the normal CD4:CD8 ratio (Catovsky et al., 1981, D'Arena et al., 2013, Gonzalez-Rodriguez et al., 2010, Pourgheysari et al., 2010, Nunes et al., 2012). This inverted CD4:CD8 ratio is associated with shorter lymphocyte doubling time, shorter TTFT and reduced PFS indicating that T-cell dysfunction contributes to disease progression in CLL (Nunes et al., 2012). Further to this inversion of CD4:CD8 T cells there is also the accumulation of terminally differentiated effector memory cells with a significant reduction

in the naïve $CD4^+$ $CD8^+$ subsets in CLL patients (Whelan et al., 1982, Gorgun et al., 2005, Nunes et al., 2012) These effector memory T cells are derived by antigen exposure indicating that repeated or chronic antigen stimulation is a feature of CLL. Precisely what antigen(s) are involved in this process remains unresolved, but a number of groups have suggested that cytomegalovirus (CMV) may play a role in driving CD4+ and CD8+ effector memory T cells (Pourgheysari et al., 2010, Mackus et al., 2003, Walton et al., 2010). These T cell defects have been shown to cause impaired immune functions in CLL patients. T cells derived from patients have shorter telomeres (Röth et al., 2008) and Nunes et al*.,* demonstrated that there was the emergence of CD8+PD1+ T cells with an 'exhaustion' phenotype (Nunes et al., 2012). Palma et al*.,* demonstrated that the numbers of Th1, Th2, Th17 and regulatory T cells were substantially increased in CLL patients (Palma et al., 2016). In summary the current literature indicates that CLL T cells display abnormal subset distribution, increased expression of immune checkpoints and impaired immune functions compared to heathy T cells .

Activated CD4 T cells have been shown to co-localise with proliferating CLL cells in CLL proliferation centres suggesting that some T-cell subpopulations promote the expansion of the CLL clone (Patten et al., 2008) and that investigating the interactions between CLL cells and T cells is essential to understand disease pathogenesis. A significant portion of these proliferation centre-localised T cells have also been shown to display CD40L, a member of the TNF superfamily that binds to CD40 on CLL cells. CD40L has been shown to rescue CLL cells from apoptosis (Kitada et al., 1999). CLL T cells also produce the chemokine IL-4 (Monserrat et al., 2014, de Totero et al., 1999) and greater levels of production has been shown to correlate with progressive disease (Rossmann et al., 2002). Recently Aquilar-Hernandez et al., demonstrated that the chemokine IL-4 augments sIgM expression and partially overcomes ibrutinib and idelalisib-mediated inhibition of sIgM signalling (Aguilar-Hernandez et al., 2016). The authors speculated the ability of IL-4 produced by T cells to enhance the effect of antigen in the tissue compartments to promote CLL tumourigenesis (Aguilar-Hernandez et al., 2016). Furthermore, in an adaptive xenograft model using primary CLL cells in mice, T cells were essential for tumour engraftment (Bagnara et al., 2011). The T cell dysfunction seen in CLL patients, coupled with data seen from IL-4 experiments, the protective effects of CD40L as well as the important role of T cells in the adaptive xenograft models suggests a key role for T cells in CLL cell biology.

As discussed previously, exosomes are emerging as an important mode of intercellular communication. CLL cells release exosomes following stimulation with the T-cell microenvironment signals, IL-4 and CD40L. These vesicles were shown to be enriched with microRNAs (miRNA). T cells exposed to these exosomes exhibited enhanced

migration, immunological synapse signalling and interactions with CLL cells (Smallwood et al., 2016) indicating that a bi-directional crosstalk also occurs between CLL cells and T cells.

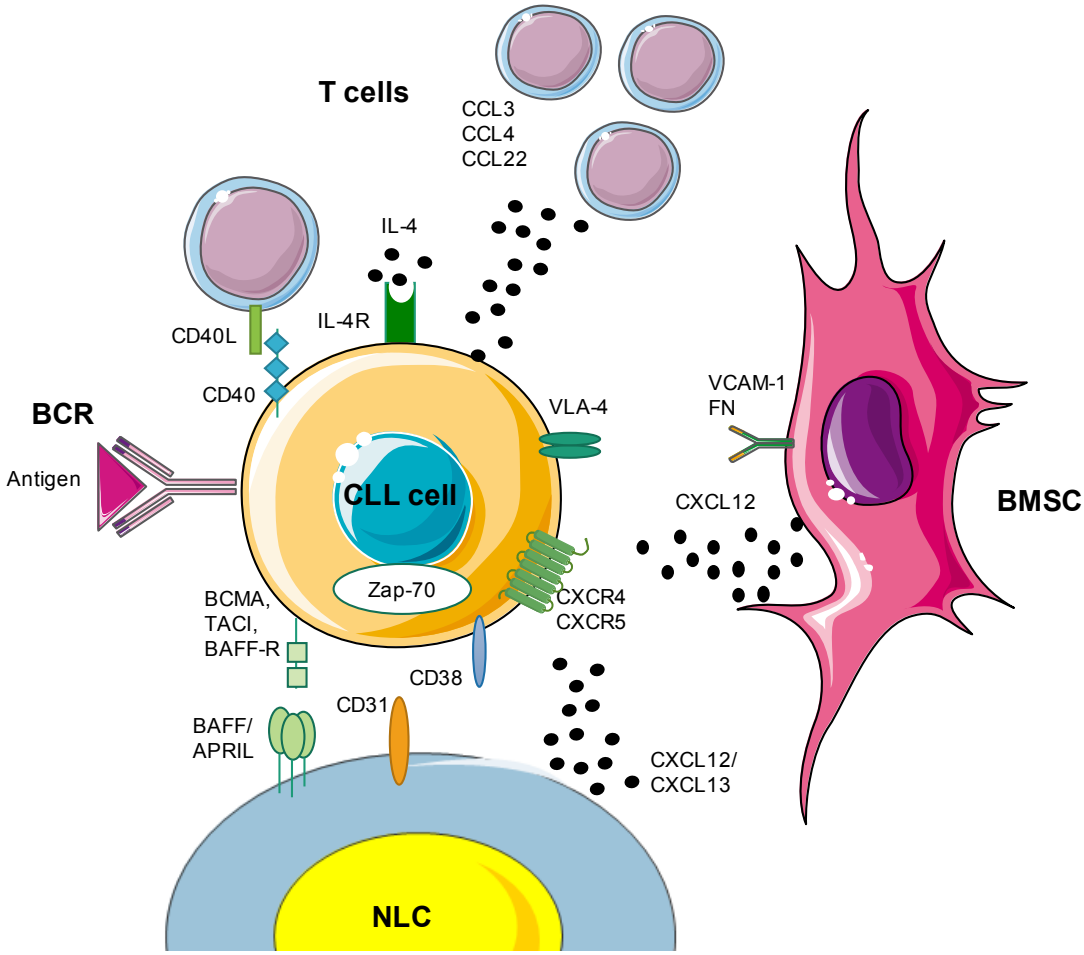

FIGURE 1-12: CELLULAR AND MOLECULAR INTERACTIONS IN THE CLL MICROENVIRONMENT (ADAPTED FROM (BURGER ET AL., 2009A)

Molecular interactions between CLL cell and stromal cells and T cells in the CLL microenvironment are important for CLL-cell survival, homing and proliferation. NLCs and BMSCs secrete the chemokines CXCL12 and CXCL13 which are important for CLL cell homing into the BM and/or SLO tissue microenvironment. NLC cells secrete both CXCL12 and CXCL13 whereas BMSC predominantly secrete CXCL12. These chemokines attract CLL cells by binding to the G protein-coupled receptors CXCR4 and CXCR5 which are highly expressed on the surface of CLL cells. Integrin receptors, particularly VLA-4 integrins which are expressed on the surface of CLL cells cooperate with the chemokine receptors in promoting tissue retention by establishing cell contact via the respective ligands (VCAM-1 and fibronectin) on stromal cells. CLL cells secrete the chemokines CCL3,4 and 22 which act as chemoattractants for T cells. These allow for T cells to move into the microenvironment and promote pro-survival signals to the CLL cells. T cells further interact with the CLL clone by ligation of CD40L and secretion of IL-4. NLC also provide survival signals to the CLL cell by the expression of the TNF family members BAFF and APRIL and via their respective receptors (BCMA, TACI, BAFF-R) expressed on CLL cells. CD38 expression on CLL cells allows CLL cells to interact with its receptor CD31 which is expressed by stromal cells and NLCs. Ligation of CD38 results in the activation of ZAP70 and downstream signalling pathways. Antigens are key in the activation and expansion of the CLL clone by the activation of the BCR and its downstream signalling pathways.

1.4.2 Microenvironment-associated signalling pathways

The CLL tissue microenvironment cellular players described above act through a number of different pathways which include surface receptors, adhesion molecules and soluble factors. A summary of molecular pathways involved in the CLL microenvironment are outlined in Table 1.3 and detailed in the sections below.

1.4.2.1 The BCR

The BCR is a key molecule on the surface of healthy B cells and as such also plays a major part in CLL cell survival and proliferation. The BCR consists of a ligand binding moiety in the form of a surface bound immunoglobulin (sIg) and a signal transduction moiety in the form of CD79a and CD79b (Igα/Igβ). The CD79a/CD79b molecules contain immunoreceptor tyrosine activation motifs (ITAMs) that undergo phosphorylation when an antigen binds to the Ig. This phosphorylation is catalyzed by LYN, and leads to the recruitment of SYK. Activation of SYK triggers formation of a membrane-associated signalling complex known as the signalosome comprising SYK, BTK, PLCγ, PI3K, as well as other adaptor molecules and co-receptors at the plasma membrane. The signalosome co-ordinates and regulates the downstream cellular signalling events. Figure 1-13 outlines the key event involved in BCR signalosome formation and some of the downstream pathways associated with BCR signalling.

In CLL cells the BCR still remains key, however signalling responses are greatly heterogeneous. sIg is always expressed, however, levels are generally lower in comparison to normal circulating B cells (Packham and Stevenson, 2010). Despite these lower levels sIg has been shown to still be highly influential on CLL cell behaviour and disease progression demonstrated by the number of new therapeutic agents acting on downstream kinases of the BCR signalling pathway. Response to engagement of the BCR differs between U-CLL and M-CLL and it has been shown that response to BCR signalling is generally higher in U-CLL (Mockridge et al., 2007, Guarini et al., 2008). Analysis of BCR signalling in the two subsets has revealed two main responses, proliferation or anergy. Anergy, defined as a failure to respond to BCR stimuli, is a mechanism of tolerance which is normally used to keep the immune system in check. Anergy functions to control self-reactive B cells and render them inactive (Cambier et al., 2007). It has been shown that it is fact the balance between 'positive' signalling and anergy which appears to determine the behaviour of CLL *in vivo* rather than expression levels, with M-CLL mainly being driven towards anergy while in U-CLL, the more aggressive of the subsets, there is more evidence for growth-promoting signalling (Packham et al., 2014, Mockridge et al., 2007, Guarini et al., 2008) (Figure 1-14). Similar to normal B cells, in CLL cells sIg activation

triggers a range of signalling pathways however this only occurs in responsive cells some of which are briefly outlined below.

One way the ability to retain signalling capacity through the BCR is associated with poor prognosis could be through the suppression of apoptosis. One target of the BCR signalling pathway that may potentially lead to suppression of apoptosis is the BCL2 family proteins which are key regulators of apoptosis. In particular, the family protein MCL1 has shown to be increased following sIgM activation *in vitro* (Petlickovski et al., 2005, Bernal et al., 2001). sIgM activation also increases phosphorylation of BIM, a BCL2 related, pro-apoptotic protein which is tightly regulated by phosphorylation (Paterson et al., 2012). In CLL, anti-IgM-induced BIM phosphorylation is correlated with U-CLL patients and progressive disease. Further to this, it is also associated with progressive disease in the M-CLL subset (Paterson et al., 2012). These data demonstrate that MCL1 and BIM play a key role in apoptosis regulation in CLL cells and may potentially be associated with progressive disease.

sIgM can also promote survival of CLL cells through activation of some components of the unfolded protein response (UPR) (Krysov et al., 2014) a stress response pathway that responds to the accumulation of unfolded proteins. In B cells, the UPR plays a key role in differentiation because the production of secreted immunoglobulin requires a compensatory increase in protein production capacity which is mediated by UPR induction (Todd et al., 2008). UPR activation is not exclusively a response of stress but has been shown to be a signal regulated pathway, as BCR stimulation has been shown to increase some UPR components. Krysov et al., demonstrated that sIgM stimulation led to the activation of the UPR and that this activation correlated with aggressive disease (Krysov et al., 2014). They also demonstrated that BCR kinase inhibitors reduced this activation indicating that this response may be related to disease progression.

Another way signalling capacity through the BCR is associated with poor prognosis, is potentially through the activation of proliferation pathways. sIgM stimulation has been shown to increase the expression of the proto-oncoprotein MYC, which is a known positive regulator of the cell cycle (Krysov et al., 2012). MYC induction was shown to be partially dependent on the MEK/ERK signalling pathway. MYC and phosphorylated ERK1/2 were demonstrated to be both expressed within proliferation centers *in vivo* (Krysov et al., 2012) suggesting that induction of MYC is likely to play a role in antigen-induced cell proliferation. Yeomans et al., demonstrated another method in which sIgM stimulation can promote disease progression in CLL. They demonstrated BCR stimulation led to an increase in messenger RNA (mRNA) translation *in vitro* and *in vivo.* They specifically demonstrated the upregulation of MYC mRNA (Yeomans et al., 2016). Again,

demonstrating that MYC may play a major role in the growth promoting effects following BCR stimulation (Yeomans et al., 2016, Krysov et al., 2012).

1.4.3 BCR crosstalk to the microenvironment

The remarkable lymphocytosis observed following treatment with the BCR kinase inhibitors ibrutinib and idelalisib (Woyach et al., 2014, Brown et al., 2014b) as well as their effects on migration, adhesion and stromal cell interactions indicated the possibility that the BCR cross talks with other microenvironment receptors such as adhesion pathways and migration and chemokine signalling (Figure 1-15). This indicates that 'BCR inhibitors' could potentially target multiple pathways all interconnected with the BCR, which would explain some of the findings seen in the clinic.

Microenvironmental stimuli are extremely important for the survival and activation of CLL cells as well as response to therapy (discussed in more detail throughout this chapter). As such research regarding new BCR kinase inhibitors has sought to evaluate the role of ibrutinib and idelalisib in regulating microenvironmental stimuli. Ibrutinib has been shown to reduce CLL viability in survival inducing co-cultures. Pre-treatment of CLL cells with ibrutinib resulted in a marked reduction in the protection seen following co-culture with the HS5 stromal cell line. Ibrutinib also has an effect on a number of other cell types in the CLL microenvironment, including T cells and macrophages (Niemann et al., 2016). Co-treatment with ibrutinib inhibited the protection induced by both CD40L, BAFF, IL-6, IL-4 and TNF-α (Herman et al., 2011). In a similar manner idelalisib reduces CLL viability even following culture with microenvironmental cells such as NLC (Hoellenriegel et al., 2011) and MSC (Herman et al., 2010). Idelalisib has been shown to modulate the CLL microenvironment in a number of different ways. Firstly, idelalisib inhibits CLL cell signalling pathways following CD40L, BAFF, and IL-4 stimulation (Herman et al., 2010). Idelalisib has also been shown to inhibit NLC- and BCR-induced secretion of the T cell chemoattractant chemokines, CCL3 and CCL4 (Hoellenriegel et al., 2011). *In vivo* investigations found that a number of chemokines and cytokines were dramatically reduced following treatment with idelalisib (CCL2, CCL7, IL-6, sCD40L, CCL22, TNF-α, and CCL17) (Hoellenriegel et al., 2011).

1.4.3.1 CXCR4

In normal cells, BCR activation reduces CXCR4 expression so it is reasonable to assume the same will occur in CLL cells; indeed signalling through the BCR reduces CXCR4 expression in CLL cells (Quiroga et al., 2009). Further to this, activation of CLL cells

through sIgM has also been shown to modulate CXCL12-mediated adhesion, chemotaxis and migration (Quiroga et al., 2009). This increased migration can be blocked through BCR kinase inhibitors such as ibrutinib and idelalisib as discussed in Section1.2.2.1. (de Rooij et al., 2012, Ponader et al., 2012, Herman et al., 2014). There are also interactions between CXCR4 signalling and CD38/ZAP70 pathway. CD38+/ZAP70+ patients are characterised by an increased migration to CXCR4 which can be blocked by anti-CD38 mAbs (Deaglio et al., 2010).

1.4.3.2 Integrin receptors

CD49d is one of the main molecules responsible for mediating both cell-cell and cell-matrix interactions by binding respectively to VCAM-1 and fibronection (Fn). As discussed in Section1.2.1 CD49d expression has an independent impact on prognosis (Gattei et al., 2008, Rossi et al., 2008, Shanafelt et al., 2008, Bulian et al., 2014, Majid et al., 2011). The binding of CLL cells on stromal cells in microenvironmental through CD49d, reflects the activity of normal B cells and CD49d-driven interactions play a key role in controlling the development of B cells (Arroyo et al., 1999, Miyake et al., 1991). These BCR-CD49d interactions are preserved in CLL (Spaargaren et al., 2003) and BCR kinase inhibitors have been shown to inhibit CD49d-mediated adhesion of CLL cells (de Rooij et al., 2012, Fiorcari et al., 2013). Blockade of BCR-CD49d interactions could be responsible for the shrinkage of LN and lymphocytosis of CLL cells into the PB following treatment with these drugs.

1.4.3.3 CCR7

The chemokine receptor CCR7 plays an important role in the migration of B cell and CLL cells across the vascular endothelium (Till et al., 2002). CCR7 is highly expressed on the surface of CLL cells and the degree of expression has been shown to be associated with ZAP70 and CD38 expression (Richardson et al., 2006). It has been shown that CCL19/CCL20 induced migration is more pronounced in ZAP70/CD38 positive CLL cells. Calpe et al., demonstrated that CCR7 is BCR regulated and in ZAP70 positive cells sIgM stimulation results in the up-regulation of CCR7. This increased expression was translated into increased signalling and migration to CCL21

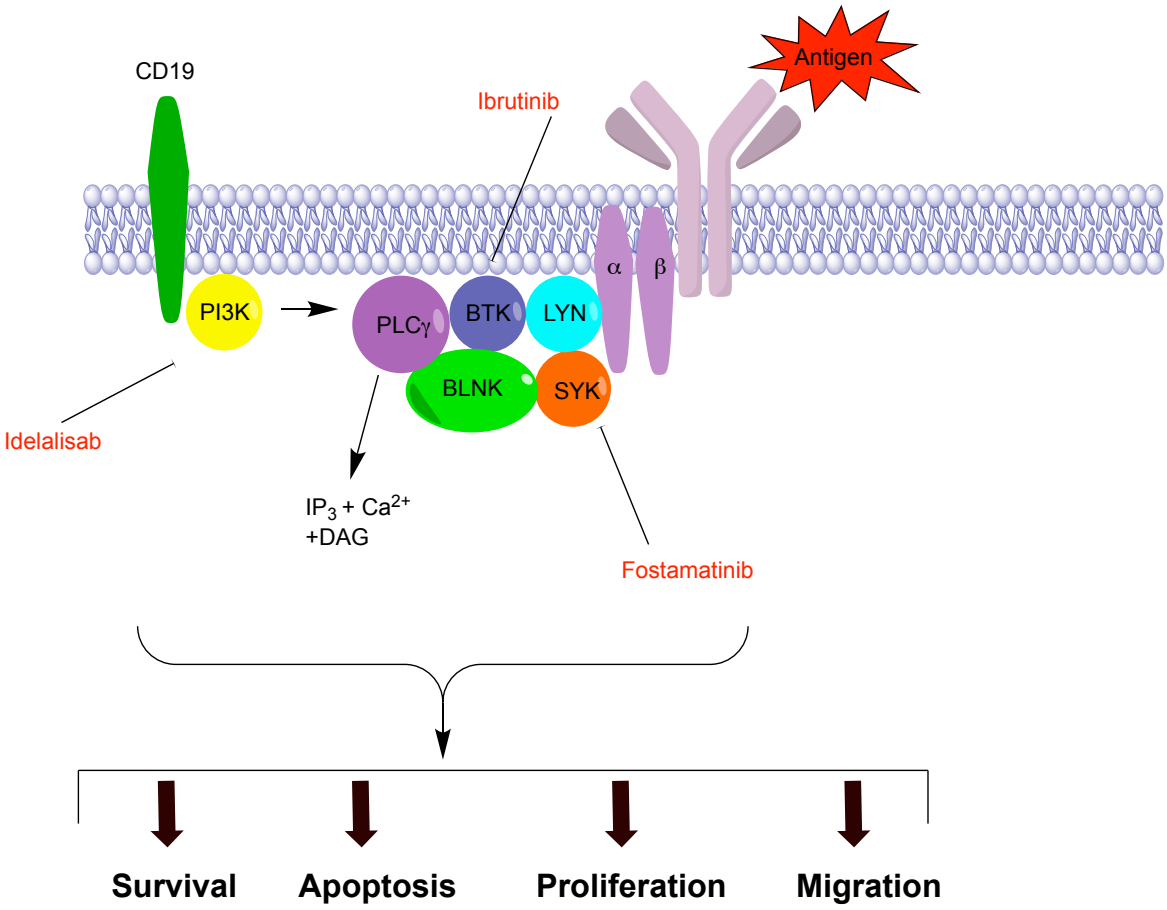

FIGURE 1-13: THE BCR SIGNALOSOME

The BCR is composed of a membrane bound immunoglobulin, bound to a signal transduction moiety, CD79α/CD79β. Both CD79α/CD79β contain immunoreceptor tyrosine activation motifs (ITAMs) that undergo phosphorylation when an antigen binds to the immunoglobulin. This phosphorylation is carried out by LYN, and leads to the recruitment of SYK. Activation of SYK produces a membrane-associated signalling complex known as the signalosome. The signalosome consists of SYK, BTK, PLCγ, PI3K as well as other adaptor molecules at the membrane surface. The activation of PI3K requires the co-activator CD19 to be phosphorylated by LYN. The signalosome co-ordinates and regulates the downstream cellular events in the cell such as survival, migration, proliferation and apoptosis.

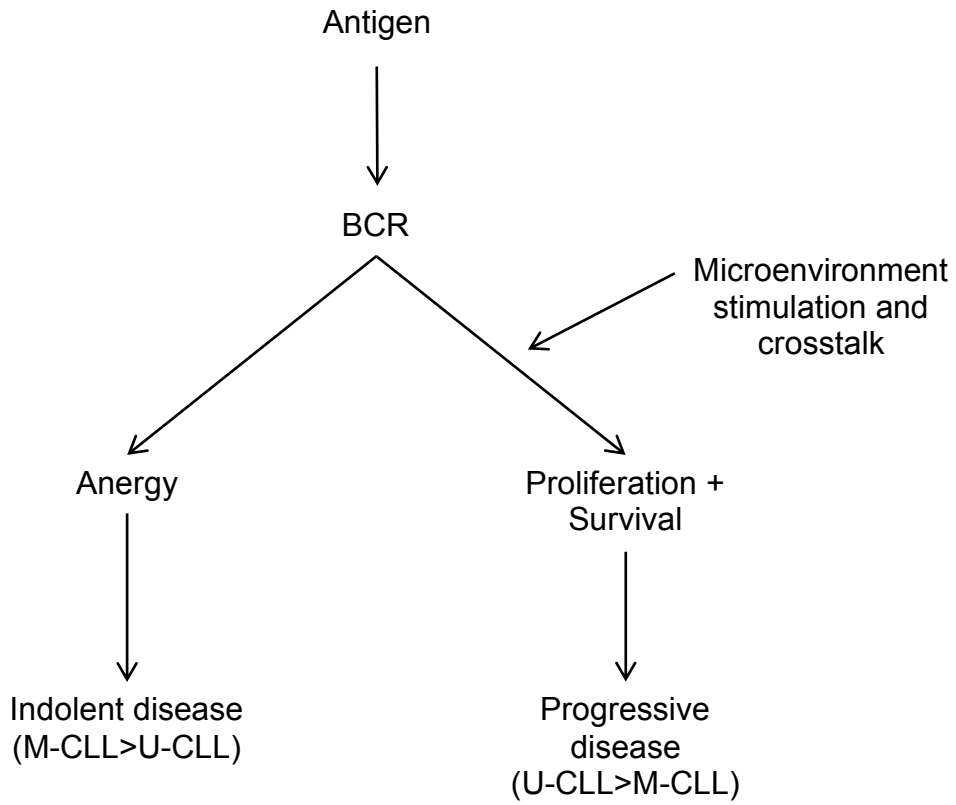

FIGURE 1-14: DIFFERENT BCR SIGNALLING RESPONSES AND VARIABLE CLINICAL OUTCOME IN CLL (ADAPTED FROM (PACKHAM ET AL., 2014)).

Analysis of surface immunoglobulin-mediated signalling in the two major disease subsets as defined by *IGHV* mutational status reveals differing responses to engagement of the BCR. Mutated CLL (M-CLL) generally of better prognosis is mainly, but not exclusively dirven towards anergy. While, in contrast, unmutatued CLL (U-CLL) retains more reponsiveness which could possibly explain the increased progression seen in U-CLL patients. Further to this, CLL cells are also protected from apoptosis from microenvironment stimulation and cross talk to the BCR such as the induction of the surival-promoting MCL-1 protein.

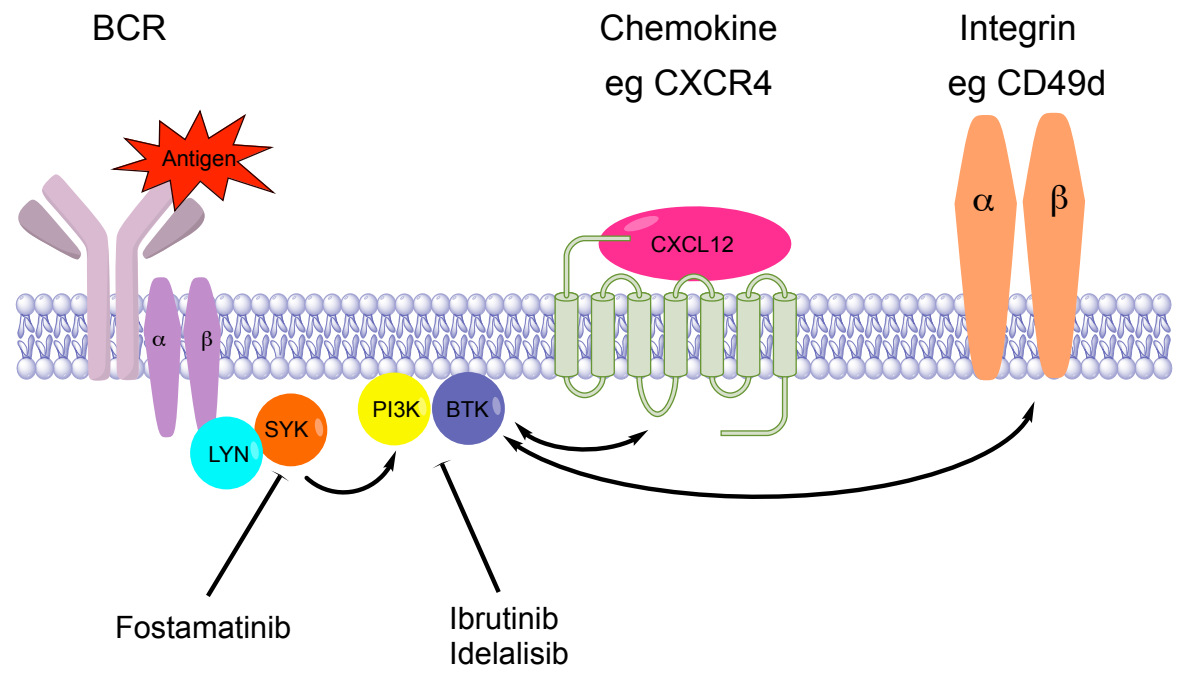

FIGURE 1-15: BCR CROSSTALK WITH MICROENVIRONMENT RECEPTORS

This schematic representation demonstrates the dual role of BTK and PI3K in BCR, chemokine and integrin signalling. Indicating how 'BCR inhibitors' could potentially target multiple pathways all interconnected with the BCR, which would explain how BCR stimulation and result in increased migration and adhesion.

1.4.4 Chemokines and cytokines secreted by stromal cells

1.4.4.1 CXCL12

Chemokines secreted by stromal cells play a critical role in the homing and retention of CLL cells in the tissue microenvironment. The most understood of these stromal chemokines is CXCL12 (also known as stromal-derived factor-1 (SDF-1)) which was originally characterised as a pre-B cell growth factor (Nagasawa et al., 1994). CXCL12 binds to the receptors CXCR4 and CXCR7 and the major role of the CXCL12 chemokine is to regulate haematopoietic cell trafficking and SLO architecture. Gene knockout mice deficient in either CXCL12 or CXCR4 results in impaired haematopoiesis, exhibited as a defect in trafficking of HSCs (Ratajczak et al., 2006, Ma et al., 1998).

CXCL12 is secreted by a number of cell types within the CLL microenvironment, including MSCs (Burger et al., 1999) and NLCs (Burger et al., 2000). CXCL12 has two major effects on CLL cells; firstly it causes migration towards stromal cells as discussed previously (Section1.4). And secondly, it provides survival signals to CLL cells (Burger et al., 2000). Both of these effects are mediated through the chemokine receptor CXCR4 which is expressed at high levels on the surface of peripheral blood CLL cells (Burger et al., 1999). CXCR4 expression is approximately three to four-fold greater on the surface of CLL cells than that of normal blood and BM B cells (Mohle et al., 1999).

Receptor internalisation by endocytosis is a major feature for most chemokine receptors. CXCR4 is downregulated via receptor endocytosis once activated by CXCL12 (Burger et al., 1999) and can therefore be used as a marker of CXCL12 'exposure'. Circulating CLL cells in the PB characteristically express high levels of surface CXCR4, while CLL cells resident in the tissue microenvironments and in close contact to CXCL12 secreting cells have lower levels of surface CXCR4 (Ghobrial et al., 2004). Moreover, circulating CLL cells with low CXCR4 and high CD5 expression have increased expression of Ki67, and altered gene expression signatures associated with proliferation, and apoptosis (Calissano et al., 2009) suggesting CXCR4 is downmodulated as cells receive tissue based stimulation. The natural recovery of CXCR4 on CLL cells in the circulation can be mimicked by incubating CLL cells *in vitro* where levels of CXCR4 increase rapidly (within hours;(Coelho et al., 2013).

CXCR4 is a G-protein coupled receptor (GPCR) and therefore the mechanism of activation is mediated by an intracellular heteroterimeric G-protein associated with the inner surface of the plasma membrane. The classic model of GPCR signalling starts with the exchange of GDP for GTP on one of the subunits of the heterotrimeric G proteins. Active GTP subsequently stimulates adenylyl cyclase to produce second messenger cAMP. cAMP in turn activates protein kinase A (PKA), which has many downstream

targets that affect the cell's behaviour. CXCR4 receptor signalling following stimulation with CXCL12 has a number of effects on the cell including activation of PI3K (Burger et al., 1999), phosphorylation of STAT3 (Burger et al., 2005) and p44/42 MAP kinases (Burger et al., 2000) and calcium mobilisation. As already stated, one of the functions of CXCL12/CXCR4 interactions is the trafficking of lymphocytes. This chemotaxis has been shown to be mediated through PI3K (Mellado et al., 2001, Ward, 2006). PI3K activation can also lead to tumour cell survival through the activation of AKT (Barbero et al., 2003). Other molecules also implicated in tumour cell survival through CXCR4 signal are p38 and Erk1/2 (Vlahakis et al., 2002).

Because CXCL12 not only directly stimulates CLL cell survival but also attracts CLL cells to the supportive microenvironment the CXCR4-CXCL12 axis is an important therapeutic target. Inhibition of the CXCR4/CXCL12 axis is well into clinical development and is holding great promise. There is growing interest in the use of CXCR4 antagonists to help mobilise cells involved in MRD out of the stroma and into the PB (Discussed in more detail Chapter5, Section5.1). Recently the CXCR4 antagonist plerixafor was used in combination with the anti-CD20 antibody rituximab and showed that plerixafor efficiently mobilises CLL cells from the stroma into the peripheral blood.

1.4.4.2 CXCL13

Another key chemokine involved in CLL trafficking is CXCL13 (also known as B cell-attracting chemokine (BCA-1)). CXCL13 binds to the receptor CXCR5 (CD185) which is highly expressed on CLL cells (Burkle et al., 2007). In normal B cell homeostasis CXCL13 gradients induce the recruitment of circulating naïve B cells into follicles (Mueller and Germain, 2009). CXCL13 has also been shown to be involved in the positioning of these naïve B cells once they are inside the follicle. CXCL13 is secreted by NLC (Burkle et al., 2007) as well as other stromal cells such as FDCs (Allen et al., 2004). As with CXCR4, binding of CXCL13 to CXCR5 leads to receptor endocytosis and a number of downstream effects. *In vitro* CLL cells show increased chemotaxis following stimulation to CXCR5 (Burkle et al., 2007).

1.4.4.3 CCL19 and CCL21

Two additional chemokines secreted by stromal cells in the CLL microenvironment are CCL19 and CCL21. As discussed previously, these chemokines serve as ligands for the CCR7 receptor on CLL cells and play an important role in the migration of CLL cells across the vascular endothelium (Till et al., 2002).

1.4.5 Chemokines and cytokines secreted by CLL cells

1.4.5.1 CCL3 and CCL4

Chemokines secreted by CLL cells also play a key role in creating a supportive microenvironment mainly through the attraction of accessory cells into the tissue. Activated CLL cells have been shown to secrete CCL3 and CCL4, two chemokines which normally play a role in the adaptive immune response by acting as chemoattractants for T cells and monocytes (Burger, 2011). Further to this CCL3/4 have been shown to be elevated in the plasma of CLL patients (Burger et al., 2009b) and are strongly associated with prognostic markers such as *IGHV* mutations, CD38 and ZAP70 (Sivina et al., 2011). CCL3/4 recruit regulatory T cells that express their cognate receptor CCR5 into close proximity of CLL cells. This movement allows T cells to efficiently provide pro-survival signals (Bystry et al., 2001). Burger et al., demonstrated that sIgM stimulation induced a dose-dependent increase in expression of CCL3 and CCL4 and that incubation with the Syk inhibitor R406 completely inhibited this induction (Burger et al., 2009b). Further to this NLC cells also induced production of the two chemokines and this NLC-induction could also be inhibited by R406 suggesting that the induction of CCL3 and CCL4 secretion in CLL-NLC co-cultures is SYK-dependent and therefore could involve the BCR. This finding reveals how BCR modulation alters the microenvironment.

Inhibiting the secretion of these pro-survival chemokines by CLL cells is a promising therapeutic target. Due to the involvement of the BCR in the production of CCL3/CCL4 (Burger et al., 2009b), there is evidence that inhibition of the BCR signalling pathways will lead to decreased secretion. Burger et al., 2009 showed that there was decreased secretion of CCL3/4 by CLL cells when cultured with NLC when they were treated with a SYK inhibitor (Burger et al., 2009b). The PI3Kδ inhibitor CAL-101 which inhibits the BCR pathway downstream of SYK was also shown to cause a marked reduction in circulating CCL3/4 in patients treated with the drug (Hoellenriegel et al., 2011).

1.4.5.2 CCL22

Another chemokine secreted by CLL cells is CCL22 (Ghia et al., 2002). CCL22 functions in a similar way to CCL3/CCL4 by recruiting T cells into the tumour microenvironment, enabling them to provide survival signals to the CLL cells. CCL22 binds to the receptor CCR4 which has been shown to be highly expressed on regulatory T cells. Unlike CCL3/CCL4, CCL22 acts as a secondary recruitment signal and is only secreted following ligation with CD40 on the T cells (Ghia et al., 2002). This fact is further supported by the fact that PB CLL cells do not secrete CCL22.

1.4.6 Chemokines and cytokines and the pathogenesis of CLL

CLL patients often present with a progressive immunodeficiency which could be due to the ability of CLL cells to escape immunosurveillance by manipulating their surrounding microenvironment. CLL cells are able to evade immune detection through different mechanisms involving the secretion of immunosuppressive cytokines and the alteration of signalling pathways (Ramsay et al., 2008). A number of chemokine and cytokines are induced in survival-supporting cultures of CLL cells and several of these have been reported to be elevated in the plasma of patients with CLL, many correlating with clinical course (Fayad et al., 2001, Wierda et al., 2003, Ferrajoli et al., 2002, Yoon et al., 2012). One of these cytokines is IL-8, which has been shown to promote the progression of several human cancers (Waugh and Wilson, 2008) including CLL (Wierda et al., 2003, Yoon et al., 2012). In patients with CLL, increased IL-8 mRNA expression has been associated *in vitro* with pro-longed cell survival (Francia di Celle et al., 1996). Functionally, IL-8 expression has been shown to be upregulated by the CXCR4/CXCL12 axis and Perbellini et al., demonstrated that CLL cells co-cultured with BMSC showed an increase in IL-8 supernatent concentration compared to CLL cells cultured alone and blockage of either CXCL12 or CXCR4 significantly inhibited this increase (Perbellini et al., 2015).

An 'inflammatory' microenvironment was shown to be induced in survival-inducing culture in the work by Schulz et al., who demonstrated that culture with survival-supportive culture conditions induced distinct gene expression changes, a high proportion of which were inflammatory cytokines (Schulz et al., 2011). The role of the immune system and chemokines and cytokines in the CLL microenvironment is further supported by the research using the immunomodulatory agent lenalidomide showing that one mechanism of action is through modulation of the microenvironment. Fiocari et al., examined the effect of lenalidomide on the monocyte/macrophage population from CLL patients and showed impaired monocyte migration response to CCL2, CCL3 and CXCL12 (Fiorcari et al., 2015a). The gene expression signature induced by lenalidomide in NLCs indicated a reduction of pivotal pro-survival signals such as CCL2 and supported a modulation towards M1 phenotype. Their data indicated a mechanism of action that mediates a pro-inflammatory switch of NLCs affecting the protective microenvironment of CLL.

1.4.7 Adhesion molecules

Survival signals may be provided to CLL cells by interactions with adhesion molecules expressed on their surfaces and cells expressing their ligands in the microenvironment. Adhesion molecules play an important role in cell-cell interactions as well as interactions

between cells and their surrounding environment such as the ECM. Integrins are a family of adhesion receptors that are essential for cells to undergo migration within tissues and are essential for the recirculation of cells. Integrins are central to many aspects of tissue localisation of both normal and malignant lymphocytes.

CLL cells express β1 and β2 integrins (CD29 and CD18) and variable amounts of α3 (CD49c), α4 (CD49d) and α5 (CD49e) chains (Munk Pedersen and Reed, 2004). β1 integrins are also known as very late activation antigens (VLAs). VLAs all have a β1subunits but various α subunits (α1-α6). As discussed earlier (Section1.2.1), surface expression of the integrin subunit CD49d can be used as a prognostic marker and is important in crosstalk with the BCR (Section1.4.3). High expression of CD49d is also associated with nodal disease (Brachtl et al., 2014). The α4β1 integrin, known as VLA-4 plays a particularly important role in interactions between normal and malignant haematopoietic cells and their BM microenvironment. VLA-4 is a receptor for fibronectin and VCAM-1. In CLL cells VLA-4 has been shown to cooperate with CXCR4 in CLL cell adhesion to MSC (Burger and Kipps, 2006). Stimulation through sIgM is associated with increased adhesion to fibronectin. CD49d is understood to be a major factor in the CLL microenvironment and is shown to have a complex interplay with other surface receptors such as CXCR4 (Burger and Kipps, 2006), the BCR (Fiorcari et al., 2013, Hoellenriegel et al., 2011) and CD38 through the chemokines CCL3/CCL4 (Zucchetto et al., 2009).

CLL cells also express variable amounts of leukocyte-function associated antigen-1 (LFA-1, CD11a). Adhesion of cells through the interaction with ICAM-1 on stromal cells has been reported to induce protection against spontaneous apoptosis (Maffei et al., 2013).

1.4.8 TNF family receptors

TNF family members are a group of cytokines that function to either provide survival signals or alternatively induce apoptosis. CD40 is a co-stimulatory protein part of the TNF-receptor superfamily that is found on antigen presenting cells and is required for their activation. CD40 is found on the surface of CLL cells (Ledbetter et al., 1987, Gruss and Dower, 1995). Binding to its ligand CD40L on T cells can induce a variety of downstream effects in CLL cells, firstly the activation of pro-survival and proliferation pathways and secondly immune recognition resulting in the induction of immune responses. T cells have been shown to modulate the survival of CLL cells through the CD40/CD40L system and within proliferation systems a significant number of T cells display CD40L.

B cell–activating factor (BAFF) of the TNF family is a type II transmembrane protein that has been shown to promote B cell survival (Mackay et al., 2003). BAFF binds to members

of the TNF receptor family such as the BAFF receptor (BAFF-R), BCMA (B cell maturation antigen) and TACI (transmembrane activator and calcium modulator and cyclophilin ligand interactor). Two of the BAFF receptors BCMA and TACI also bind APRIL, another proliferation inducing ligand, which has also been shown to contribute to B cell survival (Mackay et al., 2003). CLL cells have been shown to express the receptors for BAFF and APRIL and via these receptors NLC-derived BAFF and APRIL induce activation of the canonical NFκB pathway and protect CLL cells from spontaneous and drug induced apoptosis (Nishio et al., 2005). More recently BAFF was shown to upregulate MicroRNA-155 (miR-155) (Cui et al., 2014). High-level expression of miR-155 is associated with aggressive disease in CLL and cells with high levels of miR-155 are more responsive to BCR stimulation. Further to this cells that are $CD5^{Bright}CXCR4^{Dim}$ (cells that have just been released from the microenvironment) express higher levels of miR-155. These cells were shown to be more responsive to BCR stimulation indicating that this increased expression and sensitivity is as a result of microenvironment stimulation. Further to this, treatment with CD40L and BAFF had the same effect on miR-155 expression and BCR sensitivity. This study by Cui et al., indicates that BCR ligation can be enhanced by high levels of miR-155, which in turn can be induced by crosstalk within the tissue microenvironment, potentially contributing to its association with adverse clinical outcome in patients with CLL (Cui et al., 2014).

TABLE 1.3: POTENTIAL MOLECULAR INTERACTIONS OF THE CLL MICROENVIRONMENT

Interactions between CLL cells and bystander cells in the tissue microenvironment are important for CLL cell survival and homing and retention within the protective niche. Contact between CLL and stromal cells (NLCs and BMSCs) is established by chemokine receptors as well as adhesion molecules expressed on both cell types. The chemokine receptors CXCR4 and CXCR5 are expressed at high levels on CLL cells and bind to the chemokines CXCL12 and CXCL13 respectively which are released at high levels from NLC and MSC. CLL cells additionally express two other chemokine receptors CXCR3 and CCR7 which are involved in lymphatic tissue homing. Integrins expressed on the surface of CLL cells cooperate with the chemokine receptors to establish cell adhesion. This occurs particularly through the integrins VLA-4 (CD49d) and LFA-1 (CD11a) and their respective ligands VCAM-1, fibronectin and ICAM-1. NLC cells also express BAFF and APRIL which are part of the TNF family. BAFF and APRIL provide survival signals to CLL cells via their receptors BCMA, TACI, and BAFF-R. Contact with antigen is considered one of the key factors in the activation of the CLL cell through activation of the BCR and in turn activation of the kinases downstream of the receptor. BCR stimulation as well as co-culture with stromal cells results in the secretion of the chemokines CCL3, CCL4, and CCL22. This secretion in turn results in the recruitment of T cells which interact through CD40/CD40L and IL-4.

Ligand/Receptor	Potential source	Effect on CLL pathogenesis
BCR	CLL	The BCR is a key molecule on the surface of CLL cells and plays a major part in CLL cell survival and progression.
		Signalling through the BCR increases expression of MCL-1 leading to the suppression of apoptosis (Petlickovski et al., 2005, Bernal et al., 2001).
		Signalling through the BCR leads to the activation of the UPR (Krysov et al., 2014).
		Stimulation through sIgM leads to an increase in mRNA translation. (Yeomans et al., 2016).
		BCR activation reduces CXCR4 expression (Quiroga and Burger, 2010).
		Stimulation through the BCR results in an increased production of the chemokines CCL3/CCL4 (Burger et al., 2009b).
CXCL12	Stromal cells	CXCL12 causes homing of CLL cells into the microenvironment (Burger and Peled, 2009).
	NLCs	CXCL12 can provide survival signals to CLL cells (Burger et al., 2000).
CXCL13	NLCs	CXCL13 causes homing of CLL cells into the microenvironment (Burkle et al., 2007).
		CXCL13 causes the upregulation of the anti-apoptotic protein MCL-1 in FDCs (Pedersen et al., 2002).

CCL19 and CCL21	Stromal cells	CCL19 and CCL21 play an important role in the migration of CLL cells across the vascular endothelium (Till et al., 2005). CCL19/CCL21 induced migration is more pronounced in ZAP-70/CD38 positive CLL cells.
CCL3/CCL4	CLL cells	Act as chemoattractants for T cells which allows T cells to successfully provide pro-survival signals (Bystry et al., 2001).
CCL22	CLL cells	Acts as a chemoattractant for T cells (Ghia et al., 2002).
VLA-4	CLL cells	In CLL cells VLA-4 has been shown to cooperate with CXCR4 in CLL cell adhesion to MSC (Burger and Kipps, 2006). CD49d is now an important prognostic marker (Bulian et al., 2014).
BAFF/APRIL	NLCs	NLC derived BAFF and APRIL induce activation of the canonical NFκB pathway and protect CLL cells from spontaneous and drug induced apoptosis (Nishio et al., 2005). BAFF upregulates miR-155 which has shown to induce BCR ligation (Cui et al., 2014).
CD40L	T cells	T cells have been shown to modulate the survival of CLL cells through the CD40/CD40L system (Kitada et al., 1999). Within proliferation centres a significant number of T cells display CD40L (Stevenson and Caligaris-Cappio, 2004). CD40 activation of CLL cells can result in immune recognition resulting in the induction of immune responses.
IL-4	T cells	IL-4 increases sIgM expression (Aguilar-Hernandez et al., 2016).

1.4.9 Modelling the CLL microenvironment

As outlined in the previous sections of this chapter, interactions in the tumour microenvironment can promote CLL cell survival, proliferation and drug resistance and the importance in mimicking these interactions *in vitro* is becoming increasingly clear. Substantial proliferation rates have been observed *in vivo* (Messmer et al., 2005) and studies have tried to replicate these proliferation rates *in vitro* however, studies of CLL proliferation and the pathways involved in the critical survival signals are limited by difficulties in mimicking this complex microenvironment. This is made more difficult due to the fact that primary CLL cells are notoriously difficult to culture and many models are hindered by the poor survival of these cells *in vitro*. Considering that many different cell types are being implicated in the growth of CLL, a precise definition of which cells and through which pathways are operating *in vivo* becomes essential. There is also a need for models that incorporate other variables such as oxygen and tension so that proliferation can occur. Many pre-clinical testing of potential therapies only partly take into account the protective effect of stromal cells and T cells (Burger et al., 2009a).

Hamilton et al., characterized three different co-culture systems mimicking the CLL microenvironment (Hamilton et al., 2012). The authors co-cultured CLL cells with either fibroblasts that overexpressed CD40L or CD31, or with endothelial cells. All three of the co-culture conditions resulted in increased expression of the activation marker CD69, CD38 and the adhesion molecules CD44 and CD49d. However only the transfected fibroblasts overexpressing CD40L or CD31 were able to induce CLL cell proliferation. This study indicated that many cell types and co-culture conditions are able to provide CLL with appropriate support however only certain conditions are capable of inducing cell proliferation. Asslaber et al., further added to the work of Hamilton et al., by showing that isolated autologous and allogeneic CD4+ T cells provide the strongest proliferative stimulation to CLL cells (Asslaber et al., 2013).

Finding physiologically relevant models to study CLL microenvironment interactions is an area under intense investigation due to the fact the tissue resident CLL cells are not readily available from patients. Walsby et al., developed a dynamic *in vitro* model investigating lymphocyte trafficking in CLL using a novel endothelial flow system. They demonstrated that shear forces induced by the flow system induced a number of significant changes in endothelial and CLL cell phenotypes that had not previously been seen in *in vitro* culture models (Walsby et al., 2014). This outlines the importance for selecting an appropriate model for investigating CLL/microenvironment interactions.

A number of *in vivo* mouse models have been developed to address the issues surrounding mimicking the CLL microenvironment and the most widely utilised model is the transgenic TCL1 mouse. In this mouse model the human *TCL1* gene is expressed under the control of the *IGHV* region promoter and enhancer (Bichi et al., 2002) this leads to the enhancement of AKT signalling. Another *in vivo* model is the New Zealand Black (NZB) mice who later in life develop an *IGVH* unmutated, ZAP70 positive CLL-like disease (Phillips et al., 1992). New Zealand Black mice have been found to have a mutation which results in decreased levels of miR-16 in lymphoid tissues (Raveche et al., 2007). This is reminiscent of 13q14 del seen in human CLL. Other transgenic mice models of CLL include mice overexpressing both BCL2 and a tumour necrosis factor receptor-associated factor (Zapata et al., 2004) and MYC/BAFF transgenic mice (Zhang et al., 2010). miR-15b/16-2 knockout mice have also been generated to better understand the cluster's role *in vivo* (Lovat et al., 2015). These mice developed B-cell malignancy by age 15-18 months and flow cytometric analysis demonstrated an expanded CD19+ CD5+ population, a characteristic of the cells found in CLL indicating an important role of miR-15b/16-2 loss in the pathogenesis of CLL.

1.5 Cell culture methods

Cell culture refers to the removal of cells from a tissue into a favourable artificial environment. Cells grown in an artificial environment are typically grown as a monolayer (two dimensional (2D)) on a flat surface with medium as a source of nutrition. Medium is often supplemented to aid cell growth, thereby providing essential nutrients, growth factors, hormones and oxygen to the cells. When cells reach confluency they are sub-cultured to avoid overgrowth or nutrient exhaustion. A vast number of cell lines have been established from different tumour tissues and tumour stages. Many of these cancer cell lines are relatively easy to maintain in culture and allow modelling of important features of cancers. Thus, conventional 2D cell cultures have become a major research tool due to the consistent and reproducible results they provide.

1.5.1 Two dimensional cell culture

Although easy and convenient, 2D monolayer culture methods have several limitations (Table 1.1). In 2D culture, cells are grown on flat dishes made of a very stiff polystyrene plastic. The cells adhere and spread on this plastic surface and form unnatural cell attachments to proteins that are deposited on this synthetic surface. This stiff, unnatural

culture surface can lead to elevated tensile stress and modified phenotype/cell behaviour (von der Mark et al., 1977, Petersen et al., 1992, Kim, 2005, Ghosh et al., 2005). Moreover, when cells are cultured in a monolayer, cells are only in contact with other cells at their periphery. This lack of 3D interactions can lead to inappropriate spatially distributed cell-cell and cell-ECM signalling which is essential for control of cell proliferation and differentiation *in vivo* (Kimlin et al., 2013). Finally, the presence of a homogenous cell layer means that the oxygen, nutrient and waste gradients that are present *in vivo* are absent in 2D cultures. In fact, direct comparison of 2D cultured cells and cells cultured in 3D have revealed substantial differences in cell morphology, polarity, receptor expression and oncogene expression (Breslin and O'Driscoll, 2013). Due to these differences the ability of 2D cultures to accurately mimic the behaviour of cells *in vivo* has been questioned.

1.5.2 *In vivo* models

The last few decades have seen an increase in the use of *in vivo* mouse models to model cancer cell behaviour. Although such studies can provide many advantages compared to *in vitro* culture, they are also associated with substantial disadvantages (Table 4), including cross-species differences, cost and ethical issues.

1.5.3 Three dimensional tissue culture

Recent years have seen major developments of new technologies that allow modelling of complex human tissues and tumours in 3D cultures (Kim, 2005). These systems aim to reproduce tissue-specific structural features more accurately than conventional 2D culture methods and, overall, cells grown in 3D cultures appear to better retain key features of tissue-based cells, compared to 2D cultures (Breslin and O'Driscoll, 2013). The primary advantage 3D cultures have over 2D monolayers is their well defined geometry, which makes it possible to directly relate structure to function. 3D allows the co-culture of multiple cell types allowing for the study of interactions between cells and also cells with different phenotypes. This is particularly important in tumour biology given the crucial significance of tumour-stromal interactions. Cells grown in a 3D model have proven to be more physiologically relevant, showing improved biological mechanisms such as: viability, morphology, proliferation, differentiation, response to stimuli, migration and invasion of tumour cells into surrounding tissues, angiogenesis stimulation, and immune system evasion.

TABLE 1.4: THE MAIN ADVANTAGES AND DISADVANTAGES OF 2D AND 3D CULTURES AND *IN VIVO* ANIMAL EXPERIMENTS

Method	Advantages	Disadvantages
2D culture	Easy and convenient to set up. Relatively cheap. Generally good viability of cells. Numerous cancer cell lines available which have been derived from different tumour tissues and stages. Majority of these cancer cell lines are easy to maintain in culture and can be used to model many important feature of cancers.	Cells grown in monolayers form unnatural cell attachments to stiff tissue culture plastic and the proteins that are deposited on this synthetic surface. Lack characteristics of *in vivo* microenvironment, leading to losses of critical *in vivo* cell phenotype and cell behaviour. When cultured in 2D cells have been shown to have differences in their morphology, polarity, receptor expression and gene expression in comparison to what is observed *in vivo.* In 2D monolayers, cells experience artificially high tensile stress which has been shown to affect cell morphology, cytoskeleton arrangement and cell-cell adhesion. Cells are exposed to a uniform environment with sufficient oxygen and nutrients, which is not representative of cells in solid tumours where cells are exposed to gradients of critical chemical and biological signals.
3D culture	Cells grown in a 3D model have proven to be more physiologically relevant and showed improvements in several studies of biological mechanisms. Well defined geometry, which makes it possible to directly relate structure to function. Increased cell-cell and cell-ECM interactions. This is particularly important when studying the tumour microenvironment and the significance of tumour-stromal interactions. Oxygen and nutrient gradients exist making the tumour microenvironment more physiologically relevant. Non-uniform exposure of cells to drug compounds allows for more improved screening of potential candidates in drug development. Greater stability and longer lifespans than cell cultures in 2D. Cells are allowed to grow undisturbed compared to 2D models, where regular trypsinisation is required to passage cells.	Vary in their ability to mimic *in vivo* tissue conditions. Although 3D culture systems have increased angiogenesis stimulation, models still lack a vasculature system and the transport of small molecules such as nutrients, waste products, oxygen is limited. Mimic static or short term conditions, no progression like *in vivo.* Due to artificial components there can be reproducibility problems between batches of scaffolds. Interference from artificial components in synthetic scaffolds. Difficulties handling of post culture processing and extraction of all cells for analysis. Control of culture conditions (temperature and pH). Spheroid sizes tend to be non-uniform, making them unsuitable for high-throughput drug testing. Difficultly with real time imaging with many

		models.
In vivo	Observe overall effects of an experiment in an living organism, potentially in the presence of an intact immune system.	Animal models may not adequately reproduce features of human tumours or therapeutic responses due to differences between species. Important ethical and political issues lead to many rigorous regulations. Many experiments can be costly and timely. Mice often have compromised immune systems and the non-human stromal components do not recapitulate human pathophysiology, leading to poor prediction of drug efficacy.

1.5.4 3D culture methods

The availability of 3D culture models has increased rapidly due to advances in culturing techniques and the emerging field of tissue engineering. For example, advances in tissue engineering have allowed for the development of matrix-derived 3D tumour models while advances in microfluidic technology has also allowed for the manipulation of fluids and particles at submillimetre scales. Commonly 3D culture methods can be broadly split into two main groups: the formation of tumour spheroids and matrix embedded cultures. Advancing techniques has meant that new methods through the use of microfluidics have been developed. These will be discussed in more detail in a later section. Figure 1-16 and Table 1.5 outlines the main methods currently used for the generation of 3D cell cultures and their current use in the literature. The table is split broadly into the different strategies of 3D culture.

1.5.4.1 Spheroid based culture models

Many cell types have the natural tendency to aggregate due to ability of cells to re-establish mutual contacts between cells to express a tissue-like phenotypes. Spheroid based culture methods take advantage of the fact that many cells, in the absence of a surface with which they can attach, will self assemble into 3D spheroid structures. This property has led to the widespread use of tumour spheroids (LaBarbera et al., 2012) which represent the most common use of *ex vivo* 3D cultures. Spheroids are self-assembled clusters of cell colonies, and can be produced by various techniques, including forced floating, hanging drop, or spinner flasks (Figure 1-16). Table 1.5a outlines the formation of 3D models through the formation of tumour spheroids. Tumour spheroid based systems are relatively quick and easy. However they do often miss the essential part of ECM interactions, or interactions with other cell types. This is particularly important when considering the role of the microenvironment.

1.5.4.2 Matrix-based culture models

Although a quick and convenient method, tumour spheroid models are often deficient in ECM, and ECM interactions form a critical component of tumour microenvironments. It is possible to partially circumvent this deficit by culturing cancer cells with specific ECM constituents (Lee et al., 2007) or through the use of 3D gels such as Matrigel or 3D fibroblast-based matrices. Tissue-engineered approaches have also been used to create artificial 3D scaffolds which support cells and then may eventually be incorporated into the tissue (Figure 1-16). These pre-fabricated scaffolds are usually made of collagen, or other ECM proteins such as laminin and alginate. When seeded into culture containing

scaffolds, cells migrate between fibres of the scaffold and attach to them. As the cell grow and divide, they fill the interstices within the scaffold forming 3D structures. Cells communicate with ECM molecules in the scaffold enabling *in vivo* like cell behaviour especially cell-ECM interactions.

Table 1.5(b+c) outlines the use of scaffold or gel-based systems. Biological scaffolds are advantageous because they not only provide support for cells to attach and organise into 3D structures but they are also able to provide the correct microenvironment through growth factors and other molecules which cells can interact with. However the major disadvantages of scaffold based systems is that, especially with synthetic scaffolds, cells interact with these artificial and synthetic structures.

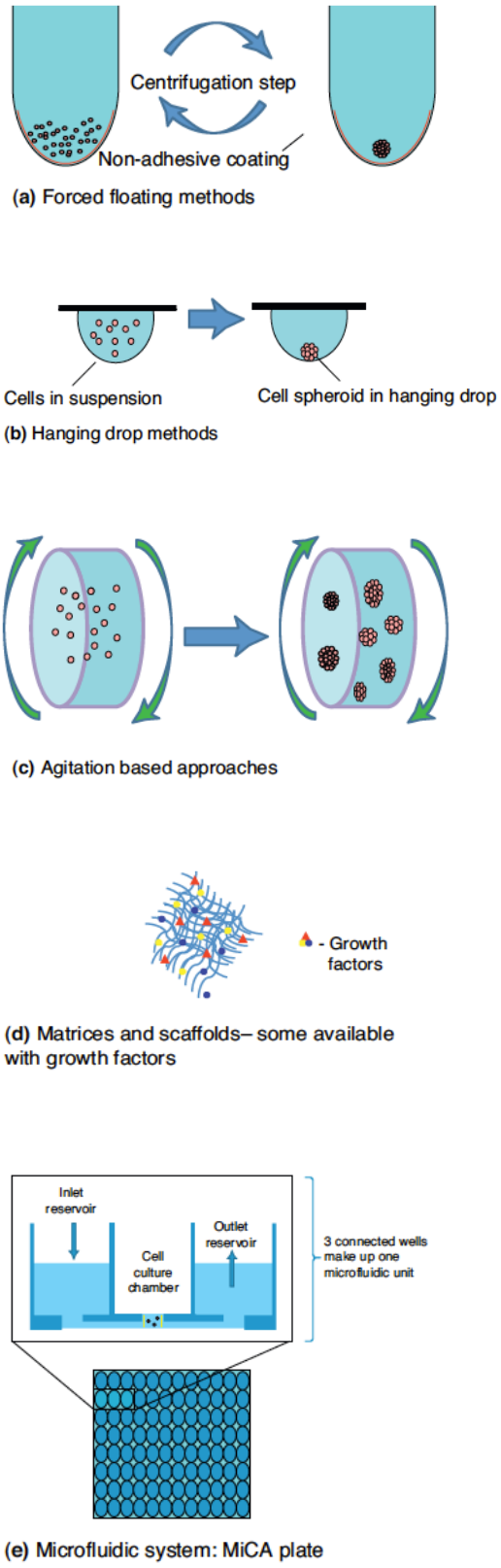

FIGURE 1-16: OVERVIEW OF THE COMMON METHODS USED FOR 3D CELL CULTURE (BRESLIN AND O'DRISCOLL, 2013)

Figure demonstrating the main methods used for the generation of 3D cultures. Methods include (a) Forced floating (b) Hanging drop (c) Agitation based approach (d) Matrices and scaffolds and (e) Microfluidic systems. A detailed description of each method can be found in Table1.5.

TABLE 1.5: MAIN METHODS CURRENTLY USED FOR THE GENERATION OF 3D CULTURES AND THEIR APPLICATION IN THE CURRENT LITERATURE

(a) Tumour spheroid methods

3D model	Description	Use in the literature
Forced Floating	Forced floating of cells is a simple method for generating 3D spheroids by preventing their attachment to the surface of the tissue culture by the modification of the culture surface. This results in the forced floating of cells in suspension which promotes cell-cell contacts due to lack of interaction with the tissue culture plastic. These cell-cell interactions force the formation of multi-cellular spheroids	Using 96-well plates coated with 0.5% poly-HEMA a panel of eight breast cancer cell lines were tested and led to the generation of tumour spheroids. The spheroids produced were easily accessible for experimentation and therefore suitable for high throughput drug testing. (Ivascu and Kubbies, 2006). 1.5% agarose in the tissue culture was used to create a thin coating over the culture dish surface preventing cell attachment to the surface, resulting in the establishment of tumour spheroids of breast cancer cell lines (Li et al., 2011).
Hanging drop	The hanging drop method uses a small aliquot of a single cell suspension which is pipetted into the wells of a MicroWell plate. Following cell seeding the plate is inverted and the aliquots of cell suspension turn into hanging drops. These drops are held in place due to surface tension and therefore cells accumulate at the tip of the drop. In a similar way to the forced floating method, the cells then form cell-cell interactions resulting in the formation of 3D spheroids	The hanging drop method was used to generate a 3D heterospheriod model of liver cancer and stromal cells which was then encapsulated into a collagen hydrogel to mimic ECM interactions. This model was used to demonstrate that the 3D model is more resistant to doxorubicin over a 2D monolayer culture (Yip and Cho, 2013). Human testis tissue was able to be cultured short term as hanging drop cultures with preserved overall morphology and continued germ line survival and proliferation. (Jorgensen et al., 2014). The hanging drop method was used to cultivate 3D tumour microtissue using non-small cell lung cancer (NSCLC) cell lines with and without human stromal cells. PBMCs and IL-2 were added after 10 days culture. (Koeck et al., 2015).
Rotary cell system	Developed by NASA, the Rotary Cell Culture System (RCCS) is a new concept in tissue engineering. By simulating microgravity, cells in liquid medium are maintained by minimal hydrodynamic forces. The culture vessel rotates on its horizontal axis, providing end over end mixing of the cells. Cells grown in RCCS are maintained in a gentle fluid orbit are able to attach to one another and form complex 3D structures.	The RCCS has enabled the production of large batches (10 to 500ml) of 3D multicellular aggregates (Hammond and Hammond, 2001). Tumour agglomerates culture in this type of bioreactor developed small areas of necrosis during continued growth (Becker and Souza, 2013).

(b) 3D gel models

3D model	Description	Use in the literature
Matrigel (or equivalent)	Gels can be used as substitute for 3D culture. Gels have a soft tissue-like stiffness and aim to mimic the ECM. Gels are most commonly made from ECM mixtures of natural origin. Matrigel is the most commonly utilised gel and is a reconstituted basement membrane preparation extracted from a mouse sarcoma.	Cancer prostate cells showed lack of organisation and increased invasiveness which is associated with cancer aggressiveness (Webber et al., 1997). Rapid proliferation of human fibrosarcoma cells was demonstrated in Matrigel (Kramer et al., 1986).
Synthetic gels	Gels made from animal sourced natural ECM may vary and change in structure over time, therefore synthetic gels such as the polyethylene glycol (PEG) based hydrogels have been developed.	Synthetic hydrogel matrixes were used to assess cell-matrix interactions using two epithelial ovarian cancer cell lines. Proliferation in 3D was dependent on cell-integrin engagement. Higher survival rates after exposure to paclitaxel was observed in the hydrogels compared to 2D monolayer (40-60% greater viability) (Loessner et al., 2010).
Fibroblast-derived matrices	Produced from CAFs this matrix resembles the stromal microenvironment.	Adenocarcinoma cell lines showed distinct aggregation, growth, proliferation and morphology profiles on fibroblast-derived 3D matrices which did not correlate to 2D behaviour (Serebriiskii et al., 2008).

(c) Scaffold based methods

3D model		Description	Use in the literature
Natural scaffolds	Collagen, Hyaluronic acid	Natural scaffolds are mainly hydrogels (colloidal gel, 99% water) made of natural materials or proteins like collagen type I, laminin or hyaluronic acid. Collagen hydrogels comprise a random mesh of collagen fibrils supporting a large amount of excess fluid (99%).	Human tumorigenic mammary cell line (MECs) formed small growth-arrested and polarised acini with adherent junctions and central lumen (Weaver et al., 1996). Collagen-based hydrogels have been widely used for the construction of 3D tumour models (Bhadriraju and Chen, 2002, Yip and Cho, 2013, Szot et al., 2011). The HA-hydrogel model was used to study the effects of heparin on tumour invasiness on 13 human cancer cell lines (David et al., 2004). The hyaluronic acid hydrogel model was also used to test camptothecin and doecetaxel which are standard therapies used in prostate cancer treatment (Gurski et al., 2009).
Synthetic scaffolds	PEG, PCL	Synthetic scaffolds have been extensively explored in tissue engineering applications to closely mimic the key features of the native ECM. Synthetic scaffolds are attractive alternatives because they offer improved batch-to-batch consistency. Scaffolds can be made from synthetic polymers including PEG. PEG-base hydrogels are prepared by chemical crosslinking polymers.	Human epithelial ovarian cells when encapsulated within a PEG-based hydrogel scaffold formed spheroids (Loessner et al., 2010). Porous PCL scaffolds were used for the culture or Ewing sarcoma cells in 3D (Fong et al., 2013)

	Microcarrier culture	Beads derived from dextran, gelatine, glycosaminoglycans and other porous polymers can be used as 3D supports for the culture of anchorage dependant cells. The primary advantage of microcarrier beads is they support the aggregation of anchorage-dependent cells that do not spontaneously aggregate. Cells growing on microcarrier beads serve as an excellent tool for studying different aspects of cell biology such as cell–cell or cell–substratum interactions	MIP-101 a human colon carcinoma cell line was shown to proliferate well in a microcarrier 3D culture and production of carcinoembryonic antigen and nonspecific cross-reacting antigen production was shown to be three to four fold greater in this 3D culture. (Jessup et al., 1997). Bovine endothelial cells attached to microcarrier beads were shown to produce endothelium-derived relaxing factor (EDRF). The use of microcarrier beads was shown to offer a good alternative for the study of endothelial cells. (Bing et al., 1992).

1.5.5 Novel 3D models

3D cultures are an invaluable research tool in tumour biology *in vitro* and, because of this, the field is ever advancing. Emerging microfabrication and microfluidics techniques offer new models that provide the opportunity to control different aspects of the tumour microenvironment for example the size of the 3D tissue constructs more efficiently. 3D model systems are also being designed to control a number of specific factors in the microenvironment which are likely to affect tumour progression and response to therapy. With the increased understanding of the importance of the tumour microenvironment, 3D models are also advancing to include multiple cellular elements. There is the need for models that include fibroblasts or other stromal cells without interference from other components such as scaffolds to truly understand the molecular interactions that occur between cellular components within the microenvironment.

1.5.5.1 Current novel 3D models in the literature

This part of the introduction will focus on the emergence of novel techniques and how these try to solve some of the disadvantages or technical problems seen with the more conventional 3D culture methods. The first part of the section with summarise some of the novel methods that have been emerging in the literature and the second part will focus on a novel method, the use of ultrasound waves to 'trap' cells, that has been utilised at the University of Southampton and how it might be useful in the modelling of the CLL microenvironment.

Liu et al., demonstrated a bladder cancer microenvironment stimulation system based on a microfluidic co-culture model. The system incorporated a perfusion system, matrigel channel units, and medium channel and four indirect contact culture chambers. They demonstrated the ability of four cells types, stromal cells, fibroblasts, endothelial cells and macrophages combined with bladder cancer cells to interact in the four chambers through soluble biological factors and metabolites. Within this system, bladder cancer cells showed a tendency to form a reticular structure (Liu et al., 2015).

Bruce et al., used a 3D microfluidic system to demonstrate a tri-culture model of the bone marrow microenvironment in acute lymphoblastic leukaemia (ALL). This 3D microfluidic tri-culture model allowed for the systematic investigation of effects of cell-cell and cell-matrix interactions on cancer progression and therapeutic intervention. The engineered 3D microfluidic tri-culture model allows precise control over the mechanical properties of matrix and fluidic shear stress. The authors then compared tumour cell viability on response to an anti-metabolite chemotherapeutic agent, cytarabine in tumour cells alone, tri-culture models for 2D static, 3D static and 3D microfluidic models (Bruce et al., 2015).

Singh et al., demonstrated the ability of a hydrogel microwell platform to successfully generate hundreds of uniform microtumours within 3-6 days from many cervical and breast carcinomas as well as head and neck squamous cell carcinoma (HNSCC) cells. They further demonstrated the ability of the platform to probe activation as well as inhibition of epidermal growth factor receptor (EGFR) signalling in 3D HNSCC microtumours in response to EGF and cetuximab treatments respectively (Singh et al., 2015). Tumour size heterogeneity can play a critical role in the establishment of different gradients within the tumour microenvironment such as hypoxia, pH, nutrients, growth factors, cytokines, and waste products. A major disadvantage of many current 3D models is the formation of a number of tumour spheroid of differing sizes leading to heterogenous effects of drug. Chambers et al., also demonstrated the use of polydimethylsiloxane (PDMS) microwells allowed for the characterisation of prostate cancer cell aggregates (Chambers et al., 2014). Further to this the system allowed the authors to consistently control for the presence or absence of an apoptotic core in the 3D cancer microaggregates.

Jaganathan et al., used a novel *in vitro* model using magnetic levitation to mimic breast tumours without the use of scaffolds while allowing for cell-cell and also tumour-fibroblast interactions. Breast cancer cells were co-cultured with fibroblasts and then magnetically levitated to allow for the formation of 3D structures which closely resemble *in vivo* tissues. The major of advantage of this system is the tumour and fibroblast cells are allowed to interact with each other and naturally form a complex matrix, thus mimicking a more relevant tumour microenvironment without externally added or other species-derived components such as Matrigel (Jaganathan et al., 2014).

One of the emerging techniques is the use of ultrasonic fields, which allows for non-contact trapping of cells in 3D agglomerates. Compared with other methods ultrasonic cell manipulation is an inexpensive non-contact method that allows simultaneous and synchronous manipulation of a large number of cells in a very short time (Bazou 2005a). Ultrasound standing wave traps (USWT) are simple in both set up and operation and have the further advantage of being non-invasive, chemically non-toxic and physically non-destructive (Kim et al., 2004). Taking into account its high efficiency and reliability and the fact in can be used with the majority of cell types, this technique holds great promise in cell manipulation techniques for a variety of applications including tumour/microenvironment interactions.

This project is primarily interested in the use of USWT to model the CLL microenvironment, therefore the method of acoustic trapping is reviewed in more detail in the following section of the Introduction.

1.6 Particle manipulation in an acoustic field

For many years it has been known that ultrasonic fields can influence the behaviour of particles in a liquid or gaseous medium. This effect relies on acoustic radiation forces that act on particles when they are within the acoustic field (Gröschl, 1998). It has been shown that these forces are generally greater in an ultrasonic standing wave (USW) (Bruus, 2012). A standing wave is a wave that remains in a constant position and is formed when two waves of identical frequency interfere with one another while traveling opposite directions through the same medium (Figure 1-17). Along the standing wave are points of minimum and maximum pressure amplitude known as nodes and anti-nodes respectively. Ultrasonic cell manipulation exploits the fact that when cells are exposed to acoustic radiation forces they are driven towards a nodal plane (Bazou et al., 2005b). Within this nodal plane there are secondary forces that cause the particles to cluster and organize into aggregates (Figure 1-18).

1.6.1 Acoustic forces

1.6.1.1 Primary radiation forces

The best understood acoustic force that particles are subjected to within an acoustic standing wave is the primary radiation force (PRF). The axial PRF is the largest force acting on the particles within the standing wave and is generated by the non-linear interaction between the acoustic field scattered by the particles and the standing wave field itself (Glynne-Jones et al., 2012). A standing ultrasonic wave will generate stationary pressure gradients and in a liquid medium, these pressure gradients will exert forces on particles distinguishable from the medium in terms of density and compressibility (Nilsson et al., 2009). Most particles and cells of interest are denser and less compressible than typical suspending fluids, this causes them to moves to the point of minimal acoustic potential, the pressure node, in response to the forces applied upon them.

1.6.1.2 Lateral forces

Stationary wave fields not only exhibit acoustic energy gradients along the axis, there are also variations in the lateral direction as well. Lateral forces cause particles to move not just to the axial pressure nodes but to particular points within the nodal plane. The lateral force is typically much weaker than the axial (Crum, 1975) yet most acoustic trapping techniques rely on these lateral forces to counteract the fluidic drag (Lierke, 1996). The application of lateral forces means that instead of having a homogenous layer of particles, particles can organise into different patterns and formations.

1.6.1.3 Interparticle forces

In addition to axial and lateral radiation forces, there are also secondary interparticle forces. These forces known as Bjerknes forces come into play when the particles are within close proximity of each other. These forces attract particles to each other and thus stabilise the cluster (Gröschl, 1998). Several studies have demonstrated that the lateral and secondary forces are at least two orders of magnitude smaller than the axial component of the primary force (Crum, 1975, Woodside et al., 1997, Spengler et al., 2003), however when the particles reach the nodal plane the axial net force is zero, and the secondary forces become increasingly important in stabilising the cluster.

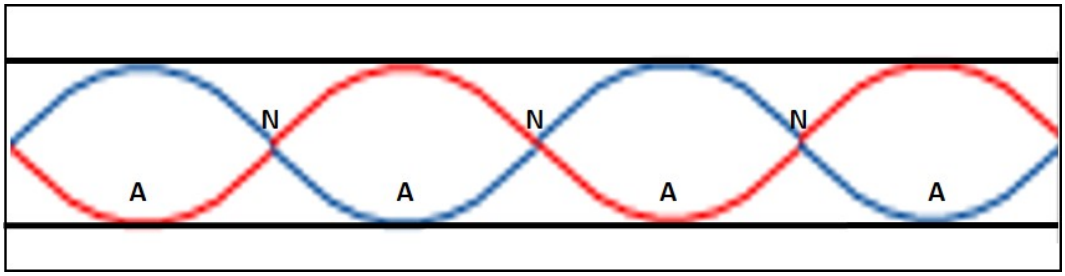

FIGURE 1-17: ULTRASOUND STANDING WAVE

A standing wave is one that remains in a constant position. Standing waves are most commonly formed when two identical waves (blue and red waves) of the same frequency interfere with each other whilst travelling in the opposite direction. Along the standing wave are points of minimum and maximum amplitude known as nodes, denoted by ‘N’ and anti-nodes denoted by ‘A’.

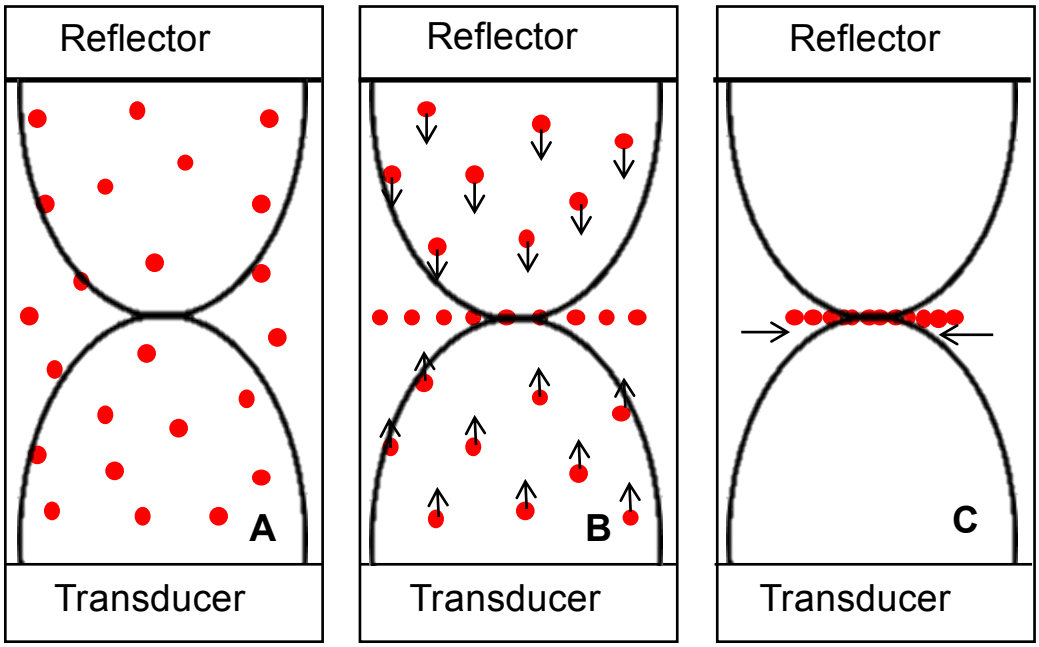

FIGURE 1-18: ACOUSTIC FORCES ACTING IN A HALF WAVELENGTH FIELD

Particles in medium (a) are subjected to a single node standing wave. Due to the fact the medium channel is a half wave length in size the node falls in the centre of the channel. Particles are directed towards the node by the primary radiation force (b). Lateral forces direct the particles to the central axis and secondary force further contribute to the agglomeration process (c).

1.6.2 Applications of acoustic trapping

Immobilisation and levitation of cells by acoustic trapping can facilitate several different applications, e.g. washing of cells, separation of cells, studies of cell-cell interactions, sonoporation and the study of non-adherent cells in a perfusion system. It is believed that acoustic trapping may give the ability to construct model systems for *in vitro* studies of cell behaviour while allowing for control over the cell microenvironment. Historically, acoustic trapping was introduced as a tool for containerless processing by NASA about 40 years ago (Lierke, 1996). The acoustic levitators developed then were aimed at levitating liquid droplets in open air.

The influence of standing ultrasonic waves on mammalian cells was first investigated by Baker who looked at erythrocytes in a liquid medium (Baker, 1972). Later, Coakley et al., (Coakley and Gallez, 1989) and Hertz (Hertz, 1995) both developed devices to utilize these effects for cell manipulation. Coakley et al., further developed the devices in the early 2000s to more miniaturised trapping systems which were aimed at studies of small cell clusters (Spengler et al., 2000). Since these early studies the majority of work using similar devices has been based on cells in suspension, moving to the nodes of the wave (Shi et al., 2009). Studies have demonstrated the ability of both single cells (Wu, 1991) and two dimensional cell aggregates (Bazou et al., 2005b, Bazou et al., 2005a) to be levitated or 'trapped' within acoustic devices. To date, acoustic trapping has been used to manipulate a number of different cell types. The formation of cell sheets within ultrasonic devices has been observed for neural cells (Bazou et al., 2005a), the prostate epithelial cell line (PZ-HPV-7) the cancerous prostate epithelial cell line (DU-145) (Bazou et al., 2006a), chondrocytes (Bazou et al., 2006b) and HepG2 (liver hepatocellular carcinoma) (Edwards et al., 2007).

Typically, functional cell assays carried out *in vitro* are based on the assumption that cells will behave in a way that is indicative of their behaviour in their natural environment. Therefore a number of studies have investigated the impact of exposure to the ultrasound frequencies in regards to cell behaviour and viability. Viability of cells exposed to ultrasound manipulation has been investigated and no indications were found to suggest that the exposure to ultrasound influenced the viability of the cells (Bazou et al., 2005b, Hultstrom et al., 2007, Evander et al., 2007). When looking at 2D neural cell aggregates within a half wavelength device Bazou et al., determined that there was no decrease in cell viability during 1 hour levitation. They added the live cell stain calcein AM, the dead cell stain ethidium homodimer-1 and the apoptosis stain Annexin V into the device during levitation and compared the uptake of the dyes by the cells at 1 minute and after 1 hour. Fluorescence analysis of the captured sheets showed no difference between the time points (Bazou et al., 2005a).

A number of other studies have investigated how the physical environment from acoustic trapping affects cell behaviour and physiology. Cockley et al., studied the initial cell-cell interactions in chondrocytes which had formed monolayers in acoustic devices. The authors looked at f-actin and gap junction communication and demonstrated that after 1 hour exposure in the devices the F-actin had accumulated at the cell-cell contact interface and the gap junctions had formed. This demonstrates the ability of cell-cell interactions to form in the devices without interacting the ECM (Coakley et al., 2004). Bazou et al., examined the physical environment experienced by levitated neural cells in an acoustic trap by monitoring a number of acoustic stimuli such as the temperature, acoustic streaming, pressure amplitudes, white noise and the inter-particular forces acting on the cells (Bazou et al., 2005b). They concluded that no adverse effects to the neural cells occurred within the devices and that acoustic stimulation did not result in any changes in the *in vitro* surface receptor interactions for these cells. Bazou et al., looked at gene expression of mouse embryonic stem cells following levitation in an USWT. Their results indicated that levitation of ES cells at the highest employed acoustic pressure for 60 minutes does not modify gene expression and cells maintained their pluripotency.

1.6.3 The acoustic trapping device

The most commonly used approach to acoustic trapping is to use a planar multilayer resonance structure which is approximately a half wavelength in size (Figure 1-19). One half-wavelength is the distance from one antinode to another. Nodes occur at intervals of half a wavelength (λ/2). Half wavelength devices can be defined as resonators in which the fluid channel is close to a half wavelength in thickness, this leads to a pressure amplitude minimum that is close to the channel centre, meaning that cells cluster and form aggregates in the channel centre away from the chamber walls. The structure, very simply consists of a transducer which couples acoustic energy into the coupling layer also known as the carrier layer. The role of the coupling layer is to improve acoustic transmission and to couple the acoustic energy more efficiently through the other layers while maintaining separation between the transducer and the fluid. Next is the fluid layer, the region where the particle manipulation is to occur. And finally the reflector layer which functions to reflect the energy back into the device. Figure 1-19 demonstrates the acoustic trapping device used throughout this project designed and made by Peter Glynne-Jones (School of Engineering, University of Southampton). It is a multi-layered half wavelength device.

Similar devices have been used in other collaborative studies at the University of Southampton ((Li et al., 2014) and Angela Tait, (PhD Thesis)). Li et al., demonstrated the

first successful application of acoustic fluidic perfusion bioreactors to bioengineer scaffold-free neocartilage grafts of human articular chondrocytes that have the potential for subsequent use in second generation autologous chondrocyte implantation for the repair of partial thickness cartilage defects. The same devices as described above, and subsequently used in this project have been used to model the airway mucosa. Levitation of single epithelial cells resulted in the formation of a cell sheet within 2 hours, which gradually contracted becoming three-dimensional by 24 hours. Contraction could be inhibited by removal of Ca^{2+} to prevent adherens junction formation or by adding cytochalasin D to prevent actin filaments or an E-cadherin neutralising antibody to prevent adherens junction formation (Angela Tait, PhD thesis).

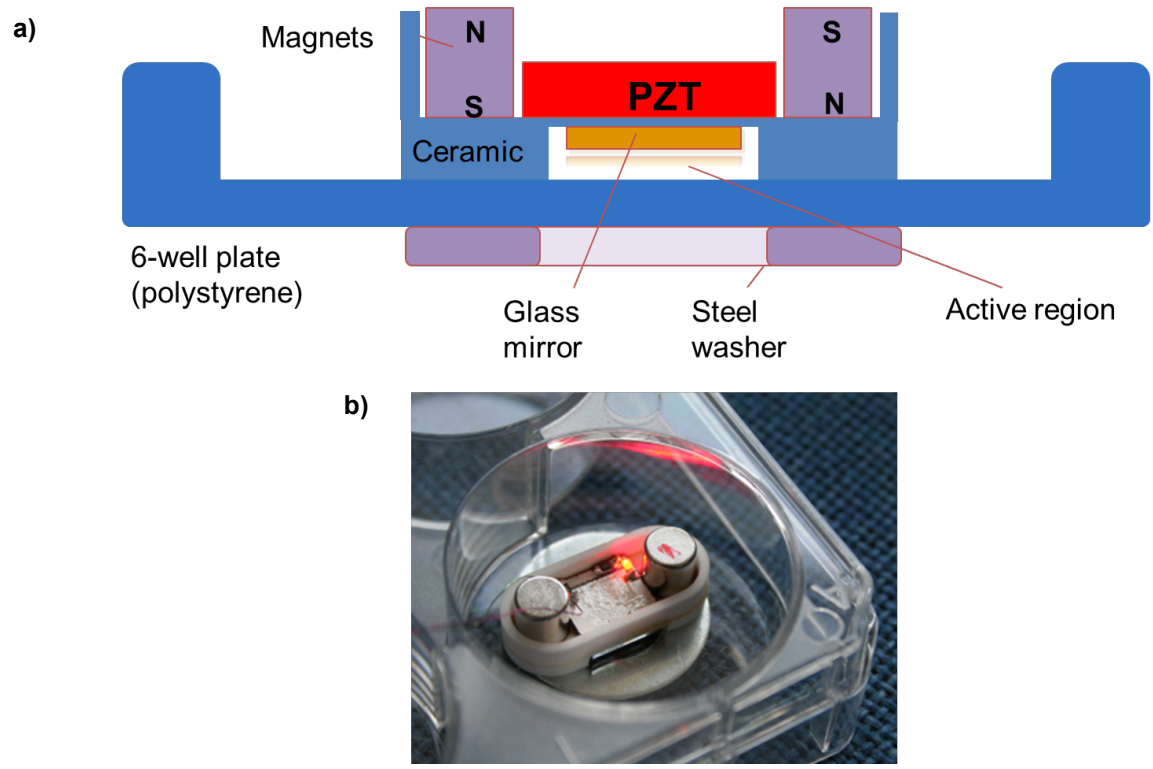

FIGURE 1-19: ACOUSTIC TRAPPING DEVICE

Figures (a) and (b) display the acoustic trapping device used throughout this project. The ultrasonic microfluidic device used in this study was designed and made by Dr Glynne-Jones, Faculty of Engineering, University of Southampton. The device is a half wavelength in size meaning that cells are levitated in the centre of the cavity. The devices very simply consists of a transducer, a coupling layer and a reflective layer. The active region of the piezoelectric PZT (lead ziconate titanate) transducer is 10 x 10 x 0.5 mm in size. The coupling layer of the device incorporates a silvered mirror (glass face towards the chamber) in order to create a dark-field background during fluorescent imaging.The device is fitted with a LED (as demonstrated in (b)) which has a current limiting resistor to indicate that power reaches the transducer. The assembled device was mounted in 6 well plate with a sheet of 1.2mm thick glass placed under it to act as an acoustic reflector. A steel washer was places the plate to attract the magnets epoxied into the devices to hold devices in position.

1.6.4 The use of acoustic trapping devices to model the CLL microenvironment

As outlined in this chapter, interactions in the tumour microenvironment promote survival and disease progression in CLL and therefore the need to mimic these interactions *in vitro* is becoming increasing apparent. A number of studies have tried using different co-culture systems (Hamilton et al., 2012, Asslaber et al., 2013) however a physically relevant model is still needed. Especially as the importance of using 3D cell culture models in becoming clear. Cells grown in 3D models have been shown to have improved biological mechanisms such as viability, morphology, proliferation and differentiation. However, 3D culture does not come without its disadvantages, the use of artificial components can lead to problems such as reproducibility and uniformity. Interference from or interactions with artificial components can also cause complications. Acoustic trapping provides a method that can 'trap' cell in 3D structures away artificial substrata thereby offering a novel, improved 3D culture method. The use of acoustic trapping therefore provides a method in which to investigate CLL/microenvironment interactions in a more physiologically, three dimensional manner. The use to acoustic forces to levitate cells, allows for the potential to truly understand molecular interactions which occur between the different cellular components.

1.7 Hypothesis and Aims

1.7.1 Hypothesis

The main hypothesis is that acoustic trapping devices can be used as a novel method to model CLL cell/microenvironmental interactions in 3D. The secondary hypothesis is that the HFFF2 cell line is a suitable model for investigating CLL/fibroblast interactions in acoustic trapping devices.

1.7.2 Aims

To investigate this hypothesis the central focus of initial experiments was the optimisation of acoustic trapping devices to levitate both CLL and fibroblasts at the same time to generate a 3D CLL microenvironment. In parallel, interactions between CLL cells and a fibroblast cell line, HFFF2, will be characterised using traditional 2D co-culture systems. This will provide a set of molecular markers of CLL/fibroblast interactions that can be assessed and compared in subsequent experiments using 3D co-cultures.

The main aims were to:

- Investigate the HFFF2 cell line as a model system for studying CLL microenvironment interactions
- Optimise acoustic trapping devices for use in modelling of CLL/stromal cell interactions in three dimensions
- Investigate the role of the chemokine receptor CXCR4 and its ligand CXCL12 in protection provided by HFFF2 cell line to CLL cells
- Analyse candidate molecules involved in HFFF2-mediated cytoprotection of CLL cells

Chapter Two

Materials and Methods

Chapter 2: Materials and Methods

2.1 Cell culture techniques

2.1.1 Materials

Material	Components
Complete RPMI-1640	RPMI 1640 (Sigma Aldrich, Missouri, United States) supplemented with 10% Foetal calf serum (FCS), 1% glutamine and 1% Penicillin/Streptomycin
Complete DMEM	Dulbecco's Modified Eagle Medium (DMEM) (Sigma Aldrich) supplemented with 10% FCS, 1% glutamine
Phosphate buffered saline (PBS)	137mM NaCl, 2.7mM KCl, 10mM Na_2HPO_4, 2mM KH_2PO_4 in 1 litre of deionised water.
MACS buffer	PBS at pH 7.2, 0.5% bovine serum albumin (BSA) (Sigma Aldrich), and 2 mM Ethylenediaminetetraacetic acid (EDTA)

2.1.2 Primary CLL samples

All CLL samples used throughout this project were taken at diagnosis or prior to treatment from patients recruited to the Lymphoproliferative disorder (LPD) study at the Department of Haematology of the Southampton University Hospital Trust. The LPD study was approved by the Institutional Review Boards of the University of Southampton (Ethics number 228/02/t) and informed consent and ethics approval was in place before the use of primary cells. Diagnosis of CLL was made according to the 2008 International Workshop on CLL/National Cancer Institute (NCI) criteria and confirmed by flow cytometery (Hallek et al., 2008). Characterisation of CLL samples including mutational status of *IGHV* gene; tumour cell population percentage ($CD19^+CD5^+$); percentage of CD38 and ZAP70 expression; calcium flux response as a percentage following stimulation was carried out by research technicians. Interphase fluorescence-in-situ-hybridisation (FISH) was performed at the Wessex Regional Genetics Laboratory in Salisbury.

CLL samples were collected by isolating peripheral blood mononuclear cells (PBMCs) by gradient density centrifugation. After PBMC isolation, samples were resuspended in FCS plus 10% (v/v) Dimethyl sulfoxide (DMSO) and frozen at a rate of 1°C per minute in a cryo freezing container before transfer to liquid nitrogen (LN_2).

Prior to use, CLL samples were removed from LN_2, quickly thawed in a 37°C water bath, added to complete RPMI-1640 (C.RPMI) and centrifuged at 350g for 5 minutes. The pellet

was re-suspended in 4mls of complete RPMI-1640 and “rested” by incubating at 37°C for 1 hour. A table of CLL patients used during this project along with their basic phenotypic characteristics are listed in Appendix A.

2.1.3 CLL cell purification

CLL cells were purified using the B-CLL cell isolation kit (MACS, Miltenyi Biotec, Germany). The B-CLL cell isolation kit is an indirect magnetic labelling system for the isolation of untouched B-CLL cells using negative selection. CLL PBMC samples were thawed and allowed to recover as described in Section 2.1.2. During B-CLL cell isolation cells were kept cold throughout the duration of the isolation and all solutions were pre-cooled. This was to prevent capping of antibodies on the cell surface and non-specific cell labelling.

2.1.3.1 Magnetic labelling

Cells were centrifuged at 350g for 5 minutes and supernatent was removed completely by aspiration. The cell pellet was resuspended in 40µl of MACS buffer per 10^7 total cells and 10µl of B-CLL cell biotin-antibody cocktail per 10^7 total cells was added. The cells were mixed thoroughly and incubated in the refrigerator (2-8°C) for 5 minutes. A further 30µl of MACS buffer was added per 10^7 total cells and 20µl of anti-biotin microbeads were added per 10^7 total cells. Cells were mixed thoroughly and incubated for a further 10 minutes in the refrigerator (2-8°C). Following incubation cells were washed in MACS buffer to remove any unbound antibody cocktail and microbeads. Cells were centrifuged at 350g for 5 minutes and resuspended in 500µl MACS buffer.

2.1.3.2 Magnetic separation with LS columns

LS columns and MidiMAC separator (both MACS, Miltenyi Biotec) were chosen for the magnetic separation for B-CLL cells as these were deemed appropriate for both the number of total and labelled cells. The LS columns were placed in the magnetic field of the MACS separator and columns were prepared by rinsing with 3mls of MACS buffer. Cell suspension was applied to the column avoiding the formation of air bubbles. Flow-through was collected containing the unlabelled cells, representing the enriched B-CLL cells. The column was washed with 3ml MACS buffer and unlabelled cells that passed through were collected and combined with the flow-through from previous step. Unlabelled cells were centrifuged at 350g for 5 minutes and cell pellet was resuspended in pre-warmed C.RPMI. Purification was confirmed for each sample via FACS using CD5/CD19 staining (detailed in Section2.3.3) (Appendix C).

2.1.4 Cell lines

The human foetal foreskin fibroblast (HFFF2) cell line (Health Protection Agency, United Kingdom) was chosen as a suitable model for the assays carried out during the course of this project, so far. The HFFF2 cell line was grown in complete DMEM (C.DMEM) unless stated otherwise. HFFF2 cells were kept at approximately 60-80% confluency to avoid spontaneous transdifferentiation from fibroblasts to myofibroblasts. HFFF2 cells were incubated at 37°C /10% CO_2.

2.1.4.1 HFFF2 transdifferentiation studies

For transdifferentiation studies, HFFF2 cells were plated at $2x10^5$cells/well into a 6-well plate and left overnight at 37°C/10% CO_2.. Cells were treated with 2ng/ml TGF-β1 (Sigma-Aldrich) in complete C.DMEM and returned to the incubator for 72 hours.

2.1.4.2 Generation of HFFF2-derived CM

To generate HFFF2-derived conditioned media (CM), HFFF2 cells were plated at $2x10^5$cells/well in complete RPMI-1640 in a 6-well plate and left for 72 hours at 37°C/10% CO_2. After 72 hours the supernatant was collected from each well, centrifuged at 350g for 5 minutes in to eliminate any detached cells or cell debris and stored at -20°C.

CM separation was carried out according to molecular weight (MW) using Amicon Ultra-15 Centrifugal Filter Units (Merck Millipore, Germany) (Figure 2-1) with a 3kDa cut off. CM (15ml) was placed in the Amicon Ultra filter device and centrifuged at 4,000g for 30minutes. Following centrifugation, the concentrated solute in the filter device was collected by inserting a gel loading pipette into the bottom of the filter device and withdrawing the sample using a side-to-side sweeping motion carefully avoiding contact with the filter membrane. The concentrated solute was resuspended in 15ml (or original volume) of complete RPMI. This formed the high molecular weight (HMW) fraction of CM. The filter device was removed leaving the ultrafiltrate. This formed the low molecular weight (LMW) fraction of the CM.

2.1.5 CLL and HFFF2 co-culture experiments

For all CLL-HFFF2 co-culture experiments cells were always cultured at a 5:1 ratio (CLL:HFFF2). HFFF2 cells were plated out in pre-warmed C.DMEM 24 hours prior to commencement of experiment to allow the cells to adhere and spread. After 24 hours, media was removed and wells gentled washed with pre-warmed PBS. CLL cells were then plated onto HFFF2 cells in pre-warmed C.RPMI.

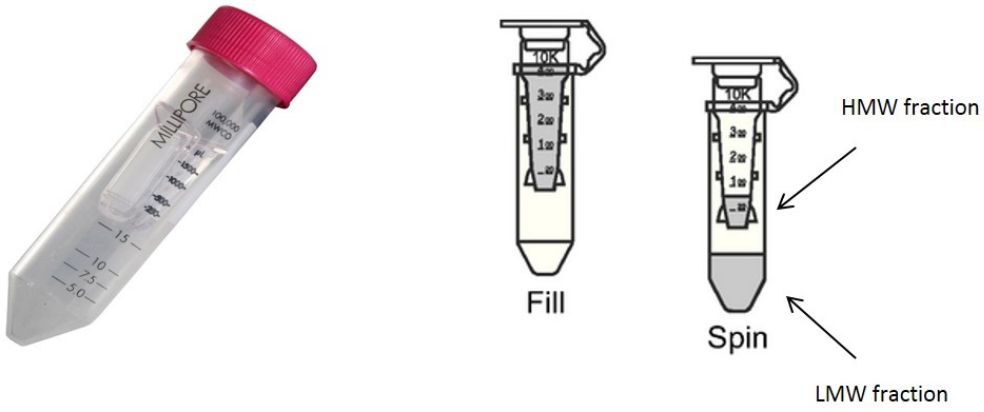

FIGURE 2-1: AMICON ULTRA-15 CENTRIFUGAL FILTER UNITS (MERCK MILLIPORE)

The Amicon Ultra-15 centrifugal filter units contain an Ultracel regenerated cellulose membrane which has a molecular weight cut off of 3kDa. The membrane chamber fits in a 15ml falcon. The CM is pipetted gently onto the membrane without touching or disturbing the membrane. Following centrifugation, the membrane unit can be removed to collect the flow through which forms the LMW fraction. Any CM left in the filter chamber forms the HMW fraction.

2.2 Protein techniques

2.2.1 Materials

Material	Components
20% Tx100	4ml PBS and 1ml Tx100
0.05% PBS-tween	PBS as detailed above (Section2.1.1) supplemented with 0.05% Tween-20
Bovine serum albumin (BSA)-PBS	PBS as detailed above (Section2.1.1) supplemented with 1% BSA
5X RIPA Buffer	0.75M NaCl, 5% NP40, 2.5% Deoxycholate, 0.5% sodium dodecyl sulfate and 0.25M Tris pH8.0
10% Acrylamide gel (separating gel)	5ml H_2O, 3.3ml 30% Acrylamide (Sigma Aldrich), 2.5ml 1.5M Tris (pH8.8), 100µl 10% SDS, 100µl 10% Ammonium Persulfate, 4µl TEMED
Stacking gel	2.7ml H_2O, 670µl 30% Acrylamide, 500µl 1.0M Tris (pH6.8), 40µl 10% SDS, 40µl 10% APS, 3µl TEMED
10x Running Buffer	250mM Tris base, 1.9M glycine, 35mM SDS
Transfer Buffer	500ml absolute ethanol, 200ml 10x running buffer, topped up 2 litres with deionised water
1% TBS-tween	10mM Tris pH8.0, 150mM NaCl diluted in 1 litre deionised water with 1ml Tween-20
5% Milk-TBS tween	1% TBS-tween as detailed above supplemented with 5% milk powder

2.2.2 α-SMA immunofluorescence

α-SMA immunofluorescence was used to determine the presence of stress fibres in the transdifferentiation assays. HFFF2 cells were plated in 6 well culture plates and treated with or without 2ng/ml TGF-β as described in Section2.1.4.1. Following 72 hours culture, media was removed and the wells were washed gently twice with PBS. Cells were then fixed with 4%(w/v) paraformaldehyde (PFA) and left at 4°C for a minimum of 1 hour. Fixative was then removed and the wells were washed twice with PBS. Cells were then permeabilised for 5 minutes at RT on an orbital shaker with 0.5% (w/v) Tx100. Cells were then washed three times for 5 minutes each in 0.5% PBS-Tween and then blocked in 1% (w/v) bovine serum albumin (BSA)-PBS for 5mins at RT. Cells were washed again three times for 5 minutes each. The α-SMA primary antibody (Sigma Aldrich) was diluted (1:1000) in 1% BSA-PBS and added to each well (100µl per well) and the plate was incubated for 1 hour at RT or overnight at 4°C. Following incubation with the primary antibody cells were washed three times for 5 minutes each. The secondary antibody (goat anti-mouse Alexa-488, In house) was diluted (1:50) in 1% BSA-PBS and incubated in the dark at RT on the shaker for 1 hour. Following incubation cells were again washed before

being counterstained with 1µg/ml 4',6-diamidino-2-phenylindole (DAPI) (Sigma Aldrich) (1:2000 diluted in 1% BSA-PBS) for 15 minutes in the dark at RT. Finally cells were washed three times for 5 minutes each before imaging on a fluorescent microscope.

2.2.3 CXCL12 enzyme-linked immunosorbent assay (ELISA)

CXCL12 ELISA's were performed on supernatants collected from HFFF2 cells that had been cultured with or without 2ng/ml TGF-β. A Human CXCL12/SDF-1 alpha Quantikine ELISA Kit was carried out as per manufacturer protocol (R&D systems, Oxford, UK). Supernatants were diluted 1:10 in calibrator diluent and all reagents and standards prepared as recommended and outlined in the protocol. 100µl assay diluent was added to each well and then 100µl of standard, sample, or control was added. The plate was then incubated for 2 hours at RT on a horizontal orbital microplate shaker set at 500rpm. Plates were washed three times in wash buffer by aspirating each well. After each wash complete removal of liquid was ensured. 200µl of CXCL12 conjugate was added to each well and the plate was incubated again at RT for 2 hours. The wash step was repeated. 200µl of substrate solution was added to each well and the plate was incubated for 30 minutes at RT protected from light. Following incubation 50µl of stop solution was added to each well. The addition of the stop solution causes a colour change from blue to yellow. To ensure thorough mixing and uniform colour the plate was tapped gently. Optical density was determined using a microplate reader set to 450nm with wavelength correction set to 570nm. CXCL12 concentrations in the supernatants were calculated using the standard curve. Background levels were 50pg/ml.

2.2.4 Western blotting

2.2.4.1 Cell harvest

CLL cells were collected from culture plates and centrifuged at 350g for 10 minutes at 4°C. Cells were transferred into eppendorfs and centrifuged at 1,520g for 5 minutes at 4°C using a bench top centrifuge. HFFF2 cells were collected in a different manner. Media was aspirated and cells were washed twice with ice cold PBS. Cells were scraped in 1ml ice cold PBS and cell pellets were collected by centrifugation at 1,520g for 5 minutes.

Supernatent was removed and cell pellets were then resuspended in 1xRIPA buffer supplemented with protease and phosphatase inhibitors (Sigma-Aldrich, 1:100) to ensure that protein integrity and phosphorylation was maintained. Cells were lysed on ice for 30

minutes. After incubation lysate were centrifuged at 16,100g at 4°C for 30 minutes. The supernatent was collected and stored at -20°C until required.

2.2.4.2 Determining protein concentration

Protein concentration was determined using the Pierce BCA protein assay kit (ThermoFisher Scientific, Massachusett, USA). The Pierce BCA protein assay uses bicinchoninic acid (BCA) for the colourmetric detection of proteins. The method uses the biuret reaction which is based on the reduction of Cu^{2+} to Cu^{1+} by a protein in an alkaline medium. The reagent buffer in the kits detects the cuprous cations resulting in a purple colour caused by the chelation of the BCA reagent molecules and cuprous ions. This colour change is proportional to the concentration of protein present and can be measured using a plate reader, set to light absorbance at 562nm. A standard curve using BSA was used to carry out protein concentration quantification (0, 15, 31, 62, 125, 250, 500 and 1000 µg/ml). BSA standards were made using RIPA diluted in water.

Lysates were diluted in Millipore ultraclean water (4µl lysate in 46µl water). 23µl BSA, or lysate was added to 200µl Pierce protein assay reagent (9.8ml BCA reagent A and 200µl BCA reagent B) in a clear 96 well plate. Final dilution of lysates was 12.5x. Absorbance was detected on the Varioskan Flash plate reader (ThermoFisher Scientific) at 562nm. Protein concentration for each sample was then determined using the standard curve.

2.2.4.3 SDS-PAGE gel electrophoresis

An equal concentration of protein sample was transferred into eppendorfs along with 0.5 volume of loading dye (Cell Signalling Technology, Massachusett, USA) containing 30x Dithiothreitol (DTT). Protein samples plus loading dye were heated to 95°C for five minutes to denature proteins, reduce protein-protein interactions (S-S bonds) and to allow the binding of SDS. During SDS-PAGE gel electrophoresis proteins migrate through a polyacrylamide gel and separate according to their stokes radius by electrophoresis due to the presence of the SDS. Smaller proteins move more easily through the gel compared to larger proteins, resulting in a resolution of larger proteins at the top of the gel and smaller proteins at the bottom of the gel.

Polyacrylamide SDS gels were made as described in Molecular Cloning: a Laboratory Manual (Sambrook 1989). Gels consisted of a separating gel with a stacking gel on top and contained either a 10 or 15 well comb. Protein was loaded onto the polyacrylamide gel and electrophoresis was carried out in running buffer at 120V for approximately 1 hour. Approximation of protein size was determined by running a PAGEruler plus protein ladder (ThermoFisher Scientific) alongside the samples.

Separated proteins were then transferred onto nitrocellulose membrane (Whatman Protran, GE Healthcare, United Kingdom) in transfer buffer at 100V for 1 hour. Protein transfer required the gel to be sandwiched between nitrocellulose membrane, filter paper and sponges. This was placed in transfer buffer which enables an electrical current to be generated resulting in the protein moving from the gel towards the nitrocellulose membrane which was closer to the positive electrode.

2.2.4.4 Antibody incubation and visualisation

The membrane was then blocked using 5% (w/v) milk powder-TBS-Tween and incubated at RT for 1 hour. Primary antibodies were added to the nitrocellulose blot diluted in 5% (w/v) milk powder-TBS-Tween. Blots were incubated with the primary antibody for 16 hours at 4°C. After incubation, blots were washed three times for 5minutes with TBS-Tween before the secondary antibodies were added and diluted as described in Table 2.1 and incubated for 1 hour RT. After washing three times with TBS-Tween, Supersignal West Pico Chemiluminescent (ThermoFisher Scientific) was added and the blot was imaged using the UVP ChemiDoc-It Imaging System with the BioChemi HR camera P/N 97-0155-02, (UVP, Cambridge, UK).

TABLE 2.1: DILUTIONS AND SUPPLIERS OF THE PRIMARY AND SECONDARY ANTIBODIES UTILISED FOR WESTERN BLOTTING

Antibody	Species	Final concentration	Company
α-SMA (clone 1A4)	Mouse	1:5000	Sigma Aldrich
HSC-70 (B-6)	Mouse	1:1000	Santa Cruz Biotechnology (Dallas, USA)
Secondary antibody	Goat anti- mouse conjugated to horse radish peroxidase	1:2000	Dako (Agilent Technologies, Denmark)

2.3 Flow cytometry techniques

2.3.1 Materials

Material	Components
Annexin-V buffer (10x)	0.1 M HEPES, pH 7.4, 1.4M NaCl, 25mM calcium chloride in deionised water
FACS buffer	1% BSA, 4mM EDTA, 0.15mM sodium azide in 1xPBS
Low-serum RMPI-1640	RPMI-1640 supplemented with 1% glutamine, 1% Penicillin Streptomycin and 0.01% FCS

2.3.2 Annexin-V/propidium iodide staining for the analysis of CLL cell viability

Annexin-V/Propidium Iodide (PI) staining via FACS was used to determine CLL cell viability. Annexin-V binds with high affinity to phosphatidylserine (PS). In normal viable cells, PS is located on the cytoplasmic surface of the plasma membrane. In apoptotic cells, however, PS is translocated from the inner to the outer leaflet of the plasma membrane, exposing PS to the external cellular environment where it can be detected by Annexin-V. PI is an intercalating agent that can be used as a DNA stain to assess cell viability. PI is impermeable to viable cells meaning it is generally excluded.

HFFF2 cells were plated at a density of $5x10^4$cells/well in a 48-well plate and left overnight at 37°C/10% CO_2 to allow cells to adhere and spread. After overnight incubation media was removed from wells containing HFFF2 cells and wells were washed gently with pre-warmed PBS to remove any detached cells. CLL cells were plated at $2x10^5$cells/well in C.RPMI alone or in wells containing HFFF2 cells and were left at 37°C/10% CO_2 for 24 or 48 hour. A portion of CLL cells were harvested and analysed via FACS immediately (0 hour timepoint).

Prior to FACS analysis, CLL cells were collected into FACS tubes and the plates washed gently with PBS to remove any CLL cells attached to either the HFFF2 cells or tissue culture plastic. FACS tubes were then centrifuged at 350g for 5 minutes. Cells were re-suspended in 300µl of 1x Annexin-V buffer containing 2.5µg/ml of Annexin-V-FITC (Protein Core Facility, University of Southampton) and 12.5µM of PI (Invitrogen, Molecular Probes, California, USA) per FACS tube. Cells were vortexed gently and left for 15 minutes in the dark prior to FACS analysis via FACSCanto I flow cytometer (BD Biosciences, New Jersey, USA). 10,000 events were recorded per tube. Results were analysed using FlowJo version 7.6.5.

2.3.2.1 CLL cell viability following culture in HFFF2-derived CM

HFFF2 cells were plated at $2x10^5$ cells/well in complete RPMI-1640 in a 6-well plate and left for 72hrs at 37°C/10% CO_2. After 72hrs the supernatant was collected from each well, centrifuged at 350g for 5 minutes to eliminate any detached cells or cell debris and stored at -20°C. The ability of CM to protect CLL cells from spontaneous apoptosis was analysed via Annexin-V/PI staining as described above. FACS tubes were prepared as detailed above and FACS analysis was carried out via FACSCanto I flow cytometer (BD Biosciences). 10,000 events were recorded per tube and results were analysed using FlowJo version 7.6.5.

2.3.2.2 CLL cell viability following culture in transwell plates

HFFF2 cells were plated $1x10^5$ cells/well in a 24 well plate and left overnight at 37°C/10% CO_2 to allow cells to adhere and spread. After overnight incubation media was removed and HFFF2 cells were gently washed with pre-warmed PBS. CLL cells were plated alone or either directly onto the HFFF2 cells at $5x10^5$ cells in 1000ul/well or plated into a transwell chamber (Corning, USA) (Figure 2-2) with a 5μm pore size at $5x10^5$ cells in 100ul/well. Cells were left for 24 or 48 hours prior to FACS analysis via Annexin-V/PI staining as described above. A portion of CLL cells were isolated and analysed immediately (0hr timepoint). At each timepoint the membrane was washed gently with PBS, to ensure all CLL cells were collected from the chamber, and no cells remained attached. FACS tubes were prepared as detailed above and FACS analysis was carried out via FACSCanto I flow cytometer (BD Biosciences). 10,000 events were recorded per tube and results were analysed using FlowJo version 7.6.5.

2.3.2.3 CXCR4/CXCL12 neutralising antibodies

Annexin-V/PI and CLL cell migration assays were carried out in the presence of neutralising antibodies to CXCL12 and CXCR4. The concentrations used for each antibody/inhibitor are described in Table 2.2. Prior to experiments CLL cells were pre-treated with the CXCR4 neutralising antibody and plerixafor for 1hr before being added to the co-culture (Annexin-V/PI) or transwell chamber (Migration). The CXCL12 neutralising antibody was added directly to the co-culture (Annexin-V/PI) and was added into the migration media in the bottom of the migration plate.

TABLE 2.2: CONCENTRATIONS AND SUPPLIERS OF THE NEUTRALISING ANTIBODIES UTILISED IN VIABILITY EXPERIMENTS

Antibody/Inhibitor	Concentrations used for migration assay	Concentraion used for viability assays	Supplier
CXCL12 neutralising antibody	40, 8, 1.6µg/ml	40, 8µg/ml	R&D systems
CXCR4 neutralising antibody	20µg/ml	10µg/ml	Biolegend

a)

b)

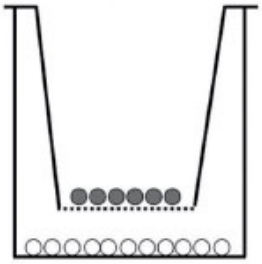

FIGURE 2-2: TRANSWELL CHAMBER PLATES

(a) Commercially available 12 well transwell plates used for migration and separation experiments as outlined in this thesis. (b) Schematic diagram of the culture of two different cell types (dark circles and white circles) for separation experiments in tranwells plates. In migration assays white circles to represent chemokine, dark circles to represent cells.

2.3.3 CXCR4 expression on CLL cells

HFFF2 cells were plated 2.5x10^5cells/well in a 6 well plate and left overnight at 37°C/10% CO_2 to allow cells to adhere and spread. After overnight incubation media was removed and HFFF2 cells were gently washed with pre-warmed PBS. CLL cells were plated either alone or onto the HFFF2 cells at 1x10^6cells/well. A portion of CLL cells were isolated and analysed immediately (0 hour timepoint), while the remainder were left at 37°C for 24 or 48 hours. For each time point CLL cells were transferred from the culture plate into FACS tubes. FACS tubes were centrifuged at 350g for 5 minutes. Cells were washed in FACS buffer and centrifuged at 350g for 5 minutes. Cells were then resuspended in 100µl of ice cold FACS buffer containing 5µl of CXCR4-APC, 1µl of CD19-Pacific blue and 2µl of CD5-PerCP (All Biolegend, San Diego, California). Two extra tubes were prepared, one containing unstained cells and one containing CD5-PerCP Cy5.5, CD19-Pacific blue and the APC isotype control antibody (Biolegend).Tubes were incubated on ice in the dark for 15 minutes. Cells were washed twice in FACS buffer at 350g for 5 minutes and finally resuspended in 200µl FACS buffer before acquisition on the FACSCanto II flow cytometer (BD Biosciences). 50,000 events were recorded per tube and results were analysed using FlowJo version 7.6.5. CXCR4 mean fluorescent intensity (MFI) was recorded on the CD5/CD19 CLL population.

2.3.4 IgM and CXCR4 phenotype and signalling experiments

To determine the effect of HFFF2 co-culture on CLL cell signalling capacity and phenotype, CLL cells were plated alone or in the presence of HFFF2 cell and expression of CXCR4 and IgM was measured at 8, 24, 48 and 72 hours and signalling capacity was determined via Calcium flux analysis at the same time points. HFFF2 cells were plated 2.5x10^5cells/well in a 6 well plate and left overnight at 37°C/10% CO_2 to allow cells to adhere and spread. CLL cells were plated either alone or onto the HFFF2 cells at 1x10^6cells/well. A portion of CLL cells were isolated and analysed immediately (0 hour timepoint), while the remainder were left at 37°C for 8, 24, 48 or 72 hours.

2.3.4.1 CXCR4 and surface IgM expression

For each time point CLL cells were transferred from the culture plate into FACS tubes. FACS tubes were centrifuged at 350g for 5 minutes. Cells were washed in FACS buffer at 350g for 5 minutes. Cells were then resuspended in 100µl of ice cold FACS buffer containing 5µl of CXCR4-APC, 5µl IgM-PE, 1µl of CD19-Pacific blue and 2µl of CD5-PerCP (All Biolegend). Again two extra tubes were prepared, one containing unstained cells and one containing CD5-PerCP Cy5.5, CD19-Pacific blue and the APC and PE isotype control antibodies (Biolegend). Tubes were incubated on ice in the dark for 15

minutes. Cells were washed twice in FACS buffer at 350g for 5 minutes and finally resuspended in 200µl FACS buffer before acquisition on the FACSCanto II flow cytometer (BD Biosciences). 50,000 events were recorded per tube and results were analysed using FlowJo version 7.6.5. CXCR4 and IgM mean fluorescent intensity (MFI) was recorded on the CD5/CD19 CLL population.

2.3.4.2 Calcium flux analysis

Experiments for calcium flux analysis were carried out in parallel with experiments outlined in Section2.3.4.1. IgM signalling capacity was determined by measuring the percentage of cells with increased intracellular calcium following stimulation with soluble goat $F(ab')_2$ anti-IgM and using a cut-off value of ≥5% responding cells to define samples as sIgM responsive (Mockridge et al., 2007).

For calcium flux analysis each tube requires $2.5x10^6$ CLL cells. Cells were plated out as outlined above ($1x10^6$ cells/well) therefore 2.5 wells were combined into one FACS tube. Cells were collected and 2µl 10% pluronic F-127 (Sigma Aldrich) and 0.8µl of Fluro3-AM (stock concentration 50µg/ml) (Life Technologies, California, USA) were added to each tube. Cells were incubated at 37°C for 30 minutes. Cells were washed once in 2ml of RT C.RPMI and centrifuged at 350g for 5 minutes. The supernatant was removed and cell pellet resuspended in 500µl C.RPMI and kept at RT in the dark.

Prior to acquisition each tube was pre-warmed for approximately 5 minutes in a 37°C water bath. Acquisition settings were as follows; all tubes were acquired on low flow rate; for IgM stimulated tubes the stopping time was set for 900 seconds, for the isotype control stimulated tubes the stopping time was set to 600 seconds. Following pre-warming, the FACS tubes were vortexed and placed on the cytometer for acquisition. Unstimulated cells were acquired and recorded for 30 seconds; after 30 seconds, the tube was carefully removed while still recording and tube was stimulated with 10µg/ml of anti-IgM or IC (both Southern Biotech, USA). The tube was vortexed and placed back on the cytometer. This process was done as quickly as possible to prevent gaps in the recording. Recording of events continued for a further 10 minutes for anti-IgM stimulated tubes or 5 minutes for IC tubes. After this period, tubes were again carefully removed while still recording and 20ng/ml of ionomycin (Sigma Aldrich) was added. The tube was vortexed and placed back on the cytometer for a further 5 minutes.

Results were analysed using FlowJo version 7.6.5 using the kinetics function. Results were corrected for the presence of Tcells/NK cells (which do not respond to anti-Ig stimulation) using the percentage of CD19+ B cells determined by the phenotyping

analysis carried out routinely before CLL samples are available for research. The following formula was used to determine the percentage of responding B cells:

$$\%\, responding\ cells = \left[\frac{Peak(All\ events)\ -\ MeanY(unstimulated)}{\%\ CD19+cells}\right] x100$$

2.3.5 CLL cell migration assay

CLL cells were thawed as detailed previously and plated 200µl/well into a 48well plate at a cell density of $1x10^7$ cells/ml and placed at 37°C. Cells were rested for 16 hours prior to migration experiments in order to allow the cells to recover their CXCR4 surface expression to enable them to migrate. After 16 hours incubation cells were removed from the plates and placed in eppendorfs and washed twice in empty media (RPMI-1640 supplemented with 0.1% FCS) by centrifugation at 350g at RT for 5 minutes. Either 200µl empty media or empty media supplemented with 400ng/ml of recombinant human CXCL12 (R&D Systems) was placed into the lower chamber of the transwell plates. Cells were then re-counted to allow for cells having been lost during wash steps. Cells were plated into the upper chamber of the transwell plate (Figure 2-2) at $5x10^5$ cells/well in 80µl/well. Cells were then placed in the incubator at 37°C for 2 hours to allow the cells to migrate.

After 2 hours, the media was removed from the lower chamber of the plate and placed into FACS tubes. The wells were then vigorously washed to remove any cells attached to the tissue culture plastic. FACS tubes were centrifuged at 350g for 5 minutes. Cells were then resuspended in 100µl of ice cold FACS buffer containing 3µl of CD19-APC and 2µl of CD5-PerCP (Biolegend). Tubes were incubated on ice in the dark for 30 minutes. Cells were washed twice in FACS buffer at 350g for 5 minutes and finally resuspended in 150µl FACS buffer before acquisition on the FACSCanto I flow cytometer (BD Biosciences). Cell samples were acquired on a high flow rate for 1minute and the number of CD5/CD19 positive cells was recorded.

2.3.6 CCL2 intracellular expression

CCL2 intracellular expression in CLL cells following co-culture with HFFF2-derived CM was determined using intracellular staining via flow cytometry. CLL PBMCs or purified

CLL cells were plated at $1x10^7$/ml in either RPMI or HFFF2-derived CM. A proportion of CLL cells in RPMI were stimulated with 7.5µg/ml CpG-ODN (Source Bioscience, Nottingham, UK) to be used as a positive control for cytokine detection. CpG-ODN binds to toll-like receptor 9 (TLR9) and is a strong stimuli to cells resulting in the production of a number of different cytokines and chemokines. Cells were then incubated for 24 hours at 37°C/10% CO_2. After 24 hours culture, all wells were stimulated with Brefeldin A (BD bioscience, 1 in 1000 dilution). Cells were incubated for a further 5 hours. Brefeldin A is a protein transport inhibitor and is commonly used as part of intracellular cytokine staining protocol to enhance signals by blocking transport processes during cell activation. BrefeldinA leads to the accumulation of most cytokines at the Golgi Complex/Endoplasmic Reticulum (Jung, et al., 1993) to enhance detection via intracellular staining.

2.3.6.1 Intracellular staining

After 5 hours, cells were transferred into a FACS tube containing 1ml FACS buffer and Brefeldin A (1 in 1000 dilution). Tubes were centrifuged at 350g for 5 minutes and supernatant removed. Cell pellets were resuspended in 100µl FACS buffer containing Brefeldin A (1:1000). 50 µl of cell suspension was transferred into a new FACS tube and 50µl of antibody mastermix containing CD5-PerCP Cy5.5 and CD19-Pacific blue was added to each tube. Tubes were incubated on ice and in the dark for 30 minutes. Cells were then washed once in FACS buffer containing Brefeldin A and tubes were centrifuged at 350g for 5 minutes. 250µl of the cytofix/cytoperm solution (Provided by the kit, BD Fix/Perm kit) was added to each tube and mixed well. Tubes were incubated on ice and in the dark for 20 minutes. Cells were washed twice in perm wash (Provided by the kit) and tubes were centrifuged at 350g for 5 minutes. 20µl of CCL2-PE antibody or PE isotype control (BD Biosciences) were added and tubes were incubated on ice, in the dark for 30 minutes. Cells were washed once in perm wash (Provided by the kit) and tubes were centrifuged at 350g for 5 minutes. Cells were resuspended in 200µl FACS buffer before acquisition on the FACSCanto II flow cytometer (BD Biosciences). 30,000 events were recorded per tube and results were analysed using FlowJo version 7.6.5. Percentage cells positive for PE were recorded on the CD5/CD19 CLL population based on the relevant isotype control tube for each sample.

2.4 Molecular biology techniques

2.4.1 CLL cell RNA extraction

RNA was extracted from CLL cell pellets using Trizol/chloroform method. 750µl Trizol (Ambion, Life Technologies) was added to cell pellets and cells were gently pipetted up and down to lyse cells and incubated at RT for 5 minutes. 200µl chloroform (Sigma Aldrich) was added to the samples and mixed thoroughly to create an emulsion. Samples were incubated at RT for 3 minutes. The RNA was separated from any proteins and DNA by centrifugation at 11,200rpm (12000g) for 15 minutes at 4°C in a bench top centrifuge. Centrifugation separated proteins into the organic phase, while RNA was collected into the aqueous phase. RNA is present in the aqueous phase due to the fact that negatively charged RNA interacts with the polar water in the aqueous phase, but does not interact with non-polar trizol in the organic phase.

The aqueous phase was carefully removed and collected into a new DNA/RNAse free microfuge tubes (Eppendorf, Hamburg, Germany) and 100% isopropanol was added to precipitate out RNA. Tubes were inverted 4-5 times to ensure thorough mixing. 5µg glycogen (Ambion, Life Technologies) was added to aid the visualisation of the RNA pellet. RNA was pelleted by centrifugation at 11,200rpm (12000g) for 10 minutes at 4°C in a bench top centrifuge. All isopropanol was removed and the RNA pellet was washed in 75% (v/v) ethanol and samples were centrifuged 8,900rpm (7500g) 5 minutes at 4°C. All ethanol was removed and RNA pellets were allowed to air dry on the bench for approximately 5 minutes. RNA was re-dissolved in 30µl RNase-free H_2O (Promega, Wisconsin, USA) before quantification on the NanoDrop (ThermoFisher Scientific).

2.4.2 RNA clean up

RNA samples were cleaned up prior to shipment for GEP experiments, to remove phenol contamination. RNA samples were diluted by adding 70µl RNase-free H_2O. 1/10 volume of ice-cold 3M sodium acetate (pH5.2) was added to the RNA sample, and mixed thoroughly. 2.5x volume of 100% ice ethanol was added to the RNA and the tube was inverted five times to mix. RNA was stored overnight at -80°C. RNA was centrifuged at 13,000rpm (16000g) at 4°C for 20 minutes in a benchtop centrifuge. RNA pelelts were washed in ice cold 75% ethanol and centrifuged again at 13,000rpm (1600g) at 4°C for 20 minutes in a benchtop centrifuge. All supernatant was removed from the RNA pellets and pellets were pulsed to ensure all ethanol was removed. RNA pellets were allowed to air dry on the bench for approximately 5 minutes. RNA was re-dissolved in 30µl RNase-free H_2O before quantification on the NanoDrop (ThermoScientific).

2.4.3 Determining RNA integrity

2.4.3.1 Nanodrop

The Thermo Nanodrop 1000 was used to determine RNA sample integrity. For accurate readings, prior to use it was ensured that the measurement pedestal surfaces were clean by loading 1-2 µL of de-ionized water onto the lower measurement pedestal. The sample arm was placed down and the "Nucleic Acid Measurement" setting was chosen and the Spectrometer was allowed to initialize. The RNA setting was selected and 1µl RNase-free H_2O was used to blank the machine. 1µl of each sample was then analysed. After measuring samples, areas around the upper and lower pedestals was cleaned thoroughly. This prevents cross-contamination from previous samples and distortion of low-level measurements.

2.4.3.2 Bioanalyzer

The Agilent RNA 6000 nano kit (Agilent, California, USA) was used to confirm quality of each RNA sample to be sent for GEP. Agilent RNA kits contain chips and reagents designed for analysis of RNA fragments. Each RNA chip contains an interconnected set of microchannels that is used for separation of nucleic acid fragments based on their size as they are driven through it electrophoretically. Agilent RNA kits are designed for use with the Agilent 2100 Bioanalyzer instrument (Agilent).

Chips were prepared as per Agilent user guide (Figure 2-3). All reagents were allowed to equilibrate to RT for 30 minutes before use. To prepare the gel 550µl of Agilent RNA 6000 Nano gel matrix was pipetted into the top receptacle of a spin filter. The spin filter was then spun in the microcentrifuge for 10 minutes at 1500g.The gel-dye was prepared by mixing 1µl RNA 6000 Nano dye into a 65µl aliquot of filtered gel as prepared above. The tube was then spun for 10 minutes at RT at 13000g. The gel-dye was loaded as per instructions 9µl of gel-dye was loaded into the bottom of the well-marked 'G'. The plunger was pushed down for 30 seconds and then released with the clip mechanisms. 9µl of the gel-dye mix was then loaded into a further two wells marked in the instruction manual. 5µl of RNA Nano marker was loaded into the well marked with ladder symbol and each of the 12 sample wells. Ladder aliquots were kept on ice prior to use and loaded into the well marked with the ladder symbol. To minimise secondary structure, the RNA samples were heat denatured to 70°C for 2 minutes before loading into the sample wells of the chip. The chip was placed into a horizontal IKA vortex mixer for 60 seconds at 2400 rpm. The chip was then loaded into the Agilent 2100 bioanalyzer.

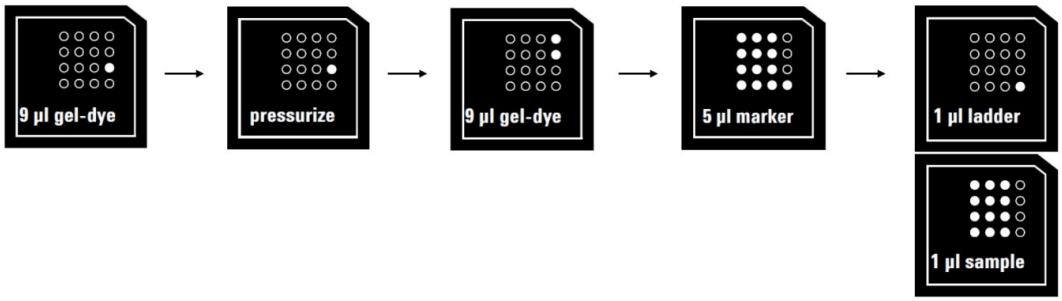

FIGURE 2-3: PREPARATION OF BIOANLYZER CHIPS

Schematic for preparation of bioanalyzer chips. The gel-dye was loaded as per instructions 9µl of gel-dye was loaded into the bottom of the well-marked 'G'. The plunger was pushed down for 30 seconds and then released with the clip mechanisms. 9µl of the gel-dye mix was then loaded into a further two wells marked in the instruction manual. 5µl of RNA Nano marker was loaded into the well marked with ladder symbol and each of the 12 sample wells.

2.4.4 First strand complementary DNA synthesis

Complementary DNA (cDNA) was synthesised from RNA collected using 220ng of RNA diluted in RNase-free H_2O water to a total volume of 14µl. 1µl of oligo-dT (Promega) was added to the samples and heated to 70°C for 5 minutes to enable the oligo-dT primer to bind to the polyA tail. The mixture was cooled to 4°C before the cDNA synthesis master mix (5µl MMLV buffer (Promega), 1.25µl 10mM dNTPs, 0.625µl RNasin ribonuclease inhibitor (Promega), 1µl MMLv polymerase (Promega) and 2.125µl H_2O) was added to each sample. The mixture was heated to 42°C for 60 minutes to generate cDNA and then the mixture was heated to 95°C to inactivate the enzyme before chilling to 4°C. The cDNA was diluted into a total of 100µl with nuclease-free H_2O and stored at -20°C. The process of cDNA synthesis is described in Figure 2-4

2.4.5 Quantitative polymerase chain reaction

Quantative polymerase chain reaction (qPCR) was carried out using TaqMan primers (Applied Bioscience, Paisely, UK). TaqMan qPCR was used as the primers and probes, specific for the gene of interest and therefore accurate quantification of the cDNA present. The TaqMan primers contained forward and reverse primers for the gene of interest along with a probe that contained a fluorophore and a quencher. qPCR reactions are based on fluorescence resonance energy transfer (FRET) reactions and are described in Figure 5.

5µl of cDNA was added to qPCR plates (Applied Biosystems) along with 4µl of nuclease-free H_2O, 4µl primer (Applied Biosystems) and 10µl of qPCR master mix (Applied Biosystems). Plates were covered with MicroAmp Optical Adhesive Film (Applied Biosystems) and pulsed in the centrifuge to ensure thorough mixing of reagents and that liquid was in the bottom of each well. qPCR plates were then placed in the Applied Biosystems, 7500 Real Time PCR system and qPCR reactions were commenced. Cycles were as follows and the cycling stage was carried out 40 times. Typical curve results are displayed in Figure 6.

Holding stage: 50°C 2 minutes

95°C 10 minutes

Cycling stage: 95°C 15 minutes

60°C 1 minutes

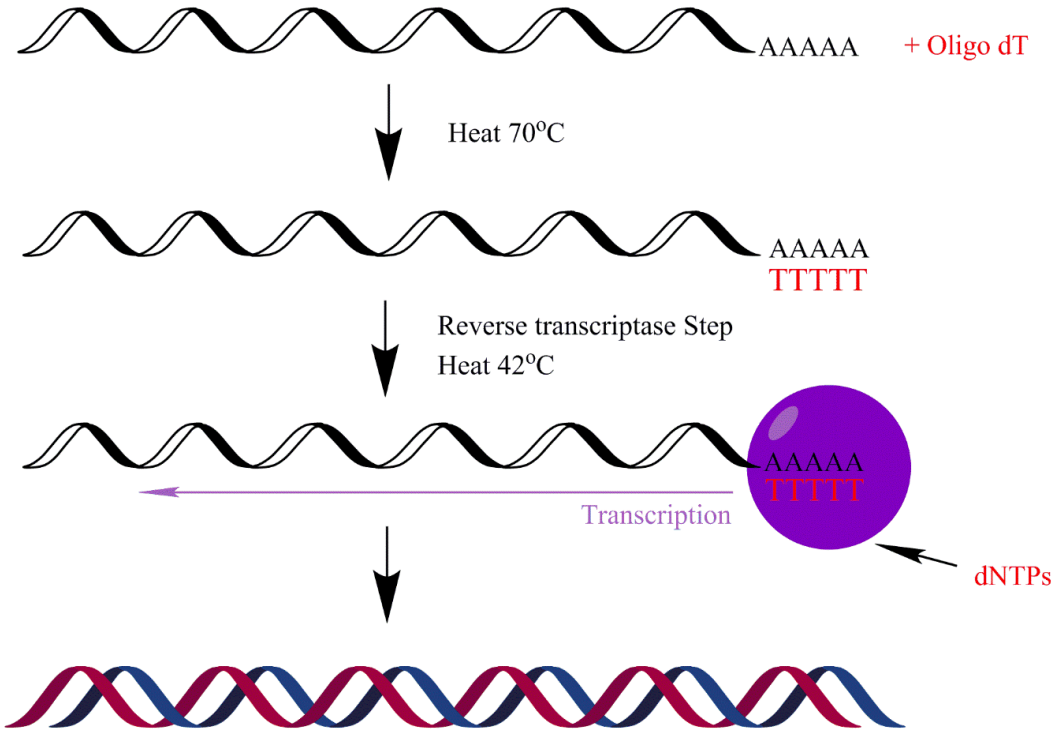

FIGURE 2-4: FIRST STRAND COMPLEMENTARY DNA SYNTHESIS

Complementary DNA (cDNA) was synthesised from RNA diluted in RNase-free H_2O water. Oligo-dT was added to the samples and heated to 70°C for 5 minutes to enable the oligo-dT primer to bind to the polyA tail. The mixture was cooled to 4°C before the cDNA synthesis master mix was added to samples. The mixture was heated to 42°C for 60 minutes to generate cDNA and then the mixture was heated to 95°C to inactivate the enzyme before chilling to 4°C. Finally cDNA was diluted with nuclease-free H_2O

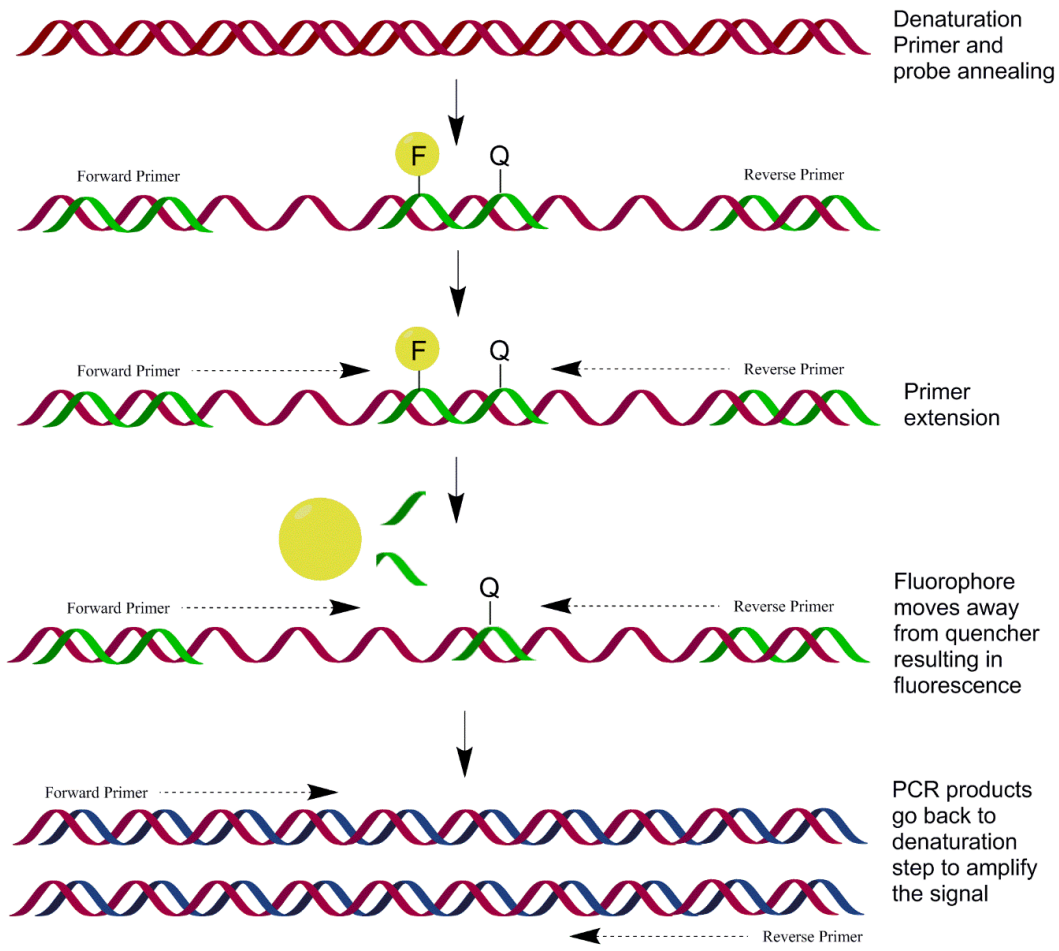

FIGURE 2-5: TAQMAN QUANTITATIVE PCR METHOD

Schematic representation of qPCR using TaqMan primers and probes. F indicates the fluorophore and Q represents the quencher. Illustration prepared in ChemBio Draw. In the initial step of the PCR the cDNA is denatured by heating to 95°C, this allowed the primers and probes access to the cDNA. Temperature is then reduced to 60°C for annealing and extension of the primer. Extension of the primer in the 5'-3' direction results in the polymerase meeting the 5'end of the probe. The polymerase degrades the probe in order to extend the primer. This degradation results in the fluorophore moving away from the quencher, resulting in fluorescence. While the fluorophore and quencher are attached to the probe, no fluorescence is detected because fluorescence resonance energy transfer (FRET) occurrs. FRET is the energy transfer between two molecules; the fluorophore becomes excited at a particular wavelength resulting in the production of light at a different wavelength, this is normally seen as fluorescence. However in close proximity to a quencher the fluorescence wavelength emitted is absorbed by the quencher, which will produce a different wavelength. This absorbance of fluorescence by the quencher is known as FRET. Therefore only when the probe is degraded by amplification of the target gene was fluorescence is detected. As your primer and probes are specific for your gene of interest, the fluorescence produced is directly proportional to the concentration of the cDNA present.

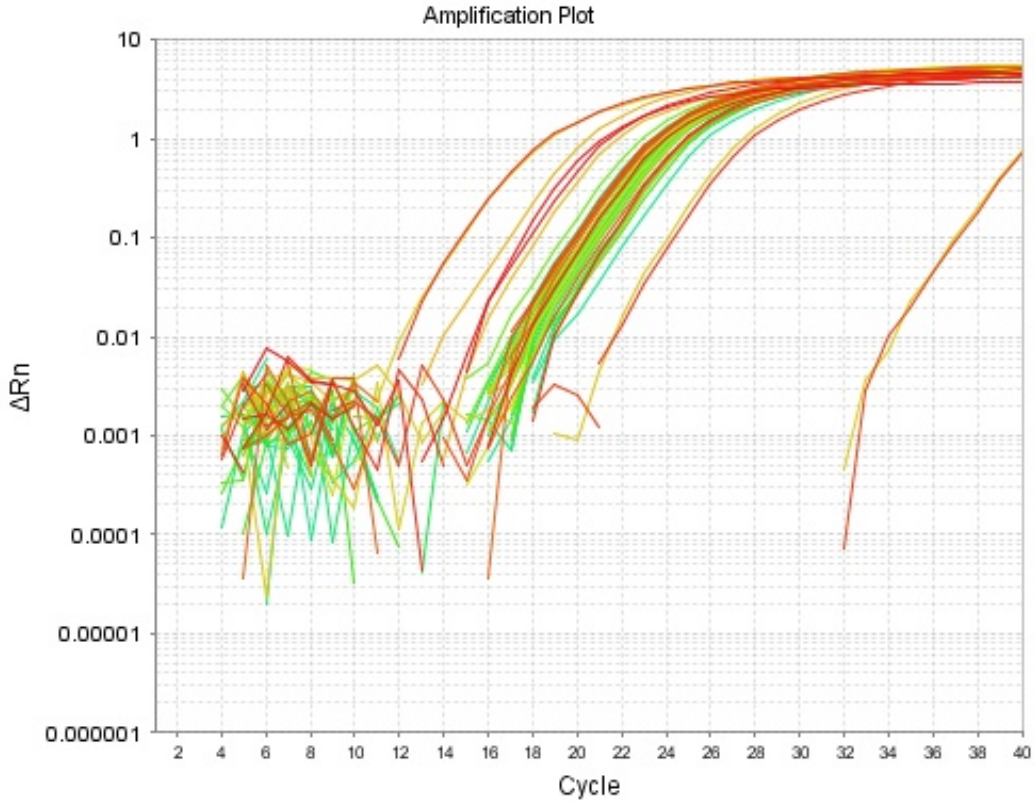

FIGURE 2-6: TYPICAL AMPLIFICATION PLOT FROM QPCR EXPERIMENTS

Typical amplification plots obtained from the Applied Biosystems, 7500 Real Time PCR system for samples analysed in this thesis.

2.5 Gene expression profiling experiments

2.5.1 Gene expression profiling experiments outline

Gene expression profiling (GEP) was carried out on RNA collected from CLL cells cultured in a number of different conditions. The culture conditions were as follows: CLL cells cultured alone, CLL cells co-cultured with HFFF2 cells, CLL cells co-cultured with HFFF2-derived CM, CLL cells stimulated with immobilised αIgM, and finally CLL cells co-cultured with HFFF2 cells and stimulated with immobilised αIgM. RNA was also collected from HFFF2 cells to be used as a control.

HFFF2 cells were plated out for the direct co-culture condition. HFFF2 cells were plated out $1x10^6$/well in a $10cm^2$ culture dish and left overnight at 37°C/10% CO_2 to allow cells to adhere and spread. $5x10^6$ CLL cells were plated into each $10cm^2$ dish and two dishes were used per condition (Total CLL cells $10x10^6$). CLL cells were either plated in C.RPMI alone, C.RPMI onto HFFF2 cell, or in HFFF2-derived CM (Section2.1.4.2). A proportion of the CLL cells were stimulated with αIgM (Southern Biotech) immobilised onto dynabeads (Life Technologies). 3µl of immobilised αIgM was used per $1x10^6$ CLL cells. All dishes were incubated for 8 hours at 37°C/5% CO_2. After 8 hours, CLL cell were collected and RNA was extracted from cell pellets. RNA was cleaned up and RNA integrity was checked using the nanodrop and bioanlyzer as described previously. Nanodrop and Bioanalyzer results for all GEA samples can be found in Appendix D.

2.5.2 Analysis of raw GEP experiment data performed by Cambridge Genomic Services

Following GEP, results were received from Cambridge. Quality control (QC) data was provided for each culture conditions. QC data included: firstly, scatter plots of the samples, each graph plot the samples against each other while the correlation and the number of point away from the x=y line by a least 2 folds (up/down); Secondly boxplots of the data, the box delimits the 25th and 75th percentile, the delimitation in the middle is the median of the data. The data should roughly have boxplots similar in shape and size. And, finally hierarchical clustering of the data, showing the relationship between them according to the most variable data point, selected by taking probes for which the standard deviation is at least 10% of the mean. Full quality control reports for each culture condition are displayed in AppendixE.

2.5.3 Multiple comparisons of GEP data

2.5.3.1 Analysis pipeline

Data was analysed by Cambridge Genomic services. First the raw data is loaded into R using the lumi package from bioconductor then is divided into subsets according to the groups being compared, only the samples involved in a given comparison were used. The subsets are then filtered to remove any non-expressed probes using the detection p-value from Illumina (if for a given probe all the detection p-value for the samples are above 0.01 it is removed from the analysis as it is considered not expressed (not detected in all samples)). Once the filtering is done, the data are transformed using the Variance Stabilization Transformation (VST, (Lin et al., 2008)) from lumi which is close to log2 transformation but without bias at low and high intensity. The last step before the comparisons is to normalise the data, to remove technical variation between arrays. The method used is quantile normalisation. Once the data are normalised, the comparisons are done using the limma package (Smyth, 2004), the results are corrected for multiple testing using FDR, the corrected value in the comparisons results table is called "adj.P.val", this is the one also used to generate the summary of the comparisons.

Prior to sample shipping to Cambridge, a list of analysis comparisons was sent for the bioinformatics team to perform their basic level of analysis. For GEP analysis the following comparisons were requested; CLL cultured alone versus CLL cultured with HFFF2 cells and CLL cells cultured with HFFF2-derived CM to determine transcriptional responses occurring in CLL cells following microenvironmental stimulation from stromal cells. CLL cells cultured alone versus CLL cell stimulated with αIgM beads and also CLL cells cultured alone versus CLL cells cultured with HFFF2 and stimulated with αIgM beads to determine how transcriptional responses to antigen might be modulated by microenvironmental co-stimulation. For each comparison requested one data file was received containing the results of the statistical analysis (AppendixE).

2.5.4 Gene set enrichment analysis using GSEA software

Gene set enrichment analysis was carried out using the GSEA software (Broad Institute). To further investigate the differences between CLL cells cultured alone and in the presence of HFFF2 cells while taking into account biological functions. GSEA is a computational method that determines whether an a priori defined set of genes shows statistically significant, concordant differences between two biological states (e.g. phenotypes). The algorithm used by the software is fully described the in The Gene Set

Enrichment Analysis PNAS paper (Subramanian et al., 2005). For all analysis carried out for this study the GSEA Preranked analysis option was used. GSEA Preranked runs the gene set enrichment analysis against a ranked list of genes, which are uploaded into the software. In this case the ranked list of genes was the expression datasets, ranked according to their fold change. The ranked list of genes was loaded into the software and analysed against a set of genes from The Molecular Signatures Database (MSigDB). MSigDB is a collection of annotated gene sets for use with GSEA software. The 10348 gene sets in the MSigDB are divided into 8 major collections, and several subcollections.

The primary result of the gene set enrichment analysis was the enrichment score (ES), which reflects the degree to which a gene set is overrepresented at the top or bottom of a ranked list of genes. GSEA calculates the ES by walking down the ranked list of genes, increasing a running-sum statistic when a gene is in the gene set and decreasing it when it is not. A positive ES indicates gene set enrichment at the top of the ranked list; a negative ES indicates gene set enrichment at the bottom of the ranked list. Each gene set was then given a normalised enrichment score (NES). The NES was the primary statistic for examining enrichment results, because by normalising the enrichment score, GSEA accounts for differences in gene set size. This means that the NES could be used to compare analysis results across the gene sets.

Analysis was carried out using the C2-curated gene set from the MsigDB. The gene sets are collected from various sources such as online pathway databases, publications in PubMed, and knowledge of domain experts. MSigDB describe the gene sets in the C2 collection as coming from the following sources: (i) Online pathway databases (Gene sets representing metabolic and signalling pathways are imported from the online pathway databases) (ii) Biomedical literature (Over the past few years, microarray studies have identified signatures of several important biological and clinical states) (iii) L2L (Gene sets compiled from published mammalian microarray studies (Newman and Weiner, Genome Biology 2005, 6(9):R81)) and (iv) MYC Target Gene Database (gene sets curated by Dr. Chi Dang from the MYC Target Gene Database at Johns Hopkins University School of Medicine). For this analysis I specifically looked at the Cannonical Pathways gene set, that is gene sets from the pathway databases. (www.broadinstitute.org/gsea). Usually, these gene sets are canonical representations of a biological process compiled by domain experts.

2.6 Acoustic trapping device techniques

2.6.1 Acoustic trapping device

The ultrasonic microfluidic device used in this study was briefly described previously (Introduction, Section1.6.3). The device was designed and made by Dr Glynne-Jones, Faculty of Engineering, University of Southampton. The device is a half wavelength in size meaning that cells are levitated in the centre of the cavity. The active region of the transducer is 10 x 10 x 0.5 mm in size. The coupling layer of the device incorporates a silvered mirror (glass face towards the chamber) in order to create a dark-field background during fluorescent imaging (Figure 2-7).

The body of the devices were designed and made by Dr Peter Glynne-Jones (Faculty of Engineering and the Environment, University of Southampton). Devices were created by micro-milling of macor, a machinable ceramic. The mirror (Edmund optics NT31-418. 9.5mm x 11.2mm x 1.2mm) was epoxied to the macor with epotek 301 and cured at a temperature of 120 °C for 1 hour. A PZT (lead ziconate titanate) tranducer (PZ27, Ferroperm, Kvistgaard, Denmark 10mm x 11mm) was also epoxied to the macor base. The transducer electrodes were connected via soldered wires, with silver paint used to make connection between the lower electrode and a small area of the top electrode isolated by micromilling. A surface mount LED (Stanley, from RS components, UK) with current limiting resistor was also attached to the transducer to indicate that power reaches the transducer (failure of the numerous connections in the system is often hard to spot otherwise).

The assembled device was mounted within a 6well plate, with a sheet of 1.2mm thick glass cut from a microscope slide placed under it to act as an acoustic reflector. A steel washer was placed under the 6-well plate attracts magnets (also epoxied into the device – see Figure 2-7) to hold devices in position. This clamping is important as small movements of the device would disrupt the acoustic resonance.

The device was initially tested in the Faculty of Engineering and the Environment using an electrical impedance analyser (Cypher graph, C60) by Dr Peter Glynne-Jones. Acoustic resonances can be identified as being close to the impedance minima in the plot. By making a measurement of a device both with and without medium under it, it is possible to identify the half-wave resonance which only exists in the presence of the medium. The devices were found to have slightly different resonance frequencies. Thus in order to drive all the devices from one signal a frequency sweep in the range 1.95Mhz to 2.12Mhz (at a rate of 50Hz) at a sweep rate of 0.05 seconds was chosen. This also has the advantage

that should the resonant frequency of an individual device shift slightly due to physical movement then the resonance will be maintained.

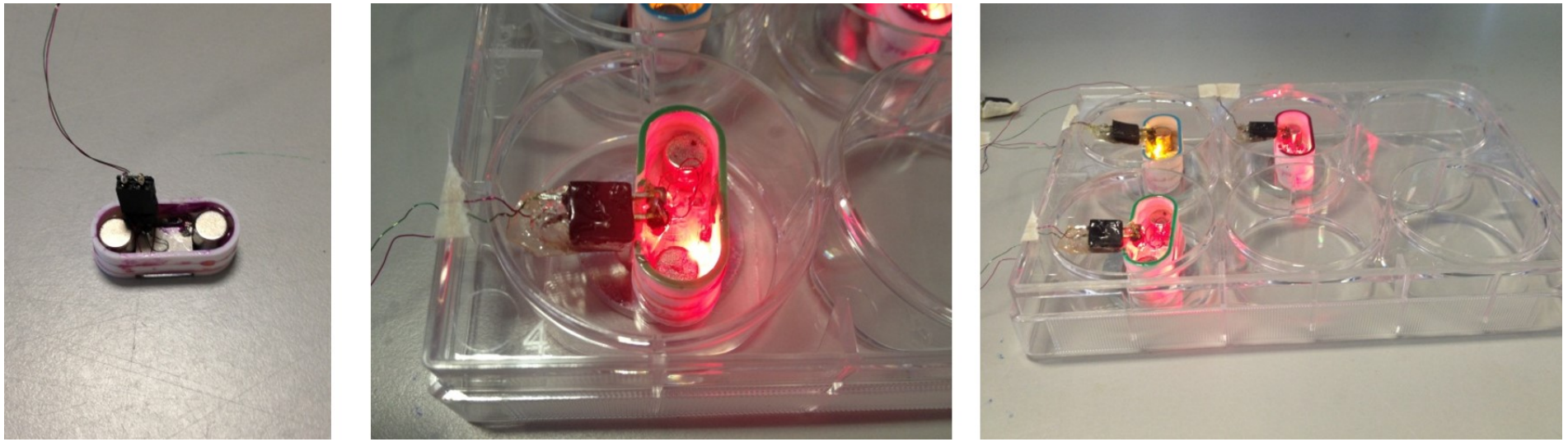

FIGURE 2-7: ACOUSTIC TRAPPING DEVICE IN A 6 WELL PLATE FORMAT

Acoustic trapping devices were optimised prior to the commencement of this project to enable each device to fit into 6 well tissue culture plates. This format allowed for multiple devices to be run per experiment. Each device is fitted with an LED light which indicates when all connections are correctly in place and the device is powered to allow for easy troubleshooting. Each device was identified by a different colour of nail varnish.

2.6.2 Set up of acoustic trapping devices and injection of cells

The device amplitude was set using an oscilloscope and Picoscope6 software (Pico Technology, Cambridgeshire UK) to 6 Vpp with a sweep from 1.95Mhz to 2.12Mhz every 0.05secs. Devices were connected and set up as shown in Figure 2-7

For ease of use, the signal generator and amplifier pictured in Figure 2-7was designed by Dr Glynne-Jones, (University of Southampton) and could be programmed to create the required frequency sweep and amplitude. Cells were injected into the device using a flat gel-loading pipette (Corning), this method ensured injection of cells under the acoustic trapping device in the centre of the PZT transducer. Correct injection of cells was vital to ensure cells were 'caught' by the ultrasound and not injected out the other side of the transducer into the well. Injection directly under the centre of the transducer was also important to avoid loss of cells out the edges as well. The microscopes were used to track injection of cells and agglomerate formation.

Two microscopes were used during the course of this project: Olympus IX81 inverted research microscope which is fitted with a Hamamatsu ORCA-ER black/white digital camera, fitted with fluorescent filters and the Nikon eclipse Ti microscope fitted with a Nikon DS-Qi1mc camera and culture chamber. The phase contrast time-lapse microscope had a heated and $C0_2$ controlled culture chamber, for which long term levitation experiments were carried out. The fluorescent microscope had a heated stage but no $C0_2$ controlled culture chamber so was only used for short-term experiments. For experiments carried out on this microscope media was buffered with the addition of 20μM HEPES (Sigma-Aldrich) to minimise any effects caused by the lack of $C0_2$ controlled culture chamber.

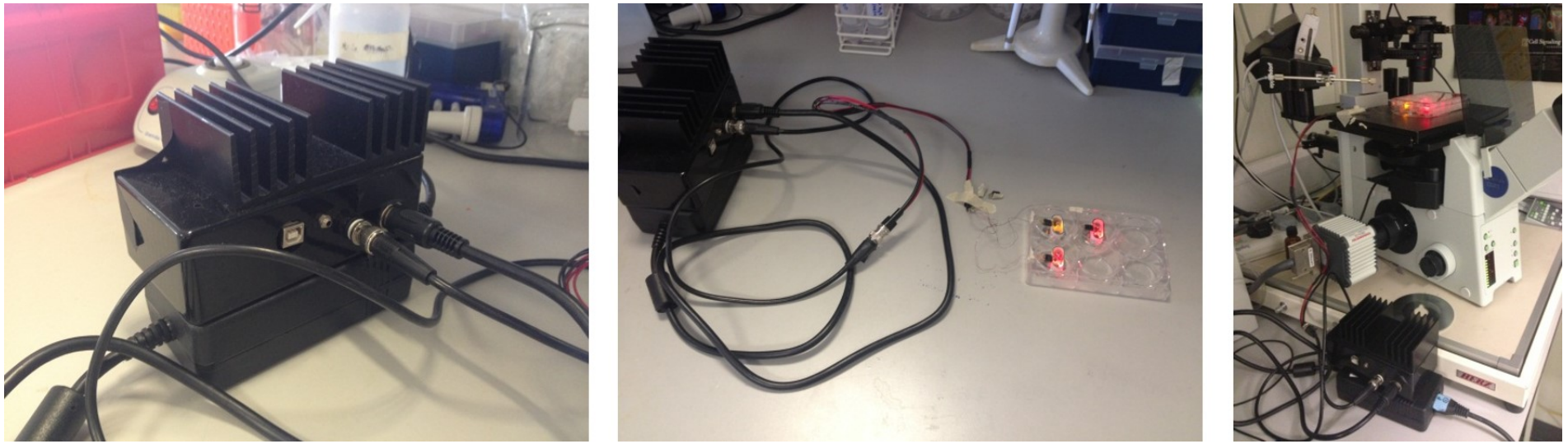

FIGURE 2-8: SET UP OF ACOUSTIC TRAPPING DEVICES

Devices were connected to the power supply by small connecters as pictured in Figure 2-7. These connecters run to drive electronics (black box) with its own power supply. The drive electronics box was custom-made by Dr Peter Glynne-Jones. Once connected, the 6 well plate and devices remained on the heated microscope stage with wires secured by tape for the duration of the experiment.

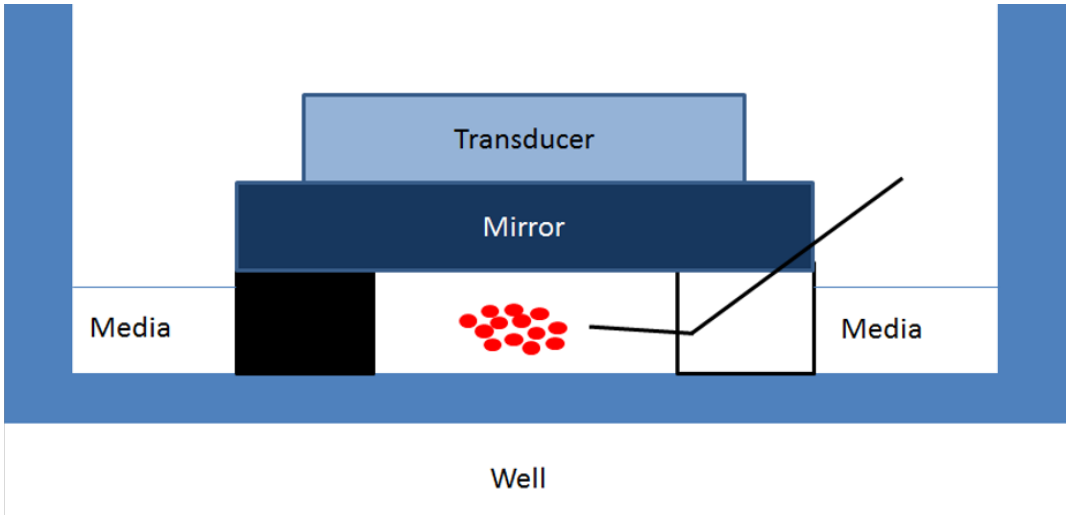

FIGURE 2-9: INJECTION OF CELLS INTO ACOUSTIC TRAPPING DEVICES

Cells were injected into the device using a flat gel-loading pipette to ensure all cells were injected under the acoustic trapping device in the centre of the PZT transducer. Correct injection of cells was vital to ensure cells were 'caught' by the ultrasound and not injected out the other side of the transducer into the well. Injection directly under the centre of the transducer was also important to avoid loss of cells out the edges as well. The microscopes were used to track injection of cells and agglomerate formation.

2.6.3 Cell labelling

Prior to entry into the acoustic trapping device, cells were fluorescently labelled to allow for better imaging and viewing of agglomerates. Different fluorescence labels were used in combinations in acoustic trapping device experiments concentrations for which are outlined in Table 2.3. CLL cells were removed from LN_2 and thawed and allowed to recover for an hour as described in Section2.1.2. CLL cells were centrifuged at 350g for 5 minutes and resuspended in 2ml pre-warmed PBS containing the fluorescent label. HFFF2 were labelled while still attached to the tissue culture flasks; in this instance, media was aspirated from the flask, cells were washed with warmed PBS and then 5ml of PBS containing the fluorescent label was added to the flask. Following the addition of the PBS/dye solution both cell types were incubated in the dark at 37°C for 45 minutes. After 45minutes incubation the PBS/dye solution was removed. CLL cells were washed in pre-warmed PBS and centrifuged at 350g for 5 minutes while HFFF2 cells were gently washed in the flask. Complete RPMI-1640 and complete DMEM were added to the CLL and HFFF2 cells respectively cells were incubated at 37°C for a further 30 minutes. HFFF2 cells were then trypsinised and detached from the flask. Both cell types were then washed twice in PBS by centrifugation at 350g for 5 minutes to remove any excess dye. Cells were counted and then resuspended at a concentration of $18x10^6$ cells/ml ready for injection into the acoustic trapping device as outlined in 4.6.2. When co-levitation experiments were carried out with both cell types, the same ratio (1:4, HFFF2:CLL) was maintained to replicate other biological co-culture experiments.

TABLE 2.3: NAMES, DILUTIONS AND SUPPLIERS OF THE CELL TRACE AND FLUORESCENT DYES USED TO LABEL CELLS IN ACOUSTIC TRAPPING DEVICE EXPERIMENTS

Fluorescent Dye	CLL concentration	HFFF2 concentration
CFSE (Invitrogen)	15μM	15μM
CellTracker Red (Invitrogen)	10μM	5μM
CellTracker Blue (Invitrogen)	50μM	50μM

2.6.4 Measurement of the minimum voltage required to levitate cells in acoustic trapping device

Measurement of the minimum voltage required to levitate cells in the devices was carried out in the Faculty of Engineering and the Environment with the help of Dr Peter Glynne-Jones. Measuring the acoustic pressure amplitude within the resonant cavity was difficult due to the confined space. The acoustic pressure amplitude inside the capillary for a given drive voltage was found by balancing the weight of a 10μm fluorescent polystyrene bead against the acoustic radiation force in the manner described by Spengler et al., (Spengler et al., 2003). Acoustic pressure was found to be related to drive voltage applied to the PZT by a factor of 26 kPa/Vpp ±30%. The low accuracy of this measurement is caused by the difficulty of ascertaining when the two forces are precisely balanced, and uncertainty in the material properties of the polystyrene beads. For analysis of the voltage required to levitate cells in the device, 10μm fluorescent beads (Polysciences, Pennsylvania, #18140-2) were levitated. Figure 2-10 shows how the minimum height of levitation was approximately calculated. The voltage was dropped until the beads were no longer levitating. This voltage was converted to the voltage output as Vpp. This was repeated to work out the voltage required to levitate an agglomerate of cells. The fluorescent beads this time were allowed to form an agglomerate and the process was repeated.

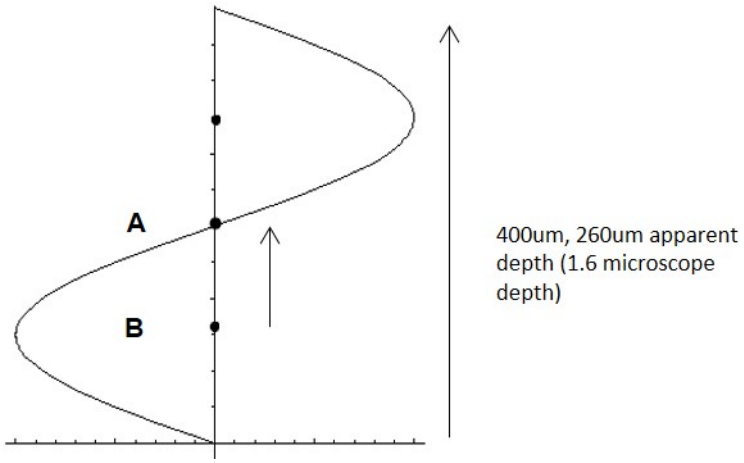

FIGURE 2-10: CALCULATION OF APPROXIMATE HEIGHT BEADS WILL NO LONGER LEVITATE IN THE ACOUSTIC TRAPPING DEVICE

Point A represents the centre of the active region. As the devices are half wavelength in height the beads will levitate in the centre of the devices. Point B is the known point at which the ultrasound will no longer be able to levitate the beads. When they pass point B the beads will drop. The distance between point A and B is approximately 400μm, this relates to an 260μm apparent depth on the microscope. This was used to approximate the point at which the beads would no longer be able to levitate and the voltage was reduced until the beads fell to this point.

2.7 Statistics

All data analysis and graphs were performed using GraphPad Prism. Data was assumed to be not normally distributed due to the small sample sizes and therefore non-parametric tests were carried out through out this project. For paired data, Wilcoxons matched-pairs signed rank test was carried out, for unpaired data Mann-Whitney tests were used.

The Pearson rank correlation coefficient was calculated to determine the strength of association between various parameters.

Chapter Three

Investigating the HFFF2 cell line as a model system for studying CLL microenvironment interactions

Chapter 3: Investigating the HFFF2 cell line as a model system for studying CLL microenvironment interactions

3.1 Introduction

Interactions with accessory cells in the tumour microenvironment promote CLL cell survival, proliferation and drug resistance. It is important therefore to investigate these interactions *in vitro*. As outlined in the introduction (Table 1.3), various cell types comprising the microenvironment promote CLL cell survival, including NLCs (Burger et al., 2000, Tsukada, 2002, Pedersen et al., 2002, Nishio et al., 2005, Burger et al., 2009b, Filip et al., 2013), MSCs (Lagneaux et al., 1999, Panayiotidis et al., 1996, Burger and Kipps, 2006, Kurtova et al., 2009, Ghia et al., 2005), FDCs (Burger et al., 2009a, Pedersen et al., 2002) and T cells (Patten et al., 2008). Further to this, *in vitro* studies have revealed bi-directional cross talk between CLL cells and MSC resulting in the activation of both cell types (Ding et al., 2009, Lutzny et al., 2013, Ghosh et al., 2010). CLL cells are able to induce stromal cells to proliferate and release mediators, which in turn promote malignant cell survival. The microenvironment is not only important for CLL progression and survival but also in drug resistance where protective microenvironmental niches “shield” malignant cells from therapy (Burger and Chiorazzi, 2013, Panayiotidis et al., 1996, Burger and Kipps, 2002). Modulation of the microenvironment has therefore become a promising drug strategy demonstrated through the use of compounds like plerixafor, lenalidomide and natalizumab.

These points underline the importance of identifying the most appropriate tissue culture models to investigate interactions operating in the CLL tumour microenvironment. Tissue-resident cells are not readily available from patients and studies to date have focused on 2D co-culture of CLL blood cells with various stromal cells of human or murine origin (Hamilton et al., 2012, Asslaber et al., 2013). However, the overall goal of this thesis was to develop a novel 3D culture system to investigate CLL cells microenvironment interactions. Therefore, the main aim of the experiments described in this chapter was to find a suitable cell line system to use with primary CLL cells in acoustic trapping devices, and to extend analysis of this model using 2D culture. Previous research in the host laboratory has investigated the use of the HFFF2 cell line as a model for CLL/fibroblast interactions *in vitro* (Samantha Dias, PhD thesis, (Blunt et al., 2015)). We therefore selected the HFFF2 cell line as a potential model cell system for use in acoustic trapping

devices. This chapter will aim to further investigate the use of the HFFF2 cell line for investigating CLL/fibroblast interactions *in vitro.*

3.2 Hypothesis

The HFFF2 cell line will be a suitable cell line for investigating CLL/fibroblast interactions in acoustic trapping devices.

3.3 Aims and objectives

The overall goal of this chapter was to determine whether the HFFF2 cell line was a suitable model for investigating CLL cell/fibroblast interactions through a more detailed characterisation of responses in 2D *in vitro* cultures. Previous work in the host laboratory has demonstrated that HFFF2 cells protect CLL cells from spontaneous apoptosis in 2D cultures (Samantha Dias, PhD thesis). The first aim was therefore to expand the cohort of CLL samples analysed in this way, to determine whether HFFF2-mediated cytoprotection was observed for all cases, and, if any, variability of responses correlated with clinical or biological features of the disease. The second aim was to determine the manner in which HFFF2-mediated cytoprotection occurred, and whether it is mediated via cell:cell contact. Finally, this chapter aimed to confirm the ability of the HFFF2 cell line to undergo transdifferentiation. The specific objectives of this chapter were:

- Confirm the ability of the HFFF2 cell line to protect CLL cells from spontaneous apoptosis using Annexin-V/PI staining
- Investigate the heterogeneity of spontaneous apoptosis in CLL cells and heterogeneity of cytoprotection from HFFF2 cells
- Determine whether HFFF2-mediated cytoprotection occurs in a contact-dependent manner
- Confirm the ability of the HFFF2 cell line to transdifferentiate following treatment with TGF-β using α-SMA as a marker of myofibroblasts

3.4 The HFFF2 fibroblast cell line protects CLL cells from spontaneous apoptosis

The first experiments described in this chapter were performed to confirm the ability of the HFFF2 cell line to protect CLL cells from spontaneous apoptosis, and to probe potential heterogeneity of response. The HFFF2 cell line is well established as a model of fibroblast transdifferentiation (Moutasim et al., 2009, Frampton et al., 2015, Bhome et al., 2015). The HFFF2 cell line does not undergo spontaneous transdifferentiation but can be stimulated to transdifferentiate following treatment with TGF-β (Moutasim et al., 2009, Frampton et al., 2015, Bhome et al., 2015, Samantha Dias, PhD Thesis) meaning that the HFFF2 cell line is a useful tool to reliably investigate the role of both fibroblasts and myofibroblast. The differing ability of fibroblasts and their differentiated counterpart, the myofibroblast, to protect CLL cells from spontaneous apoptosis has previously been investigated (Samantha Dias, PhD Thesis). It was found that both cell types protected CLL cells from apoptosis, however, fibroblasts protected CLL cells to a greater extent than myofibroblasts (Samantha Dias, PhD Thesis). Therefore, these experiments were performed using undifferentiated HFFF2 cells.

CLL cell apoptosis was quantified using Annexin-V/PI staining and flow cytometry. Annexin-V/PI staining is a convenient, quick and reliable detection method for studying cell viability (Section2.3.2). Viability was assessed immediately after recovery of CLL samples from cryopreservation (0 hours), and at 24 and 48 hours after culture in media alone or in the presence of HFFF2 cells. 48 hours was selected as the latest time point for study, based on previous experiments in the laboratory and published literature for other models of stromal cell protection (Lagneaux et al., 1998, Kurtova et al., 2009).

The gating strategy used for all Annexin-V/PI viability experiments is described in Figure 3-1. A gate was first applied on the lymphocyte population via the forward and side scatter values (FSC,SSC) to select for the lymphocyte population and minimise potential contaminations from detached HFFF2 cells in co-culture experiments (Figure 3-1a). The majority of samples chosen comprised ≥80% (apart from patients that are denoted in red in the patient table, AppendixA) CD5+CD19+ cells to minimise potential contamination from non-malignant cells. A large gate was used on the FSC/SSC plots incorporating both live and dead CLL cells (Figure 3-1b). The proportion of cells in each quadrant of the Annexin-V/PI (FITC/PerCP respectively) plot and the percentage of viable cells (ie, FITC/PerCP negative cells) was recorded for each sample (Figure 3-1c). Overall, CLL cell viability was quantified for a total of 42 patient samples cultured alone or in the presence of HFFF2 cells. Samples were a mixture of U/M-CLL, and had a range of signalling capabilities and surface IgM expression.

3.4.1 Differences in levels of spontaneous apoptosis of CLL samples

As well documented in the literature (Coscia et al., 2011), CLL cells cultured alone exhibited substantial spontaneous cell death over the 48 hours. Due to varying rates of spontaneous apoptosis, all samples were normalised for comparison. For comparing decrease in viability over time, the 0 hour time point was set to 100% and the viability at the 24 and 48 hour time points was calculated as percentage decrease. The average decrease in CLL cell viability of the 42 CLL samples was 37% (range 11-66%) and 46% (range 32 to 73%) at 24 and 48 hours, respectively. The large range of the percentage decrease in viability between patients indicates substantial heterogeneity between different CLL samples. Therefore further analysis was carried out to determine whether certain subsets of disease displayed greater spontaneous apoptosis. CLL samples were split into groups depending in *IGHV* mutational status, sIgM signalling capability (measured by anti-IgM-induced calcium mobilisation; signallers and non-signallers were determined using the cut off of 5% ((Mockridge et al., 2007), Methods Section2.3.4.2) and sIgM expression levels (Figure 3-2). Consistent with a previous study (Coscia et al., 2011), there was a tendency for a greater loss of viability in U-CLL compared to M-CLL especially at 48 hours. However this difference did not reach statistical significance (Figure 3-2a). There was also no significant difference in spontaneous cell death when the samples were split according to their sIgM signalling capability or sIgM expression levels) (Figure 3-2b and c).

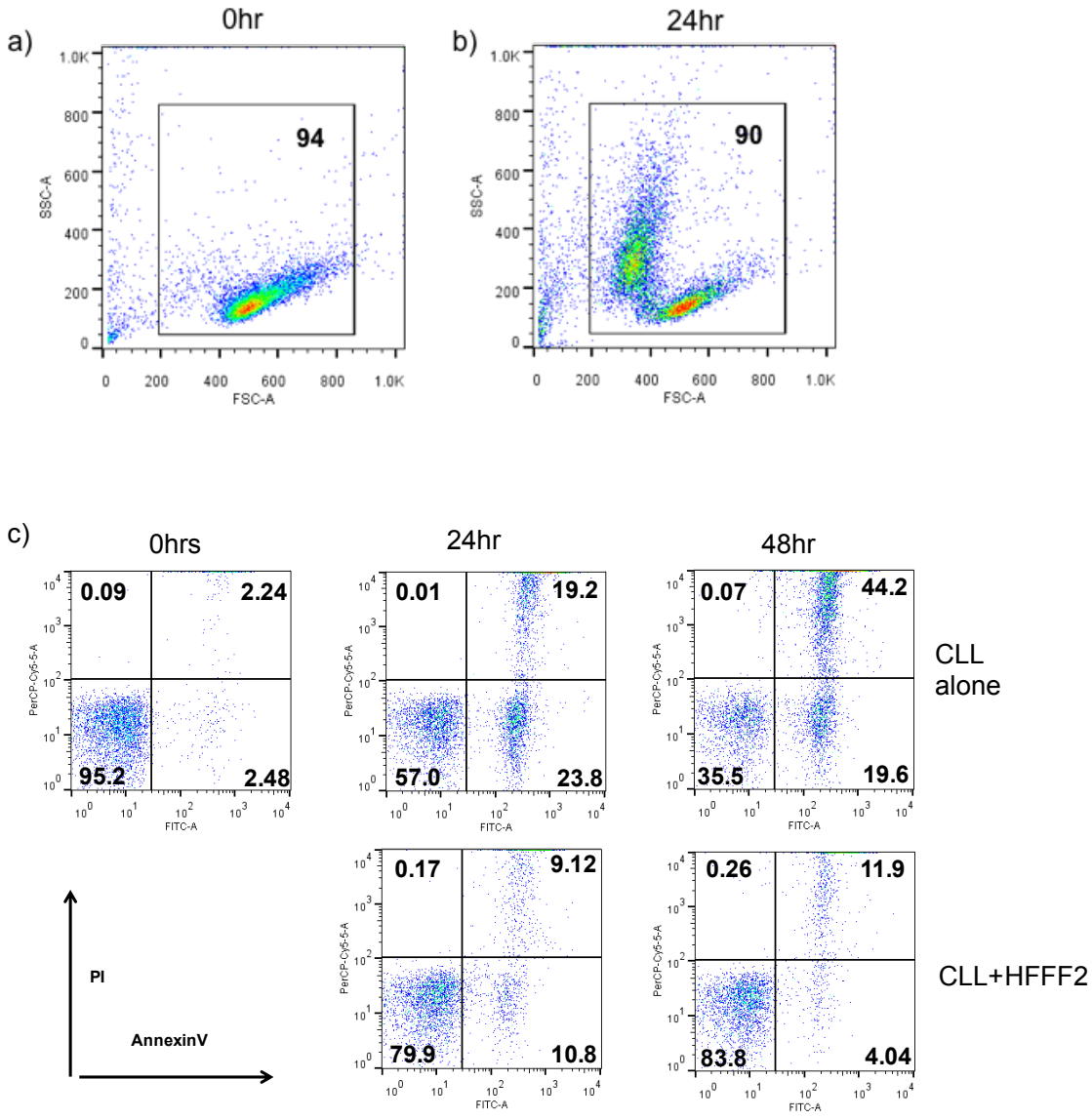

FIGURE 3-1: GATING STRATEGY FOR ANNEXIN-V/PI EXPERIMENTS

CLL cells were cultured alone or in the presence of HFFF2 fibroblasts for 24 or 48 hours prior to analysis of apoptosis. Viability was measured using Annexin-V/PI staining and FACS at the start of experiment (0 hours), and 24 and 48 hours. The lymphocyte population was gated to ensure only CLL cells were analysed by minimising potential contamination from detached HFFF2 cells. A large FSC/SSC gate was used to incorporate both live and dead cells. (a) Lymphocyte gate at 0 hrs. (b) Lymphocyte gate at 48 hrs, showing the accumulation of dead cells with increased side scatter axis (SSC). (c) Annexin-V/PI staining for gated lymphocyte population. Top row indicates CLL cultured alone at 0, 24 and 48 hrs, while bottom row indicates CLL cells cultured with HFFF2 cells. Numbers indicate percentage events per quadrant. Bottom left quadrant (FITC/PerCP negative) contains viable CLL cells, the bottom right quadrant contains CLL cells going through early stage apoptosis (FITC-positive/PerCP-negative) and the top right quadrant contains apoptotic cells (FITC/PerCP positive). FACS analysis in FlowJo Version 9.9.3.

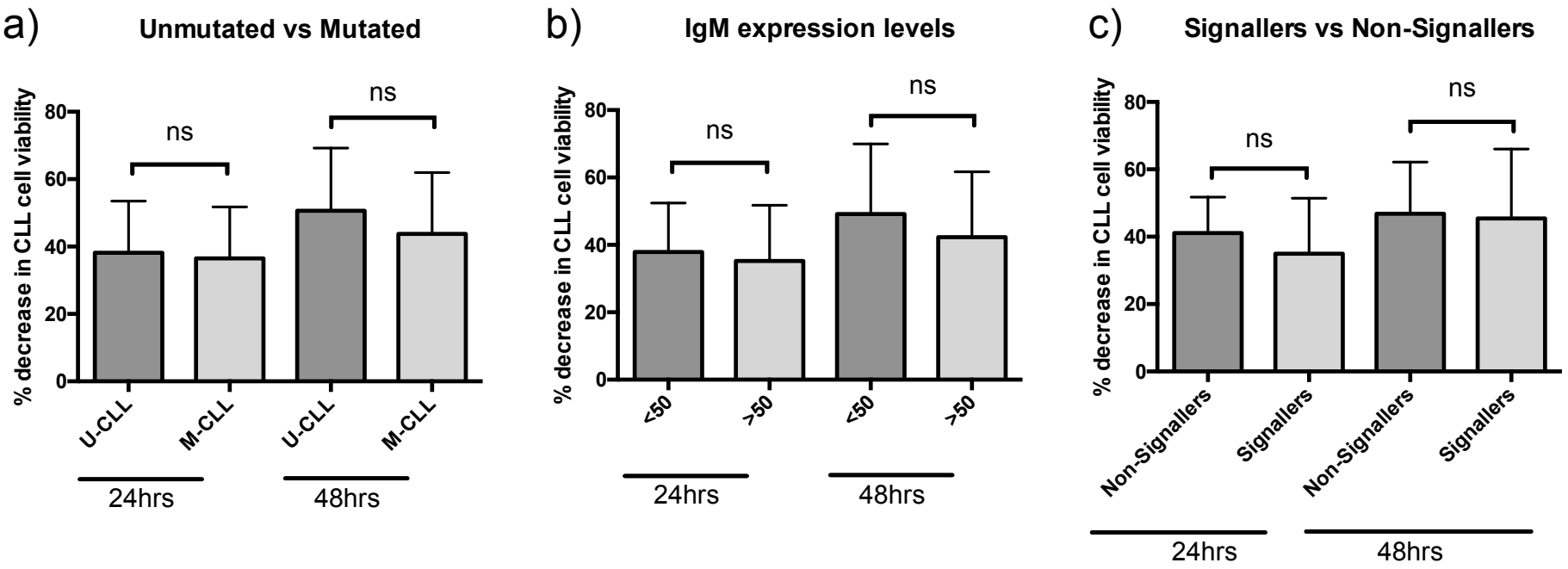

FIGURE 3-2: COMPARISON OF SPONTANEOUS APOPTOSIS LEVELS BETWEEN THE DIFFERENT CLL PROGNOSTIC SUBGROUPS

Summary of data for all samples analysed (n=42). CLL samples were split into different prognostic subgroups and percentage decrease in CLL cell viability was plotted for each group for both 24 and 48 hours. (a) CLL samples were split into two groups based upon their *IGHV* mutation status. Statistical significance is indicated (Mann-Whitney; ns = non-significant). (b) CLL samples were split into two groups based on their sIgM expression levels. Low IgM expression was termed a sample with a IgM MFI of less than 50. Statistical significance is indicated (Mann-Whitney; ns = non-significant). (c) CLL samples were split into two groups based upon their signalling ability. A 'signaller' was termed a sample with an anti-IgM-induced calcium flux >5% of cells (Mockridge 2007, Methods Section2.3.4.2). Statistical significance is indicated (Mann-Whitney; ns = non-significant). All Error bars are SD. Analysis and graphs created using Graphad prism 6.

3.4.2 Ability of the HFFF2 cell line to protect CLL cells from spontaneous apoptosis

The addition of HFFF2 cells into the culture significantly enhanced CLL cell viability confirming the ability of the HFFF2 cell line to protect CLL cells from spontaneous apoptosis. Figure 3-3 displays the results seen from six representative patients and a summary for all 42 patients' samples is shown in Figure 3-4.

Figure 3-4 confirms that HFFF2 cells improved CLL cell viability by 20 – 30% at the 24 and 48 hour time points. Increased survival was observed for all patients, however, because of the intersample variation in spontaneous CLL cell death, data for all patients were corrected to show percentage change in cell viability for CLL cells co-cultured with fibroblasts compared to CLL cells cultured alone (Figure 3-4). In this analysis, CLL cell viability was significantly higher when cultured in the presence of the HFFF2 cells at both 24 and 48 hours (P=<0.0001).

In Figure 3-3, it seems surprising that cell viability appears to increase at the later time point in sample 660. However, rather than being due to cell proliferation, this likely reflects the transient nature of apoptotic cells. Thus, cells that die early and are quantified at 24 hours, will later become debris/fragments which are not detected in the assay. Therefore the apparent increase in viability more likely reflects selection of more robust cells during the culture.

3.4.3 Heterogeneity in levels of cytoprotection from the HFFF2 cell line

I also investigated whether variation in the cytoprotective effects of HFFF2 cells differed between subsets of disease (Figure 3-5). Similar to spontaneous apoptosis (Figure 3-2), there was no statistically significant difference in the cytoprotective effects of HFFF2 cells between M-CLL and U-CLL, and between groups of samples separated on the basis of sIgM expression or signalling capacity. It was also investigated whether the levels of HFFF2 cytoprotection correlated to the levels of spontaneous apoptosis for the same patient sample (Figure 3-6). Data indicate that there is a significant correlation between levels of apoptosis and levels of cytoprotection. This positive correlation indicates that patients with greater spontaneous apoptosis have greater protection from HFFF2 cells. This indicates that these patients that are more dependent on microenvironmental stimulation i.e. patients that have greater levels of spontaneous apoptosis will require more protection from HFFF2 cells.

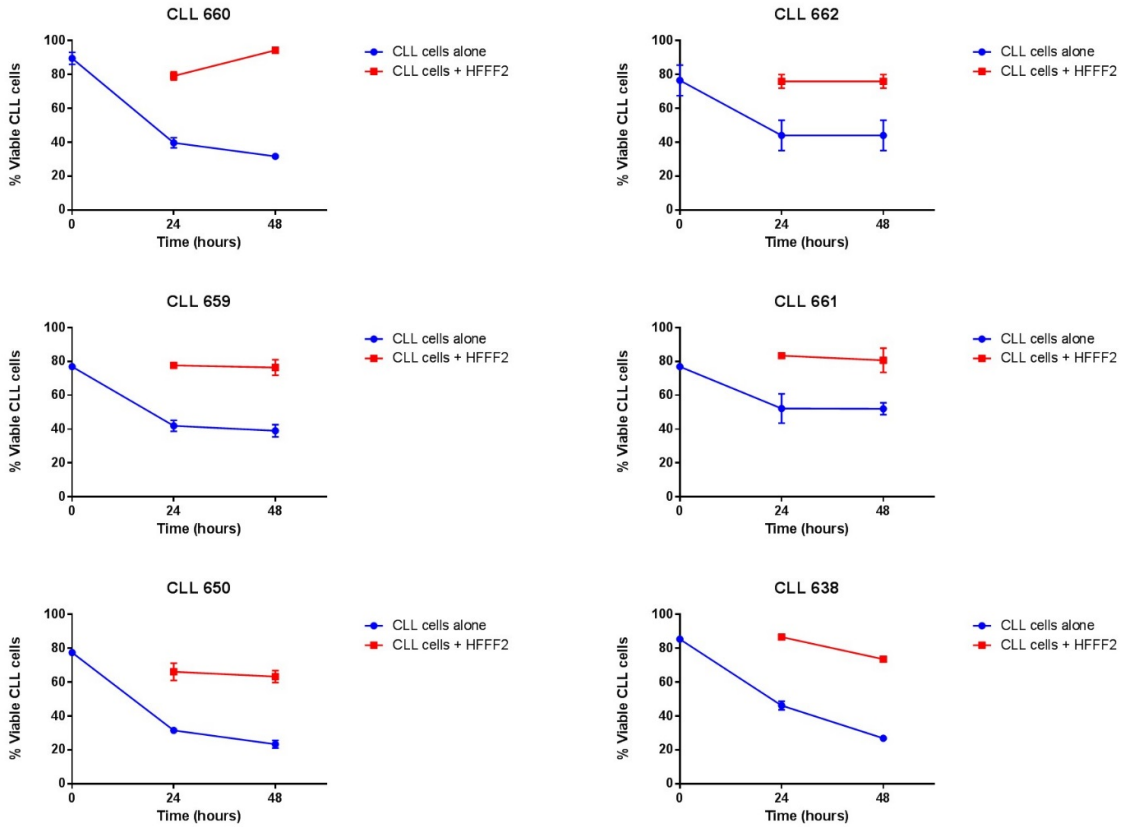

FIGURE 3-3: EFFECT OF HFFF2 CO-CULTURE ON CLL CELL SURVIVAL

Viability results for six representative CLL patients. CLL samples were cultured alone (blue line) or in the presence of HFFF2 fibroblasts (red line) for 0, 24 or 48 hours prior to analysis of CLL cell viability. Cell viability was measured by Annexin-V/PI staining with gating as outlined in Figure 3-1. Analysis and graphs created using Graphad prism 6.

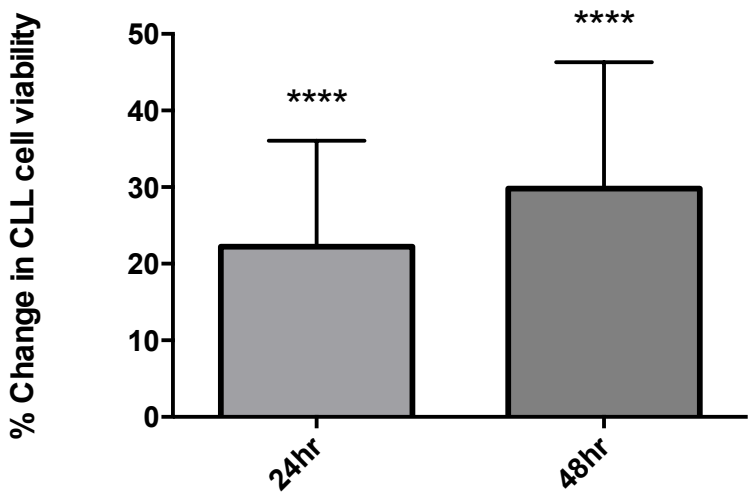

FIGURE 3-4: EFFECT OF HFFF2 CO-CULTURE ON CLL CELL SURVIVAL

Summary of data for all samples analysed (n=42). Due to the variation in rates of spontaneous apoptosis between CLL samples data were corrected to show percent change in CLL cell viability for CLL cells co-cultured with fibroblasts compared to CLL cells cultured alone. Statistical significance is indicated (Wilcoxon Test; ****P=<0.0001) the percentage change in CLL viability was compared to CLL cell cultured alone at the same time point. Error bars are SD. Analysis and graphs created using Graphad prism 6.

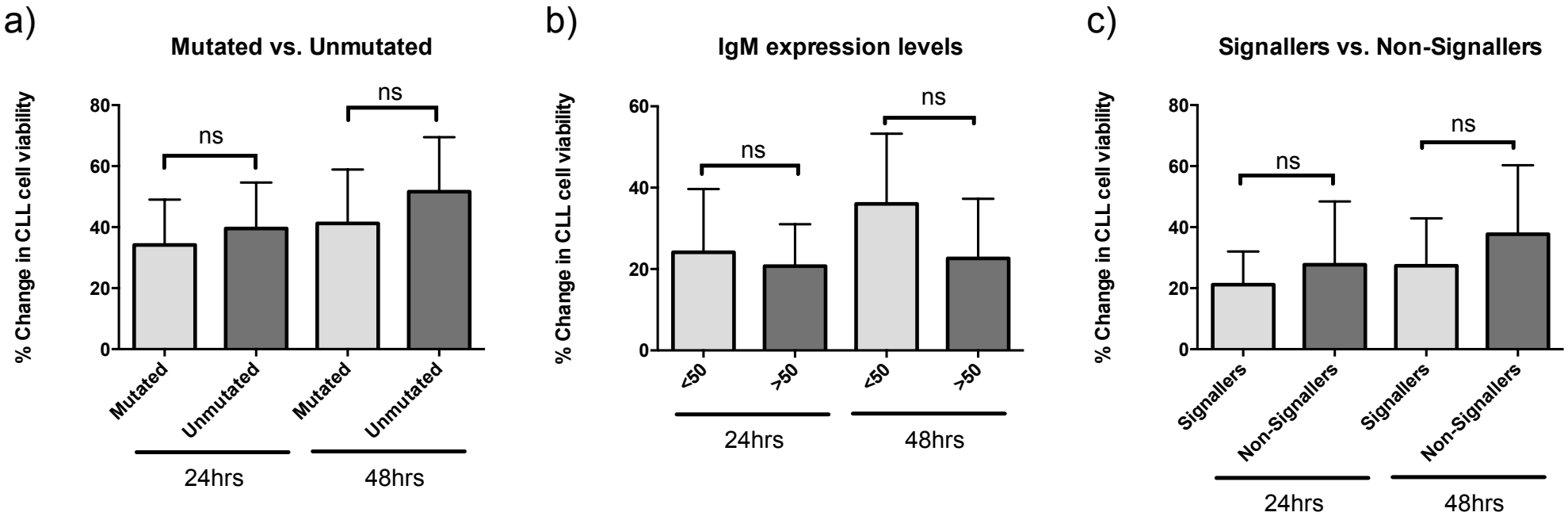

FIGURE 3-5: COMPARISON OF HFFF2-CYTOPROTECTION LEVELS BETWEEN DIFFERENT CLL PROGNOSTIC SUBGROUPS

Summary of data for all samples analysed (n=42). CLL samples were split into different prognostic subgroups as per Figure 3-2 and percentage change in CLL cell viability was plotted for each group for both 24 and 48 hours. Analysis and graphs created using Graphad prism 6.

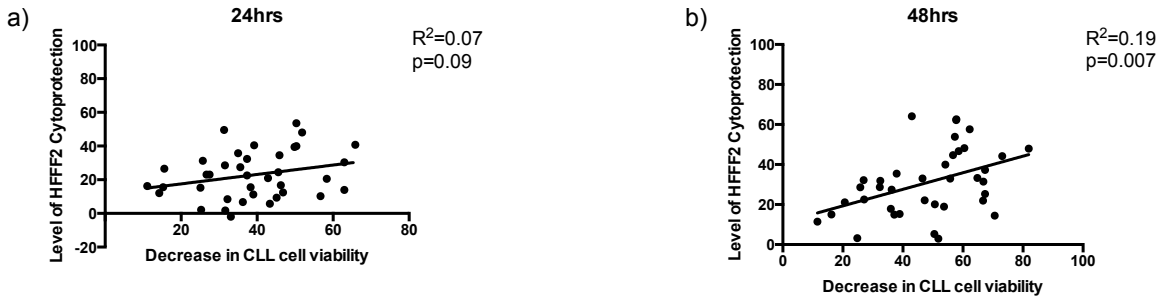

FIGURE 3-6: CORRELATION BETWEEN SPONTANEOUS APOPTOSIS AND HFFF2-CELL-MEDIATED CYTOPROTECTION AT 24 AND 48 HOURS

Correlation analysis was carried out using linear regression for the levels of spontaneous apoptosis (normalised values from Figure 2) and levels of HFFF2 cytoprotection (normalised values from Figure 4). R values and P values are indicated on each individual graph. Analysis and graphs created using Graphad prism 6

3.5 Primary lymph node fibroblasts protect CLL cells in a similar way to the HFFF2 cell line

Although the HFFF2 cell line is widely used for researching fibroblasts and fibroblast transdifferentiation (Moutasim et al., 2009, Frampton et al., 2015, Bhome et al., 2015), its suitability for investigating CLL/stroma interactions could be limited due to the fact that these cells are derived from the skin. We therefore performed comparative experiments using primary fibroblasts derived from a healthy LN. The cells that grew out of the LN tissue were thin and spindle-shaped typical of the morphology of fibroblasts (Figure 3-7). Preliminary experiments also analysed expression of the myofibroblast marker α-SMA following treatment with TGF-β which is a known inducer of transdiffrentiation *in vitro* (Figure 6). These initial experiments along with the cell morphology helped confirmed that the cells being used in these experiments where fibroblasts.

Viability studies using Annexin-V/PI staining were repeated using the LN-derived fibroblasts using identical cell numbers and experimental conditions as tested for HFFF2 cells. The experiment was performed using two different CLL samples (both U-CLL). Similar to HFFF2 cells, LN fibroblasts protected CLL cells from spontaneous apoptosis at both 24 and 48 hours (Figure 3-8). Therefore, the protective effect of HFFF2 cells also appears to be a property of LN-derived fibroblasts. However, experiments using LN-derived cells were particularly demanding, due to difficulties in cell culture, and future experiments were performed using HFFF2 cells

.

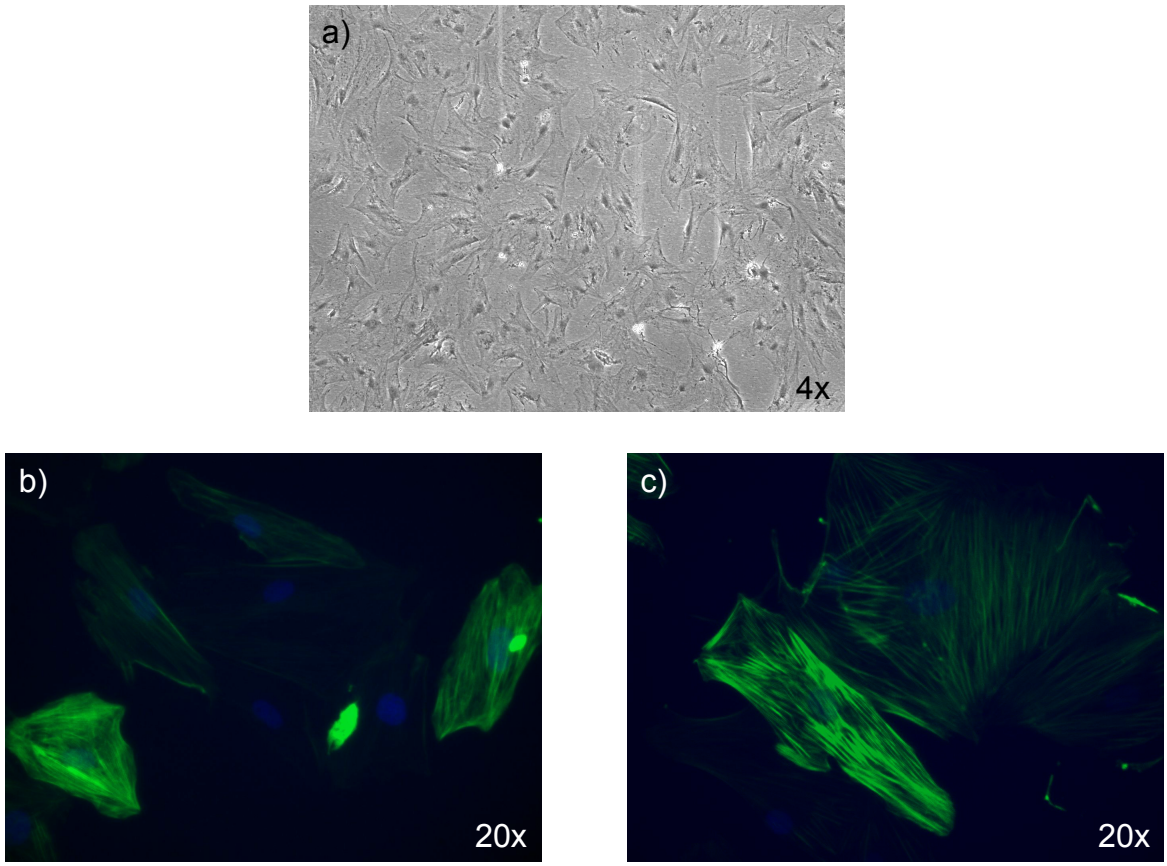

FIGURE 3-7: CHARACTERISATION OF LYMPH NODE FIBROBLASTS

(a) Adherent cells that grew out of the healthy lymph node (LN) tissue were imaged to check their morphology. Images were taken at 4x (b,c) Fibroblasts were seeded into 6 well plates and left to adhere and spread. After 24 hours media was replaced with either C.DMEM or C.DMEM supplemented with 2ng/ml TGF-β. After 72 hours cells were stained with DAPI to detect live cells (blue) and α-SMA (green) and immunofluorescence was carried out on cells cultured alone (b) or in the presence of 2 ng/ml TGF-β (c). Images were taken at 20x

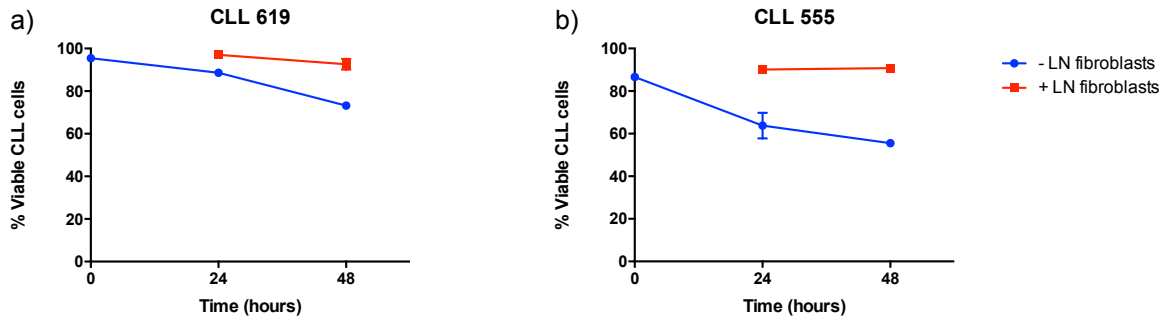

FIGURE 3-8: EFFECT OF PRIMARY LYMPH NODE FIBROBLAST CO-CULTURE ON CLL CELL SURVIVAL

CLL cells were cultured alone (blue line) or in the presence of LN fibroblasts (red line) for 0, 24 or 48 hours prior to analysis of CLL cell viability. Cell viability was measured by Annexin-V/PI staining with gating as outlined in Figure 3-1. Results are shown for two patients' samples. Analysis and graphs created using Graphad prism 6.

3.6 HFFF2-cytoprotection occurs in a contact-independent manner

I next investigated whether the cytoprotection provided by the HFFF2 fibroblasts occurred via direct contact or through soluble factors. This is a particularly important question, especially in determining how mechanisms might differ in 3D co-culture systems where different cell:cell interactions may form. HFFF2-derived CM was generated by collecting HFFF2 culture supernatant (Methods Section2.1.4.2).

3.6.1 Generation of HFFF2-derived CM

Preliminary experiments determined whether HFFF2-derived CM was capable of providing protection to CLL cells. Three time-points were used to generate the CM in these early experiments, to investigate, which, if any provided the greatest protection to CLL cells. HFFF2 cells were therefore cultured for either 24, 48 or 72 hours before culture supernatant was collected to generate HFFF2-derived CM. Care was taken to ensure that supernatant was collected when HFFF2 cells (i) were still attached to the tissue culture, (ii) were not over confluent and (iii) appeared healthy with similar morphology as seen in other cultures. The supernatant was centrifuged twice to ensure any detached cells or cell fragments were removed.

Cells from two CLL samples (CLL 513 and CLL 661) were cultured alone or in the presence of HFFF2-derived CM and viability was assessed at time of recovery (0 hours), and at 24 and 48 using Annexin-V/PI staining (as outlined in Section3.4). All CM protected CLL cells from spontaneous apoptosis in the two patients tested, with perhaps the greatest protection afforded by the CM collected from 72 hour HFFF2 cell cultures, especially at the later time point of analysis (48 hours) (Figure 3-9). Large error bars in Figure 9b are largely due to the two patients having differing levels of spontaneous apoptosis. Therefore 72 hours was used to generate HFFF2-CM for all experiments.

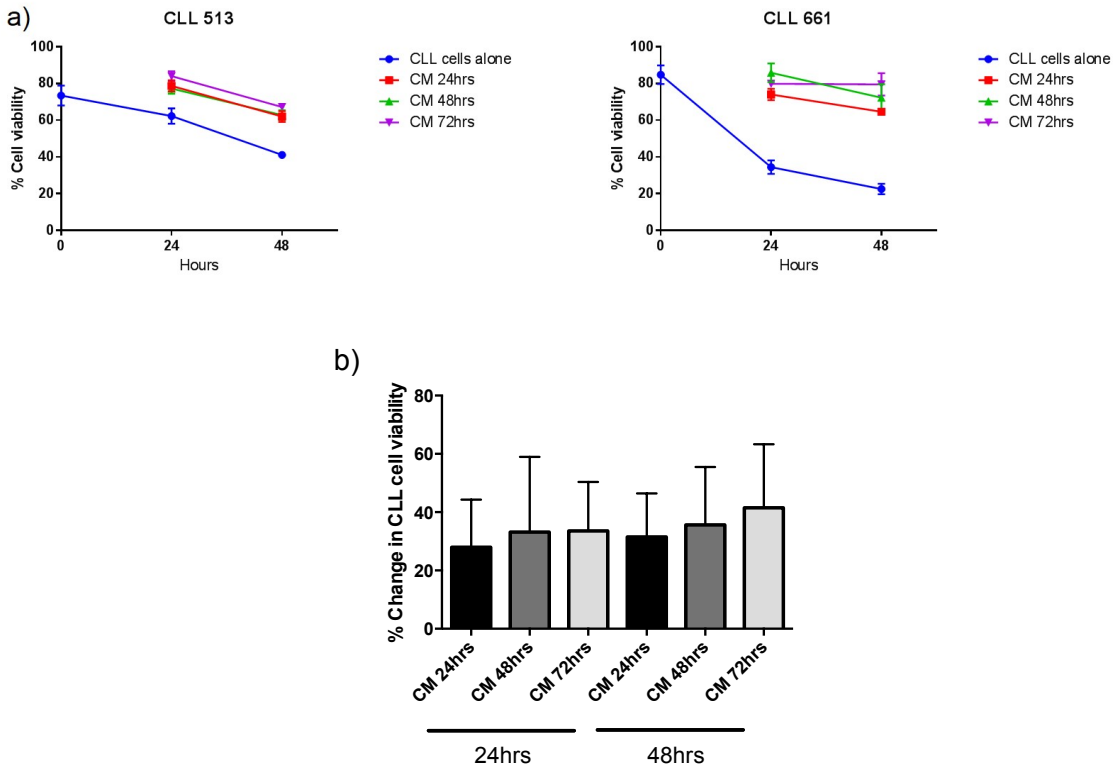

FIGURE 3-9: COMPARISON OF DIFFERENT HFFF2 CULTURE PERIODS USED TO GENERATE HFFF2-DERIVED CM

HFFF2 cells were cultured for either 24, 48 or 72hrs before culture supernatant was collected to generate HFFF2-derived CM. (a) CLL cells were cultured alone (blue line), in the presence of HFFF2-derived CM generated for 24hrs (red line), 48hrs (green line) or 72hrs (purple line) for 0, 24 or 48 hours prior to analysis of CLL cell viability. Cell viability was measured by Annexin-V/PI staining with gating as outlined in Figure 1. (b) Combined results for two patients tested. Due to the variation in rates of spontaneous apoptosis between CLL samples data were corrected to show percentage change in CLL cell viability for CLL cells cultured in the presence of the different HFFF2-derived CM compared to CLL cells cultured alone. Error bars are SD. Analysis and graphs created using Graphad prism 6.

3.6.2 Ability of HFFF2-derived CM to protect CLL cells from spontaneous apoptosis

The data obtained from the first two CLL patients indicated that HFFF2-cytoprotection occurred in a contact-independent way. The cohort of patients was expanded to 24 patients. Samples were a mixture of U/M-CLL, generally comprised ≥70% CD5+CD19+ cells (apart from three samples 674, 656 and 577a; AppendixA) and had a range of signalling capabilities and surface IgM expression. CLL cells were cultured alone or in the presence of HFFF2-CM. As with previous survival experiments viability was measured at time of recovery (0 hours) and 24 and 48 hours. CLL cells were also directly co-cultured with HFFF2 as a control and for comparison between the two culture conditions. As before, data were corrected to show percentage increase in cell viability for CLL cells co-cultured with fibroblasts or CM compared to CLL cells cultured alone to allow for variation in spontaneous apoptosis between patients. Results from six representative patients are shown in Figure 3-10. Overall, HFFF2 cell-derived CM suppressed spontaneous apoptosis in all samples. The protective effect of CM was similar to HFFF2 cell co-culture in 4/6 samples tested in parallel, but appeared less effective in the other two samples.

The results demonstrated that CM protected all CLL samples from spontaneous apoptosis at both time points, although, again, there was substantial inter-sample variation in the extent of protection (Figure 3-11). Similar to direct co-culture, there was not significant difference in extend of CM-mediated protection between different disease subsets (Figure 3-12).

3.6.3 Direct comparison between direct co-culture and CM

Parallel data for HFFF2 CM-mediated and direct co-culture-mediated CLL cell protection was available for all 24 samples analysed in the CM experiments, allowing direct comparison between the two culture methods (Figure 3-13). At 24 hours, interestingly there was a significant increase in the protection provided by HFFF2-CM. However, by 48 hours here was no significant difference in the extent of cytoprotection provided by the two experimental conditions.

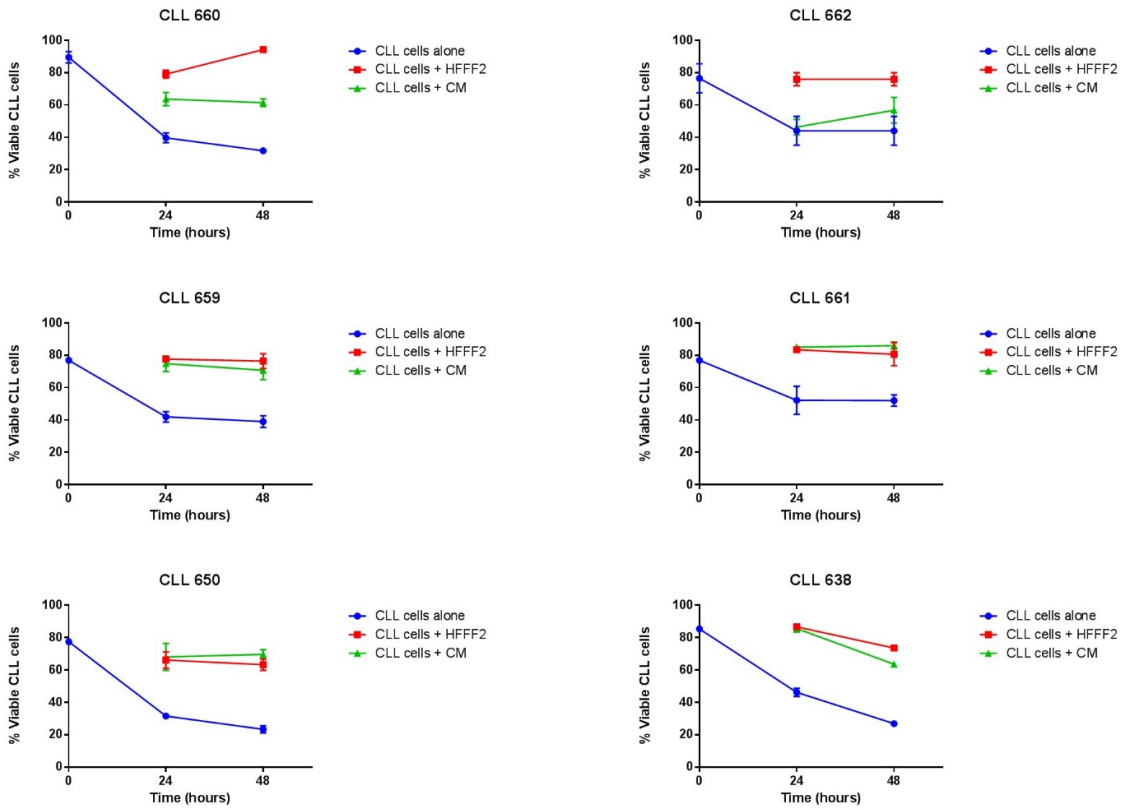

FIGURE 3-10: EFFECT OF HFFF2-DERIVED CM ON CLL CELL SURVIVAL

Viability results for six representative CLL patients. CLL cells were cultured alone (blue line), in the presence of HFFF2 fibroblasts (red line) or in the presence of HFFF2-derived CM (green line) for 0, 24 or 48 hours prior to analysis of CLL cell viability. Cell viability was measured by Annexin-V/PI staining with gating as outlined in Figure 3-1. HFFF2-CM was derived for 72hours. Analysis and graphs created using Graphad prism 6.

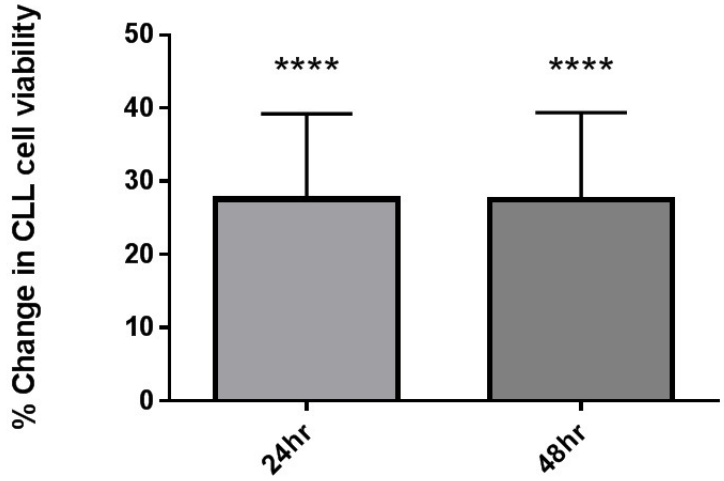

FIGURE 3-11: EFFECT OF HFFF2-DERIVED CM ON CLL CELL SURVIVAL

Summary of data for all samples analysed (n=24). Due to the variation in rates of spontaneous apoptosis between CLL samples data were corrected to show percentage change in CLL cell viability for CLL cells cultured in the presence of HFFF2-derived CM compared to CLL cells cultured alone. Statistical significance is indicated (Wilcoxon Test; ****P=<0.0001). Error bars are SD. Analysis and graphs created using Graphad prism. 6.

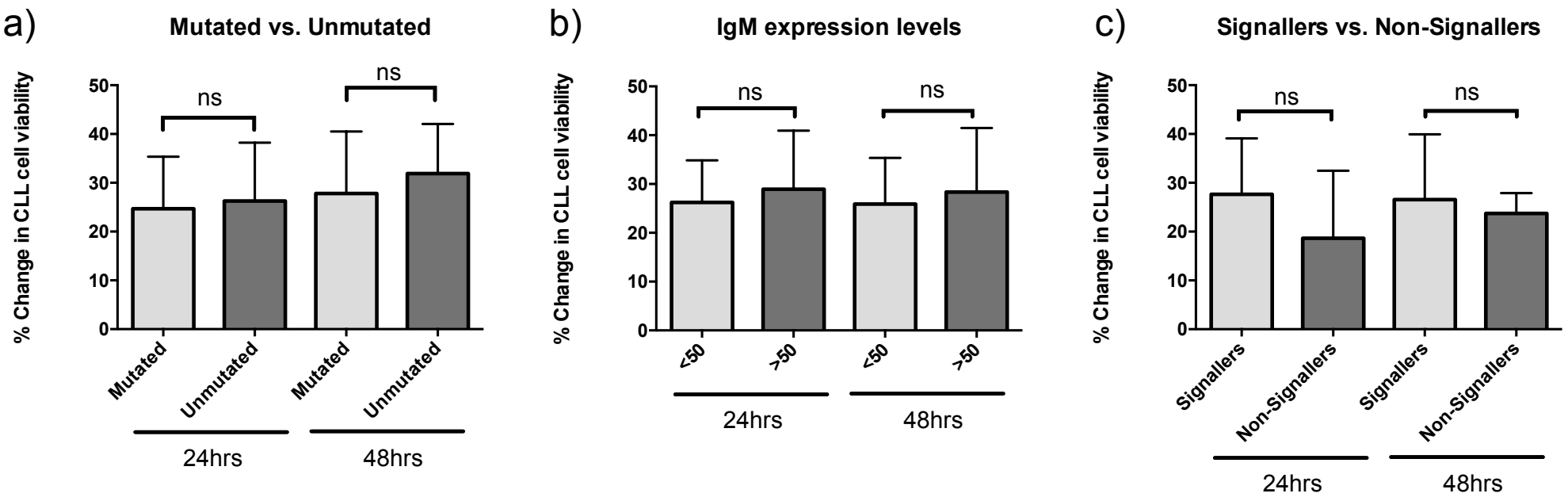

FIGURE 3-12: COMPARISON OF HFFF2-DERIVED CM PROTECTION LEVELS BETWEEN DIFFERENT CLL DISEASE SUBSETS

Summary of data for all samples analysed (n=24). CLL samples were split into different prognostic subgroups as per Figure 3-2 and percentage change in CLL cell viability was plotted for each group for both 24 and 48 hours. Analysis and graphs created using Graphad prism 6.

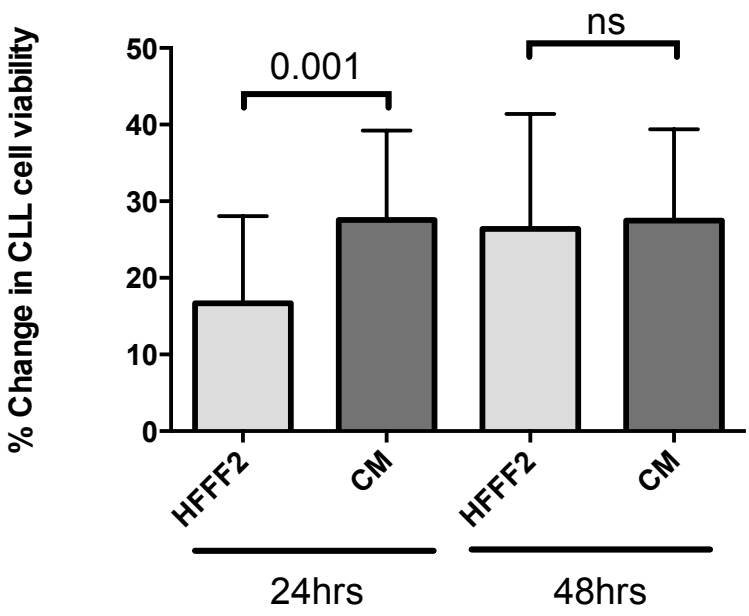

FIGURE 3-13: COMPARISON OF PROTECTION TO CLL CELLS BETWEEN HFFF2 DIRECT CO-CULTURE AND HFFF2-DERIVED CM

Summary of data for all samples analysed for HFFF2 direct contact and HFFF2-derived CM (n=24). Percentage change in CLL viability is plotted. Statistical significance is indicated (Wilcoxon Test; ns = non-significant). Error bars are SD. Analysis and graphs created using Graphad prism 6.

3.6.4 HFFF2 cells protect CLL cells from spontaneous apoptosis through a microporous membrane

To further investigate the potential role of soluble factors in the support of CLL cells in vitro, additional experiments were performed using microporous membranes to separate the two cell types. HFFF2 cells were seeded into tissue culture wells and CLL cells were added either directly on top of the HFFF2 cells (i.e. co-culture) or into a transwell chamber with a 5μm membrane preventing direct contact between the two cell types. CLL cells were also cultured alone in a normal 48 well plate or in the transwell chamber without underlying HFFF2 cells as additional controls. CLL cell viability was quantified using Annexin-V/PI staining. Four representative patients are displayed in Figure 3-14. Figure 3-15demonstrates corrected data to show the percentage increase in CLL cell viability which indicates that, consistent with the CM data, HFFF2 cells separated from CLL cells via a membrane protect CLL cells from spontaneous apoptosis (P=0.006 and P=0.008 at 24 and 48 hours respectively).

The data obtained so far indicate that direct contact between the two cell types is not required for CLL cell protection to be observed. The difference in protection to CLL cells was compared between the three culture conditions (Figure 3-16). Figure 3-16 demonstrates corrected data to show the percentage increase in CLL cell viability which indicates, as observed previously, at 24 hours, there is a significant difference between direct co-culture and CM, which is not observed at 48 hours (P=0.006 and P=0.4). There is also a significant difference between CM and membrane separation at both timepoints (P=0.008 and P=0.04) and a significant difference between direct co-culture and membrane separation at 48 hours (P=0.02).

These data indicate that all three experimental conditions: direct cell contact, HFFF2-derived CM and microporous membrane separation, protect CLL cells from spontaneous apoptosis. Therefore these data indicate that protection from HFFF2 cells is to at least some extent mediated via soluble factor(s), secreted into the CM, which are able to diffuse through the membrane of a transwell plate. The results do show a significant difference between the protection seen from direct contact/CM and separation through a micro-porous, however the protection to CLL cells is still significant.

3.7 Summary of survival data

Overall, these experiments demonstrated the ability of the HFFF2 cell line to protect CLL cells from spontaneous apoptosis. The cytoprotection provided by the cell line was compared to that seen from primary LN fibroblasts, a more physiologically relevant system and the protection was comparable. Large heterogeneity was observed in the cytoprotection provided to the CLL cell however there was no obvious differences between subsets or other prognostic subgroups. Further to this, CM and transwell plate experiments demonstrate that the protection from the HFFF2 cell line is mediated at least in part via soluble factors. Overall, the results obtained so far confirms the suitability of the HFFF2 cell line for survival measurements in 3D models.

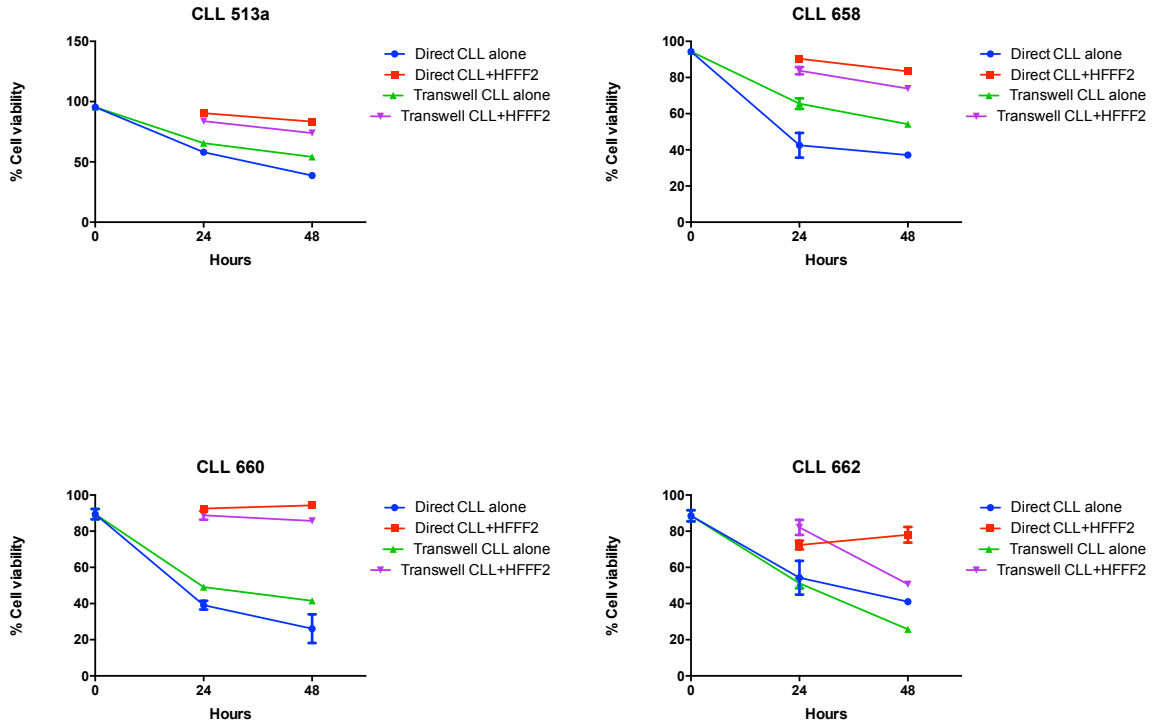

FIGURE 3-14: EFFECT OF HFFF2-CYTOPROTECTION FOLLOWING SEPARATION OF BOTH CELL TYPES BY A MICROPOROUS MEMBRANE

Viability results for four representative CLL patients. CLL cells were cultured alone (blue line), in the presence of HFFF2 fibroblasts (red line) or in the presence of HFFF2 separated by a 5µm microporous membrane (purple line) for 0, 24 or 48 hours prior to analysis of CLL cell viability. Cell viability was measured by Annexin-V/PI staining with gating as outlined inFigure 3-1. CLL cells cultured in the transwell chamber were included as a control (green line) to account of any effect from cultured in the chamber itself. Analysis and graphs created using Graphad prism 6.

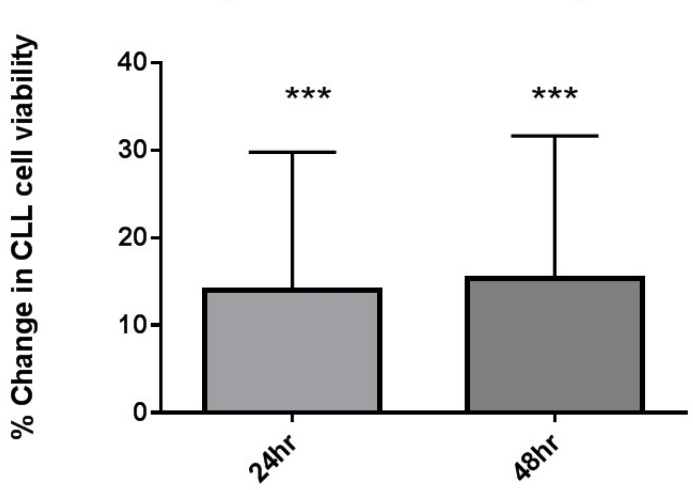

FIGURE 3-15: EFFECT OF HFFF2-CYTOPROTECTION FOLLOWING SEPARATION OF BOTH CELL TYPES BY A MICROPOROUS MEMBRANE

Summary of data for all samples analysed (n=17). Due to the variation in rates of spontaneous apoptosis between CLL samples, data were corrected to show percent change in CLL cell viability for CLL cells cultured in the presence of HFFF2 cells either direct or separated compared to CLL cells cultured alone. Differences were calculated using the appropriate CLL alone control (CLL alone in Tranwells vs. HFFF2 separated by membrane) Statistical significance is indicated (Wilcoxon Test; 24 hour ***P=0.006 and 48 hour *** P=0.008). Error bars are SD. Analysis and graphs created using Graphad prism 6.

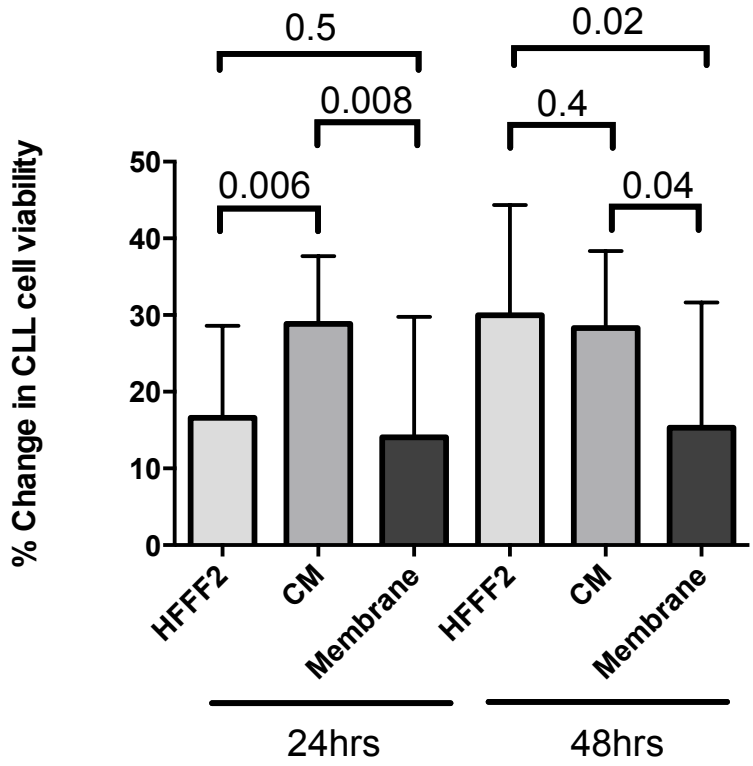

FIGURE 3-16: COMPARISON OF THE ABILITY OF DIFFERENT CULTURE METHODS USING THE HFFF2 CELL LINE TO PROVIDE PROTECTION FROM SPONTANEOUS APOPTOSIS TO CLL CELLS

Summary of data for all samples analysed for HFFF2 direct contact and HFFF2-derived CM and microporous membrane separation (n=17). Percentage change in CLL viability is plotted. Statistical significance is indicated (Wilcoxon Test; individual pvalues are shown on the graph). Error bars are SD. Analysis and graphs created using Graphad prism 6.

3.8 Characterisation of the HFFF2 cell line

Having confirmed the suitability of the HFFF2 cell line for enhancing CLL cell survival, and identifying a substantial role for soluble factors, the final goal was to complete additional characterisation prior to embarking on the development of acoustic devices for 3D co-culture experiments using this cell line. In particular, it was important to confirm that these cells could undergo a controlled transdifferentiation to myofibroblasts. For example, a secondary aim of the microdevices could be to investigate the effect of acoustic forces on transdifferentiation in these cells, in the presence or absence of CLL cells.

HFFF2 cells are adherent cells derived from the foreskin of a 14-18 week old human foetus (ATCC). Consistent with this derivation, the cells adhered in culture and had a typical fibroblast morphology with a spindle shape. Moreover, the cells expressed low levels of alpha smooth muscle actin (α-SMA) a marker of transdifferentiation.

To confirm that HFFF2 cells could be induced to transdifferentiate, cells were treated with TGF-β (2 ng/ml), a known inducer of myofibroblast transdifferentiation, for 72 hours. 72 hours was chosen as a suitable time point due to the fact that treatment for this time is well documented to cause transdifferentiation (Desmouliere et al., 1993, Ronnov-Jessen and Petersen, 1993). Both immunoblot and immunofluorescence analysis revealed an increase in α-SMA expression in TGF-β treated cells, compared to control cells cultured for 72 hours without TGF-β (Figure 3-17 and Figure 3-18). For immunoblotting, a representable experiment is shown in Figure 3-17a and Figure 3-17b shows quantitation for multiple experiments (n=11). Moreover, immunofluorescence demonstrated that α-SMA was incorporated into stress fibres (Figure 3-18), a key feature of the differentiated myofibroblast (Gabbiani et al., 1971).

These data confirm that HFFF2 cells can be easily and consistently induced to transdifferentiate into myofibroblasts as well as remain undifferentiated during long term cell culture. To conclude, in addition to its effects on CLL cell survival, the HFFF2 cell line is also a useful model to investigate effects on transdifferentiation in the acoustic device.

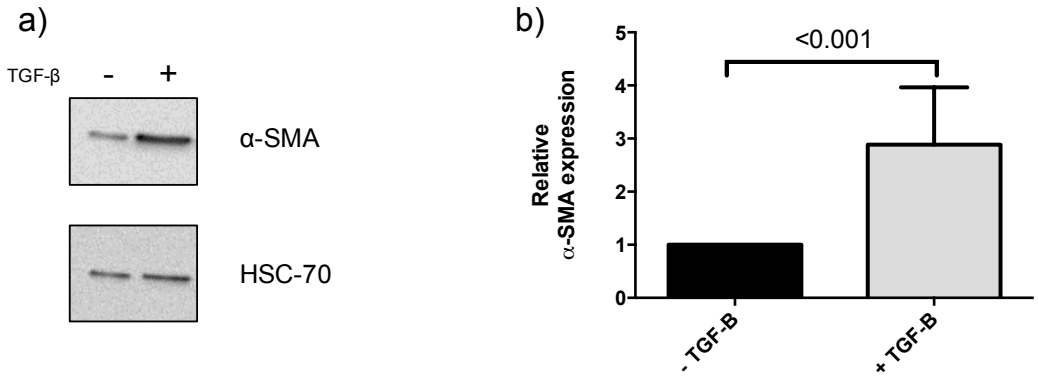

FIGURE 3-17: CHARACTERISATION OF THE HFFF2 CELL LINE

(a) Representative α-SMA western blot for one experiment. HFFF2 cells were seeded and treated in the same way as for immunofluorescence experiments prior to protein extraction and western blot analysis. (b) Data were first normalised to HSC-70 and then HFFF2 untreated control to show increase in α-SMA following treatment with TGF-β (n=11). Statistical significance of difference is shown (Wilcoxon test; ***P<0.001) Error bars displayed are standard deviation (SD).

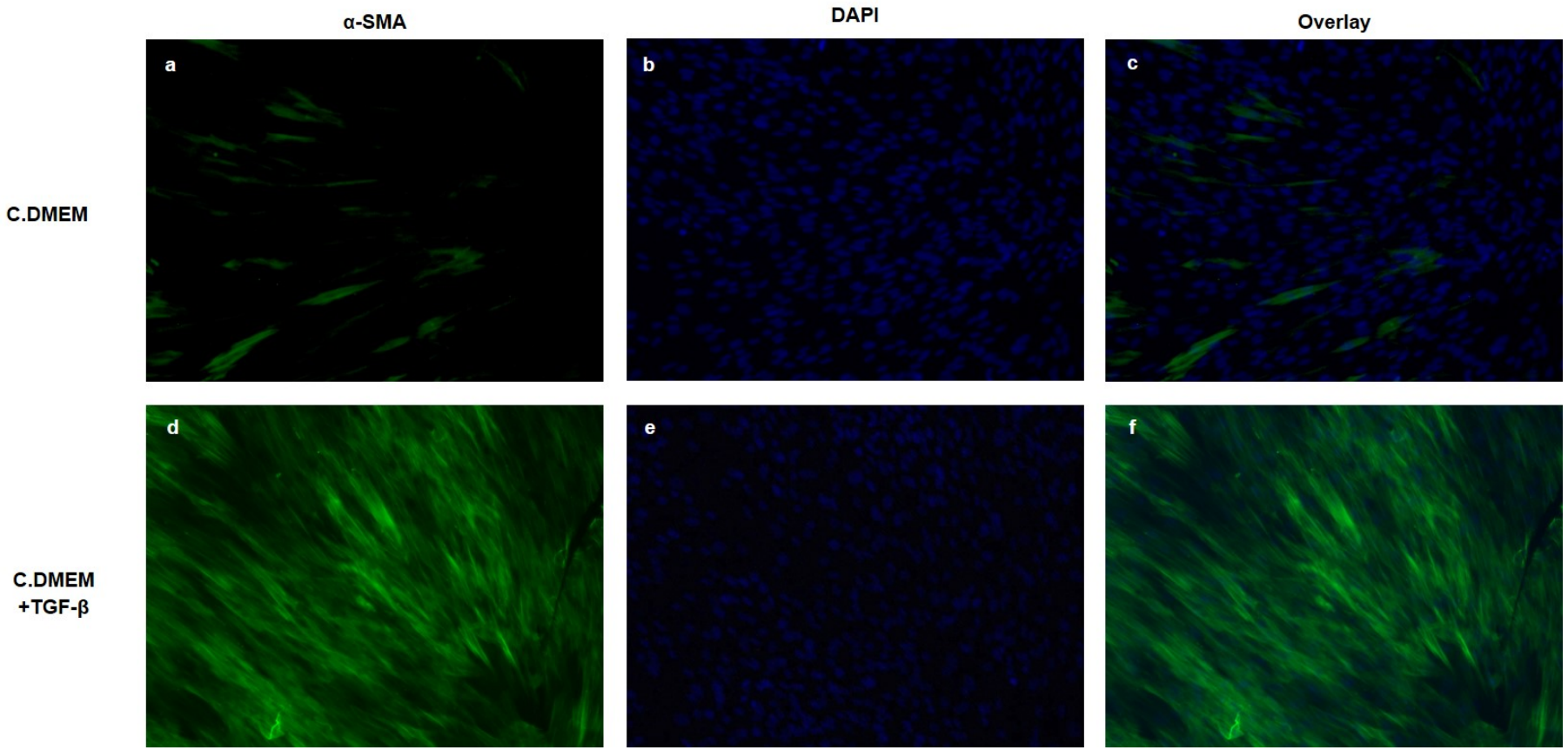

FIGURE 3-18: CHARACTERISATION OF THE HFFF2 CELL LINE

Representative images of HFFF2 immunofluorescence (n=11). HFFF2 cells were seeded into 6 well plates and left to adhere and spread. After 24 hours media was replaced with either C.DMEM or C.DMEM supplemented with 2ng/ml TGF-β. After 72 hours cells were stained with DAPI to detect live cells (blue) and α-SMA (green) and immunofluorescence was carried out on cells cultured alone (a,b,c) or in the presence of 2 ng/ml TGF-β (d,e,f). Images were taken at 4x.

3.9 Key Findings

- The HFFF2 cells protect CLL cells from spontaneous apoptosis
- Heterogeneity of the protective effects of HFFF2 cells is not related to major disease subsets such as *IGHV* mutations, surface IgM expression or sIgM signalling capability
- HFFF2 cells protect CLL cells in a contact-independent manner
- HFFF2 cells are able to undergo transdifferentiation and express α-SMA and stress fibres

3.10 Discussion

3.10.1 HFFF2 cells protect CLL cells from spontaneous apoptosis

To test for its suitability as a model for studying CLL cell and fibroblast interactions the HFFF2 cell line was initially tested for its ability to protect CLL cells from spontaneous apoptosis. Various cell types comprising the CLL microenvironment have been shown to positively regulate CLL cell survival including NLCs (Burger et al., 2000, Tsukada, 2002, Pedersen et al., 2002, Nishio et al., 2005, Burger et al., 2009b, Filip et al., 2013), MSCs (Lagneaux et al., 1999, Panayiotidis et al., 1996, Burger and Kipps, 2006, Kurtova et al., 2009, Ghia et al., 2005), FDCs (Burger et al., 2009a, Pedersen et al., 2002) and T cells (Patten et al., 2008). Many of the experiments carried out to date have been performed using poorly defined "stromal" cells. We have used the HFFF2 model as it is a relatively well-characterised cell line and a model we can modulate in the laboratory to transdifferentiate.

The first aim of this chapter was to further characterise the HFFF2 cell line to analyse its potential use in acoustic trapping devices. Since the ability of the HFFF2 cell line to protect CLL cells from spontaneous apoptosis had previously been demonstrated, my main goal was to extend the analysis to a larger cohort to probe for potential differences in response between cells from different subsets of disease. As documented in the literature there was substantial spontaneous apoptosis when CLL cells were cultured alone *in vitro* which differed substantially between individual patients' samples. Coscia et al., demonstrated using Annexin-V/PI staining that U-CLL are more prone to spontaneous apoptosis and more subjective to pro-survival signals from the microenvironment (Coscia

et al., 2011). In this data set there was a trend towards increased spontaneous apoptosis in U-CLL, but overall, responses between different disease subsets were not different.

Data obtained consistently demonstrated that the HFFF2 cell line is capable of protecting CLL cells at both 24 and 48 hours post recovery (Figure 3-4). As with the levels of spontaneous apoptosis there was also heterogeneity in the levels of cytoprotection provided by the HFFF2 cell line, indicating that some CLL samples are more dependent on the microenvironment than others. HFFF2-mediated protection was not clearly linked to disease subsets (Figure 3-5); rather, samples with the greatest levels of spontaneous apoptosis showed the strongest survival response to HFFF2 cells (Figure 3-6). The reasons for this are not clear. It may reflect a technical issue of quantitation of improved viability in samples where the overall levels of apoptosis are low. By contrast, it may reveal a functional link between susceptibility to spontaneous apoptosis *in vitro* and microenvironmental effects operating *in vivo.* Thus, those samples with the greatest susceptibility to spontaneous apoptosis may be those which are most receptive or dependent on microenvironmental signals *in vivo.* Identifying samples that are more dependent on stromal cells could help determine patients that could potentially benefit treatment strategies that directly target microenvironment interactions.

The mechanisms by which HFFF2 cells promote CLL cell survival were not studied, but are likely to involve changes in expression of BCL2 family proteins. In particular expression of the BCL2 family protein MCL1 is increased following IgM activation (Petlickovski et al., 2005, Bernal et al., 2001) or co-culture with FDC-derived cells (Pedersen et al., 2002). Work in our laboratory has shown that MCL1 expression is significantly higher in CLL cells that were cultured in fibroblast derived-CM compared to cells cultured in complete RPMI, after 8 and 24 hours of culture. Moreover, expression of the pro-apoptotic family protein Bim_{EL} is lower in CLL cells cultured in fibroblast derived CM compared to cells cultured in complete RPMI, after 8 and 24 hours of culture (Samantha Dias, PhD Thesis).

3.10.2 Suitability of the HFFF2 cell line as a model system for investigating CLL/microenvironment interactions

Although the HFFF2 cell line is widely utilised and characterised system for researching fibroblasts (Moutasim et al., 2009, Frampton et al., 2015, Bhome et al., 2015), its suitability to investigate CLL cell fibroblast interactions could be potentially limited due to the fact that these cells have been derived from the skin. As CLL cells do not accumulate in dermal tissue, we next aimed to see if we could utilise a more physiologically relevant

cell line. Bone marrow derived primary stromal cells (STRO-1 cells) isolated from patients undergoing hip replacements have previously been characterised in the laboratory (Samantha Dias, PhD thesis). However, the cell line was shown to spontaneously differentiate and were unstable *in vitro* so were therefore not a reliable model to investigate CLL cell/fibroblast interactions. It was next aimed to characterise fibroblasts from a healthy LN. These LN fibroblasts demonstrated the capability to promote CLL survival confirming that the response to HFFF2 cells is not a peculiarity of this cell line (Figure 3-8). However there was a low number of cells and the cells grew extremely poorly even after 21 days+ in culture. Due to this we can conclude that although more physiologically relevant they are not a feasible cell line to be used in future experiments optimising the acoustic trapping devices.

3.10.3 HFFF2 cells protect CLL cells in a non-contact dependent manner

I next aimed to determine whether protection from HFFF2 cells is mediated by direct contact or soluble factors. This is a particularly important question, especially in determining how mechanisms might differ in 3D co-culture systems where different cell:cell interactions may form. Therefore It was investigated whether HFFF2-mediated cytoprotection is mediated by direct contact or soluble factors through the use of HFFF2-derived CM, and separation of the two cell types by a microporous membrane. Many studies have shown that contact is required for other CLL microenvironment cells to protect CLL cells from spontaneous apoptosis (Lagneaux et al., 1999, Burger et al., 1999, Pedersen et al., 2002, Panayiotidis et al., 1996, Lagneaux et al., 1998). Several studies have shown that the protective effects of BMSCs require close proximity (Kurtova et al., 2009, Burger et al., 1999, Lagneaux et al., 1998) while Pederson et al., showed that FDCs rescue leukemic cells from spontaneous apoptosis, a process that is dependant by direct cell contact (Pedersen et al., 2002).

CM experiments indicated HFFF2-derived CM was adequate to protect CLL cells from spontaneous apoptosis (Figure 3-11) and further to this there was no significant difference between the protection from spontaneous apoptosis when CLL cells were cultured with HFFF2 derived CM in comparison to CLL cells cultured with direct contact with HFFF2 cells. Parallel data for HFFF2-CM-mediated and direct co-culture mediated CLL cell protection was available for all 24 patients analysed in the CM experiments, allowing for direct comparison between the two culture methods (Figure 3-12). At 24 hours there was a significant increase in the protection provided by HFFF2-CM. However by 48 hours there was significant difference in the extent of cytoprotection although there was a trend for greater protection in the co-culture. Several studies have shown that CM was not

sufficient to protect CLL cells from spontaneous apoptosis. Pederson et al., demonstrated that CM derived from a FDC line was not adequate to protect CLL cells from spontaneous apoptosis (Pedersen et al., 2002) while Burger et al., showed that CM derived from CLL PBMC cultures did not improved the viability of CLL cells (Burger et al., 2000). However in line with the results seen in this project, Zhang et al., demonstrated that CM from HS-5 stromal cells was able to protect CLL cell viability (Zhang et al., 2012).

When other studies have investigated the need for contact between cells types in the CLL microenvironment, many have used microporous membranes to separate the different cell types. It was aimed to replicate these experiments by culturing CLL cells and HFFF2 separated by a microporous membrane containing 5μm pores. Results indicated that although there was a decrease in protection when compared to direct contact, HFFF2 cells were still able to protect CLL cells from apoptosis through the membrane (Figure 3-15). These results are indicative that the protection is at least partially due to a soluble factor that is able to pass through the 5μm pores. The decrease seen in protection could be due to CLL cells not being 'happy' cultured in the transwell inserts. There may also be unstable proteins which would not be present in the HFFF2-derived CM. Several studies have conversely shown that separation by a membrane is enough to inhibit the protection from stromal cells (Lagneaux et al., 1999, Pedersen et al., 2002, Panayiotidis et al., 1996, Lagneaux et al., 1998). Lagneux et al., showed that microporous membrane not only blocked the protective effect of stromal cells but strikingly, the percentage of apoptotic cells was increased (Lagneaux et al., 1999). This observation suggests that the cell line used for those experiments secretes a soluble factor that can diffuse through the membrane and is able to induce apoptosis. Conversely, Zhang et al., again was able to show that three different cell lines (HS-5, StromaNKtert, and KUSA-H1) were able promote CLL cell survival and conferred significant survival when CLL cells were treated with F-ara-A, oxaliplatin or H_20_2 when using a membrane to prevent direct contact supplementing the data observed in this experiment (Zhang et al., 2012). The conflicting results in the literature outline the importance of the model system chosen for experiment and highlights how different models provide support through different mechanisms.

3.10.4 Ability of HFFF2 cell line to transdifferentiate into myofibroblasts

Having confirmed the suitability of the HFFF2 cell line for enhancing CLL cell survival, and identifying a substantial role for soluble factors, the final goal was to complete additional characterisation prior to embarking on the development of acoustic devices for 3D co-culture experiments using this cell line. We therefore secondly aimed to demonstrate the

ability of the HFFF2 cell line to transdifferentiate into its activated counterpart the myofibroblast. It was important to determine whether the cell line was able to undergo controlled transdifferentiation as a secondary aim of the microdevices could be to investigate the effect of acoustic forces on transdifferentiation in these cells, in the presence or absence of CLL cells.

The HFFF2 cell line is a widely utilised and well-characterised system for researching both fibroblasts and myofibroblasts. One of the main key factors thought to induce natural transdifferentiation of HFFF2 cells is confluency (ATCC), and subsequently the cells were kept at around 60-80% confluency during the course of this project. Kept like this HFFF2 can be maintained in their undifferentiated phenotype for a few months until, eventually they will lose their fibroblast phenotype. The main features of transdifferentiation include an increase in α-SMA expression and the formation of stress fibres (Gabbiani et al., 1971, Darby et al., 1990). It is well documented that when HFFF2 cells are treated with TGF-β they consistently fully transdifferentiate into myofibroblasts within 48-72 hours (Moutasim et al., 2009, Frampton et al., 2015, Bhome et al., 2015). We first aimed to confirm these finding by culturing HFFF2 cells with and without TGF-β for 72 hours before carrying out western blotting and immunofluorescence to determine α-SMA expression. The results from Figure 3-17 and Figure 3-18 confirmed that TGF-β treated HFFF2 cells have a greater expression of α-SMA as shown by both western blot and immunofluorescence. The immunofluorescence also demonstrated the formation of stress fibres.

3.10.5 Final Comments

Although the HFFF2 cell line may not be the most physiologically relevant cell line for investigating CLL:microenvironmental interactions, this chapter has demonstrated the ability of the HFFF2 cell line to consistently protect CLL cells from spontaneous apoptosis. This protection was comparable to that seen from primary LN fibroblast, and levels are also comparable to what others have demonstrated in the literature. Further to this, CM and transwell plate experiments demonstrate that the protection from the HFFF2 cell line is mediated at least in part via soluble factors. I was unable to identify a link between the extent of HFFF2 cell –mediated protection and different disease subsets, however, use of an extended cohort did clearly show that cytoprotection was a general phenomenon observed in all samples. Overall, the results obtained confirmed the suitability of the HFFF2 cell line for use in the subsequent development of 3D culture models.

Chapter Four

Optimisation of acoustic trapping devices for modelling CLL/microenvironment interactions in three dimensions

Chapter 4: Optimisation of acoustic trapping devices for modelling CLL/microenvironmental interactions in three dimensions

4.1 Introduction

In the experiments described in this chapter, I investigated the potential utility of novel acoustic trapping devices to probe CLL/stromal cell interactions in 3D. These acoustic devices were initially developed in the Faculty of Engineering and the Environment at the University of Southampton and use ultrasound standing waves to 'levitate' cells away from interactions with solid tissue culture substrata (Introduction, Section1.6). Based on results described in the previous chapter, my studies of acoustic devices were performed using primary CLL cells and HFFF2 fibroblasts.

It has been known for many years that acoustic radiation forces influence the behaviour of particles in ultrasonic fields in both liquid and gaseous phases (Gröschl, 1998). The majority of work using such acoustic devices have studied cells in suspension and have demonstrated the movement of cells to the nodal plane of an US standing wave (Shi et al., 2009). Both single cells (Wu, 1991) and 2D cell aggregates (Bazou et al., 2005b) have been levitated or 'trapped' in this way. The behaviour of multiple cell types has been probed in these devices and formation of cell sheets has been observed for; neural cells (Bazou et al., 2005a); the prostate epithelial cell line, PZ-HPV-7 (Bazou et al., 2006a); the cancerous prostate epithelial cell line, DU-145 (Bazou et al., 2006a); chondrocytes (Bazou et al., 2006b, Li et al., 2014); and HepG2 liver hepatocellular carcinoma cells (Edwards et al., 2007). However, no studies have investigated "co-levitation" of two cell types in a single device. Therefore, an important goal of my study was to determine whether it was possible to find conditions in which both CLL and HFFF2 cells could be co-levitated despite the substantial difference in the size (and thus the influence of acoustic forces) of these two cell types.

Another important question for consideration is the potential direct influence of ultrasound waves on cell behaviour and viability. Several studies have investigated effects of US waves on cell viability and have not observed deleterious effects (Bazou et al., 2005b, Hultstrom et al., 2007, Evander et al., 2007). In addition, Bazou et al., examined the physical environment experienced by levitated neural cells in an acoustic trap by monitoring the temperature, acoustic streaming, pressure amplitudes, white noise and the inter-particular forces acting on the cells (Bazou et al., 2005b). Adverse effects or changes

on *in vitro* surface receptor interactions were not detected in these studies. However, it is clearly important to continue to consider effects of US on cell viability in these experiments, before moving on to detailed functional characterisation.

4.2 Hypothesis

CLL cells and HFFF2 can "co-levitate" in acoustic trapping devices forming a 3D mixed cell agglomerate that will be allow us to probe mechanisms of CLL/stromal cell interactions in follow-on studies.

4.3 Aims and objectives

The overall aim of this chapter was to determine the potential utility of acoustic trapping devices to probe CLL/stromal cell interactions in 3D. More specifically, I aimed to determine whether it is possible to find conditions in which both CLL and HFFF2 cells can be co-levitated. And finally, to determine whether there is any direct influence of US waves on CLL and HFFF2 cell viability or cell behaviour. The specific objectives of this chapter were:

- Investigate the ability of CLL and HFFF2 cells alone to levitate in an US standing wave within the acoustic trapping devices
- Investigate the ability of CLL and HFFF2 cells to 'co-levitate' in the acoustic trapping device
- Analyse formation of 3D structures within the devices
- Determine the viability of both cell types within the devices

4.4 Initial assessment of CLL and HFFF2 cell levitation in acoustic trapping devices

To determine the ability of CLL and HFFF2 cells to levitate in the acoustic trapping device, both cell types were individually injected into the device. Cells were visualised using fluorescent or visible light microscopy, including time-lapse imaging. Devices were set-up as outlined in the methods (Methods, Section2.6) and acoustic frequency was previously

determined and set. Devices were set at 6Vpp and due to the fact devices are found to have slightly different resonance frequencies as a result of manufacturing, a frequency sweep was used to enable us to drive all devices from one signal. A sweep frequency of 1.95Mhz to 2.12Mhz (steps of 50Hz) at a sweep rate of 0.05 seconds was chosen. The performance of each device was routinely confirmed before cell analysis by analysing levitation of fluorescent beads (not shown). These parameters were chosen based on previous cell work carried out in similar devices at the University of Southampton (Angela Tait, PhD thesis, Siwei Li, PhD thesis).

In the first experiments, primary CLL cells were fluorescently labelled with CFSE (15μM) and 20μl of a $7x10^6$ cell/ml suspension was injected into the acoustic trapping device using a gel loading tip. A high concentration of cells was used to firstly help visualisation and the basis that the more concentrated the injection solution was, the better chance of levitation and agglomerate formation. CLL samples were not selected based on any specific clinical features but analysis was restricted to samples with a high proportion of malignant ($CD5^+CD19^+$) B cells (>88%). The experiment also used standard complete RPMI with 10% FCS as the culture medium. CLL cells were successfully levitated in the device and within seconds of being injected cells started moving to the nodal plane where they formed several small agglomerates (Figure 4-1 and AppendixB, Video 1 and Video 2). The agglomerates remain levitated for a substantial period of time (~15 minutes) until the ultrasound generator was turned off and the cells sunk onto the glass slide at the bottom of the device.

These initial experiments uncovered some substantial technical difficulties, especially associated with introduction of cells into the device. Video 2 records some of these; Injection of cells was particularly difficult and accurate placing of the gel loading tip was important to ensure that cells are ‘caught’ by the ultrasound field and not injected out the other side of the transducer. Injection of cells directly under the centre of the transducer was also important to avoid loss of cells beyond the edges of the ultrasound field. It was also essential to remove the loading pipette very gently to prevent ‘pulling’ cells out of the ultrasound field; movement of cells during removal of the pipette can also be seen in Video 2.

Similar experiments were performed using CFSE-labelled HFFF2 cells. HFFF2 cells at the same concentration as above were also successfully levitated in the device using identical culture and ultrasound conditions as used for CLL cells (Figure 4-2). In contrast to CLL cells, HFFF2 cells tended to form a single, larger agglomerate.

These results demonstrate the ability of the device to not only successfully levitate both cell types under identical conditions, but also for the cells to form agglomerates. This was

particularly impressive due to the differing sizes of the two cell types and opened up the possibility of culturing both cell types together. At the time points analysed in these experiments (typically up to 15 minutes), agglomerates were generally planar and ~1-2 cells thick. However, there were differences in the size of agglomerates formed by the two cell types; the multiple agglomerates formed by CLL cells were typically much smaller than the single agglomerate formed by the HFFF2 cells. Differences in agglomerates between CLL and HFFF2 cells may be due to the difference in size of these cell types.

4.5 Co-levitation of CLL and HFFF2 cells

4.5.1 Optimisation of cell numbers injected into acoustic trapping devices

We next investigated the effect of co-injection of CLL and HFFF2 cells into the devices. In these experiments, as all this work was greatly experimental and lots of optimisation was required we varied the number of introduced cells to determine whether this influenced formation of CLL/HFFF2 cell co-agglomerates. For example, we hypothesised that higher initial cell densities could encourage cell packing following levitation and perhaps drive formation of a 3D agglomerate, rather than the planar structures observed in initial experiments. Therefore, I tested a range of cell concentrations in these experiments. The ratio of CLL to HFFF2 cells was maintained at 5:1 (as for other *in vitro* studies) and injections were performed using mixed cells at concentrations of $3x10^6$, $6x10^6$, $9x10^6$ and $18x10^6$ cells/ml. The volume injected was 20μl so the introduced total cell numbers were $6x10^4$, $1.2x10^5$, $1.8x10^5$ and $3.6x10^5$, respectively. Unfortunately, fluorescence imaging capacity was not available at the time of this study. Therefore, cells were imaged using light microscopy and the structure of the agglomerates was noted at times up to 5 minutes post-injection. A summary of observations is presented in Table 4.1.

Although agglomerates formed under all conditions, there appeared to be a substantial influence of cell numbers on agglomerate morphology. With higher cell numbers, agglomerates formed rapidly and appeared to be tightly packed. At lower cell numbers, agglomerates formed more slowly and appeared to be packed less densely. These results revealed the importance of cell concentration for effective formation of agglomerates and all further experiments were performed using the higher cell concentration tested here. However, even under these conditions, the formed agglomerates were predominantly planar, comprising bilayer structures, rather than more 3D “tissue-like” structures.

Although I was not able to individually track CLL and HFFF2 cells in this experiment, at most concentrations very few single cells were present suggesting that the agglomerates contained both cell types.

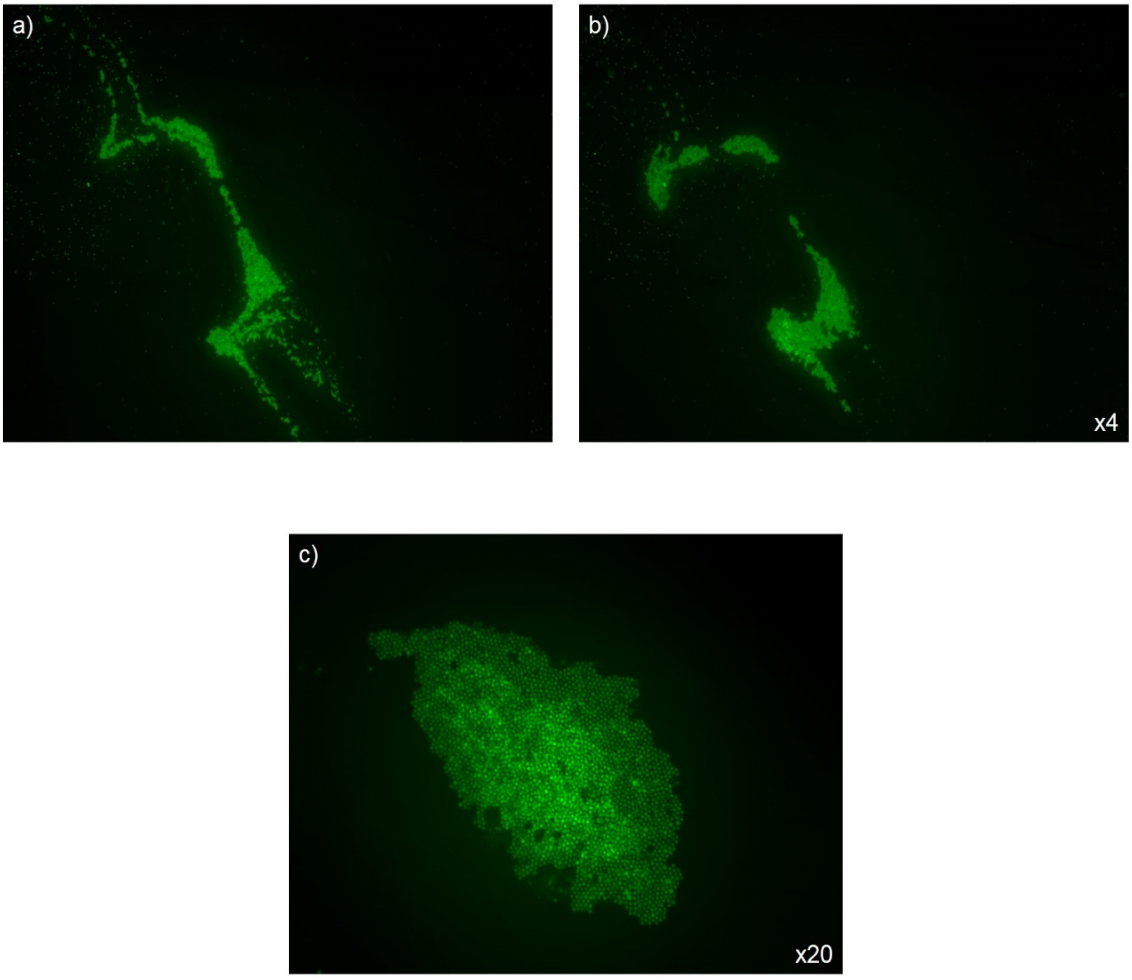

FIGURE 4-1: SHORT-TERM LEVITATION OF CLL CELLS IN ACOUSTIC TRAPPING DEVICE

CLL cells were fluorescently labelled with CFSE (15μM) and introduced into the acoustic trapping device. Images are representative of multiple experiments performed using various CLL samples and show (a) initial movement of cells towards nodal plane (~30 seconds, 4x original magnification) and (b,c) levitated CLL cell agglomerates (~ 5 minutes) at x4 and x20 original magnification respectively.

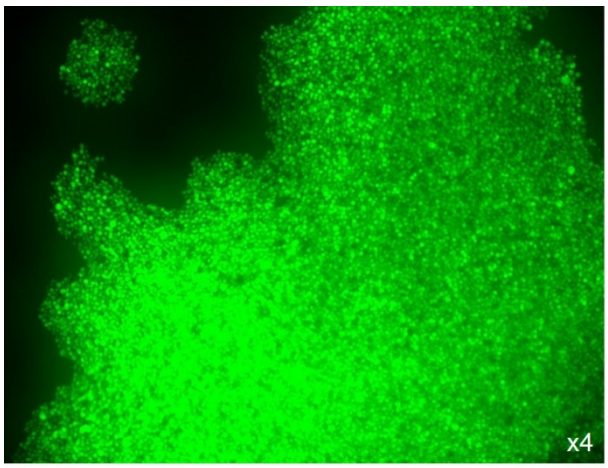

FIGURE 4-2: SHORT TERM LEVITATION OF HFFF2 CELLS IN ACOUSTIC TRAPPING DEVICE

HFFF2 cells were fluorescently labelled with CFSE (15μM) and introduced into the acoustic trapping device. Image is representative of multiple experiments and shows levitation and movement of HFFF2 cells towards the nodal plane after ~5 minutes. Original magnification 4x.

TABLE 4.1: SUMMARY OF MORPHOLOGY OF AGGLOMERATES FORMED IN THE ULTRASOUND DEVICES USING DIFFERENT INITIAL CELL CONCENTRATIONS

Cell concentration	Number of cell injected into devices	Morphology observations
$3x10^6$/ml	$6x10^4$ cells	Very slow forming agglomerate (~5mins) One very small agglomerate formed on the edge of the acoustic field. Agglomerate appeared loosely formed, with many voids between cell clusters. Cells formed two monolayer sheet, agglomerate appeared planar in nature.
$6x10^6$/ml	$1.2x10^5$ cells	Agglomerate formed quicker than $3x10^6$/ml concentration. Larger agglomerate formed in centre of acoustic field. Agglomerate still appeared loosely formed, with voids between cell clusters. Cells formed two monolayer sheets, agglomerate appeared planar in nature.
$9x10^6$/ml	$1.8x10^5$ cells	Agglomerate formed in less than ~1 minute of injection into devices. Large agglomerate formed in centre of acoustic field. Agglomerate tightly formed. Cells formed two monolayer sheets, agglomerate appeared planar in nature.
$18x10^6$/ml	$3.6x10^5$ cells	Agglomerate rapidly formed (~30secs). Large agglomerate formed in centre of acoustic field. Agglomerate tightly formed. Cells formed two monolayer sheets, agglomerate appeared planar in nature.

4.5.2 Co-levitation of CLL and HFFF2 cells using different fluorescent dyes

I next directly investigated whether CLL and HFFF2 cells could co-levitate, and whether the cells formed distinct or mixed agglomerates. CLL cells were labelled with CFSE and HFFF2 fibroblasts were labelled with CellTracker Red (5μM) allowing separate imaging of the two cell types. Cells were combined at a 5:1 ratio (CLL:HFFF2) and injected into the device using the higher cell concentration of $18x10^6$ cells/ml. Agglomerate formation was imaged in real-time using fluorescent microscopy. Images obtained at early time points (~5 minutes) revealed that CLL and HFFF2 co-levitated and accumulated in mixed agglomerates. These agglomerates also appeared to be planar with the two different cell types forming distinct, adjacent monolayer sheets. Interestingly, at later time points (~60 minutes), the CLL and HFFF2 cells appeared to have started to intermingle; the distinct planar cell layers were less apparent (Figure 4-3). This provided the first evidence of motility and potential interaction amongst the two cell types within the device. Future experiments therefore focused on longer levitation periods to determine whether this led to “restructuring” of agglomerates, using fluorescent dyes to separately track CLL and HFFF2 cells.

4.5.3 Co-levitation of CLL and HFFF2 cells at later time points

My next experiments were designed to investigate effects of longer (~hours) levitation times on CLL and HFFF2 cells. CLL cells and HFFF2 cells were fluorescently labelled as before and injected into acoustic trapping devices. Two devices were used, one contained CLL cells alone and one containing a mixture of CLL and HFFF2 cells. Agglomerates were allowed to form and then left levitating for 4 hours. At this time, agglomerates were observed in devices injected with both CLL cells alone and co-injected with CLL and HFFF2 cells (Figure 4-4). Overall, the agglomerates appeared similar to those observed at 60 minutes, although there was some indication of a slight compaction of the CLL cell-only agglomerate in this experiment. This decrease in size could be because the agglomerates are becoming sparser as edge-cells are no longer held by the acoustic field (and therefore lost from the agglomerate), or because the agglomerates are contracting and becoming more three-dimensional. Such a “contraction” phenomenon has been observed previously when 16-HBE (an epithelial cell line) cells were imaged using these devices (Angela Tait, PhD thesis).

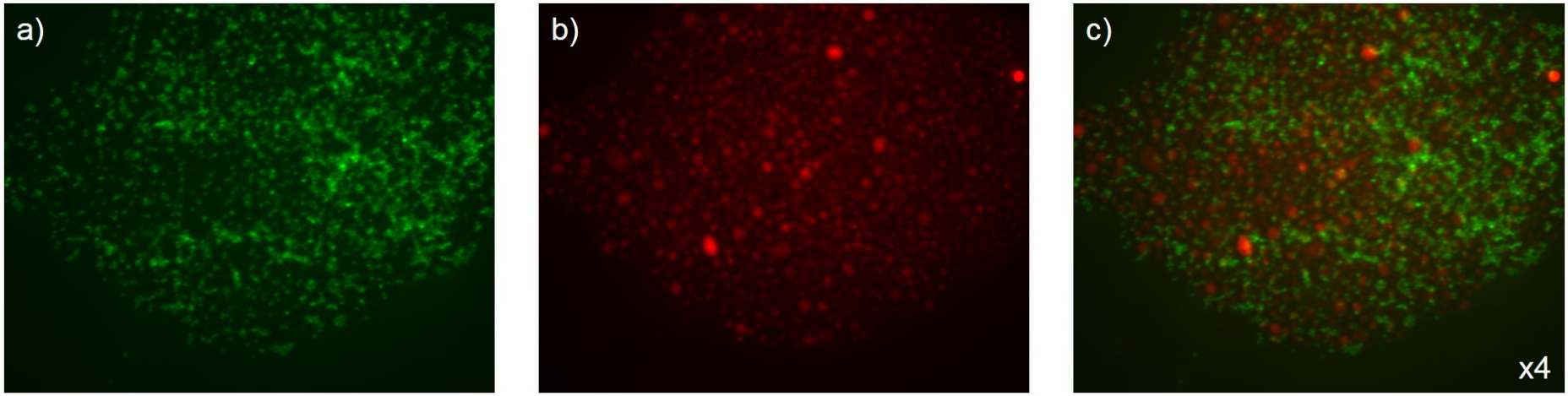

FIGURE 4-3: CO-LEVITATION OF CLL AND HFFF2 CELLS IN ACOUSTIC TRAPPING DEVICES

CLL and HFFF2 cells were labelled with CFSE or CellTracker Red, respectively, mixed at a 5:1 ratio, and introduced into the device. Images are representative of multiple experiments and show agglomerates of mixed CLL and HFFF2 cells at ~5 minutes. Original magnification x4. (a) CFSE fluorescence (CLL cells); (b) CellTracker Red (HFFF2 cells); and (c) merged images.

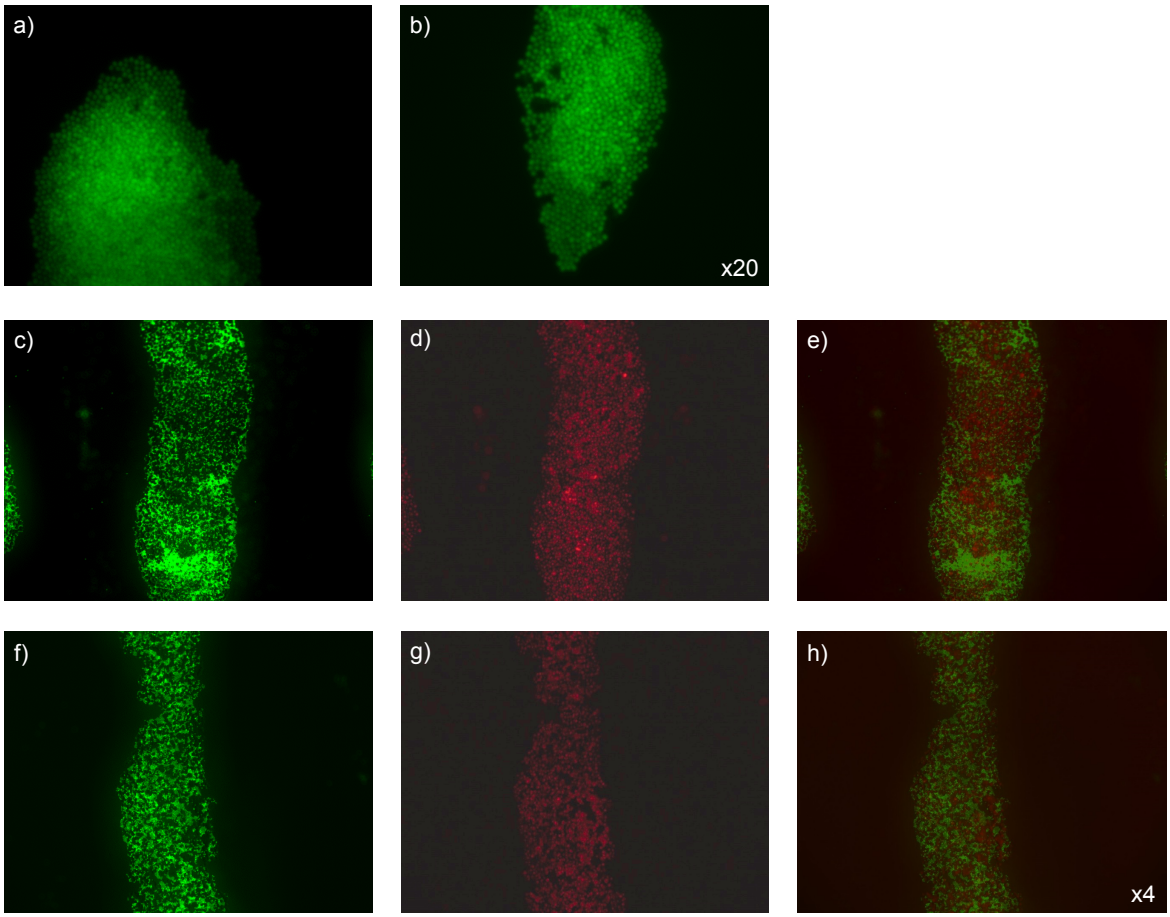

FIGURE 4-4: LEVITATION OF CLL CELLS IN THE ACOUSTIC TRAPPING DEVICE; 4 HOUR ANALYSIS

CLL cells and HFFF2 cells were fluorescently labelled with CFSE and CellTracker Red respectively and introduced into the acoustic trapping devices as CLL cells alone or a mixture of both cell types at a ratio of 5:1. (a) CLL cells at ~5 minutes and (b) 4 hours. Original magnification x20. CLL cells. A mixture CLL and HFFF2 cells were also injected simultaneously. (c-e) ~5 minutes and (f-h) ~4 hours. Original magnification x4. (c,f) CFSE fluorescence (CLL cells); (d,g) CellTracker Red (HFFF2 cells); and (e,h) merged images.

4.6 Effect of extended levitation on CLL and HFFF2 cells

These initial experiments provided encouragement that the acoustic devices could be used to model CLL/stromal cells interactions in 3D. However, biological communication is likely to take place over relatively extended periods of time. Indeed, maximal effects of HFFF2 on CLL cell survival in 2D culture required incubation periods of 48 hours or more (Chapter 3, Section3.6.2). Therefore, the next experiments investigated the effect of levitation time on agglomerate morphology up to 48 hours.

CLL cells were injected into the device alone or mixed with HFFF2 fibroblasts (at a 5:1 ratio) and agglomerates were imaged using the time-lapse facility on the Nikon eclipse Ti microscope. Unfortunately, fluorescent imaging was not available for this experiment. Therefore, cells were left unlabelled and imaging was performed using light microscopy. Images were taken at 30 minute intervals and the study was performed with parallel analysis of several devices to probe inter-device variability. These longer experiments revealed a number of practical difficulties with the devices. Power to the devices was temperamental, with devices failing half-way through experiments. Once power is lost to the devices, cells will no longer levitate and fall onto the cover slips. Once this had occurred there was no way to 'rescue' experiments, meaning a number of experiments were lost due to this technical issue. Another problem encountered was with the time lapse imaging. Fluorescent imaging was not available for these experiments and due to the structure of devices, on inverted microscopes the devices rely on natural light for imaging and tracking of agglomerates. A number of time lapse images could be lost due to simply issues like the room light being turned off. These are just a couple of practical issues encountered when running the devices. Others are discussed further in the discussion section of this chapter (Section 4.12)

Figure 4-5 shows results obtained for one representative patient sample (CLL 589) of 7 tested. The left hand panels of Figure 4-5 demonstrate agglomerates at the start of the experiment (ie, directly after formation of agglomerates). Similar to previous experiments, CLL cells appeared to form smaller multiple agglomerates. By contrast, mixed cell samples tended to form a single larger agglomerate similar to agglomerates formed by HFFF2 cells alone. The right hand panels of Figure 4-5 shows agglomerates after 48 hours of levitation and Video 3,4 and 5 shows the time-lapse imaging of the agglomerates. For CLL cells alone, the smaller agglomerates remained largely unchanged throughout this time period with only small amounts of possible contraction. By contrast, mixed agglomerates containing CLL and HFFF2 cells contracted substantially over this time

period. At 48 hours, the co-agglomerates appeared to have a dense core surrounded by a monolayer of cells. This morphology might be due to segregation of the two cell types with the HFFF2 cells forming the 3D core (similar to the agglomerate seen when HFFF2 cells are cultured alone) with a surrounding monolayer of CLL cells sheet. An alternate possibility is the agglomerate morphology shows separation of live and dead cells, with dead cells being 'ejected' from the agglomerate core.

Following these experiments, I investigated levitation of HFFF2 cells alone at times up to 48 hours, using the Nikon eclipse Ti microscope as described above (Figure 4-6 and Video 6). Similar to co-agglomerates of CLL and HFFF2 cells, HFFF2 cell-only agglomerates contracted over the incubation period resulting in a dense agglomerate with a significantly reduced cross-sectional area at 48 hours (Figure 4-6 n=7). However, in contrast to the mixed agglomerates, HFFF2 cell-only agglomerates lacked a surrounding monolayer of cells. This supports the idea that the structure observed previously in co-agglomerates of CLL and HFFF2 cells was due to segregation of cells, with HFFF2 cells comprising the dense core. This outlined one disadvantage of only using light microscopy. Fluorescent labelling of the two cell types would enable us to easily answer this question. Similar results were obtained in each the 7 independent experiments.

Overall, these results were encouraging and suggested that acoustic devices could be used to model CLL/stromal interactions in 3D. Despite substantial differences in cell sizes, both cell types could be levitated under identical conditions (see Figure 4-7 and Figure 4-8 for a summary of results). CLL cells alone formed multiple, small agglomerates which remained substantially unchanged at times up to 48 hours post-injection. HFFF2 cells alone, and mixtures of HFFF2 and CLL cells, formed an initial large agglomerate which contracted over time. Contraction appeared to begin at ~6 hours post-injection and stopped at ~24 hours. Whereas HFFF2/CLL cell co-agglomerates had a dense core surrounded by a "skirt" of cells in a thin layer, HFFF2 cells alone were maintained as a dense agglomerate lacking the surrounding monolayer of cells. Given these encouraging results, the next experiments were designed to investigate the viability of cells within the device. Previous studies of acoustic devices have not revealed significant effects of ultrasound on cell viability (Bazou et al., 2005b, Hultstrom et al., 2007, Evander et al., 2007, Ankrett et al., 2013). However, these studies only investigated responses at times up to 1 hour post-injection so analysis of later time points was critical.

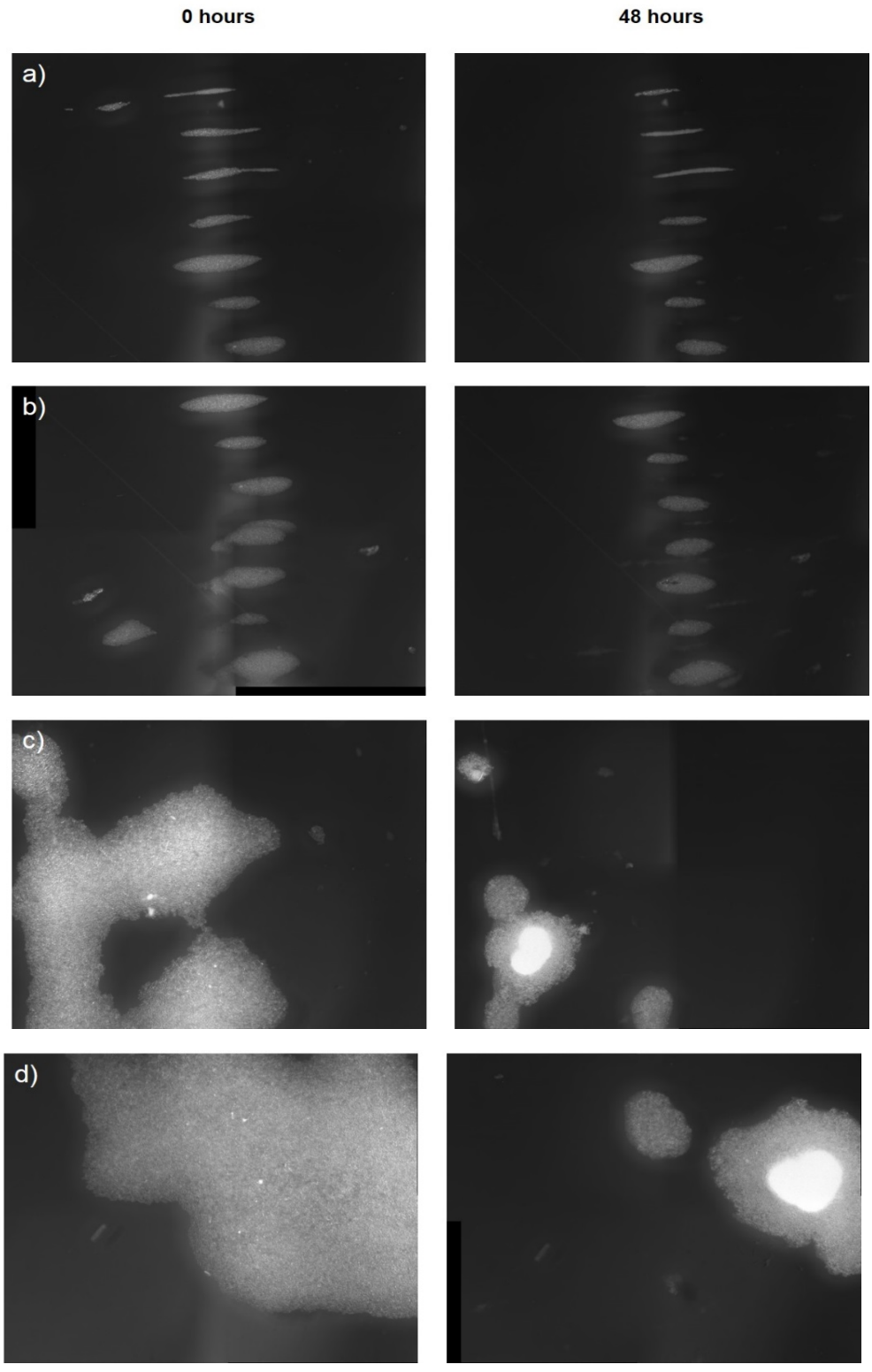

FIGURE 4-5: CO-LEVITATION OF CLL AND HFFF2 CELLS FOR 48 HOURS; PARALLEL ANALYSIS IN MULTIPLE IN ACOUSTIC TRAPPING DEVICES.

CLL cells (sample 589) were levitated in acoustic trapping devices for 48 hours in the presence or absence of HFFF2 cells. Images were taken directly after formation of agglomerates (0 hours; left panel) and at 48 hours (right panels). (a,b) CLL cells alone, obtained with two different devices (c,d) CLL and HFFF2 cells, obtained with two different devices. Original magnification 4x.

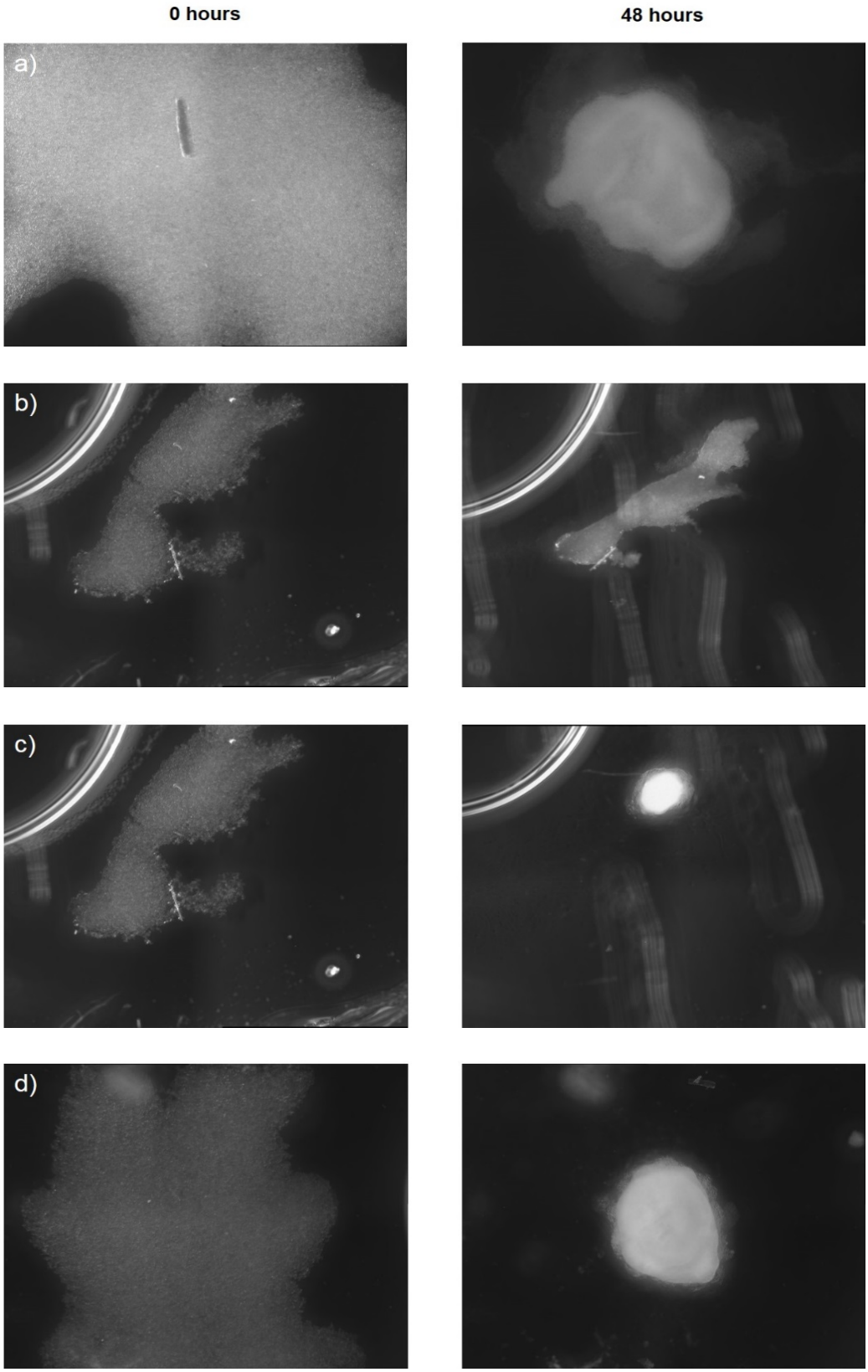

FIGURE 4-6: LEVITATION OF HFFF2 CELLS FOR 48 HOURS; PARALLEL ANALYSIS IN MULTIPLE IN ACOUSTIC TRAPPING DEVICES.

HFFF2 cells were levitated in acoustic trapping devices. Images were taken directly after formation of agglomerates (0 hours; left panel) and at 48 hours (right panel). (a-d) Results obtained with 4 different devices. Original magnification 4x. The bright particles in (b) and (c) are air bubbles.

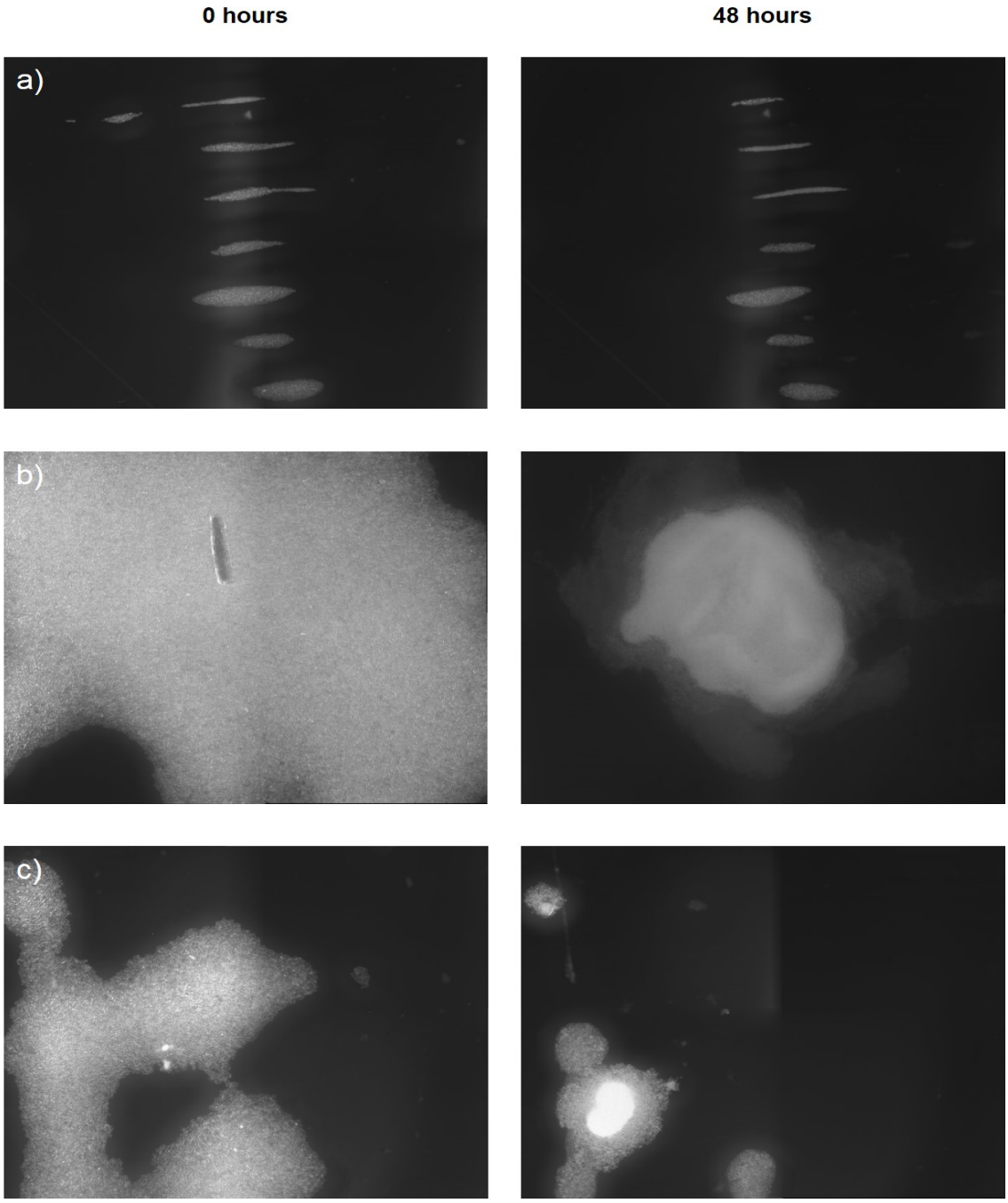

FIGURE 4-7: DIRECT COMPARISON OF CLL, HFFF2 AND MIXED AGGLOMERATE MORPHOLOGY AFTER 48 HOURS LEVITATION IN DEVICES.

CLL cells were levitated in acoustic trapping devices for 48 hours in the presence or absence of HFFF2 cells. HFFF2 cells were also levitated alone. Images were taken at the start of experiment (directly after formation of agglomerates, left panel) and at 48 hours (right panel). (a) CLL cells alone (b) HFFF2 cells alone (c) CLL and HFFF2 cells co-levitated. Original magnification 4x.

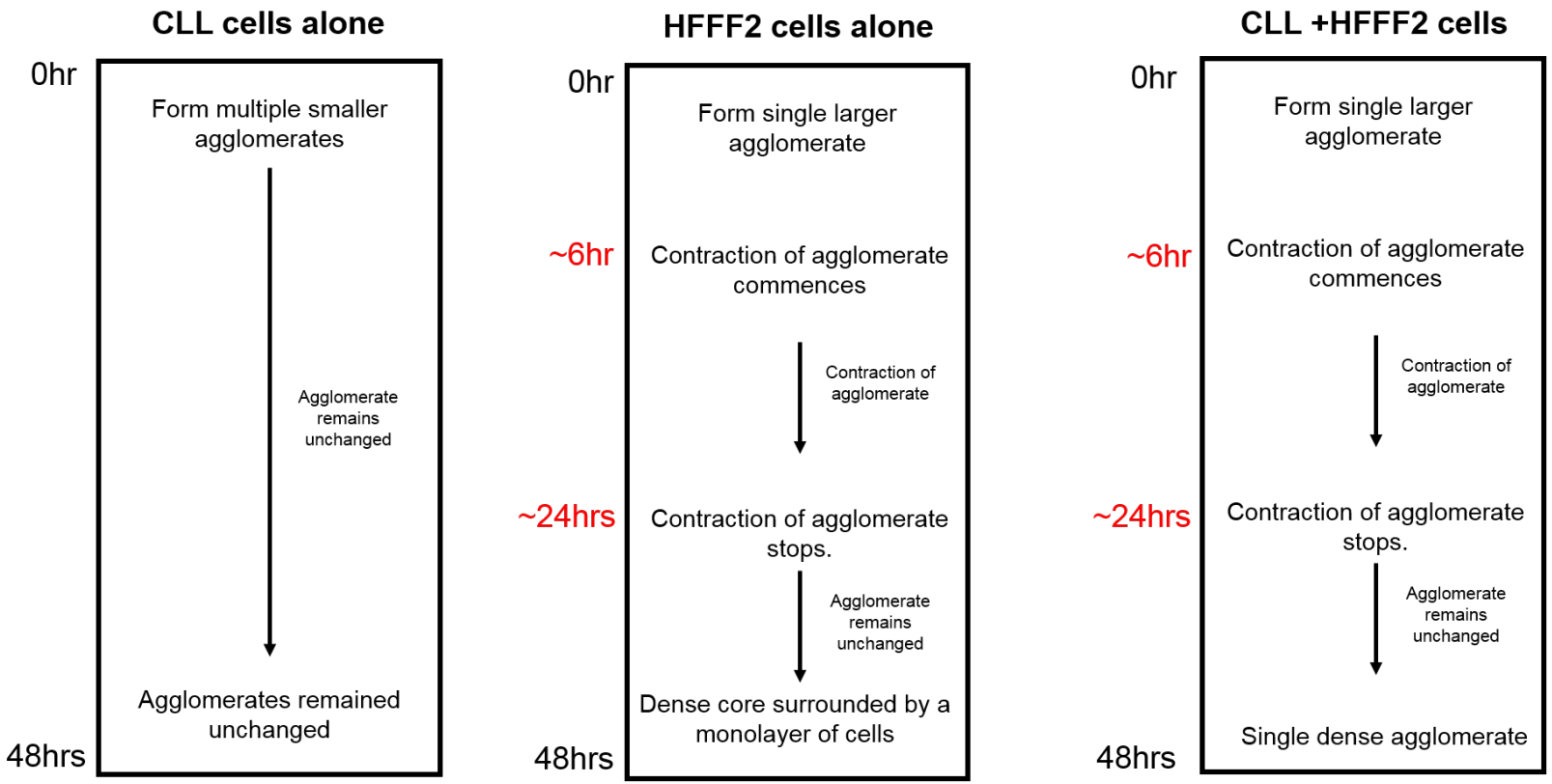

FIGURE 4-8: SUMMARY OF LEVITATION FINDINGS COMPARING AGGLOMERATES CONTAINING CLL CELLS ALONE, HFFF2 CELLS ALONE AND CLL AND HFFF2 CELLS

Summary schematic demonstrated the differences in morphology along with approximating timings seen when levitating CLL cells alone, HFFF2 cells alone and co-levitation of CLL and HFFF2 together.

4.7 Analysis of CLL and HFFF2 cell viability using propidium iodide exclusion

I next aimed to determine whether there is any direct influence of US waves on CLL and HFFF2 cell viability. The first experiments used the viable cell-impermeable fluorescent probe propidium iodide (PI) to discriminate between cells with intact and non-intact plasma membranes (Chapter 3, Section3.4). CLL cells were labelled with CFSE and injected into the device. In these experiments, the culture medium was supplemented with HEPES to improve CO_2-buffering since gassed incubation chambers were not available for these experiments. The ultrasound generator was activated and cells were allowed to form agglomerates. PI was then gently injected into the side of the devices and the cells were left for 8 hours before fluorescent imaging (Figure 4-9). Analysis revealed that essentially all CLL cells were PI-positive showing loss of plasma membrane integrity, suggesting extensive cell death.

One possibility was that the apparent cell death was associated with the culture conditions per se, rather than being a specific feature induced in the acoustic devices. For example, fluctuations in temperature or pH of the tissue culture medium of cells due to lack of incubation chamber on the microscope stage may result in cell death. Therefore, additional CLL cells were plated directly into tissue culture plates and cultured in parallel on the microscope stage (i.e., not in acoustic devices) or in a standard tissue culture incubator (37°C/10% $C0_2$). PI analysis of these parallel cultures revealed very low levels of PI-positive cells, indicating that CLL cell death is a specific feature of the acoustic devices, rather than temperature/pH fluctuations associated with the imaging platform (Figure 4-9c,d).

Similar experiments were performed in time-course format to investigate kinetics of PI-staining of cells in the acoustic devices. PI-positive CLL cells started appearing after only 1hour ultrasound exposure in the acoustic devices (Figure 4-10 and Figure 4-11). The proportion of PI-positive cells increased over the duration of the experiment, with the majority of cells being PI positive by 8 hours. This was seen in all samples tested (n=5). Similar results were obtained for levitated CLL cells in multiple devices and in multiple agglomerates. By contrast, control tissue-culture plates incubated in parallel on the microscope stage or in a standard tissue culture incubator consistently showed only very small number of PI-positive cells.

Similar experiments were used to investigate viability of HFFF2 cells. Similar to CLL cells, microscopy showed that PI-positive HFFF2 cells were abundant at 8 hours post-levitation.

The overall proportion of PI-positive HFFF2 cells was lower than CLL cells (where essentially all cells were PI-positive at this time), and time-course experiments showed that accumulation of PI-positive HFFF2 cells was delayed compared to CLL cells; PI-positive HFFF2 cells appeared at ~4 hours post-levitation (Figure 4-12 and Figure 4-13). Control cultures had very few PI-positive HFFF2 cells again indicating that loss of plasma membrane integrity is a specific feature of the acoustic devices.

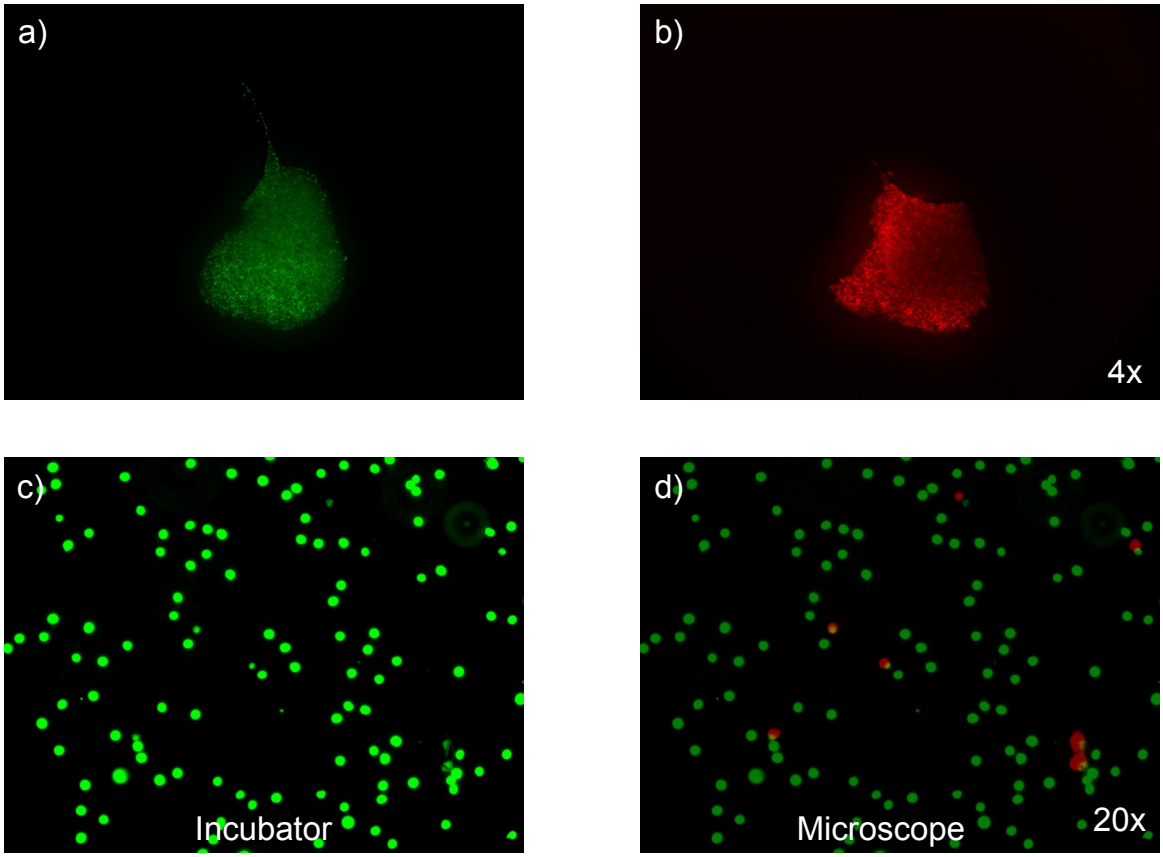

FIGURE 4-9: ANALYSIS OF CLL CELL VIABILITY USING PROPIDIUM IODIDE FOLLOWING LEVITATION IN ACOUSTIC TRAPPING DEVICES

Fluorescently labelled CLL cells (Green staining, sample 513a) were introduced into acoustic trapping devices for 8 hours. Propidium iodide (PI, 10µg/ml) was gently injected into the side of the device (Red staining). In parallel, CLL cells were cultured in conventional tissue culture plates as a control. One was kept on the microscope stage and one at normal culture conditions (37°C/10% $C0_2$). Images above were taken at 8 hours. (a) CFSE stained agglomerate (b) PI staining of agglomerate (c,d) Incubator control plate and microscope control plate respectively. Original magnification 4x. and 20x as displayed on image.

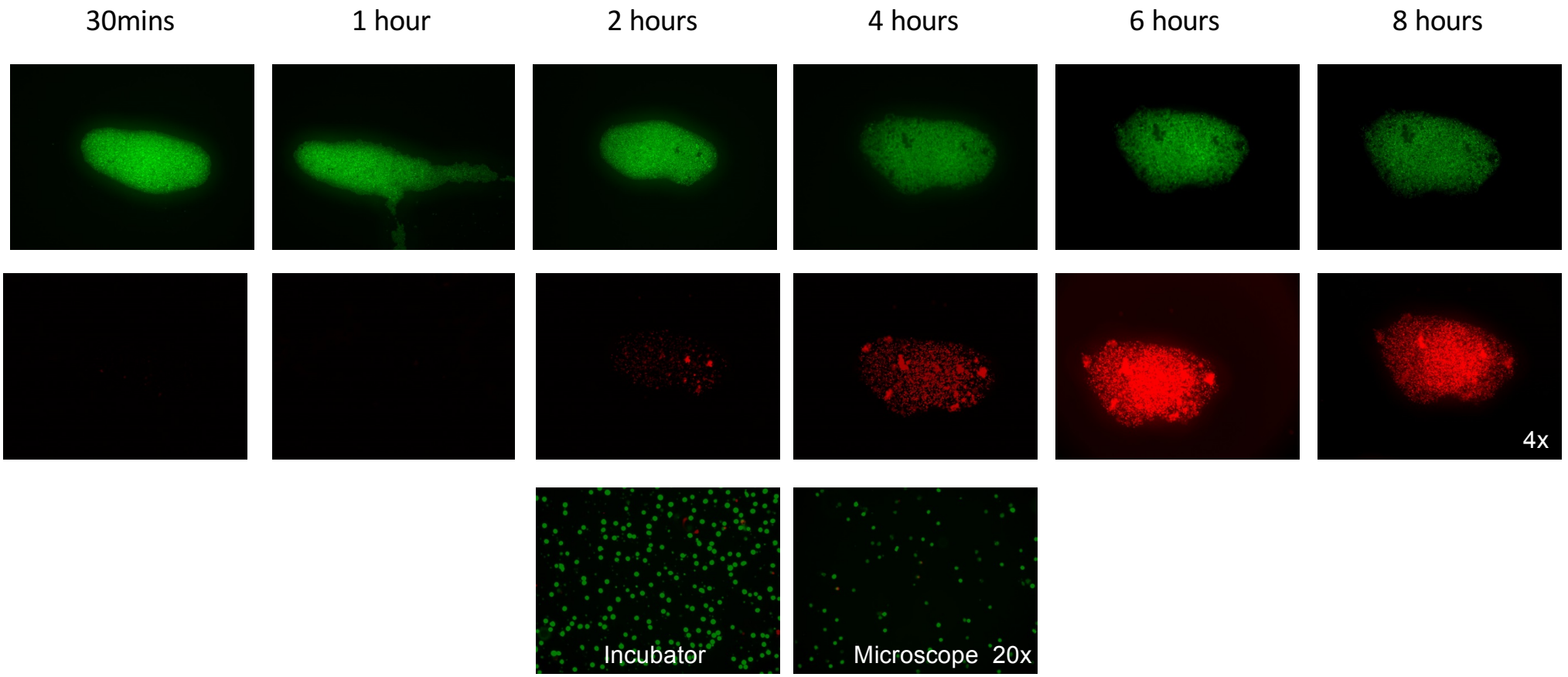

FIGURE 4-10: VIABILITY OF CLL CELLS FOLLOWING 8 HOURS LEVITATION IN ACOUSTIC TRAPPING DEVICES

As for Figure 4-9, but using CLL sample 656 and images were taken at 30 minutes, 1 hour and then every 2 hourly until 8 hours. Increasing levitation time goes from left to right. Control plates, bottom row. Original magnification 4x. and 20x as displayed on image.

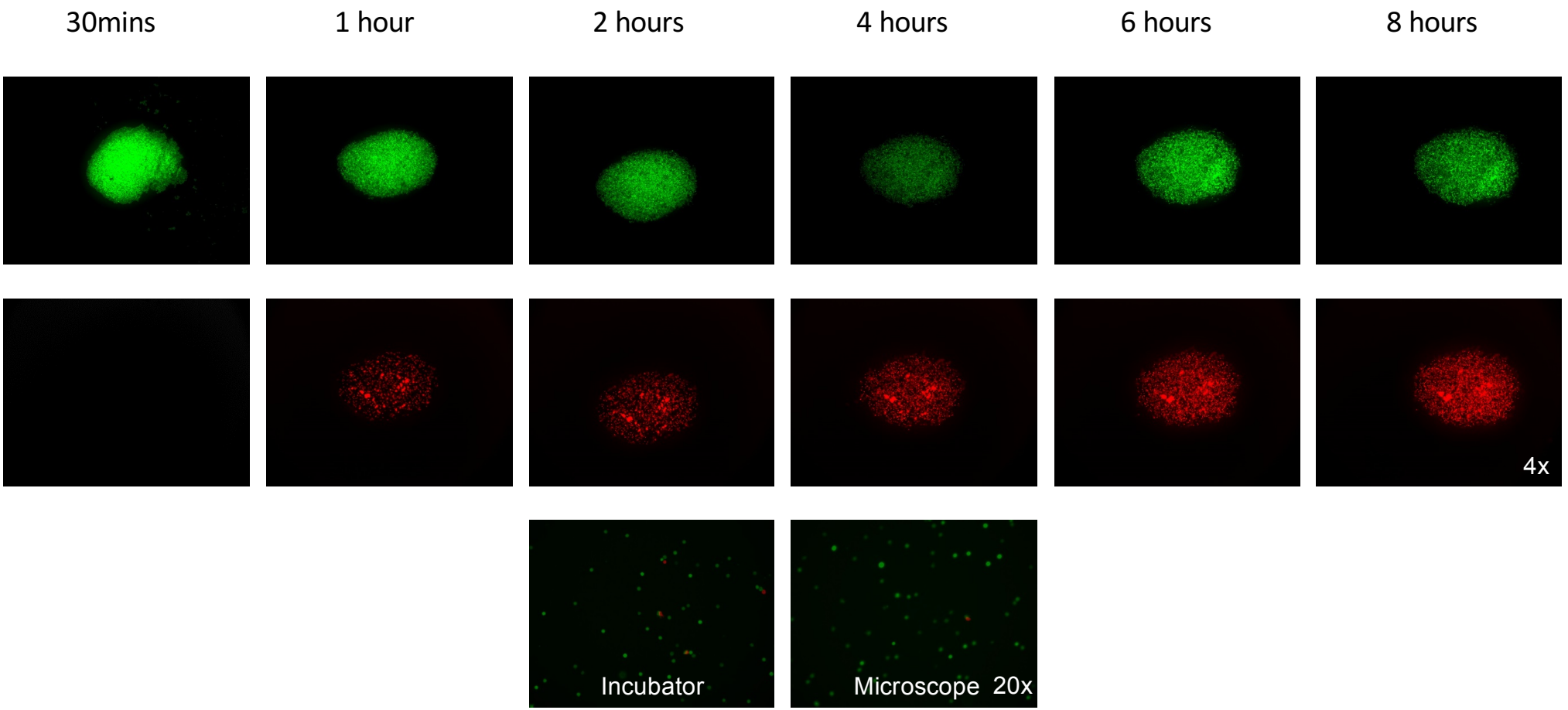

FIGURE 4-11: VIABILITY OF CLL CELLS FOLLOWING 8 HOURS LEVITATION IN ACOUSTIC TRAPPING DEVICE

As for Figure 4-10, but using CLL sample 650. Original magnification 4x. and 20x as displayed on image.

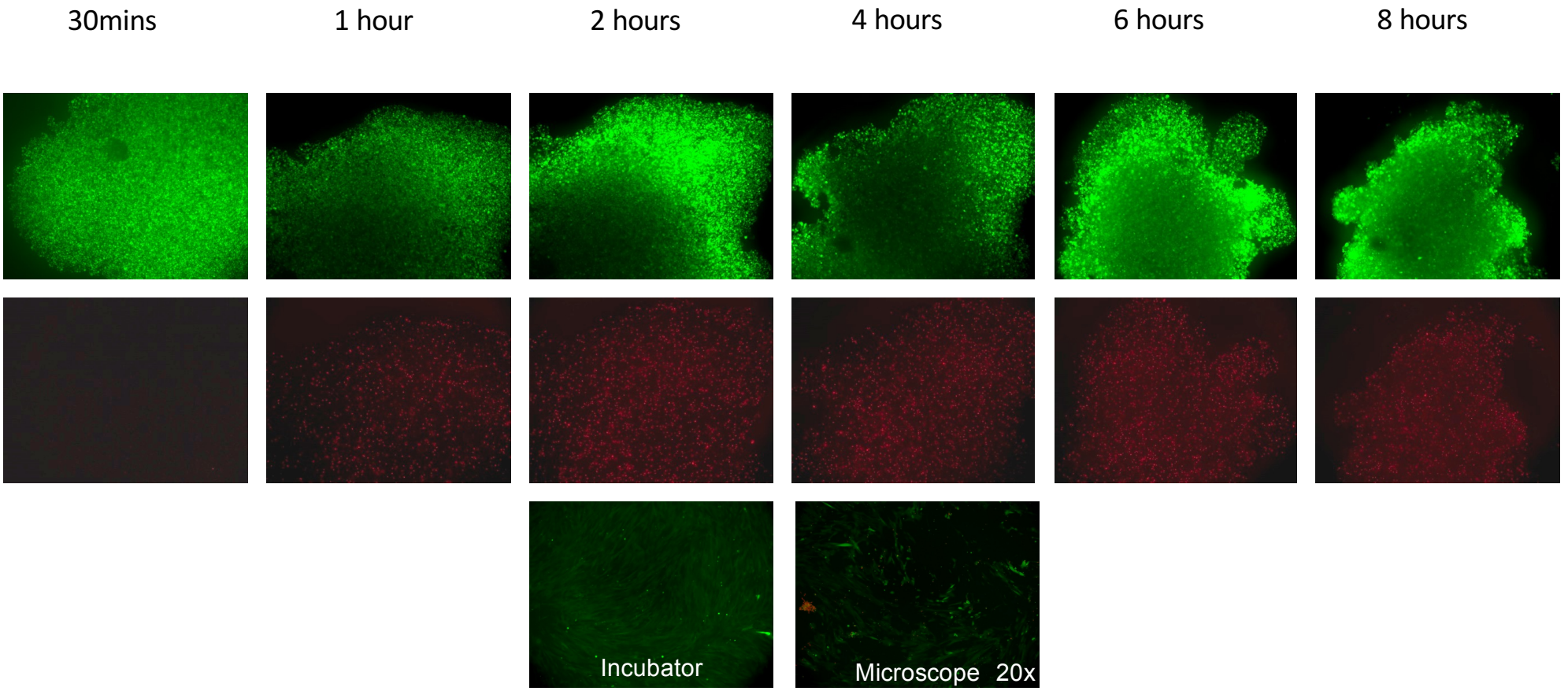

FIGURE 4-12: VIABILITY OF HFFF2 CELLS FOLLOWING 8 HOURS LEVITATION IN ACOUSTIC TRAPPING DEVICE

Fluorescently labelled HFFF2 cells (Green staining) were introduced into acoustic trapping devices for 8 hours. Propidium iodide (PI, 10µg/ml) was gently injected into the side of the device (Red staining). In parallel, HFFF2 cells were cultured in conventional tissue culture plates as a control. One was kept on the microscope stage and one at normal culture conditions in the incubator (37°C/10% C02). Images were taken at 30 minutes, 1 hour and then every 2 hourly until 8 hours. Increasing levitation time goes from left to right. . Control plates, bottom row. Original magnification 4x. and 20x as displayed on image.

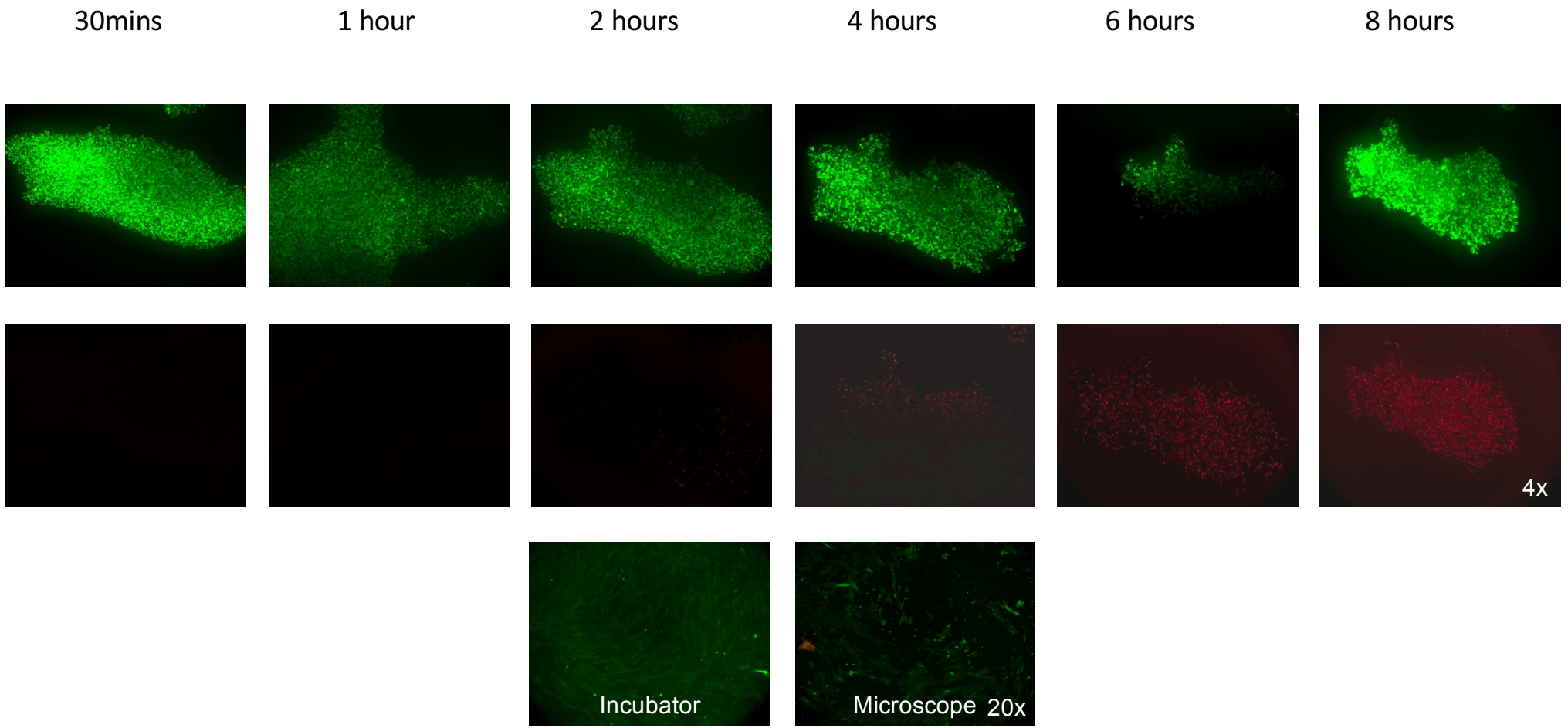

FIGURE 4-13: VIABILITY OF HFFF2 CELLS FOLLOWING 8 HOURS LEVITATION IN ACOUSTIC TRAPPING DEVICE

As for Figure 4-12, repeat experiment with HFFF2 cells. Original magnification 4x. and 20x as displayed on image.

4.8 Analysis of caspase 3/7 activation in CLL cells following levitation in acoustic trapping devices

Studies with PI suggested that both CLL and HFFF2 cells were readily killed within the acoustic devices. However, interpretation of PI-staining is complicated due to the potential impact of sonoporation whereby ultrasound waves can directly rupture plasma membranes. Indeed, this has been proposed as a method of cell transfection (Miller et al., 1996, Ng and Liu, 2002, Ankrett et al., 2013). Therefore, it was not clear if PI uptake was due to direct (perhaps temporary) disruption of plasma membranes by ultrasound, or was a consequence of cell death. We therefore developed additional approaches to quantify cell killing in the devices, including of co-cultured CLL and HFFF2 cells.

An initial series of experiments was performed using Annexin-V which stains phosphatidyl serine exposed on the outer membrane of apoptotic cells (Methods, Section2.3.2). Agglomerates were recovered from the device, disrupted and then stained with Annexin-V/PI prior to flow cytometry (data not shown). Although Annexin-V positive cells were detected in these experiments, it proved difficult to reliably quantify staining separately on CLL or HFFF2 cells. Some experiments were performed using CLL cells pre-labelled with CFSE prior to injection into the device (using APC-conjugated Annexin-V to avoid the CFSE fluorescent signal in FL1), but even under these conditions it proved difficult to reliably gate on CLL or HFFF2 cells to specifically quantify apoptosis in the individual cell types (data not shown).

We also investigated the CellEvent caspase 3/7 detection reagent (Invitrogen) to quantify apoptosis in the agglomerates. Caspase-3 is a key effector caspase that amplifies signal from initiator caspases and irreversibly commits cells to apoptosis. The CellEvent caspase 3/7 detection reagent is a four amino acid caspase 3-target peptide (DEVD), conjugated to a nucleic acid binding fluorescent probe. When intact, the DEVD peptide inhibits the ability of the dye to bind to DNA. Following caspase-cleavage of the DEVD target peptide, the released fluorescent probe is free to bind DNA, resulting in a strong fluorogenic response. The fluorescence emission of the dye when bound to DNA is ~530 nm and can be observed using a standard “FITC" filter set. Initial validation experiments were performed using CLL cells in standard culture. CLL cells were cultured for 48 hours without stromal support to promote spontaneous apoptosis. This was associated with strong activation of caspases 3/7, detected using the fluorogenic reporter peptide. Titration experiments were performed to determine the optimal probe concentrations for use in experiments with the acoustic devices (Figure 4-14). For all future experiments 5μM of the CellEvent reagent was used.

The CellEvent caspase 3/7 reagent was then used to further investigate cell viability in acoustic trapping devices. CLL cells were fluorescently labelled with CellTracker Red, injected into the acoustic device and levitated as agglomerates for 8 hours. As in previous experiments, cell culture media was supplemented with HEPES to improve buffering capacity. After 7.5 hours, caspase 3/7 detection reagent was gently added to the side of the devices and the cells were incubated for an additional 30 minutes prior to imaging. Similar to the experiments performed using PI-staining, analysis of fluorescence revealed that the majority of cells in the agglomerate contained active caspase 3/7 (Figure 4-15) indicating a significant increase in apoptotic cell death at this time. Parallel analysis of control tissue culture samples on the microscope stage and in a standard incubator revealed only low levels of apoptosis.

We also performed experiments with co-analysis of PI-staining and caspase 3/7 activation, to directly compare results using these two approaches. CLL cells were labelled with CellTracker Blue and injected into the acoustic device. Cells were allowed to form agglomerates and levitated for 7.5 hours. A mixture of caspase 3/7 detection reagent and PI was gently added to the side of the devices and the cells were levitated for a further 30 minutes prior to imaging. Imaging revealed similar patterns of fluorescence with the two probes. Figure 4-15 shows an agglomerate from three CLL samples analysed.

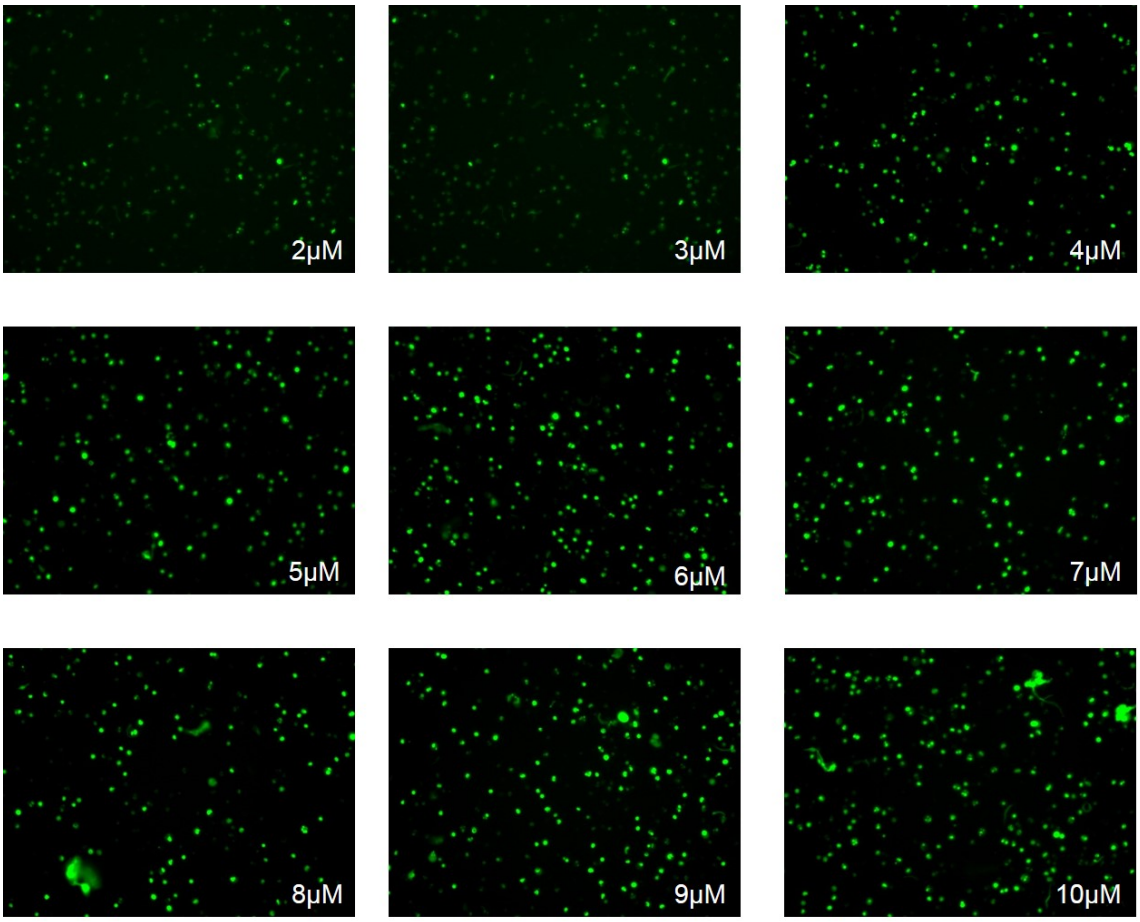

FIGURE 4-14: OPTIMISATION OF CASPASE 3/7 REAGENT STAINING

CLL cells were cultured in tissue culture plates for 48 hours to induce spontaneous apoptosis. Viability was determined using the CellEvent caspase 3/7 detection reagent (Invitrogen). The CellEvent Caspase 3/7 detection reagent from Invitrogen detects activated caspase3/7. Increasing concentrations of the Caspase 3/7 fluorescent dye was added to the CLL cells and cells were 30 minutes prior to imaging on the fluorescent microscope using the FITC filter. Original magnification 4x.

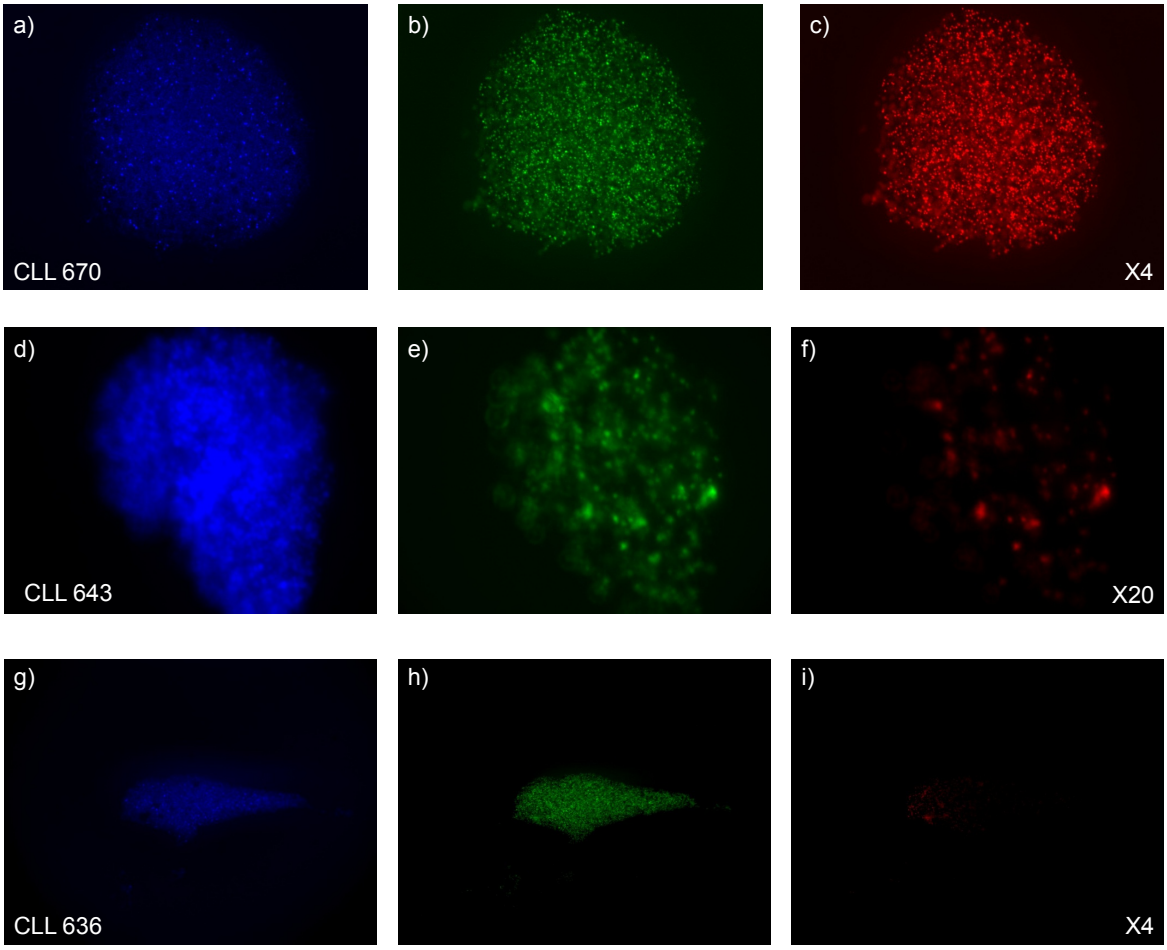

FIGURE 4-15: VIABILITY OF CLL CELLS FOLLOWING 8 HOURS LEVITATION IN ACOUSTIC TRAPPING DEVICE USING CELLEVENT CASPASE 3/7 REAGENT

CLL cells were fluorescently labelled with CellTracker Blue (Blue staining, CLL sample 670, 643 and 636), and levitated in acoustic trapping devices for 8 hours. caspase 3/7 (5 µM, Green staining) and propidium iodide (10µg/ml ,PI) (Red staining) was gently injected into the side of the device 30 minutes prior to imaging. (a,d,g) CellTracker Blue staining (b,e,h) caspase 3/7 reagent staining (g,h,i) PI staining. Original magnification is noted on individual patient experiments.

4.9 Analysis of caspase 3/7 activation in HFFF2 cells in acoustic trapping devices

The same approach was used to investigate HFFF2 cell apoptosis. HFFF2 cells were labelled with CellTracker Blue and analysed using PI and the caspase 3/7 probe as described for CLL cells (Section4.8, Figure 4-15). Imaging at 8 hours post-levitation revealed the overall pattern of PI and caspase 3/7 probe fluorescence was very similar, and that a large proportion of HFFF2 cells had undergone apoptosis at this time point (Figure 4-16). Parallel control cultures showed very low levels of PI-staining/caspase 3/7 probe fluorescence.

We wondered to what extent the cell death of HFFF2 cells was due to their being deprived of supporting substrate interactions normally provided by tissue culture plasticware. For example, anchorage dependent cells undergo a form of apoptosis termed anoikis (Frisch and Francis, 1994) when detached from supporting ECM. To determine directly whether lack of cell attachment to tissue culture surface was sufficient to promote cell killing, HFFF2 (and CLL) cells were cultured for 8 hours on conventional plastic petri dishes not coated for tissue culture. Cell death was measured using PI staining and the experiment was performed using five independent CLL samples, and two separate repeats with HFFF2 cells. Representative data are shown in Figure 4-17 and Figure 4-18. Microscopic analysis confirmed that HFFF2 cells did not adhere to non-coated petri-dishes, and CLL cells remained unattached in both tissue culture vessels. However, there was no difference in the levels of PI-staining for either cell type between the two culture conditions. Therefore, the substantial apoptosis of CLL and HFFF2 cells observed in the devices is not due to lack of attachment per se, but may be a direct effect of ultrasound waves.

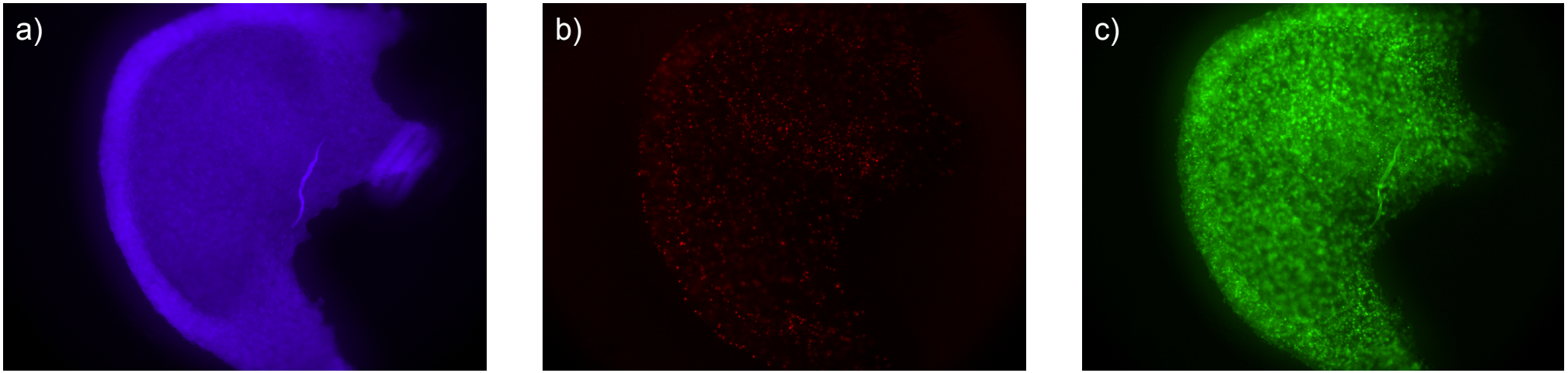

FIGURE 4-16: VIABILITY OF HFFF2 CELLS FOLLOWING 8 HOURS LEVITATION IN ACOUSTIC TRAPPING DEVICE USING CELLEVENT CASPASE 3/7 REAGENT

HFFF2 cells were fluorescently labelled with CellTracker Blue, and levitated in acoustic trapping devices for 8 hours. caspase 3/7 (Green staining) and Propidium Iodide (PI) (Red staining) was gently injected into the side of the device 30 minutes prior to imaging. (a) CellTracker Blue staining (b) caspase 3/7 reagent staining (c) PI staining. Original magnification 4x.

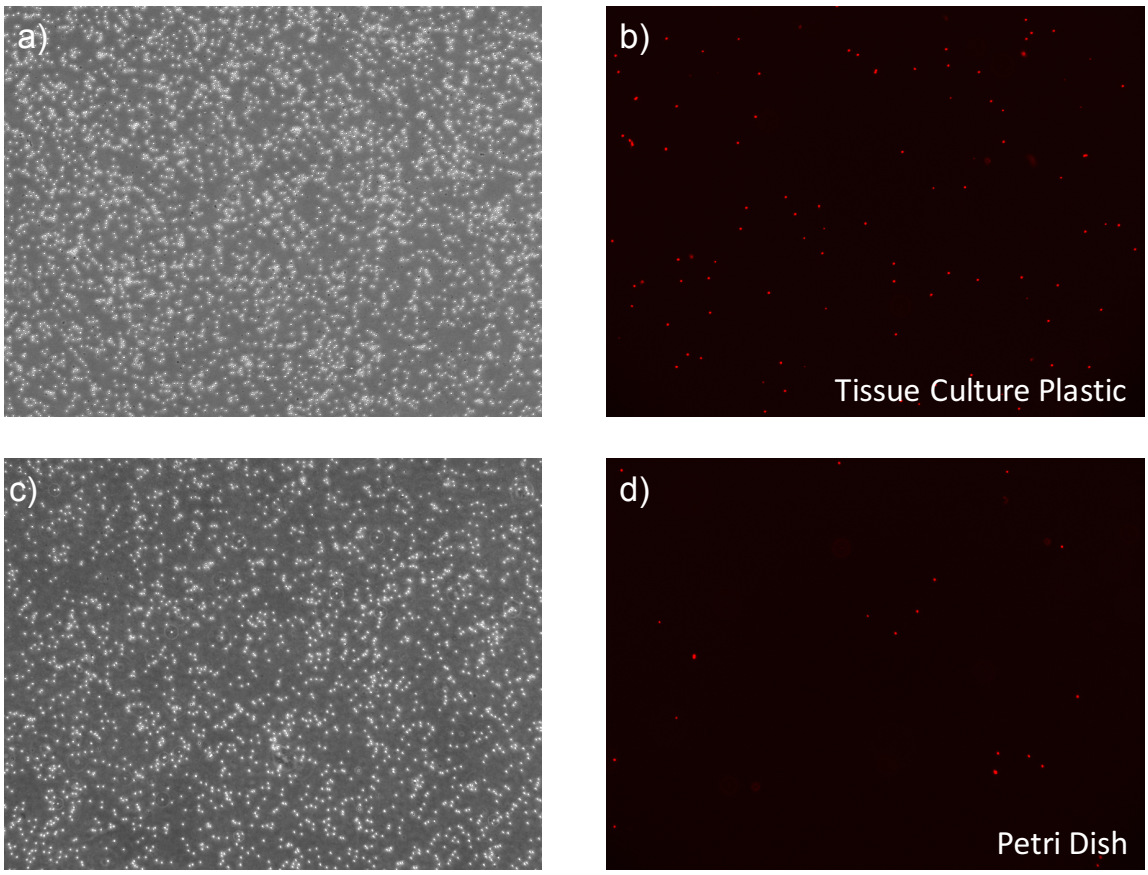

FIGURE 4-17: VIABILITY OF CLL CELLS FOLLOWING CULTURE ON CONVENTIONAL TISSUE CULTURE PLASTIC VERSUS NON-TREATED PETRI DISHES

CLL cells (sample 668) were cultured on conventional tissue culture plates and non-treated petri dishes for 8 hours. Viability was tested by adding propidium iodide (PI) to each plate and imaging on the fluorescent microscope. Top panel displays images from conventional tissue culture plate, bottom row displays images from petri dishes. (a,c) Phase contrast of CLL cells cultured plastic (b,d) PI staining of CLL cells. Original magnification x4.

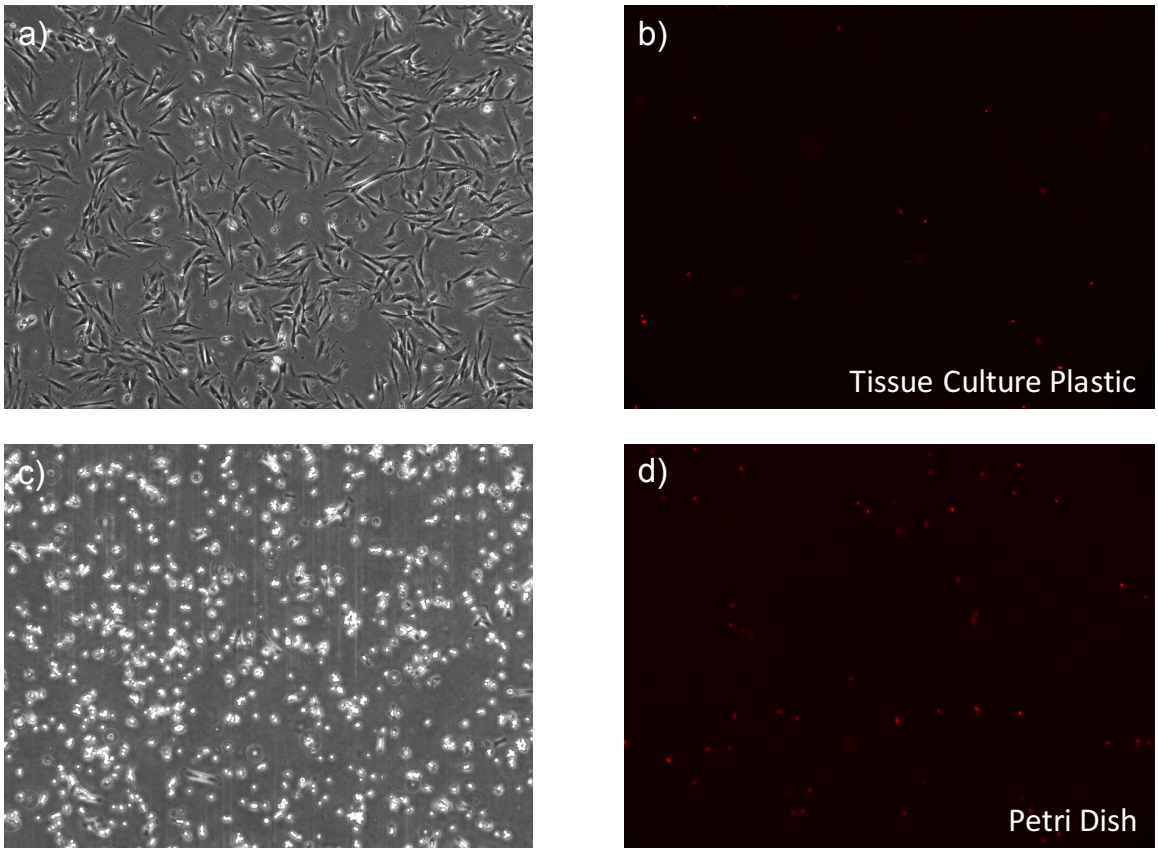

FIGURE 4-18: VIABILITY OF HFFF2 CELLS FOLLOWING CULTURE ON CONVENTIONAL TISSUE CULTURE PLASTIC VERSUS NON-TREATED PETRI DISHES

HFFF2 cells were cultured on conventional tissue culture plates and non-treated petri dishes for 8 hours. Viability was tested by adding propidium iodide (PI) to each plate and imaging on the fluorescent microscope. Top panel displays images from conventional tissue culture plate, bottom row displays images from petri dishes. (a,c) Phase contrast of CLL cells cultured plastic (b,d) PI staining of CLL cells. Original magnification x4.

4.10 Exploration of physical stimuli

In light of these results, I began to explore features that might account for the dramatic loss of viability observed when cells were levitated in the devices.

One possibility was that heating of the transducer was causing a localised increase in media temperature leading to cell death. To investigate this, the temperature of the media directly under the transducer was measured using temperature probes at times up to 8 hours (Table 4.2). This was repeated three times. This analysis showed that the temperature of the media increased by an average of just 1.8°C during the experiment (from 22.4°C to 24.2°C). Therefore, local heating is unlikely to be a substantial trigger for extensive cell death. Although the temperature recorded in the device is lower than standard conditions (37°C) this is also unlikely to be the cause of the cell death, since similar levels of killing were not observed in parallel cultures incubated on the microscope stage but without acoustic devices.

All experiments to this point had been performed using an ultrasound amplitude of 6 Vpp, based on previous studies using these devices to levitate epithelial cells and chondrocytes (Angela Tait, PhD thesis, Siwei PhD thesis). In an attempt to reduce the strength of the ultrasound field in the devices, I set out to identify the minimum ultrasound amplitude that was required for levitation (Methods, Section2.6.4). Initial experiments were performed using fluorescent beads as a well validated approach to explore physical features associated with levitation (Table 4.3). In fact, this analysis showed that the average voltage required to levitate the beads is ~2 Vpp. A similar amplitude was required to levitate cell agglomerates. Thus, one option would be to reduce the ultrasound amplitude used in the devices. However, in these experiments it was also observed that there was significant inter-device variation in ultrasound amplitude needed for bead levitation. Moreover, it was noted that the minimum amplitude needed for levitation of pre-formed agglomerates was not sufficient to drive *de novo* agglomerate formation.

TABLE 4.2: MEASUREMENT OF TEMPERATURE CHANGES OVER 8 HOUR PERIOD IN THE ACOUSTIC TRAPPING DEVICES

Liquid medium temperature directly under the transducer was monitored for 8 hours using temperature probes placed directly under the PZT transducer. Table displays three repeats performed.

Time	Repeat1 (°C)	Repeat2 (°C)	Repeat3 (°C)
0hr	21.9	22.8	22.4
1hr	22.5	23.9	23.2
2hr	23.2	24.2	23.9
3hr	23.5	24.0	24.2
4hr	23.9	24.1	24.5
5hr	24.2	24.0	23.9
6hr	24.3	24.0	24.0
7hr	24.0	24.0	24.2
8hr	24.3	24.0	24.2

TABLE 4.3: DETERMINATION OF THE MINIMUM VOLTAGE REQUIRED FOR LEVITATION OF FLUORESCENT BEADS

Fluorescent beads were used to determine the minimum voltage required for levitation in each device (Methods, Section2.6.4). The voltage was lowered until the beads starting to drop. Using the z position on the microscope and the fact that the approximate apparent depth that each bead would travel until it would no longer be able to levitate we were able to predict the approximate z position at which levitation would cease.The voltage on the signal generator was then converted to an output voltage (Vpp).

Device	H_{3Vpp}	Predicted H_{drop}	V_{drop}	Output (Vpp)
1	3671	3606	0.84	2.02
2	3646	3581	1.1	2.64
	3661	3596	0.86	2.06
3	3689	3624	0.40	0.96
Agglomerate	4605	4670	0.70	1.68

4.11 Key findings

The main goal of these experiments was to determine the ability of acoustic trapping devices to model the CLL/stromal cell microenvironment. Optimisation focussed on the ability of both cell types to co-levitate in the devices and secondly the affect of acoustic forces on cell viability. The key findings in this chapter were:

- Both CLL and HFFF2 cells are able to levitate in acoustic trapping devices
- CLL and HFFF2 cells can 'co-levitate' forming an agglomerate containing a mixture of both cell types
- CLL cells characteristically form multiple smaller agglomerates while HFFF2 cells and a mixture of both CLL and HFFF2 form single large agglomerates
- Over 48 hours agglomerates containing HFFF2 cells and a mixture of CLL and HFFF2 cells contract to form 3D structures
- Over 48 hours agglomerates containing CLL cells remain unchanged
- Viability of both CLL cells and HFFF2 cells is dramatically reduced after 8 hours levitation in acoustic trapping devices
- Transducer heating, ultrasound stimuli and lack of contact are unlikely to be the cause of the dramatic decrease in cell viability

4.12 Discussion

4.12.1 Ability of CLL and HFFF2 cells to levitate in acoustic trapping device

The main aim of this chapter was to determine the ability of acoustic trapping devices to levitate CLL and HFFF2 cells. The majority of work using similar acoustic trapping devices have primarily looked at the levitation of single cells (Wu, 1991) or 2D cell aggregates (Bazou et al., 2005b) which have 'trapped' or levitated at a signal node. This work has used a variety of different cell lines including COS-7 monkey fibroblasts (Hultstrom et al., 2007), neural cells (Bazou et al., 2005a), chrondocytes (Bazou et al., 2006b), prostate epithelial cell line (PZ-HPV-7 cells) and prostate cancer cell line (DU-145) (Bazou et al., 2006a), HepG2 cells, a liver hepatocellular carcinoma (Edwards et al., 2007), 16HBE a respiratory epithelial cell line (Angela Tait, PhD thesis) and human articular chondrocytes (Li et al., 2014).

We initially showed that both CLL cells and HFFF2 cell line could individually levitate in the device (Figure 4-1 and Figure 4-2). To the best of our knowledge this is the first time primary lymphocytes have been levitated in a device of this nature. Both cell types formed aggregates of cells within a couple of minutes levitation which is in line with other cellular work carried out in similar devices (Video 1 and Video 2). In order to determine whether we could use the acoustic trapping devices for modelling the CLL microenvironment we next aimed to determine whether two different cell types could be levitated in the same device simultaneously. Figure 4-3 demonstrates the ability of both cell types to not only simultaneously levitate in the devices but to also 'co-levitate' in the same agglomerate of cells. Again to the best of our knowledge, this is the first time this has been demonstrated.

4.12.2 Morphology of agglomerates following levitation in acoustic trapping devices for longer period of time

To determine the ability of devices to drive the formation of 3D structures I next investigated the morphology of agglomerates in the device for both cell types as well as a mixture of both over longer levitation periods. CLL cells were levitated for four hours in the presence or absence of HFFF2 cells. Figure 4-4 revealed that there was no real change in agglomerate morphology over this period of time. However, microscope analysis revealed what appeared to be the movement of CLL cells between the HFFF2 monolayer indicating that there is the potential for the two cells types to start interacting with each other (Data not shown). This led to the possibility that this was the start of the formation of structures which are more 3D in nature.

To determine whether devices could lead to the formation of 3D structures agglomerates were next levitated for 48 hours and changes in morphology were tracked using time lapse. Videos 3, 4, 5 and 6 indicate the ability of the agglomerates to be maintained for this length of time and also demonstrated that agglomerates containing HFFF2 cells and a mixture of HFFF2 and CLL cells contracted to form denser structures that appeared 3D in nature. The results indicated a difference in the way the two different cell types behaved in the devices. HFFF2 cells and a mixture of both cell types showed a contraction of the agglomerate to form a dense core with mixed agglomerates being surrounded by a 'skirt' formed by single cells. In comparison agglomerates containing CLL cells alone did not change in morphology over the levitation time (Figure 4-5).

Work by another research laboratory at the University of Southampton, using the same devices demonstrated a similar contraction using a respiratory epithelial cell line, 16HBE cells. They further demonstrated that this contraction was likely to be caused by the

formation of adheren junctions and their associated actin filaments due to the fact that after 2 hours levitation the 16HBE cells started to form adheren junctions which coincided with the contraction of the agglomerate beginning (Angela Tait, PhD Thesis). Other investigators have also looked at cell-cell interactions and have showed that F-actin had accumulated at the cell-cell contact interface and gap junctions had formed (Bazou et al., 2006b). Edwards et al., investigated HepG2 cells levitated over 1 hour. The HepG2 cells formed a 2D aggregate within 30 seconds and by 10 minutes the morphology of the cells had changed losing their roundness. The F-actin staining became localised at regions of cell-cell contact after 4 minutes, becoming more defined at the cell-cell interface after 11 minutes (Edwards et al., 2007). Although most papers have investigated the formation of cell sheets rather than 3D structures as seen in this project, they all showed that the morphology of cells when levitated was not the same as cells grown on a solid substrate. These data indicate the ability of cells to interact with each other within the acoustic trapping devices and demonstrate that the formation and maintenance of the agglomerates after formation may be held together through cell-cell interactions as well as acoustic trapping forces. This was confirmed by the fact that when the ultrasound was turned off and agglomerates drop the agglomerate is maintained and the 3D structure is still visible. This phenomenon is not visible when agglomerates were levitated for shorter time periods where agglomerates quickly dispersed. This would potentially allow for us to study CLL cell and fibroblast interactions with both cell types hopefully forming cell-cell interactions.

4.12.3 Viability of CLL and HFFF2 cells in acoustic trapping device

The second aim of the chapter was to investigate whether there was any direct influence of ultrasound waves on CLL and HFFF2 cell viability or cell behaviour. We first aimed to determine the viability of both cell types within the devices. Viability of cells in similar ‘trapping’ devices has been investigated using many different methods (Bazou et al., 2005a, Bazou et al., 2005b, Bazou et al., 2006b, Bazou et al., 2006a, Evander et al., 2007, Ankrett et al., 2013).Current data from these studies indicate there is no decrease in viability for cell levitated for up to 1 hour. However, no published studies so far have looked at the viability of cells being levitated in such device for longer than 1 hour. A number of methods were used in this study to determine the viability of both cell types in the acoustic trapping device and revealed the major drawback encountered during this project; poor viability of cells in the acoustic trapping device. Data indicate that after 8 hours levitation of both CLL and HFFF2 cells in the devices, the majority of cells within the

agglomerates were dead. Cell apoptosis was detected as early as 2 hours for CLL cells and 4 hours for HFFF2 cells.

Ankrett et al., investigated viability of single H9c2 cardiac myoblasts within an ultrasound standing wave in identical devices as used in this project. Viability was found to be unaffected between 0-15Vpp (Ankrett et al., 2013). Our devices are run at 6Vpp so this falls nicely into the 'safe' voltage range so was not expected to affect viability of the cells. However the current work differs as the cell types studied are different, they were levitated for a longer time period and were allowed to form agglomerates as opposed to single cells. The minimum voltage required for levitation was determined and the results demonstrated that once agglomerates had formed in the devices that the voltage could in fact be reduced to 2Vpp. Reducing the voltage to 2Vpp could potentially help reduce levels of cell death however analysis showed that agglomerates struggled to form at this lower voltage (Table 4.3). Ankrett et al., next investigated the effect of varying the sweep frequency . They showed that at fixed amplitude (29Vpp) but with varying frequency sweep period (tsw = 0.02-0.50 sec), cell viability remained relatively constant at tsw ≥ 0.08 sec, whilst viability was reduced at tsw < 0.08 sec with the lowest viability being recorded at tsw = 0.05 sec(Ankrett et al., 2013). We are currently using a sweep frequency of 0.05 seconds where the lowest viability was recorded (minimum viability of ~41% after 1 hour). The transducers used in this study are set with a sweeping frequency around the resonate frequency (1.7 to 1.85 MHz kHz). Sweeping needs to occur and at a rate of 0.05 seconds to allow for variation between the transducers of the different devices and to allow for variation over time for the transducer. By using sweep frequencies it allows us to maintain levitation of the cells over the time period required.

Another possibility of the cause of the decrease in cell viability seen could be because of acoustic streaming. Acoustic streaming was not characteristically seen in the devices due to the fact that the transducer amplitude was reduced to a level where streaming was not seen. Acoustic streaming can also be caused due to bubbles in the media, however measures were taken to ensure bubbles were not pipetted into the device along with cells and although bubbles were witnessed in some experiments no acoustic streaming was witnessed throughout the duration of experiments making it unlikely that acoustic streaming was the cause of the decrease in viability.

Overall, the ultrasound stimuli we are using in this project are already very low and should create a gentle acoustic environment for the cells. By reducing any of the parameters any more it is likely that reliable levitation may be compromised and most probably will not have any effect on the viability of the cells. The same devices have been used with 16HBE a respiratory epithelial cell line and viability was shown to be moderate up to 6 hours (Angela Tait, PhD Thesis). Therefore it is likely that overall the acoustic conditions

are not likely to be the cause of cell death in the devices but more likely reflect the specific nature of the cell types being examined in these experiments.

Another possibility is that the cell death may rather be due to the cells lacking contact to a solid substrata. The HFFF2 cells are an adherent cell line, and therefore lack of contact to tissue culture plastic may be detrimental to their viability. Fibroblasts like to adhere and spread along tissue culture plastic. CLL cells, although not adherent in nature, have been shown to preferentially adhere to tissue culture plates. One possibility is the cells are going through programmed cell death known as anoikis (Frisch and Francis, 1994). This occurs when anchorage dependant cells become detached from the ECM and the ECM can no longer provide survival and growth signals. Another possibility is that the cell shape is changing. This has been shown to signal to whether a cell would survive or undergo apoptosis. Chen et al., demonstrated that in bovine capillary endothelial cells, there was significantly increased cell death in cells which were rounded in morphology compared to those which were able to spread on the surface (Chen et al., 1997). However analysis using petri dishes to prevent attachment showed that this was not the case as there was no dramatic reduction in cell viability when cell attachment was prevented compared to conventional tissue culture plastic and petri dishes (Figure 4-17 and Figure 4-18).

Based on all these considerations, minimizing the levitation time cells undergo was deemed the best way to maintain viability. However, viability has been shown to be affected in as little as 2 hours in the devices. This led to the question of whether in this short period of time, we would be able to investigate CLL/fibroblast interactions.

4.12.4 Final comments

Along with the major viability problems, there are also other factors that need to be taken into consideration when optimising the acoustic trapping devices for modelling the CLL microenvironment. The device has already progressed well to allow for the devices to fit into 6 well plates, which allows for easy injection and easy access and retrieval to the aggregates of cells formed. The addition of a mirrored reflector under the transducer allowed for easy visualisation. However there are still some issues with the need for constant maintenance with the devices as small wires become detached on a regular basis, requiring the need for soldering. The connectors also come detached from the device itself requiring regular gluing and maintenance. The reliability needs to be improved to stop the constant need for soldering and repairing. The devices are also limited in the fact that they cannot be used under sterile conditions and cells need to be

added when the devices are *in situ* as the devices cannot be moved without the disruption of agglomerates in the devices. This also means that devices need to stay on the microscope for the duration of the experiment, leading to issues with temperature and $C0_2$. Optimisation should allow for devices to be set up and used within a sterile environment. This would allow for devices to be set up and cells injected into the devices in tissue culture hood, before the devices are moved to an incubator for the duration of the experiment.

All these considerations along with the significant loss of viability in the devices, lead to the conclusion that at present acoustic trapping devices could not be sufficiently optimised to allow robust modelling of CLL microenvironment interactions. In light of this, the goal of the project was refocused to investigate in more detail the basis of HFFF2-mediated CLL cell protection in standard 2D cultures.

Chapter Five

Role of the chemokine receptor CXCR4 and its ligand CXCL12 in HFFF2-cytoprotection

Chapter 5: Role of the chemokine receptor CXCR4 and its ligand CXCL12 in HFFF2-cytoprotection

5.1 Introduction

Chemokines secreted by stromal cells play a critical role in the homing and retention of CLL cells in tissues. The most characterised of these stromal chemokines is CXCL12. As outlined in the Introduction (Section1.4.4.1) the main receptor for this chemokine is CXCR4 and the major role of CXCL12 is to regulate haematopoietic cell trafficking and SLO architecture (Cyster, 2005, Peled et al., 1999, Broxmeyer et al., 2005). CXCL12 has two major effects on CLL cells; firstly it causes migration towards stromal cells, and secondly, it provides survival signals to CLL cells (Burger et al., 2000). These effects are mediated through the chemokine receptor CXCR4, a GPCR which is expressed on the surface of peripheral blood CLL cells (Burger et al., 1999, Burger and Peled, 2009, Mohle et al., 1999). Surface expression of CXCR4 on CLL cells is approximately three to four-fold greater than that of normal blood and bone marrow B cells (Mohle et al., 1999).

Receptor internalization by endocytosis is a major feature for most chemokine receptors. CXCR4 is no different and binding of CXCL12 to the receptor induces a dose dependent endocytosis of CXCR4 (Burger et al., 1999). CXCR4 can therefore be used as a marker of CXCL12 'exposure' in CLL cells. Circulating CLL cells in the peripheral blood characteristically express variable levels of surface CXCR4, while CLL cells resident in the tissue microenvironments and in close contact to CXCL12 secreting cells have lower levels of surface CXCR4 (Ghobrial et al., 2004). These differences in CXCR4 expression have led a model of cell re-circulation through the tissues (Introduction Figure, (Calissano et al., 2009)). Thus, peripheral blood CLL cells express variable levels of CXCR4 depending on whether they have recently left the CXCL12-expressing tissues or have recovered receptor expression and are preparing to re-enter with CLL cells in the blood (Coelho et al., 2013). Indeed, within individual samples, cells with low CXCR4 typically express low levels of sIgM indicating that at least some of these cells have recently engaged antigen (Coelho et al., 2013). Moreover, cells with low CXCR4 and high CD5 have increased expression of Ki67, and altered gene expression signatures associated with proliferation, apoptosis and oxidative damage (Calissano et al., 2009). The natural recovery of CXCR4 on CLL cells in the circulation can be mimicked by incubating CLL cells *in vitro* where levels of CXCR4 increase rapidly (within hours; (Coelho et al., 2013)).

The CXCL12-CXCR4 axis is also important for CLL cell survival with a number of studies linking the chemokine CXCL12 to survival *in vitro*. Burger et al., demonstrated that recombinant CXCL12 protects CLL cells against spontaneous apoptosis (Burger et al., 2000) and in the same study showed that blocking antibodies against CXCL12 blocked NLC-mediated protection (Burger et al., 2000).

Due to the fact that CXCL12 not only attracts CLL cells to the supportive microenvironment but also directly stimulates CLL cell survival, the CXCR4-CXCL12 axis is an important therapeutic target. Blocking CXCR4/CXCL12 interactions could potentially have a number of effects. It would firstly disrupt the adhesion of CLL cells to protective stromal interactions that confer survival via multiple mechanisms. Secondly it would cause the mobilisation of CLL cells from the tissues sites into the peripheral blood making them much more susceptible to other therapies. Thirdly, it would block the migration of cells back into the protective microenvironment. Finally, blocking the CXCL12/CXCR4 axis would block CXCR4-mediated survival signals (Burger and Peled, 2009).

For the reasons outlined above, inhibition of the CXCR4/CXCL12 axis has advanced well into clinical development and is holding great promise. CXCR4 antagonists inhibit CLL-cell activation by CXCL12 and can reverse, at least in part, stromal cell-mediated drug resistance (Burger et al., 2005). There are four main classes of CXCR4 antagonists; small peptide antagonists, non-peptide antagonists, antibodies to CXCR4 and RNA oligonucleotides. Antagonists of CXCR4 effectively block CXCL12-induced activation, migration and signalling of CLL cells as well as reverse stromal-mediated protection (Burger et al., 2005). Plerixafor, a bicyclam is a specific small molecule antagonist of CXCR4 which is licenced for stem cell mobilisation and is currently in clinical trials for CLL (Introduction, Table 1.2). Plerixafor inhibits CXCL12-mediated calcium mobilisation and chemotaxis and shows no cross reactivity with other chemokine receptors. A phase I clinical trial of plerixafor used in combination with rituximab showed a plerixafor dose-dependent mobilization of CLL cells into the peripheral blood (Andritsos et al., 2010).

5.2 Hypothesis

The chemokine CXCL12 is produced by the HFFF2 cell line and acts via CXCR4 to protect CLL cells from apoptosis *in vitro*.

5.3 Aims and objectives

The aim of this chapter was to determine whether the chemokine receptor CXCR4 along with its ligand CXCL12 plays a role in the cytoprotection provided by the HFFF2 cell line to CLL cells *in vitro*. I also investigated the effect of HFFF2 co-culture on the expression and recovery of CXCR4 on CLL cells *in vitro*. The specific objectives were:

- Separate HFFF2-derived CM into different molecular weight fractions to determine an approximate molecular weight of any molecules responsible for protection provided to CLL cells in HFFF2-derived CM
- Investigate production of CXCL12 by HFFF2 cells
- Determine the effect of HFFF2 cell co-culture on CXCR4 expression and recovery on CLL cells *in vitro*
- Determine the effect of HFFF2-derived CM on CXCR4 expression and recovery on CLL cells *in vitro*
- Investigate any differences in the effect of direct HFFF2 cell contact and HFFF2-derived CM on CXCR4 expression and recovery on CLL cells *in vitro*
- Investigate the role of CXCR4 and CXCL12 on CLL cell survival in the HFFF2 culture model using neutralising antibodies and antagonists towards CXCR4 and CXCL12.

5.4 Separation of HFFF2-CM to determine approximate molecular weight of candidate molecules responsible for HFFF2-mediated cytoprotection

Due to the ability of HFFF2-derived CM to increase survival of CLL cells (Section 3.6) the first aim was to investigate the soluble factor(s) present in the CM which mediate increased CLL cell survival. This was initially addressed by separating HFFF2-CM into low (<3kDa) and high (>3kDa) molecular weight (MW) fractions to probe the nature of the active factor(s). For example, Zhang et al., has previously shown that when using a cut-off of 3kDa, it was the low MW fraction (LMW) of stromal cell-derived CM that promoted cell survival, an effect mediated via cysteine (Zhang et al., 2010). By contrast, if protection was mediated via chemokines and cytokine (typically 8-10kDa) as in line with my hypothesis, then the high MW (HMW) fraction would be expected to contain the survival promoting activity.

HFFF2-CM was separated into high and low MW fractions using Millipore separation columns with a 3kDa cut off. CLL cells were co-cultured as per previous survival experiments prior to Annexin-V/PI staining and FACS analysis at 24 and 48 hours. CLL cells were either cultured alone, in the presence of HFFF2 cells, with unseparated HFFF2-CM, or with the LMW and HMW fractions. As an additional control CLL cells were also treated with a 'recombined CM' formed by adding equal quantities of the HMW and LMW fractions.

Three samples were selected for an initial pilot study (Figure 5-1). As expected HFFF2 cell co-culture and HFFF2-CM effectively protected CLL cells from spontaneous apoptosis *in vitro*. Results obtained using the CM fractions were more variable. For samples CLL 663 and CLL 661, the LMW fractions did not enhance survival, whereas for sample CLL 656 a slight improvement in cell viability was observed. By contrast, the HMW fraction enhanced cell survival of all three samples, although the extent of protection was variable. Extent of protection provided by the 'recombined CM' was generally similar to unfractionated CM.

The study was expanded to an additional 5 samples but restricting analysis to the 48 hour time point where differences between LMW and HMW CM fractions were most apparent in the pilot experiments. A summary for all samples analysed is shown in Figure 5-2. In this larger analysis, there was, overall, no substantial protective effects mediated by LMW-CM. By contrast, HMW-CM significantly increased CLL cell survival, although not to the same extent as HFFF2 cell co-culture or HFFF2-CM. Protection mediated by the 'recombined CM' was also reduced compared to unfractionated CM, suggesting that the process of fractionation may have had a modest inhibitory effect on the survival promoting activity, perhaps explaining why the survival advantage provided by the HMW-CM did not reach the levels obtained with unfractionated CM.

Overall, the results suggest that HFFF2 cell-mediated cytoprotection is not consistently mediated by low molecular weight factors such as cysteine. By contrast, the results are consistent with a potential role for soluble chemokine and/or cytokines, including CXCL12 (MW ~8kDa).

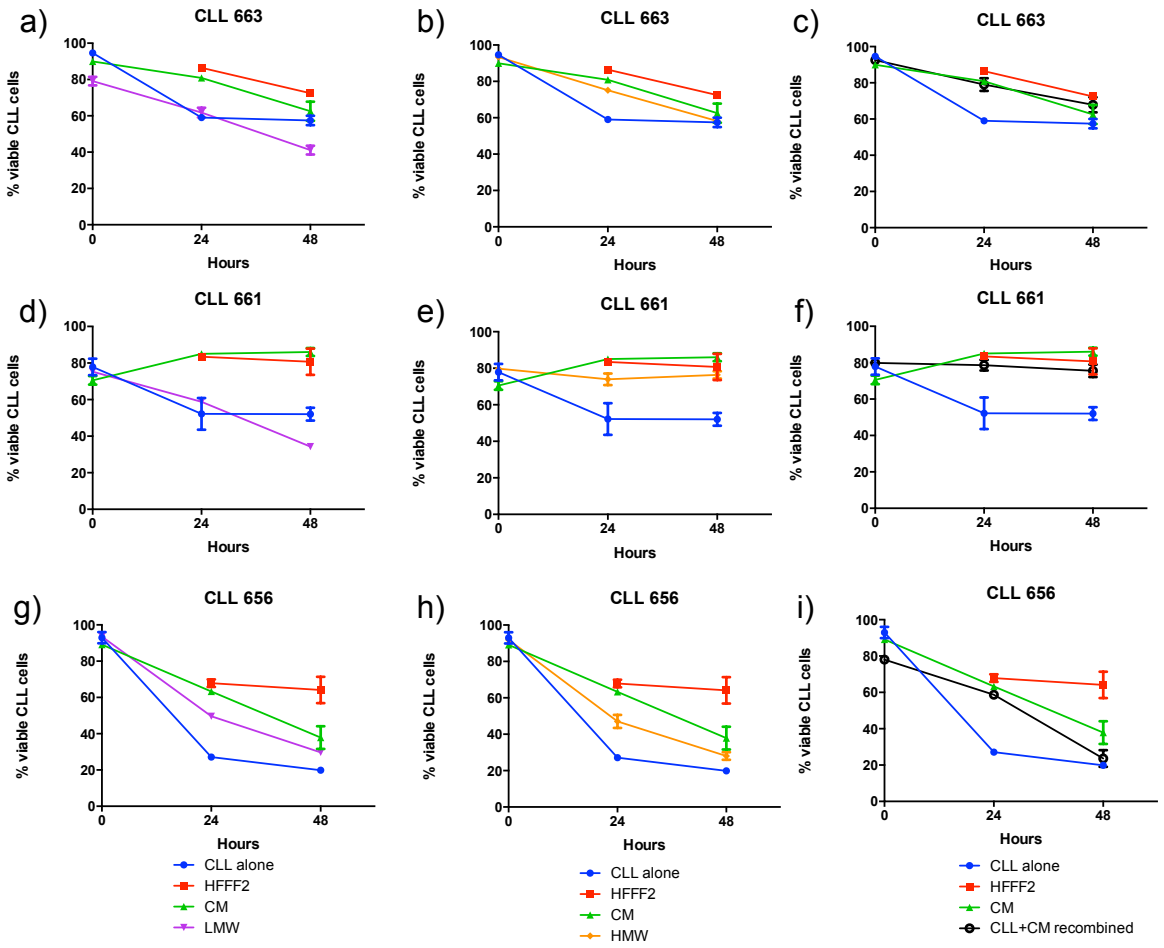

FIGURE 5-1: SEPARATION OF HFFF2-CM USING MILLIPORE SEPARATION COLUMNS WITH A 3KDA CUT-OFF

Viability results for three CLL samples. HFFF2-CM was separated into low and high molecular weight fractions (LMW and HMW respectively) using a 3 kDa cut off filter. CLL cells were cultured alone (blue line) or in the presence of CM (green line) for 0, 24 or 48 hours prior to analysis of CLL cell viability. Results for each patient are shown in three graphs. All graphs show CLL cells cultured alone (blue line), CLL cells cultured with HFFF2 cells (red line) and CLL cells cultured with CM (green line). The separated fractions are then split across the three graphs. (a,d,g) CLL cells cultured with the LMW fraction (purple line). (b,e,h) CLL cells cultured with the HMW fraction (orange line) and (c,f,i) 'CM recombined' (black line). Cell viability was measured by Annexin-V/PI staining with gating as outlined in previous chapter (Figure 3-1).

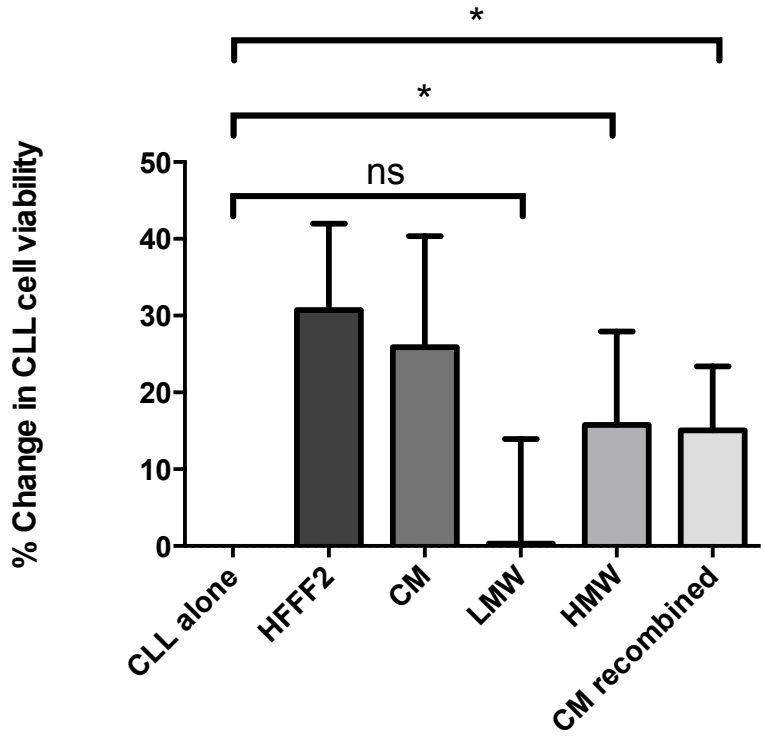

FIGURE 5-2: EFFECT OF LOW AND HIGH MOLECULAR WEIGHT FRACTIONS OF HFFF2-CM ON CLL CELL SURVIVAL

CM was separated into low and high MW fractions using a 3KDa cut off. CLL cells were cultured alone or in the presence of CM for 48 hours prior to analysis of CLL cell viability. Summary for all samples analysed (n=8). Due to the variation in rates of spontaneous apoptosis between CLL samples data were corrected to show percentage change in CLL cell viability for CLL cells co-cultured with either unfractionated CM, LMW CM, HMW CM, or recombined CM, compared to CLL cells cultured alone. Statistical significance of differences are indicated (Wilcoxon Test; *P=0.0313). Error bars are SD. Analysis and graphs created using Graphad prism 6.

5.5 Ability of the HFFF2 cell line to secrete CXCL12

An ELISA assay was next used to quantify secretion of CXCL12 by HFFF2 cells, and to determine whether expression was altered when cells were induced to transdifferentiate by exposure to TGF-β. Cells were cultured under the various conditions for 72 hours and before the culture supernatant was collected and CXCL12 quantified (Figure 5-3). CXCL12 was detected in the cell supernatants under all conditions at concentrations >1 ng/ml. Although variation in experimental conditions make comparisons to other studies difficult, the levels of CXCL12 secreted by HFFF2 cells appeared high (Table 5.1), consistent with the idea that this chemokine may play a significant role in HFFF2 cell mediated survival of CLL cells.

Interestingly, treatment with TGF-β reduced CXCL12 secretion by ~30% (Figure 5-3). Previous results from the host laboratory have shown that the survival promoting effects of HFFF2 cells for CLL cells is reduced when cells are induced to undergo TGF-β-induced transdifferentiation (Samantha Dias, unpublished data). Although correlative, this observation is consistent with the reduced secretion of CXCL12 by transdifferentiated HFFF2 cells. Therefore, further experiments were performed to directly investigate the role of the CXCL12/CXCR4 axis in CLL cell cytoprotection.

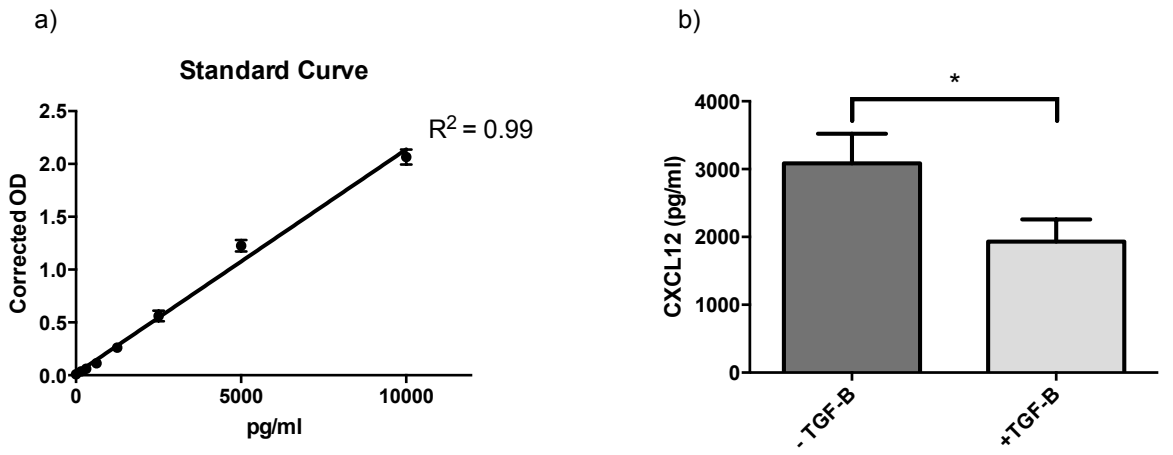

FIGURE 5-3: QUANTIFICATION OF CXCL12 LEVELS IN HFFF2 CELL CULTURE SUPERNATANT

HFFF2 cells were cultured for 72hrs with or without TGF-β (2ng/ml). After 72 hours culture supernatant was collected from each of the wells and CXCL12 was quantifies using an ELISA assay. CXCL12 concentrations were calculated using a standard curve (a). (b) Summary of CXCL12 levels determined from standard curve in all experimental repeats (n=9). The bars show data for non-treated HFFF2 cells and those treated with TGF-β. Statistical significance is indicated (Wilcoxon Test; *P=0.0391). Error bars are SD. Analysis and graphs created using Graphad prism 6.

TABLE 5.1: LEVELS OF CXCL12 SECRETED FROM VARIOUS STROMAL CELL TYPES IN THE LITERATURE

Cell Type	CXCL12 Level	Culture conditions	Reference
Human Osteoblasts	Ranged from 138±36 to 787±48pg/ml	96hrs/10^4 cells	(Taichman et al., 2002)
Human Osteoblasts	~400pg/ml	72hrs	(Sun et al., 2003)
Mouse embryonic fibroblasts	50 to 1,000pg/ml	48hrs	(Moskovits et al., 2006)
W1-38 human diploid embryonic fibroblasts	50 to 1,000pg/ml	48hrs	(Moskovits et al., 2006)
Human umbilical vein endothelial cells	10.36±0.2ng/ml	2 to 120 hrs/ 3×10^4/ml	(Salvucci et al., 2002)
Caco-2 cells	Ranged from 830 and 4900 ng/ml	-	(Brand et al., 2005)
Prostate stromal fibroblasts	3.70 to 17.47 pg/ml	72hrs	(Begley et al., 2005)
MSCs	1147.7±310.2pg/ml	24hrs/10^5 cells	(Sorrentino et al., 2008)
Synovial Fibroblasts	300pg/ml	48hrs	(Hitchon et al., 2002)

5.6 The effect of HFFF2 cell co-culture on CXCR4 expression on CLL cells

I next investigated the effect of HFFF2 cells on expression of CXCR4 by CLL cells. As described (Section4.1), downmodulation of CXCR4 is a useful “biomarker” of exposure to CXCL12. Therefore, CXCR4 expression was quantified to determine whether the secretion of CXCL12 by HFFF2 cells was sufficient to engage and downmodulate CXCR4 on CLL cells. The first experiments were performed using co-culture of CLL and HFFF2 cells. CXCR4 expression on CLL cells naturally recovers with time (Coelho et al., 2013). Therefore, time course experiments were performed to monitor recovery of CXCR4 in the presence or absence of HFFF2 cells over a 48 hour culture period. CXCR4 was quantified using flow cytometric analysis of CD5+CD19+ cells. CXCR4 recovery is relatively rapid (Coelho et al., 2013) and expression was therefore analysed at the start of the experiment and at 8 hours. CXCR4 expression was measured by gating on the CD5+CD19+ positive population to ensure only the expression of CXCR4 on CLL cells was being measured. Data were corrected to the isotype control to account for any background fluorescence and then normalised to baseline expression MFI levels at time of recovery to firstly demonstrate the recovery of CLL cells over culture *in vitro* and secondly to demonstrate any reductions in receptor expression seen following culture with HFFF2 cells. Figure 5-4 demonstrates the results obtained for the six samples analysed. As expected, there was a clear increase in expression of CXCR4 at 8 hours in each sample. However, co-culture with HFFF2 cells effectively suppressed CXCR4 recovery. In 4/6 samples, there was no increase in CXCR4 expression in co-cultured CLL cells compared to cells at the start of the experiment. In the other 2 samples, inhibitory effects of HFFF2 cell co-culture was partial. Figure 5-5 shows summarised data for all samples, confirming that HFFF2 cell co-culture significantly reduced the recovery of CXCR4 on CLL cells at 8 hours. The graph also shows that HFFF2 cell co-culture also reduced CXCR4 expression at later time points (24 and 48 hours). Here, CXCR4 expression was typically reduced below the levels observed at the start of the experiment, although the recovery of CXCR4 on control CLL cells (without HFFF2 cells) is quite variable at these times.

These results indicate that CXCR4 is down-modulated on CLL cells co-cultured with HFFF2 fibroblasts, providing further support for the hypothesis that CXCL12 mediates cytoprotectible effects of HFFF2 cells.

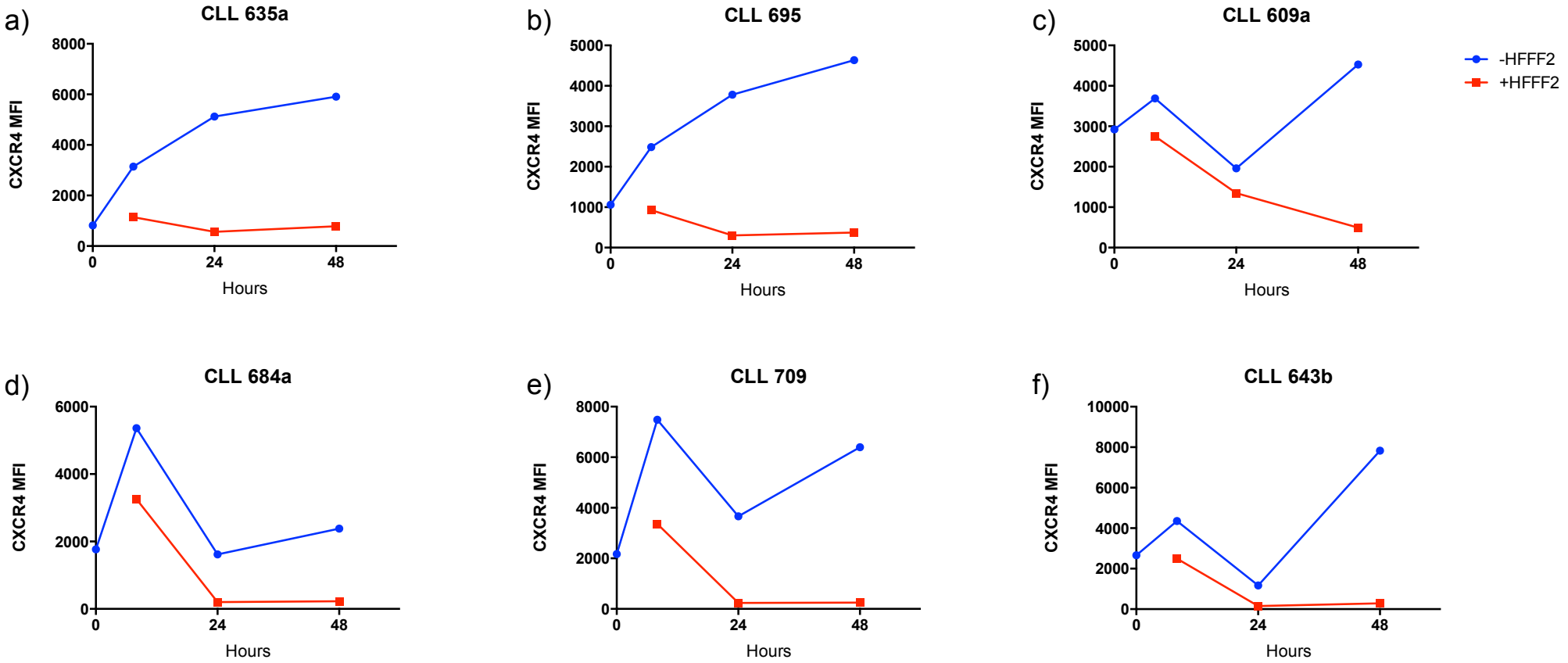

FIGURE 5-4: EFFECT OF HFFF2 CELL CULTURE ON CXCR4 EXPRESSION ON CLL CELLS

CLL cells were cultured alone (blue line) or co-cultured with HFFF2 cell line (red line) for 48 hours. CXCR4 expression was quantified by flow cytometry at the start of the experiment (0 hours) and at 8, 24 and 48 hours. Graphs show data obtained for the six samples investigated. Analysis and graphs created using Graphad prism 6.

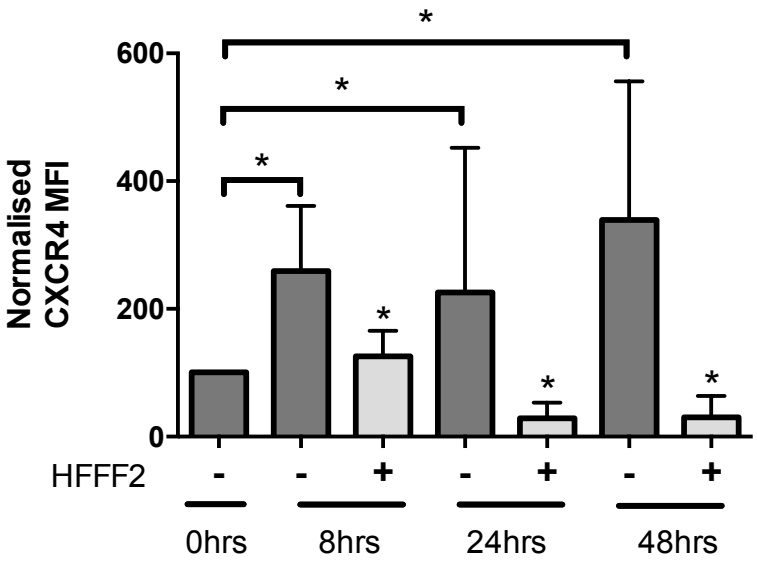

FIGURE 5-5: EFFECT OF HFFF2 CELL CO-CULTURE ON CXCR4 EXPRESSION ON CLL CELLS

The ability of the CLL cells to recover the chemokine receptor CXCR4 *in vitro* was measured in the presence or absence of the HFFF2 cell line. Summary of data for all samples analysed (n=6). Data was normalised to CXCR4 expression of CLL cells at the start of the experiment (set to 100 for each sample). Statistical significance of differences is indicated (Wilcoxon Test; *P=0.0313). Error bars are SD. Analysis and graphs created using Graphad prism 6.

5.7 Effect of HFFF2-derived CM on CXCR4 expression on CLL cells

Additional experiments were performed to investigate the effect of HFFF2-CM on CXCR4 expression of CLL cells. Experiments were performed as for Figure 5-4 and Figure 5-5 except that HFFF2-CM was used in place of HFFF2 cell co-culture and analysis focused on 24 and 48 hour time points. The 8 hour was excluded from these preliminary studies due to the fact that the greatest fold change between the conditions was seen at the later time points of 24 and 48 hours. Figure 5-6 demonstrates results obtained for the five samples investigated. There was a clear increase in CXCR4 expression in 3/5 samples analysed (643b being the only patient common to the HFFF2 and CM experiments), whereas CXCR4 expression did not increase in the other two samples. Intersample variation in CXCR4 recovery has been reported previously (Coelho et al., 2013). Surprisingly, in the 3 samples which showed CXCR4 recovery, addition of HFFF2-CM had no substantial effect on CXCR4 expression.

The differences observed in experiments analysing effects of HFFF2 cell co-culture and HFFF2-CM on CXCR4 expression were surprising since they suggested that the secretion of CXCL12 by HFFF2 cells, and the survival promoting effects of HFFF2 cells were "uncoupled". However, direct comparison between the two studies is difficult since they were performed using largely independent sample cohorts. Therefore, to confirm this result, additional experiments were performed to directly compare the effects of HFFF2 cell co-culture and HFFF2-CM on CXCR4 recovery on CLL cells. Five CLL samples were cultured either alone, co-cultured with HFFF2 cells or with HFFF2-CM. Data for individual samples is shown in Figure 5-7 and Figure 5-8 shows a summary for all samples analysed in parallel. As shown previously, there was an increase in CXCR4 expression in control CLL cells at 8 hours. CXCR4 expression varied at later time points, but was generally maintained at the levels measured at the start of the experiment in all samples. Consistent with the previous studies, CXCR4 expression was consistently downmodulated by co-culture with HFFF2 cells, but not by HFFF2-CM. In fact, these data suggest that HFFF2-CM may have modestly increased CXCR4 expression on CLL cells, especially at 24 hours.

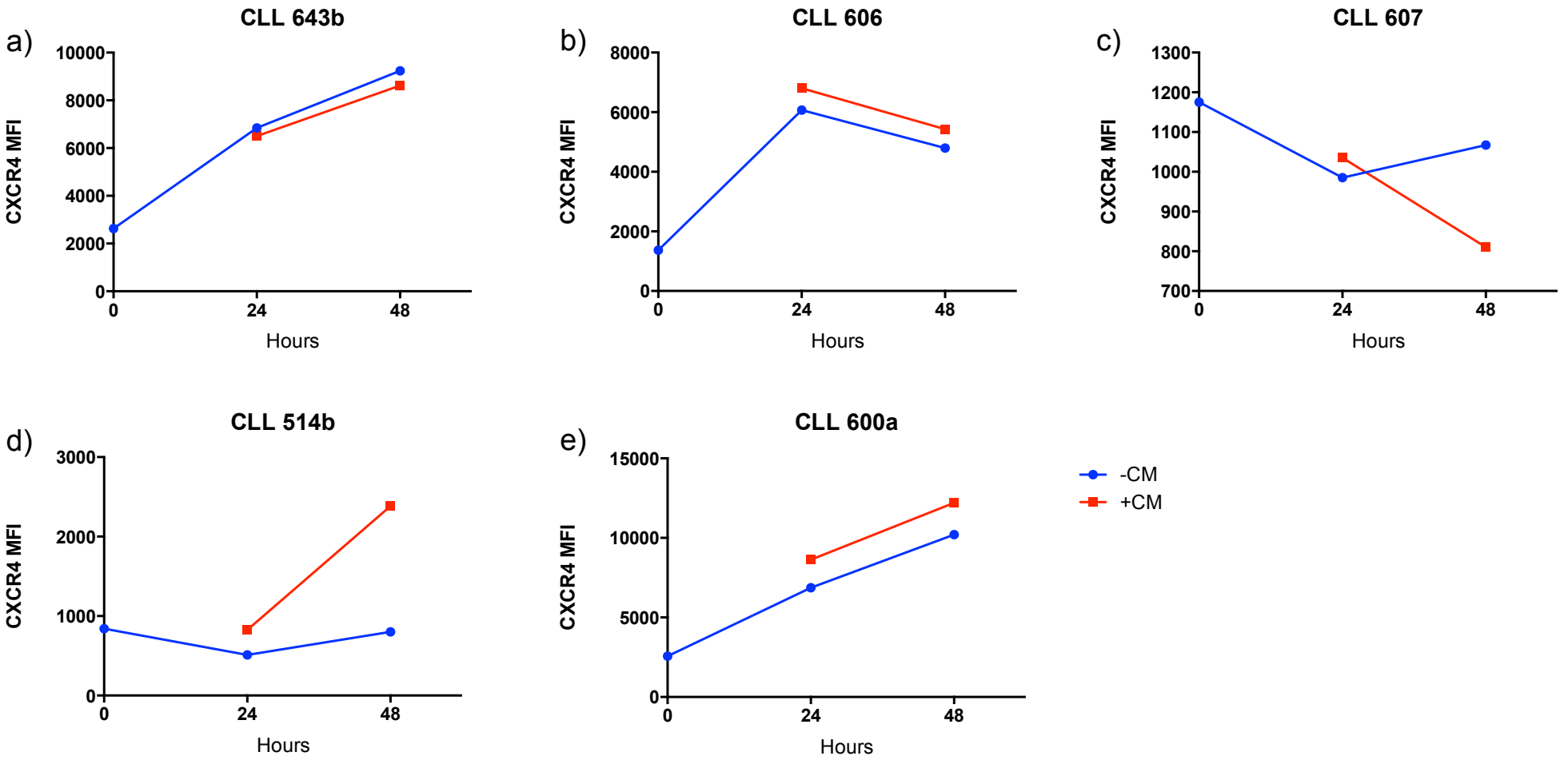

FIGURE 5-6: EFFECT OF HFFF2-DERIVED CM ON CXCR4 EXPRESSION ON CLL CELLS

CLL cells were cultured alone (blue line) or with HFFF2-CM (red line) for up to 48 hours. CXCR4 expression was measured at time of recovery (0 hours), 8, 24 and 48 hours via flow cytometry. Graphs show results for the five patients investigated. Analysis and graphs created using Graphad prism 6.

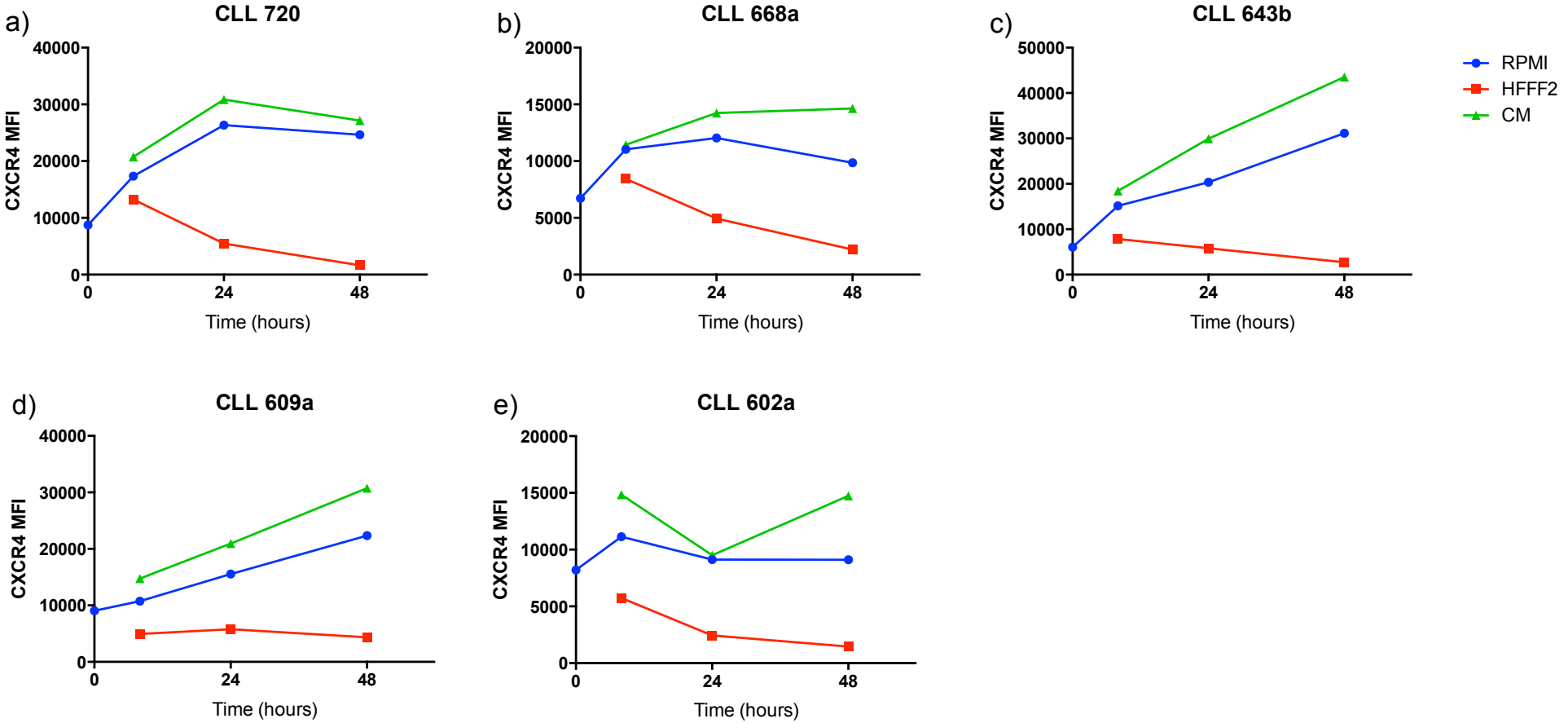

FIGURE 5-7: COMPARISON OF HFFF2 DIRECT CO-CULTURE AND HFFF2-DERIVED CM ON CXCR4 EXPRESSION ON CLL CELLS

A direct comparison was carried out to determine the difference between direct HFFF2 cell contact and HFFF2-derived CM on CXCR4 expression *in vitro*. CLL cells were either cultured alone (blue line), co-cultured with HFFF2 cells (red line) or cultured with HFFF2-derived CM (green line) for 48 hours. CXCR4 was measure at time of recovery (0 hours), 8, 24 and 48 hours via flow cytometry. Graphs display results for the five patients investigated. Analysis and graphs created using Graphad prism 6.

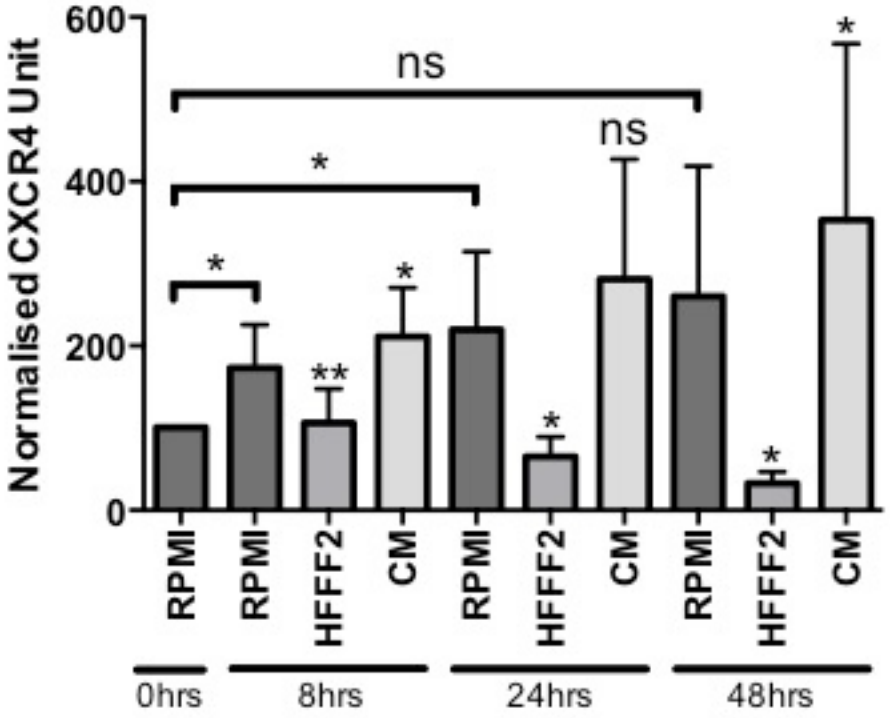

				Pvalue
CXCR4 recovery	RPMI 0hr	RPMI 8hr	*	0.0351
	RPMI 0hr	RPMI 24hr	*	0.0473
	RPMI 0hr	RPMI 48hr	ns	0.0866
HFFF2 co-culture	RPMI 8hr	HFFF2 8hr	**	0.0092
	RPMI 24hr	HFFF2 24hr	*	0.0113
	RPMI 48hr	HFFF2 48hr	*	0.0281
HFFF2-CM	RPMI 8hr	CM 8hr	*	0.0106
	RPMI 24hr	CM 24hr	ns	0.0779
	RPMI	CM 48hr	*	0.0351

FIGURE 5-8: COMPARISON OF HFFF2 DIRECT CO-CULTURE AND HFFF2-DERIVED CM ON CXCR4 EXPRESSION ON CLL CELLS

A direct comparison was carried out to determine the difference between direct HFFF2 cell contact and HFFF2-derived CM on CXCR4 expression *in vitro*. Summary of data for all samples analysed (n=5). Data was normalised to CXCR4 expression at time of recovery (0 hours) to firstly display the recovery of CXCR4 *in vitro* in CLL cells and secondly the effect of HFFF2 cell co-culture and HFFF2-derived CM culture on this increase in receptor expression. Statistical significance is indicated on the graph and individual p values are reported in the table (Wilcoxon Test; ns = non significant). On the graph, statistical significance displayed directly above the bars indicates result compared to RPMI of the same time point. Error bars are SD. Analysis and graphs created using Graphad prism 6.

5.8 Effect of neutralising antibodies to CXCR4 and CXCL12 on HFFF2-mediated CLL cell survival

To directly investigate the role of CXCR4 and CXCL12 in HFFF2-mediated cell survival, I performed a series of experiments using neutralising antibodies to specifically block the function of the chemokine and receptor. Antibody selection was based on the literature where previous studies have shown that neutralising CXCR4 and CXCL12 antibodies suppress CXCR4 mediated apoptosis in HPB-ALL cells, gp120- and gp160-induced apoptosis in cultured endothelial cells and CXCL12 induced migration of CLL cells, respectively (Berndt et al., 1998, Ullrich et al., 2000, Mohle et al., 1999, Burger et al., 1999, Petty et al., 2007, Ouwehand et al., 2008).

Prior to analysis of effects on HFFF2-mediated survival, the antibodies were tested for their ability to inhibit CXCL12-induced migration of CLL cells in transwell assays. CLL cells were cultured for 16 hours overnight to allow recovery of CXCR4 and then pre-treated with the CXCR4 neutralising or isotype control antibody. Cells were then placed in the upper chamber of the transwell plates and CXCL12-supplemented media was placed in the lower chamber. For CXCL12 neutralising experiments, CLL cells were cultured for 16 hours and then placed in the top chamber, and CXCL12-supplemented media with anti-CXCL12 or control antibody was placed in the lower chamber. As an additional control, all experiments were also performed with media (without added CXCL12) in the lower chamber to quantify migration in the absence of chemokine. Migration was analysed after 2 hours incubation, using flow cytometric quantitation of CD5+CD19+ cells. Concentration ranges for both antibodies were determined using data sheets supplied with the antibodies along with published literature.

Figure 5-9 demonstrates results obtained with one CLL sample; very similar results were obtained using another sample (not shown). The experiments confirm the ability of the neutralising antibodies to inhibit CXCL12-induced CLL cell migration. Responses to either antibody were dose-responsive, with reduced inhibitory activity at lower concentrations. Control antibodies had no effect on CXCL12-mediated migration (data not shown). Based on these results, the CXCL12 specific antibody was tested in further experiments at 40 or 8μg/ml. For the CXCR4 neutralising antibody, further experiments were performed using the antibody at 10μg/ml. Although, not optimal for inhibition, this concentration was selected due to cost levels.

To investigate the effects of CXCR4 or CXCL12 neutralising antibodies on HFFF2 cell mediated protection of CLL cells, CLL cells were cultured alone or co-cultured with HFFF2

cells, in the presence of neutralising antibodies or relevant control antibody. CLL cell survival was measured using Annexin-V/PI staining at the start of the experiment (0hr) and at 24 and 48 hours. Twelve samples were analysed using the CXCR4 neutralising antibody. Figure 5-10a-f shows data from 6 representative samples and data for all samples is summarised in Figure 5-10g. The results demonstrate that the CXCR4 neutralising antibody has no effect on the ability of HFFF2 cell co-culture to suppress spontaneous apoptosis of CLL cells.

Similar experiments were performed using the CXCL12 neutralising antibody. The experiment was performed using only two CLL samples, due to the high cost of the antibody. Figure 5-11a,b shows the separate data from the two samples and data for both samples is summarised in Figure 5-11c. Similar to studies using the CXCR4 neutralising antibody, the CXCL12 neutralising antibody has no effect on the ability of HFFF2 cell co-culture to suppress spontaneous apoptosis of CLL cells. These experiments, demonstrate that, despite secretion of high levels of CXCL12 by HFFF2 cells, this chemokine appears not to play a substantial role in the survival promoting effects induced by these cells.

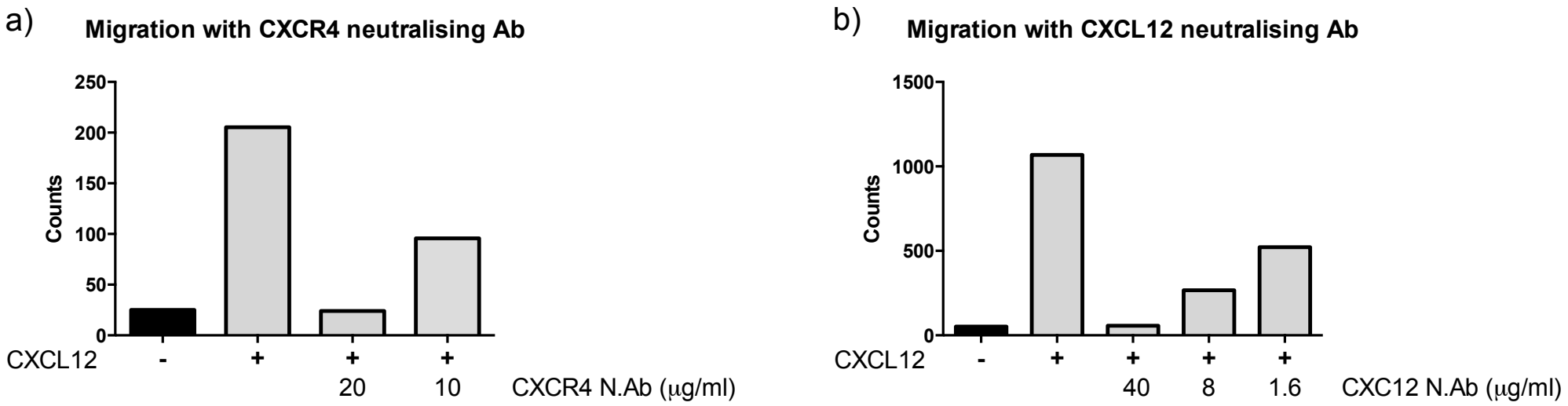

FIGURE 5-9: EFFECT OF NEUTRALISING ANTIBODIES TO CXCR4 AND CXCL12 ON CLL CELL MIGRATION

Figure shows data from one patient of two studied. CLL cells were cultured for 16 hours overnight to allow recovery of CXCR4. (a) CLL cells were then treated with either the CXCR4 neutralising antibody or left untreated as a control and plated into the upper chamber of transwell plates. (b) CLL were plated in the top chambers of a transwell plates treated and tested for migration towards standard media, or CXCL12-supplementred media in the presence of various concentrations of CXCL12 neutralising antibody. For both experiments, CLL cells were allowed to migrate for 2 hours and the number of migrated CD5+/CD19+ cells were determined using flow cytometry. Analysis and graphs created using Graphad prism 6.

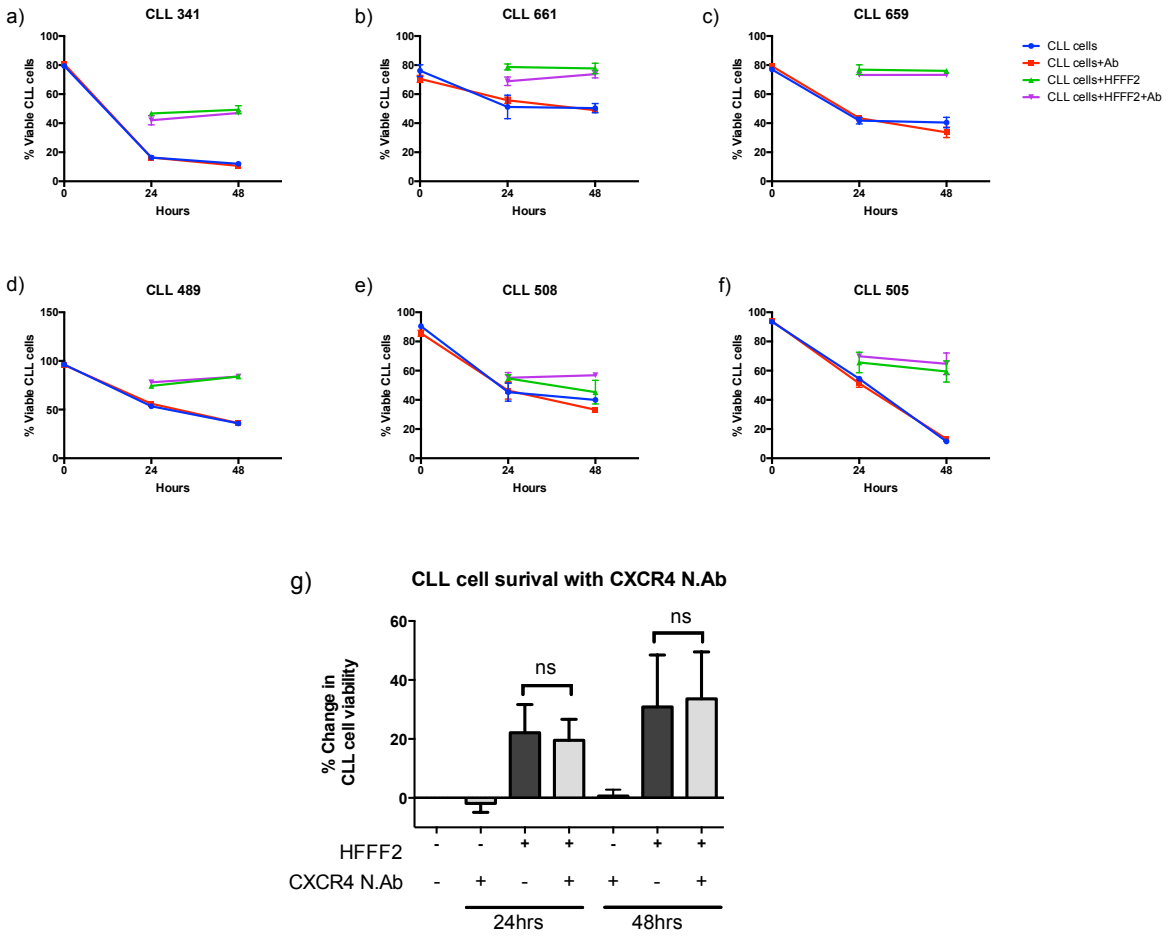

FIGURE 5-10: EFFECT OF A CXCR4-SPECIFIC NEUTRALISING ANTIBODY ON THE CYTOPROTECTIVE EFFECTS OF HFFF2 CELLS ON CLL CELLS

CLL cells were cultured alone, or co-cultured with HFFF2 cells in the presence or absence of a neutralising CXCR4 antibody or control antibody (10 µg/ml). CLL cell survival was measured using Annexin-V/PI staining at time of recovery (0 hr), and at 24 and 48 hours. (a-f) Raw Annexin-V/PI results. CLL cells were cultured alone (blue line) or with the neutralising antibody (red line) and also co-cultured with HFFF2 cells (green line) and with HFFF2 cells and the antibody (purple line). Each determination was performed in triplicate; Error bars are SD. (g) Summary of data for all samples analysed (n=12). Due to the variation in rates of spontaneous apoptosis between CLL samples data were corrected to show percent change in CLL cell viability for CLL cells co-cultured with fibroblasts compared to CLL cells cultured alone. Statistical significance is indicated (Mann Whitney test; ns indicates non significant differences, p=0.5221 and 0.8729 respectively). Error bars are SD. Analysis and graphs created using Graphad prism 6.

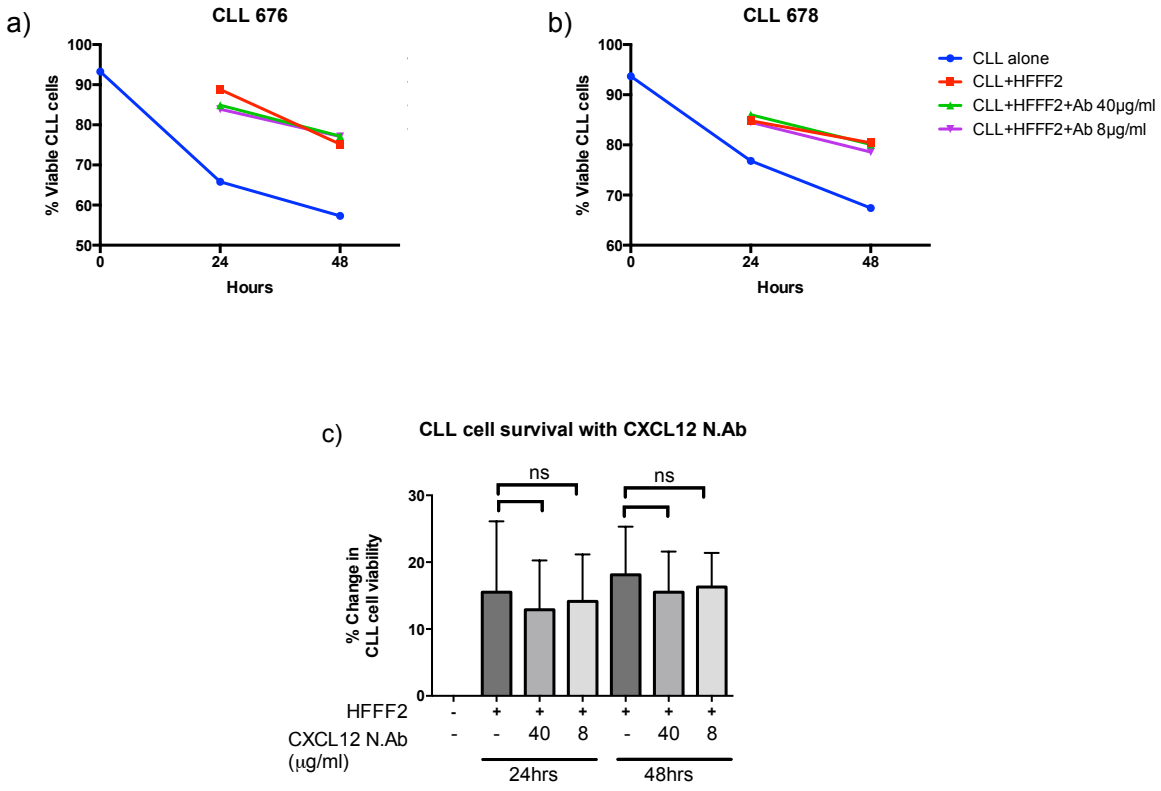

FIGURE 5-11: EFFECT OF A NEUTRALISING ANTIBODY TO CXCL12 ON THE PROTECTION PROVIDED BY THE HFFF2 CELL LINE

CLL cells were cultured in the presence or absence of HFFF2 and were treated with a neutralising antibody to CXCL12 or appropriate isotype control antibody (40 and 8µg/ml). CLL cell survival was measured using annexin-V/PI staining at the start of time of recovery (0 hr), and at 24 and 48 hours. (a,b) Raw Annexin-V/PI results. CLL cells were cultured alone (blue line) or with the neutralising antibody 40µg/ml (green line), neutralising antibody 8µg/ml (purple line) and also co-cultured with HFFF2 cells (red line). Each determination was performed in triplicate; Error bars are SD. (c) Summary of data for all samples analysed (n=2). Due to the variation in rates of spontaneous apoptosis between CLL samples data were corrected to show percent change in CLL cell viability for CLL cells co-cultured with fibroblasts compared to CLL cells cultured alone. Statistical significance is indicated (Mann Whitney test; ns indicates non significant data). Error bars are SD. Analysis and graphs created using Graphad prism 6.

5.9 Key findings

The results from Chapter3 indicated that a soluble factor was, at least to some extent, responsible for the protection against spontaneous apoptosis seen when CLL cells were cultured with HFFF2 cells or HFFF2-derived CM. Given previous studies implicating CXCL12 in stromal cell-mediated survival of CLL cells, the main aim of the experiments described in this chapter was to investigate the significance of this chemokine for HFFF2 cell-mediated protection. Overall, the results demonstrate that CXCL12/CXCR4 interactions do not significantly contribute to the survival promoting effects of HFFF2 cells.

- Separation of HFFF2-derived CM revealed that the HMW fraction protected CLL cells from spontaneous apoptosis more than the LMW fraction
- The HFFF2 cell line secretes the chemokine CXCL12
- Co-culture of CLL cells with HFFF2 cells prevents recovery of the chemokine receptor CXCR4
- Co-culture of CLL cells with HFFF2-derived CM increases expression of the chemokine receptor CXCR4
- Neutralising antibodies to CXCR4 and CXCL12 decrease CXCL12-mediated migration but do not reduce protection against spontaneous apoptosis mediated by HFFF2 cells or HFFF2-derived CM

5.10 Discussion

5.10.1 The potential role of a HMW molecule in HFFF2-derived CM-mediated protection of CLL cells

As discussed in Chapter 3 a number of studies demonstrated the ability of soluble factors to promote CLL cell survival. In particular Zhang et al*.,* had previously shown that three different cell lines (HS-5, StromaNKtert, and KUSA-H1) were able to promote CLL cell survival through a microporous membrane to prevent direct contact when treated with F-ara-A, oxaliplatin or H_20_2 (Zhang et al., 2010). These experiments firstly aimed to try and determine any candidate molecules involved in HFFF2 CM-mediated protection through the separation of HFFF2-derived CM. The preliminary experiment aimed to replicate what was demonstrated by Zhang and colleagues in the HS-5 cell line. Zhang et al., separated stromal conditioned media at 3kDa and demonstrated that the LMW fraction of the stromal CM enhanced GSH synthesis in CLL cells and promoted cell survival (Zhang et al., 2010).

They went on to discover that cysteine was the soluble factor secreted by HS-5 stromal cells responsible for protecting CLL cells from apoptosis. This revealed an important metabolic interaction between CLL cells and stromal cells allowing CLL cells to maintain the redox balance ultimately promoting cell survival and drug resistance (Zhang et al., 2010). Conversely, demonstrated in Figure 5-2, I have shown in the HFFF2 cell model that the HMW fraction conferred the greatest protection to CLL cells over a 48 hour period. This excludes the possibility that the soluble factor in HFFF2-CM could be cysteine or another low molecular weight metabolic molecule and that HFFF2-mediated protection is probably not through a metabolic pathway. Further to this, it has been shown previously in the host laboratory that culture in the presence of HFFF2 cells does not affect the levels of reactive oxygen species (ROS) in CLL cells, indicating that in this model, HFFF2 cells are not effecting the redox balance and this is not contributing to CLL cell survival (Samantha Dias, PhD thesis). The differing results from what was demonstrated by Zhang et al., may again firstly demonstrate the importance of choosing the correct model when characterising CLL/microenvironmental interactions and secondly underline the fact that microenvironment-mediated survival signals to CLL cells most probably occur through a number of cell types and a number of different molecules and pathways.

The tendency for greater protection seen after culture with the HMW fraction of HFFF2-derived CM, indicates that potential candidate molecules involved in HFFF2-mediated protection have a molecular weight greater than 3kDa. A number of chemokines and cytokines are shown to be present in the CLL microenvironment and serum of CLL patients and have a molecular weight of between 8 and 10kDa. Chemokines and cytokines play a critical role on the homing and retention of CLL cells and some have also been implicated with CLL cell survival and disease prognosis including but not exclusively IL-8 (Wierda et al., 2003, Yoon et al., 2012), CCL2 (Fiorcari et al., 2015b, Burgess et al., 2012), CXCL2 (Burgess et al., 2012), CCL3/CCL4 (Burger et al., 2009b) and CXCL12 (Burger et al., 2000). This led to the hypothesis that a chemokine or cytokine, or potentially a number of different cytokines/chemokines could be responsible for the CM-mediated protection to CLL cells.

Perhaps the most characterised of chemokines in the CLL microenvironment is CXCL12 (discussed in detail Introduction, Section1.4.4.1). CXCL12 is secreted from a number of cells in the CLL microenvironment (Burger et al., 2000, Burger et al., 1999) and has been shown in other studies to not only be involved in the homing of CLL cells to the microenvironment but also in directly providing survival signals to the CLL cells (Burger et al., 2000). CXCL12 has an active isoform of 8kDa which fits with the separation data so it was next aimed to determine whether the CXCR4/CXCL12 axis was playing a role in HFFF2-mediated protection.

5.10.2 The HFFF2 cell line secretes the chemokine CXCL12

In order to determine the role of CXCL12 in HFFF2 cytoprotection I first aimed to establish whether the cell line produced CXCL12. A quantakine ELISA kit to CXCL12 revealed that both HFFF2 cells and HFFF2 cells treated with TGF-β produced CXCL12 (Figure 5-3). These data show that HFFF2 cells produce higher levels of the chemokine than their activated counterpart (Figure 2). This fits with other data observed in the host laboratory and discussed in detail in Chapter3, Section3.4.2, showing that HFFF2 cells protect CLL cells more than myofibroblast (Samantha Dias, unpublished data). These data confirm that ability of the HFFF2 cell line to produce the chemokine and supports the hypothesis that CXCL12 could potentially play a role in the protection of CLL cells in the HFFF2 model.

5.10.3 Co-culture with HFFF2 cells prevents recovery of CXCR4 while HFFF2-CM increases CXCR4 expression

The CXCR4 receptor is downregulated via receptor endocytosis once activated by CXCL12 (Burger 1999) and can therefore be used as a marker of CXCL12 'exposure', as discussed at the beginning of this chapter (Section5.1). Here we have shown that CXCR4 expression levels are significantly reduced when CLL cells are co-cultured with HFFF2 cells suggesting that the CLL cells have been 'exposed' to CXCL12 during co-culture.

The results from the CXCR4 expression experiments indicate that the expression of CXCR4 is reduced following co-culture with HFFF2 cells and suggests the possibility the CXCL12 downstream signalling pathways are activated (Figure 5-5). CXCR4 receptor signalling following stimulation with CXCL12 has a number of different effects on the cell including activation of PI3K (Burger et al., 1999), phosphorylation of STAT3 (Burger et al., 2005) and p44/42 MAP kinases (Burger et al., 2000) and finally effects on calcium homeostasis. It has been shown that CXCL12 can promote cell survival through PI3K and MAPK signalling pathways. Genes associated with cell survival have also been shown to be upregulated upon CXCL12 exposure (Teicher and Fricker, 2010). Future experiments should aim to look at whether this decrease in CXCR4 is biologically significant and downstream signalling molecules are upregulated.

Conversely data shown here demonstrate that culture with HFFF2-derived CM does the reverse and modestly increases CXCR4 expression (Figure 5-6). A direct comparison between the two culture conditions was carried out to confirm these findings and revealed that in the same patients HFFF2 direct contact reduced CXCR4 expression while HFFF2-

derived CM increased expression (Figure 5-7 and Figure 5-8). These data could indicate that there is a difference in the way CXCL12 is presented to the receptor. HFFF2 could provide a proteoglycan-bound CXCL12, immobilized on the surface of cells while the secreted form in the CM could be inactive. It is likely that the functional form of CXCL12 is a proteoglycan-bound CXCL12, immobilized on the surface of cells (Amara et al., 1999). The secreted form, if inactivate would not cause down-regulation of the CXCR4, and the receptor could be up-regulated due to other signals from the CM preparing the cell for entry into the protective niche. It is important to note here that binding of the CXCR4 antibody is not thought to be blocked by CXCL12 as it has been demonstrated that CXCL12 does not block 12G5 binding to CXCR4 (Tan et al., 2006).

The results from the CXCR4 recovery experiments continue to indicate the possibility of CXCL12 playing a role in CLL cell survival in the HFFF2 direct co-culture model, however show that the protection from HFFF2-derived CM is likely to be far more complicated with the CM containing a large 'cocktail' of different soluble factors. We have shown that CXCL12 is present in the HFFF2-derived CM, but as discussed this may be in an inactive form, and although a chemokine, CXCL12 may be more active bound to the surface of the fibroblasts.

5.10.4 Neutralising antibodies to CXCL12 and CXCR4 prevent CXCL12-mediated migration but are unable to block HFFF2-mediated protection to CLL cells

It was hypothesised that if CXCL12 was at least partially responsible for HFFF2-cytoprotection that neutralising antibodies to CXCL12 or CXCR4 could be used to inhibit this protection. Burger et al., demonstrated that NLCs firstly induced down modulation of CXCR4 in a similar fashion demonstrated here and they showed that a neutralising antibody to CXCL12 inhibits this protection. Neutralising antibodies were therefore used to try and block HFFF2-mediated protection, but although able to block CLL cell migration to CXCL12 they had no effect on CLL survival (Figure 5-10 and Figure 5-11). The neutralising antibody to CXCR4 was the same clone as used in the study carried out by Burger et al., (12G5 clone) however did not have an effect in our culture model (Burger et al., 2000).

Plerixafor has been previously shown to disrupt the cross-talk between CLL cells and a MSC- or NLC-based microenvironment (Stamatopoulos et al., 2012) and therefore might be a more reliable method to block the CXCR4 axis. However recent studies have shown that extended exposure to plerixafor may actually lead to increased interactions between surviving leukaemic cells and the bone marrow microenvironment (Sison et al., 2014).

Sison and colleagues demonstrated that exposure to plerixafor over 72 hours increased surface CXCR4 expression and modulated surface expression of additional adhesion molecules (CXCR7, CD49d and CXCR3) on acute lymphoblastic leukaemia (ALL) cell lines. They also demonstrated that this increase in surface CXCR4 was functional by showing enhanced CXCL12-induced chemotaxis. This studies indicates that careful investigation needs to be performed using CXCR4 inhibitors to determine their optimal use and therefore plerixafor was not used in the HFFF2 co-culture model due to these this confusing interactions and also the longer culture times used in the survival assay during this project.

5.10.5 Final comments

Overall, data in this chapter demonstrate that CXCL12 is unlikely to be the primary molecule in HFFF2-CM or in HFFF2 direct co-culture responsible for the protection mediated to CLL cells. However, this does not rule out other chemokines and cytokines in the HFFF2-derived CM. Results in this chapter have also revealed a difference in the effects of direct co-culture and HFFF2-CM on CXCR4 expression. Future experiments could be designed to determine whether the CXCL12 present in HFFF2-CM is active by looking at CXCR4 signalling. This would help to better understand the differences seen in CXCR4 expression following co-culture with HFFF2 cells or HFFF2-CM. There is also the possibility that CXCR4 down-modulation following HFFF2 co-culture isn't through CXCL12 binding. Other research in our laboratory have shown that stimulation with a number of different stimuli including α-IgM and IL-4 (Aguilar-Hernandez et al., 2016) causes CXCR4 down-modulation indicating that cross talk between a number of different receptors in the CLL microenvironment occurs as discussed in Introduction, Figure 1-12. These data reveal a potentially complex interplay of molecules in the HFFF2 and HFFF2-CM model but indicate although HFFF2 co-culture causes down modulation of the receptor, CXCR4/CXCL12 is not responsible for HFFF2-mediated cytoprotection.

Chapter Six

Candidate molecules involved in HFFF2-mediated cytoprotection to CLL cells

Chapter 6: Candidate molecules involved in HFFF2-mediated cytoprotection to CLL cells

6.1 Introduction

Interactions with the tumour microenvironment promote CLL cell survival, proliferation and drug resistance; understanding these interactions is therefore an important goal. My previous experiments indicated that CXCL12 and its receptor CXCR4 did not play a substantial role in promoting CLL cell survival in the HFFF2 cell culture model. Therefore further experiments were designed to identify other molecules that might mediate HFFF2 cell-mediated cytoprotection.

These experiments were based on gene expression profiling (GEP). GEP analysis has led to many advances in our understanding of CLL, including identification of the prognostic marker ZAP70 (Wiestner et al., 2003b) and identification of pathways activated by the BCR, including *in vivo*. (Vallat et al., 2007, Herishanu et al., 2011). GEP has also shed the light on the nature of the possible B-cell-of-origin of CLL susbets (Damle et al., 2002) and that Ig-mutated and Ig-unmutated CLL can be readily distinguished from each other by the expression of different genes (Klein et al., 2001, Rosenwald et al., 2001). Important studies have also revealed distinct gene expression changes occurring following culture in survival-supportive conditions, including co-culture with chemokines such as stromal cell co-culture (HS-5 cell) and stromal cell CM and NLC (Schulz et al., 2011, Burger et al., 2009b). Overall, GEP has proved a valuable approach to probe mechanisms of regulation in CLL, including microenvironmental cross-talk.

6.2 Hypothesis

Gene expression analysis will reveal differences in transcription following co-culture with HFFF2 cells. This in turn will uncover candidate molecules that could potentially promote CLL cell survival *in vitro*.

6.3 Aims and objectives

The aim of this chapter was to use GEP to further investigate the interactions between CLL cells and the HFFF2 cell line, to reveal candidate molecules involved in the survival of CLL cells. I also investigated whether CLL response to activation of the cell surface BCR might be modulated by microenvironment co-stimulation. The specific objectives of this chapter were:

- Determine transcription responses in CLL cells following co-culture with HFFF2 cells using GEP.
- Determine whether transcriptional responses following sIgM stimulation are modulated by HFFF2 cell co-culture using GEP.
- Confirm differentially expressed genes using qPCR
- Investigate functional consequences of transcriptional changes

6.4 GEP experiment outline

RNA was collected from CLL cells following culture for 8 hours in various experimental conditions. 8 hours was chosen as the culture period since other experiments carried out in our research laboratory previously identified increases in expression of some BCL2 family proteins following co-culture with HFFF2 cell at this time (unpublished; Samantha Dias, Elizabeth Lemm, Graham Packham) suggesting it was a reasonable time point to probe broader modulatory effects.

The central aim of the GEP experiments was to identify transcriptional changes that occur following stimulation of CLL cells in the HFFF2 cell culture model. Therefore, the first culture conditions investigated were CLL cells alone and CLL cells cultured with HFFF2 cells. Due to the fact that HFFF2 cells are adherent we expected little contamination from HFFF2 cell RNA. However, to control for this, I also performed GEP of CLL cells treated with HFFF2-derived CM.

An additional aim of these experiments was to determine how transcriptional responses to antigen might be modulated by microenvironmental co-stimulation. Therefore, I also performed GEP of CLL cells stimulated with bead-bound αIgM for 8 hours in the presence or absence of HFFF2 cells. Finally, the GEP of HFFF2 cells alone was also analysed.

GEP was performed at Cambridge Genomic Services using triplicate RNA samples for each condition.

Three CLL samples were used for GEP experiments (CLL 635, 567 and 481;Table 6.1). This small cohort included one U-CLL sample and 2 M-CLL samples. CLL cells were not purified prior to analysis to avoid potential confounding factors associated with additional cell handling. Further to this, analysis of unpurified cells has the potential to reveal processes dependent on additional cell types within the PBMC preparation that would be missed using purified CLL cells. However, the selected samples comprised ≥83% CD5+CD19+ cells to minimise potential contamination from non-malignant cells. Samples were also selected based on (i) their ability to signal (Ca^{2+} fluxes) in response to sIgM stimulation since this was a pre-requisite to determine whether anti-IgM responses were modulated by HFFF2 cell co-culture and (ii) their ability to be protected by HFFF2 co-culture and HFFF2-derived CM (all samples were tested prior to GEP experiments for their viability at 8 hours to confirm cells were still viable and for their ability to be protected (AppendixE).

6.5 Analysis of raw GEP data performed by Cambridge Genomic services

As part of the GEP service, Cambridge Genomic Services provided detailed quality control (QC) analysis for all expression data (AppendixE). Hierarchical clustering demonstrated that, for each experimental condition, datasets from triplicates were closely clustered (Figure 6-1a-e). As expected there was biological variability between the patients. Interestingly, data derived from patient 3's samples consistently clustered away from the other two samples for all conditions.

Further analysis of the individual triplicates was performed using hierarchical clustering and multi-dimensional scaling (MDS) for all data sets. Hierarchical clustering (Figure 6-2) revealed that the clearest separation was between CLL cell-derived and HFFF2 cell-derived samples. For example, CLL PBMC only samples were clearly separated away from CLL cells co-cultured with HFFF2 cells. CLL cell derived samples were relatively closely correlated, but again, there was separate clustering of patient 3 derived samples, compared to samples from the other two patients, in the presence or absence of HFFF2 cells. There was evidence for clustering between samples between different culture conditions (ie, with anti-IgM, or with HFFF-2 derived CM), but overall clustering was dominated by interpatient variability. Similar results were obtained using MDS (Figure 6-3).

Overall, this initial analysis indicates that the analysis is robust since triplicate samples were closely correlated. However, it indicated that any differences between stimulation (particularly for anti-IgM and CM) were small compared to inter-patient variability; patient 3 in particular had GEPs that were relatively distinct to patient 1 and 2, which clustered more tightly. Based on these findings, Cambridge Genomic Services summarised the triplicates for each sample and condition into a single representative “Sample” by normalising expression values across the triplicates and calculating a mean expression value for each individual probe.

TABLE 6.1: CHARACTERISTICS OF PATIENTS SELECTED FOR GEP EXPERIMENTS

Patient	Sample	*IGHV* status	V gene usage	Zap-70 (%)	$CD5^+$/ $CD19^+$ (%)	IgM (MFI)	IgD (MFI)	IgM Ca^{2+} (%)	IgD Ca^{2+} (%)
Patient 1	635b	U	V3-21*01	2	83	135	60	90	94
Patient 2	567b	M	V3-33*01 or V3-33*06	2	91	198	39	72	71
Patient 3	481	M	V4-59*01	0	86	188	132	67	75

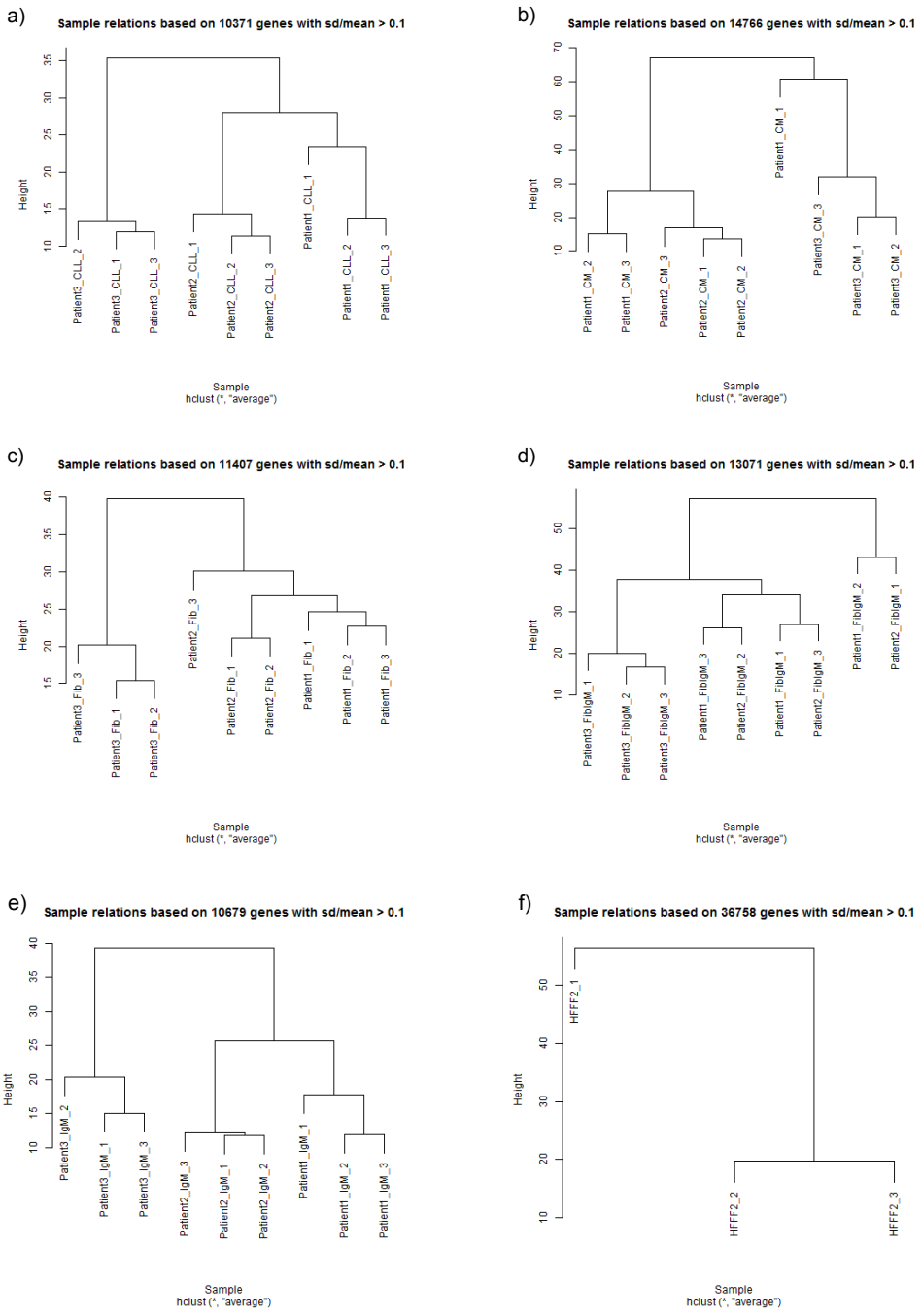

FIGURE 6-1: HIERARCHICAL CLUSTERING OF RNA SAMPLES FOR GEP ANALYSIS

Hierarchical clustering of the data, showing the relationship between them according to the most variable data point, selected by taking probes for which the standard deviation is at least 10% of the mean. Data is from three technical replicates from the three different samples studied. Each replicate was performed as separate experiment. Graphs demonstrate samples from each of the conditions tested. (a) CLL cells cultured alone (b)CLL cells cultured with HFFF2-derived CM (c) CLL cells co-cultured with HFFF2 cells (d) CLL cells cultured with HFFF2 cells and stimulated with αIgM beads (e) CLL cells stimulated with αIgM beads and (f) HFFF2 cells.

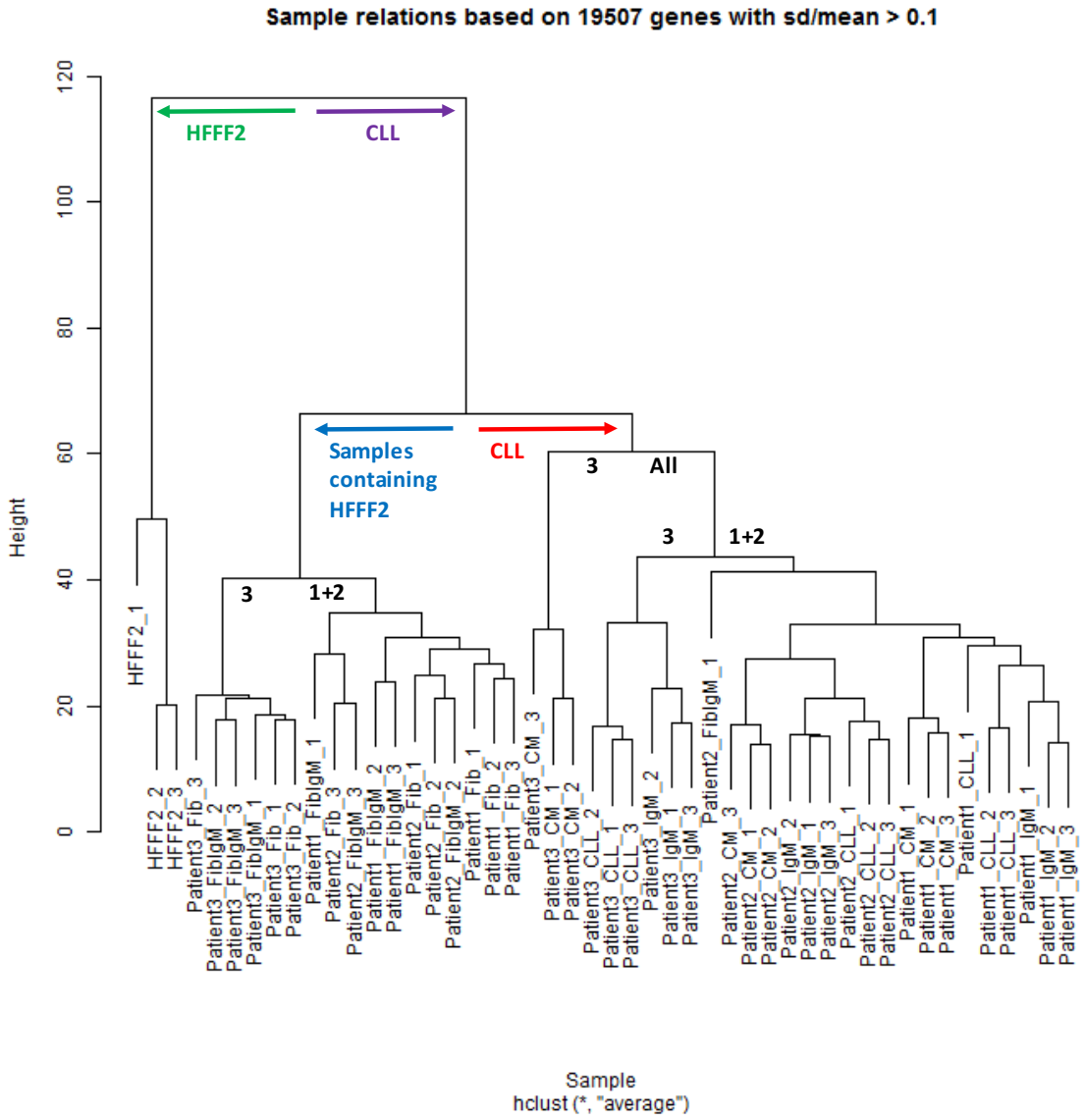

FIGURE 6-2: HIERARCHICAL CLUSTERING OF ALL RNA SAMPLES

Hierarchical clustering of all data showing the relationship between them according to the most variable data point, selected by taking probes for which the standard deviation is at least 10% of the mean. Graph shows clustering of all RNA samples sent for analysis. The samples are split into two main branches, the HFFF2 cells (Green) and CLL samples (Purple). The CLL RNA samples are then further split into two main branches, samples that have been cultured with HFFF2 cells (blue) and samples that had CLL cells cultured alone (red). From each of the CLL RNA samples branches, patients 2 and 1 cluster together and patient 3 clusters alone.

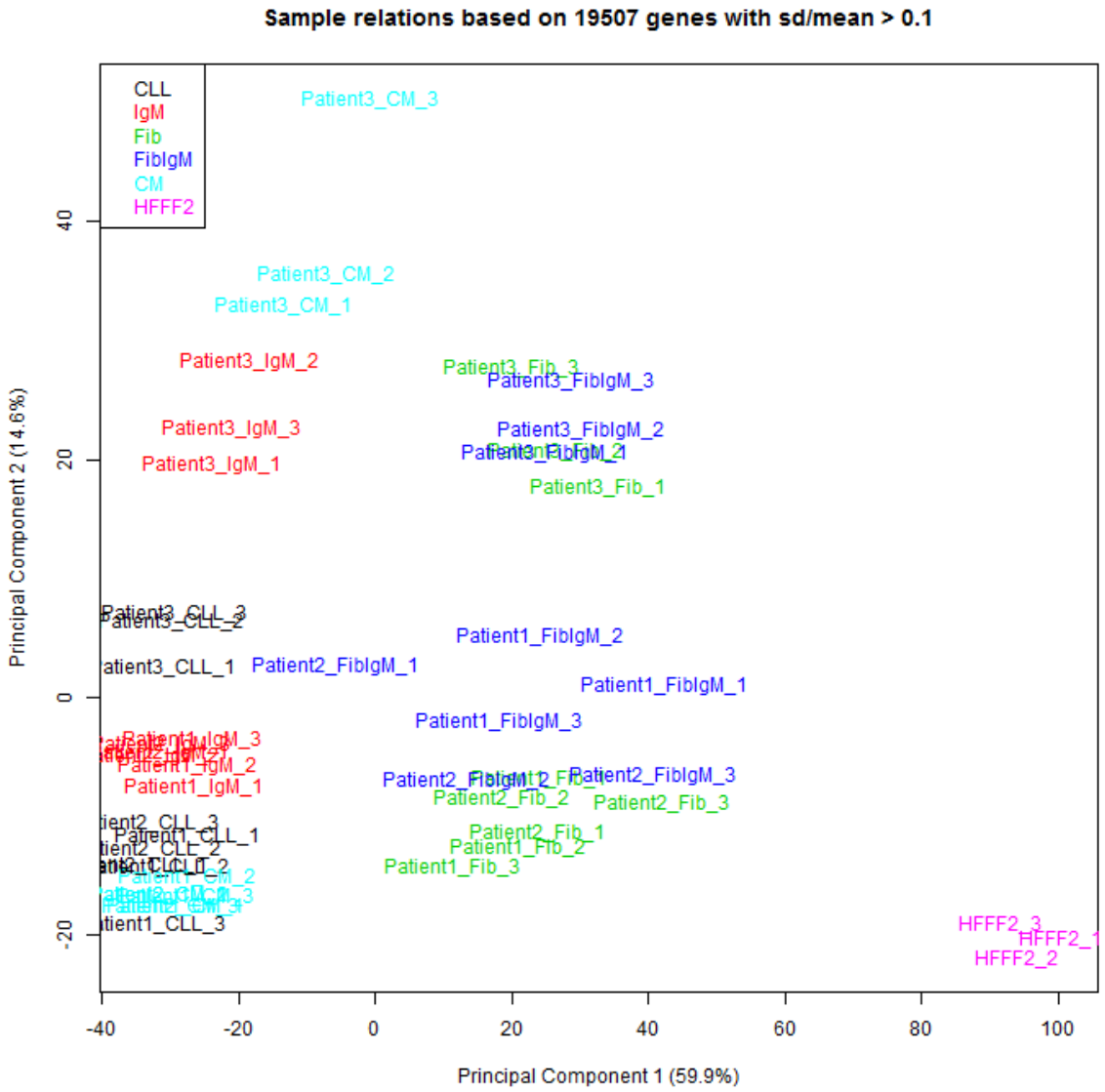

FIGURE 6-3: MULTI-DIMENSIONAL SCALING PLOT OF ALL RNA SAMPLES

Multi-dimensional scaling (MDS) plot plotting the variation between all the RNA samples in two dimensions. HFFF2 cell RNA samples cluster to the far right (purple) and CLL RNA samples cluster to the left. CLL samples that have cultured with HFFF2 cells fall in the middle of the plot (blue and green).

6.6 Multiple comparisons of GEP data

Detailed description of the analysis pipeline used for analysis of the expression data set is outlined in the Methods Section2.5.2 Due to the fact that the technical repeats were highly correlated (Figure 3-1), the replicates were summarised to a single 'sample'; in particular, the values across the three replicates were normalised and then the mean value for each probe was calculated.

The next step in data analysis was to compare expression for individual probes to identify RNAs that were differentially regulated between different conditions. Analysis was restricted to probes that were considered to be expressed; the data set was filtered to remove any non-expressed probes using the detection p value from Illumina (Methods Section2.5.2). Several statistical values were reported for each probe including LogFC (the log2 fold change between the two conditions), and the P.value and adjusted P.value (adj.P.value). The adj.P.value was the primary filtering parameter used to identify differentially regulated RNAs to minimise the potential for "false positives" associated with multiple testing. LogFC is determined for each RNA such that negative and positive LogFC values indicate RNAs that were upregulated or downregulated respectively following co-culture of CLL cells with HFFF2 cell.

A summary of results from the multiple comparison analysis performed by Cambridge Genomic Services is shown in Table 6.2. The table shows the number of differentially expressed RNAs at two levels of significance (adj.P <0.05 and <0.01, respectively) for the four major comparisons. Consistent with clustering shown in Figure 6-2 and Figure 6-3, the greatest numbers of regulated RNAs were detected in comparisons between CLL cells alone and CLL cells co-cultured with HFFF2 cells (with or without anti-IgM). Anti-IgM stimulation of CLL cells resulted in ~300 differentially expressed genes (at adj.P <0.01) suggesting a rather selective effect on transcriptional reprogramming, as previously described (Vallat et al., 2007). Surprisingly, there were no statistically significance differences in RNA expression between CLL cells alone and CLL cells with HFFF2-derived CM.

TABLE 6.2: RESULTS OF MULTIPLE COMPARISONS CARRIED OUT BY CAMBRIDGE GENOMIC SERVICE

Summary outline of statistics performed by Cambridge Genomic Service using the analysis pipeline as described in Methods Section2.5.2. Number of selected probes is the number of expressed probes used to comparision after filtering to remove all non-expressed probes.The final two columns denote the number of significant results using adjusted p value at 0.01 and 0.05 respectively (1% and 5% confidence intervals).

Multiple comparisons			
Comparisons	**Number of selected probes**	**Significant results at 0.01**	**Significant results at 0.05**
CLL vs CM	22480	0	0
CLL vs Fib	23912	5758	10562
CLL vs FibIgM	23803	7508	11594
CLL vs IgM	22309	282	2567

6.7 Transcriptional differences between CLL cells cultured alone and in the presence of the HFFF2 cell line

The main aim of these experiments was to determine transcriptional responses following co-culture with HFFF2 cells. As seen in Table 6.2, comparison of CLL cells alone and CLL cells co-cultured with HFFF2 revealed a relatively high number of differentially expressed genes. These RNAs are presented graphically in the Volcano Plot shown in Figure 6-4a. In this graph format, the log fold change and adj.P value is plotted for each individual probe. RNAs with adj.P values <0.05 are plotted in red, whereas RNAs with adj.P values ≥0.05 (ie, not considered significant in this analysis) are plotted in blue. The graph reveals that the majority of RNAs with statistically significant differential expression between the conditions lie in the top left quadrant, indicating that differential expression is generally associated with upregulation in the presence of HFFF2 cells. Similar results were obtained when the 100 most differentially expressed RNAs (based on adj.P value) were displayed using a heatmap (Figure 6-4b).

The next step in the analysis was to identify the specific RNAs which were differentially regulated between CLL cells alone and CLL cells co-cultured with HFFF2 cells. Filtering of expression datasets was carried out as recommended by Cambridge Genomic Service and outlined in Methods, Section2.5.3. Genes were then ranked according to the logFC such that negative and positive LogFC values indicate RNAs that were upregulated or downregulated respectively following co-culture of CLL cells with HFFF2 cells. Table 6.3 indicates the “top 50” most highly regulated RNAs for both up- and down-regulation. Overall, the FC was greater for up-regulated compared to down-regulated RNAs, consistent with the results presented in the volcano plot (Figure 6-4a).

Visual inspection of the list of up-regulated RNAs revealed several cytokines of potential interest, including IL6, the top ranked RNA by FC (~150-fold increase). However, many of the apparently increased RNAs were not classically expressed in haematological cells, including collagen type I and SMA. This suggested that, despite the HFFF2 cells being tightly adherent, that RNA samples derived from CLL cells co-cultured with HFFF2 cells may have been contaminated with a significant amount of HFFF2 cell-derived RNA. This is consistent with the clustering of CLL and HFFF2 co-cultured samples with HFFF2 cells alone in hierarchial clustering and MDS (Figure 6-2 and Figure 6-3).

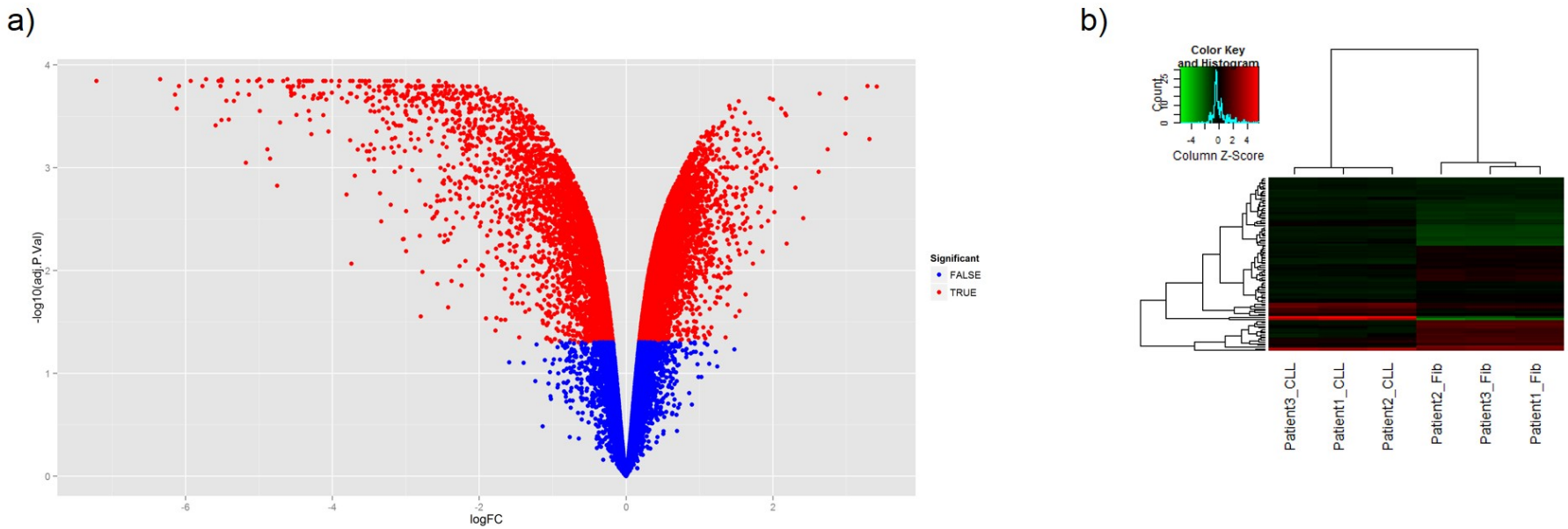

FIGURE 6-4: COMPARISON OF CLL CELLS CULTURED ALONE AND CLL CELLS CULTURED IN THE PRESENCE OF THE HFFF2 CELL LINE

Graphical overview of the multiple comparison analysis performed by Cambridge Genomic service comparing CLL cells cultured alone and CLL cells cultured in the presence of the HFFF2 cell line (a) Volcano Plot. Significance as a function of the log fold change, the adjusted p-value is transformed to a negative log10 scale and plotted on the y axis, results are significant if above 1.3 (adj.P.Val<0.05), 2 for higher significance (adj.P.val<0.01). Positive results are denoted by red while negative values are blue. (b) Heatmap plot. Top 100 genes sorted by adj.P.Val were grouped using hierarchical clustering. Note that not all of the 100 genes are necessarily significant. Intensity values were centered and scaled across samples. Green color indicates lower intensity and Red color indicates higher intensity. A light blue traceback line in the color key indicates the distribution of scaled intensity values.

TABLE 6.3: TOP 50 DIFFERENTIALLY EXPRESSED GENES FOLLOWING COMPARISON BETWEEN CLL CELLS CULTURED ALONE AND CLL CELLS CULTURED IN THE PRESENCE OF HFFF2 CELLS

(a) Genes upregulated in CLL cells in the presence of HFFF2s in comparision to CLL cells cultured alone. (b) Genes downregulated in CLL cells in the presence of HFFF2s in comparision to CLL cells cultured alone.

a) Upregulated in CLL cells following co-culture with HFFF2 cells

Target ID	Name	LogFC	FC	Adj. Pvalue
IL6	Interleukin 6 (B-Cell Stimulatory Factor)	-7.22	148.5	0.0001434
TM4SF1	Transmembrane 4 L Six Family Member 1	-6.35	81.42	0.0001377
TPM2	Tropomyosin 2 (Beta)	-6.14	70.72	0.0001946
TPM2	Tropomyosin 2 (Beta)	-6.12	69.57	0.0002663
PTRF	Polymerase I And Transcript Release Factor	-6.09	68.05	0.0001606
COL1A2	Collagen, Type I, Alpha 2	-5.93	60.93	0.0001434
PTGS2	Prostaglandin-Endoperoxide Synthase 2	-5.77	54.54	0.0001606
DKK3	Dickkopf WNT Signalling Pathway Inhibitor 3	-5.72	52.73	0.0001377
MT2A	Metallothionein 2A	-5.59	48.16	0.0003873
BGN	Biglycan	-5.55	46.82	0.0001434
CAV1	Caveolin 1, Caveolae Protein, 22kDa	-5.53	46.04	0.0001606
SERPINE2	Serpin Peptidase Inhibitor, Clade E (Nexin, Plasminogen Activator Inhibitor Type 1), Member 2	-5.51	45.59	0.0003442
DKK3	Dickkopf WNT Signalling Pathway Inhibitor 3	-5.51	45.56	0.0001377
TMEM158	Transmembrane Protein 158 (Gene/Pseudogene)	-5.51	45.41	0.0001434
COL1A2	Collagen, Type I, Alpha 2	-5.44	43.55	0.0002236
CCL2	Chemokine (C-C Motif) Ligand 2	-5.41	42.54	0.0003408
LOC100134134	N/A	-5.34	40.56	0.0002244
COL6A3	Collagen, Type VI, Alpha 3	-5.29	39.21	0.0001434
PLAU	Plasminogen Activator, Urokinase	-5.29	39.06	0.0001904
MT1E	Metallothionein 1E	-5.18	36.22	0.0008963
ACTA2	Actin, Alpha 2, Smooth Muscle, Aorta	-5.14	35.29	0.0001434
TNFRSF11B	Tumor Necrosis Factor Receptor Superfamily, Member 11b	-5.13	35.10	0.0001941
CXCL1	C-X-C Motif Chemokine 1	-5.03	32.59	0.0001434
CCND1	Cyclin D1	-5.00	31.88	0.0001377
CSF2	Colony Stimulating Factor 2 (Granulocyte-Macrophage)	-4.99	31.77	0.000281
COL4A1	Collagen, Type IV, Alpha 1	-4.97	31.36	0.0001627
IL1B	Interleukin 1, Beta	-4.89	29.59	0.0006625
CALD1	Caldesmon 1	-4.86	29.01	0.0001434
MT1A	Metallothionein 1A	-4.85	28.82	0.0008147
CDH2	Cadherin 2, Type 1, N-Cadherin	-4.82	28.32	0.0001434
IFIT1	Interferon-Induced Protein With Tetratricopeptide Repeats 1	-4.75	26.95	0.0014989
LOC387882	N/A	-4.71	26.21	0.0003624
TPM1	Tropomyosin 1 (Alpha)	-4.67	25.47	0.0001434
RND3	Rho Family GTPase 3	-4.61	24.46	0.0001377
MFGE8	Milk Fat Globule-EGF Factor 8 Protein	-4.61	24.40	0.0001627
CTGF	Connective Tissue Growth Factor	-4.59	24.01	0.0001627
COL1A1	Collagen, Type I, Alpha 1	-4.57	23.67	0.0001724
TPM1	Tropomyosin 1 (Alpha)	-4.56	23.66	0.0001855
CDC20	Cell Division Cycle 20	-4.56	23.59	0.000199
LUM	Lumican	-4.55	23.46	0.0001904
FSTL1	Follistatin-Like 1	-4.54	23.20	0.0001606
IGFBP5	Insulin-Like Growth Factor Binding Protein 5	-4.52	22.89	0.0001904
CYR61	Cysteine-Rich, Angiogenic Inducer, 61	-4.49	22.46	0.0003061
PLOD2	Procollagen-Lysine, 2-Oxoglutarate 5-Dioxygenase 2	-4.46	22.01	0.0001627
THY1	Thy-1 Cell Surface Antigen	-4.46	21.98	0.0001434
FSCN1	Fascin Actin-Bundling Protein 1	-4.45	21.87	0.0001496
GREM1	Gremlin 1, DAN Family BMP Antagonist	-4.45	21.86	0.0001434
COL6A3	Collagen, Type VI, Alpha 3	-4.40	21.04	0.0001606

b) Downregulated in CLL cells following co-culture with HFFF2 cells

Target ID	Name	LogFC	FC	Adj. Pvalue
LYZ	Lysozyme	3.31	9.95	0.0005275
RGS2	Regulator Of G-Protein Signalling 2, 24kDa	3.29	9.77	0.0001606
S100A9	S100 Calcium Binding Protein A9	2.99	7.97	0.0002111
CD14	CD14 molecule	2.99	7.94	0.0004672
TSC22D3	TSC22 Domain Family, Member 3	2.74	6.70	0.0006625
TSC22D3	TSC22 Domain Family, Member 3	2.64	6.22	0.0001904
CXCR4	Chemokine (C-X-C Motif) Receptor 4	2.62	6.15	0.0010948
FUCA1	Fucosidase, Alpha-L- 1, Tissue	2.41	5.33	0.0031022
CXCR4	Chemokine (C-X-C Motif) Receptor 4	2.31	4.94	0.0015613
CSF1R	Colony Stimulating Factor 1 Receptor	2.19	4.56	0.0054732
CYP1B1	Cytochrome P450, Family 1, Subfamily B, Polypeptide 1	2.18	4.53	0.0003103
TYROBP	TYRO Protein Tyrosine Kinase Binding Protein	2.17	4.49	0.0002962
FAM46C	Family With Sequence Similarity 46, Member C	2.11	4.33	0.0002663
YPEL2	Yippee-Like 2 (Drosophila)	2.04	4.13	0.0009864
S1PR1	Sphingosine-1-Phosphate Receptor 1	2.02	4.05	0.002705
CXCL16	Chemokine (C-X-C Motif) Ligand 16	2.00	4.00	0.0002166
LOC65130	N/A	1.98	3.94	0.0008249
EDG1	Sphingosine-1-Phosphate Receptor 1	1.97	3.93	0.0015647
RCSD1	RCSD Domain Containing 1	1.97	3.91	0.0016455
MAFB	V-Maf Avian Musculoaponeurotic Fibrosarcoma Oncogene Homolog...	1.96	3.89	0.0002111
EBI2	G Protein-Coupled Receptor 183	1.94	3.83	0.00071
FCN1	S100 Calcium Binding Protein A9	1.94	3.82	0.0032965
MBP	Lysozyme	1.91	3.76	0.0010224
CHST15	Carbohydrate (N-Acetylgalactosamine 4-Sulfate 6-O) Sulfotransferase 15	1.88	3.68	0.0009529
EBI2	Epstein-Barr Virus Induced Gene 2 (Lymphocyte-Specific G Protein-Coupled Receptor)	1.87	3.66	0.0006464
SPOCK2	Sparc/Osteonectin, Cwcv And Kazal-Like Domains Proteoglycan (Testican) 2	1.86	3.63	0.0065715
C13ORF15	Chromosome 13 Open Reading Frame 15, Regulator Of Cell Cycle	1.85	3.60	0.0014622
ACSM3	Acyl-CoA Synthetase Medium-Chain Family Member 3	1.84	3.59	0.0007013
ALOX5AP	Arachidonate 5-Lipoxygenase-Activating Protein	1.84	3.59	0.0037394
CD6	CD6 molecule, T-Cell Differentiation Antigen CD6	1.84	3.57	0.0010041
HVCN1	Hydrogen Voltage Gated Channel 1	1.84	3.57	0.0010785
PSCDBP	Cytohesin 1 Interacting Protein	1.83	3.56	0.0024096
FCER1G	Fc Fragment Of IgE, High Affinity I, Receptor For; Gamma Polypeptide	1.83	3.54	0.0005275
KIAA1683	KIAA1683	1.81	3.51	0.0007404
ARRDC2	Arrestin Domain Containing 2	1.81	3.50	0.0004623
TMEM71	Transmembrane Protein 71	1.80	3.49	0.002718
PPFIBP2	Protein Tyrosine Phosphatase Receptor Type F Polypeptide-Interacting Protein-Binding Protein 2	1.79	3.45	0.0008507
YPEL3	Yippee-Like 3 (Drosophila)	1.78	3.42	0.0013948
LFNG	LFNG O-Fucosylpeptide 3-Beta-N-Acetylglucosaminyltransferase	1.77	3.42	0.0011877
LOC728014	N/A	1.77	3.42	0.0011714
HRK	Harakiri, BCL2 Interacting Protein	1.75	3.37	0.0007668
LAPTM5	Lysosomal Protein Transmembrane 5	1.75	3.37	0.0008968
PDE4B	Phosphodiesterase 4B, CAMP-Specific	1.73	3.33	0.0012597
ABHD15	Abhydrolase Domain Containing 15	1.73	3.32	0.0004811
LOC100132564	N/A	1.73	3.32	0.0085596
SESN3	Sestrin 3	1.72	3.29	0.0011043
KLHL24	Kelch-Like Family Member 24	1.72	3.29	0.0012479
C13ORF18	KIAA0226-Like	1.71	3.27	0.0015903
GPT2	Glutamic Pyruvate Transaminase (Alanine Aminotransferase) 2	1.70	3.26	0.0016976

6.7.1 Assessment of HFFF2 cell contamination

Further analysis was performed to assess the degree of potential contamination of CLL cell RNA by HFFF2-derived RNA. The left column of Table 6.4 shows the “top 50” RNAs upregulated in HFFF2 control cell sample in comparison to CLL cells. The right column shows the top 50” RNAs apparently upregulated in CLL cells co-cultured with HFFF2 cells compared to CLL cells alone. The RNAs in red indicate the genes that were also upregulated in HFFF2 cell RNA. The table clearly shows that the vast majority of RNA apparently induced in co-cultured CLL cells are actually most highly expressed in HFFF2 cells relative to CLL cells. Therefore, it appears that there is a substantial contamination of CLL cells from the co-cultured HFFF2 cells.

TABLE 6.4: HFFF2 CELL CONTAMINATION

Table to demonstrate most differentially expressed genes in HFFF2 cells compared to CLL cells and also the most differentially expressed genes in CLL cells following co-culture with HFFF2 cells as a way of determining the level of HFFF2 contamination Filtering of data tables was used to determine the level of contamination from HFFF2 cell RNA in co-cultures that contain both CLL and HFFF2 cells. Column one displays the top 50 upregulated genes in HFFF2 cells in comparison to CLL cells. The second column displays the top 50 upregulated genes in CLL cells following co-culture with HFFF2 in comparison to CLL cells cultured alone. The red colour denotes similarities between columns.

Upregulated in HFFF2 cells compared to CLL cells	Upregulated in CLL cells following HFFF2 co-culture
COL1A2	IL6
COL1A2	TM4SF1
LOC100134134	TPM2
TPM2	TPM2
PTRF	PTRF
BGN	COL1A2
DKK3	PTGS2
COL1A1	DKK3
COL4A1	MT2A
DKK3	BGN
COL6A3	CAV1
TPM2	SERPINE2
SERPINE2	DKK3
CTGF	TMEM158
MFGE8	COL1A2
IGFBP5	CCL2
TM4SF1	LOC100134134
LUM	COL6A3
FSTL1	PLAU
COL6A3	MT1E
CAV1	ACTA2
IGFBP5	TNFRSF11B
ACTA2	CXCL1
COL6A1	CCND1
CYR61	CSF2
CALD1	COL4A1
IGFBP7	IL1B
SPARC	CALD1
CDH2	MT1A
TPM1	CDH2
TPM1	IFIT1
DKK1	LOC387882
COL5A2	TPM1
FBLN1	RND3
FLNC	MFGE8
FSCN1	CTGF
CCND1	COL1A1
TNFRSF11B	TPM1
TMEM158	CDC20
CD248	LUM
MT2A	FSTL1
MEG3	IGFBP5
PLOD2	CYR61
SERPINE1	PLOD2
GAS6	THY1
PLAU	FSCN1
IFITM3	GREM1

6.8 Transcriptional differences between CLL cells cultured alone and in the presence of HFFF2-CM

Due to the contamination of co-cultured CLL cell RNA with HFFF2 cell-derived RNA, we shifted the focus of the analysis of the GEP data to the experiments using HFFF2 cell-derived CM. As shown in Table 6.2, initial analysis did not reveal any significantly regulated RNAs using our standard statistical cut-offs of adj. P value of P=0.01 and P=0.05. This is confirmed in the volcano plot shown in Figure 6-5a. However, the volcano plot also shows that, although not reaching statistical significance, there were a substantial number of RNAs that were differentially regulated (LogFC>2), especially up-regulated following treatment of CLL cells with CM. Similar results are shown in the heat map (Figure 6-5b) which reveals some (non-significant) differences between the grouped samples (ie ±CM)

Based on these results, we reasoned that CM did alter gene expression profiles of CLL cells, but that these differences did not reach statistical significance, likely due to the interpatient variation revealed in Figure 6-2. One strategy to increase the robustness of the analysis would be to simply increase the number of samples analysed, to increase the capacity to detected potentially small differences in gene expression between conditions. However, due to cost constraints, we pursued an alternate strategy and performed a cross-comparison of the data sets generated by (i) co-culture of CLL cells with HFFF2 cells and (ii) treatment of CLL cells with HFFF2-derived CM. The goal was to only select RNAs which were regulated under both conditions, independently of strict statistical considerations, to eliminate the confounding effects of contamination of CLL cells by HFFF2 cells.

Similar to the HFFF2 co-culture experiments we prepared two lists of genes. These lists show the “top 50” genes upregulated or downregulated following culture of CLL cells with CM (Table 6.5a and Table 6.5b, respectively). In this case, RNAs were simply ranked according to their FC, regardless of the adj.Pvalue (>0.05 for all RNAs in this analysis). In contrast to the CLL/HFFF2 cell co-culture experiment, the resultant list of “upregulated” genes was dominated by chemokines and cytokines, with no clear signature of non-haematological RNAs. Interestingly, IL6, also revealed in the CLL/HFFF2 co-culture experiment, was strongly induced (~14-fold) following incubation of CLL cells with HFFF2 cell derived CM.

Finally, we compared the list of specific upregulated RNAs revealed in the CM experiment, with the results obtained previously from direct co-culture of CLL and HFFF2 cells (Table 6.6). Table 6.6 shows the “top 50” genes upregulated in CLL cells treated with

CM, ranked according to FC (as in Table 6.5a). Alongside are the corresponding values for each RNA selected from the data obtained from the HFFF2 co-culture experiment (Table 6.3). Green colour denotes a greater FC in the CM condition, while red colour denotes a lower FC in the CM condition. Overall, 46/50 of the candidates genes identified in the CM experiment were significantly upregulated (adj.Pvalue <0.05) in the CLL/HFFF2 co-culture experiment. Interestingly there are two genes that have a positive FC (i.e. are downregulated following HFFF2 co-culture in comparison to CLL cells cultured alone), these are denoted by the bold in the column and are PPBP, better known as CXCL7, a chemoattractant for neutrophils and NLRP3 an upstream activator of NF_KB which has been shown to play a role in the regulation of inflammation.

Overall, we believe the combined analysis of the co-culture and CM experiments has allowed us to define a list of candidate-regulated genes for further analysis. Detailed analysis has revealed that the co-culture experiment is complicated by a higher than expected degree of contamination of CLL RNA samples by HFFF2 cell derived RNA. Responses to CM appear moderate and are overwhelmed by inter-patient variability. However, combining the data sets increases power to detect small changes, and eliminates HFFF2 cell contamination.

Visual inspection of the “top 50” candidate upregulated genes reveals that a large number of chemokines and cytokines are upregulated in CLL cells when co-cultured with HFFF2 cells and/or HFFF2-derived CM, including CCL3, IL6, CXCL5, IL1α, CCL2, IL24, CXCL1, CXCL2 and IL8. This pattern of regulation is further apparent when considering the “top 100” upregulated RNAs (AppendixE) where many more chemokines and cytokines are present. This is of potential interest since chemokines and cytokines are clearly of critical importance to the biology of CLL cells, including for suppression of apoptosis. Table 6.7 summarises the function, including previous work in CLL, of some of these candidate regulatory molecules.

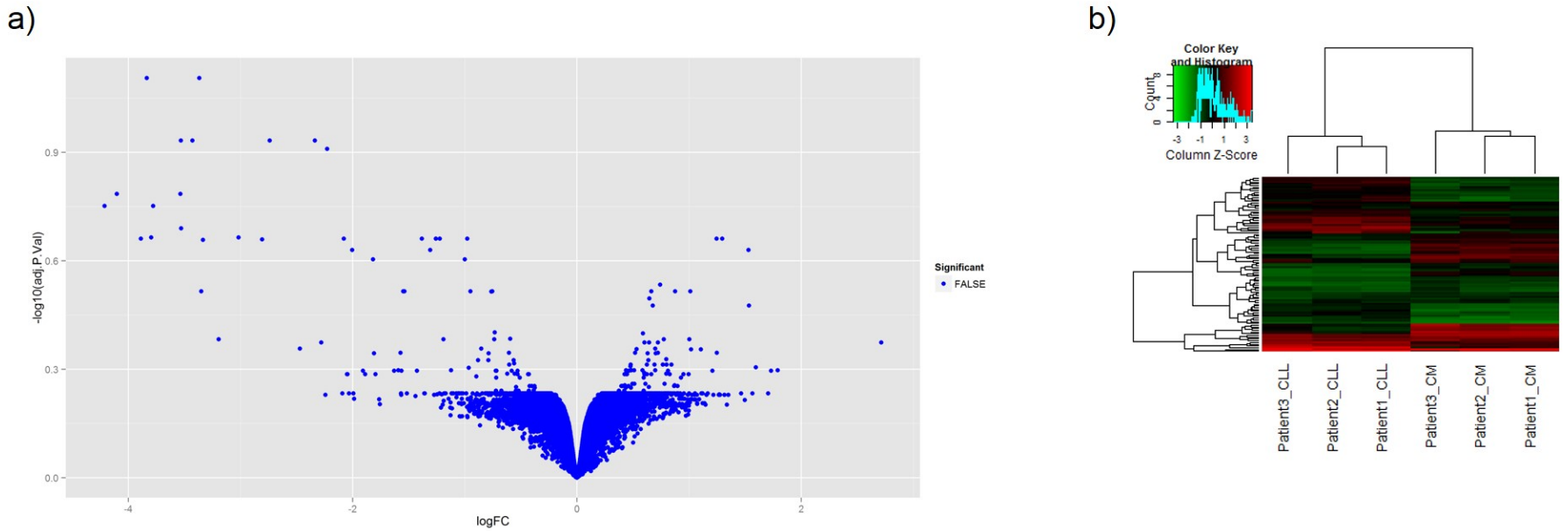

FIGURE 6-5: COMPARISON OF CLL CELLS CULTURED ALONE AND CLL CELLS CULTURED IN THE PRESENCE OF HFFF2-DERIVED CM

Graphical overview of the multiple comparison analysis performed by Cambridge Genomic service comparing CLL cells cultured alone and CLL cells cultured in the presence of the HFFF2 derived CM. (a) Volcano Plot. Significance as a function of the log fold change, the adjusted p-value is transformed to a negative log10 scale and plotted on the y axis, results are significant if above 1.3 (adj.P.Val<0.05), 2 for higher significance (adj.P.val<0.01). Positive results are denoted by red while negative values are blue. (b) Heatmap plot. Top 100 genes sorted by adj.P.Val were grouped using hierarchical clustering. Intensity values were centered and scaled across samples. Green color indicates lower intensity and Red color indicates higher intensity. A light blue traceback line in the color key indicates the distribution of scaled intensity value.

TABLE 6.5: TOP 50 DIFFERENTIALLY EXPRESSED GENES FOLLOWING COMPARISON BETWEEN CLL CELLS CULTURED ALONE AND CLL CELLS CULTURED IN THE PRESENCE OF HFFF2-DERIVED CM

(a) Genes upregulated in CLL cells in the presence of HFFF2-derived CM in comparision to CLL cells cultured alone. (b) Genes upregulated in CLL cells cultured alone in comparison to CLL cells cultured in the presence of HFFF2-derived CM.

a) Upregulated in CLL cells following culture with HFFF2-derived CM

Target ID	Name	LogFC	FC	Adj. Pvalue
CCL3L3	Chemokine (C-C Motif) Ligand 3-Like 3	-4.21	18.54	0.1769746
CCL3	Chemokine (C-C Motif) Ligand 3	-4.10	17.19	0.1638881
IL1B	Interleukin 1, Beta	-3.89	14.82	0.2181392
LOC728835	N/A	-3.84	14.30	0.0783518
CCL3L1	Chemokine (C-C Motif) Ligand 3-Like 1	-3.80	13.91	0.2162378
IL6	Interleukin 6	-3.78	13.73	0.1769746
CCL3L1	Chemokine (C-C Motif) Ligand 3-Like 1	-3.54	11.61	0.1638881
CCL4L1	Chemokine (C-C Motif) Ligand 4-Like 1	-3.53	11.58	0.1166725
CXCL5	Chemokine (C-X-C Motif) Ligand 5	-3.53	11.55	0.2041741
CCL4L2	Chemokine (C-C Motif) Ligand 4-Like 2	-3.43	10.78	0.1166725
CCL3L1	Chemokine (C-C Motif) Ligand 3-Like 1	-3.37	10.33	0.0783518
IL1A	Interleukin 1, Alpha	-3.35	10.20	0.3050602
PTGS2	Prostaglandin-Endoperoxide Synthase 2	-3.34	10.10	0.2196855
CCL2	Chemokine (C-C Motif) Ligand 2	-3.19	9.16	0.4136674
TNF	Tumor Necrosis Factor	-3.02	8.10	0.2162378
IL1RN	Interleukin 1 Receptor Antagonist	-2.81	7.00	0.2191212
IL24	Interleukin 24	-2.74	6.68	0.1166725
CXCL1	Chemokine (C-X-C Motif) Ligand 1	-2.47	5.55	0.4396678
CXCL2	Chemokine (C-X-C Motif) Ligand 2	-2.34	5.05	0.1166725
IL1RN	IL1RN	-2.28	4.86	0.422328
IER3	Immediate Early Response 3	-2.23	4.69	0.1231396
IL8	Interleukin 8	-2.08	4.23	0.2181392
PTGS2	Prostaglandin-Endoperoxide Synthase 2	-2.00	4.02	0.2344008
IL8	Interleukin 8	-1.82	3.53	0.2489002
CXCL5	Chemokine (C-X-C Motif) Ligand 5	-1.81	3.50	0.452448
SOD2	Superoxide Dismutase 2	-1.63	3.09	0.5055476
CTSL1	Cathepsin L	-1.59	3.02	0.5045323
CTSL1	Cathepsin L	-1.57	2.98	0.4515607
PPBP	Pro-Platelet Basic Protein (Chemokine (C-X-C Motif) Ligand 7)	-1.57	2.96	0.5055476
SOD2	Superoxide Dismutase 2	-1.55	2.93	0.3050602
SLC25A24	Solute Carrier Family 25 (Mitochondrial Carrier; Phosphate Carrier), Member 24	-1.54	2.91	0.3050602
RIN2	Ras And Rab Interactor 2	-1.43	2.69	0.5055476
NLRP3	NLR Family, Pyrin Domain Containing 3	-1.38	2.61	0.2181392
IL24	Interleukin 24	-1.31	2.48	0.2344008
LOC728830	N/A	-1.26	2.39	0.2181392
IL24	Interleukin 24	-1.22	2.34	0.2181392
NLRP3	NLR Family, Pyrin Domain Containing 3	-1.19	2.28	0.4136674
NFKBIZ	Nuclear Factor Of Kappa Light Polypeptide Gene Enhancer In B-Cells Inhibitor, Zeta	-1.12	2.18	0.5045323
MIR302C	MicroRNA 302c	-1.00	2.00	0.2489002
ID2	Inhibitor Of DNA Binding 2, Dominant Negative Helix-Loop-Helix Protein	-0.98	1.97	0.2181392
MAFF	V-Maf Avian Musculoaponeurotic Fibrosarcoma Oncogene Homolog F	-0.97	1.95	0.4966027
CYP4B1	Cytochrome P450, Family 4, Subfamily B, Polypeptide 1	-0.95	1.93	0.3050602
CD40	CD40 Molecule, TNF Receptor Superfamily Member 5	-0.88	1.84	0.4727872
PLAUR	Plasminogen Activator, Urokinase Receptor	-0.85	1.81	0.4396678
BST2	Bone Marrow Stromal Cell Antigen 2	-0.79	1.73	0.4727872
TPM2	Tropomyosin 2 (Beta)	-0.79	1.73	0.452448
LOC100129681	N/A	-0.76	1.70	0.3053888
ID2	Inhibitor Of DNA Binding 2, Dominant Negative Helix-Loop-Helix Protein	-0.76	1.69	0.3050602
GNLY	Granulysin	-0.74	1.67	0.41366574

b) Downregulated in CLL cells following culture with HFFF2-derived CM

Target ID	Name	LogFC	FC	Adj. Pvalue
RGS2	Regulator Of G-Protein Signalling 2	2.71	6.56	0.422328
TSC22D3	TSC22 Domain Family, Member 3	1.79	3.46	0.5045323
LYZ	Lysozyme	1.73	3.32	0.5055476
TSC22D3	TSC22 Domain Family, Member 3	1.71	3.26	0.5845561
CSF1R	Colony Stimulating Factor 1 Receptor	1.59	3.02	0.495173
S100A8	S100 Calcium Binding Protein A8	1.57	2.96	0.5845561
FUCA1	Fucosidase, Alpha-L- 1, Tissue	1.53	2.89	0.3341525
OLR1	Oxidized Low Density Lipoprotein (Lectin-Like) Receptor 1	1.53	2.89	0.2344008
CXCR4	Chemokine (C-X-C Motif) Receptor 4	1.50	2.82	0.6097805
NDRG1	N-Myc Downstream Regulated 1	1.46	2.76	0.5845561
MT1F	Metallothionein 1F	1.35	2.55	0.5896915
CXCR4	Chemokine (C-X-C Motif) Receptor 4	1.38	2.53	0.628517
STMN3	Stathmin-Like 3	1.31	2.49	0.5896915
TGFBI	Transforming Growth Factor, Beta-Induced	1.29	2.45	0.2181392
FAM43A	Family With Sequence Similarity 43, Member A	1.27	2.42	0.5896915
HPCAL1	Hippocalcin-Like 1	1.27	2.41	0.5880197
HVCN1	Hydrogen Voltage Gated Channel 1	1.27	2.40	0.5896915
FCN1	Ficolin (Collagen/Fibrinogen Domain Containing) 1	1.25	2.37	0.4515607
KIAA1683	N/A	1.25	2.37	0.2181392
TMEM71	N/A	1.22	2.32	0.5901506
LOC339192	N/A	1.21	2.31	0.5055476
INPP5A	Inositol Polyphosphate-5-Phosphatase	1.17	2.25	0.5845561
APOD	Apolipoprotein D	1.15	2.23	0.5896915
SPOCK2	Sparc/Osteonectin	1.15	2.21	0.628517
LOC100132564	N/A	1.14	2.20	0.622227
CLEC5A	C-Type Lectin Domain Family 5, Member A	1.12	2.17	0.5845561
ALOX5AP	Arachidonate 5-Lipoxygenase-Activating Protein	1.12	2.17	0.622227
FAM46C	Family With Sequence Similarity 46, Member C	1.11	2.16	0.5845561
LOC100129550	N/A	1.10	2.15	0.4413648
TRIB1	Tribbles Pseudokinase 1	1.09	2.13	0.6070699
MAD1L1	Mitotic Arrest Deficient-Like 1	1.07	2.10	0.6247382
LY9	Lymphocyte Antigen 9	1.07	2.10	0.6220767
HVCN1	Hydrogen Voltage Gated Channel 1	1.07	2.10	0.5896915
YPEL2	Yippee-Like 2	1.06	2.08	0.6079884
ARRDC2	Arrestin Domain Containing 2	1.05	2.07	0.5845561
C7orf50	Chromosome 7 Open Reading Frame 50	1.05	2.07	0.5896915
LY9	Lymphocyte Antigen 9	1.05	2.07	0.6079884
C9orf103	chromosome 9 open reading frame 103	1.03	2.04	0.5896915
PIK3IP1	Phosphoinositide-3-Kinase Interacting Protein 1	1.02	2.03	0.6066041
HMGB2	High Mobility Group Box 2	1.02	2.02	0.4413648
PDE4B	Phosphodiesterase 4B, CAMP-Specific	1.01	2.02	0.6070054
TSC22D3	TSC22 Domain Family, Member 3	1.01	2.02	0.3050602
KLF2	Kruppel-Like Factor 2	1.01	2.01	0.6191233
CD36	CD36 Molecule (Thrombospondin Receptor)	1.00	2.00	0.4136674
CCPG1	Cell Cycle Progression 1	1.00	2.00	0.5845561
S1PR1	Sphingosine-1-Phosphate Receptor 1	1.00	2.00	0.6521658
EBI2	EBV-Induced G-Protein Coupled Receptor 2	1.00	2.00	0.6317781
SH3PXD2A	SH3 And PX Domains 2A	1.00	1.99	0.5170737
CCR6	Chemokine (C-C Motif) Receptor 6	0.99	1.99	0.6688774

TABLE 6.6: FOLD CHANGES OF THE TOP 50 REGULATED GENES IN CLL CELLS IN THE PRESENCE OF HFFF2-DERIVED CM IN COMPARISON TO THE FOLD CHANGES FOLLOWING DIRECT CULTURE WITH HFFF2 CELLS

The LogFC of the top 50 upregulated genes following culture with HFFF2-derived CM were compared to the LogFC of the same genes following direct culture with HFFF2 cells. Green colour indicates a lower fold change following HFFF2 direct co-culture and red colour indicates a greater upregulation.

	HFFF2-derived CM		HFFF2 co-culture	
TargetID	**logFC**	**adj.P.Val**	**logFC**	**adj.P.Val**
CCL3L3	-4.21	0.176975	-3.50	0.000835
CCL3	-4.10	0.163888	-3.43	0.000825
IL1B	-3.89	0.218139	-4.89	0.000662
CCL3L1	-3.80	0.216238	-2.42	0.000436
IL6	-3.78	0.176975	-7.21	0.000143
CCL3L1	-3.54	0.163888	-2.42	0.000436
CCL4L1	-3.53	0.116673	-2.66	0.002405
CXCL5	-3.53	0.204174	-2.26	0.000537
CCL4L2	-3.43	0.116673	-2.81	0.004597
CCL3L1	-3.37	0.078352	-2.42	0.000436
IL1A	-3.35	0.30506	-2.34	0.000447
PTGS2	-3.34	0.219685	-4.29	0.000143
CCL2	-3.19	0.413667	-5.41	0.000341
TNF	-3.02	0.216238	-2.59	0.002781
IL1RN	-2.81	0.219121	-1.83	0.002389
IL24	-2.74	0.116673	-0.09	0.336669
CXCL1	-2.47	0.439668	-5.03	0.000143
CXCL2	-2.34	0.116673	-3.28	0.000159
IL1RN	-2.28	0.422328	-1.83	0.002389
IFIT1	-2.24	0.589692	-4.75	0.001499
IER3	-2.23	0.12314	-4.32	0.000281
IL19	-2.09	0.584556	-0.66	0.028809
IL8	-2.08	0.218139	-3.87	0.000211
SERPINB2	-2.05	0.517074	-1.19	0.015344
SERPINB2	-2.04	0.517074	-1.19	0.015344
MX1	-2.03	0.584556	-2.99	0.002653
PTGS2	-2.01	0.234401	-4.29	0.000143
IL19	-1.99	0.584556	-0.66	0.028809
IFI44L	-1.99	0.604513	-2.77	0.010332
TNFAIP6	-1.91	0.505548	-1.14	0.030636
AQP9	-1.89	0.517074	-0.74	0.13876
IL8	-1.82	0.2489	-3.87	0.000211
CXCL5	-1.81	0.452448	-2.26	0.000537
CCL20	-1.80	0.517074	-2.18	0.000674
MIR155HG	-1.76	0.607005	-1.78	0.038401
CCL22	-1.76	0.625712	-1.03	0.167301
SOD2	-1.63	0.505548	-2.05	0.003034
CTSL1	-1.59	0.504532	-0.64	0.002798
CTSL1	-1.57	0.451561	-0.65	0.002798
BATF	-1.57	0.584556	-1.51	0.00657
IFIT3	-1.57	0.589692	-4.75	0.001499
PPBP	**-1.57**	**0.505548**	**0.75**	**0.006857**
SOD2	-1.55	0.30506	-2.05	0.003034
SLC25A24	-1.54	0.30506	-0.36	0.049417
EIF2AK2	-1.52	0.584556	-2.02	0.002357
XAF1	-1.44	0.594231	-1.77	0.006137
RIN2	-1.43	0.505548	-2.02	0.002764
NLRP3	**-1.38**	**0.218139**	**0.17**	**0.079272**
IFITM1	-1.36	0.584556	-2.32	0.000365

TABLE 6.7: CHEMOKINE AND CYTOKINES UPREGULATED FOLLOWING CO-CULTURE WITH HFFF2 CELLS OR HFFF2-DERIVED CM AND THEIR FUNCTION IN CLL CELL BIOLOGY

Target	Name	Function	CLL Literature
IL6	Interleukin 6 (B-Cell Stimulatory Factor)	Functions in inflammation and the maturation of B cells. It is a potent inducer of the acute phase response. Plays an essential role in the final differentiation of B-cells into Ig-secreting cells Involved in lymphocyte and monocyte differentiation.	Increased in CLL serum compared to healthy controls (Fayad et al., 2001). Inhibits spontaneous apoptosis in CLL cells (Reittie et al., 1996). Inhibited proliferation of CLL cells induced by TNF (Aderka et al., 1993). Tumour-derived IL-6 may contribute to immunological defect in CLL (Buggins et al., 2008).
CCL2	Chemokine (C-C Motif) Ligand 2, Monocyte Chemotactic Protein 1	Recruits monocytes, memory T cells, and dendritic cells to the sites of inflammation produced by either tissue injury or infection.	CLL cells produce CCL2 but only in the presence of accessory cells (Burgess et al., 2012). Enhances CLL cells survival *in vitro* (Burgess et al., 2012). Upregulated following cultured with HS-5 stromal cells (Schulz et al., 2011).
CXCL1	C-X-C Motif Chemokine 1	CXCL1 is a secreted growth factor that signal through the G-protein coupled receptor, CXCR2. Plays a role in inflammation and as a chemoattractant for neutrophils.	N/A
IL1B	Interleukin 1, Beta	IL-1 is produced by activated macrophages as a proprotein, which is proteolytically processed to its active form by caspase 1. This cytokine is an important mediator of the inflammatory response, and is involved in a variety of cellular activities, including cell proliferation, differentiation, and apoptosis.	Isolated cells from progressive disease produce less IL-1 compared to patients with indolent disease (Aguilar-Santelises et al., 1992). IL-1 induces differentiation and activation of CLL cells (Takeuchi and Katayama, 1994).
IL8	Interleukin 8	Also known as CXCL8; One of the major mediators of the inflammatory response. This chemokine is secreted by several cell types. It functions as a chemoattractant, and is also a potent angiogenic factor.	High levels of IL-8 are associated with shorter survival (Wierda et al., 2003). IL-8 promotes CLL cell survival (Wierda et al., 2003, Binsky et al., 2007).

CCL3	Chemokine (C-C Motif) Ligand 3	Also known as macrophage inflammatory protein 1 alpha, plays a role in inflammatory responses through binding to the receptors CCR1, CCR4 and CCR5. One of the major HIV-suppressive factors produced by CD8+ T-cells.	Plasma concentrations are strongly associated with established prognostic markers (Sivina et al., 2011). NLC co-culture induces CCL3 expression in CLL cells (Burger et al., 2009b). BCR triggering induces robust CCL3 secretion (Burger et al., 2009b).
CXCL2	Chemokine (C-X-C Motif) Ligand 2	Produced by activated monocytes and neutrophils and expressed at sites of inflammation. Haematoregulatory chemokine, which, *in vitro*, suppresses hematopoietic progenitor cell proliferation.	CLL cells produce CXCL2 but only in the presence of accessory cells (Burgess et al., 2012). Enhances CLL cells survival *in vitro* (Burgess et al., 2012).
IL11	Interleukin 11	This cytokine is shown to stimulate the T-cell-dependent development of immunoglobulin-producing B cells. It is also found to support the proliferation of hematopoietic stem cells and megakaryocyte progenitor cells.	Recombinant IL-11 activates CLL cells leading to morphologic alterations of the cell and increase in cell number and size (Tsimanis et al., 2001).
CXCL12	Chemokine (C-X-C Motif) Ligand 12	Chemoattractant for T-lymphocytes and monocytes. Activates the C-X-C chemokine receptor CXCR4 to induce a rapid chemotaxis. Plays a role in many diverse cellular functions, including embryogenesis, immune surveillance, inflammation response, tissue homeostasis, and tumor growth and metastasis.	Causes migration of CLL cells into microenvironment (Burger et al., 1999). Provides survival signals to CLL cells (Burger et al., 2000).
IL1A	Interleukin 1, Alpha	Similar to IL1B; Produced by activated macrophages, IL-1 stimulates thymocyte proliferation by inducing IL-2 release, B-cell maturation and proliferation, and fibroblast growth factor activity.	See IL-1β.
CXCL5	Chemokine (C-X-C Motif) Ligand 5	Binds to the G-protein coupled receptor chemokine (C-X-C motif) receptor 2 to recruit neutrophils. Recruits and activates leukocytes, to promote angiogenesis and to remodel connective tissues.	N/A
CXCL6	Chemokine (C-X-C Motif) Ligand 6	Chemotactic for neutrophil granulocytes. Signals through binding and activation of its receptors (CXCR1 and CXCR2).	N/A

CCL20	Chemokine (C-C Motif) Ligand 20	Chemotactic factor that attracts lymphocytes and neutrophils although only weakly. Inhibits proliferation of myeloid progenitors in colony formation assays. May be involved in formation and function of the mucosal lymphoid tissues by attracting lymphocytes and dendritic cells towards epithelial cells.	N/A
CXCL10	Chemokine (C-X-C Motif) Ligand 10	Binding of this protein to its receptor CXCR3 results in pleiotropic effects, including stimulation of monocytes, natural killer and T-cell migration, and modulation of adhesion molecule expression.	N/A
IL24	Interleukin 24	A member of the IL10 family of cytokines. Can induce apoptosis selectively in various cancer cells. Has anti-proliferative properties on melanoma cells and may contribute to terminal cell differentiation.	IL-24 mRNA silencing promotes CLL cell apoptosis, indicating that IL-24 is a survival factor in CLL (Sainz-Perez et al., 2006). Recombinant IL-24 resulted in transcription, protein synthesis and phosphorylation of p53 (Sainz-Perez et al., 2008). IL-24 was not detected in 28/28 CLL patients but 100-500pg/ml is commonly detected in healthy controls (Sainz-Perez et al., 2008).
IL19	Interleukin 19	Belongs to the IL10 cytokine subfamily. This cytokine is found to be preferentially expressed in monocytes. It can bind the IL20 receptor complex and lead to the activation of the signal transducer and activator of transcription 3 (STAT3). Reported to up-regulate the expression of IL6 and TNF-alpha and induce apoptosis, which suggests a role of this cytokine in inflammatory responses.	N/A
CCL22	Chemokine (C-C Motif) Ligand 22	The cytokine encoded by this gene displays chemotactic activity for monocytes, dendritic cells, natural killer cells and for chronically activated T lymphocytes. This chemokine may play a role in the trafficking of activated T lymphocytes to inflammatory sites and other aspects of activated T lymphocyte physiology.	Chemoattractant for T lymphocytes and monocytes (Ghia et al., 2002).

6.9 Transcriptional responses to anti-IgM stimulation

A second aim of this study was to determine whether HFFF2 cells influence transcriptional responses following sIgM stimulation of CLL cells. As shown in Table 6.2, there were 282 RNAs that were differentially expressed between CLL cells cultured alone and CLL cells treated with anti-IgM for 8 hours (adj.Pvalue<0.01). These differentially expressed genes are equally distributed between the two phenotypes as demonstrated by the volcano plots (Figure 6-6), however the data points on the left hand of the plot (those in the second phenotype, stimulated with anti-IgM) have a far greater FC. Table 6.8 shows the "top 50" RNAs which were up-regulated in CLL cells following anti-IgM stimulation. All RNAs shown had adj.Pvalues<0.05 and RNAs are ranked according to descending FC. Visual inspection revealed that the list contained many RNAs that have been demonstrated previously to be induced following sIgM stimulation of CLL cells, including CCL3, EGR1/2/3, MYC, GLA, NR4A2/3, mIR155 and DDX21 (Burger et al., 2009b, Krysov et al., 2012, Pede et al., 2013, Guarini et al., 2008, Cui et al., 2014, Yeomans et al., 2016).

6.9.1 Modulation of transcriptional responses

Due to the contamination of CLL RNA samples by HFFF2 cell-derived RNA revealed in previous analyses, we did not directly compare the gene expression profiles of CLL cells stimulated with anti-IgM in the presence or absence of HFFF2 cell co-culture. Instead, we adopted the strategy that appeared successful for analysis of CM-regulated genes, and investigated the effect of HFFF2 cell co-culture on anti-IgM regulated genes on a per-RNA basis. Table 6.9 displays the "top 50" anti-IgM-responsive genes from Table 6.8 comparing expression between CLL cells stimulated with anti-IgM and CLL cells alone. The second data column in Table 6.9 shows the FC for each of these "top 50" RNAs comparing expression between CLL cells stimulated with anti-IgM and CLL cells stimulated with anti-IgM and co-cultured with HFFF2. Many of the "top 50" RNAs were as discussed previously EGR1/2/3, MYC, CCL3, NR4A3/2, DDX21 and miR-155HG. Of these, CCL3 and miR-155HG have a greater upregulation following co-culture with HFFF2 cell and stimulation with anti-IgM compared to CLL cells just stimulated with anti-IgM. This suggests that HFFF2 cells may modulate response to anti-IgM. However, because of the technical difficulties associated with the GEP of co-cultured cells, additional experiments were performed using flow cytometry to directly investigate sIgM expression and function specifically on CLL cells.

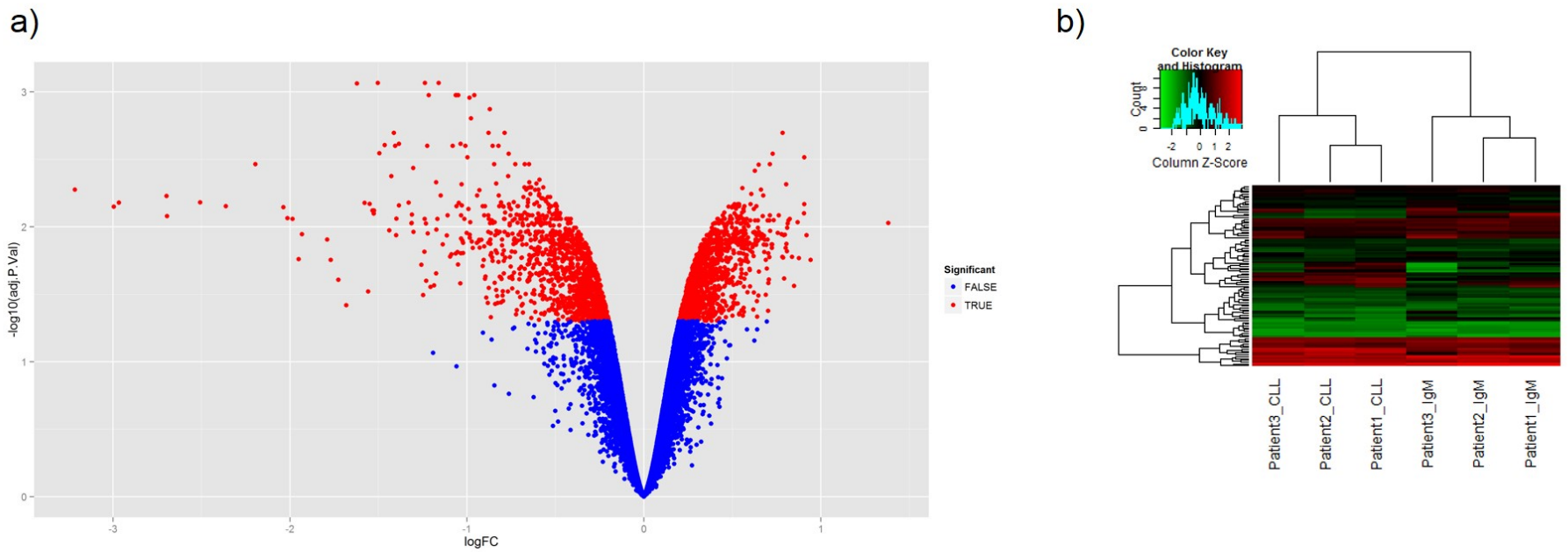

FIGURE 6-6: COMPARISON OF CLL CELLS CULTURED ALONE AND CLL CELLS CULTURED IN THE PRESENCE OF αIGM BEADS

Graphical overview of the multiple comparison analysis performed by Cambridge Genomic service comparing CLL cells cultured alone and CLL cells stimulated with αIgM beads (a) Volcano Plot. Significance as a function of the log fold change, the adjusted p-value is transformed to a negative log10 scale and plotted on the y axis, results are significant if above 1.3 (adj.P.Val<0.05), 2 for higher significance (adj.P.val<0.01). Positive results are denoted by red while negative values are blue. (b) Heatmap plot. Top 100 genes sorted by adj.P.Val were grouped using hierarchical clustering. Note that not all of the 100 genes are necessarily significant. Intensity values were centered and scaled across samples. Green color indicates lower intensity and Red color indicates higher intensity. A light blue traceback line in the color key indicates the distribution of scaled intensity values.

TABLE 6.8: TOP 50 DIFFERENTIALLY EXPRESSED GENES FOLLOWING COMPARISON BETWEEN CLL CELLS CULTURED ALONE AND CLL CELLS STIMULATED αIGM BEADS

(a) Genes upregulated in CLL cells following stimulation with αIgM beads in comparision to CLL cells cultured alone. (b) Genes upregulated in CLL cells cultured alone in comparison to CLL cells stimulated with with αIgM beads.

a) Upregulated in CLL cells following stimulation with αIgM

Target ID	Name	LogFC	FC	Adj. Pvalue
CCL4L1	Chemokine (C-C Motif) Ligand 4-Like 1	-3.00	7.97	0.0070975
CCL4L2	Chemokine (C-C Motif) Ligand 4-Like 2	-2.97	7.82	0.0066193
CCL3	Chemokine (C-C Motif) Ligand 3	-2.70	6.49	0.0059106
CCL3L3	Chemokine (C-C Motif) Ligand 3-Like 3	-2.70	6.47	0.0083396
EGR1	Early Growth Response 1	-2.51	5.68	0.0065831
CCL3L1	Chemokine (C-C Motif) Ligand 3-Like 1	-2.36	5.14	0.0070162
LRRC32	Leucine Rich Repeat Containing 32	-2.19	4.58	0.0034337
CCL3L1	Chemokine (C-C Motif) Ligand 3-Like 1	-2.04	4.1	0.0071477
EGR2	Early Growth Response 2	-2.01	4.04	0.0086178
EGR3	Early Growth Response 3	-1.99	3.96	0.0087239
SGK	Serum/Glucocorticoid Regulated Kinase 1	-1.95	3.87	0.0173487
SERPINE2	Serpin Peptidase Inhibitor, Clade E (Nexin, Plasminogen Activator Inhibitor Type 1), Member 2	-1.93	3.82	0.011362
MYC	V-Myc Avian Myelocytomatosis Viral Oncogene Homolog	-1.79	3.46	0.0124472
MYC	V-Myc Avian Myelocytomatosis Viral Oncogene Homolog	-1.77	3.41	0.0175517
SGK1	Serum/Glucocorticoid Regulated Kinase 1	-1.73	3.31	0.024635
SGK1	Serum/Glucocorticoid Regulated Kinase 1	-1.68	3.21	0.0382033
SLAMF7	SLAM Family Member 7	-1.62	3.08	0.0008641
BACE2	Beta-Site APP-Cleaving Enzyme 2	-1.58	2.98	0.0066388
FOSB	FBJ Murine Osteosarcoma Viral Oncogene Homolog B	-1.56	2.95	0.0301997
CKS2	CDC28 Protein Kinase Regulatory Subunit 2	-1.55	2.93	0.0067537
ADM	Adrenomedullin	-1.53	2.89	0.0075796
NR4A3	Nuclear Receptor Subfamily 4, Group A, Member 3	-1.53	2.88	0.0079789
MX1	MX Dynamin-Like GTPase 1	-1.52	2.88	0.0075796
ADCY3	Adenylate Cyclase 3	-1.50	2.83	0.0008572
TXN	Thioredoxin	-1.49	2.82	0.0028448
GLA	Galactosidase, Alpha	-1.46	2.76	0.0024741
IRF4	Interferon Regulatory Factor 4	-1.44	2.71	0.0106129
ATF3	Activating Transcription Factor 3	-1.42	2.69	0.0042087
KIAA0251	N/A	-1.41	2.66	0.0020133
TXN	Thioredoxin	-1.40	2.65	0.0025049
NME1	NME/NM23 Nucleoside Diphosphate Kinase 1	-1.40	2.64	0.0115242
SLC7A5	Solute Carrier Family 7 (Amino Acid Transporter Light Chain, L System), Member 5	-1.40	2.64	0.0087054
SRXN1	Sulfiredoxin 1	-1.38	2.61	0.0069301
PHACTR1	Phosphatase And Actin Regulator 1	-1.38	2.61	0.0024292
BACE2	Beta-Site APP-Cleaving Enzyme 2	-1.33	2.51	0.0066193
CKS2	CDC28 Protein Kinase Regulatory Subunit 2	-1.31	2.48	0.0094153
MTHFD2	Methylenetetrahydrofolate Dehydrogenase (NADP+ Dependent) 2, Methenyltetrahydrofolate Cyclohydrolase 2 3	-1.31	2.48	0.009372
METTL1	Methyltransferase Like 1	-1.31	2.48	0.0081278
TNF	Tumor Necrosis Factor	-1.30	2.47	0.0036642
NR4A2	Nuclear Receptor Subfamily 4, Group A, Member 2	-1.30	2.47	0.0109157
LGALS3	Lectin, Galactoside-Binding, Soluble, 3	-1.26	2.39	0.0191241
MIR155HG	MIR155 Host Gene	-1.25	2.37	0.0320512
NR4A2	Nuclear Receptor Subfamily 4, Group A, Member 2	-1.24	2.36	0.0153076
SLC7A1	Solute Carrier Family 7 (Cationic Amino Acid Transporter, Y+ System), Member 1	-1.24	2.36	0.0087292
LY9	Lymphocyte Antigen 9	-1.24	2.36	0.0008572
TNFRSF18	Tumor Necrosis Factor Receptor Superfamily, Member 18	-1.23	2.35	0.0094324
PTGER4	Prostaglandin E Receptor 4 (Subtype EP4)	-1.23	2.35	0.0251295
LY9	Lymphocyte Antigen 9	-1.22	2.34	0.0025049

b) Downregualted in CLL cells following stimulation with αIgM

Target ID	Name	LogFC	FC	Adj. Pvalue
CD14	CD14 Molecule	1.38	2.6	0.009372
VCAN	Versican	0.94	1.92	0.0175517
RCSD1	RCSD Domain Containing 1	0.92	1.89	0.0115242
TGFBI	Transforming Growth Factor, Beta-Induced, 68kDa	0.91	1.87	0.0067977
ALOX5	Arachidonate 5-Lipoxygenase	0.91	1.87	0.0030539
S100A8	S100 Calcium Binding Protein A8	0.90	1.87	0.0079539
LOC90925	N/A	0.88	1.84	0.0170493
SEMA4B	Sema Domain, Immunoglobulin Domain (Ig), Transmembrane Domain (TM) And Short Cytoplasmic Domain, (Semaphorin) 4B	0.87	1.83	0.0092618
CD79B	CD79b Molecule, Immunoglobulin-Associated Beta	0.85	1.8	0.0273893
CD79B	CD79b Molecule, Immunoglobulin-Associated Beta	0.84	1.79	0.016708
CD14	CD14 Molecule	0.82	1.77	0.0087239
PVRIG	Poliovirus Receptor Related Immunoglobulin Domain Containing	0.82	1.76	0.0089839
VPREB3	Pre-B Lymphocyte 3	0.81	1.76	0.0094324
GAPT	GRB2-Binding Adaptor Protein, Transmembrane	0.81	1.75	0.0101513
TBC1D10C	TBC1 Domain Family, Member 10C	0.81	1.75	0.0151769
CD79B	CD79b Molecule, Immunoglobulin-Associated Beta	0.81	1.75	0.0133972
UCP2	Uncoupling Protein 2 (Mitochondrial, Proton Carrier)	0.80	1.75	0.0048439
PTPRCAP	Protein Tyrosine Phosphatase, Receptor Type, C-Associated Protein	0.80	1.74	0.0143322
ITGB7	Integrin, Beta 7	0.80	1.74	0.0114301
HSH2D	Hematopoietic SH2 Domain Containing	0.79	1.73	0.0241105
C4ORF34	Small Integral Membrane Protein 14	0.79	1.73	0.0115222
SPOCK2	Sparc/Osteonectin, Cwcv And Kazal-Like Domains Proteoglycan (Testican) 2	0.79	1.73	0.0168844
C6ORF105	Androgen-Dependent TFPI-Regulating Protein	0.78	1.72	0.0020133
AIM2	Absent In Melanoma 2	0.78	1.72	0.016729
CD27	CD27 Molecule	0.78	1.72	0.011362
C1ORF162	Chromosome 1 Open Reading Frame 162	0.76	1.7	0.0082268
GUCY2C	Guanylate Cyclase 2C	0.76	1.69	0.011076
IL10RA	Interleukin 10 Receptor, Alpha	0.73	1.66	0.0089215
S100A9	S100 Calcium Binding Protein A9	0.73	1.66	0.0028679
CXXC5	CXXC Finger Protein 5	0.73	1.65	0.0134966
CD24	CD24 Molecule	0.72	1.65	0.0143322
INPP5D	Inositol Polyphosphate-5-Phosphatase, SHIP	0.72	1.65	0.0134966
LY86	Lymphocyte Antigen 86	0.71	1.64	0.010727
C13ORF18	N/A	0.71	1.64	0.0082268
TOP1MT	Topoisomerase (DNA) I, Mitochondrial	0.71	1.64	0.0034337
STMN3	Stathmin-Like 3	0.71	1.64	0.0167531
PYCARD	PYD And CARD Domain	0.71	1.63	0.0089868
SIGLEC10	Sialic Acid Binding Ig-Like Lectin 10	0.71	1.63	0.0246076
CCM2	Cerebral Cavernous Malformation 2	0.70	1.63	0.015714
LTB	Lymphotoxin Beta (TNF Superfamily, Member 3)	0.70	1.63	0.0261019
SUSD3	Sushi Domain Containing 3	0.70	1.63	0.0418713
RASGRP2	RAS Guanyl Releasing Protein 2 (Calcium And DAG-Regulated)	0.70	1.62	0.0089839
ETS1	Cytohesin 4	0.70	1.62	0.0124472
TXNIP	Thioredoxin Interacting Protein	0.70	1.62	0.0203606
PLAC8	Placenta-Specific 8	0.69	1.62	0.0136402
S1PR1	Sphingosine-1-Phosphate Receptor 1	0.69	1.61	0.0175517
GAPT	GRB2-Binding Adaptor Protein, Transmembrane	0.69	1.61	0.031899
CD6	CD6 Molecule	0.68	1.61	0.0124728
PSCD4	Cytohesin 4	0.68	1.6	0.0153876

TABLE 6.9: EFFECT OF HFFF2 CO-CULTURE ON CLL CELL RESPONSE TO ANTI-IGM STIMULATION

The first column contains the FC for the top 50 upregulated genes in CLL cells following stimulation with α-IgM beads in comparison to CLL cells cultured alone. The far column denotes the FC of these genes following co-culture with HFFF2 cells (i.e. FibIgM versus IgM alone) to determine modulation of transcriptional response to antigen by microenvironment co-stimulation. Red colour denotes upregulation following microenvironment co-stimulation; green colour denotes upregulation following IgM stimulation alone.

	Upregulated in CLL cells following stimulation with αIgM		Effect of HFFF2 co-stimulation
TargetID	Name	LogFC	LogFC
CCL4L1	Chemokine (C-C Motif) Ligand 4-Like 1	9.29	
CCL4L2	Chemokine (C-C Motif) Ligand 4-Like 2	7.97	3.15
CCL3	Chemokine (C-C Motif) Ligand 3	7.82	3.29
CCL3L3	Chemokine (C-C Motif) Ligand 3-Like 3	6.49	6.10
EGR1	Early Growth Response 1	6.47	6.29
CCL3L1	Chemokine (C-C Motif) Ligand 3-Like 1	5.68	2.77
LRRC32	Leucine Rich Repeat Containing 32	5.14	5.82
CCL3L1	Chemokine (C-C Motif) Ligand 3-Like 1	4.58	2.25
EGR2	Early Growth Response 2	4.1	
EGR3	Early Growth Response 3	4.04	2.78
SGK	Serum/Glucocorticoid Regulated Kinase 1	3.96	2.99
SERPINE2	Serpin Peptidase Inhibitor, Clade E (Nexin, Plasminogen Activator Inhibitor Type 1), Member 2	3.87	
MYC	V-Myc Avian Myelocytomatosis Viral Oncogene Homolog	3.82	2434.85
MYC	V-Myc Avian Myelocytomatosis Viral Oncogene Homolog	3.46	
SGK1	Serum/Glucocorticoid Regulated Kinase 1	3.41	
SGK1	Serum/Glucocorticoid Regulated Kinase 1	3.31	
SLAMF7	SLAM Family Member 7	3.21	
BACE2	Beta-Site APP-Cleaving Enzyme 2	3.08	
FOSB	FBJ Murine Osteosarcoma Viral Oncogene Homolog B	2.98	2.77
CKS2	CDC28 Protein Kinase Regulatory Subunit 2	2.95	5.09
ADM	Adrenomedullin	2.93	5.05
NR4A3	Nuclear Receptor Subfamily 4, Group A, Member 3	2.89	13.39
MX1	MX Dynamin-Like GTPase 1	2.88	3.79
ADCY3	Adenylate Cyclase 3	2.88	9.58
TXN	Thioredoxin	2.83	2.39
GLA	Galactosidase, Alpha	2.82	2.70
IRF4	Interferon Regulatory Factor 4	2.76	
ATF3	Activating Transcription Factor 3	2.71	2.87
KIAA021	N/A	2.69	2.78
TXN	Thioredoxin	2.66	
NME1	NME/NM23 Nucleoside Diphosphate Kinase 1	2.65	2.70
SLC7A5	Solute Carrier Family 7 (Amino Acid Transporter Light Chain, L System), Member 5	2.64	2.46
SRXN1	Sulfiredoxin 1	2.64	
PHACTR1	Phosphatase And Actin Regulator 1	2.61	2.78
BACE2	Beta-Site APP-Cleaving Enzyme 2	2.61	2.60
CKS2	CDC28 Protein Kinase Regulatory Subunit 2	2.51	2.47
MTHFD2	Methylenetetrahydrofolate Dehydrogenase (NADP+ Dependent) 2, Methenyltetrahydrofolate Cyclohydrolase 2 3	2.48	5.05
METTL1	Methyltransferase Like 1	2.48	2.29
TNF	Tumor Necrosis Factor	2.48	2.65
NR4A2	Nuclear Receptor Subfamily 4, Group A, Member 2	2.47	5.33
LGALS3	Lectin, Galactoside-Binding, Soluble, 3	2.47	10.90
MIR155HG	MIR155 Host Gene	2.39	2.71
NR4A2	Nuclear Receptor Subfamily 4, Group A, Member 2	2.37	2.60
SLC7A1	Solute Carrier Family 7 (Cationic Amino Acid Transporter, Y+ System), Member 1	2.36	10.90
LY9	Lymphocyte Antigen 9	2.36	
TNFRSF18	Tumor Necrosis Factor Receptor Superfamily, Member 18	2.36	4.34

6.9.2 Gene set enrichment analysis using GSEA software

When looking at the identification of genes that are differentially expressed in two conditions like the experiment performed here the most common statistical approach is to quantify the interest of each gene with a *p*-value, adjust these *p*-values for multiple comparisons, chose an appropriate cut-off, and create a list of *candidate genes* which can be further investigated as carried out previously above. However, this approach has been criticized for ignoring biological knowledge regarding how genes work together. Recently a series of methods, that do incorporate biological knowledge, have been proposed by looking at whether sets of genes show significant concordant differences between the two biological groups. We have used a gene set enrichment software called GSEA (Gene Set Enrichment Analysis) to carry out this analysis to further investigate the differences between CLL cells cultured alone and in the presence of HFFF2 cells while taking into account biological functions.

GSEA is a computational method that determines whether an a priori defined set of genes shows statistically significant, concordant differences between two biological states (phenotypes). The algorithm used by the software is fully described the in 'The Gene Set Enrichment Analysis' PNAS paper (Subramanian et al., 2005). For all analysis carried out for this study the GSEA Preranked analysis option was used. GSEA Preranked runs the gene set enrichment analysis against a ranked list of genes, which are uploaded into the software. In this case the ranked list of genes was the expression datasets, ranked according to their fold change. Detailed analysis strategy is outlined in Methods Section2.5.3

It was aimed to investigate enrichment of gene sets within phenotypes using the C2-curated gene set from Msig database. This gene set is collected from various sources such as online pathway databases, publications in PubMed, and knowledge of domain experts. For this analysis I specifically looked at the Canonical Pathways gene set. Using GSEA to firstly look at the effect of anti-IgM stimulation will help to confirm the data set and methods used as there is extensive evidence for the upregulation of certain genes and gene sets following anti-IgM stimulation. I therefore used GSEA to compare the anti-IgM-induced gene signature revealed in my experiment for similarity to other signatures in public databases (Figure 6-7). There was an upregulation of signalling pathways including:

SIG_PIP3_SIGNALLING_IN_B_LYMPHOCYTES,

SIG_BCR_SIGNALLING_ PATHWAY

REACTOME_ANTIGEN_ACTIVATES_B_CELL_RECEPTOR_LEADING_TO_GENERATION_OF_SECOND_MESSENGERS.

The results revealed a large number of BCR signalling pathways confirming the approach adopted.

GSEA was also used to confirm the findings from the data set analysis looking at the effect of HFFF2-CM culture (Figure 6-8, AppendixE). Results from the GSEA indicated that 614/1067 gene sets were enriched in the CLL cells cultured alone while 453 gene sets were enriched in the CLL cells cultured in HFFF2-derived CM phenotype. Looking at the gene sets, out of those with a positive ES i.e. enriched in the first phenotype, CLL cells cultured alone, 45 are significant at FDR less than 25% and 41 gene set are significant at nominal pvalue less than 1%. Looking at the gene sets with a negative ES i.e. enriched in the second phenotype, CLL cells cultured in the presence of HFFF2-derived CM, 316 are significant at FDR less than 25% and 147 gene sets are significant at nominal pvalue less than 1%. This indicates that although the spread in upregulation is fairly even between the two phenotypes, far more are significantly enriched in the second phenotype. The top hit with the greatest NES is REACTOME_ CHEMOKINE_ RECEPTORS_ BIND_ CHEMOKINES. Further to this there a whole plethora of gene sets related to inflammation and/or chemokines:

KEGG_CYTOKINE_CYTOKINE_RECEPTOR_INTERACTION

KEGG_CHEMOKINE_ SIGNALLING_PATHWAY

BIOCARTA_INFLAM_PATHWAY

REACTOME_CYTOKINE _SIGNALLING_IN_IMMUNE_SYSTEM

This confirms a substantial upregulation of inflammatory chemokine and cytokine following culture with HFFF2-derived CM, as identified by analysis of lists of individual regulated genes.

FIGURE 6-7: SCHEMATIC REPRESENTING THE GSEA RESULTS USING THE CANNONICAL PATHWAYS DATA SET

Schematic representing the GSEA results using the Cannonical Pathways data set comparing CLL cells cultured alone and CLL cells stimulated with αIgM beads. The Cannonical Pathways data set contains 1067 gene sets. Each circle indicates the number of gene sets that were upregulated under that culture conditon and also the number that were significantly upregualted. Under each diagram is a selection of important gene sets that are significantly upregulated.

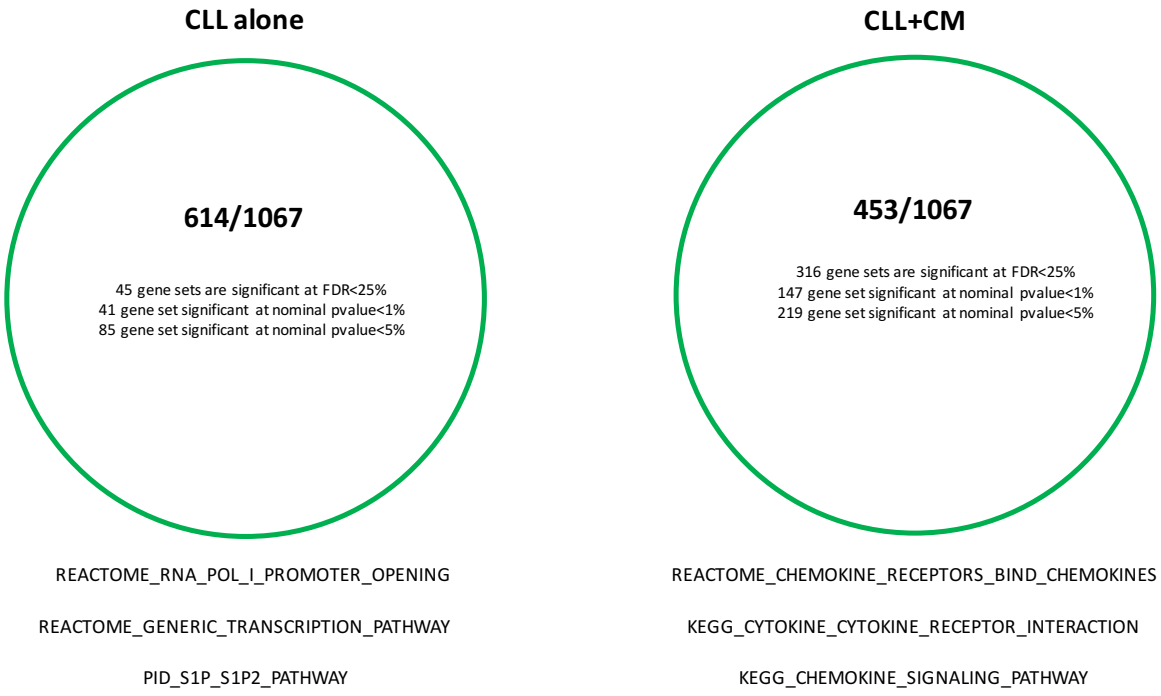

FIGURE 6-8: SCHEMATIC REPRESENTING THE GSEA RESULTS USING THE CANNONICAL PATHWAYS DATA SET

Schematic representing the GSEA results using the Cannonical Pathways data set comparing CLL cells cultured alone and CLL cells co-cutlured in the presence of HFFF2-derived CM. The Cannonical Pathways data set contains 1067 gene sets. Each circle indicates the number of gene sets that were upregulated under that culture conditon and also the number that were significantly upregualted. Under each diagram is a selection of important gene sets that are significantly upregulated.

6.10 Effect of co-culture of CLL cells with HFFF2 cells on surface IgM expression and signal capacity

Due to the technical difficulties associated with GEP of co-cultured cells I next aimed to directly investigate the effect of co-culture of CLL cells with HFFF2 cells on sIgM expression and signal capacity. Previous experiments (Mockridge et al., 2007) have shown that *in vitro* incubation of CLL cells is associated with increased sIgM expression/signal capacity. I therefore cultured CLL cells alone or in the presence of HFFF2 cells and analysed (i) sIgM expression on CD5+CD19+ CLL cells and (ii) anti-IgM-induced calcium fluxes at 8, 24 or 48 hours using flow cytometry. This analysis was performed using a total of 6 CLL samples selected to encompass a range of basal sIgM expression and signal responses (Table 6.10).

Representative flow cytometry results for sIgM expression are shown for two samples (CLL 635 and CLL 695) in Figure 6-9. Quantitation for the 6 samples analysed in total and a summary for all data is shown in Figure 6-10 and Figure 6-11. Results demonstrate that *in vitro* culture of CLL cells is generally associated with a recovery of sIgM expression, particularly at 48 hours (observed in 4/6 samples). sIgM expression was increased in the presence of HFFF2 cells in 4/6 samples (684a, 709, 609a, 643b). In the other two samples, HFFF2 cells either appeared to have no effect (635a) or reduced sIgM expression (CLL 695). These results appear to suggest that HFFF2 co-culture enhances sIgM expression. However, it is notable that the two samples where HFFF2 cells did not enhance sIgM (both U-CLL) had the strongest recovery of sIgM in the absence of HFFF2 cells. It is possible that the pathways which allow sIgM recovery are operating maximally in these cells, and can not be enhanced by HFFF2 co-culture. However, decreasing viability of CLL cells *in vitro* is likely to reduce recovery of sIgM. Thus, as apoptosis was not quantified directly in these experiments, an alternate explanation is that HFFF2 cell co-culture acts indirectly to maintain CLL cell viability/metabolic activity to promote sIgM recovery.

Results for parallel analysis of anti-IgM-induced signal responses are shown in Figure 6-12 and Figure 6-13. Similar to sIgM expression, the analysis did not reveal a consistent response to HFFF2 co-culture across all samples studied and, in general, anti-IgM-induced Ca^{2+} fluxes were not different between cells in the presence or absence of HFFF2 co-culture. There is a tendency for increased calcium flux at 8 hours following co-culture but results were varied between patients as demonstrated by the large error bars Overall microenvironmental co-stimulation, at least in this model does not appear to have a substantial effect on anti-IgM mediated signalling responses. Future experiments therefore focused on the effects of HFFF2 cells on CLL without sIgM stimulation.

TABLE 6.10: CHARACTERISTICS OF PATIENTS USED IN HFFF2/IGM EXPERIMENTS

Patient	M/U-CLL	$CD5^+/CD19^+$(%)	IgM (MFI)	Ca flux (%)
635a	U	89	67	82
695	U	98	80	82
684a	M	92	31	14
709	M	92	101	46
609a	M	89	25	57
643b	M	92	15	25

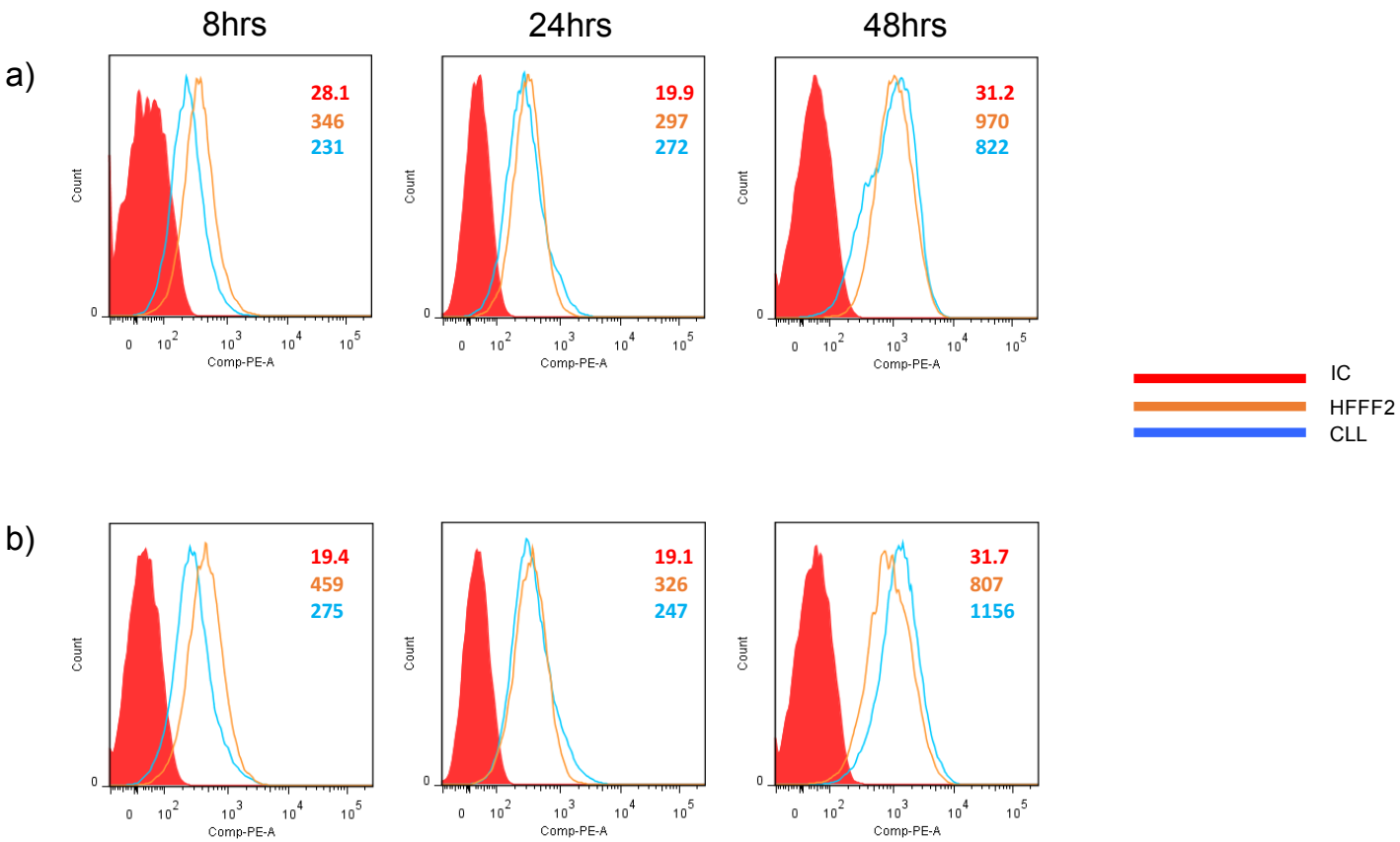

FIGURE 6-9: SURFACE IGM EXPRESSION FOLLOWING CO-CULTURE WITH THE HFFF2 CELL LINE

FACS histograms displaying IgM expression for two representative patients CLL 635 and CLL 695 ((a) and (b) respectively). Solid peak (red) represents isotype control. CLL cells were either cultured alone (blue line) or in the presence of HFFF2 cells (orange line) for 8, 24 or 48hrs. Increasing culture length goes from left to right. Reported values are Mean fluorescence intensity (MFI).

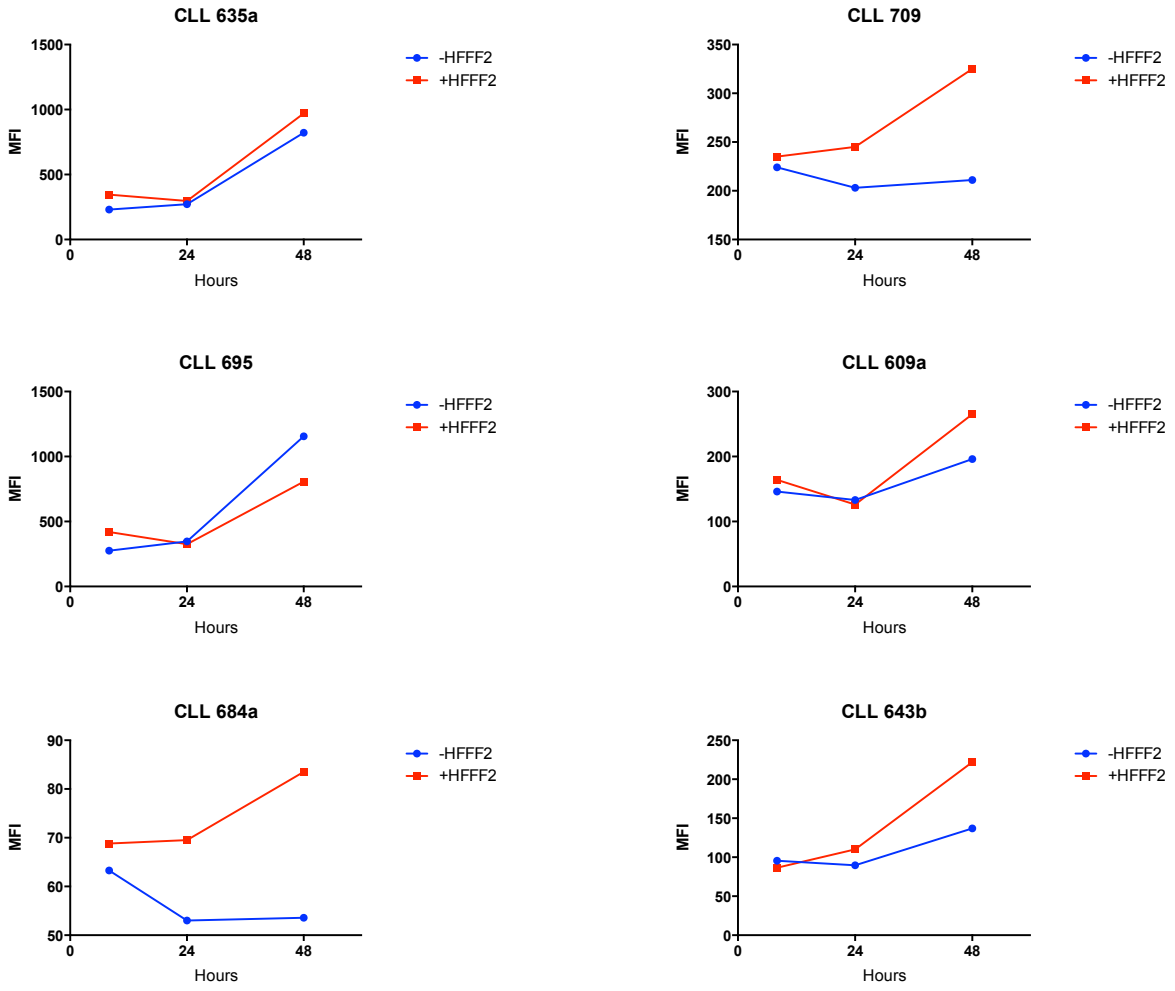

FIGURE 6-10: SURFACE IGM EXPRESSION FOLLOWING CO-CULTURE WITH THE HFFF2 CELL LINE

Surface IgM expression results for all six CLL patients studied. CLL cells were cultured alone (blue line) or in the presence of HFFF2 fibroblasts (red line) for 8, 24 or 48 hours prior to analysis of IgM expression levels via FACS. Plotted values are IgM mean fluorescent intensity (MFI).

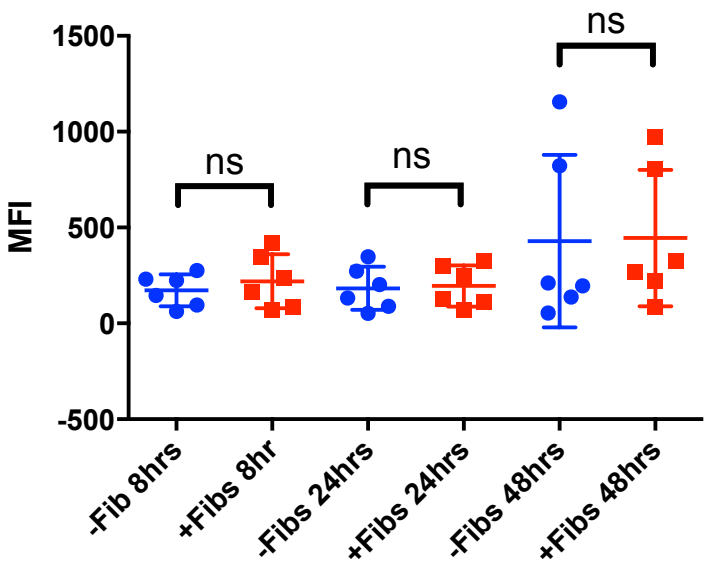

FIGURE 6-11: SURFACE IGM EXPRESSION FOLLOWING CO-CULTURE WITH THE HFFF2 CELL LINE

Summary of data for all samples analysed (n=6). Surface IgM expression is plotted as mean fluorescence intensity (MFI) normalised to CLL alone MFI for each individual timepoint. Statistical significance is indicated (Wilcoxon Test; ns non-significant). Error bars are SD.

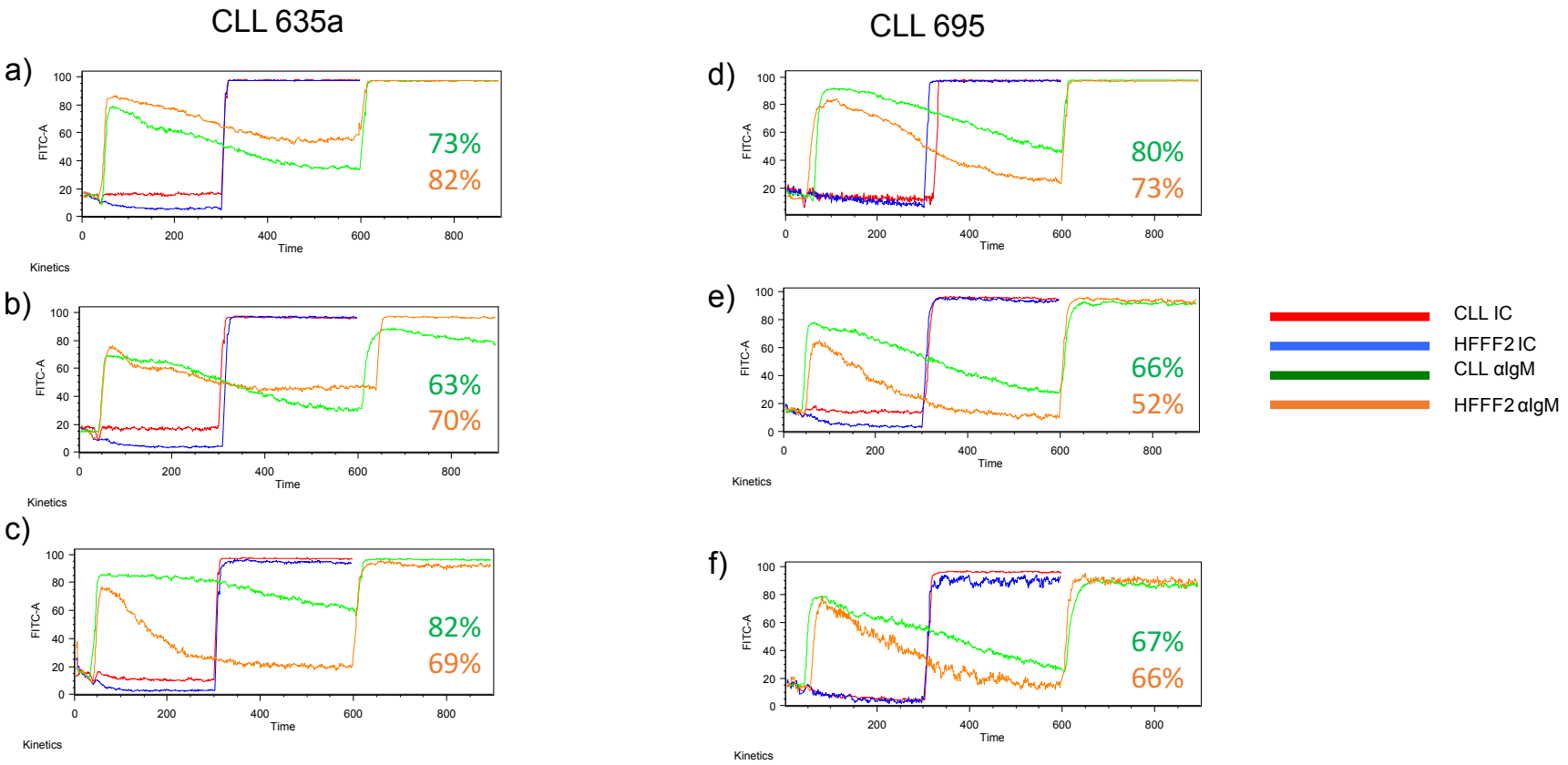

FIGURE 6-12: CALCIUM FLUX ANALYSIS FOR TWO REPRESENTATIVE PATIENTS (CLL 635A AND CLL 695) FOLLOWING CO-CULTURE WITH THE HFFF2 CELL LINE

Two representative patients. CLL cells were cultured alone (red and green line) or in the presence of HFFF2 cells (blue and orange line) for 8 hours (a,d) 24 hours (b,e) and 48 hours (c,f). CLL cells were stimulated with either αIgM (green and orange line) or isotype control (IC, red and blue line) and calcium flux was measured for 5 or 10 minutes (isotype and αIgM respectively) before ionomycin was added as a positive control.

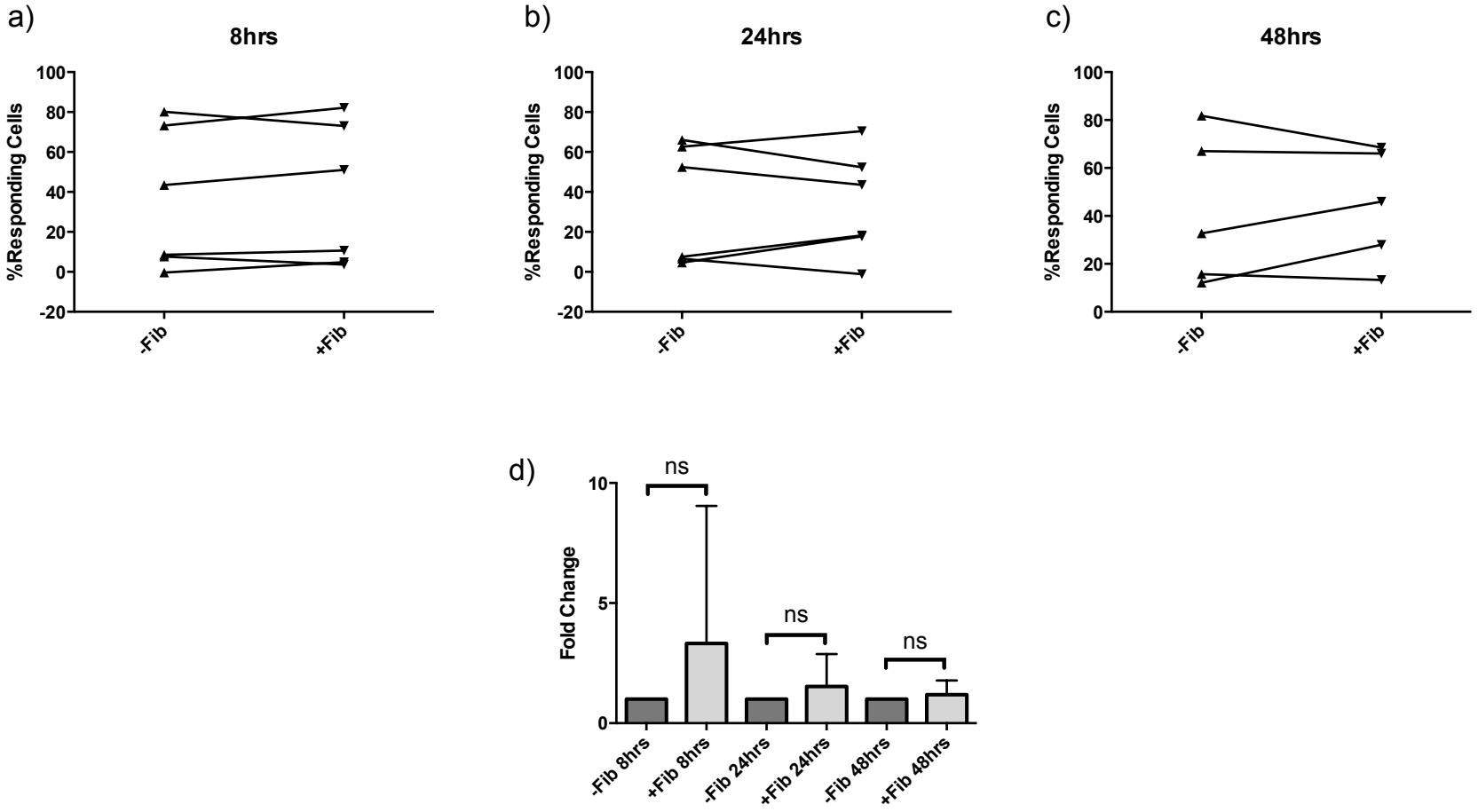

FIGURE 6-13: CALCIUM FLUX ANALYSIS FOLLOWING CO-CULTURE WITH HFFF2 CELLS

Grouped data for all patients analysed (n=6). Percent responding cells are plotted at the three time points analysed (a) 8, (b) 24 and (c) 48 hours. (d) Combined fold change for all patients analysed. Samples were normalised to CLL cells cultured alone. Statistical significance is indicated (Wilcoxon Test; ns non-significant). Error bars are SD.

6.11 Analysis of *IL6, IL8, CCL2* and *CXCL2* mRNA expression following co-culture of CLL cells with HFFF2-derived CM

Following the GEP results demonstrating that a large number of chemokines and cytokines are upregulated following co-culture with HFFF2 cells or HFFF2-CM a select number were chosen for further analysis. Regulation of the expression of IL6, IL8, CCL2 and CXCL2 RNAs by HFFF2 CM was confirmed using q-PCR. These RNAs were selected since they were among some of the most strongly induced RNAs identified by GEP in HFFF2-stimulated CLL cells and have potential roles in CLL biology (Table 6.7). For example, IL-6 which had the greatest FC following co-culture with HFFF2 cells has been shown to increased in CLL serum compared to healthy controls (Fayad et al., 2001), has been shown to prevent spontaneous apoptosis (Reittie et al., 1996) and tumour-derived IL-6 may contribute to immunological defects in CLL (Buggins et al., 2008). Another interesting chemokine with an emerging role in CLL is CCL2. CCL2 is a chemoattractant for monocytes and T cells and enhances CLL cells survival *in vitro* (Burgess et al., 2012).

The first step in confirmation was to investigate expression in the same RNA samples that were analysed by GEP. Results from q-PCR analysis confirmed that co-culture of CLL cells with HFFF2 cell-derived CM was associated with a statistically significant increase in expression of all four RNAs (Figure 6-14). Overall the fold change was similar to results from GEP. A greater FC was seen in IL-6, CCL2 and IL-8 (FC of 27, 22 and 14 compared to 14, 10 and 5 respectively), while CXCL2 was comparable (FC of 4 compared to 5).

The second step for confirmation was to quantify RNA expression in an additional 10 samples, two of which were repeats from the GEP samples (481 and 567) for QC purposes. Samples were a mixture of U/M-CLL (6 M-CLL and 4 U-CLL). CLL samples were treated with HFFF2 cell-derived CM for 8 hours (see left two bars for each of the graphs shown in Figure 6-15 and Figure 6-16 labelled as “PBMC”). Data is displayed as raw ΔCt values to indicate where samples were ‘undetectable’ by qPCR (Figure 6-15) and secondly following normalisation to the CLL ‘PBMC’ condition (Figure 6-16). This analysis further confirmed that HFFF2-CM treatment of CLL PBMC samples was associated with increased expression of IL6, IL8, CCL2 and CXCL2 RNAs. In this extended cohort, the increases in IL8, CCL2 and CXCL2 RNAs were significant (P=0.002, P=0.004 and P=0.01 respectively). However, the fold induction of IL6 RNA was much reduced compared to the original 4 samples analysed by GEP (FC of 27 verses 2) and the difference in expression between control and HFFF2-CM-treated cells was not significant. In part this was because IL6 RNA was not detectable in 4 samples under either condition.

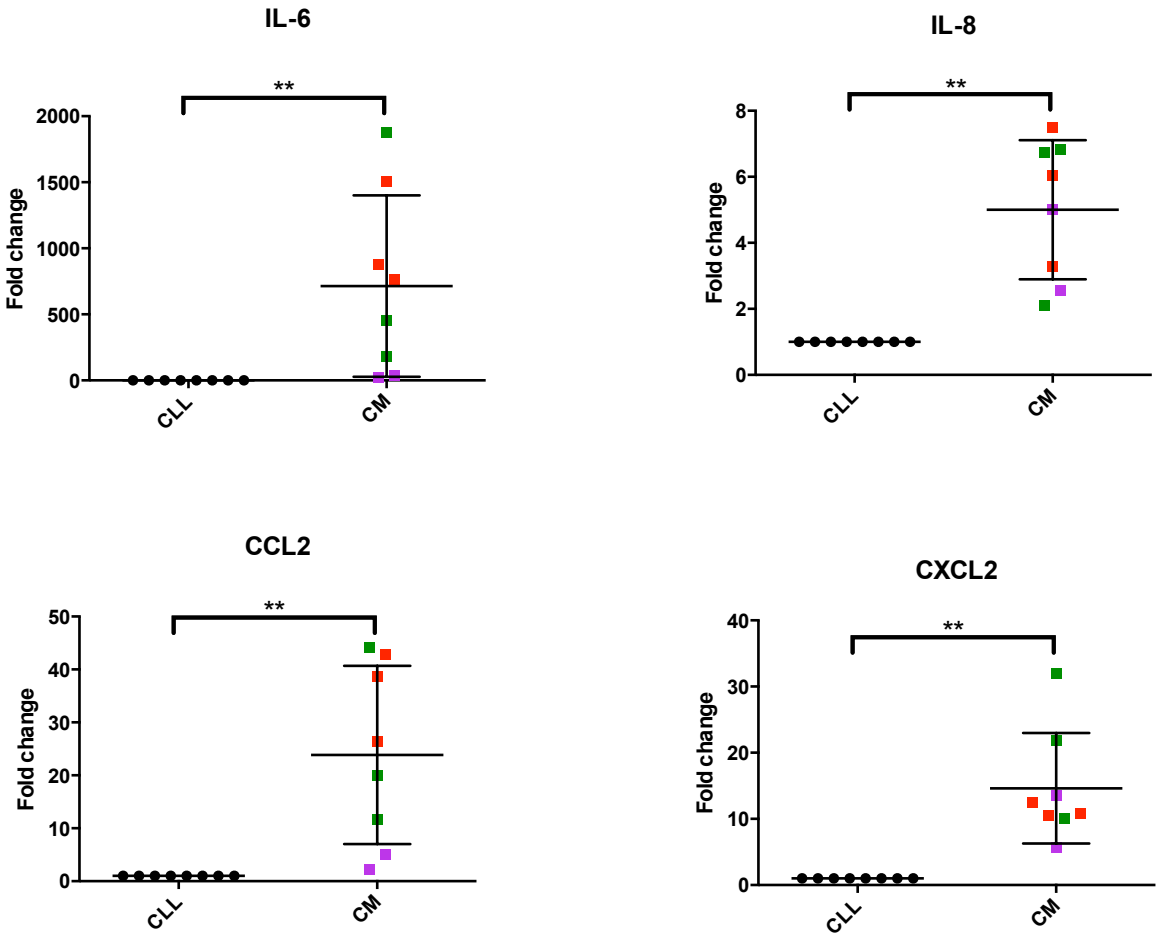

FIGURE 6-14: ABUNDANCE OF *IL6, IL8, CCL2* AND *CXCL2* MRNA EXPRESSION IN CLL CELLS FOLLOWING CO-CULTURE WITH HFFF2-DERIVED CM

Following GEP, the same RNA samples were used to confirm the results seen. Data from three replicates of three different CLL patients (indicated by different colours). Following co-culture of CLL cells with HFFF2-derived CM qPCR analysis was undertaken to investigate the abundance of *IL6, IL8, CCL2* and *CXCL2* mRNA levels. Plots represent fold change relative to CLL cultured in RPMI ΔΔCT value. ΔΔCT value were calculated relative to B2M. Error bars indicate the standard deviation and statistical significance is indicated (Wilcoxon Test; ** P=0.0008).

6.11.1 Comparison of responses between CLL PBMC and purified CLL cells

Microenvironmental cross-talk may involve multiple cells types, some of which may act as obligate intermediates in the ability of HFFF2 cells to modulate gene expression in CLL cells. All experiments to this point were performed using CLL PBMCs in order for us to "capture" both direct and indirect effects of HFFF2 cells on CLL cells. Therefore, in parallel with the experiment described above, I also investigated the effect of HFFF2-CM on purified CLL cells to determine the potential role of accessory cells in mediating CLL/HFFF2 cell cross-talk. CLL cells were purified by negative selection using the MACS CLL cell isolation kit (Purification data, AppendixC). For some experiments, PBMCs were also passed down the isolation column without antibodies, to control for possible effects associated with the prolonged processing time associated with purification. Whereas expression of CCL2, CXCL12 and IL8 RNAs was increased in CLL PBMCs incubated with HFFF2-CM, expression of these RNAs was unaltered in purified CLL cells following co-culture with HFFF2-CM (Figure 6-16). By contrast, the modest increase in IL6 RNA observed in these samples following incubation with HFFF2-CM was similar in CLL PBMCs and purified CLL cells. Results obtained in PBMCs were similar between experiments where PBMCs were used directly, or following passage down the MACS isolation column (data not shown). Overall, these results suggested that HFFF2-CM directly induces *IL6* RNA expression in CLL cells. By contrast, for *CCL2*, *CXCL12* and *IL8* RNAs, it is possible that induction in CLL cells is dependent on an intermediate cell type, or that these RNAs are actually being induced by HFFF2-CM in a small fraction of non-CLL cells present with the PBMC samples.

To begin to address these possibilities, we investigated whether the extent of RNA induction depended on the number of non-malignant cells present in the PBMCs, which ranged from 3 to 26% for the samples used in these experiments. For example, if the chemokines/cytokines were derived from third cell type, there may be a correlation between the response and proportion of non-malignant cells. This analysis may also reveal if production is by CLL cells but is dependent on the third cell type. There was no clear relationship between the extent of RNA induction following HFFF2-CM treatment and the proportion of non-malignant cells for any of the RNAs analysed (Figure 6-17). However removal of a outlier with a large FC in the CCL2 dataset revealed a potential relationship which was significant suggesting that the increase in CCL2 expression following culture with HFFF2-CM may be dependent on a third cell type. There is also an indication of this in the CXCL2 dataset.

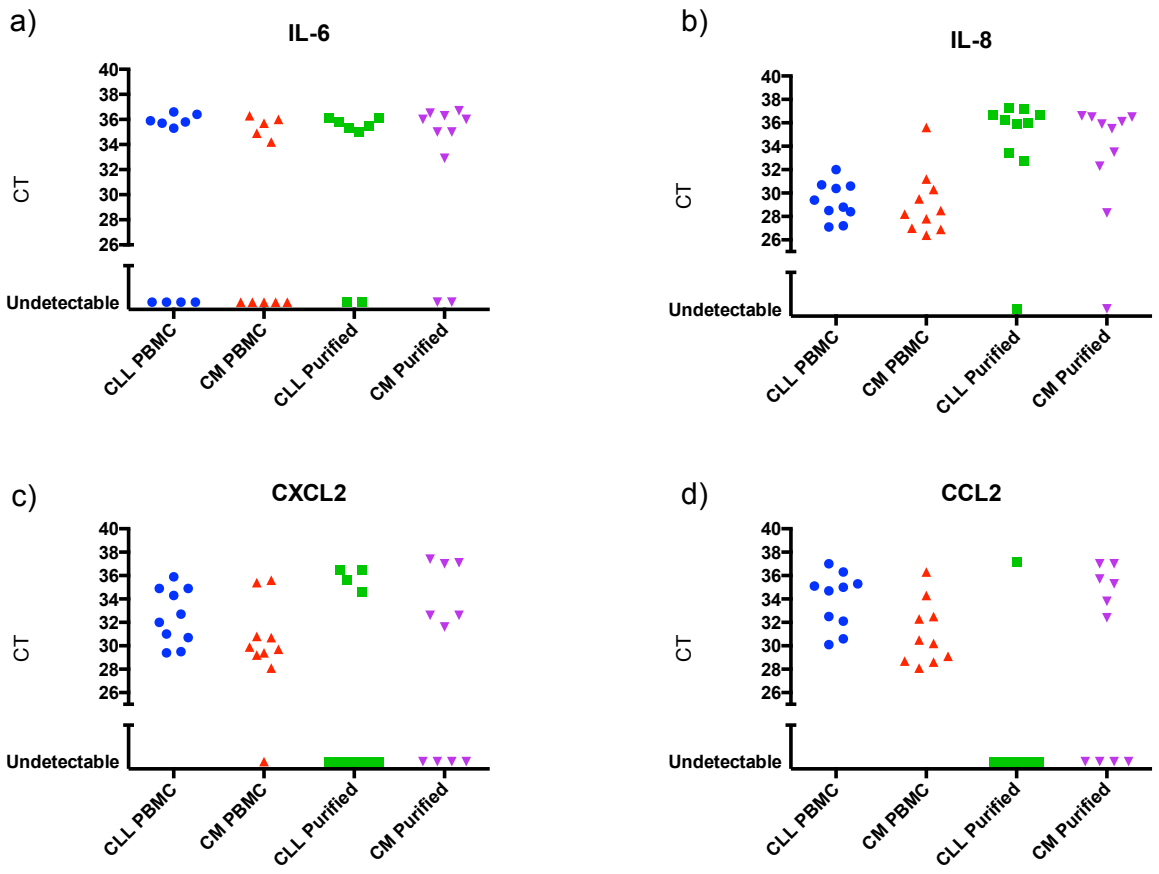

FIGURE 6-15: ABUNDANCE OF *IL6, IL8, CCL2* AND *CXCL2* MRNA EXPRESSION IN CLL CELLS FOLLOWING CO-CULTURE WITH HFFF2-DERIVED CM

Summary of data for all samples analysed (n=10). Following co-culture of CLL cells with HFFF2-derived CM qPCR analysis was undertaken to investigate the abundance of *IL6, IL8, CCL2* and *CXCL2* mRNA levels. Plots represent raw ΔCt values.

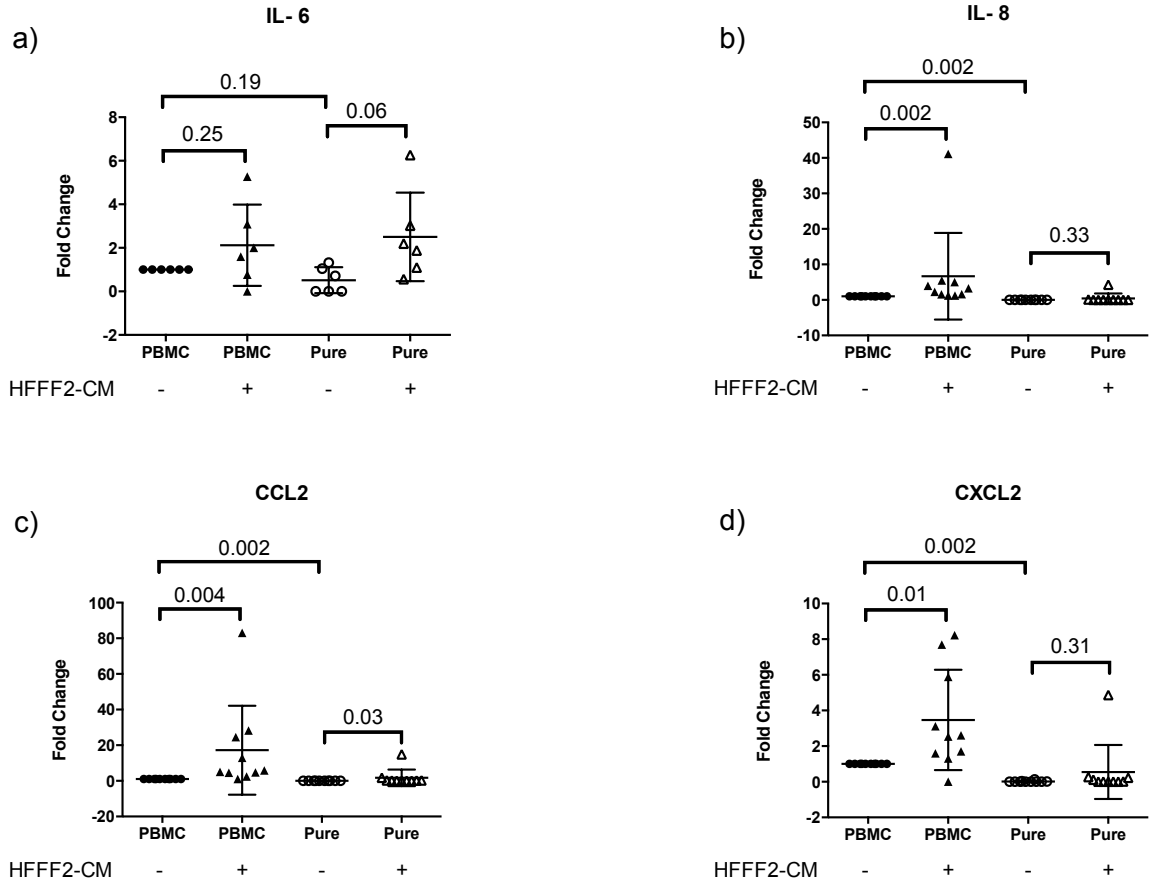

FIGURE 6-16: ABUNDANCE OF *IL6, IL8, CCL2* AND *CXCL2* MRNA EXPRESSION IN CLL CELLS FOLLOWING CO-CULTURE WITH HFFF2-DERIVED CM

Summary of data for all samples analysed (n=6 *IL6* and n=10 *IL8, CCL2* and *CXCL2*). Following co-culture of CLL cells with HFFF2-derived CM qPCR analysis was undertaken to investigate the abundance of *IL6, IL8, CCL2* and *CXCL2* mRNA levels. Plots represent fold change relative to CLL cultured in RPMI ΔΔCT value. ΔΔCT value were calculated relative to B2M. Error bars indicate the standard deviation and statistical significance is indicated (Wilcoxon Test).

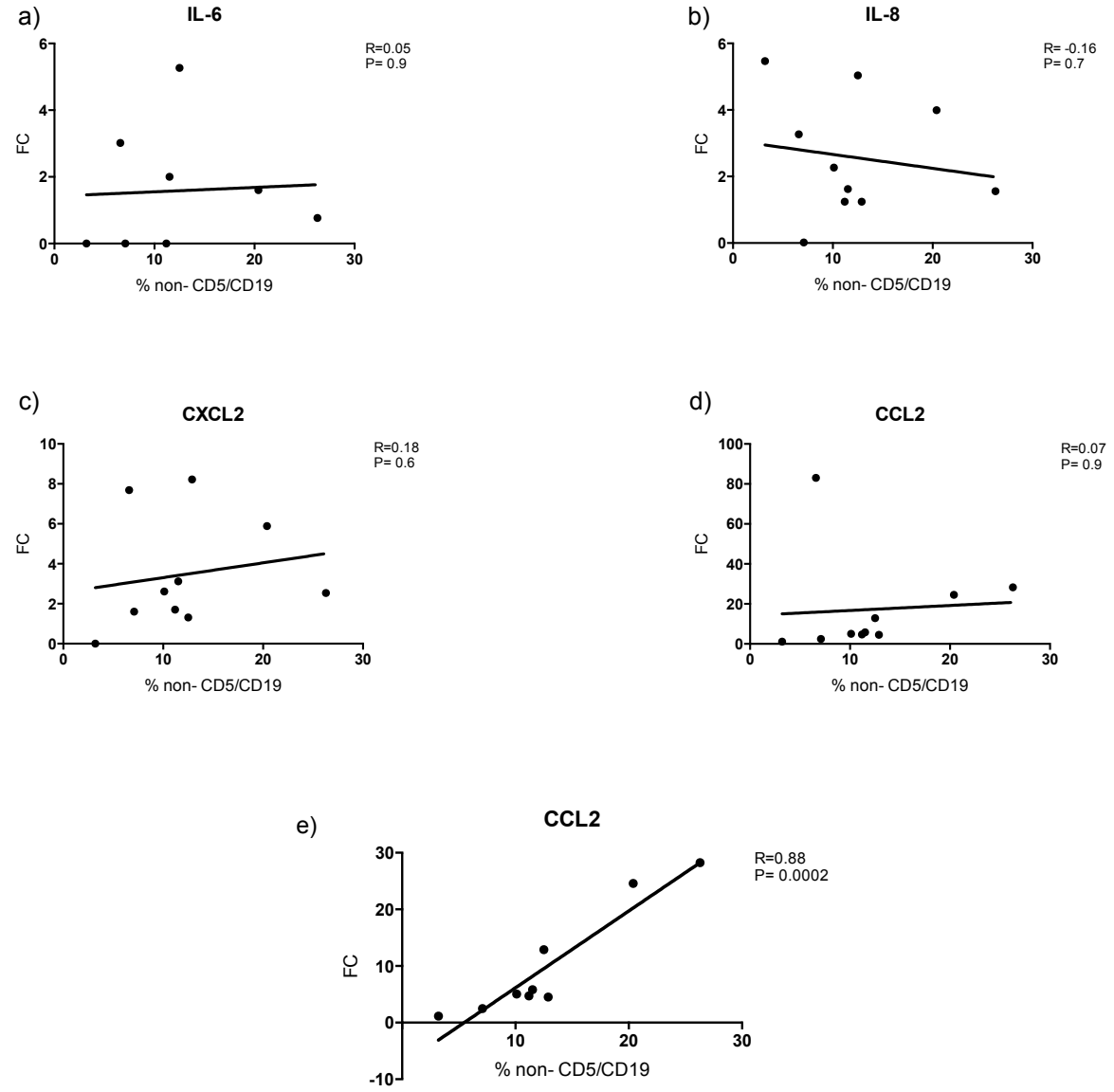

FIGURE 6-17: RELATIONSHIP BETWEEN PERCENTAGE NON-CD5/CD19 CELLS AND FOLD CHANGE OF *IL6, IL8, CCL2* AND *CXCL2* ABUNDANCE FOLLOWING CULTURE WITH HFFF2-DERIVED CM

Correlation analysis was carried out using Pearsons Test between FC values (normalised values from Figure 6-15) and percentage non $CD5^{+}CD19^{+}$ cells for all four genes analysed. R values and P values are indicated on each individual graph.

6.12 Quantitation of intracellular levels of CCL2 by flow cytometry

I next used intracellular staining to directly quantify cytokine expression in CLL cells to resolve whether the cytokines were induced in CLL cells, but via a pathway dependent on a third cell type, or were induced by HFFF2-CM in non CLL cells. This analysis focused on CCL2 because (i) possible interesting relationship between upregulation of CCL2 and the percentage of non-malignant cells indicating a potential role of a third cell type, (ii) two recent studies which have explored the upregulation of the chemokine following culture with stromal cells (Schulz et al., 2011, Burgess et al., 2012) (iii) CCL2 had the greatest fold change (20-fold) and (iv) availability of reagents/antibodies

CLL PBMCs and purified CLL cells were treated with HFFF2-CM for 24 hours, and then stained for intracellular CCL2, CD19 and CD5 to allow for quantitation of CCL2 in malignant cells. In addition purified CLL cells and CLL PBMCs were treated with CpG-ODN (7.5μg/ml) as a positive control. Figure 6-18 displays results obtained with one representative sample. Although the signals obtained using intracellular staining were weak and differed widely between individual samples, quantitation of the FACS data confirmed a modest 5-fold overall increase in CCL2 expression in PBMCs and a 2-fold increase in purified cells (Figure 6-19). This was in comparison to a 20-fold and 2-fold increase from the qPCR data. Although the increase in CCL2 expression was not significant, the results mirrored what was seen in the q-PCR experiments. CpG-ODN stimulation resulted in a overall 7-fold and 4-fold in PBMCs and purified CLL cells respectively. However, this difference was statistical significant only for purified cells. In particular, there was one outlier, which had much stronger response for PBMC but overall the response between PBMCs and purified CLL cells was similar.

In summary, this suggests, as hinted in the correlation analysis from the qPCR data that, the increase in CCL2 expression following culture with HFFF2-CM may be dependent on a third cell type. However, low level of response observed using intracellular staining prevented us from drawing firm conclusions from this data.

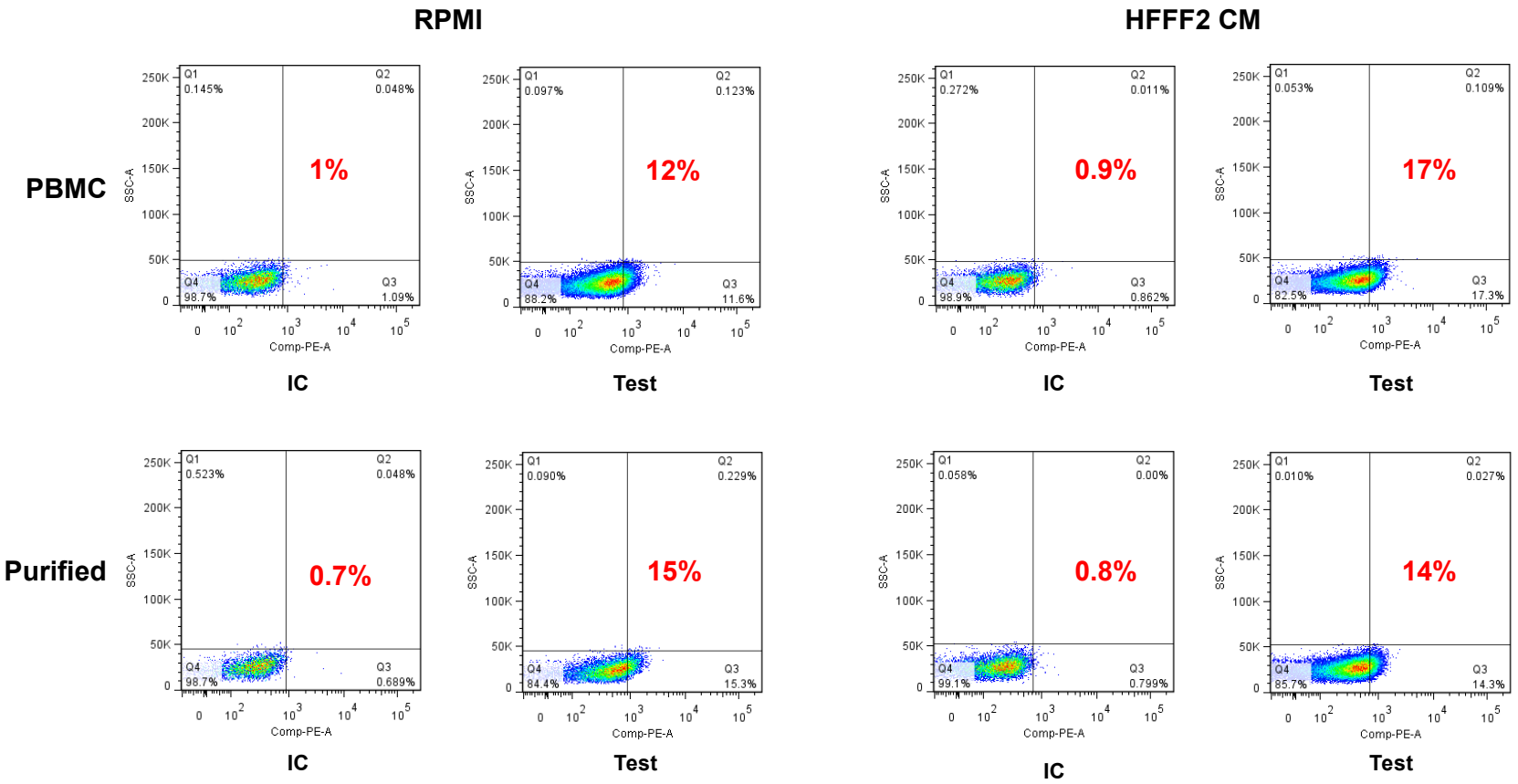

FIGURE 6-18: INTRACELLULAR STAINING OF CCL2 IN CLL CELLS

FACS plots displaying intracellular expression of CCL2 for one representative patient (CLL 575d). CLL cells were cultured as PBMCs or purified CLL cells in either C.RPMI or HFFF2-derived CM for 24 hours. CCL2 expression (PE) was measured on the CD5+CD19+ population. Values in red indicate percentage number of cells producing CCL2. Gates for PE expression was determined using IC for each sample.

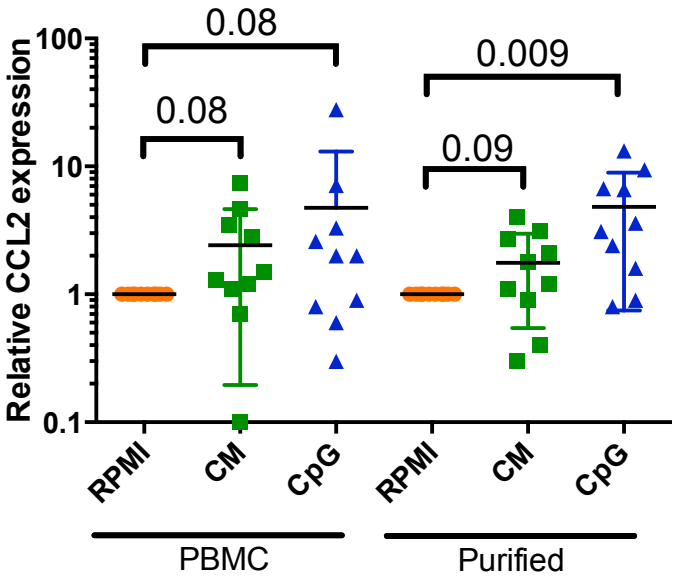

FIGURE 6-19: LEVEL OF CCL2 EXPRESSION IN CLL CELLS VIA INTRACELLULAR STAINING USING FLOW CYTOMETRY

Normalised FACS data. CLL cells were cultured as PBMCs or purified cells in either C.RPMI or HFFF2-derived CM. CCL2 expression was normalised to the RPMI conditions for the respective condtion (PBMC and purified). Error bars indicate the standard deviation and statistical significance is indicated (Wilcoxon Test).

6.13 Viability of purified CLL cells compared to CLL PBMC cultures

To further investigate the role of third-party “accessory cells”, we compared the effects of HFFF2 cells on survival of purified CLL cells and CLL PBMCs. Purified CLL cells or CLL PBMCs were cultured alone, in the presence of HFFF2 cells or HFFF2-derived CM and viability was assessed at 0, 24 and 48 hours (Figure 6-20). There was no significant difference in the spontaneous apoptosis of purified CLL cells versus CLL cells in the PBMC culture, however there was a trend for an increase in cell viability at both timepoints for CLL PBMCs (62% versus 68% and 52% versus 58% at 24 and 48 hours respectively). As expected, both HFFF2 cell co-culture and HFFF2-CM promoted CLL cell survival in both conditions (co-culture > CM). However, similar survival promoting effects were observed for both purified CLL cells and CLL PBMCs (Figure 6-20c), suggesting survival effects mediated by HFFF2 cells is not dependent on an intermediate accessory cell.

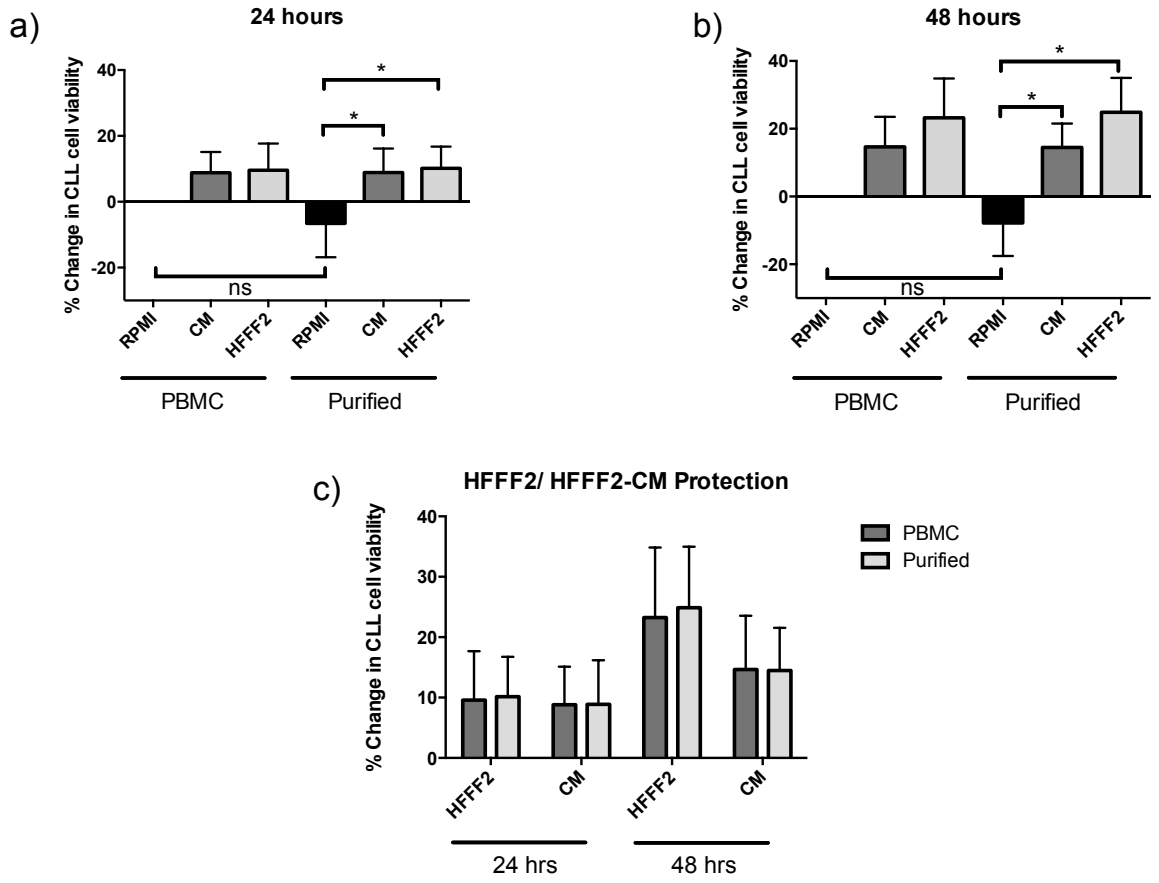

FIGURE 6-20: COMPARISON OF VIABILITY AND HFFF2 PROTECTION LEVELS IN CLL PBMC AND PURIFIED CLL CULTURES

Summary of data for all samples analysed (n=7). (a,b) Effect of PBMC culture on CLL cell viability at 24 and 48 hours respectively. Due to variation in rates of spontaneous apoptosis data were corrected to show percent change in CLL cell viability for CLL PBMCs compared to purified CLL cells. (c) Levels of HFFF2 and HFFF2-CM protection in CLL PBMCs and purified CLL cells. Due to the variation in rates of spontaneous apoptosis between CLL samples data were corrected to show percent change for CLL cell viability for CLL cells co-cultured with HFFF2 cells or HFFF2-CM compared to CLL cells cultured alone either as PBMCs or purified. Statistical significance is indicated (Wilcoxon Test; ns= non significant). Error bars are SD.

6.14 Key Findings

- HFFF2 co-culture and HFFF2-derived CM caused widespread transcriptional reprogramming in CLL cells
- Chemokines and cytokines RNAs were commonly upregulated in CLL cells following co-culture with HFFF2 cells
- Co-culture of CLL cells with HFFF2 cells does not consistently effect surface IgM expression/Ca^{2+} signal capacity
- HFFF2-derived CM increases expression of the chemokines and cytokines IL-6, IL-8, CXCL2 and CCL2
- An intermediate cell type appears to be required for HFFF2-CM induced expression of CXCL2, CCL2 and IL-8 RNAs, but not HFFF2-CM-induced CLL cell survival.
- IL-6 expression does not appear to require an intermediate cell type

6.15 Discussion

6.15.1 Data quality from GEP experiment

The data quality analysis performed by Cambridge Genomic services, indicated that the RNA samples collected for GEA were of good quality. Figure 6-1 demonstrated how the three technical repeats performed for each patient tested were closely correlated indicating the robustness of the experimental conditions performed. This allowed for an average of the repeats to be taken for each patient. The hierarchical clustering (Figure 6-2) and MDS clustering (Figure 6-3) indicated that patient 1 and 2 cluster together, but patient 3 clusters away from the other two patients. There is no obvious differences between patient 3 and the other patients to explain this clustering (Table 6.1). This indicates one of the weaknesses of the GEA experiments, the sample size. CLL is an extremely heterogeneous disease and there is also heterogeneity in terms of CLL patient response to HFFF2 cell culture as indicated in previous experiments (Chapter 3). This initial QC analysis indicated that the experiment and sample collection was robust since triplicate samples were closely correlated. However, it indicated that any differences between stimulation (particularly for anti-IgM and CM) were small compared to inter-

patient variability. Further GEA experiments looking into transcriptional changes following stromal cell culture could take into account other prognostic factors when choosing patients and also level of HFFF2-mediated protection to individual CLL patients.

6.15.2 HFFF2 cell contamination in CLL cell RNA

Analysis of GEA data revealed that there was potential contamination from HFFF2 cell RNA in CLL samples. MDS clustering of all samples analysed (Figure 6-3) revealed that the HFFF2 cell RNA samples cluster together and samples containing only CLL cells in the culture cluster away from these. The CLL samples containing HFFF2 cell culture were revealed to cluster between these two groups, indicating the potential of the samples containing both CLL and HFFF2 cell RNA. When collecting CLL cells care was taken to ensure that only CLL cells were removed, gentle washing was used and following collection plates were checked to ensure all HFFF2 cells were left adhered to the bottom of the plate to ensure potential contamination was low. Visual inspection revealed many of the upregulated RNAs were not classically expressed in haematological cells indicating that a large number of the highly upregulated genes in the co-culture RNA may in fact be from HFFF2 cell RNA. This is consistent with the clustering observed in the quality control data. Contamination was further confirmed by comparing the top 50 differentially expressed genes between HFFF2 cell RNA and CLL cell RNA to the HFFF2/CLL cell co-culture. Results indicated that the vast majority of RNAs apparently upregulated in CLL cells following co-culture are actually among the most highly expressed in HFFF2 cells (Table 6.4). All of these results, from the MDS clustering and data set analysis indicated that caution must be applied when interpreting results from CLL/HFFF2 co-culture. All results were therefore used alongside and compared to CLL/HFFF2-derived CM results.

6.15.3 Transcriptional differences following survival-inducing culture with HFFF2 cells and HFFF2-derived CM

Following the results of the HFFF2 contamination analysis, it is necessary to talk about HFFF2 direct contact and HFFF2-derived CM as a whole and focus was shifted to analysis of the HFFF2-CM experiments. Table 6.2 indicated that analysis did not reveal any significantly upregulated RNAs following culture in HFFF2-CM. We reasoned that there were differences in the gene expression profiles, however these did not reach statistical significance most likely due to the interpatient variability. We applied a combined approach to the analysis by performing a cross-comparison between the

dataset for CLL cells co-cultured with HFFF2 and CLL cells cultured with CM. The combined analysis defined a list of candidate regulated genes.

Visual inspection of the data sets revealed that a large number of the upregulated RNAs following co-culture were chemokines and cytokines (Table 6.3 and Table 6.5). GSEA confirmed this finding, with the top hits coming from gene sets such as chemokine receptors, cytokine receptor interactions, chemokine signalling pathways, and cytokine signalling in the immune system (AppendixE). Revealing that a large number of chemokines and cytokines were upregulated in the survival-inducing condition.

6.15.4 Modulation of transcriptional responses to antigen by microenvironmental co-stimulation

A secondary aim of the GEP experiments was to determine whether HFFF2 co-culture influenced the transcriptional response to antigen. Other studies have looked at the effect of microenvironment and BCR cross talk (Introduction, Section1.4.3). For example stimulation of CD40L and BAFF was shown to increase miR-155 expression which was in turn shown to enhance BCR ligation (Cui et al., 2014). Table 6.2 demonstrated that there was 282 genes that were differentially expressed between CLL cells cultured alone and CLL cells stimulated with anti-IgM. This dataset allowed for confirmation of the methods used in these experiments by revealing many RNAs that had been previously demonstrated to be induced following anti-IgM stimulation (Burger et al., 2009b, Krysov et al., 2012, Pede et al., 2013, Guarini et al., 2008, Cui et al., 2014, Yeomans et al., 2016).

Due to the potential issue of HFFF2 RNA contamination, to determine the effect of micronvironmental stimulation of the transcriptional response to antigen we adapted a similar approach as with the CM experiments. Analysis revealed that many of the top 50 genes implicated in previous literature, such as MYC, CCL3, and miR-155 had a greater upregulation following co-culture with HFFF2 cells, indicating that HFFF2 co-culture may modulate the transcriptional response to antigen.

6.15.5 Surface IgM expression and CLL signal capacity following co-culture with HFFF2 cells

sIgM and sIgM Ca^{2+} signalling capacity was measured following co-culture with HFFF2 cells for 8, 24 and 48 hours and compared to levels on CLL cells cultured alone. Results first demonstrated the ability of sIgM to recover *in vitro* (Figure 6-10, Blue line). This was

explored further in Figure 6-11. Mockridge et al., had previously described how partially or completely anergized sIgM responses from each subset can recover both sIgM expression and signal capacity spontaneously *in vitro* or following capping/endocytosis (Mockridge et al., 2007). In this study there is a trend for receptor recovery at 48 hours however this is not significant.

Results indicated there was no change in sIgM levels following co-culture with HFFF2 cell (Figure 6-12 and Figure 6-13). There was however a trend for increased expression at the 48 hour time point and to some extent the 24 hour time point although neither were significant. However there is also the implication of CLL cell viability to be considered at this later time point so no real conclusions can be drawn from this. Looking at sIgM Ca^{2+} signalling, there was no difference between signal capacity following co-culture with HFFF2 cells. These results would indicate that there is no effect on CLL signalling ability following microenvironment co-stimulation at least in this *in vitro* model.

6.15.6 Enrichment of chemokines and cytokines following culture with HFFF2 cells or HFFF2-derived CM

The dataset and GSEA analysis revealed that a number of the enriched gene sets in both culture conditions involved the inflammatory response and chemokines/cytokines. Schulz et al., demonstrated a similar result in their study looking at gene expression following culture with HS-5 stromal cells (Schulz et al., 2011). They demonstrated that upregulated genes included many encoding for chemokines such as IL6, CCL2, CXCL1, CXCL5 all of which were also upregulated in this study (Table 6.3 and Table 6.5). Burger et al., also demonstrated the chemokines CCL3 and CCL4 were induced in CLL cells following NLC co-culture (Burger et al., 2009b). Again CCL3 was shown to be upregulated in this study however CCL4 was not. Further comparison of our results with data published by Edelmann et al., who cultured CLL cells with the murine fibroblast cell line M2-10B4 again revealed that the most significantly upregulated genes were CCL2 and IL-8 among many other chemokines and cytokines which overlap with the results seen in this study (Edelmann et al., 2008). The confirmation with all of these studies, which are all using different culture conditions indicate that there is a general importance of these genes in the survival of CLL cells.

A number of genes were then chosen for confirmatory studies. Selection of genes were based on (i) their fold change (ii) their potential functional relevance based on current literature and (iii) the availability of reagents (antibodies etc.). qRT-PCR confirmed that there was an increase in abundance of *IL6, IL8, CCL2* and *CXCL2* genes in the RNA sent

for GEA at Cambridge (Figure 6-14). This cohort was expanded (n=10) and firstly demonstrated the ability of CLL cells to produce all four chemokines/cytokines and secondly the ability of HFFF2-derived CM to increase abundance of mRNA. CLL cells cultured alone showed expression of *IL8, CCL2* and *CXCL2* in all ten patients tested, however expression of *IL6* was more variable with only six patients having detectable levels of mRNA (Figure 6-15).

It was next aimed to firstly confirm whether it was the CLL cells producing the chemokines/cytokines and secondly determine the role of accessory cells in the PBMC culture by purifying CLL cells prior to culture. The level of expression in the purified culture was more variable between the genes, for example *IL8* mRNA was detectable in the majority purified CLL cells while in comparison *CCL2* was only detected in one patient following purification. There was a variable ability of purified CLL cells to express *IL6* and *CXCL2* (six and four patients respectively). The ability of purified CLL cells to produce *IL8, IL6* and *CXCL2* indicates the ability of the CLL cells to produce the cytokine/chemokines, however there is a decrease in expression for all four indicating either a potential role for accessory cells within in the PBMC culture or other accessory cells are producing and contributing to the levels of the chemokine/cytokine. Correlation statistics confirmed that there was a trend between the number of accessory cells in the PBMC culture and the level of cytokine/chemokine produced (Figure 6-17). This could be because accessory cells are contributing to the levels produces or because they are needed to stimulate CLL cells to produce the chemokines. Because of this further experiments are needed to confirm the production of chemokines and cytokines is by the CLL cells.

CCL2 was chosen to carry forward for further investigation firstly due to the emerging evidence in the literature ((Burgess et al., 2012) and secondly to try and probe the interesting relationship between HFFF2 cells and other accessory cells. Intracellular staining of CCL2 via flow cytometry confirmed the ability of CLL to produce CCL2 and confirmed results seen via qRT-PCR confirming HFFF2-derived CM increased CCL2 at both a transcriptional and protein level. Although CM was able to induce CCL2 production in the purified cells, the FC was lower (FC of 4 compared to 7) indicating there may be a role for a third cell type.

Burgess et al*.,* demonstrated the ability of CLL cells to produce the chemokine CCL2 and CXCL2 but only in the presence of accessory cells. They concluded that the presence of accessory cells was vital for survival as culturing pure CLL cells resulted in poor survival, this has also been demonstrated to a certain extent in this study (Figure 6-20). They explored this further and showed that the addition of CCL2 or CXCL2 to purified cells did not rescues them from apoptosis (Burgess et al., 2012). Results here have indicated that IL-6 is potentially acting in a different manner to IL-8, CCL2 and CXCL2 due to the fact

that HFFF2-CM was still able to directly induce expression in purified CLL cells whereas it appears from these data that induction of CCL2, CXCL2 and IL-8 is dependent on an intermediate cell type present in the PBMC culture. This opens the possibility that these chemokine and cytokines are involved in a complex pro-survival model involving paracrine and autocrine signals and involving accessory cells and potentially HFFF2 stromal cells all acting in a feedback loop to promote CLL survival (Figure 6-21).

6.15.7 Viability of purified CLL cells

It was next aimed to try and further the understanding of these four chemokines/cytokines along with accessory cells in the PBMC culture by determining the role of cells in the PBMC culture on firstly CLL cell survival and secondly HFFF2-mediated protection. This was done by comparing firstly the viability of purified cells versus PBMC and secondly the levels of HFFF2-mediated protection in both cultures. Purified CLL cells or CLL PBMCs were cultured alone, in the presence of HFFF2 cells or HFFF2-derived CM and viability was assessed at 0, 24 and 48 hours (Figure 6-20). Results indicated that there was an increase in spontaneous apoptosis when purified CLL cells were cultured in comparison to CLL PBMC cultures. Although this was not significant it indicates that “accessory cells” in the PBMC culture may play a role in promoting CLL cell viability. These data may not be significant due to the fact that there are already very low levels of ‘non-malignant’ cells in the PBMC so differences may be limited. When cultured with HFFF2 cells or HFFF2-CM however, similar survival promoting effects were observed for both purified CLL cells and CLL PBMCs (Figure 6-20c), suggesting survival effects mediated by HFFF2 cells are not dependent on an intermediate accessory cell. These results indicate that although the expression of CCL2, CXCL2 and IL-8 is dependent on an intermediate cell type that is present in the PBMC culture these chemokines/cytokines are unlikely to be promoting CLL survival in the HFFF2-model. These data coupled with the qPCR results indicate that IL-6 might be the candidate molecule involved in HFFF2-mediated protection.

IL-6 is a cytokine that functions in inflammation and the maturation of B cells. It has been implicated in a host of chronic diseases that are associated with chronic inflammation. Chronic IL-6 signalling has also been linked to tumourigenesis and several studies have suggested a possible role for dysregulated production of IL-6 in malignant lymphomas (Yee et al., 1989, Chang et al., 1992, Takeshita et al., 1993, Hsu et al., 1992, Freeman et al., 1989, Müller et al., 1991). There are elevated serum levels of IL-6 in CLL patients and levels have been shown to correlate with phenotypic characteristics and outcome (Fayad et al., 2001). IL-6 has been shown to reduce spontaneous apoptosis in CLL (Reittie et al.,

1996) and activated STAT3 and NF-κB maintain the levels of the anti-apoptotic proteins MCL1 and BCL-$_{XL}$ and autocrine production of IL-6 (Hirt et al., 2014). There have been studies indicating a potential role of a stroma-mediated activation of the PI3K/NF-κB pathway in CLL cells (Cuni et al., 2004) and interestingly both of these pathways were enriched following culture with HFFF2 cells or HFFF2-derived CM (AppendixE). GSEA analysis by Edelmann et al., also demonstrated that direct contact culture with a stromal cell line (M2-10B4) resulted in the upregulation of PI3K/NF-κB/Akt pathway genes (Edelmann et al., 2008). Activation of PI3K signalling in CLL cells following culture with the fibroblast cell line led to the translocation and subsequent phosphorylation of Akt (Cuni et al., 2004). Previous research in our laboratory demonstrated that pAKT^{473} expression is higher following culture with HFFF2-CM. This data indicated that HFFF2 fibroblasts release soluble factors that induce AKT/PI3K signal transduction pathways (Samantha Dias, PhD thesis). Transcription factors of the NF-κB family are key regulators of differentiation and survival in B cells and NF-κB target genes include: *IL1B*, *IL6* and *IL8* all of which were detected in this GSEA study. Target genes of NF-κB such as IL-8 and IL-6 have been shown to have a number of different effects on CLL survival (Table 7 and Table 8). Levels of NF-κB activity in CLL cells are variable but higher compared to normal B cells and, NF-κB activity in CLL cells has been shown to affect survival (Furman et al., 2000, Cuni et al., 2004, Hewamana et al., 2008, Lopez-Guerra and Colomer, 2010).

6.15.8 Final comments

Data have revealed that HFFF2 co-culture and culture with HFFF2-derived CM caused a widespread transcriptional reprogramming in CLL cells and chemokines/cytokines were commonly upregulated following co-culture with HFFF2 cells or HFFF2-derived CM. Further analysis using qPCR and intracellular staining using flow cytometry revealed a potential pro-survival loop involving HFFF2 cells, chemokines and other 'intermediate' cells (Figure 6-21). Data revealed that although not necessary for survival, these 'intermediate' cells are needed for the production of the chemokines/cytokines IL-8, CCL2 and CXCL2 following co-culture with HFFF2 cells or HFFF2-derived CM. Conversely, IL-6 was produced by CLL cells independently of cells present in the PBMC culture and IL-6 production is increased following co-culture with HFFF2 cells. These results indicate that IL-6 may potentially promote survival through PI3K/NF-κB signalling pathways, whereas CCL2, CXCL2, IL-8 may work to enhance migration of other accessory cells into the microenvironment which in turn may also promote CLL cell survival.

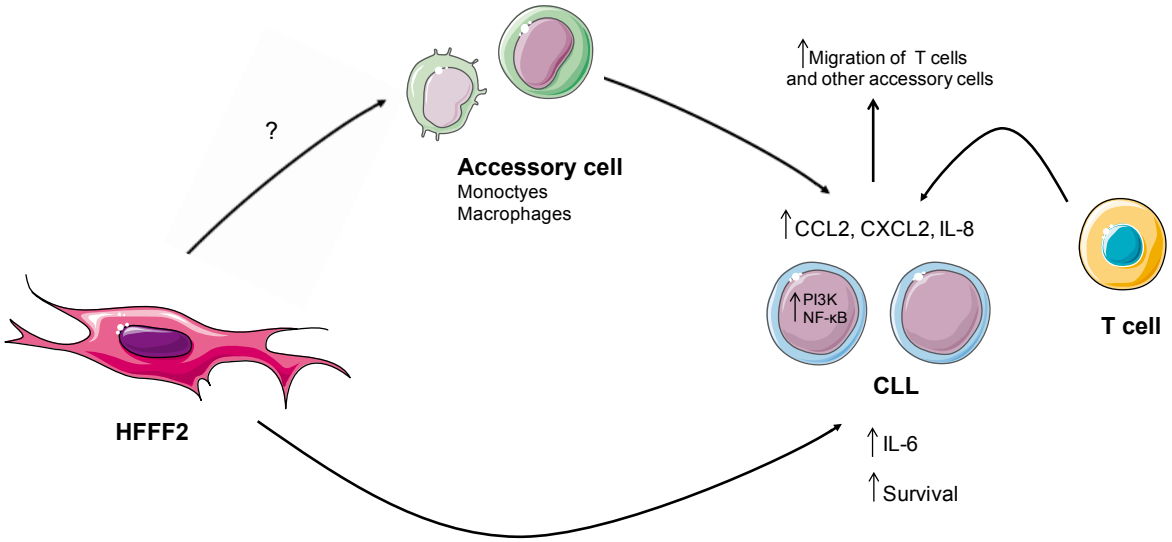

FIGURE 6-21: PROPOSED MODEL FOR A PRO-SURVIVAL MECHANISM INVOLVING HFFF2 CELLS, ACCESSORY CELLS AND CHEMOKINES/CYTOKINES

Following co-culture with HFFF2 or HFFF2 CM results in the upregulation of the chemokine CCL2 and CXCL2 and the cytokines IL-6 and IL-8. Upregulation of IL-6 by co-culture is independent of accessory cells such as monocytes, macrophages and T cell, whereas conversely the upregulation of CCL2, CXCL2 and IL-8 is dependent on the presence of a third intermediate cell type present in CLL PBMC cultures. In this proposed model, we hypothesise that IL-6 functions to promote CLL cell survival potentially through the upregulation of the PI3K/NF-κB signalling pathways conversely IL-6 may induce PI3K/NF-κB signalling pathways in an autocrine manner resulting in an increase in cell survival, while CCL2, CXCL2 and IL-8 function to attract other survival promoting accessory cells to the microenvironment.

Chapter Seven

Final discussion

Chapter 7: Final discussion

7.1 Overview of findings

At the beginning of this thesis my primary hypothesis was that acoustic trapping devices could be used as a novel method to model CLL microenvironment interactions in 3D. The secondary hypothesis was that the HFFF2 cell line is a suitable model for investigating CLL/fibroblast interactions in acoustic trapping devices. In order to investigate these hypotheses I had several aims. Listed below are the key findings related to each aim.

Aim: Investigate the HFFF2 cell line as a model system for studying CLL microenvironment interactions

Key findings:

- The HFFF2 cell line protects CLL cells from spontaneous apoptosis in a contact-independent manner
- Heterogeneity of the protective effects of HFFF2 cells is not related to major disease subsets such as *IGHV* mutation status, surface IgM expression or sIgM signalling capability

Aim: Optimise acoustic trapping devices for use in modelling of CLL/stromal cell interactions in three dimensions

Key findings:

- Both CLL and HFFF2 cells are able to levitate in acoustic trapping devices and co-levitate' forming an agglomerate containing a mixture of both cell types
- CLL cells characteristically form multiple smaller agglomerates while HFFF2 cells and agglomerates containing a mixture of both CLL and HFFF2 form single large agglomerates which contract to form 3D-structures over longer levitation times
- Viability of both CLL cells and HFFF2 cells is dramatically reduced after 8 hours levitation in acoustic trapping devices

Aim: Investigate the role of the chemokine receptor CXCR4 and its ligand CXCL12 in the protection provided by HFFF2 cell line to CLL cells

Key findings:

- The HFFF2 cell line secretes the chemokine CXCL12 and co-culture with HFFF2 cells *in vitro* prevents recovery of the chemokine receptor CXCR4
- Neutralising antibodies to CXCR4 and CXCL12 decrease CXCL12-mediated migration but do not reduce protection against spontaneous apoptosis mediated by HFFF2 cells or HFFF2-derived CM

Aim: Analyse candidate molecules involved in HFFF2-mediated cytoprotection to CLL cells

Key findings:

- HFFF2 co-culture and culture with HFFF2-derived CM caused a widespread transcriptional reprogramming in CLL cells.
- Chemokine and cytokine RNAs were commonly upregulated in CLL cells following co-culture with HFFF2 cells
- HFFF2 co-culture increased expression of many of the top upregulated genes following αIgM stimulation indicating that the BCR response may be modulated by microenvironment co-stimulation although co-culture had no effect on sIgM expression and signalling response
- HFFF2-derived CM increases expression of the chemokines and cytokines IL-6, IL-8, CXCL2 and CCL2
- An intermediate cell type appears to be required for HFFF2-CM induced expression of CXCL2 and IL-8 RNAs, but not HFFF2-CM-induced CLL cell survival
- IL-6 expression and CCL2 expression to a certain extent does not appear to require an intermediate cell type

Data revealed a significant loss of viability of both CLL and HFFF2 cells when levitated in acoustic trapping devices meaning that that, at present, acoustic trapping devices are not optimised enough to allow for modelling of the CLL microenvironment which unfortunately does not support my original hypothesis. Data secondly showed that the HFFF2 cell line and HFFF2-derived CM significantly protect CLL cells from spontaneous apoptosis and this protection is at least partially due to a soluble factor. In particular, a number of

chemokines and cytokines were shown to be upregulated in these survival-promoting conditions. Overall these data are consistent with the secondary hypothesis that the HFFF2 cell line is a suitable model for investigating CLL/fibroblast interactions *in vitro*.

7.2 Use of acoustic trapping devices to model the CLL microenvironment

Modelling the CLL microenvironment has been an area under intense investigation since the discovery that novel BCR kinase inhibitors such as ibrutinib and idelalisib cause a lymphocytosis of malignant cells into the peripheral blood indicating a complex crosstalk between microenvironment pathways *in vivo*. When trying to recapitulate the CLL microenvironment *in vitro* studies have primarily used co-culture with a number of different cell types including stromal cells, NLCs and T cells. Studies have also progressed to look at a combination of the cell types above as well as soluble factors to try and create a more physiologically relevant model (Plander et al., 2009, Purroy et al., 2014, Hamilton et al., 2012, Asslaber et al., 2013). However no study to date has looked at modelling the CLL microenvironment in 3D.

The main aim of this project was the optimisation of acoustic trapping devices to levitate both CLL and HFFF2 cells simultaneously to create a 3D model of the CLL microenvironment. The majority of work using similar acoustic trapping devices to those used for the duration of this project have primarily looked at the levitation of single cells (Wu, 1991) or 2D cell aggregates (Bazou et al., 2005b). This work has used a variety of different cell lines including COS-7 monkey fibroblasts (Hultström et al., 2007), Neural cells (Bazou et al., 2005a), Chrondocytes (Bazou et al., 2006b), prostate epithelial cell line (PZ-HPV-7 cells) and prostate cancer cell line (DU-145) (Bazou et al., 2006a), HepG2 cells a liver hepatocellular carcinoma (Edwards et al., 2007), 16HBE a respiratory epithelial cell line (Angela Tait, PhD thesis) and human articular chondrocytes (Li et al., 2014). It was first important to determine whether two different cell types could be simultaneously levitated in the same agglomerate. Chapter 4 addressed this, and it was demonstrated that firstly both CLL cells and the HFFF2 cell line could individually levitate in the device. Chapter 4 then demonstrated the ability of both cell types to simultaneously levitate in the same agglomerate. To the best of our knowledge, this was the first time primary leukaemia cells and a fibroblast cell line have been levitated within an ultrasonic trap and the first time two different cell types have been levitated simultaneously in the same device. This was a particularly surprising and pleasing result considering the differing sizes of the two cell types (and thus influence of acoustic forces).

Chapter 4 further demonstrated the ability of the agglomerates containing both cell types to contract over longer levitation periods to form 3D structures. The ability of the devices to form 3D structures reveals opportunities to model different accessory cells together with CLL cells and other soluble factors to create a more physically relevant model of the tissue microenvironment in CLL.

The second main aim of this part of the project was to determine whether levitation in the acoustic trapping devices had any effect on viability or cell characteristics. A number of studies have investigated effects of ultrasound waves on cell viability and have not observed deleterious effects (Bazou et al., 2005b, Hultstrom et al., 2007, Evander et al., 2007). In addition, Bazou et al., examined the physical environment experienced by levitated neural cells in an acoustic trap by monitoring the temperature, acoustic streaming, pressure amplitudes, white noise and the inter-particular forces acting on the cells (Bazou et al., 2005b). Adverse effects or changes on *in vitro* surface receptor interactions were not detected in these studies. Chapter 4 revealed that levitation in the devices for as little as 2 hours had a major detrimental effect on both CLL and HFFF2 cell viability. Further investigation revealed that the lack of contact to a solid surface, transducer heating or lack of proper incubation during experiments was not causing this dramatic reduction in cell viability. Ankrett et al., used similar devices to investigate the effect a number of physical stimuli on the viability of H9c2 cardiac myoblasts. The transducers used throughout this study are set with a sweeping frequency around the resonate frequency (1.7 to 1.85 MHz kHz). Sweeping needs to occur and at a rate of 0.05 seconds to allow for variation between the transducers of the different devices and to allow for variation over time for the transducer. Ankrett et al., demonstrated that the lowest viability of cells was witnessed at the greatest sweep frequency of 0.05 seconds (~41% reduction in viability) (Ankrett et al., 2013). These results indicate that the sweep frequency could be contributing to the decrease in cell viability, however sweeping needs to occur and at a rate of 0.05 seconds to allow for variation between the transducers of the different devices and to allow for variation over time for the transducer. By using sweep frequencies it allows us to maintain levitation of the cells over the time period required. This is one part of the devices that could be optimised to allow for future use.

The work carried out to optimise the acoustic trapping devices carried out in Chapter 4 revealed that at present the devices are not optimised enough for use in modelling the CLL microenvironment. However, data did demonstrate the ability of devices to levitate two different cell types in the same agglomerate, and the ability of the agglomerate to contract other time. This reveals the potential of the devices to be used in the manner we originally hypothesised; this would be greatly advantageous in not only the investigation of CLL microenvironment interactions but also in terms of other types of malignancies with

the potential for a number of different cell types to be modelled in a 3D manner. This would hopefully provide a physically relevant model with the potential for investigating the interactions between a number of different cells in the tumour microenvironment.

7.3 Suggestions for future work to investigate the use of acoustic trapping devices to model the CLL microenvironment

As there was very little knowledge of the use of acoustic trapping devices for 3D tissue culture and no information concerning the behaviour of CLL or HFFF2 cell fibroblasts during acoustic trapping prior to the beginning of this project, much of this aspect of the project was exploratory. While the project demonstrated the feasibility of the approach for forming 3D structures containing both CLL and HFFF2 cells, there is still work to be done to firstly address the viability problems and secondly to create a robust system that has day-to-day utility.

Prior to commencement of this project development of acoustic trapping devices had progressed well to a '6 well device', which allowed for easy visualisation of the cell agglomerates due to the mirrored reflector under the transducer and easy access to the agglomerates as well as the possibility or multiple devices to be run for larger experiments. However, one of the main problems encountered was that devices required constant maintenance with small wires becoming detached on a regular basis leading to repeated soldering of these wires back onto the connectors. The devices need to be developed further to avoid this constant maintenance and to allow for a robust system that can be used on a regular basis and by a user with a 'non-engineering' background. The devices also need improved sterile handling due to the fact that cells need to be added when the devices were *in situ* as the devices cannot be moved without disruption of the agglomerates. The devices and method should allow for devices to be set up and used within a sterile environment and also allow for the transfer of devices into incubators.

The main problem encountered during this part of the project was the dramatic loss of viability seen after cells were levitated in the acoustic trapping devices. Further optimisation of acoustic parameters of the devices could be changed to try and minimise the decrease in viability observed. One of the main parameters which could be further optimised is the sweep frequency. By increasing the sweep time we could hopefully reduce the forces acting on the cells which could potentially increase cell viability.

One possibility to try and over come the viability issues, is the potential to try and levitate a scaffold along with the cells. This would help overcome any reductions in viability

caused by a lack of contact. However, data from Chapter 4, indicate that the lack of contact is not an issue and likely to be the cause of the cell death. The inclusion of a scaffold would also add in the complication of interactions with artificial substrates in the scaffold, and one of the main advantages of acoustic trapping is the lack of these interactions.

7.4 The role of chemokine and cytokines in HFFF2-mediated cytoprotection using the HFFF2 cell line model

Work in our lab has previously shown that the HFFF2 cell line is able to protect CLL cells from spontaneous apoptosis however, it was important to further characterise the HFFF2 cell co-culture model to determine whether certain prognostic markers could be used to predict the levels of cytoprotection from HFFF2 to help when optimising the acoustic trapping devices. Chapter 3 addressed this question and demonstrated that the HFFF2 cell line protected CLL cells in a contact independent manner. There was great heterogeneity in the levels of cytoprotection between patients. However the level of protection could not be correlated to *IGHV* mutational status or signalling capacity of the CLL sample. It would however be interesting to correlate the level of protection against other prognostic markers such as CD49d as this is a more clinically relevant marker.

It was important to try and understand the mechanism of survival in the HFFF2 co-culture model as this could help determine future therapeutic targets. Given previous studies implicating CXCL12 in stromal cell-mediated survival of CLL cells (Burger et al., 2000), the main aim of the experiments described in Chapter 5 was to investigate the significance of this chemokine for HFFF2 cell-mediated protection. Chapter 5 demonstrated that the although CXCR4 was strongly downmodulated following co-culture with HFFF2 cells, the chemokine receptor CXCR4 and its respective ligand CXCL12 were not playing a role in the protection mediated by the HFFF2 cell line. The difference between what other studies have found demonstrating that the chemokine CXCL12 promotes CLL cell survival and the data presented here most likely outlines the difference between the models used when characterising CLL/microenvironment interactions *in vitro*. However, the advantage when using the HFFF2 cell line is that it is an relatively well defined model and other stromal cell lines used for investigating CLL/microemvironment issues are often poorly defined in terms of cell phenotype.

Following the data regarding CXCR4, I secondly looked more broadly at the gene expression profile following co-culture with HFFF2 cells. Chapter 6 demonstrated that following co-culture with HFFF2 cells or HFFF2-CM the gene expression profile revealed an enrichment of chemokines and cytokines confirming similar findings in the literature

(Burger et al., 2009b, Edelmann et al., 2008, Schulz et al., 2011). Further work concentrated on four specific chemokines/cytokines namely CCL2, CXCL2, IL-8 and IL-6 as these chemokines/cytokines were among the most highly upregulated following co-culture and had previously been investigated in the literature (Burgess et al., 2012, Schulz et al., 2011). qPCR and FACS analysis revealed a potentially different mechanism of action for the four chemokines demonstrating the possibility that these chemokine and cytokines are involved in a complex pro-survival model involving paracrine and autocrine signals and involving accessory cells and HFFF2 stromal cells all acting in a feedback loop to promote CLL survival. qPCR analysis revealed that there was little difference between IL-6 expression in CLL cells following culture in HFFF2-derived CM in either purified cells or PMBC cultures indicating that unlike IL-8, CCL2 or CXCL2 the production of IL-6 did not rely on an third intermediate cell type. This proposed pro-survival model is demonstrated in Figure 6-21. The qPCR data and viability data using purified CLL cells indicated that IL-8, CXCL2 and CCL2 were not linked to survival. These molecules are probably more likely to be involved with migration of other accessory cells into the microenvironment. Interestingly, data indicate that IL-6 could potentially be responsible for HFFF2-mediated protection as the production of this cytokine by CLL cells did not rely on a third cell type in the PBMC culture.

IL-6 has been shown to reduce spontaneous apoptosis in CLL (Reittie et al., 1996) and activated STAT3 and NF-κB maintain the levels of the anti-apoptotic proteins MCL1 and BCL-$_{XL}$ and autocrine production of IL-6 (Liu et al., 2016). There have been studies indicating a potential role of a stroma-mediated activation of the PI3K/NF-κB pathway in CLL cells (Cuni et al., 2004) and interesting both of these pathways were enriched following culture with HFFF2 cells or HFFF2-derived CM. Previous research in our laboratory demonstrated that pAKT^{473} expression is higher following culture with HFFF2-CM. This data indicated that HFFF2 fibroblasts release soluble factors that induce AKT/PI3K signal transduction pathways (Samantha Dias, PhD thesis). The PI3K inhibitor Cal-101 was then used to inhibit the signalling pathway and was shown to block HFFF2-mediated cytoprotection. These data indicate that blocking the PI3K pathway within CLL cells significantly blocks fibroblast-mediated protection of CLL cells (Samantha Dias, PhD thesis). These data, coupled with the GEP and qPCR results demonstrated in this project indicate that activation of the PI3K/NF-κB pathways and production of IL-6 by CLL cells could potential contribute to HFFF2-mediated cytoprotection.

7.5 Suggestions for future work to investigate the role of chemokine and cytokines in HFFF2-mediated cytoprotection using the HFFF2 cell line model

More samples are required to analyse the effect of PBMC culture versus purified CLL on CM-mediated increases in the expression of the chemokines/cytokines IL-6, IL-8, CCL2 and CXCL2. Greater sample numbers will provide a better insight into the correlation between the increase in expression and the number of non-malignant cells in the CLL sample as the numbers used during this experiment are quite small and it is therefore difficult to see any correlations although there were trends.

It would be important to determine which, if any, accessory cells are involved in the proposed survival loop (Figure 6-21). The identification of which intermediate cell type is involved in the survival of CLL cells will help us further our understanding of CLL/microenvironmental interactions. A better understanding of these complex interactions could lead to new, more effective treatment strategies for CLL by disrupting the microenvironmental support mechanism. One way of determining whether other accessory cells are involved in the support mechanism is by depleting them individually from the PBMC culture using the MACS isolation kits. Burgess et al., did a similar experiment and T cells and macrophages were depleted from CLL PBMCs using CD3 and CD14 microbeads, respectively (Burgess et al., 2012). This work could be replicated and we could look at the induced expression of the given chemokine/cytokines following culture with HFFF2-CM after depleting the different cell populations.

Finally, the question of whether these cytokines particularly IL-6 are playing a role in CLL cell survival mediated by HFFF2 co-culture or HFFF2-CM still requires further investigation. The data presented from the GEA indicated that these chemokines/cytokines were upregulated in the survival inducing-conditions, and current literature has linked these to CLL cell survival. However, whether these chemokines/cytokines are promoting CLL cells survival in the HFFF2 model and whether they are they only factors still requires further investigation. This could firstly be carried out adding exogenous forms of each of the cytokines/chemokines to CLL cells and determining their effect on CLL cell survival. Further work could involve the addition of neutralising antibodies to the HFFF2 co-culture or HFFF2-CM and then also determine their effect on CLL cell survival. The effect of neutralizing antibodies on survival could also be extended to looking at the effect of blocking these chemokines/cytokines on the PI3K/NF-κB pathways in CLL cells to try and confirm the link between HFFF2-protection and previous data seen in our laboratory (Samantha Dias, PhD thesis). This could help to

further our understanding of the role of the described signalling pathways in the HFFF2-mediated cytoprotection and ultimately microenvironmental interactions *in vivo*.

Chapter 8

References

Chapter 8: List of References

ABE, R., DONNELLY, S. C., PENG, T., BUCALA, R. & METZ, C. N. 2001. Peripheral Blood Fibrocytes: Differentiation Pathway and Migration to Wound Sites. *The Journal of Immunology,* 166**,** 7556-7562.

ADERKA, D., MAOR, Y., NOVICK, D., ENGELMANN, H., KAHN, Y., LEVO, Y., WALLACH, D. & REVEL, M. 1993. Interleukin-6 inhibits the proliferation of B-chronic lymphocytic leukemia cells that is induced by tumor necrosis factor-alpha or -beta. *Blood,* 81**,** 2076-84.

ADVANI, R. H., BUGGY, J. J., SHARMAN, J. P., SMITH, S. M., BOYD, T. E., GRANT, B., KOLIBABA, K. S., FURMAN, R. R., RODRIGUEZ, S., CHANG, B. Y., SUKBUNTHERNG, J., IZUMI, R., HAMDY, A., HEDRICK, E. & FOWLER, N. H. 2013. Bruton tyrosine kinase inhibitor ibrutinib (PCI-32765) has significant activity in patients with relapsed/refractory B-cell malignancies. *J Clin Oncol,* 31**,** 88-94.

AGUILAR-HERNANDEZ, M. M., BLUNT, M. D., DOBSON, R., YEOMANS, A., THIRDBOROUGH, S., LARRAYOZ, M., SMITH, L. D., LINLEY, A., STREFFORD, J. C., DAVIES, A., JOHNSON, P. M., SAVELYEVA, N., CRAGG, M., FORCONI, F., PACKHAM, G., STEVENSON, F. K. & STEELE, A. J. 2016. IL-4 enhances expression and function of surface IgM in CLL cells. *Blood*.

AGUILAR-SANTELISES, M., LOFTENIUS, A., LJUNGH, C., SVENSON, S. B., ANDERSSON, B., MELLSTEDT, H. & JONDAL, M. 1992. Serum levels of helper factors (IL-1 alpha, IL-1 beta and IL-6), T-cell products (sCD4 and sCD8), sIL-2R and beta 2-microglobulin in patients with B-CLL and benign B lymphocytosis. *Leuk Res,* 16**,** 607-13.

ALLEN, C. D., ANSEL, K. M., LOW, C., LESLEY, R., TAMAMURA, H., FUJII, N. & CYSTER, J. G. 2004. Germinal center dark and light zone organization is mediated by CXCR4 and CXCR5. *Nat Immunol,* 5**,** 943-52.

ALLEN, C. D. C. & CYSTER, J. G. 2008. Follicular dendritic cell networks of primary follicles and germinal centers: phenotype and function. *Seminars in immunology,* 20**,** 14-25.

AMARA, A., LORTHIOIR, O., VALENZUELA, A., MAGERUS, A., THELEN, M., MONTES, M., VIRELIZIER, J. L., DELEPIERRE, M., BALEUX, F., LORTAT-JACOB, H. & ARENZANA-SEISDEDOS, F. 1999. Stromal cell-derived factor-1alpha associates with heparan sulfates through the first beta-strand of the chemokine. *J Biol Chem,* 274**,** 23916-25.

ANDRITSOS, L., BYRD, J. C., JONES, J. A., HEWES, B., KIPPS, T. J., HSU, F. J. & BURGER, J. A. 2010. Preliminary results from a phase I dose escalation study to determine the maximum tolerated dose of plerixafor in combination with rituximab in patients with relapsed chronic lymphocytic leukemia. *Haematologica,* 95**,** 321.

ANKRETT, D. N., CARUGO, D., LEI, J., GLYNNE-JONES, P., TOWNSEND, P. A., ZHANG, X. & HILL, M. 2013. The effect of ultrasound-related stimuli on cell viability in microfluidic channels. *Journal of Nanobiotechnology,* 11**,** 1-5.

ARROYO, A. G., YANG, J. T., RAYBURN, H. & HYNES, R. O. 1999. Alpha4 integrins regulate the proliferation/differentiation balance of multilineage hematopoietic progenitors in vivo. *Immunity,* 11**,** 555-66.

ASSLABER, D., GROSSINGER, E. M., GIRBL, T., HOFBAUER, S. W., EGLE, A., WEISS, L., GREIL, R. & HARTMANN, T. N. 2013. Mimicking the microenvironment in chronic lymphocytic leukaemia - where does the journey go? *Br J Haematol,* 160**,** 711-4.

BAGNARA, D., KAUFMAN, M. S., CALISSANO, C., MARSILIO, S., PATTEN, P. E. M., SIMONE, R., CHUM, P., YAN, X.-J., ALLEN, S. L., KOLITZ, J. E., BASKAR, S., RADER, C., MELLSTEDT, H., RABBANI, H., LEE, A., GREGERSEN, P. K., RAI, K. R. & CHIORAZZI, N. 2011. A novel adoptive transfer model of chronic lymphocytic leukemia suggests a key role for T lymphocytes in the disease. *Blood,* 117**,** 5463-5472.

BAKER, N. V. 1972. Segregation and Sedimentation of Red Blood Cells in Ultrasonic Standing Waves. *Nature,* 239**,** 398-399.

BARBERO, S., BONAVIA, R., BAJETTO, A., PORCILE, C., PIRANI, P., RAVETTI, J. L., ZONA, G. L., SPAZIANTE, R., FLORIO, T. & SCHETTINI, G. 2003. Stromal cell-derived factor 1alpha stimulates human glioblastoma cell growth through the activation of both extracellular signal-regulated kinases 1/2 and Akt. *Cancer Res,* 63**,** 1969-74.

BAZOU, D., DAVIES, G., JIANG, W. G. & COAKLEY, T. 2006a. Rapid molecular and morphological responses of prostate cell lines to cell-cell contact. *Cell Commun Adhes,* 13**,** 279-94.

BAZOU, D., DOWTHWAITE, G. P., KHAN, I. M., ARCHER, C. W., RALPHS, J. R. & COAKLEY, W. T. 2006b. Gap junctional intercellular communication and cytoskeletal organization in chondrocytes in suspension in an ultrasound trap. *Mol Membr Biol,* 23**,** 195-205.

BAZOU, D., FOSTER, G. A., RALPHS, J. R. & COAKLEY, W. T. 2005a. Molecular adhesion development in a neural cell monolayer forming in an ultrasound trap. *Mol Membr Biol,* 22**,** 229-40.

BAZOU, D., KUZNETSOVA, L. A. & COAKLEY, W. T. 2005b. Physical enviroment of 2-D animal cell aggregates formed in a short pathlength ultrasound standing wave trap. *Ultrasound Med Biol,* 31**,** 423-30.

BECKER, J. L. & SOUZA, G. R. 2013. Using space-based investigations to inform cancer research on Earth. *Nat Rev Cancer,* 13**,** 315-27.

BEGLEY, L., MONTELEON, C., SHAH, R. B., MACDONALD, J. W. & MACOSKA, J. A. 2005. CXCL12 overexpression and secretion by aging fibroblasts enhance human prostate epithelial proliferation in vitro. *Aging Cell,* 4**,** 291-8.

BERGFELD, S. A. & DECLERCK, Y. A. 2010. Bone marrow-derived mesenchymal stem cells and the tumor microenvironment. *Cancer Metastasis Rev,* 29**,** 249-61.

BERNAL, A., PASTORE, R. D., ASGARY, Z., KELLER, S. A., CESARMAN, E., LIOU, H. C. & SCHATTNER, E. J. 2001. Survival of leukemic B cells promoted by engagement of the antigen receptor. *Blood,* 98**,** 3050-7.

BERNDT, C., MOPPS, B., ANGERMULLER, S., GIERSCHIK, P. & KRAMMER, P. H. 1998. CXCR4 and CD4 mediate a rapid CD95-independent cell death in CD4(+) T cells. *Proc Natl Acad Sci U S A,* 95**,** 12556-61.

BHADRIRAJU, K. & CHEN, C. S. 2002. Engineering cellular microenvironments to improve cell-based drug testing. *Drug Discov Today,* 7**,** 612-20.

BHOME, R., GOH, R., PRIMROSE, J., SAYAN, A. & MIRNEZAMI, A. 2015. PTH-321 Exosomes and microparticles: distinct extracellular compartments which convey genetic information in the colorectal tumour microenvironment. *Gut,* 64**,** A550-A551.

BICHI, R., SHINTON, S. A., MARTIN, E. S., KOVAL, A., CALIN, G. A., CESARI, R., RUSSO, G., HARDY, R. R. & CROCE, C. M. 2002. Human chronic lymphocytic leukemia modeled in mouse by targeted TCL1 expression. *Proc Natl Acad Sci U S A,* 99**,** 6955-60.

BINET, J. L., AUQUIER, A., DIGHIERO, G., CHASTANG, C., PIGUET, H., GOASGUEN, J., VAUGIER, G., POTRON, G., COLONA, P., OBERLING, F., THOMAS, M., TCHERNIA, G., JACQUILLAT, C., BOIVIN, P., LESTY, C., DUAULT, M. T., MONCONDUIT, M., BELABBES, S. & GREMY, F. 1981. A new prognostic classification of chronic lymphocytic leukemia derived from a multivariate survival analysis. *Cancer,* 48**,** 198-206.

BING, R. J., DUDEK, R., KÄHLER, J., NARAYAN, K. S. & INGRAM, M. 1992. Cytokine production from freshly harvested human mononuclear cells attached to plastic beads. *Tissue and Cell,* 24**,** 203-209.

BINSKY, I., HARAN, M., STARLETS, D., GORE, Y., LANTNER, F., HARPAZ, N., LENG, L., GOLDENBERG, D. M., SHVIDEL, L., BERREBI, A., BUCALA, R. & SHACHAR, I. 2007. IL-8 secreted in a macrophage migration-inhibitory factor- and CD74-dependent manner regulates B cell chronic lymphocytic leukemia survival. *Proc Natl Acad Sci U S A,* 104**,** 13408-13.

BIRNBAUM, T., ROIDER, J., SCHANKIN, C. J., PADOVAN, C. S., SCHICHOR, C., GOLDBRUNNER, R. & STRAUBE, A. 2007. Malignant gliomas actively recruit bone marrow stromal cells by secreting angiogenic cytokines. *J Neurooncol,* 83**,** 241-7.

BLUNT, M. D., CARTER, M. J., LARRAYOZ, M., SMITH, L. D., AGUILAR-HERNANDEZ, M., COX, K. L., TIPTON, T., REYNOLDS, M., MURPHY, S., LEMM, E., DIAS, S., DUNCOMBE, A., STREFFORD, J. C., JOHNSON, P. W., FORCONI, F., STEVENSON, F. K., PACKHAM, G., CRAGG, M. S. & STEELE, A. J. 2015. The PI3K/mTOR inhibitor PF-04691502 induces apoptosis and inhibits microenvironmental signaling in CLL and the Emicro-TCL1 mouse model. *Blood,* 125**,** 4032-41.

BOISSARD, F., FOURNIE, J. J., LAURENT, C., POUPOT, M. & YSEBAERT, L. 2015. Nurse like cells: chronic lymphocytic leukemia associated macrophages. *Leuk Lymphoma,* 56**,** 1570-2.

BRACHTL, G., PINON HOFBAUER, J., GREIL, R. & HARTMANN, T. N. 2014. The pathogenic relevance of the prognostic markers CD38 and CD49d in chronic lymphocytic leukemia. *Ann Hematol,* 93**,** 361-74.

BRAND, S., DAMBACHER, J., BEIGEL, F., OLSZAK, T., DIEBOLD, J., OTTE, J. M., GOKE, B. & EICHHORST, S. T. 2005. CXCR4 and CXCL12 are inversely expressed in colorectal cancer cells and modulate cancer cell migration, invasion and MMP-9 activation. *Exp Cell Res,* 310**,** 117-30.

BRASELMANN, S., TAYLOR, V., ZHAO, H., WANG, S., SYLVAIN, C., BALUOM, M., QU, K., HERLAAR, E., LAU, A., YOUNG, C., WONG, B. R., LOVELL, S., SUN, T., PARK, G., ARGADE, A., JURCEVIC, S., PINE, P., SINGH, R., GROSSBARD, E. B., PAYAN, D. G. & MASUDA, E. S. 2006. R406, an orally available spleen tyrosine kinase inhibitor blocks fc receptor signaling and reduces immune complex-mediated inflammation. *J Pharmacol Exp Ther,* 319**,** 998-1008.

BRESLIN, S. & O'DRISCOLL, L. 2013. Three-dimensional cell culture: the missing link in drug discovery. *Drug Discov Today,* 18**,** 240-9.

BROUTY-BOYÉ, D. 2005. Developmental Biology of Fibroblasts and Neoplastic Disease. *In:* MACIEIRA-COELHO, A. (ed.) *Developmental Biology of Neoplastic Growth.* Springer Berlin Heidelberg.

BROWN, J. R., BYRD, J. C., COUTRE, S. E., BENSON, D. M., FLINN, I. W., WAGNER-JOHNSTON, N. D., SPURGEON, S. E., KAHL, B. S., BELLO, C., WEBB, H. K., JOHNSON, D. M., PETERMAN, S., LI, D., JAHN, T. M., LANNUTTI, B. J., ULRICH, R. G., YU, A. S., MILLER, L. L. & FURMAN, R. R. 2014a. Idelalisib, an inhibitor of phosphatidylinositol 3-kinase p110delta, for relapsed/refractory chronic lymphocytic leukemia. *Blood,* 123**,** 3390-7.

BROWN, J. R., BYRD, J. C., COUTRE, S. E., BENSON, D. M., FLINN, I. W., WAGNER-JOHNSTON, N. D., SPURGEON, S. E., KAHL, B. S., BELLO, C., WEBB, H. K., JOHNSON, D. M., PETERMAN, S., LI, D., JAHN, T. M., LANNUTTI, B. J., ULRICH, R. G., YU, A. S., MILLER, L. L. & FURMAN, R. R. 2014b. Idelalisib, an inhibitor of phosphatidylinositol 3-kinase p110δ, for relapsed/refractory chronic lymphocytic leukemia. *Blood,* 123**,** 3390-3397.

BROWN, J. R., FURMAN, R. R., FLINN, I., COUTRE, S. E., WAGNER-JOHNSTON, N. D., KAHL, B. S., SPURGEON, S. E. F., BENSON, D. M., PETERMAN, S. & JOHNSON, D. M. Final results of a phase I study of idelalisib (GSE1101) a selective inhibitor of PI3K {delta}, in patients with relapsed or refractory CLL. ASCO Annual Meeting Proceedings, 2013. 7003.

BROXMEYER, H. E., ORSCHELL, C. M., CLAPP, D. W., HANGOC, G., COOPER, S., PLETT, P. A., LILES, W. C., LI, X., GRAHAM-EVANS, B., CAMPBELL, T. B., CALANDRA, G., BRIDGER, G., DALE, D. C. & SROUR, E. F. 2005. Rapid mobilization of murine and human hematopoietic stem and progenitor cells with AMD3100, a CXCR4 antagonist. *J Exp Med,* 201**,** 1307-18.

BRUCE, A., EVANS, R., MEZAN, R., SHI, L., MOSES, B. S., MARTIN, K. H., GIBSON, L. F. & YANG, Y. 2015. Three-Dimensional Microfluidic Tri-Culture Model of the Bone Marrow Microenvironment for Study of Acute Lymphoblastic Leukemia. *PLoS One,* 10**,** e0140506.

BRUUS, H. 2012. Acoustofluidics 7: The acoustic radiation force on small particles. *Lab Chip,* 12**,** 1014-21.

BUGGINS, A. G., PATTEN, P. E., RICHARDS, J., THOMAS, N. S., MUFTI, G. J. & DEVEREUX, S. 2008. Tumor-derived IL-6 may contribute to the immunological defect in CLL. *Leukemia,* 22**,** 1084-7.

BULIAN, P., SHANAFELT, T. D., FEGAN, C., ZUCCHETTO, A., CRO, L., NUCKEL, H., BALDINI, L., KURTOVA, A. V., FERRAJOLI, A., BURGER, J. A., GAIDANO, G., DEL POETA, G., PEPPER, C., ROSSI, D. & GATTEI, V. 2014. CD49d is the strongest flow cytometry-based predictor of overall survival in chronic lymphocytic leukemia. *J Clin Oncol,* 32**,** 897-904.

BURGER, J. A. 2011. Nurture versus nature: the microenvironment in chronic lymphocytic leukemia. *Hematology Am Soc Hematol Educ Program,* 2011**,** 96-103.

BURGER, J. A., BURGER, M. & KIPPS, T. J. 1999. Chronic lymphocytic leukemia B cells express functional CXCR4 chemokine receptors that mediate spontaneous migration beneath bone marrow stromal cells. *Blood,* 94**,** 3658-67.

BURGER, J. A. & CHIORAZZI, N. 2013. B cell receptor signaling in chronic lymphocytic leukemia. *Trends Immunol,* 34**,** 592-601.

BURGER, J. A., GHIA, P., ROSENWALD, A. & CALIGARIS-CAPPIO, F. 2009a. The microenvironment in mature B-cell malignancies: a target for new treatment strategies. *Blood,* 114**,** 3367-75.

BURGER, J. A. & KIPPS, T. J. 2002. Chemokine receptors and stromal cells in the homing and homeostasis of chronic lymphocytic leukemia B cells. *Leuk Lymphoma,* 43**,** 461-6.

BURGER, J. A. & KIPPS, T. J. 2006. CXCR4: a key receptor in the crosstalk between tumor cells and their microenvironment. *Blood,* 107**,** 1761-7.

BURGER, J. A. & PELED, A. 2009. CXCR4 antagonists: targeting the microenvironment in leukemia and other cancers. *Leukemia,* 23**,** 43-52.

BURGER, J. A., QUIROGA, M. P., HARTMANN, E., BURKLE, A., WIERDA, W. G., KEATING, M. J. & ROSENWALD, A. 2009b. High-level expression of the T-cell chemokines CCL3 and CCL4 by chronic lymphocytic leukemia B cells in nurselike cell cocultures and after BCR stimulation. *Blood,* 113**,** 3050-8.

BURGER, J. A., TSUKADA, N., BURGER, M., ZVAIFLER, N. J., DELL'AQUILA, M. & KIPPS, T. J. 2000. Blood-derived nurse-like cells protect chronic lymphocytic leukemia B cells from spontaneous apoptosis through stromal cell-derived factor-1. *Blood,* 96**,** 2655-63.

BURGER, M., HARTMANN, T., KROME, M., RAWLUK, J., TAMAMURA, H., FUJII, N., KIPPS, T. J. & BURGER, J. A. 2005. Small peptide inhibitors of the CXCR4 chemokine receptor (CD184) antagonize the activation, migration, and antiapoptotic responses of CXCL12 in chronic lymphocytic leukemia B cells. *Blood,* 106**,** 1824-30.

BURGESS, M., CHEUNG, C., CHAMBERS, L., RAVINDRANATH, K., MINHAS, G., KNOP, L., MOLLEE, P., MCMILLAN, N. A. & GILL, D. 2012. CCL2 and CXCL2 enhance survival of primary chronic lymphocytic leukemia cells in vitro. *Leuk Lymphoma,* 53**,** 1988-98.

BURKLE, A., NIEDERMEIER, M., SCHMITT-GRAFF, A., WIERDA, W. G., KEATING, M. J. & BURGER, J. A. 2007. Overexpression of the CXCR5 chemokine receptor, and its ligand, CXCL13 in B-cell chronic lymphocytic leukemia. *Blood,* 110**,** 3316-25.

BYRD , J. C., BROWN , J. R., O'BRIEN , S., BARRIENTOS , J. C., KAY , N. E., REDDY , N. M., COUTRE , S., TAM , C. S., MULLIGAN , S. P., JAEGER , U., DEVEREUX , S., BARR , P. M., FURMAN , R. R., KIPPS , T. J., CYMBALISTA , F., POCOCK , C., THORNTON , P., CALIGARIS-CAPPIO , F., ROBAK , T., DELGADO , J., SCHUSTER , S. J., MONTILLO , M., SCHUH , A., DE VOS , S., GILL , D., BLOOR , A., DEARDEN , C., MORENO , C., JONES , J. J., CHU , A. D., FARDIS , M., MCGREIVY , J., CLOW , F., JAMES , D. F. & HILLMEN , P. 2014. Ibrutinib versus Ofatumumab in Previously Treated Chronic Lymphoid Leukemia. *New England Journal of Medicine,* 371**,** 213-223.

BYRD, J. C., FURMAN, R. R., COUTRE, S., FLINN, I. W., BURGER, J. A., BLUM, K. A., SHARMAN, J., GRANT, B., JONES, J. A. & WIERDA, W. G. The Bruton's tyrosine kinase (BTK) inhibitor ibrutinib (PCI-32765) promotes high response rate, durable remissions, and is tolerable in treatment naive (TN) and relapsed or refractory (RR) chronic lymphocytic leukemia (CLL) or small lymphocytic lymphoma (SLL) patients including patients with high-risk (HR) disease: new and updated results of 116 patients in a phase Ib/II study. ASH annual meeting abstracts, 2012. 189.

BYRD, J. C., FURMAN, R. R., COUTRE, S. E., BURGER, J. A., BLUM, K. A., COLEMAN, M., WIERDA, W. G., JONES, J. A., ZHAO, W., HEEREMA, N. A., JOHNSON, A. J., SHAW, Y., BILOTTI, E., ZHOU, C., JAMES, D. F. & O'BRIEN, S. 2015. Three-year follow-up of treatment-naive and previously treated patients with CLL and SLL receiving single-agent ibrutinib. *Blood,* 125**,** 2497-506.

BYRD, J. C., FURMAN, R. R., COUTRE, S. E., FLINN, I. W., BURGER, J. A., BLUM, K. A., GRANT, B., SHARMAN, J. P., COLEMAN, M., WIERDA, W. G., JONES, J. A., ZHAO, W., HEEREMA, N. A., JOHNSON, A. J., SUKBUNTHERNG, J., CHANG, B. Y., CLOW, F., HEDRICK, E., BUGGY, J. J., JAMES, D. F. & O'BRIEN, S. 2013. Targeting BTK with ibrutinib in relapsed chronic lymphocytic leukemia. *N Engl J Med,* 369**,** 32-42.

BYSTRY, R. S., ALUVIHARE, V., WELCH, K. A., KALLIKOURDIS, M. & BETZ, A. G. 2001. B cells and professional APCs recruit regulatory T cells via CCL4. *Nat Immunol,* 2**,** 1126-32.

CALIGARIS-CAPPIO, F. 2003. Role of the microenvironment in chronic lymphocytic leukaemia. *British Journal of Haematology,* 123**,** 380-388.

CALIGARIS-CAPPIO, F. & GHIA, P. 2008. Novel insights in chronic lymphocytic leukemia: are we getting closer to understanding the pathogenesis of the disease? *J Clin Oncol,* 26**,** 4497-503.

CALIN, G. A., DUMITRU, C. D., SHIMIZU, M., BICHI, R., ZUPO, S., NOCH, E., ALDLER, H., RATTAN, S., KEATING, M., RAI, K., RASSENTI, L., KIPPS, T., NEGRINI, M., BULLRICH, F. & CROCE, C. M. 2002. Frequent deletions and down-regulation of micro- RNA genes miR15 and miR16 at 13q14 in chronic lymphocytic leukemia. *Proc Natl Acad Sci U S A,* 99**,** 15524-9.

CALIN, G. A., FERRACIN, M., CIMMINO, A., DI LEVA, G., SHIMIZU, M., WOJCIK, S. E., IORIO, M. V., VISONE, R., SEVER, N. I., FABBRI, M., IULIANO, R., PALUMBO, T., PICHIORRI, F., ROLDO, C., GARZON, R., SEVIGNANI, C., RASSENTI, L., ALDER, H., VOLINIA, S., LIU, C. G., KIPPS, T. J., NEGRINI, M. & CROCE, C. M. 2005. A MicroRNA signature associated with prognosis and progression in chronic lymphocytic leukemia. *N Engl J Med,* 353**,** 1793-801.

CALISSANO, C., DAMLE, R. N., HAYES, G., MURPHY, E. J., HELLERSTEIN, M. K., MORENO, C., SISON, C., KAUFMAN, M. S., KOLITZ, J. E., ALLEN, S. L., RAI, K. R. & CHIORAZZI, N. 2009. In vivo intraclonal and interclonal kinetic heterogeneity in B-cell chronic lymphocytic leukemia. *Blood,* 114**,** 4832-42.

CAMBIER, J. C., GAULD, S. B., MERRELL, K. T. & VILEN, B. J. 2007. B-cell anergy: from transgenic models to naturally occurring anergic B cells? *Nat Rev Immunol,* 7**,** 633-643.

CAPLAN, A. I. 1994. The mesengenic process. *Clin Plast Surg,* 21**,** 429-35.

CATOVSKY, D., FOOKS, J. & RICHARDS, S. 1989. Prognostic factors in chronic lymphocytic leukaemia: the importance of age, sex and response to treatment in survival. A report from the MRC CLL 1 trial. MRC Working Party on Leukaemia in Adults. *Br J Haematol,* 72**,** 141-9.

CATOVSKY, D., LAURIA, F., MATUTES, E., FOA, R., MANTOVANI, V., TURA, S. & GALTON, D. A. G. 1981. Increase in Ty Lymphocytes in B-Cell Chronic Lymphocytic Leukaemia. *British Journal of Haematology,* 47**,** 539-544.

CHAMBERS, K. F., MOSAAD, E. M., RUSSELL, P. J., CLEMENTS, J. A. & DORAN, M. R. 2014. 3D Cultures of prostate cancer cells cultured in a novel high-throughput

culture platform are more resistant to chemotherapeutics compared to cells cultured in monolayer. *PLoS One,* 9**,** e111029.

CHANAN-KHAN, A., MILLER, K. C., MUSIAL, L., LAWRENCE, D., PADMANABHAN, S., TAKESHITA, K., PORTER, C. W., GOODRICH, D. W., BERNSTEIN, Z. P., WALLACE, P., SPANER, D., MOHR, A., BYRNE, C., HERNANDEZ-ILIZALITURRI, F., CHRYSTAL, C., STAROSTIK, P. & CZUCZMAN, M. S. 2006. Clinical efficacy of lenalidomide in patients with relapsed or refractory chronic lymphocytic leukemia: results of a phase II study. *J Clin Oncol,* 24**,** 5343-9.

CHANG, H., JAMAL, N., WANG, X. H., MINDEN, M. D. & MESSNER, H. A. 1992. Constitutive production of the interleukins IL-5 and IL-6 by the lymphoma cell line OCI-Ly 17 derived from a patient with malignant lymphoma and hypereosinophilia. *Leuk Lymphoma,* 8**,** 97-107.

CHEN, C. S., MRKSICH, M., HUANG, S., WHITESIDES, G. M. & INGBER, D. E. 1997. Geometric control of cell life and death. *Science,* 276**,** 1425-8.

CHUAYSRI, C., THUWAJIT, P., PAUPAIROJ, A., CHAU-IN, S., SUTHIPHONGCHAI, T. & THUWAJIT, C. 2009. Alpha-smooth muscle actin-positive fibroblasts promote biliary cell proliferation and correlate with poor survival in cholangiocarcinoma. *Oncol Rep,* 21**,** 957-69.

CIMMINO, A., CALIN, G. A., FABBRI, M., IORIO, M. V., FERRACIN, M., SHIMIZU, M., WOJCIK, S. E., AQEILAN, R. I., ZUPO, S., DONO, M., RASSENTI, L., ALDER, H., VOLINIA, S., LIU, C. G., KIPPS, T. J., NEGRINI, M. & CROCE, C. M. 2005. miR-15 and miR-16 induce apoptosis by targeting BCL2. *Proc Natl Acad Sci U S A,* 102**,** 13944-9.

COAKLEY, W. & GALLEZ, D. 1989. Membrane-membrane contact: involvement of interfacial instability in the generation of discrete contacts. *Bioscience reports,* 9**,** 675-691.

COAKLEY, W. T., BAZOU, D., MORGAN, J., FOSTER, G. A., ARCHER, C. W., POWELL, K., BORTHWICK, K. A., TWOMEY, C. & BISHOP, J. 2004. Cell-cell contact and membrane spreading in an ultrasound trap. *Colloids Surf B Biointerfaces,* 34**,** 221-30.

COELHO, V., KRYSOV, S., STEELE, A., SANCHEZ HIDALGO, M., JOHNSON, P. W., CHANA, P. S., PACKHAM, G., STEVENSON, F. K. & FORCONI, F. 2013. Identification in CLL of circulating intraclonal subgroups with varying B-cell receptor expression and function. *Blood,* 122**,** 2664-72.

COLLINS, R. J., VERSCHUER, L. A., HARMON, B. V., PRENTICE, R. L., POPE, J. H. & KERR, J. F. R. 1989. Spontaneous programmed death (apoptosis) of B-chronic lymphocytic leukaemia cells following their culture in vitro. *British Journal of Haematology,* 71**,** 343-350.

COSCIA, M., PANTALEONI, F., RIGANTI, C., VITALE, C., RIGONI, M., PEOLA, S., CASTELLA, B., FOGLIETTA, M., GRIGGIO, V., DRANDI, D., LADETTO, M., BOSIA, A., BOCCADORO, M. & MASSAIA, M. 2011. IGHV unmutated CLL B cells are more prone to spontaneous apoptosis and subject to environmental prosurvival signals than mutated CLL B cells. *Leukemia,* 25**,** 828-37.

CRESPO, M., BOSCH, F., VILLAMOR, N., BELLOSILLO, B., COLOMER, D., ROZMAN, M., MARCÉ, S., LÓPEZ-GUILLERMO, A., CAMPO, E. & MONTSERRAT, E. 2003. ZAP-70 Expression as a Surrogate for Immunoglobulin-Variable-Region Mutations in Chronic Lymphocytic Leukemia. *New England Journal of Medicine,* 348**,** 1764-1775.

CRUM, L. A. 1975. Bjerknes forces on bubbles in a stationary sound field. *The Journal of the Acoustical Society of America,* 57**,** 1363-1370.

CUI, B., CHEN, L., ZHANG, S., MRAZ, M., FECTEAU, J. F., YU, J., GHIA, E. M., ZHANG, L., BAO, L., RASSENTI, L. Z., MESSER, K., CALIN, G. A., CROCE, C. M. & KIPPS, T. J. 2014. MicroRNA-155 influences B-cell receptor signaling and associates with aggressive disease in chronic lymphocytic leukemia. *Blood,* 124**,** 546-54.

CUNI, S., PEREZ-ACIEGO, P., PEREZ-CHACON, G., VARGAS, J., SANCHEZ, A., MARTIN-SAAVEDRA, F., BALLESTER, S., GARCIA-MARCO, J., JORDA, J. & DURANTEZ, A. 2004. A sustained activation of PI3K/NF-κB pathway is critical for the survival of chronic lymphocytic leukemia B cells. *Leukemia,* 18**,** 1391-1400.

CURRIE, K. S., KROPF, J. E., LEE, T., BLOMGREN, P., XU, J., ZHAO, Z., GALLION, S., WHITNEY, J. A., MACLIN, D., LANSDON, E. B., MACIEJEWSKI, P., ROSSI, A. M., RONG, H., MACALUSO, J., BARBOSA, J., DI PAOLO, J. A. & MITCHELL, S. A. 2014. Discovery of GS-9973, a selective and orally efficacious inhibitor of spleen tyrosine kinase. *J Med Chem,* 57**,** 3856-73.

CYSTER, J. G. 1999. Chemokines and Cell Migration in Secondary Lymphoid Organs. *Science,* 286**,** 2098-2102.

CYSTER, J. G. 2005. Chemokines, sphingosine-1-phosphate, and cell migration in secondary lymphoid organs. *Annu Rev Immunol,* 23**,** 127-59.

CYSTER, J. G., ANSEL, K. M., REIF, K., EKLAND, E. H., HYMAN, P. L., TANG, H. L., LUTHER, S. A. & NGO, V. N. 2000. Follicular stromal cells and lymphocyte homing to follicles. *Immunol Rev,* 176**,** 181-93.

CYSTER, J. G. & SCHWAB, S. R. 2012. Sphingosine-1-phosphate and lymphocyte egress from lymphoid organs. *Annu Rev Immunol,* 30**,** 69-94.

D'ARENA, G., SIMEON, V., D'AURIA, F., STATUTO, T., SANZO, P. D., MARTINO, L. D., MARANDINO, A., SANGIORGIO, M., MUSTO, P. & FEO, V. D. 2013. Regulatory T-cells in chronic lymphocytic leukemia: actor or innocent bystander? *American Journal of Blood Research,* 3**,** 52-57.

DAMLE, R. N., GHIOTTO, F., VALETTO, A., ALBESIANO, E., FAIS, F., YAN, X. J., SISON, C. P., ALLEN, S. L., KOLITZ, J., SCHULMAN, P., VINCIGUERRA, V. P., BUDDE, P., FREY, J., RAI, K. R., FERRARINI, M. & CHIORAZZI, N. 2002. B-cell chronic lymphocytic leukemia cells express a surface membrane phenotype of activated, antigen-experienced B lymphocytes. *Blood,* 99**,** 4087-93.

DAMLE, R. N., WASIL, T., FAIS, F., GHIOTTO, F., VALETTO, A., ALLEN, S. L., BUCHBINDER, A., BUDMAN, D., DITTMAR, K., KOLITZ, J., LICHTMAN, S. M., SCHULMAN, P., VINCIGUERRA, V. P., RAI, K. R., FERRARINI, M. & CHIORAZZI, N. 1999. Ig V gene mutation status and CD38 expression as novel prognostic indicators in chronic lymphocytic leukemia. *Blood,* 94**,** 1840-7.

DARBY, I., SKALLI, O. & GABBIANI, G. 1990. a-Smooth muscle actin is transiently expressed by myofibroblasts during experimental wound healing. *Lab Invest,* 63**,** 21-29.

DAVID, L., DULONG, V., LE CERF, D., CHAUZY, C., NORRIS, V., DELPECH, B., LAMACZ, M. & VANNIER, J. P. 2004. Reticulated hyaluronan hydrogels: a model for examining cancer cell invasion in 3D. *Matrix Biol,* 23**,** 183-93.

DE ROOIJ, M. F., KUIL, A., GEEST, C. R., ELDERING, E., CHANG, B. Y., BUGGY, J. J., PALS, S. T. & SPAARGAREN, M. 2012. The clinically active BTK inhibitor PCI-

32765 targets B-cell receptor- and chemokine-controlled adhesion and migration in chronic lymphocytic leukemia. *Blood,* 119**,** 2590-4.

DE TOTERO, D., REATO, G., MAURO, F., CIGNETTI, A., FERRINI, S., GUARINI, A., GOBBI, M., GROSSI, C. E. & FOA, R. 1999. IL4 production and increased CD30 expression by a unique CD8+ T-cell subset in B-cell chronic lymphocytic leukaemia. *Br J Haematol,* 104**,** 589-99.

DEAGLIO, S., AYDIN, S., GRAND, M. M., VAISITTI, T., BERGUI, L., D'ARENA, G., CHIORINO, G. & MALAVASI, F. 2010. CD38/CD31 interactions activate genetic pathways leading to proliferation and migration in chronic lymphocytic leukemia cells. *Mol Med,* 16**,** 87-91.

DEAGLIO, S., VAISITTI, T., BERGUI, L., BONELLO, L., HORENSTEIN, A. L., TAMAGNONE, L., BOUMSELL, L. & MALAVASI, F. 2005. CD38 and CD100 lead a network of surface receptors relaying positive signals for B-CLL growth and survival. *Blood,* 105**,** 3042-50.

DELGADO, J., ESPINET, B., OLIVEIRA, A. C., ABRISQUETA, P., DE LA SERNA, J., COLLADO, R., LOSCERTALES, J., LOPEZ, M., HERNANDEZ-RIVAS, J. A., FERRA, C., RAMIREZ, A., RONCERO, J. M., LOPEZ, C., AVENTIN, A., PUIGGROS, A., ABELLA, E., CARBONELL, F., COSTA, D., CARRIO, A., GONZALEZ, M., GRUPO ESPANOL DE LEUCEMIA LINFATICA, C. & GRUPO ESPANOL DE CITOGENETICA, H. 2012. Chronic lymphocytic leukaemia with 17p deletion: a retrospective analysis of prognostic factors and therapy results. *Br J Haematol,* 157**,** 67-74.

DESMOULIERE, A., GEINOZ, A., GABBIANI, F. & GABBIANI, G. 1993. Transforming growth factor-beta 1 induces alpha-smooth muscle actin expression in granulation tissue myofibroblasts and in quiescent and growing cultured fibroblasts. *J Cell Biol,* 122**,** 103-11.

DI GIOVANNI, S., VALENTINI, G., CARDUCCI, P. & GIALLONARDO, P. 1989. Beta-2-Microglobulin Is a Reliable Tumor Marker in Chronic Lymphocytic Leukemia. *Acta Haematologica,* 81**,** 181-185.

DIJKSTRA, M. K., VAN LOM, K., TIELEMANS, D., ELSTRODT, F., LANGERAK, A. W., VAN 'T VEER, M. B. & JONGEN-LAVRENCIC, M. 2009. 17p13/TP53 deletion in B-CLL patients is associated with microRNA-34a downregulation. *Leukemia,* 23**,** 625-7.

DING, W., NOWAKOWSKI, G. S., KNOX, T. R., BOYSEN, J. C., MAAS, M. L., SCHWAGER, S. M., WU, W., WELLIK, L. E., DIETZ, A. B., GHOSH, A. K., SECRETO, C. R., MEDINA, K. L., SHANAFELT, T. D., ZENT, C. S., CALL, T. G. & KAY, N. E. 2009. Bi-directional Activation between Mesenchymal Stem Cells and CLL B-Cells: Implication for CLL Disease Progression. *British journal of haematology,* 147**,** 471-483.

DOHNER, H., STILGENBAUER, S., BENNER, A., LEUPOLT, E., KROBER, A., BULLINGER, L., DOHNER, K., BENTZ, M. & LICHTER, P. 2000. Genomic aberrations and survival in chronic lymphocytic leukemia. *N Engl J Med,* 343**,** 1910-6.

DÜHRSEN, U. & HOSSFELD, D. K. 1996. Stromal abnormalities in neoplastic bone marrow diseases. *Annals of Hematology,* 73**,** 53-70.

DÜRIG, J., NÜCKEL, H., CREMER, M., FÜHRER, A., HALFMEYER, K., FANDREY, J., MÖRÖY, T., KLEIN-HITPASS, L. & DÜHRSEN, U. 2003. ZAP-70 expression is a prognostic factor in chronic lymphocytic leukemia. *Leukemia,* 17**,** 2426-2434.

DVORAK, H. F. 1986. Tumors: wounds that do not heal. Similarities between tumor stroma generation and wound healing. *N Engl J Med,* 315**,** 1650-9.

DWYER, R. M., POTTER-BEIRNE, S. M., HARRINGTON, K. A., LOWERY, A. J., HENNESSY, E., MURPHY, J. M., BARRY, F. P., O'BRIEN, T. & KERIN, M. J. 2007. Monocyte chemotactic protein-1 secreted by primary breast tumors stimulates migration of mesenchymal stem cells. *Clin Cancer Res,* 13**,** 5020-7.

EDELMANN, J., KLEIN-HITPASS, L., CARPINTEIRO, A., FUHRER, A., SELLMANN, L., STILGENBAUER, S., DUHRSEN, U. & DURIG, J. 2008. Bone marrow fibroblasts induce expression of PI3K/NF-kappaB pathway genes and a pro-angiogenic phenotype in CLL cells. *Leuk Res,* 32**,** 1565-72.

EDWARDS, G. O., BAZOU, D., KUZNETSOVA, L. A. & COAKLEY, W. T. 2007. Cell adhesion dynamics and actin cytoskeleton reorganization in HepG2 cell aggregates. *Cell Commun Adhes,* 14**,** 9-20.

EVANDER, M., JOHANSSON, L., LILLIEHORN, T., PISKUR, J., LINDVALL, M., JOHANSSON, S., ALMQVIST, M., LAURELL, T. & NILSSON, J. 2007. Noninvasive acoustic cell trapping in a microfluidic perfusion system for online bioassays. *Analytical chemistry,* 79**,** 2984-2991.

FARAHANI, M., RUBBI, C., LIU, L., SLUPSKY, J. R. & KALAKONDA, N. 2015. CLL Exosomes Modulate the Transcriptome and Behaviour of Recipient Stromal Cells and Are Selectively Enriched in miR-202-3p. *PLOS ONE,* 10**,** e0141429.

FAYAD, L., KEATING, M. J., REUBEN, J. M., O'BRIEN, S., LEE, B. N., LERNER, S. & KURZROCK, R. 2001. Interleukin-6 and interleukin-10 levels in chronic lymphocytic leukemia: correlation with phenotypic characteristics and outcome. *Blood,* 97**,** 256-63.

FENG, B. & CHEN, L. 2009. Review of mesenchymal stem cells and tumors: executioner or coconspirator? *Cancer Biother Radiopharm,* 24**,** 717-21.

FERRAJOLI, A., KEATING, M. J., MANSHOURI, T., GILES, F. J., DEY, A., ESTROV, Z., KOLLER, C. A., KURZROCK, R., THOMAS, D. A. & FADERL, S. 2002. The clinical significance of tumor necrosis factor-α plasma level in patients having chronic lymphocytic leukemia. *Blood,* 100**,** 1215-1219.

FILIP, A. A., CISEŁ, B., KOCZKODAJ, D., WĄSIK-SZCZEPANEK, E., PIERSIAK, T. & DMOSZYŃSKA, A. 2013. Circulating microenvironment of CLL: Are nurse-like cells related to tumor-associated macrophages? *Blood Cells, Molecules, and Diseases,* 50**,** 263-270.

FIORCARI, S., BROWN, W. S., MCINTYRE, B. W., ESTROV, Z., MAFFEI, R., O'BRIEN, S., SIVINA, M., HOELLENRIEGEL, J., WIERDA, W. G., KEATING, M. J., DING, W., KAY, N. E., LANNUTTI, B. J., MARASCA, R. & BURGER, J. A. 2013. The PI3-kinase delta inhibitor idelalisib (GS-1101) targets integrin-mediated adhesion of chronic lymphocytic leukemia (CLL) cell to endothelial and marrow stromal cells. *PLoS One,* 8**,** e83830.

FIORCARI, S., MARTINELLI, S., BULGARELLI, J., AUDRITO, V., ZUCCHINI, P., COLACI, E., POTENZA, L., NARNI, F., LUPPI, M., DEAGLIO, S., MARASCA, R. & MAFFEI, R. 2015a. Lenalidomide interferes with tumor-promoting properties of nurse-like cells in chronic lymphocytic leukemia. *Haematologica,* 100**,** 253-62.

FIORCARI, S., MARTINELLI, S., BULGARELLI, J., AUDRITO, V., ZUCCHINI, P., COLACI, E., POTENZA, L., NARNI, F., LUPPI, M., DEAGLIO, S., MARASCA, R. &

MAFFEI, R. 2015b. Lenalidomide interferes with tumor-promoting properties of nurse-like cells in chronic lymphocytic leukemia. *Haematologica,* 100**,** 253-262.

FONG, E. L. S., LAMHAMEDI-CHERRADI, S.-E., BURDETT, E., RAMAMOORTHY, V., LAZAR, A. J., KASPER, F. K., FARACH-CARSON, M. C., VISHWAMITRA, D., DEMICCO, E. G., MENEGAZ, B. A., AMIN, H. M., MIKOS, A. G. & LUDWIG, J. A. 2013. Modeling Ewing sarcoma tumors in vitro with 3D scaffolds. *Proceedings of the National Academy of Sciences of the United States of America,* 110**,** 6500-6505.

FORCONI, F., POTTER, K. N., WHEATLEY, I., DARZENTAS, N., SOZZI, E., STAMATOPOULOS, K., MOCKRIDGE, C. I., PACKHAM, G. & STEVENSON, F. K. 2010. The normal IGHV1-69-derived B-cell repertoire contains stereotypic patterns characteristic of unmutated CLL. *Blood,* 115**,** 71-7.

FORSTER, R., SCHUBEL, A., BREITFELD, D., KREMMER, E., RENNER-MULLER, I., WOLF, E. & LIPP, M. 1999. CCR7 coordinates the primary immune response by establishing functional microenvironments in secondary lymphoid organs. *Cell,* 99**,** 23-33.

FRAMPTON, S. J., JENEI, V., MELLONE, M., HANLEY, C. J., RUCKA, M. M., TOD, J., MOUTASIM, K. A., KING, E. V. & THOMAS, G. 2015. Abstract 2389: Eps8: a negative regulator of myofibroblast differentiation and function. *Cancer Research,* 75**,** 2389.

FRANCIA DI CELLE, P., MARIANI, S., RIERA, L., STACCHINI, A., REATO, G. & FOA, R. 1996. Interleukin-8 induces the accumulation of B-cell chronic lymphocytic leukemia cells by prolonging survival in an autocrine fashion. *Blood,* 87**,** 4382-9.

FREEMAN, G. J., FREEDMAN, A. S., RABINOWE, S. N., SEGIL, J. M., HOROWITZ, J., ROSEN, K., WHITMAN, J. F. & NADLER, L. M. 1989. Interleukin 6 gene expression in normal and neoplastic B cells. *J Clin Invest,* 83**,** 1512-8.

FRIEDBERG, J. W., SHARMAN, J., SWEETENHAM, J., JOHNSTON, P. B., VOSE, J. M., LACASCE, A., SCHAEFER-CUTILLO, J., DE VOS, S., SINHA, R., LEONARD, J. P., CRIPE, L. D., GREGORY, S. A., STERBA, M. P., LOWE, A. M., LEVY, R. & SHIPP, M. A. 2010. Inhibition of Syk with fostamatinib disodium has significant clinical activity in non-Hodgkin lymphoma and chronic lymphocytic leukemia. *Blood,* 115**,** 2578-85.

FRISCH, S. M. & FRANCIS, H. 1994. Disruption of epithelial cell-matrix interactions induces apoptosis. *J Cell Biol,* 124**,** 619-26.

FURMAN, R. R., ASGARY, Z., MASCARENHAS, J. O., LIOU, H. C. & SCHATTNER, E. J. 2000. Modulation of NF-kappa B activity and apoptosis in chronic lymphocytic leukemia B cells. *J Immunol,* 164**,** 2200-6.

FURMAN, R. R., SHARMAN, J. P., COUTRE, S. E., CHESON, B. D., PAGEL, J. M., HILLMEN, P., BARRIENTOS, J. C., ZELENETZ, A. D., KIPPS, T. J., FLINN, I., GHIA, P., ERADAT, H., ERVIN, T., LAMANNA, N., COIFFIER, B., PETTITT, A. R., MA, S., STILGENBAUER, S., CRAMER, P., AIELLO, M., JOHNSON, D. M., MILLER, L. L., LI, D., JAHN, T. M., DANSEY, R. D., HALLEK, M. & O'BRIEN, S. M. 2014. Idelalisib and Rituximab in Relapsed Chronic Lymphocytic Leukemia. *New England Journal of Medicine,* 370**,** 997-1007.

GABBIANI, G., RYAN, G. B. & MAJNE, G. 1971. Presence of modified fibroblasts in granulation tissue and their possible role in wound contraction. *Experientia,* 27**,** 549-50.

GANGHAMMER, S., GUTJAHR, J., HUTTERER, E., KRENN, P. W., PUCHER, S., ZELLE-RIESER, C., JÖHRER, K., WIJTMANS, M., LEURS, R., SMIT, M. J., GATTEI, V., GREIL, R. & HARTMANN, T. N. 2016. Combined CXCR3/CXCR4 measurements are of high prognostic value in chronic lymphocytic leukemia due to negative co-operativity of the receptors. *Haematologica,* 101**,** e99-e102.

GATTEI, V., BULIAN, P., DEL PRINCIPE, M. I., ZUCCHETTO, A., MAURILLO, L., BUCCISANO, F., BOMBEN, R., DAL-BO, M., LUCIANO, F., ROSSI, F. M., DEGAN, M., AMADORI, S. & DEL POETA, G. 2008. Relevance of CD49d protein expression as overall survival and progressive disease prognosticator in chronic lymphocytic leukemia. *Blood,* 111**,** 865-73.

GENTILE, M., CUTRONA, G., NERI, A., MOLICA, S., FERRARINI, M. & MORABITO, F. 2009. Predictive value of β2-microglobulin (β2-m) levels in chronic lymphocytic leukemia since Binet A stages. *Haematologica,* 94**,** 887-888.

GHIA, P., CIRCOSTA, P., SCIELZO, C., VALLARIO, A., CAMPOREALE, A., GRANZIERO, L. & CALIGARIS-CAPPIO, F. 2005. Differential effects on CLL cell survival exerted by different microenvironmental elements. *Curr Top Microbiol Immunol,* 294**,** 135-45.

GHIA, P., STROLA, G., GRANZIERO, L., GEUNA, M., GUIDA, G., SALLUSTO, F., RUFFING, N., MONTAGNA, L., PICCOLI, P., CHILOSI, M. & CALIGARIS-CAPPIO, F. 2002. Chronic lymphocytic leukemia B cells are endowed with the capacity to attract CD4+, CD40L+ T cells by producing CCL22. *Eur J Immunol,* 32**,** 1403-13.

GHOBRIAL, I. M., BONE, N. D., STENSON, M. J., NOVAK, A., HEDIN, K. E., KAY, N. E. & ANSELL, S. M. 2004. Expression of the chemokine receptors CXCR4 and CCR7 and disease progression in B-cell chronic lymphocytic leukemia/ small lymphocytic lymphoma. *Mayo Clin Proc,* 79**,** 318-25.

GHOSH, A. K., SECRETO, C. R., KNOX, T. R., DING, W., MUKHOPADHYAY, D. & KAY, N. E. 2010. Circulating microvesicles in B-cell chronic lymphocytic leukemia can stimulate marrow stromal cells: implications for disease progression. *Blood,* 115**,** 1755-64.

GHOSH, S., SPAGNOLI, G. C., MARTIN, I., PLOEGERT, S., DEMOUGIN, P., HEBERER, M. & RESCHNER, A. 2005. Three-dimensional culture of melanoma cells profoundly affects gene expression profile: a high density oligonucleotide array study. *J Cell Physiol,* 204**,** 522-31.

GLYNNE-JONES, P., BOLTRYK, R. J. & HILL, M. 2012. Acoustofluidics 9: Modelling and applications of planar resonant devices for acoustic particle manipulation. *Lab Chip,* 12**,** 1417-26.

GONZALEZ-RODRIGUEZ, A. P., CONTESTI, J., HUERGO-ZAPICO, L., LOPEZ-SOTO, A., FERNANDEZ-GUIZAN, A., ACEBES-HUERTA, A., GONZALEZ-HUERTA, A. J., GONZALEZ, E., FERNANDEZ-ALVAREZ, C. & GONZALEZ, S. 2010. Prognostic significance of CD8 and CD4 T cells in chronic lymphocytic leukemia. *Leuk Lymphoma,* 51**,** 1829-36.

GORGUN, G., HOLDERRIED, T. A., ZAHRIEH, D., NEUBERG, D. & GRIBBEN, J. G. 2005. Chronic lymphocytic leukemia cells induce changes in gene expression of CD4 and CD8 T cells. *J Clin Invest,* 115**,** 1797-805.

GRÖSCHL, M. 1998. Ultrasonic separation of suspended particles-Part I: Fundamentals. *Acta Acustica united with Acustica,* 84**,** 432-447.

GRUSS, H. J. & DOWER, S. K. 1995. Tumor necrosis factor ligand superfamily: involvement in the pathology of malignant lymphomas. *Blood,* 85**,** 3378-404.

GUARINI, A., CHIARETTI, S., TAVOLARO, S., MAGGIO, R., PERAGINE, N., CITARELLA, F., RICCIARDI, M. R., SANTANGELO, S., MARINELLI, M., DE PROPRIS, M. S., MESSINA, M., MAURO, F. R., DEL GIUDICE, I. & FOA, R. 2008. BCR ligation induced by IgM stimulation results in gene expression and functional changes only in IgV H unmutated chronic lymphocytic leukemia (CLL) cells. *Blood,* 112**,** 782-92.

GUNN, M. D., KYUWA, S., TAM, C., KAKIUCHI, T., MATSUZAWA, A., WILLIAMS, L. T. & NAKANO, H. 1999. Mice lacking expression of secondary lymphoid organ chemokine have defects in lymphocyte homing and dendritic cell localization. *J Exp Med,* 189**,** 451-60.

GUNN, M. D., TANGEMANN, K., TAM, C., CYSTER, J. G., ROSEN, S. D. & WILLIAMS, L. T. 1998. A chemokine expressed in lymphoid high endothelial venules promotes the adhesion and chemotaxis of naive T lymphocytes. *Proc Natl Acad Sci U S A,* 95**,** 258-63.

GURSKI, L. A., JHA, A. K., ZHANG, C., JIA, X. & FARACH-CARSON, M. C. 2009. Hyaluronic acid-based hydrogels as 3D matrices for in vitro evaluation of chemotherapeutic drugs using poorly adherent prostate cancer cells. *Biomaterials,* 30**,** 6076-85.

HALLEK, M., CHESON, B. D., CATOVSKY, D., CALIGARIS-CAPPIO, F., DIGHIERO, G., DOHNER, H., HILLMEN, P., KEATING, M. J., MONTSERRAT, E., RAI, K. R. & KIPPS, T. J. 2008. Guidelines for the diagnosis and treatment of chronic lymphocytic leukemia: a report from the International Workshop on Chronic Lymphocytic Leukemia updating the National Cancer Institute-Working Group 1996 guidelines. *Blood,* 111**,** 5446-56.

HALLEK, M., FISCHER, K., FINGERLE-ROWSON, G., FINK, A., BUSCH, R., MAYER, J., HENSEL, M., HOPFINGER, G., HESS, G. & VON GRÜNHAGEN, U. 2010. Addition of rituximab to fludarabine and cyclophosphamide in patients with chronic lymphocytic leukaemia: a randomised, open-label, phase 3 trial. *The Lancet,* 376**,** 1164-1174.

HALLEK, M., LANGENMAYER, I., NERL, C., KNAUF, W., DIETZFELBINGER, H., ADORF, D., OSTWALD, M., BUSCH, R., KUHN-HALLEK, I., THIEL, E. & EMMERICH, B. 1999. Elevated serum thymidine kinase levels identify a subgroup at high risk of disease progression in early, nonsmoldering chronic lymphocytic leukemia. *Blood,* 93**,** 1732-7.

HAMBLIN, T. J., DAVIS, Z., GARDINER, A., OSCIER, D. G. & STEVENSON, F. K. 1999. Unmutated Ig V(H) genes are associated with a more aggressive form of chronic lymphocytic leukemia. *Blood,* 94**,** 1848-54.

HAMILTON, E., PEARCE, L., MORGAN, L., ROBINSON, S., WARE, V., BRENNAN, P., THOMAS, N. S., YALLOP, D., DEVEREUX, S., FEGAN, C., BUGGINS, A. G. & PEPPER, C. 2012. Mimicking the tumour microenvironment: three different co-culture systems induce a similar phenotype but distinct proliferative signals in primary chronic lymphocytic leukaemia cells. *Br J Haematol,* 158**,** 589-99.

HAMMOND, T. G. & HAMMOND, J. M. 2001. Optimized suspension culture: the rotating-wall vessel. *Am J Physiol Renal Physiol,* 281**,** F12-25.

HANADA, M., DELIA, D., AIELLO, A., STADTMAUER, E. & REED, J. C. 1993. bcl-2 gene hypomethylation and high-level expression in B-cell chronic lymphocytic leukemia. *Blood,* 82**,** 1820-8.

HANAHAN, D. & COUSSENS, L. M. 2012. Accessories to the crime: functions of cells recruited to the tumor microenvironment. *Cancer Cell,* 21**,** 309-22.

HANAHAN, D. & WEINBERG, R. A. 2000. The hallmarks of cancer. *Cell,* 100**,** 57-70.

HANAHAN, D. & WEINBERG, R. A. 2011. Hallmarks of cancer: the next generation. *Cell,* 144**,** 646-74.

HARA, M., MURAKAMI, T. & KOBAYASHI, E. 2008. In vivo bioimaging using photogenic rats: Fate of injected bone marrow-derived mesenchymal stromal cells. *Journal of Autoimmunity,* 30**,** 163-171.

HE, L., HE, X., LOWE, S. W. & HANNON, G. J. 2007. microRNAs join the p53 network [mdash] another piece in the tumour-suppression puzzle. *Nat Rev Cancer,* 7**,** 819-822.

HERISHANU, Y., PEREZ-GALAN, P., LIU, D., BIANCOTTO, A., PITTALUGA, S., VIRE, B., GIBELLINI, F., NJUGUNA, N., LEE, E., STENNETT, L., RAGHAVACHARI, N., LIU, P., MCCOY, J. P., RAFFELD, M., STETLER-STEVENSON, M., YUAN, C., SHERRY, R., ARTHUR, D. C., MARIC, I., WHITE, T., MARTI, G. E., MUNSON, P., WILSON, W. H. & WIESTNER, A. 2011. The lymph node microenvironment promotes B-cell receptor signaling, NF-kappaB activation, and tumor proliferation in chronic lymphocytic leukemia. *Blood,* 117**,** 563-74.

HERMAN, S. E., GORDON, A. L., HERTLEIN, E., RAMANUNNI, A., ZHANG, X., JAGLOWSKI, S., FLYNN, J., JONES, J., BLUM, K. A., BUGGY, J. J., HAMDY, A., JOHNSON, A. J. & BYRD, J. C. 2011. Bruton tyrosine kinase represents a promising therapeutic target for treatment of chronic lymphocytic leukemia and is effectively targeted by PCI-32765. *Blood,* 117**,** 6287-96.

HERMAN, S. E., GORDON, A. L., WAGNER, A. J., HEEREMA, N. A., ZHAO, W., FLYNN, J. M., JONES, J., ANDRITSOS, L., PURI, K. D., LANNUTTI, B. J., GIESE, N. A., ZHANG, X., WEI, L., BYRD, J. C. & JOHNSON, A. J. 2010. Phosphatidylinositol 3-kinase-delta inhibitor CAL-101 shows promising preclinical activity in chronic lymphocytic leukemia by antagonizing intrinsic and extrinsic cellular survival signals. *Blood,* 116**,** 2078-88.

HERMAN, S. E., NIEMANN, C. U., FAROOQUI, M., JONES, J., MUSTAFA, R. Z., LIPSKY, A., SABA, N., MARTYR, S., SOTO, S., VALDEZ, J., GYAMFI, J. A., MARIC, I., CALVO, K. R., PEDERSEN, L. B., GEISLER, C. H., LIU, D., MARTI, G. E., AUE, G. & WIESTNER, A. 2014. Ibrutinib-induced lymphocytosis in patients with chronic lymphocytic leukemia: correlative analyses from a phase II study. *Leukemia,* 28**,** 2188-96.

HERTZ, H. M. 1995. Standing-wave acoustic trap for nonintrusive positioning of microparticles. *Journal of Applied Physics,* 78**,** 4845-4849.

HEWAMANA, S., LIN, T. T., JENKINS, C., BURNETT, A. K., JORDAN, C. T., FEGAN, C., BRENNAN, P., ROWNTREE, C. & PEPPER, C. 2008. The novel nuclear factor-κB inhibitor LC-1 is equipotent in poor prognostic subsets of chronic lymphocytic leukemia and shows strong synergy with fludarabine. *Clinical Cancer Research,* 14**,** 8102-8111.

HEYN, H., MORAN, S., HERNANDO-HERRAEZ, I., SAYOLS, S., GOMEZ, A., SANDOVAL, J., MONK, D., HATA, K., MARQUES-BONET, T. & WANG, L. 2013.

DNA methylation contributes to natural human variation. *Genome research,* 23**,** 1363-1372.

HINZ, B. 2007. Formation and Function of the Myofibroblast during Tissue Repair. *Journal of Investigative Dermatology,* 127**,** 526-537.

HINZ, B., PHAN, S. H., THANNICKAL, V. J., GALLI, A., BOCHATON-PIALLAT, M. L. & GABBIANI, G. 2007. The myofibroblast: one function, multiple origins. *Am J Pathol,* 170**,** 1807-16.

HIRT, C., PAPADIMITROPOULOS, A., MELE, V., MURARO, M. G., MENGUS, C., IEZZI, G., TERRACCIANO, L., MARTIN, I. & SPAGNOLI, G. C. 2014. "In vitro" 3D models of tumor-immune system interaction. *Adv Drug Deliv Rev,* 79-80**,** 145-54.

HITCHON, C., WONG, K., MA, G., REED, J., LYTTLE, D. & EL-GABALAWY, H. 2002. Hypoxia-induced production of stromal cell–derived factor 1 (CXCL12) and vascular endothelial growth factor by synovial fibroblasts. *Arthritis & Rheumatism,* 46**,** 2587-2597.

HOELLENRIEGEL, J., MEADOWS, S. A., SIVINA, M., WIERDA, W. G., KANTARJIAN, H., KEATING, M. J., GIESE, N., O'BRIEN, S., YU, A., MILLER, L. L., LANNUTTI, B. J. & BURGER, J. A. 2011. The phosphoinositide 3'-kinase delta inhibitor, CAL-101, inhibits B-cell receptor signaling and chemokine networks in chronic lymphocytic leukemia. *Blood,* 118**,** 3603-12.

HSU, S. M., XIE, S. S. & WALDRON, J. A., JR. 1992. Functional heterogeneity and pathogenic significance of interleukin-6 in B-cell lymphomas. *Am J Pathol,* 141**,** 915-23.

HULTSTROM, J., MANNEBERG, O., DOPF, K., HERTZ, H. M., BRISMAR, H. & WIKLUND, M. 2007. Proliferation and viability of adherent cells manipulated by standing-wave ultrasound in a microfluidic chip. *Ultrasound Med Biol,* 33**,** 145-51.

HULTSTRÖM, J., MANNEBERG, O., DOPF, K., HERTZ, H. M., BRISMAR, H. & WIKLUND, M. 2007. Proliferation and viability of adherent cells manipulated by standing-wave ultrasound in a microfluidic chip. *Ultrasound in medicine & biology,* 33**,** 145-151.

HWANG, R. F., MOORE, T., ARUMUGAM, T., RAMACHANDRAN, V., AMOS, K. D., RIVERA, A., JI, B., EVANS, D. B. & LOGSDON, C. D. 2008. Cancer-associated stromal fibroblasts promote pancreatic tumor progression. *Cancer Res,* 68**,** 918-26.

IVASCU, A. & KUBBIES, M. 2006. Rapid generation of single-tumor spheroids for high-throughput cell function and toxicity analysis. *J Biomol Screen,* 11**,** 922-32.

JAGANATHAN, H., GAGE, J., LEONARD, F., SRINIVASAN, S., SOUZA, G. R., DAVE, B. & GODIN, B. 2014. Three-dimensional in vitro co-culture model of breast tumor using magnetic levitation. *Sci Rep,* 4**,** 6468.

JAMES, D. F., WERNER, L., BROWN, J. R., WIERDA, W. G., BARRIENTOS, J. C., CASTRO, J. E., GREAVES, A., JOHNSON, A. J., RASSENTI, L. Z., RAI, K. R., NEUBERG, D. & KIPPS, T. J. 2014. Lenalidomide and rituximab for the initial treatment of patients with chronic lymphocytic leukemia: a multicenter clinical-translational study from the chronic lymphocytic leukemia research consortium. *J Clin Oncol,* 32**,** 2067-73.

JANEWAY CA JR, T. P., WALPORT M, ET AL. 2001. *Immunobiology, 5th edition*, Garland Science.

JENKINS, M. K., KHORUTS, A., INGULLI, E., MUELLER, D. L., MCSORLEY, S. J., REINHARDT, R. L., ITANO, A. & PAPE, K. A. 2001. In vivo activation of antigen-specific CD4 T cells. *Annu Rev Immunol,* 19**,** 23-45.

JESSUP, J. M., BROWN, D., FITZGERALD, W., FORD, R. D., NACHMAN, A., GOODWIN, T. J. & SPAULDING, G. 1997. Induction of carcinoembryonic antigen expression in a three-dimensional culture system. *In Vitro Cell Dev Biol Anim,* 33**,** 352-7.

JORGENSEN, A., YOUNG, J., NIELSEN, J. E., JOENSEN, U. N., TOFT, B. G., RAJPERT-DE MEYTS, E. & LOVELAND, K. L. 2014. Hanging drop cultures of human testis and testis cancer samples: a model used to investigate activin treatment effects in a preserved niche. *Br J Cancer,* 110**,** 2604-14.

KALLANDER, C. F., SIMONSSON, B., HAGBERG, H. & GRONOWITZ, J. S. 1984. Serum deoxythymidine kinase gives prognostic information in chronic lymphocytic leukemia. *Cancer,* 54**,** 2450-5.

KALLURI, R. & ZEISBERG, M. 2006. Fibroblasts in cancer. *Nat Rev Cancer,* 6**,** 392-401.

KALOS, M., LEVINE, B. L., PORTER, D. L., KATZ, S., GRUPP, S. A., BAGG, A. & JUNE, C. H. 2011. T cells with chimeric antigen receptors have potent antitumor effects and can establish memory in patients with advanced leukemia. *Sci Transl Med,* 3**,** 95ra73.

KIDD, S., SPAETH, E., KLOPP, A., ANDREEFF, M., HALL, B. & MARINI, F. C. 2008. The (in) auspicious role of mesenchymal stromal cells in cancer: be it friend or foe. *Cytotherapy,* 10**,** 657-67.

KIM, D. H., HAAKE, A., SUN, Y., NEILD, A. P., IHM, J. E., DUAL, J., HUBBELL, J. A., JU, B. K. & NELSON, B. J. 2004. High-throughput cell manipulation using ultrasound fields. *Conf Proc IEEE Eng Med Biol Soc,* 4**,** 2571-4.

KIM, J. B. 2005. Three-dimensional tissue culture models in cancer biology. *Semin Cancer Biol,* 15**,** 365-77.

KIMLIN, L., KASSIS, J. & VIRADOR, V. 2013. 3D in vitro tissue models and their potential for drug screening. *Expert Opin Drug Discov,* 8**,** 1455-66.

KITADA, S., ZAPATA, J. M., ANDREEFF, M. & REED, J. C. 1999. Bryostatin and CD40-ligand enhance apoptosis resistance and induce expression of cell survival genes in B-cell chronic lymphocytic leukaemia. *Br J Haematol,* 106**,** 995-1004.

KLEIN, U., LIA, M., CRESPO, M., SIEGEL, R., SHEN, Q., MO, T., AMBESI-IMPIOMBATO, A., CALIFANO, A., MIGLIAZZA, A., BHAGAT, G. & DALLA-FAVERA, R. 2010. The DLEU2/miR-15a/16-1 cluster controls B cell proliferation and its deletion leads to chronic lymphocytic leukemia. *Cancer Cell,* 17**,** 28-40.

KLEIN, U., TU, Y., STOLOVITZKY, G. A., MATTIOLI, M., CATTORETTI, G., HUSSON, H., FREEDMAN, A., INGHIRAMI, G., CRO, L., BALDINI, L., NERI, A., CALIFANO, A. & DALLA-FAVERA, R. 2001. Gene expression profiling of B cell chronic lymphocytic leukemia reveals a homogeneous phenotype related to memory B cells. *J Exp Med,* 194**,** 1625-38.

KOECK, S., ZWIERZINA, M., LORENZ, E., GAMERITH, G., ZWIERZINA, H. & AMANN, A. 2015. Infiltration of immune cells into cancer cell/stroma cell 3D microtissues. *Journal for ImmunoTherapy of Cancer,* 3**,** P75.

KRAMER, R. H., BENSCH, K. G. & WONG, J. 1986. Invasion of reconstituted basement membrane matrix by metastatic human tumor cells. *Cancer Res,* 46**,** 1980-9.

KRYSOV, S., DIAS, S., PATERSON, A., MOCKRIDGE, C. I., POTTER, K. N., SMITH, K. A., ASHTON-KEY, M., STEVENSON, F. K. & PACKHAM, G. 2012. Surface IgM stimulation induces MEK1/2-dependent MYC expression in chronic lymphocytic leukemia cells. *Blood,* 119**,** 170-9.

KRYSOV, S., STEELE, A. J., COELHO, V., LINLEY, A., SANCHEZ HIDALGO, M., CARTER, M., POTTER, K. N., KENNEDY, B., DUNCOMBE, A. S., ASHTON-KEY, M., FORCONI, F., STEVENSON, F. K. & PACKHAM, G. 2014. Stimulation of surface IgM of chronic lymphocytic leukemia cells induces an unfolded protein response dependent on BTK and SYK. *Blood,* 124**,** 3101-9.

KULIS, M., HEATH, S., BIBIKOVA, M., QUEIROS, A. C., NAVARRO, A., CLOT, G., MARTINEZ-TRILLOS, A., CASTELLANO, G., BRUN-HEATH, I., PINYOL, M., BARBERAN-SOLER, S., PAPASAIKAS, P., JARES, P., BEA, S., RICO, D., ECKER, S., RUBIO, M., ROYO, R., HO, V., KLOTZLE, B., HERNANDEZ, L., CONDE, L., LOPEZ-GUERRA, M., COLOMER, D., VILLAMOR, N., AYMERICH, M., ROZMAN, M., BAYES, M., GUT, M., GELPI, J. L., OROZCO, M., FAN, J. B., QUESADA, V., PUENTE, X. S., PISANO, D. G., VALENCIA, A., LOPEZ-GUILLERMO, A., GUT, I., LOPEZ-OTIN, C., CAMPO, E. & MARTIN-SUBERO, J. I. 2012. Epigenomic analysis detects widespread gene-body DNA hypomethylation in chronic lymphocytic leukemia. *Nat Genet,* 44**,** 1236-42.

KURTOVA, A. V., BALAKRISHNAN, K., CHEN, R., DING, W., SCHNABL, S., QUIROGA, M. P., SIVINA, M., WIERDA, W. G., ESTROV, Z., KEATING, M. J., SHEHATA, M., JAGER, U., GANDHI, V., KAY, N. E., PLUNKETT, W. & BURGER, J. A. 2009. Diverse marrow stromal cells protect CLL cells from spontaneous and drug-induced apoptosis: development of a reliable and reproducible system to assess stromal cell adhesion-mediated drug resistance. *Blood,* 114**,** 4441-50.

LABARBERA, D. V., REID, B. G. & YOO, B. H. 2012. The multicellular tumor spheroid model for high-throughput cancer drug discovery. *Expert Opin Drug Discov,* 7**,** 819-30.

LAGNEAUX, L., DELFORGE, A., BRON, D., DE BRUYN, C. & STRYCKMANS, P. 1998. Chronic lymphocytic leukemic B cells but not normal B cells are rescued from apoptosis by contact with normal bone marrow stromal cells. *Blood,* 91**,** 2387-96.

LAGNEAUX, L., DELFORGE, A., DE BRUYN, C., BERNIER, M. & BRON, D. 1999. Adhesion to bone marrow stroma inhibits apoptosis of chronic lymphocytic leukemia cells. *Leuk Lymphoma,* 35**,** 445-53.

LEDBETTER, J. A., SHU, G., GALLAGHER, M. & CLARK, E. A. 1987. Augmentation of normal and malignant B cell proliferation by monoclonal antibody to the B cell-specific antigen BP50 (CDW40). *J Immunol,* 138**,** 788-94.

LEE, G. Y., KENNY, P. A., LEE, E. H. & BISSELL, M. J. 2007. Three-dimensional culture models of normal and malignant breast epithelial cells. *Nat Methods,* 4**,** 359-65.

LI, H., FAN, X. & HOUGHTON, J. 2007. Tumor microenvironment: The role of the tumor stroma in cancer. *Journal of Cellular Biochemistry,* 101**,** 805-815.

LI, Q., CHEN, C., KAPADIA, A., ZHOU, Q., HARPER, M. K., SCHAACK, J. & LABARBERA, D. V. 2011. 3D models of epithelial-mesenchymal transition in breast cancer metastasis: high-throughput screening assay development, validation, and pilot screen. *J Biomol Screen,* 16**,** 141-54.

LI, S., GLYNNE-JONES, P., ANDRIOTIS, O. G., CHING, K. Y., JONNALAGADDA, U. S., OREFFO, R. O., HILL, M. & TARE, R. S. 2014. Application of an acoustofluidic perfusion bioreactor for cartilage tissue engineering. *Lab Chip,* 14**,** 4475-85.

LIERKE, E. 1996. Acoustic levitation–a comprehensive survey of principles and applications. *Acta Acustica united with Acustica,* 82**,** 220-237.

LIN, S. M., DU, P., HUBER, W. & KIBBE, W. A. 2008. Model-based variance-stabilizing transformation for Illumina microarray data. *Nucleic Acids Res,* 36**,** e11.

LIU, F. T., JIA, L., WANG, P., WANG, H., FARREN, T. W. & AGRAWAL, S. G. 2016. STAT3 and NF-kappaB cooperatively control in vitro spontaneous apoptosis and poor chemo-responsiveness in patients with chronic lymphocytic leukemia. *Oncotarget*.

LIU, P. F., CAO, Y. W., ZHANG, S. D., ZHAO, Y., LIU, X. G., SHI, H. Q., HU, K. Y., ZHU, G. Q., MA, B. & NIU, H. T. 2015. A bladder cancer microenvironment simulation system based on a microfluidic co-culture model. *Oncotarget,* 6**,** 37695-705.

LOESSNER, D., STOK, K. S., LUTOLF, M. P., HUTMACHER, D. W., CLEMENTS, J. A. & RIZZI, S. C. 2010. Bioengineered 3D platform to explore cell-ECM interactions and drug resistance of epithelial ovarian cancer cells. *Biomaterials,* 31**,** 8494-506.

LOPEZ-GUERRA, M. & COLOMER, D. 2010. NF-kappaB as a therapeutic target in chronic lymphocytic leukemia. *Expert Opin Ther Targets,* 14**,** 275-88.

LOVAT, F., FASSAN, M., GASPARINI, P., RIZZOTTO, L., CASCIONE, L., PIZZI, M., VICENTINI, C., BALATTI, V., PALMIERI, D., COSTINEAN, S. & CROCE, C. M. 2015. miR-15b/16-2 deletion promotes B-cell malignancies. *Proc Natl Acad Sci U S A,* 112**,** 11636-41.

LUTZNY, G., KOCHER, T., SCHMIDT-SUPPRIAN, M., RUDELIUS, M., KLEIN-HITPASS, L., FINCH, A. J., DURIG, J., WAGNER, M., HAFERLACH, C., KOHLMANN, A., SCHNITTGER, S., SEIFERT, M., WANNINGER, S., ZABORSKY, N., OOSTENDORP, R., RULAND, J., LEITGES, M., KUHNT, T., SCHAFER, Y., LAMPL, B., PESCHEL, C., EGLE, A. & RINGSHAUSEN, I. 2013. Protein kinase c-beta-dependent activation of NF-kappaB in stromal cells is indispensable for the survival of chronic lymphocytic leukemia B cells in vivo. *Cancer Cell,* 23**,** 77-92.

MA, Q., JONES, D., BORGHESANI, P. R., SEGAL, R. A., NAGASAWA, T., KISHIMOTO, T., BRONSON, R. T. & SPRINGER, T. A. 1998. Impaired B-lymphopoiesis, myelopoiesis, and derailed cerebellar neuron migration in CXCR4- and SDF-1-deficient mice. *Proc Natl Acad Sci U S A,* 95**,** 9448-53.

MACEYKA, M. & SPIEGEL, S. 2014. Sphingolipid metabolites in inflammatory disease. *Nature,* 510**,** 58-67.

MACKAY, F., SCHNEIDER, P., RENNERT, P. & BROWNING, J. 2003. BAFF AND APRIL: a tutorial on B cell survival. *Annu Rev Immunol,* 21**,** 231-64.

MACKUS, W. J., FRAKKING, F. N., GRUMMELS, A., GAMADIA, L. E., DE BREE, G. J., HAMANN, D., VAN LIER, R. A. & VAN OERS, M. H. 2003. Expansion of CMV-specific CD8+CD45RA+CD27- T cells in B-cell chronic lymphocytic leukemia. *Blood,* 102**,** 1057-63.

MACLENNAN, I. C. 1994. Germinal centers. *Annu Rev Immunol,* 12**,** 117-39.

MAFFEI, R., BULGARELLI, J., FIORCARI, S., BERTONCELLI, L., MARTINELLI, S., GUARNOTTA, C., CASTELLI, I., DEAGLIO, S., DEBBIA, G., DE BIASI, S., BONACORSI, G., ZUCCHINI, P., NARNI, F., TRIPODO, C., LUPPI, M., COSSARIZZA, A. & MARASCA, R. 2013. The monocytic population in chronic lymphocytic leukemia shows altered composition and deregulation of genes involved in phagocytosis and inflammation. *Haematologica,* 98**,** 1115-1123.

MAJID, A., LIN, T. T., BEST, G., FISHLOCK, K., HEWAMANA, S., PRATT, G., YALLOP, D., BUGGINS, A. G., WAGNER, S., KENNEDY, B. J., MIALL, F., HILLS, R., DEVEREUX, S., OSCIER, D. G., DYER, M. J., FEGAN, C. & PEPPER, C. 2011. CD49d is an independent prognostic marker that is associated with CXCR4 expression in CLL. *Leuk Res,* 35**,** 750-6.

MALEK, S. 2013. Molecular Biomarkers in Chronic Lymphocytic Leukemia. *In:* MALEK, S. (ed.) *Advances in Chronic Lymphocytic Leukemia.* Springer New York.

MARASCA, R., MAFFEI, R., MARTINELLI, S., FIORCARI, S., BULGARELLI, J., DEBBIA, G., ROSSI, D., ROSSI, F. M., RIGOLIN, G. M., MARTINELLI, S., GATTEI, V., DEL POETA, G., LAURENTI, L., FORCONI, F., MONTILLO, M., GAIDANO, G. & LUPPI, M. 2013. Clinical heterogeneity of de novo 11q deletion chronic lymphocytic leukaemia: prognostic relevance of extent of 11q deleted nuclei inside leukemic clone. *Hematological Oncology,* 31**,** 88-95.

MATRAI, Z. 2001. CD38 expression and Ig VH gene mutation in B-cell chronic lymphocytic leukemia. *Blood,* 97**,** 1902-1902.

MELLADO, M., RODRIGUEZ-FRADE, J. M., MANES, S. & MARTINEZ, A. C. 2001. Chemokine signaling and functional responses: the role of receptor dimerization and TK pathway activation. *Annu Rev Immunol,* 19**,** 397-421.

MESSMER, B. T., MESSMER, D., ALLEN, S. L., KOLITZ, J. E., KUDALKAR, P., CESAR, D., MURPHY, E. J., KODURU, P., FERRARINI, M., ZUPO, S., CUTRONA, G., DAMLE, R. N., WASIL, T., RAI, K. R., HELLERSTEIN, M. K. & CHIORAZZI, N. 2005. In vivo measurements document the dynamic cellular kinetics of chronic lymphocytic leukemia B cells. *Journal of Clinical Investigation,* 115**,** 755-764.

MILLER, M. W., MILLER, D. L. & BRAYMAN, A. A. 1996. A review of in vitro bioeffects of inertial ultrasonic cavitation from a mechanistic perspective. *Ultrasound Med Biol,* 22**,** 1131-54.

MIYAKE, K., WEISSMAN, I. L., GREENBERGER, J. S. & KINCADE, P. W. 1991. Evidence for a role of the integrin VLA-4 in lympho-hemopoiesis. *J Exp Med,* 173**,** 599-607.

MIYASAKA, M. & TANAKA, T. 2004. Lymphocyte trafficking across high endothelial venules: dogmas and enigmas. *Nat Rev Immunol,* 4**,** 360-370.

MOCKRIDGE, C. I., POTTER, K. N., WHEATLEY, I., NEVILLE, L. A., PACKHAM, G. & STEVENSON, F. K. 2007. Reversible anergy of sIgM-mediated signaling in the two subsets of CLL defined by VH-gene mutational status. *Blood,* 109**,** 4424-31.

MOHLE, R., FAILENSCHMID, C., BAUTZ, F. & KANZ, L. 1999. Overexpression of the chemokine receptor CXCR4 in B cell chronic lymphocytic leukemia is associated with increased functional response to stromal cell-derived factor-1 (SDF-1). *Leukemia,* 13**,** 1954-9.

MONSERRAT, J., SANCHEZ, M. A., DE PAZ, R., DIAZ, D., MUR, S., REYES, E., PRIETO, A., DE LA HERA, A., MARTINEZ, A. C. & ALVAREZ-MON, M. 2014. Distinctive patterns of naive/memory subset distribution and cytokine expression in CD4 T lymphocytes in ZAP-70 B-chronic lymphocytic patients. *Cytometry B Clin Cytom,* 86**,** 32-43.

MOSKOVITS, N., KALINKOVICH, A., BAR, J., LAPIDOT, T. & OREN, M. 2006. p53 Attenuates cancer cell migration and invasion through repression of SDF-1/CXCL12 expression in stromal fibroblasts. *Cancer Res,* 66**,** 10671-6.

MOUTASIM, K. A., MIRZA, D., MARSH, D., JENEI, V., DICKINSON, S., TILAKARATNE, W. & THOMAS, G. J. 2009. Integrin αvβ6 promotes TGF-β1-dependent myofibroblastic transdifferentiation in oral submucous fibrosis. *Head & Neck Oncology,* 1**,** 1.

MUELLER, S. N. & GERMAIN, R. N. 2009. Stromal cell contributions to the homeostasis and functionality of the immune system. *Nat Rev Immunol,* 9**,** 618-629.

MÜLLER, H., TAKESHITA, M., KRAUSE, J., SCHUSTER, K., KIKUCHI, M. & STUTTE, H. 1991. [Immunohistochemical in situ demonstration of cytokines in Hodgkin and non-Hodgkin lymphoma]. *Verhandlungen der Deutschen Gesellschaft fur Pathologie,* 7**6,** 164-168.

MUNK PEDERSEN, I. & REED, J. 2004. Microenvironmental interactions and survival of CLL B-cells. *Leuk Lymphoma,* 45**,** 2365-72.

NAGASAWA, T. 2006. Microenvironmental niches in the bone marrow required for B-cell development. *Nat Rev Immunol,* 6**,** 107-16.

NAGASAWA, T., KIKUTANI, H. & KISHIMOTO, T. 1994. Molecular cloning and structure of a pre-B-cell growth-stimulating factor. *Proceedings of the National Academy of Sciences of the United States of America,* 91**,** 2305-2309.

NAGIRA, M., IMAI, T., YOSHIDA, R., TAKAGI, S., IWASAKI, M., BABA, M., TABIRA, Y., AKAGI, J., NOMIYAMA, H. & YOSHIE, O. 1998. A lymphocyte-specific CC chemokine, secondary lymphoid tissue chemokine (SLC), is a highly efficient chemoattractant for B cells and activated T cells. *Eur J Immunol,* 28**,** 1516-23.

NAKAO, M., ISHII, G., NAGAI, K., KAWASE, A., KENMOTSU, H., KON-NO, H., HISHIDA, T., NISHIMURA, M., YOSHIDA, J. & OCHIAI, A. 2009. Prognostic significance of carbonic anhydrase IX expression by cancer-associated fibroblasts in lung adenocarcinoma. *Cancer,* 115**,** 2732-2743.

NG, K. Y. & LIU, Y. 2002. Therapeutic ultrasound: its application in drug delivery. *Med Res Rev,* 22**,** 204-23.

NIEMANN, C. U., HERMAN, S. E., MARIC, I., GOMEZ-RODRIGUEZ, J., BIANCOTTO, A., CHANG, B. Y., MARTYR, S., STETLER-STEVENSON, M., YUAN, C. M., CALVO, K. R., BRAYLAN, R. C., VALDEZ, J., LEE, Y. S., WONG, D. H., JONES, J., SUN, C., MARTI, G. E., FAROOQUI, M. Z. & WIESTNER, A. 2016. Disruption of in vivo Chronic Lymphocytic Leukemia Tumor-Microenvironment Interactions by Ibrutinib - Findings from an Investigator-Initiated Phase II Study. *Clin Cancer Res,* 22**,** 1572-82.

NILSSON, J., EVANDER, M., HAMMARSTRÖM, B. & LAURELL, T. 2009. Review of cell and particle trapping in microfluidic systems. *Analytica Chimica Acta,* 649**,** 141-157.

NISHIO, M., ENDO, T., TSUKADA, N., OHATA, J., KITADA, S., REED, J. C., ZVAIFLER, N. J. & KIPPS, T. J. 2005. Nurselike cells express BAFF and APRIL, which can promote survival of chronic lymphocytic leukemia cells via a paracrine pathway distinct from that of SDF-1alpha. *Blood,* 106**,** 1012-20.

NUNES, C., WONG, R., MASON, M., FEGAN, C., MAN, S. & PEPPER, C. 2012. Expansion of a CD8(+)PD-1(+) replicative senescence phenotype in early stage CLL patients is associated with inverted CD4:CD8 ratios and disease progression. *Clin Cancer Res,* 18**,** 678-87.

OLUMI, A. F., GROSSFELD, G. D., HAYWARD, S. W., CARROLL, P. R., TLSTY, T. D. & CUNHA, G. R. 1999. Carcinoma-associated fibroblasts direct tumor progression of initiated human prostatic epithelium. *Cancer Res,* 59**,** 5002-11.

OSCIER, D. G., GARDINER, A. C., MOULD, S. J., GLIDE, S., DAVIS, Z. A., IBBOTSON, R. E., CORCORAN, M. M., CHAPMAN, R. M., THOMAS, P. W. & COPPLESTONE, J. A. 2002. Multivariate analysis of prognostic factors in CLL: clinical stage, IGVH gene mutational status, and loss or mutation of the p53 gene are independent prognostic factors. *Blood,* 100**,** 1177-1184.

OUWEHAND, K., SANTEGOETS, S. J., BRUYNZEEL, D. P., SCHEPER, R. J., DE GRUIJL, T. D. & GIBBS, S. 2008. CXCL12 is essential for migration of activated Langerhans cells from epidermis to dermis. *Eur J Immunol,* 38**,** 3050-9.

PACKHAM, G., KRYSOV, S., ALLEN, A., SAVELYEVA, N., STEELE, A. J., FORCONI, F. & STEVENSON, F. K. 2014. The outcome of B-cell receptor signaling in chronic lymphocytic leukemia: proliferation or anergy. *Haematologica,* 99**,** 1138-48.

PACKHAM, G. & STEVENSON, F. 2010. The role of the B-cell receptor in the pathogenesis of chronic lymphocytic leukaemia. *Semin Cancer Biol,* 20**,** 391-9.

PAGGETTI, J., HADERK, F., SEIFFERT, M., JANJI, B., DISTLER, U., AMMERLAAN, W., KIM, Y. J., ADAM, J., LICHTER, P., SOLARY, E., BERCHEM, G. & MOUSSAY, E. 2015. Exosomes released by chronic lymphocytic leukemia cells induce the transition of stromal cells into cancer-associated fibroblasts. *Blood,* 126**,** 1106-17.

PALMA, M., GENTILCORE, G., HEIMERSSON, K., MOZAFFARI, F., NÄSMAN-GLASER, B., YOUNG, E., ROSENQUIST, R., HANSSON, L., ÖSTERBORG, A. & MELLSTEDT, H. 2016. T cells in chronic lymphocytic leukemia display dysregulated expression of immune checkpoints and activation markers. *Haematologica*.

PAN, Z., SCHEERENS, H., LI, S. J., SCHULTZ, B. E., SPRENGELER, P. A., BURRILL, L. C., MENDONCA, R. V., SWEENEY, M. D., SCOTT, K. C., GROTHAUS, P. G., JEFFERY, D. A., SPOERKE, J. M., HONIGBERG, L. A., YOUNG, P. R., DALRYMPLE, S. A. & PALMER, J. T. 2007. Discovery of selective irreversible inhibitors for Bruton's tyrosine kinase. *ChemMedChem,* 2**,** 58-61.

PANAYIOTIDIS, P., JONES, D., GANESHAGURU, K., FORONI, L. & HOFFBRAND, A. V. 1996. Human bone marrow stromal cells prevent apoptosis and support the survival of chronic lymphocytic leukaemia cells in vitro. *Br J Haematol,* 92**,** 97-103.

PARKER, H., ROSE-ZERILLI, M. J., PARKER, A., CHAPLIN, T., WADE, R., GARDINER, A., GRIFFITHS, M., COLLINS, A., YOUNG, B. D., OSCIER, D. G. & STREFFORD, J. C. 2011. 13q deletion anatomy and disease progression in patients with chronic lymphocytic leukemia. *Leukemia,* 25**,** 489-97.

PATERSON, A., MOCKRIDGE, C. I., ADAMS, J. E., KRYSOV, S., POTTER, K. N., DUNCOMBE, A. S., COOK, S. J., STEVENSON, F. K. & PACKHAM, G. 2012. Mechanisms and clinical significance of BIM phosphorylation in chronic lymphocytic leukemia. *Blood,* 119**,** 1726-36.

PATTEN, P. E., BUGGINS, A. G., RICHARDS, J., WOTHERSPOON, A., SALISBURY, J., MUFTI, G. J., HAMBLIN, T. J. & DEVEREUX, S. 2008. CD38 expression in chronic lymphocytic leukemia is regulated by the tumor microenvironment. *Blood,* 111**,** 5173-81.

PAULSSON, J. & MICKE, P. 2014. Prognostic relevance of cancer-associated fibroblasts in human cancer. *Semin Cancer Biol,* 25**,** 61-8.

PEDE, V., ROMBOUT, A., VERMEIRE, J., NAESSENS, E., MESTDAGH, P., ROBBERECHT, N., VANDERSTRAETEN, H., VAN ROY, N., VANDESOMPELE, J., SPELEMAN, F., PHILIPPE, J. & VERHASSELT, B. 2013. CLL cells respond to B-Cell receptor stimulation with a microRNA/mRNA signature associated with MYC activation and cell cycle progression. *PLoS One,* 8**,** e60275.

PEDERSEN, I. M., KITADA, S., LEONI, L. M., ZAPATA, J. M., KARRAS, J. G., TSUKADA, N., KIPPS, T. J., CHOI, Y. S., BENNETT, F. & REED, J. C. 2002. Protection of CLL B cells by a follicular dendritic cell line is dependent on induction of Mcl-1. *Blood,* 100**,** 1795-801.

PELED, A., PETIT, I., KOLLET, O., MAGID, M., PONOMARYOV, T., BYK, T., NAGLER, A., BEN-HUR, H., MANY, A., SHULTZ, L., LIDER, O., ALON, R., ZIPORI, D. & LAPIDOT, T. 1999. Dependence of human stem cell engraftment and repopulation of NOD/SCID mice on CXCR4. *Science,* 283**,** 845-8.

PEPPER, C., BUGGINS, A. G. S., JONES, C. H., WALSBY, E. J., FORCONI, F., PRATT, G., DEVEREUX, S., STEVENSON, F. K. & FEGAN, C. 2015. Phenotypic heterogeneity in IGHV-mutated CLL patients has prognostic impact and identifies a subset with increased sensitivity to BTK and PI3K[delta] inhibition. *Leukemia,* 29**,** 744-747.

PERBELLINI, O., CIOFFI, F., MALPELI, G., ZANOLIN, E., LOVATO, O., SCARPA, A., PIZZOLO, G. & SCUPOLI, M. T. 2015. Up-regulation of CXCL8/interleukin-8 production in response to CXCL12 in chronic lymphocytic leukemia. *Leuk Lymphoma,* 56**,** 1897-900.

PETERSEN, O. W., RØNNOV-JESSEN, L., HOWLETT, A. R. & BISSELL, M. J. 1992. Interaction with basement membrane serves to rapidly distinguish growth and differentiation pattern of normal and malignant human breast epithelial cells. *Proceedings of the National Academy of Sciences of the United States of America,* 89**,** 9064-9068.

PETLICKOVSKI, A., LAURENTI, L., LI, X., MARIETTI, S., CHIUSOLO, P., SICA, S., LEONE, G. & EFREMOV, D. G. 2005. Sustained signaling through the B-cell receptor induces Mcl-1 and promotes survival of chronic lymphocytic leukemia B cells. *Blood,* 105**,** 4820-7.

PETTY, J. M., SUEBLINVONG, V., LENOX, C. C., JONES, C. C., COSGROVE, G. P., COOL, C. D., RAI, P. R., BROWN, K. K., WEISS, D. J., POYNTER, M. E. & SURATT, B. T. 2007. Pulmonary stromal-derived factor-1 expression and effect on neutrophil recruitment during acute lung injury. *J Immunol,* 178**,** 8148-57.

PHILLIPS, J. A., MEHTA, K., FERNANDEZ, C. & RAVECHE, E. S. 1992. The NZB mouse as a model for chronic lymphocytic leukemia. *Cancer Res,* 52**,** 437-43.

PITTENGER, M. F., MACKAY, A. M., BECK, S. C., JAISWAL, R. K., DOUGLAS, R., MOSCA, J. D., MOORMAN, M. A., SIMONETTI, D. W., CRAIG, S. & MARSHAK, D. R. 1999. Multilineage potential of adult human mesenchymal stem cells. *Science,* 284**,** 143-7.

PLANDER, M., SEEGERS, S., UGOCSAI, P., DIERMEIER-DAUCHER, S., IVANYI, J., SCHMITZ, G., HOFSTADTER, F., SCHWARZ, S., ORSO, E., KNUCHEL, R. & BROCKHOFF, G. 2009. Different proliferative and survival capacity of CLL-cells in a newly established in vitro model for pseudofollicles. *Leukemia,* 23**,** 2118-28.

PONADER, S., CHEN, S. S., BUGGY, J. J., BALAKRISHNAN, K., GANDHI, V., WIERDA, W. G., KEATING, M. J., O'BRIEN, S., CHIORAZZI, N. & BURGER, J. A. 2012. The

Bruton tyrosine kinase inhibitor PCI-32765 thwarts chronic lymphocytic leukemia cell survival and tissue homing in vitro and in vivo. *Blood,* 119**,** 1182-9.

PORTER, D. L., HWANG, W. T., FREY, N. V., LACEY, S. F., SHAW, P. A., LOREN, A. W., BAGG, A., MARCUCCI, K. T., SHEN, A., GONZALEZ, V., AMBROSE, D., GRUPP, S. A., CHEW, A., ZHENG, Z., MILONE, M. C., LEVINE, B. L., MELENHORST, J. J. & JUNE, C. H. 2015. Chimeric antigen receptor T cells persist and induce sustained remissions in relapsed refractory chronic lymphocytic leukemia. *Sci Transl Med,* 7**,** 303ra139.

POURGHEYSARI, B., BRUTON, R., PARRY, H., BILLINGHAM, L., FEGAN, C., MURRAY, J. & MOSS, P. 2010. The number of cytomegalovirus-specific CD4+ T cells is markedly expanded in patients with B-cell chronic lymphocytic leukemia and determines the total CD4+ T-cell repertoire. *Blood,* 116**,** 2968-74.

PUIGGROS, A., PUIGDECANET, E., SALIDO, M., FERRER, A., ABELLA, E., GIMENO, E., NONELL, L., HERRANZ, M. J., GALVAN, A. B., RODRIGUEZ-RIVERA, M., MELERO, C., PAIRET, S., BELLOSILLO, B., SERRANO, S., FLORENSA, L., SOLE, F. & ESPINET, B. 2013. Genomic arrays in chronic lymphocytic leukemia routine clinical practice: are we ready to substitute conventional cytogenetics and fluorescence in situ hybridization techniques? *Leuk Lymphoma,* 54**,** 986-95.

PURROY, N., ABRISQUETA, P., CARABIA, J., CARPIO, C., CALPE, E., PALACIO, C., CASTELLVI, J., CRESPO, M. & BOSCH, F. 2014. Targeting the proliferative and chemoresistant compartment in chronic lymphocytic leukemia by inhibiting survivin protein. *Leukemia,* 28**,** 1993-2004.

QUEIROS, A. C., VILLAMOR, N., CLOT, G., MARTINEZ-TRILLOS, A., KULIS, M., NAVARRO, A., PENAS, E. M., JAYNE, S., MAJID, A., RICHTER, J., BERGMANN, A. K., KOLAROVA, J., ROYO, C., RUSSINOL, N., CASTELLANO, G., PINYOL, M., BEA, S., SALAVERRIA, I., LOPEZ-GUERRA, M., COLOMER, D., AYMERICH, M., ROZMAN, M., DELGADO, J., GINE, E., GONZALEZ-DIAZ, M., PUENTE, X. S., SIEBERT, R., DYER, M. J., LOPEZ-OTIN, C., ROZMAN, C., CAMPO, E., LOPEZ-GUILLERMO, A. & MARTIN-SUBERO, J. I. 2015. A B-cell epigenetic signature defines three biologic subgroups of chronic lymphocytic leukemia with clinical impact. *Leukemia,* 29**,** 598-605.

QUIROGA, M. P., BALAKRISHNAN, K., KURTOVA, A. V., SIVINA, M., KEATING, M. J., WIERDA, W. G., GANDHI, V. & BURGER, J. A. 2009. B-cell antigen receptor signaling enhances chronic lymphocytic leukemia cell migration and survival: specific targeting with a novel spleen tyrosine kinase inhibitor, R406. *Blood,* 114**,** 1029-37.

QUIROGA, M. P. & BURGER, J. A. 2010. BCR-Mediated Decrease of CXCR4 and CD62L in CLL – Letter. *Cancer Research,* 70**,** 5194.

RAI, K. R., SAWITSKY, A., CRONKITE, E. P., CHANANA, A. D., LEVY, R. N. & PASTERNACK, B. S. 1975. Clinical staging of chronic lymphocytic leukemia. *Blood,* 46**,** 219-34.

RAMSAY, A. G., JOHNSON, A. J., LEE, A. M., GORGUN, G., LE DIEU, R., BLUM, W., BYRD, J. C. & GRIBBEN, J. G. 2008. Chronic lymphocytic leukemia T cells show impaired immunological synapse formation that can be reversed with an immunomodulating drug. *J Clin Invest,* 118**,** 2427-37.

RATAJCZAK, M. Z., ZUBA-SURMA, E., KUCIA, M., RECA, R., WOJAKOWSKI, W. & RATAJCZAK, J. 2006. The pleiotropic effects of the SDF-1-CXCR4 axis in organogenesis, regeneration and tumorigenesis. *Leukemia,* 20**,** 1915-24.

RAVECHE, E. S., SALERNO, E., SCAGLIONE, B. J., MANOHAR, V., ABBASI, F., LIN, Y. C., FREDRICKSON, T., LANDGRAF, P., RAMACHANDRA, S., HUPPI, K., TORO, J. R., ZENGER, V. E., METCALF, R. A. & MARTI, G. E. 2007. Abnormal microRNA-16 locus with synteny to human 13q14 linked to CLL in NZB mice. *Blood,* 109**,** 5079-86.

REIF, K., EKLAND, E. H., OHL, L., NAKANO, H., LIPP, M., FORSTER, R. & CYSTER, J. G. 2002. Balanced responsiveness to chemoattractants from adjacent zones determines B-cell position. *Nature,* 416**,** 94-9.

REITTIE, J. E., YONG, K. L., PANAYIOTIDIS, P. & HOFFBRAND, A. V. 1996. Interleukin-6 inhibits apoptosis and tumour necrosis factor induced proliferation of B-chronic lymphocytic leukaemia. *Leuk Lymphoma,* 22**,** 83-90, follow. 186, color plate VI.

RICHARDSON, S. J., MATTHEWS, C., CATHERWOOD, M. A., ALEXANDER, H. D., CAREY, B. S., FARRUGIA, J., GARDINER, A., MOULD, S., OSCIER, D., COPPLESTONE, J. A. & PRENTICE, A. G. 2006. ZAP-70 expression is associated with enhanced ability to respond to migratory and survival signals in B-cell chronic lymphocytic leukemia (B-CLL). *Blood,* 107**,** 3584-92.

RONNOV-JESSEN, L. & PETERSEN, O. W. 1993. Induction of alpha-smooth muscle actin by transforming growth factor-beta 1 in quiescent human breast gland fibroblasts. Implications for myofibroblast generation in breast neoplasia. *Lab Invest,* 68**,** 696-707.

ROSENWALD, A., ALIZADEH, A. A., WIDHOPF, G., SIMON, R., DAVIS, R. E., YU, X., YANG, L., PICKERAL, O. K., RASSENTI, L. Z., POWELL, J., BOTSTEIN, D., BYRD, J. C., GREVER, M. R., CHESON, B. D., CHIORAZZI, N., WILSON, W. H., KIPPS, T. J., BROWN, P. O. & STAUDT, L. M. 2001. Relation of gene expression phenotype to immunoglobulin mutation genotype in B cell chronic lymphocytic leukemia. *J Exp Med,* 194**,** 1639-47.

ROSSI, D., RASI, S., FABBRI, G., SPINA, V., FANGAZIO, M., FORCONI, F., MARASCA, R., LAURENTI, L., BRUSCAGGIN, A., CERRI, M., MONTI, S., CRESTA, S., FAMA, R., DE PAOLI, L., BULIAN, P., GATTEI, V., GUARINI, A., DEAGLIO, S., CAPELLO, D., RABADAN, R., PASQUALUCCI, L., DALLA-FAVERA, R., FOA, R. & GAIDANO, G. 2012. Mutations of NOTCH1 are an independent predictor of survival in chronic lymphocytic leukemia. *Blood,* 119**,** 521-9.

ROSSI, D., RASI, S., SPINA, V., BRUSCAGGIN, A., MONTI, S., CIARDULLO, C., DEAMBROGI, C., KHIABANIAN, H., SERRA, R., BERTONI, F., FORCONI, F., LAURENTI, L., MARASCA, R., DAL-BO, M., ROSSI, F. M., BULIAN, P., NOMDEDEU, J., DEL POETA, G., GATTEI, V., PASQUALUCCI, L., RABADAN, R., FOA, R., DALLA-FAVERA, R. & GAIDANO, G. 2013. Integrated mutational and cytogenetic analysis identifies new prognostic subgroups in chronic lymphocytic leukemia. *Blood,* 121**,** 1403-12.

ROSSI, D., ZUCCHETTO, A., ROSSI, F. M., CAPELLO, D., CERRI, M., DEAMBROGI, C., CRESTA, S., RASI, S., DE PAOLI, L., BODONI, C. L., BULIAN, P., DEL POETA, G., LADETTO, M., GATTEI, V. & GAIDANO, G. 2008. CD49d expression is an independent risk factor of progressive disease in early stage chronic lymphocytic leukemia. *Haematologica,* 93**,** 1575-1579.

ROSSMANN, E. D., LEWIN, N., JEDDI-TEHRANI, M., OSTERBORG, A. & MELLSTEDT, H. 2002. Intracellular T cell cytokines in patients with B cell chronic lymphocytic leukaemia (B-CLL). *Eur J Haematol,* 68**,** 299-306.

RÖTH, A., DE BEER, D., NÜCKEL, H., SELLMANN, L., DÜHRSEN, U., DÜRIG, J. & BAERLOCHER, G. M. 2008. Significantly shorter telomeres in T-cells of patients

with ZAP-70+/CD38+ chronic lymphocytic leukaemia. *British Journal of Haematology,* 143**,** 383-386.

ROZMAN, C. & MONTSERRAT, E. 1995. Chronic lymphocytic leukemia. *N Engl J Med,* 333**,** 1052-7.

SAINZ-PEREZ, A., GARY-GOUY, H., GAUDIN, F., MAAROF, G., MARFAING-KOKA, A., DE REVEL, T. & DALLOUL, A. 2008. IL-24 induces apoptosis of chronic lymphocytic leukemia B cells engaged into the cell cycle through dephosphorylation of STAT3 and stabilization of p53 expression. *The Journal of Immunology,* 181**,** 6051-6060.

SAINZ-PEREZ, A., GARY-GOUY, H., PORTIER, A., DAVI, F., MERLE-BERAL, H., GALANAUD, P. & DALLOUL, A. 2006. High Mda-7 expression promotes malignant cell survival and p38 MAP kinase activation in chronic lymphocytic leukemia. *Leukemia,* 20**,** 498-504.

SALVUCCI, O., YAO, L., VILLALBA, S., SAJEWICZ, A., PITTALUGA, S. & TOSATO, G. 2002. Regulation of endothelial cell branching morphogenesis by endogenous chemokine stromal-derived factor-1. *Blood,* 99**,** 2703-2711.

SCHICHOR, C., BIRNBAUM, T., ETMINAN, N., SCHNELL, O., GRAU, S., MIEBACH, S., ABOODY, K., PADOVAN, C., STRAUBE, A., TONN, J. C. & GOLDBRUNNER, R. 2006. Vascular endothelial growth factor A contributes to glioma-induced migration of human marrow stromal cells (hMSC). *Exp Neurol,* 199**,** 301-10.

SCHMID, C. & ISAACSON, P. G. 1994. Proliferation centres in B-cell malignant lymphoma, lymphocytic (B-CLL): an immunophenotypic study. *Histopathology,* 24**,** 445-51.

SCHROEDER, H. W., JR. & DIGHIERO, G. 1994. The pathogenesis of chronic lymphocytic leukemia: analysis of the antibody repertoire. *Immunol Today,* 15**,** 288-94.

SCHULZ, A., TOEDT, G., ZENZ, T., STILGENBAUER, S., LICHTER, P. & SEIFFERT, M. 2011. Inflammatory cytokines and signaling pathways are associated with survival of primary chronic lymphocytic leukemia cells in vitro: a dominant role of CCL2. *Haematologica,* 96**,** 408-16.

SEREBRIISKII, I., CASTELLO-CROS, R., LAMB, A., GOLEMIS, E. A. & CUKIERMAN, E. 2008. Fibroblast-derived 3D matrix differentially regulates the growth and drug-responsiveness of human cancer cells. *Matrix Biol,* 27**,** 573-85.

SERINI, G., BOCHATON-PIALLAT, M.-L., ROPRAZ, P., GEINOZ, A., BORSI, L., ZARDI, L. & GABBIANI, G. 1998. The Fibronectin Domain ED-A Is Crucial for Myofibroblastic Phenotype Induction by Transforming Growth Factor-β1. *The Journal of Cell Biology,* 142**,** 873-881.

SERRANO, D., MONTEIRO, J., ALLEN, S. L., KOLITZ, J., SCHULMAN, P., LICHTMAN, S. M., BUCHBINDER, A., VINCIGUERRA, V. P., CHIORAZZI, N. & GREGERSEN, P. K. 1997. Clonal expansion within the CD4+CD57+ and CD8+CD57+ T cell subsets in chronic lymphocytic leukemia. *J Immunol,* 158**,** 1482-9.

SEYMOUR, J. F., GERECITANO, J. F., KAHL, B. S., PAGEL, J. M., WIERDA, W. G., ANDERSON, M.-A., RUDERSDORF, N. K., GRESSICK, L. A., MONTALVO, N. P., YANG, J., BUSMAN, T. A., DUNBAR, M., CERRI, E., ENSCHEDE, S. H., HUMERICKHOUSE, R. A. & ROBERTS, A. W. 2013. The Single-Agent Bcl-2 Inhibitor ABT-199 (GDC-0199) In Patients With Relapsed/Refractory (R/R) Non-

Hodgkin Lymphoma (NHL): Responses Observed In All Mantle Cell Lymphoma (MCL) Patients. *Blood,* 122**,** 1789-1789.

SHAIN, K. H., DALTON, W. S. & TAO, J. 2015. The tumor microenvironment shapes hallmarks of mature B-cell malignancies. *Oncogene,* 34**,** 4673-4682.

SHANAFELT, T. D., GEYER, S. M., BONE, N. D., TSCHUMPER, R. C., WITZIG, T. E., NOWAKOWSKI, G. S., ZENT, C. S., CALL, T. G., LAPLANT, B., DEWALD, G. W., JELINEK, D. F. & KAY, N. E. 2008. CD49d expression is an independent predictor of overall survival in patients with chronic lymphocytic leukaemia: a prognostic parameter with therapeutic potential. *Br J Haematol,* 140**,** 537-46.

SHARMAN, J., HAWKINS, M., KOLIBABA, K., BOXER, M., KLEIN, L., WU, M., HU, J., ABELLA, S. & YASENCHAK, C. 2015. An open-label phase 2 trial of entospletinib (GS-9973), a selective spleen tyrosine kinase inhibitor, in chronic lymphocytic leukemia. *Blood,* 125**,** 2336-43.

SHI, J., AHMED, D., MAO, X., LIN, S. C., LAWIT, A. & HUANG, T. J. 2009. Acoustic tweezers: patterning cells and microparticles using standing surface acoustic waves (SSAW). *Lab Chip,* 9**,** 2890-5.

SINGH, M., CLOSE, D. A., MUKUNDAN, S., JOHNSTON, P. A. & SANT, S. 2015. Production of Uniform 3D Microtumors in Hydrogel Microwell Arrays for Measurement of Viability, Morphology, and Signaling Pathway Activation. *Assay Drug Dev Technol,* 13**,** 570-83.

SISON, E. A., MAGOON, D., LI, L., ANNESLEY, C. E., RAU, R. E., SMALL, D. & BROWN, P. 2014. Plerixafor as a chemosensitizing agent in pediatric acute lymphoblastic leukemia: efficacy and potential mechanisms of resistance to CXCR4 inhibition. *Oncotarget,* 5**,** 8947-58.

SIVINA, M., HARTMANN, E., KIPPS, T. J., RASSENTI, L., KRUPNIK, D., LERNER, S., LAPUSHIN, R., XIAO, L., HUANG, X., WERNER, L., NEUBERG, D., KANTARJIAN, H., O'BRIEN, S., WIERDA, W. G., KEATING, M. J., ROSENWALD, A. & BURGER, J. A. 2011. CCL3 (MIP-1alpha) plasma levels and the risk for disease progression in chronic lymphocytic leukemia. *Blood,* 117**,** 1662-9.

SMALLWOOD, D. T., APOLLONIO, B., WILLIMOTT, S., LEZINA, L., ALHARTHI, A., AMBROSE, A. R., DE ROSSI, G., RAMSAY, A. G. & WAGNER, S. D. 2016. Extracellular vesicles released by CD40/IL-4-stimulated CLL cells confer altered functional properties to CD4+ T cells. *Blood,* 128**,** 542-52.

SMYTH, G. K. 2004. Linear models and empirical bayes methods for assessing differential expression in microarray experiments. *Stat Appl Genet Mol Biol,* 3**,** Article3.

SORRENTINO, A., FERRACIN, M., CASTELLI, G., BIFFONI, M., TOMASELLI, G., BAIOCCHI, M., FATICA, A., NEGRINI, M., PESCHLE, C. & VALTIERI, M. 2008. Isolation and characterization of CD146+ multipotent mesenchymal stromal cells. *Experimental hematology,* 36**,** 1035-1046.

SOTIROPOULOU, P. A. & PAPAMICHAIL, M. 2007. Immune properties of mesenchymal stem cells. *Methods Mol Biol,* 407**,** 225-43.

SPAARGAREN, M., BEULING, E. A., RURUP, M. L., MEIJER, H. P., KLOK, M. D., MIDDENDORP, S., HENDRIKS, R. W. & PALS, S. T. 2003. The B cell antigen receptor controls integrin activity through Btk and PLCgamma2. *J Exp Med,* 198**,** 1539-50.

SPAETH, E., KLOPP, A., DEMBINSKI, J., ANDREEFF, M. & MARINI, F. 2008. Inflammation and tumor microenvironments: defining the migratory itinerary of mesenchymal stem cells. *Gene Ther,* 15**,** 730-8.

SPENGLER, J., COAKLEY, W. & CHRISTENSEN, K. 2003. Microstreaming effects on particle concentration in an ultrasonic standing wave. *AIChE journal,* 49**,** 2773-2782.

SPENGLER, J. F., JEKEL, M., CHRISTENSEN, K. T., ADRIAN, R. J., HAWKES, J. J. & COAKLEY, W. T. 2000. Observation of yeast cell movement and aggregation in a small-scale MHz-ultrasonic standing wave field. *Bioseparation,* 9**,** 329-41.

STAMATOPOULOS, B., MEULEMAN, N., DE BRUYN, C., PIETERS, K., MINEUR, P., LE ROY, C., SAINT-GEORGES, S., VARIN-BLANK, N., CYMBALISTA, F., BRON, D. & LAGNEAUX, L. 2012. AMD3100 disrupts the cross-talk between chronic lymphocytic leukemia cells and a mesenchymal stromal or nurse-like cell-based microenvironment: pre-clinical evidence for its association with chronic lymphocytic leukemia treatments. *Haematologica,* 97**,** 608-15.

STEVENSON, F. K. & CALIGARIS-CAPPIO, F. 2004. Chronic lymphocytic leukemia: revelations from the B-cell receptor. *Blood,* 103**,** 4389-95.

STEVENSON, F. K., KRYSOV, S., DAVIES, A. J., STEELE, A. J. & PACKHAM, G. 2011. B-cell receptor signaling in chronic lymphocytic leukemia. *Blood,* 118**,** 4313-20.

STILGENBAUER, S., BULLINGER, L., LICHTER, P. & DOHNER, H. 2002. Genetics of chronic lymphocytic leukemia: genomic aberrations and V(H) gene mutation status in pathogenesis and clinical course. *Leukemia,* 16**,** 993-1007.

STILGENBAUER, S., LICHTER, P. & DOHNER, H. 2000. Genetic features of B-cell chronic lymphocytic leukemia. *Rev Clin Exp Hematol,* 4**,** 48-72.

STILGENBAUER, S., ZENZ, T., WINKLER, D., BUHLER, A., SCHLENK, R. F., GRONER, S., BUSCH, R., HENSEL, M., DUHRSEN, U., FINKE, J., DREGER, P., JAGER, U., LENGFELDER, E., HOHLOCH, K., SOLING, U., SCHLAG, R., KNEBA, M., HALLEK, M., DOHNER, H. & GERMAN CHRONIC LYMPHOCYTIC LEUKEMIA STUDY, G. 2009. Subcutaneous alemtuzumab in fludarabine-refractory chronic lymphocytic leukemia: clinical results and prognostic marker analyses from the CLL2H study of the German Chronic Lymphocytic Leukemia Study Group. *J Clin Oncol,* 27**,** 3994-4001.

SUBRAMANIAN, A., TAMAYO, P., MOOTHA, V. K., MUKHERJEE, S., EBERT, B. L., GILLETTE, M. A., PAULOVICH, A., POMEROY, S. L., GOLUB, T. R., LANDER, E. S. & MESIROV, J. P. 2005. Gene set enrichment analysis: a knowledge-based approach for interpreting genome-wide expression profiles. *Proc Natl Acad Sci U S A,* 102**,** 15545-50.

SULJAGIC, M., LONGO, P. G., BENNARDO, S., PERLAS, E., LEONE, G., LAURENTI, L. & EFREMOV, D. G. 2010. The Syk inhibitor fostamatinib disodium (R788) inhibits tumor growth in the Emu- TCL1 transgenic mouse model of CLL by blocking antigen-dependent B-cell receptor signaling. *Blood,* 116**,** 4894-905.

SUN, Y. X., WANG, J., SHELBURNE, C. E., LOPATIN, D. E., CHINNAIYAN, A. M., RUBIN, M. A., PIENTA, K. J. & TAICHMAN, R. S. 2003. Expression of CXCR4 and CXCL12 (SDF-1) in human prostate cancers (PCa) in vivo. *J Cell Biochem,* 89**,** 462-73.

SZOT, C. S., BUCHANAN, C. F., FREEMAN, J. W. & RYLANDER, M. N. 2011. 3D in vitro bioengineered tumors based on collagen I hydrogels. *Biomaterials,* 32**,** 7905-12.

TAICHMAN, R. S., COOPER, C., KELLER, E. T., PIENTA, K. J., TAICHMAN, N. S. & MCCAULEY, L. K. 2002. Use of the stromal cell-derived factor-1/CXCR4 pathway in prostate cancer metastasis to bone. *Cancer Res,* 62**,** 1832-7.

TAKESHITA, M., SUMIYOSHI, Y., MASUDA, Y., OHSHIMA, K., YOSHIDA, T., KIKUCHI, M. & MULLER, H. 1993. Cytokine (interleukin-1 alpha, interleukin-1 beta, tumor necrosis factor alpha, and interleukin-6)-possessing cells in lymph nodes of malignant lymphoma. *Pathol Res Pract,* 189**,** 18-25.

TAKEUCHI, H. & KATAYAMA, I. 1994. Interleukin 1 (IL-1 alpha and IL-1 beta) induces differentiation/activation of B cell chronic lymphoid leukemia cells. *Cytokine,* 6**,** 243-6.

TAN, Y., DU, J., CAI, S., LI, X., MA, W., GUO, Z., CHEN, H., HUANG, Z., XIAO, J., CAI, L. & CAI, S. 2006. Cloning and characterizing mutated human stromal cell-derived factor-1 (SDF-1): C-terminal α-helix of SDF-1α plays a critical role in CXCR4 activation and signaling, but not in CXCR4 binding affinity. *Experimental Hematology,* 34**,** 1553-1562.

TEICHER, B. A. & FRICKER, S. P. 2010. CXCL12 (SDF-1)/CXCR4 pathway in cancer. *Clin Cancer Res,* 16**,** 2927-31.

THOMPSON, P. A., KEATING, M. J., HINOJOSA, C., SMITH, S. C., DAVER, N. G., JAIN, N., BURGER, J. A., ESTROV, Z., O'BRIEN, S. & WIERDA, W. G. 2014. Lenalidomide and rituximab in combination as initial treatment of chronic lymphocytic leukemia: initial results of a phase II study. *Blood,* 124**,** 1988-1988.

THOMPSON, P. A., STINGO, F., KEATING, M. J., FERRAJOLI, A., BURGER, J. A., WIERDA, W. G., KADIA, T. M. & O'BRIEN, S. M. 2016. Outcomes of patients with chronic lymphocytic leukemia treated with first-line idelalisib plus rituximab after cessation of treatment for toxicity. *Cancer*.

TILL, K. J., LIN, K., ZUZEL, M. & CAWLEY, J. C. 2002. The chemokine receptor CCR7 and α4 integrin are important for migration of chronic lymphocytic leukemia cells into lymph nodes. *Blood,* 99**,** 2977-2984.

TILL, K. J., SPILLER, D. G., HARRIS, R. J., CHEN, H., ZUZEL, M. & CAWLEY, J. C. 2005. CLL, but not normal, B cells are dependent on autocrine VEGF and alpha4beta1 integrin for chemokine-induced motility on and through endothelium. *Blood,* 105**,** 4813-9.

TODD, D. J., LEE, A. H. & GLIMCHER, L. H. 2008. The endoplasmic reticulum stress response in immunity and autoimmunity. *Nat Rev Immunol,* 8**,** 663-74.

TSIMANIS, A., SHVIDEL, L., KLEPFISH, A., SHTALRID, M., KALINKOVICH, A. & BERREBI, A. 2001. Over-expression of the functional interleukin-11 alpha receptor in the development of B-cell chronic lymphocytic leukemia. *Leuk Lymphoma,* 42**,** 195-205.

TSIMBERIDOU, A. M., TAM, C., ABRUZZO, L. V., O'BRIEN, S., WIERDA, W. G., LERNER, S., KANTARJIAN, H. M. & KEATING, M. J. 2009. Chemoimmunotherapy may overcome the adverse prognostic significance of 11q deletion in previously untreated patients with chronic lymphocytic leukemia. *Cancer,* 115**,** 373-80.

TSUKADA, N. 2002. Distinctive features of "nurselike" cells that differentiate in the context of chronic lymphocytic leukemia. *Blood,* 99**,** 1030-1037.

TSUKADA, N., BURGER, J. A., ZVAIFLER, N. J. & KIPPS, T. J. 2002. Distinctive features of "nurselike" cells that differentiate in the context of chronic lymphocytic leukemia. *Blood,* 99**,** 1030-7.

ULLRICH, C. K., GROOPMAN, J. E. & GANJU, R. K. 2000. HIV-1 gp120- and gp160-induced apoptosis in cultured endothelial cells is mediated by caspases. *Blood,* 96**,** 1438-42.

UNDERWOOD, T. J., HAYDEN, A. L., DEROUET, M., GARCIA, E., NOBLE, F., WHITE, M. J., THIRDBOROUGH, S., MEAD, A., CLEMONS, N., MELLONE, M., UZOHO, C., PRIMROSE, J. N., BLAYDES, J. P. & THOMAS, G. J. 2015. Cancer-associated fibroblasts predict poor outcome and promote periostin-dependent invasion in oesophageal adenocarcinoma. *J Pathol,* 235**,** 466-77.

VALLAT, L. D., PARK, Y., LI, C. & GRIBBEN, J. G. 2007. Temporal genetic program following B-cell receptor cross-linking: altered balance between proliferation and death in healthy and malignant B cells. *Blood,* 109**,** 3989-97.

VAUGHAN, M. B., HOWARD, E. W. & TOMASEK, J. J. 2000. Transforming growth factor-beta1 promotes the morphological and functional differentiation of the myofibroblast. *Exp Cell Res,* 257**,** 180-9.

VLAHAKIS, S. R., VILLASIS-KEEVER, A., GOMEZ, T., VANEGAS, M., VLAHAKIS, N. & PAYA, C. V. 2002. G protein-coupled chemokine receptors induce both survival and apoptotic signaling pathways. *J Immunol,* 169**,** 5546-54.

VON ANDRIAN, U. H. & MACKAY, C. R. 2000. T-cell function and migration. Two sides of the same coin. *N Engl J Med,* 343**,** 1020-34.

VON DER MARK, K., GAUSS, V., VON DER MARK, H. & MULLER, P. 1977. Relationship between cell shape and type of collagen synthesised as chondrocytes lose their cartilage phenotype in culture. *Nature,* 267**,** 531-2.

WAGNER, W. & HO, A. D. 2007. Mesenchymal stem cell preparations--comparing apples and oranges. *Stem Cell Rev,* 3**,** 239-48.

WALSBY, E., BUGGINS, A., DEVEREUX, S., JONES, C., PRATT, G., BRENNAN, P., FEGAN, C. & PEPPER, C. 2014. Development and characterization of a physiologically relevant model of lymphocyte migration in chronic lymphocytic leukemia. *Blood,* 123**,** 3607-17.

WALTON, J. A., LYDYARD, P. M., NATHWANI, A., EMERY, V., AKBAR, A., GLENNIE, M. J. & PORAKISHVILI, N. 2010. Patients with B cell chronic lymphocytic leukaemia have an expanded population of CD4 perforin expressing T cells enriched for human cytomegalovirus specificity and an effector-memory phenotype. *Br J Haematol,* 148**,** 274-84.

WARD, S. G. 2006. T lymphocytes on the move: chemokines, PI 3-kinase and beyond. *Trends Immunol,* 27**,** 80-7.

WAUGH, D. J. & WILSON, C. 2008. The interleukin-8 pathway in cancer. *Clin Cancer Res,* 14**,** 6735-41.

WAWRZYNIAK, E., KOTKOWSKA, A., BLONSKI, J. Z., SIEMIENIUK-RYS, M., ZIOLKOWSKA, E., GIANNOPOULOS, K., ROBAK, T. & KORYCKA-WOLOWIEC, A. 2014. Clonal evolution in CLL patients as detected by FISH versus chromosome banding analysis, and its clinical significance. *European Journal of Haematology,* 92**,** 91-101.

WEAVER, V. M., FISCHER, A. H., PETERSON, O. W. & BISSELL, M. J. 1996. The importance of the microenvironment in breast cancer progression: recapitulation of mammary tumorigenesis using a unique human mammary epithelial cell model and a three-dimensional culture assay. *Biochemistry and cell biology = Biochimie et biologie cellulaire,* 74**,** 833-851.

WEBBER, M. M., BELLO, D., KLEINMAN, H. K. & HOFFMAN, M. P. 1997. Acinar differentiation by non-malignant immortalized human prostatic epithelial cells and its loss by malignant cells. *Carcinogenesis,* 18**,** 1225-31.

WEI, J. S., SONG, Y. K., DURINCK, S., CHEN, Q. R., CHEUK, A. T., TSANG, P., ZHANG, Q., THIELE, C. J., SLACK, A., SHOHET, J. & KHAN, J. 2008. The MYCN oncogene is a direct target of miR-34a. *Oncogene,* 27**,** 5204-13.

WHELAN, C. A., WILLOUGHBY, R. & MCCANN, S. R. 1982. T-cell function in chronic lymphocytic leukaemia. *British Journal of Haematology,* 50**,** 111-121.

WIERDA, W. G., JOHNSON, M. M., DO, K.-A., MANSHOURI, T., DEY, A., O'BRIEN, S., GILES, F. J., KANTARJIAN, H., THOMAS, D., FADERL, S., LERNER, S., KEATING, M. & ALBITAR, M. 2003. Plasma interleukin 8 level predicts for survival in chronic lymphocytic leukaemia. *British Journal of Haematology,* 120**,** 452-456.

WIESTNER, A., ROSENWALD, A., BARRY, T. S., WRIGHT, G., DAVIS, R. E., HENRICKSON, S. E., ZHAO, H., IBBOTSON, R. E., ORCHARD, J. A. & DAVIS, Z. 2003a. ZAP-70 expression identifies a chronic lymphocytic leukemia subtype with unmutated immunoglobulin genes, inferior clinical outcome, and distinct gene expression profile. *Blood,* 101**,** 4944-4951.

WIESTNER, A., ROSENWALD, A., BARRY, T. S., WRIGHT, G., DAVIS, R. E., HENRICKSON, S. E., ZHAO, H., IBBOTSON, R. E., ORCHARD, J. A., DAVIS, Z., STETLER-STEVENSON, M., RAFFELD, M., ARTHUR, D. C., MARTI, G. E., WILSON, W. H., HAMBLIN, T. J., OSCIER, D. G. & STAUDT, L. M. 2003b. ZAP-70 expression identifies a chronic lymphocytic leukemia subtype with unmutated immunoglobulin genes, inferior clinical outcome, and distinct gene expression profile. *Blood,* 101**,** 4944-51.

WOODSIDE, S. M., BOWEN, B. D. & PIRET, J. M. 1997. Measurement of ultrasonic forces for particle–liquid separations. *AIChE journal,* 43**,** 1727-1736.

WOYACH, J. A., SMUCKER, K., SMITH, L. L., LOZANSKI, A., ZHONG, Y., RUPPERT, A. S., LUCAS, D., WILLIAMS, K., ZHAO, W., RASSENTI, L., GHIA, E., KIPPS, T. J., MANTEL, R., JONES, J., FLYNN, J., MADDOCKS, K., O'BRIEN, S., FURMAN, R. R., JAMES, D. F., CLOW, F., LOZANSKI, G., JOHNSON, A. J. & BYRD, J. C. 2014. Prolonged lymphocytosis during ibrutinib therapy is associated with distinct molecular characteristics and does not indicate a suboptimal response to therapy. *Blood,* 123**,** 1810-7.

WU, J. 1991. Acoustical tweezers. *The Journal of the Acoustical Society of America,* 89**,** 2140-2143.

WU, Y. & ZHAO, R. C. H. 2012. The Role of Chemokines in Mesenchymal Stem Cell Homing to Myocardium. *Stem Cell Reviews and Reports,* 8**,** 243-250.

WYNN, R. F., HART, C. A., CORRADI-PERINI, C., O'NEILL, L., EVANS, C. A., WRAITH, J. E., FAIRBAIRN, L. J. & BELLANTUONO, I. 2004. A small proportion of mesenchymal stem cells strongly expresses functionally active CXCR4 receptor capable of promoting migration to bone marrow. *Blood,* 104**,** 2643-5.

XU, W. T., BIAN, Z. Y., FAN, Q. M., LI, G. & TANG, T. T. 2009. Human mesenchymal stem cells (hMSCs) target osteosarcoma and promote its growth and pulmonary metastasis. *Cancer Lett,* 281**,** 32-41.

YAMASHITA, M., OGAWA, T., ZHANG, X., HANAMURA, N., KASHIKURA, Y., TAKAMURA, M., YONEDA, M. & SHIRAISHI, T. 2012. Role of stromal myofibroblasts in invasive breast cancer: stromal expression of alpha-smooth muscle actin correlates with worse clinical outcome. *Breast Cancer,* 19**,** 170-6.

YANG, J. & LIU, Y. 2001. Dissection of Key Events in Tubular Epithelial to Myofibroblast Transition and Its Implications in Renal Interstitial Fibrosis. *The American Journal of Pathology,* 159**,** 1465-1475.

YEE, C., BIONDI, A., WANG, X. H., ISCOVE, N. N., DE SOUSA, J., AARDEN, L. A., WONG, G. G., CLARK, S. C., MESSNER, H. A. & MINDEN, M. D. 1989. A possible autocrine role for interleukin-6 in two lymphoma cell lines. *Blood,* 74**,** 798-804.

YEOMANS, A., THIRDBOROUGH, S. M., VALLE-ARGOS, B., LINLEY, A., KRYSOV, S., HIDALGO, M. S., LEONARD, E., ISHFAQ, M., WAGNER, S. D., WILLIS, A. E., STEELE, A. J., STEVENSON, F. K., FORCONI, F., COLDWELL, M. J. & PACKHAM, G. 2016. Engagement of the B-cell receptor of chronic lymphocytic leukemia cells drives global and MYC-specific mRNA translation. *Blood,* 127**,** 449-57.

YIP, D. & CHO, C. H. 2013. A multicellular 3D heterospheroid model of liver tumor and stromal cells in collagen gel for anti-cancer drug testing. *Biochem Biophys Res Commun,* 433**,** 327-32.

YOON, J. Y., LAFARGE, S., DAWE, D., LAKHI, S., KUMAR, R., MORALES, C., MARSHALL, A., GIBSON, S. B. & JOHNSTON, J. B. 2012. Association of interleukin-6 and interleukin-8 with poor prognosis in elderly patients with chronic lymphocytic leukemia. *Leuk Lymphoma,* 53**,** 1735-42.

YSEBAERT, L. & FOURNIE, J. J. 2011. Genomic and phenotypic characterization of nurse-like cells that promote drug resistance in chronic lymphocytic leukemia. *Leuk Lymphoma,* 52**,** 1404-6.

ZAPATA, J. M., KRAJEWSKA, M., MORSE, H. C., 3RD, CHOI, Y. & REED, J. C. 2004. TNF receptor-associated factor (TRAF) domain and Bcl-2 cooperate to induce small B cell lymphoma/chronic lymphocytic leukemia in transgenic mice. *Proc Natl Acad Sci U S A,* 101**,** 16600-5.

ZENZ, T., BENNER, A., DOHNER, H. & STILGENBAUER, S. 2008. Chronic lymphocytic leukemia and treatment resistance in cancer: the role of the p53 pathway. *Cell Cycle,* 7**,** 3810-4.

ZENZ, T., EICHHORST, B., BUSCH, R., DENZEL, T., HÄBE, S., WINKLER, D., BÜHLER, A., EDELMANN, J., BERGMANN, M., HOPFINGER, G., HENSEL, M., HALLEK, M., DÖHNER, H. & STILGENBAUER, S. 2010. TP53 Mutation and Survival in Chronic Lymphocytic Leukemia. *Journal of Clinical Oncology,* 28**,** 4473-4479.

ZHANG, W., KATER, A. P., WIDHOPF, G. F., 2ND, CHUANG, H. Y., ENZLER, T., JAMES, D. F., POUSTOVOITOV, M., TSENG, P. H., JANZ, S., HOH, C., HERSCHMAN, H., KARIN, M. & KIPPS, T. J. 2010. B-cell activating factor and v-Myc myelocytomatosis viral oncogene homolog (c-Myc) influence progression of chronic lymphocytic leukemia. *Proc Natl Acad Sci U S A,* 107**,** 18956-60.

ZHANG, W., TRACHOOTHAM, D., LIU, J., CHEN, G., PELICANO, H., GARCIA-PRIETO, C., LU, W., BURGER, J. A., CROCE, C. M., PLUNKETT, W., KEATING, M. J. & HUANG, P. 2012. Stromal control of cystine metabolism promotes cancer cell survival in chronic lymphocytic leukaemia. *Nat Cell Biol,* 14**,** 276-86.

ZUCCHETTO, A., BENEDETTI, D., TRIPODO, C., BOMBEN, R., DAL BO, M., MARCONI, D., BOSSI, F., LORENZON, D., DEGAN, M., ROSSI, F. M., ROSSI, D., BULIAN, P., FRANCO, V., DEL POETA, G., DEAGLIO, S., GAIDANO, G., TEDESCO, F., MALAVASI, F. & GATTEI, V. 2009. CD38/CD31, the CCL3 and CCL4 chemokines, and CD49d/vascular cell adhesion molecule-1 are interchained by sequential events sustaining chronic lymphocytic leukemia cell survival. *Cancer Res,* 69**,** 4001-9.

Appendix A

CLL patient data

Sample[a]	IGHV gene	*IGHV* status[b]	CLL population (% CD5+ CD19+)	Zap-70 (%)	CD38 (%)	IgM expression (MFI)	sIgM signal (% cells)[c]	Experiments used for
194	IGHV1-69*01 F	M	88	-	13	26	53	Device Levitation, Device Co-levitation
341	IGHV5-51*01 F	M	95	0	82	534	38	CXCR4 Ab survival
431	IGHV3-21*01 F	M	86	58	8	119	67	Transwell, CXCR4 Ab survival
446	IGHV3-7*01 F	M	88	0	8	33	-	Basal Apoptosis, Transwell
469b	IGHV4-34*01 F	M	43	2	9	180	57	Basal Apoptosis, HFFF2 CM
481	V4-59*01	M	86	0	0	188	67	Basal Apoptosis, GEP, qPCR
489	IGHV4-30-4*03 F, or IGHV4-31*03 F	M	92	2	6	26	4	Basal Apoptosis, HFFF2 CM, CXCR4 Ab survival
489a	IGHV4-30-4*03 F, or IGHV4-31*03 F	M	90	7	0	34	34	Transwell
494	-	M	-	-	-	29	6	Basal Apoptosis, Transwell
498	IGHV3-48*03 F	M	85	2	1	16	3	Basal Apoptosis, HFFF2 Contact
500c	IGHV3-48*03 F	U	92	32	56	60	12	qPCR, CCL2 expression
505	IGHV1-69*01 F	U	96	14	16	45	15	Basal Apoptosis, HFFF2 Contact, Transwell, CXCR4 Ab survival
506	-	-	89	0	0	10	3	Basal Apoptosis, HFFF2 Contact, HFFF2 CM
508	IGHV2-26*01 F	U	93	7	13	46	1	Basal Apoptosis, HFFF2 Contact, Transwell, CXCR4 Ab Survival
513	IGHV1-69*02 F	U	98		1	80	38	Basal Apoptosis, HFFF2 Contact, HFFF2 CM, CM generation, Transwell
513a	IGHV1-69*02 F	U	98	75	1	45	39	Basal Apoptosis, HFFF2 Contact, Transwell, 10hr Device Viablity
514b	IGHV3-7*01 F	M	91	45	2	81	69	CXCR4 CM
528b	IGHV4-39*07 F	U	92	56	3	151	59	qPCR, CCL2 Expression
531a	IGHV4-39*01 F	U	97	17	0	40	43	Device Levitation, CXCR4 Ab Migration
542	IGHV3-23*04 F	M	93	0	1	22	2	Basal Apoptosis, HFFF2 Contact, Transwell
551a	IGHV3-33*01 F, or IGHV3-33*06 F	U	95	8	100	125	59	CXCL12 Ab Migration
555	IGHV3-11*01 F	U	99	2	25	38	68	LN Fibroblasts
566	IGHV3-11*05 F	U	95	57	8	70	8	Basal Apoptosis, HFFF2 Contact, CXCR4 Ab Survival
567	V3-33*01 or V3-33*06	M	86	73	85	97	46	qPCR
567b	V3-33*01 or V3-33*06	M	91	2	80	198	72	GEP, qPCR
575d	IGHV3-15*01 F	M	98	1	1	116	52	qPCR, CCL2 expression
577	IGHV1-46*01 F, or IGHV1-46*03 F	M	68	23	0	26	29	Basal Apoptosis
577a	IGHV1-46*01 F, or IGHV1-46*03 F	M	40	16	3	22	31	HFFF2 CM
568	IGHV4-61*01 F	M	95	7	0	2364	86	Basal Apoptosis, HFFF2 Contact, 48hr Device levitation
589	IGHV1-18*04 F	M	94	0	0	64	82	Basal Apoptosis, HFFF2 Contact, Device Levitation, 48hr Device Levitation
598b	IGHV3-7*01 F	M	95	3	76	38	20	CCL2 Expression
600a	IGHV4-34*01 F	M	95	0	0	13	22	CXCR4 Recovery CM
602	IGHV5-51*03 F	U	98	0	36	19	24	Transwell
602a	IGHV5-51*03 F	U	99	0	13	76	44	Petri Dish Exps, CXCR4 Comparison
604b	IGHV3-30*03 F, or IGHV3-30*05 F or IGHV3-30*06 F or IGHV3-30*13 F or IGHV3-30*18 F or IGHV3-30*19 F	M	88	0	1	59	73	Basal Apoptosis, HFFF2 CM, qPCR, CCL2 Expression
606	IGHV3-30*01 F	M	91	0	3	1270	68	CXCR4 Recovery CM
607	IGHV5-51*01 F	U	82	23	90	26	60	Basal Apoptosis, HFFF2 Contact, Transwell, CXCR4 recovery CM, CXCR4 Ab survival
609a	IGHV3-72*01 F	M	89	0	18	25	57	Petri Dish Exps, CXCR4 Recovery HFFF2, CXCR4 comaprison, IgM Experiments, qPCR, CCL2 Expression
615	IGHV4-39*01 F	M	93	5	8	32	69	48hr Device Levitation, CXCR4 Ab Survival
618a	IGHV3-11*01 F	U	87	53	40	145	68	Basal Apoptosis, HFFF2 CM

619	IGHV3-30*03 F, or IGHV3-30*18 F	U	95	4	91	IgG case		LN Fibroblasts, CXCR4 Ab Survival
635	IGHV3-21*01 F	U	87	12	1	67	82	48hr Device Levitation
635a	IGHV3-21*01 F	U	89	7	2	67	82	Basal Apoptosis, HFFF2 CM, CXCR4 Recovery HFFF2, IgM Experiments
635b	IGHV3-21*01 F	U	83	2	2	135	90	GEP, qPCR
636	IGHV4-34*02 F	M	94	0	0	24	2	10hr Device Viability
637	IGHV1-69*06 F	M	83	2	0	25	17	48hr Device Levitation
643	IGHV6-1*01 F	M	91	0	0	25	26	10hr Device Viability
643b	IGHV6-1*01 F	M	91	0	0	15	25	Petri Dish Exps, CXCR4 Recovery HFFF2, CXCR4 Recovery CM, CXCR4 Comparison, IgM Experiments, CCL2
644	IGHV4-39*01 F	U	90	46	26	48	31	Basal Apoptosis, HFFF2 CM, 48hr Device Levitation
645	IGHV1-18*04 F	M	96	0	0	43	66	Basal Apoptosis, HFFF2 Contact, HFFF2 CM, 48hr Device Levitation
650	IGHV3-72*01 F	M	79	30	1	45	10	Basal Apoptosis, HFFF2 Contact, HFFF2 CM, 10hr Viabililty Exps
650a	IGHV3-72*01 F	M	82	1	0	71	18	CCL2 Expression
653	IGHV3-7*01 F	M	71	1	0	28	3	Basal Apoptosis, HFFF2 Contact, HFFF2 CM, 10hr Device Viability
656	IGHV3-30*01 F, or IGHV3-30-3*01 F	M	52	0	86	11	11	Basal Apoptosis, HFFF2 Contact, HFFF2 CM, 10hr Device Viability
658	-	-	95	5	14	6.4	26	Basal Apoptosis, HFFF2 Contact, Transwell, CXCL12 Ab Migration
659	IGHV3-53*02F	M	80	16	1	97	80	Basal Apoptosis, HFFF2 Contact, HFFF2 CM, CXCR4 Ab Survival
660	IGHV3-33*01 F, or Homsap IGHV3-33*0	U	86	89	97	21	2	Basal Apoptosis, HFFF2 Contact, HFFF2 CM, Transwell
661	IGHV1-2*04 F	M	81	7	1	98	73	Basal Apoptosis, HFFF2 Contact, HFFF2 CM, CM Generation, CXCR4 Ab Survival, CXCL12 Ab Migration
662	NOT DETERMINED	ot determine	71	1	8	28	3	Basal Apoptosis, HFFF2 Contact, HFFF2 CM, Transwell
665	IGHV3-11*01 F	M	85	0	89	468	68	CXCL12 Ab Migration
668	IGHV3-30*03 F, or IGHV3-30*18 F	U	92	35	0	71	54	Petri Dish Exps
668a	IGHV3-30*03 F, or IGHV3-30*18 F	U	92	18	1	138	47	CXCR4 Comparison, CCL2 Expression
663	IGHV4-39*01 F	M	75	18	68	52	43	Basal Apoptosis, HFFF2 Contact, HFFF2 CM
670	IGHV3-33*01 F, or Homsap IGHV3-33*0	U	78	79	65	155	73	Basal Apoptosis, HFFF2 CM, 10hr Device Viability, CXCL12 Ab Migration
674	IGHV3-21*01 F, or Homsap IGHV3-21*0	U	78	40	9	285	99	CXCL12 Ab Migration
676	IGHV6-1*02 F	M	56	3	100	918	100	Basal Apoptosis, HFFF2 Contact, HFFF2 CM, CXCL12 Ab Survival
678	IGHV4-34*12 F	M	37	12	5	49	21	CXCL12 Ab Survival
679	IGHV3-15*01 F	M	80	13	0	70	13	CXCL12 Ab Migration
684a	IGHV3-15*07 F	M	92	8	8	31	14	CXCR4 Recovery HFFF2, IgM Experiments
684b	IGHV3-15*07 F	M	86	2	10	28	14	qPCR, CCL2 expression
695	IGHV3-21*01 F, or Homsap IGHV3-21*0	U	98	-	7	80	82	CXCR4 Recovery HFFF2, IgM Experiments
709	IGHV3-7*01 F	M	92	17	0	101	46	CXCR4 Recovery HFFF2, IgM Experiments
716	IGHV3-7*01 F	M	80	1	0	77	85	CCL2 Expression
720	IGHV1-69*01 F	U	92	67	50	63	11	Petri Dish Exps, CXCR4 Comaprison
731	IGHV3-64*05 F, or Homsap IGHV3-64D*	U	94	4	5	42	19	qPCR

[a]Where suffix is not shown, this is the first sample obtained from that patient, typically obtained shortly after diagnosis. a indicate subsequent samples
[b]*IGHV* mutation status. M, mutated; U, unmutated.
[c]Maximal percentage of cells with increased intracellular calcium following treatment with soluble anti-IgM (Mockridge 2007)

Appendix B

Acoustic trapping device videos

VIDEO 1: LEVITATION OF CLL CELLS IN ACOUSTIC TRAPPING DEVICES

CLL sample 194 was fluorescently labelled with CFSE and 20 μl of a $7x10^6$ cell/ml suspension was injected into the acoustic trapping device using a gel loading tip. CLL cells were successfully levitated in the device and within minutes of being injected cells started moving to the nodal plane where they formed several small agglomerates. Movement of the cells towards the nodal plane took approximately one minute. Video speed 4x and x4 original magnification.

VIDEO 2: INJECTION OF CLL CELLS INTO ACOUSTIC TRAPPING DEVICES

CLL sample 194 was fluorescently labelled with CFSE and 20 μl of a $7x10^6$ cell/ml suspension was injected into the acoustic trapping device using a gel loading tip. Accurate placing of the gel loading tip was important to ensure that cells are 'caught' by the ultrasound field. Gentle, slow pipetting of cells was important to avoid loss of cells beyond the edge of the ultrasound field. This video also highlights the difficulty associated with removing the pipette from the devices after injection. Movement of the cells during removal can be observed, refocusing of the microscope demonstrates the extent of 'pulling' seen when the pipette was removed. Video speed 4x and x4 original magnification.

VIDEO 3: TIME LAPSE OF AGGLOMERATE CONTAINING CLL CELLS ALONE OVER 48 HOURS

CLL sample 589 was injected into the acoustic trapping devices at a cell concentration of $18x10^6$/ml. 20μl of cell sample was injected, giving a total number of cells in the device of $3.6x10^7$. Agglomerates were allowed to form and imaged using the time-lapse facility on the Nikon eclipse Ti microscope. Imaging was performed using natural light due to the manufacturing of the devices therefore due to natural light changing there are dips of lighting in the video. Images were taken at 30 minute intervals for 48 hours and placed together to form a time lapse video. Video speed 4x.

VIDEO 4: TIME LAPSE OF AGGLOMERATE CONTAINING A MIXTURE OF CLL AND HFFF2 CELLS OVER 48 HOURS

CLL sample 589 and HFFF2 cells were injected in the acoustic trapping devices at a cell concentration of $18x10^6$/ml and at a cell ratio of 5:1 (CLL:HFFF2). Agglomerates were allowed to form and then imaged using time lapse (as described for Video 3). Video speed 4x.

VIDEO 5: TIME LAPSE OF AGGLOMERATE CONTAINING A MIXTURE OF CLL AND HFFF2 CELLS OVER 48 HOURS

As for Video 4 but using CLL sample194.

VIDEO 6: TIME LAPSE OF AGGLOMERATE CONTAINING HFFF2 CELLS ALONE OVER 48 HOURS

HFFF2 cells were injected into the acoustic trapping devices at a cell concentration of $18x10^6$/ml. Agglomerates were allowed to form and then imaged using time lapse (as described for Video 3). Video speed 4.

*Note: Video media files can be found on attached CD

Appendix C

Purification data

TABLE C-1: PURIFICATION DATA DETERMINED BY FLOW CYTOMETRY

CD5+/CD19+ population was determined using flow cytometry pre- and post-purification

Sample	Pre-purification (%)	Post-purification (%)
609a	79.6	99.2
575d	96.8	98.8
604b	93.4	97.5
500c	88.8	99.2
528b	92.9	98
550b	88.5	97.8
481	87.5	98.3
567	73.7	98.4
684b	87.1	97.4
731	89.9	99.4
604b	89.3	98.6
609a	80.9	98.8
684b	87.1	97.4

CLL 528b

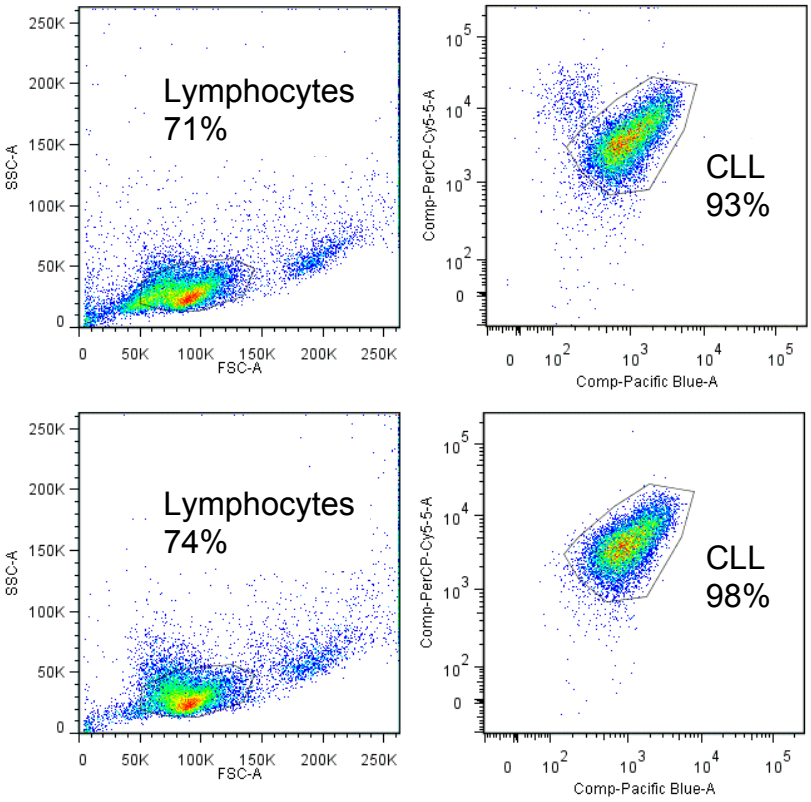

CLL 550b

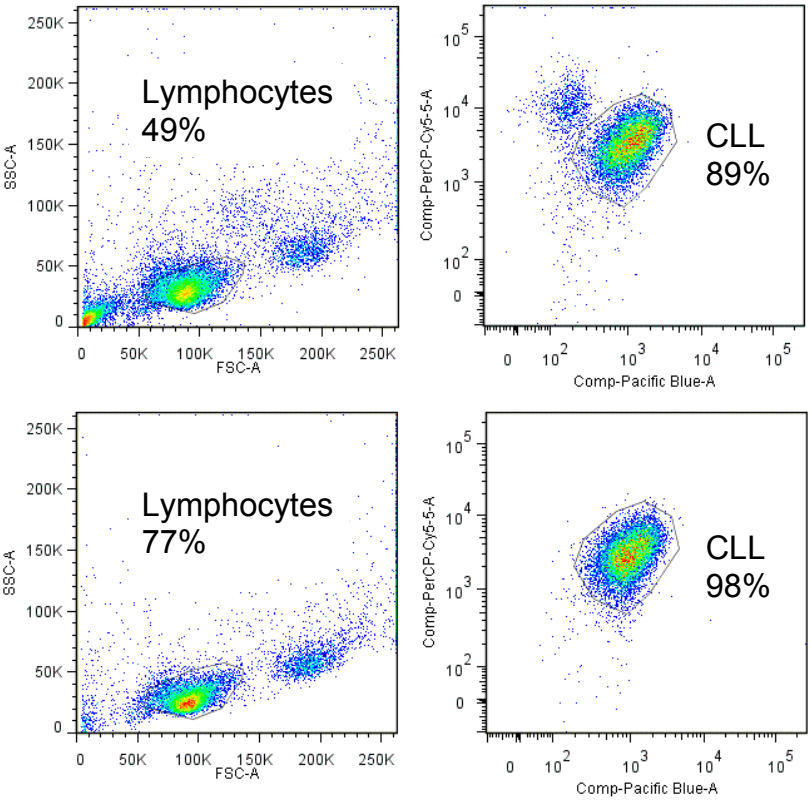

CLL 481

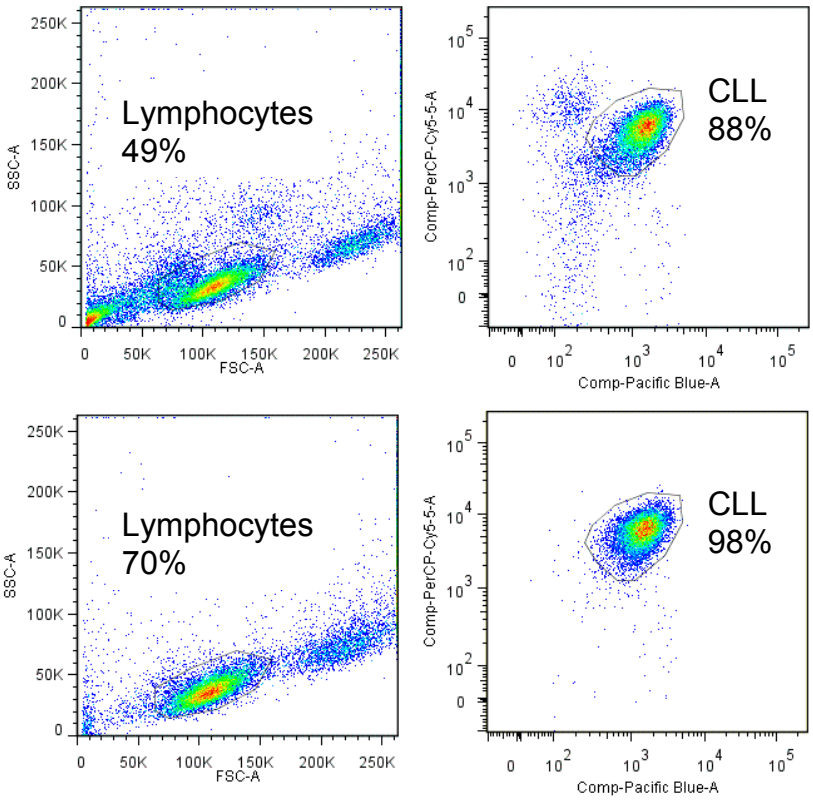

CLL 500c

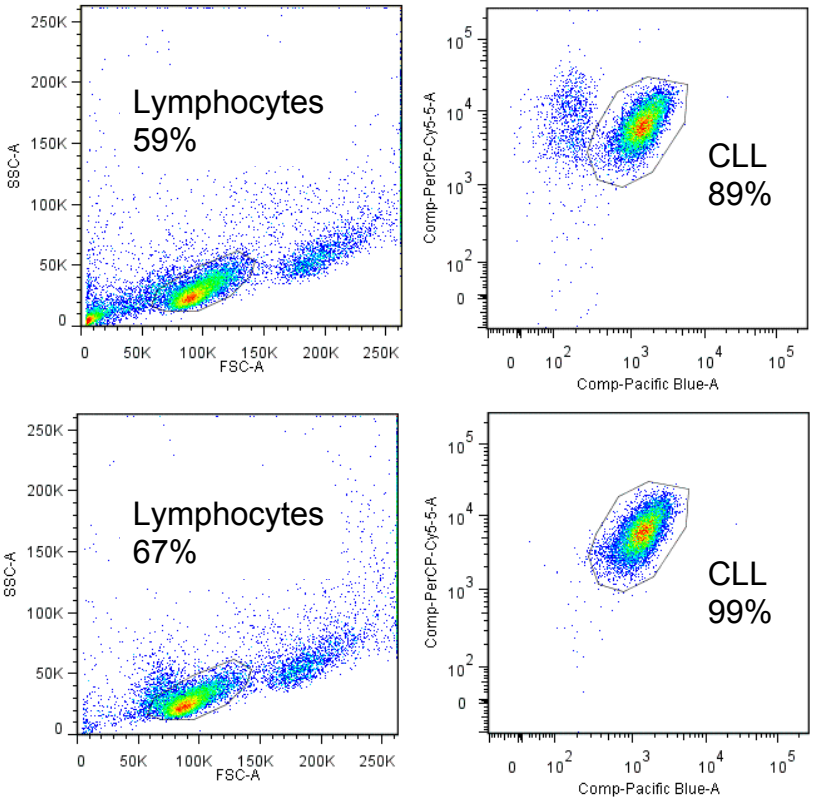

CLL 575d

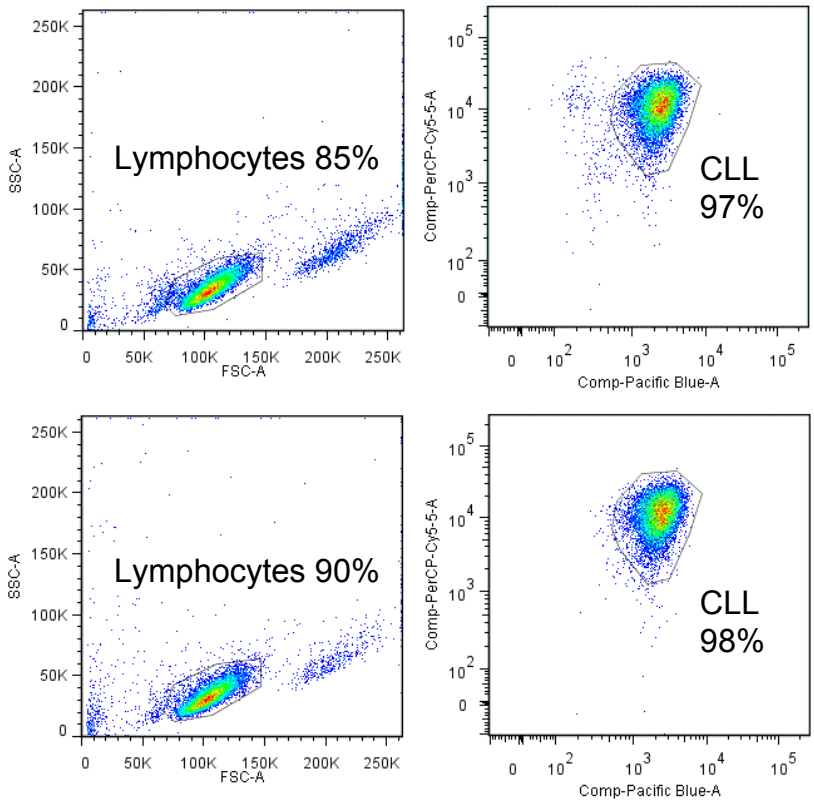

CLL 604b

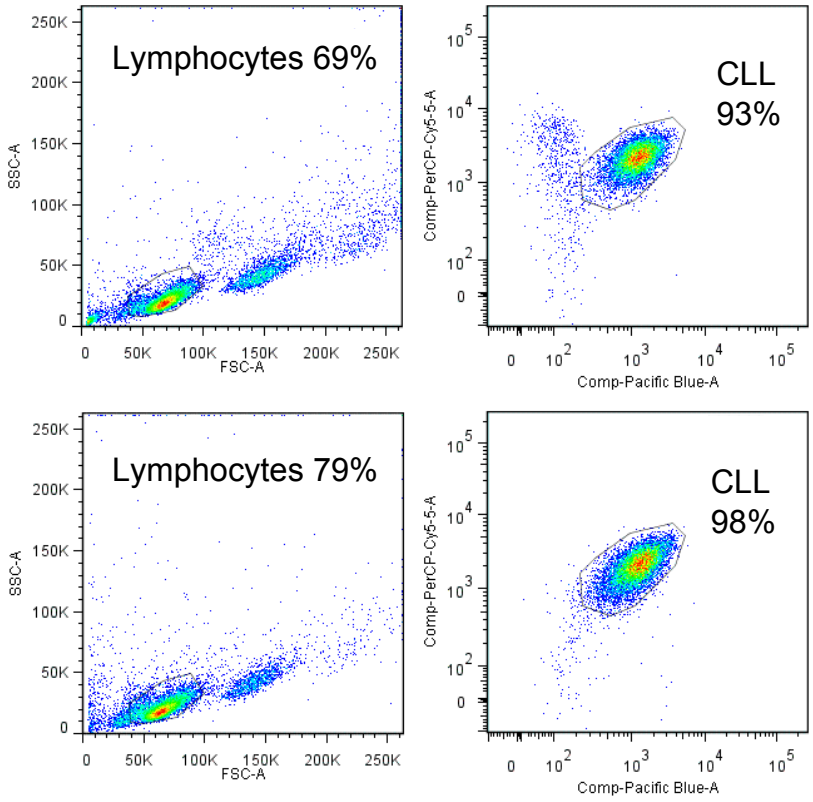

CLL 567b

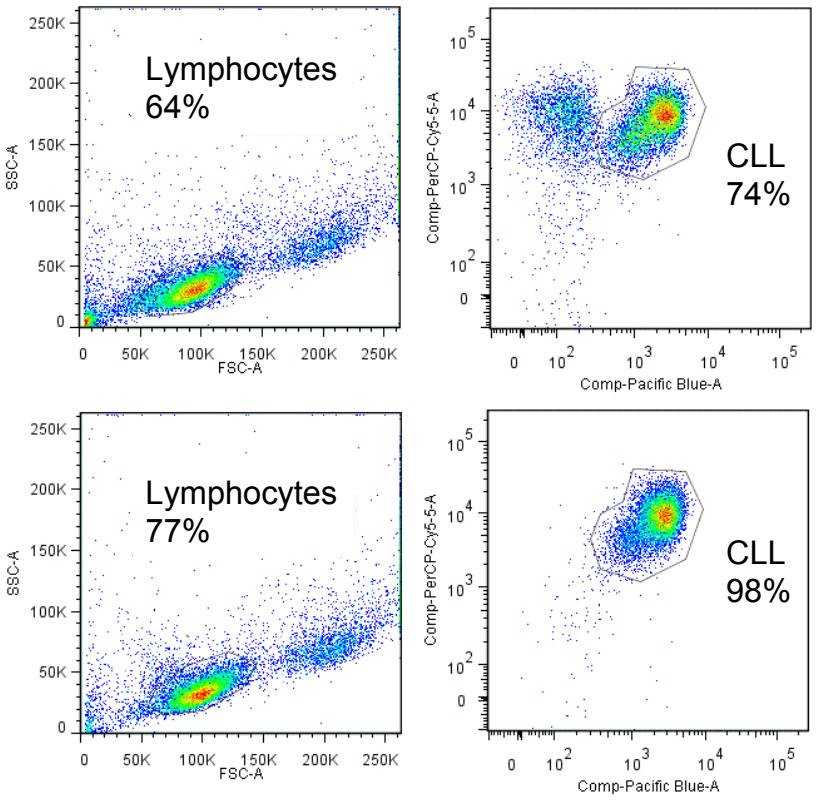

CLL 575c

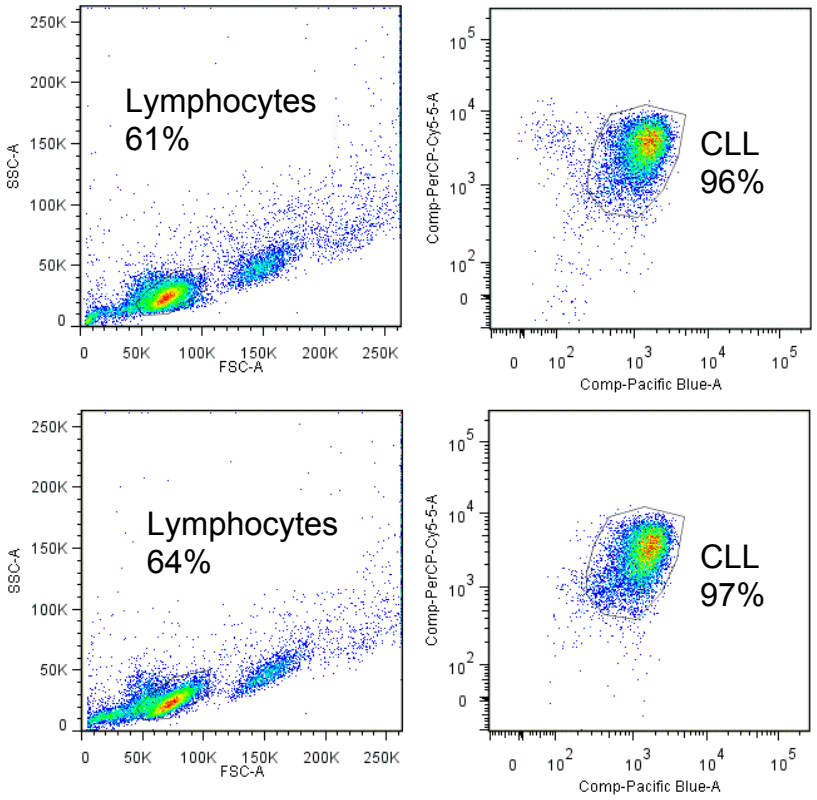

CLL 731

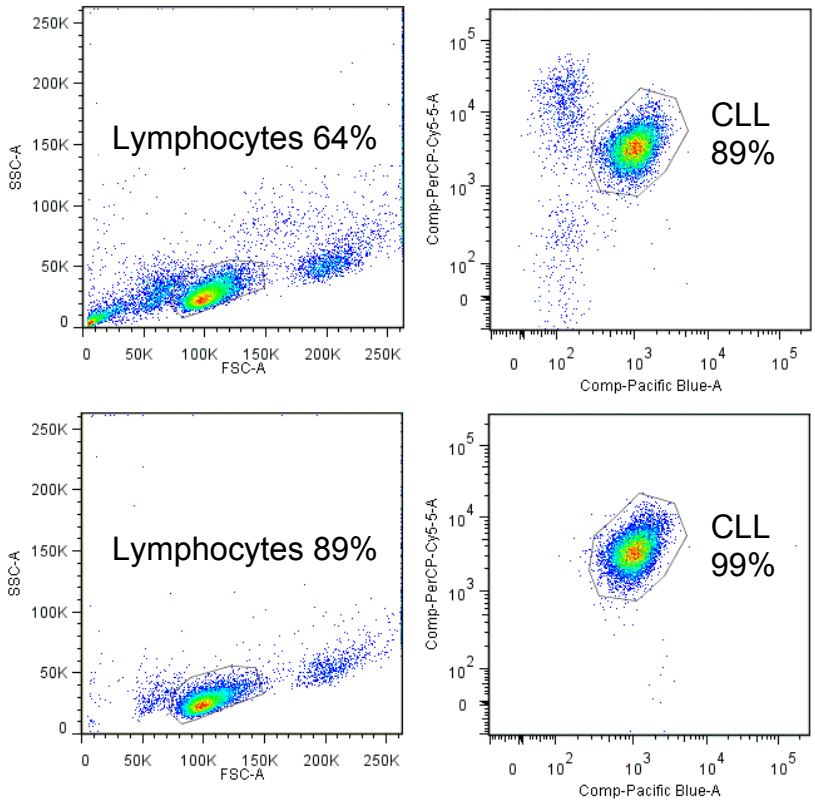

CLL 684b

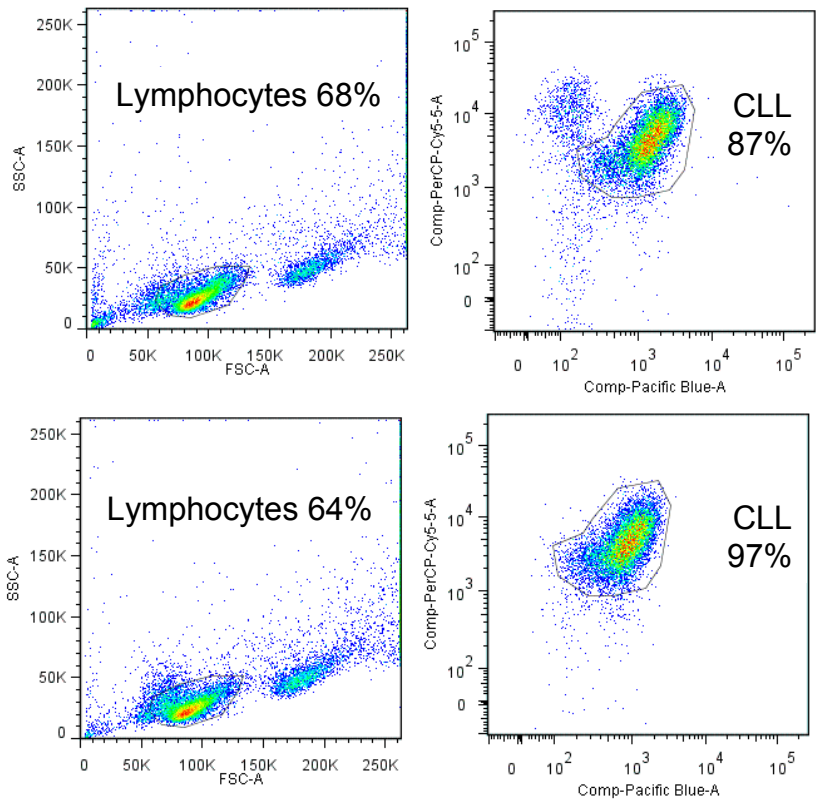

CLL 609a

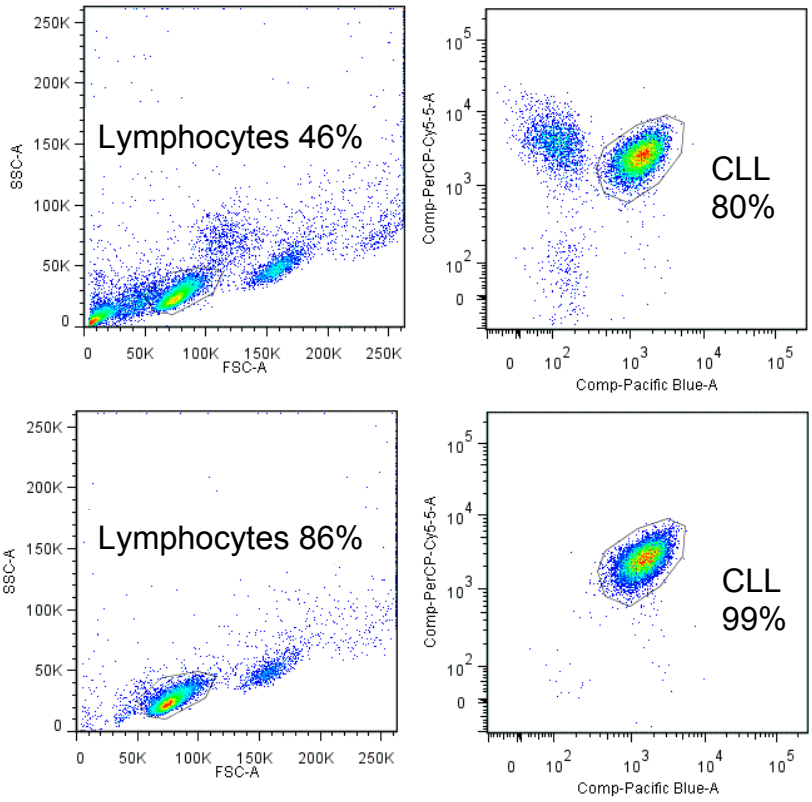

CLL 684b

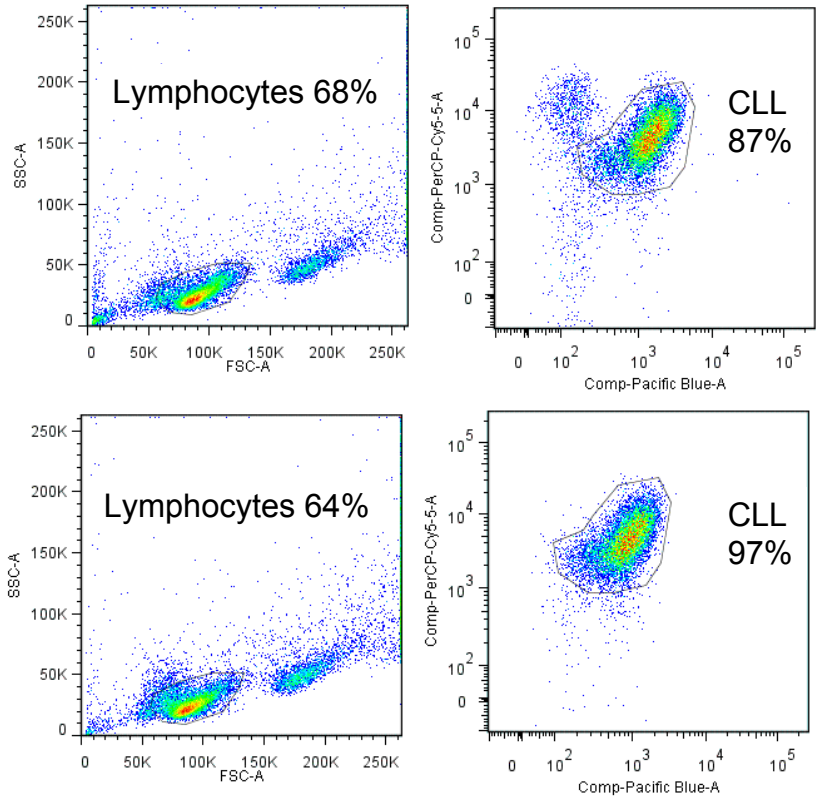

Appendix D

RNA integrity results

TABLE D-1: NANODROP RESULTS FOR RNA SENT FOR GEP ANALYSIS

Original Results				Clean up Results			
635b r1 28/08/14				**635b r1 28/08/14**			
	ng/ul	**260/280**	**260/230**		**ng/ul**	**260/280**	**260/230**
CLL alone	183.6	1.69	0.75	CLL alone	96.4	1.6	1.63
CLL+IgM	76.2	1.57	1.37	CLL+IgM	45.7	1.51	1.62
CLL+HFFF2	198.2	1.74	1.09	CLL+HFFF2	119.5	1.6	1.72
CLL+HFFF2+IgM	372.3	1.82	1.62	CLL+HFFF2+IgM	245.1	1.7	1.78
CLL+CM	164.5	1.66	1.4	CLL+CM	108.5	1.6	1.92
HFFF2	218.6	1.68	1.38	HFFF2	125.1	1.6	1.7
635b r2 04/09/14				**635b r2 04/09/14**			
	ng/ul	**260/280**	**260/230**		**ng/ul**	**260/280**	**260/230**
CLL alone	183.3	1.72	0.65	CLL alone	80.8	1.49	1.51
CLL+IgM	201.2	1.74	0.71	CLL+IgM	91.5	1.51	2.31
CLL+HFFF2	377	1.83	1.38	CLL+HFFF2	230.5	1.62	1.91
CLL+HFFF2+IgM	342.8	1.82	1.62	CLL+HFFF2+IgM	236.2	1.61	1.97
CLL+CM	187.1	1.71	1.22	CLL+CM	106.9	1.51	2.37
635b r3 12/09/14				**635b r3 12/09/14**			
	ng/ul	**260/280**	**260/230**		**ng/ul**	**260/280**	**260/230**
CLL alone	87.9	1.55	1.49	CLL alone	48.5	1.49	1.76
CLL+IgM	143.9	1.64	1.3	CLL+IgM	78.5	1.5	2
CLL+HFFF2	202.5	1.69	1.49	CLL+HFFF2	102.3	1.51	1.76
CLL+HFFF2+IgM	295.5	1.77	1.37	CLL+HFFF2+IgM	178.4	1.56	1.72
CLL+CM	157.4	1.68	1.01	CLL+CM	82.5	1.53	2.18
567b r1 02/10/14				**567b r1 02/10/14**			
	ng/ul	**260/280**	**260/230**		**ng/ul**	**260/280**	**260/230**
CLL alone	231.1	1.72	1.43	CLL alone	146.1	1.55	1.84
CLL+IgM	194.5	1.7	1.55	CLL+IgM	133	1.54	1.81
CLL+HFFF2	410.9	1.8	1.56	CLL+HFFF2	281	1.66	1.79
CLL+HFFF2+IgM	191.9	1.67	1.45	CLL+HFFF2+IgM	88.5	1.54	1.6
CLL+CM	245.8	1.73	1.22	CLL+CM	150.4	1.55	1.76
HFFF2 r1	218.6	1.68	1.38	HFFF2	125.1	1.6	1.7
567b r2 22/10/14				**567b r2 22/10/14**			
	ng/ul	**260/280**	**260/230**		**ng/ul**	**260/280**	**260/230**
CLL alone	251	1.75	1.87	CLL alone	182	1.59	1.9
CLL+IgM	209	1.74	1.82	CLL+IgM	136	1.55	1.99
CLL+HFFF2	435.8	1.79	1.59	CLL+HFFF2	298.4	1.69	2.22
CLL+HFFF2+IgM	262.2	1.73	1.56	CLL+HFFF2+IgM	146.6	1.57	1.89
CLL+CM	228	1.75	1.69	CLL+CM	151.7	1.57	2.05
HFFF2 r2	361.3	1.77	1.79	HFFF2	257.2	1.62	1.95
567b r3 23/10/14				**567b r3 23/10/14**			
	ng/ul	**260/280**	**260/230**		**ng/ul**	**260/280**	**260/230**
CLL alone	90.1	1.6	1.7	CLL alone	61.3	1.51	1.61
CLL+IgM	119.4	1.58	1.98	CLL+IgM	83.8	1.49	1.68
CLL+HFFF2	475.6	1.79	1.87	CLL+HFFF2	334.9	1.67	2.01

CLL+HFFF2+IgM	545.2	1.88	1.83	CLL+HFFF2+IgM	408	1.7	2
CLL+CM	127.2	1.71	0.66	CLL+CM	87.7	1.48	1.86
HFFF2 r3	109.2	1.6	1.66	HFFF2	61.4	1.51	1.66
431 r1				**431 r1**			
	ng/ul	**260/280**	**260/230**		**ng/ul**	**260/280**	**260/230**
CLL alone	99	1.57	1.98	CLL alone	58.8	1.5	1.77
CLL+IgM	63.4	1.52	1.8	CLL+IgM	30.4	1.48	1.81
CLL+HFFF2	454.9	1.82	1.93	CLL+HFFF2	298.6	1.65	1.98
CLL+HFFF2+IgM	507	1.9	1.98	CLL+HFFF2+IgM	332	1.68	2.17
CLL+CM	508.7	1.84	1.83	CLL+CM	96.2	1.5	1.96
431 r2				**431 r2**			
	ng/ul	**260/280**	**260/230**		**ng/ul**	**260/280**	**260/230**
CLL alone	152.6	1.69	1.68	CLL alone	87.9	1.54	2
CLL+IgM	228.1	1.73	1.71	CLL+IgM	128.4	1.57	1.96
CLL+HFFF2	459.2	1.83	1.85	CLL+HFFF2	307.6	1.63	1.95
CLL+HFFF2+IgM	483.8	1.9	1.91	CLL+HFFF2+IgM	305.5	1.63	1.86
CLL+CM	72.1	1.54	1.48	CLL+CM	10.9	1.48	2.42
431 r3				**431 r3**			
	ng/ul	**260/280**	**260/230**		**ng/ul**	**260/280**	**260/230**
CLL alone	156	1.63	1.71	CLL alone	86.5	1.51	1.89
CLL+IgM	288	1.77	1.61	CLL+IgM	123.4	1.54	2.06
CLL+HFFF2				CLL+HFFF2	233	1.65	2.03
CLL+HFFF2+IgM	435.5	1.8	1.86	CLL+HFFF2+IgM	219.5	1.65	2.05
CLL+CM	95.7	1.63	1.08	CLL+CM	30.6	1.49	1.94

Assay Class: Eukaryote Total RNA Nano
Data Path: C:\...Eukaryote Total RNA Nano_DE34903288_2014-11-07_11-30-01.xad

Created: 07/11/2014 11:30:00
Modified: 07/11/2014 12:12:51

Electrophoresis File Run Summary

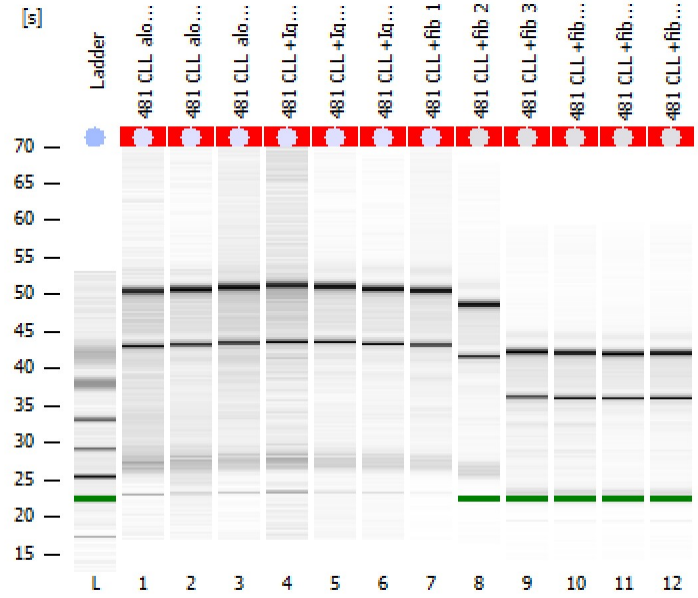

Instrument Information:

Instrument Name: DE34903288 Firmware: C.01.069
Serial#: DE34903288 Type: G2938C

Assay Information:

Assay Origin Path: C:\Program Files (x86)\Agilent\2100 bioanalyzer\2100 expert\assays\RNA\Eukaryote Total RNA Nano Series II.xsy

Assay Class: Eukaryote Total RNA Nano

Version: 2.6

Assay Comments: Total RNA Analysis ng sensitivity (Eukaryote)

Chip Information:

Chip Lot #:

Reagent Kit Lot #:

Chip Comments:

481 CLL alone 1
RIN: 6.60

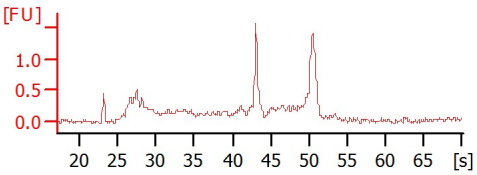

481 CLL alone 2
RIN: 7.60

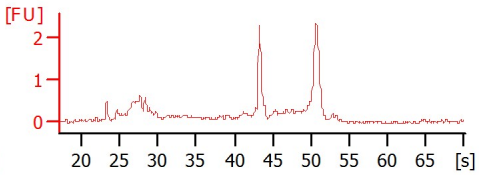

481 CLL alone 3
RIN: 7.10

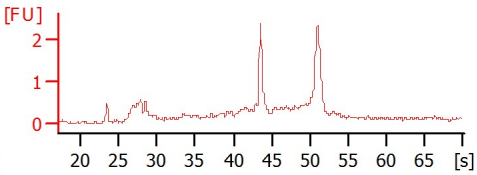

481 CLL+IgM 1
RIN: 7.60

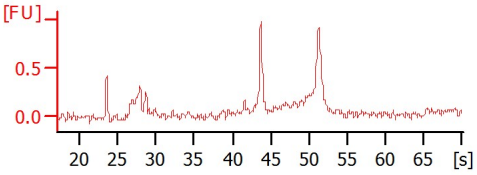

481 CLL+IgM 2
RIN: 8.30

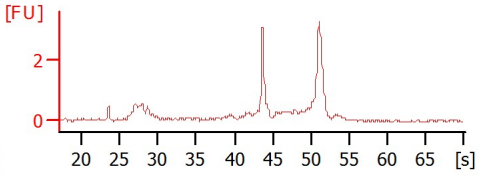

481 CLL+IgM 3
RIN: 8.20

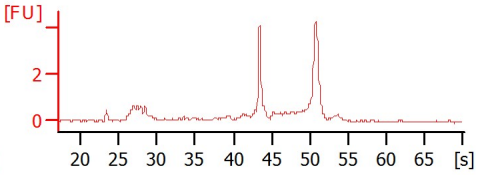

481 CLL+fib 1
RIN: 7.70

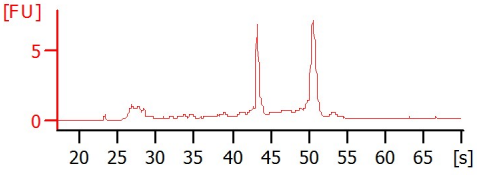

481 CLL+fib 2
RIN N/A

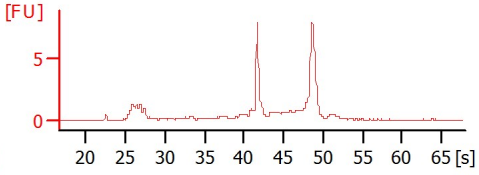

481 CLL+fib 3
RIN N/A

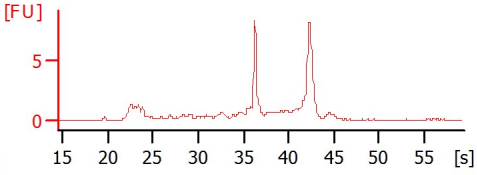

481 CLL+fib+IgM 1
RIN N/A

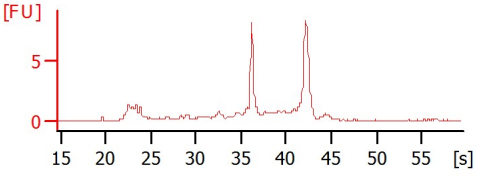

481 CLL+fib+IgM 2
RIN N/A

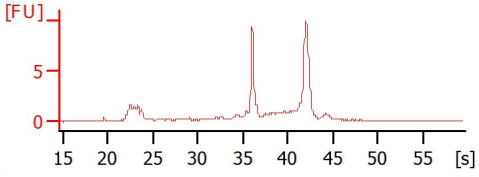

481 CLL+fib+IgM 3
RIN N/A

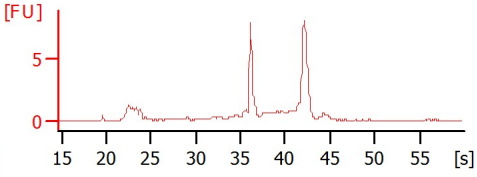

Assay Class: Eukaryote Total RNA Nano
Data Path: C:\...Eukaryote Total RNA Nano_DE34903288_2014-11-07_12-35-53.xad

Created: 07/11/2014 12:35:52
Modified: 07/11/2014 12:58:55

Electrophoresis File Run Summary

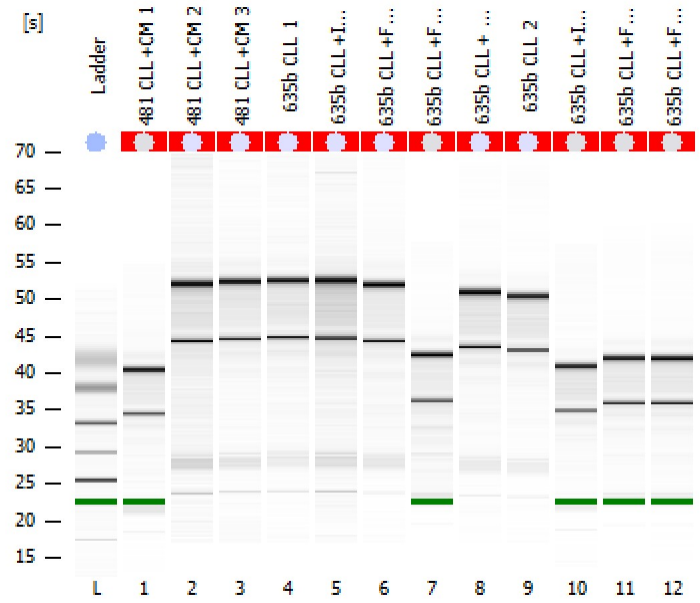

Instrument Information:

Instrument Name: DE34903288 Firmware: C.01.069
Serial#: DE34903288 Type: G2938C

Assay Information:

Assay Origin Path: C:\Program Files (x86)\Agilent\2100 bioanalyzer\2100 expert\assays\RNA\Eukaryote Total RNA Nano Series II.xsy

Assay Class: Eukaryote Total RNA Nano

Version: 2.6

Assay Comments: Total RNA Analysis ng sensitivity (Eukaryote)

Chip Information:

Chip Lot #:

Reagent Kit Lot #:

Chip Comments:

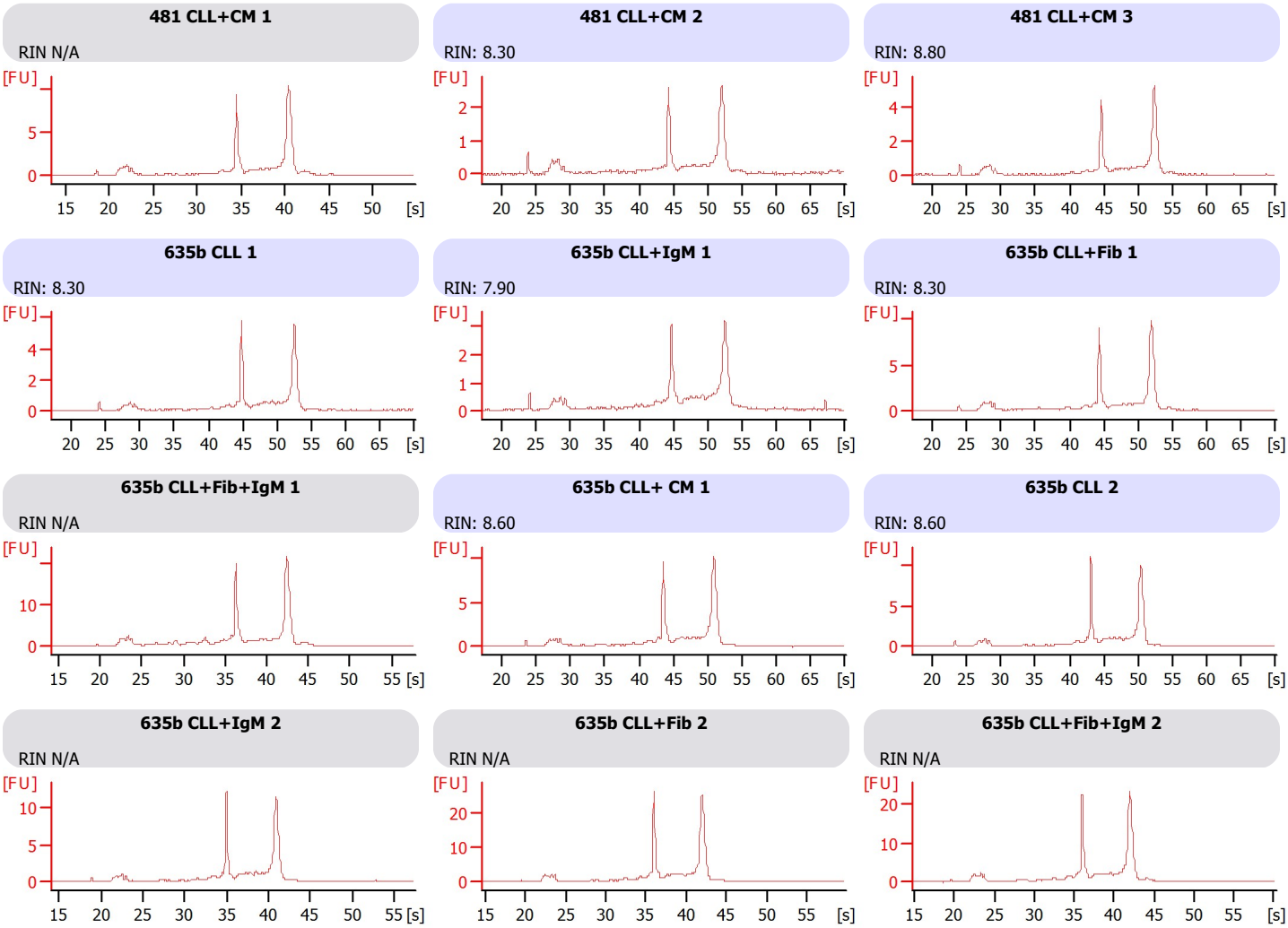

Assay Class: Eukaryote Total RNA Nano
Data Path: C:\...Eukaryote Total RNA Nano_DE34903288_2014-11-10_12-02-48.xad

Created: 10/11/2014 12:02:47
Modified: 10/11/2014 12:26:39

Electrophoresis File Run Summary

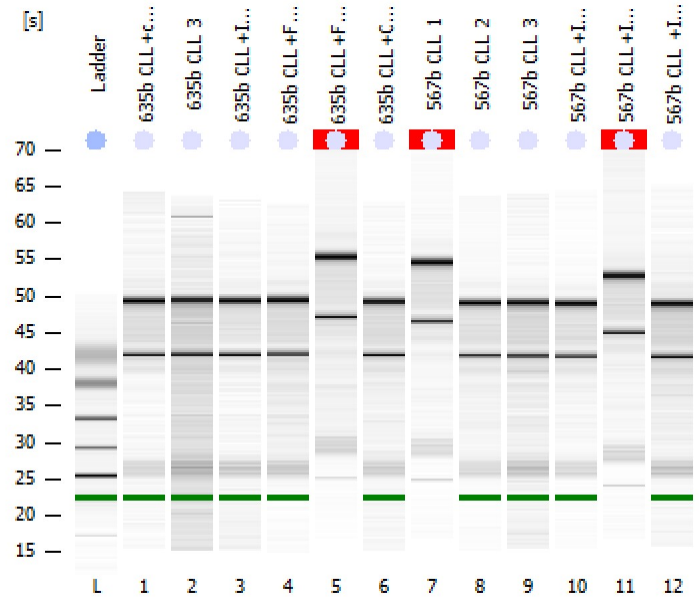

Instrument Information:

Instrument Name: DE34903288 Firmware: C.01.069
Serial#: DE34903288 Type: G2938C

Assay Information:

Assay Origin Path: C:\Program Files (x86)\Agilent\2100 bioanalyzer\2100 expert\assays\RNA\Eukaryote Total RNA Nano Series II.xsy

Assay Class: Eukaryote Total RNA Nano

Version: 2.6

Assay Comments: Total RNA Analysis ng sensitivity (Eukaryote)

Chip Information:

Chip Lot #:

Reagent Kit Lot #:

Chip Comments:

635b CLL+cm 2
RIN: 8.50

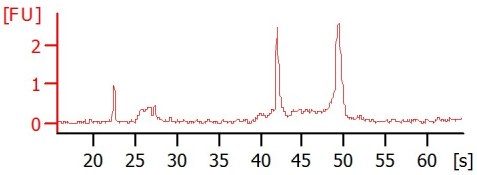

635b CLL 3
RIN: 7.30

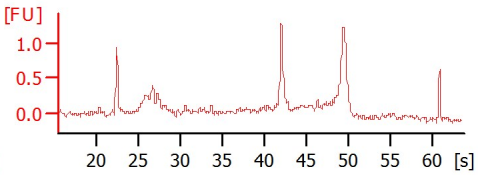

635b CLL+IgM 3
RIN: 9.10

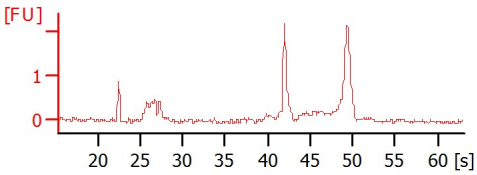

635b CLL+Fib 3
RIN: 7.40

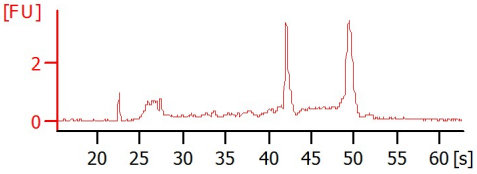

635b CLL+Fib+IgM 3
RIN: 7.70

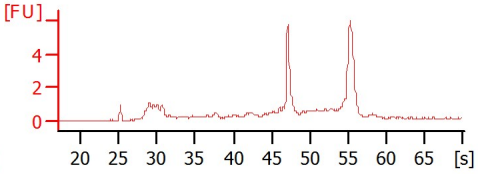

635b CLL+CM 3
RIN: 7.90

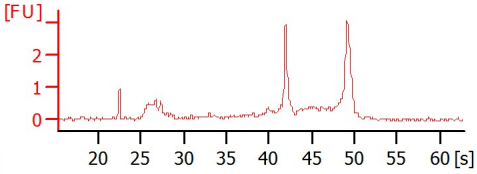

567b CLL 1
RIN: 8.20

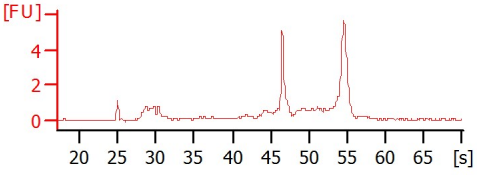

567b CLL 2
RIN: 7.80

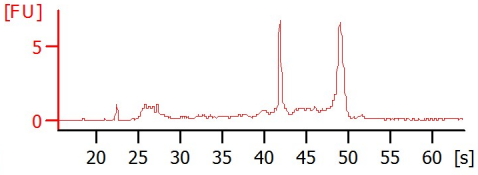

567b CLL 3
RIN: 7.90

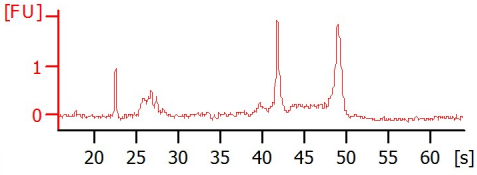

567b CLL+IgM 1
RIN:8

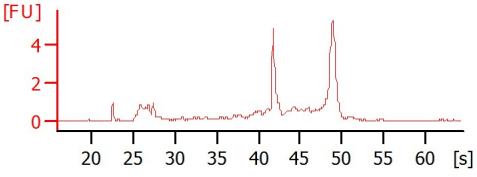

567b CLL+IgM 2
RIN: 8.50

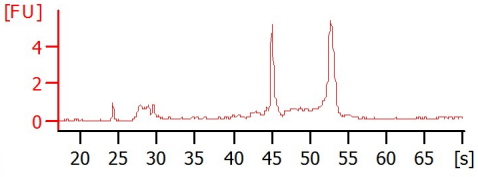

567b CLL +IgM 3
RIN: 7.30

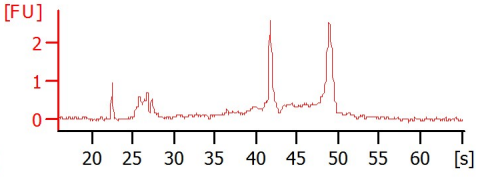

Assay Class: Eukaryote Total RNA Nano
Data Path: C:\...Eukaryote Total RNA Nano_DE34903288_2014-11-11_09-16-20.xad

Created: 11/11/2014 09:16:20
Modified: 11/11/2014 09:40:11

Electrophoresis File Run Summary

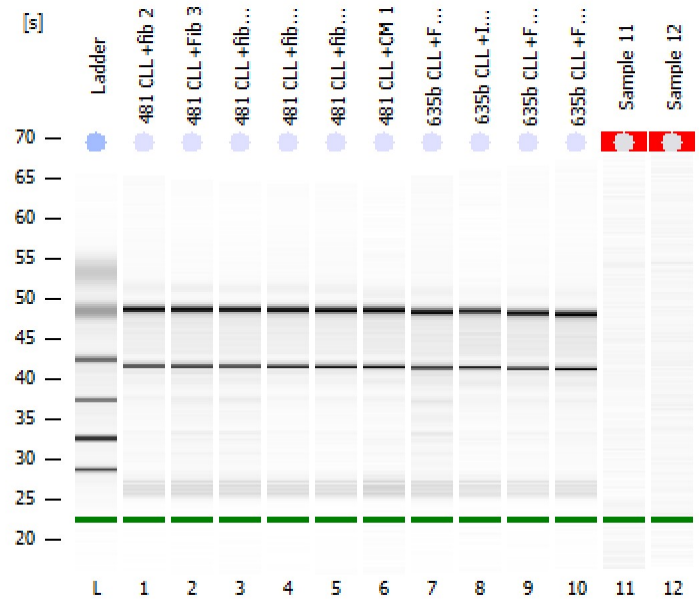

Instrument Information:

Instrument Name: DE34903288 Firmware: C.01.069
Serial#: DE34903288 Type: G2938C

Assay Information:

Assay Origin Path: C:\Program Files (x86)\Agilent\2100 bioanalyzer\2100 expert\assays\RNA\Eukaryote Total RNA Nano Series II.xsy

Assay Class: Eukaryote Total RNA Nano

Version: 2.6

Assay Comments: Total RNA Analysis ng sensitivity (Eukaryote)

Chip Information:

Chip Lot #:

Reagent Kit Lot #:

Chip Comments:

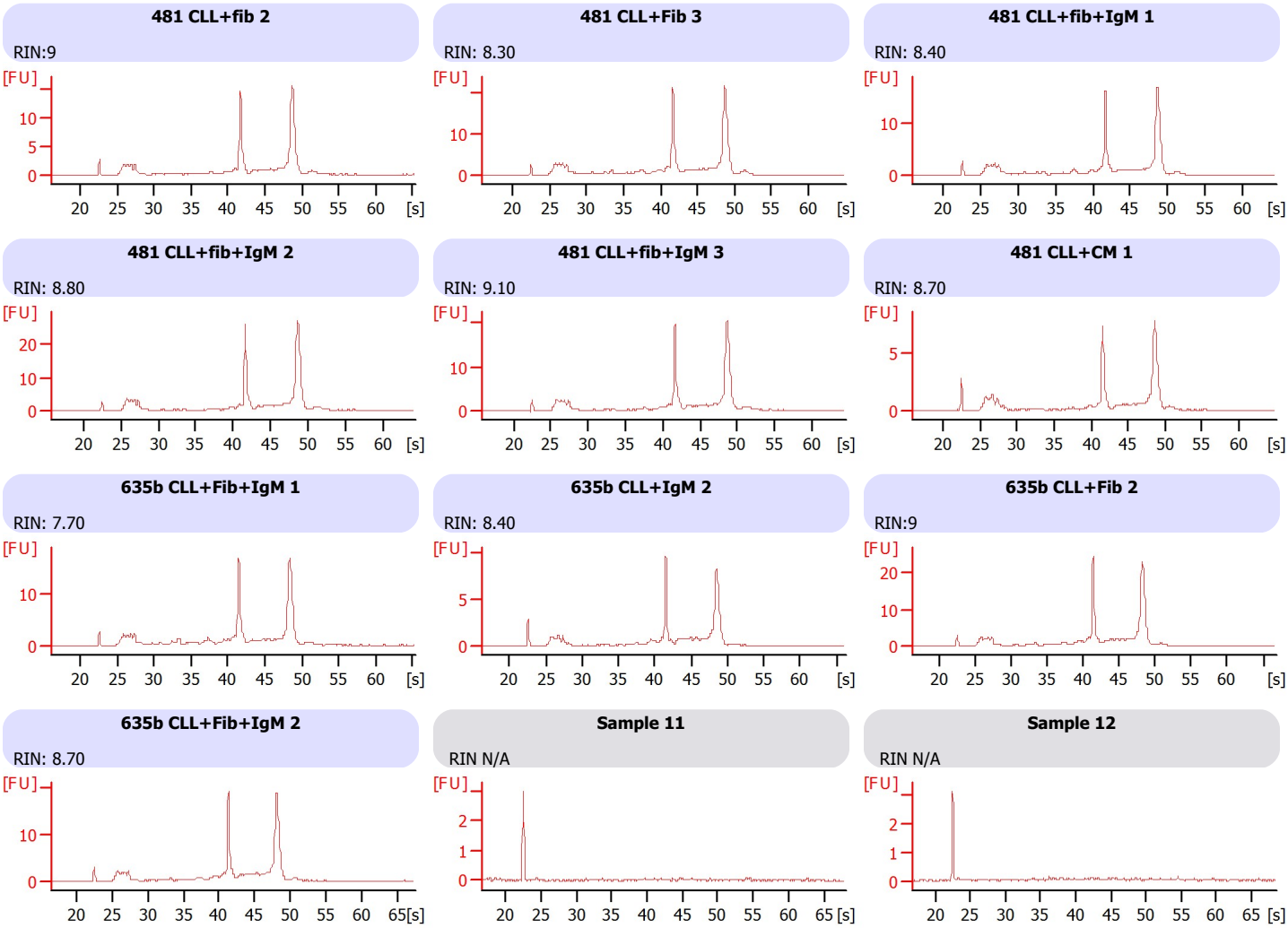

  Printed: 11/11/2014 09:55:52

Assay Class: Eukaryote Total RNA Nano
Data Path: C:\...Eukaryote Total RNA Nano_DE34903288_2014-11-11_10-14-49.xad

Created: 11/11/2014 10:14:49
Modified: 11/11/2014 10:38:39

Electrophoresis File Run Summary

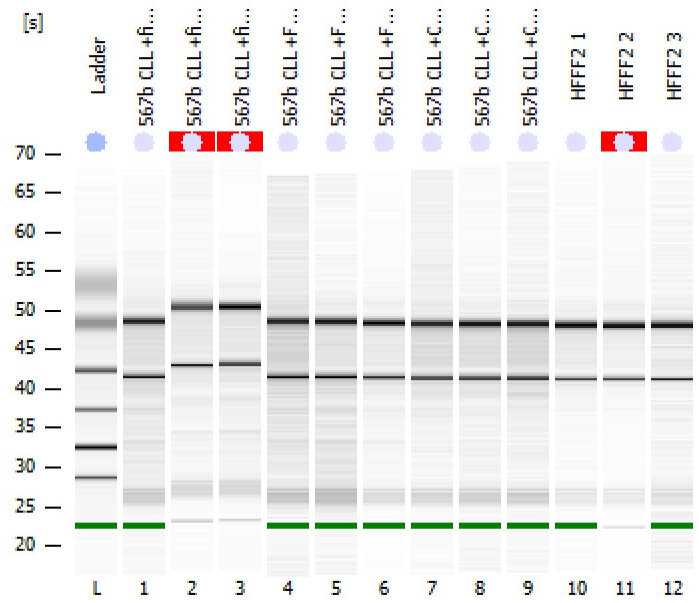

Instrument Information:

Instrument Name: DE34903288
Serial#: DE34903288
Firmware: C.01.069
Type: G2938C

Assay Information:

Assay Origin Path: C:\Program Files (x86)\Agilent\2100 bioanalyzer\2100 expert\assays\RNA\Eukaryote Total RNA Nano Series II.xsy

Assay Class: Eukaryote Total RNA Nano

Version: 2.6

Assay Comments: Total RNA Analysis ng sensitivity (Eukaryote)

Chip Information:

Chip Lot #:

Reagent Kit Lot #:

Chip Comments:

567b CLL+fib 1
RIN:7

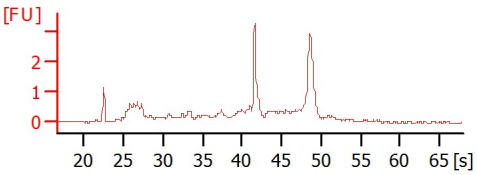

567b CLL+fib 2
RIN: 7.80

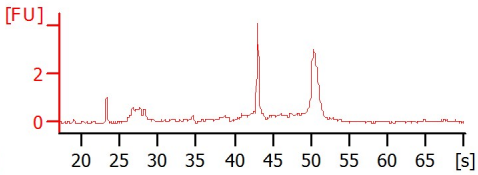

567b CLL+fib 3
RIN: 7.50

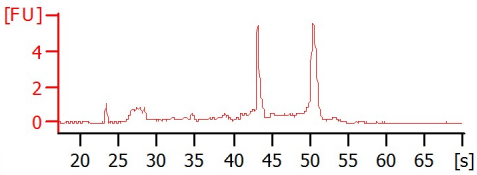

567b CLL+Fib+IgM 1
RIN: 7.20

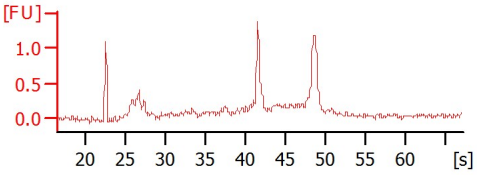

567b CLL+Fib+IgM 2
RIN: 7.10

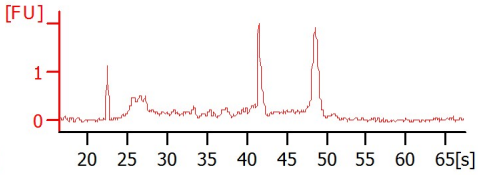

567b CLL+Fib+IgM 3
RIN: 7.90

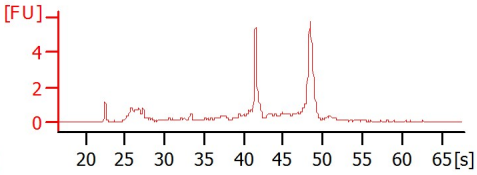

567b CLL+CM 1
RIN: 8.10

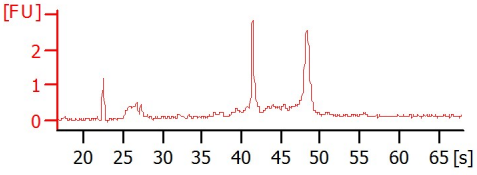

567b CLL+CM 2
RIN: 8.10

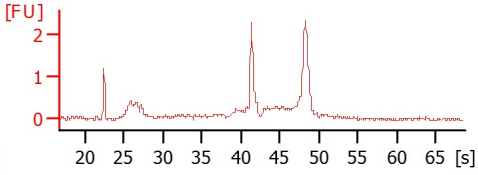

567b CLL+CM 3
RIN: 7.80

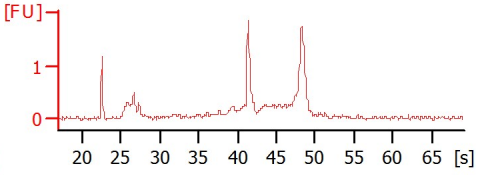

HFFF2 1
RIN: 8.70

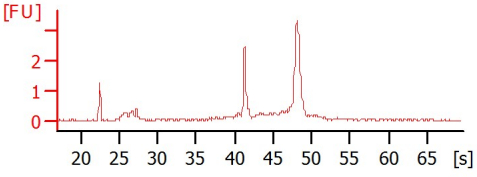

HFFF2 2
RIN: 9.30

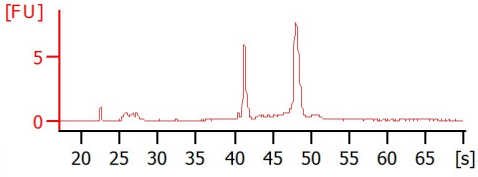

HFFF2 3
RIN: 9.30

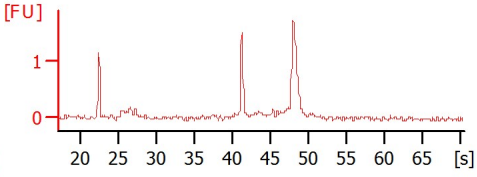

Appendix E

GEP supplementary data

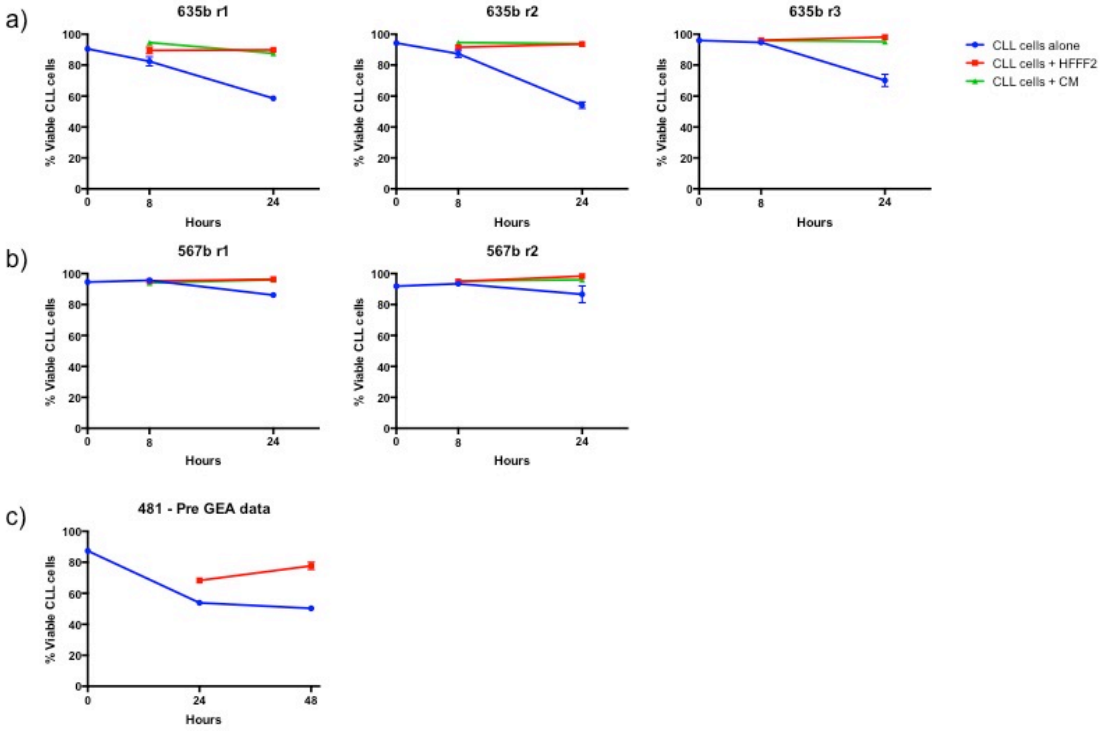

FIGURE E-1: VIABILITY AND PROTECTION DATA FROM CLL SAMPLES USED IN THE GEP EXPERIMENTS

CLL samples were selected for inclusion into the GEP experiments based on their ability to be protected by HFFF2 co-culture. Viability of each sample was also checked using Annexin-V/PI staining at 8 hours (point of RNA collection) to confirm viability of the cells was good enough for analysis. (a) Patient 1 (CLL sample 635a) viability results from three experimental repeats. (b) Patient 2 (CLL sample 567b) viability results from two experimental repeats due to inadequate number of cells for the final repeat. (c) Patient 3 (CLL sample 481) had already be tested for its ability to be protected by HFFF2 co-culture and viability was good at 24 hours. So was adequate to be included in GEA experiments.

Quality Control Data

For each condition there is a 'quality control data report' and a 'raw data report'. The quality control (QC) data is formed of technical controls which includes hybridisation controls, stringency controls, negative labelling controls and biological controls which include, the hierarchical and MDS clustering, outlier detection, boxplot of microarray intensity and density plot. Each control is explained in detail in the reports. The raw data reports includes scatterplots displaying pairwise plot with sample correlation and then repeats of the boxplots and clustering. Again each control is explained in detail on the reports.

All the samples pass on technical QC data. QC demonstrates that replicates are highly correlated, the majority of scatter plots show correlations >0.99. The scatter plots also confirm what was discussed in detail in Chapter 6 that in general samples from patient 3 are more variable when compared to their corresponding samples from patient 1 and 2. There was evidence from the scatter plots and hierarchical clustering for some outlier samples Patient1_CM_1 and Patient1_FibIgM_2. Looking at the scatter plots, Cambridge Genomic Services, believed there was evidence of a sampleID swap. Therefore they proceeded by changing the ID of these samples for subsequent next steps and were kept in the analysis due to the strong evidence.

*Note: QC data files can be found on attached CD

Multicomparison Data

A list of analysis comparisons was sent to the bioinformatics team at Cambidge to perform their basic level of analysis. For GEP analysis the following comparisons were requested; CLL cultured alone versus CLL cultured with HFFF2 cells and CLL cells cultured with HFFF2-derived CM to determine transcriptional responses occurring in CLL cells following microenvironmental stimulation from stromal cells. CLL cells cultured alone versus CLL cell stimulated with αIgM beads and also CLL cells cultured alone versus CLL cells cultured with HFFF2 and stimulated with αIgM beads to determine how transcriptional responses to antigen might be modulated by microenvironmental co-stimulation.

For each comparison requested one data file was received containing the results of the statistical analysis. The multiple comparison table at the top shows the number of differentially expressed RNAs at two levels of significance (adj.P <0.05 and <0.01, respectively) for all the comparisons. For each comparison there is a volcano plot, which displays significance as a function of the log fold change, the adjusted p-value is transformed to a negative log10 scale and plotted on the y axis, results are significant if above 1.3 (adj.P.Val<0.05), 2 for higher significance (adj.P.val<0.01). And secondly, a heatmap plot which displays the top 100 genes sorted by adj.P.Val were grouped using hierarchical clustering. (Note that not all of the 100 genes are necessarily significant. Intensity values were centered and scaled across samples). Green color indicates lower intensity and Red color indicates higher intensity. A light blue traceback line in the color key indicates the distribution of scaled intensity values.

,

*Note: Multiple comparison data files can be found on attached CD

Data set tables additional data– Top 100 genes

The following tables are extensions of the top 50 upregulated RNAs from Chapter 6. Tables display the top 100 differentially expressed RNA following comparisons and filtering as detailed in the original Table legends.

(a) Upregulated in CLL cells following co-culture with HFFF2 cells. (Extension of Table 6.3a). Chemokine and cytokines are highlighted in red.

(b) Upregulated in CLL cells following culture with HFFF2-derived CM. (Extension of Table 6.5b). Chemokine and cytokines are highlighted in red.

a) Upregulated in CLL cells following Co-culture with HFFF2 cells				
TargetID	**Name**	**logFC**	**FC**	**adj.P.Val**
IL6	**Interleukin 6 (B-Cell Stimulatory Factor)**	**-7.2**	**148.5**	**0.00014335**
TM4SF1	Transmembrane 4 L Six Family Member 1	-6.3	81.4	0.000137683
TPM2	Tropomyosin 2 (Beta)	-6.1	70.7	0.00019458
TPM2	Tropomyosin 2 (Beta)	-6.1	69.6	0.000266295
PTRF	Polymerase I And Transcript Release Factor	-6.1	68.0	0.000160592
COL1A2	Collagen, Type I, Alpha 2	-5.9	60.9	0.00014335
PTGS2	Prostaglandin-Endoperoxide Synthase 2	-5.8	54.5	0.000160592
DKK3	Dickkopf WNT Signalling Pathway Inhibitor 3	-5.7	52.7	0.000137683
MT2A	Metallothionein 2A	-5.6	48.2	0.000387321
BGN	Biglycan	-5.5	46.8	0.00014335
CAV1	Caveolin 1, Caveolae Protein, 22kDa	-5.5	46.0	0.000160592
SERPINE2	Serpin Peptidase Inhibitor, Clade E (Nexin, Plasminogen Activator Inhibitor Type 1), Member 2	-5.5	45.6	0.000344236
DKK3	Dickkopf WNT Signalling Pathway Inhibitor 3	-5.5	45.6	0.000137683
TMEM158	Transmembrane Protein 158 (Gene/Pseudogene)	-5.5	45.4	0.00014335
COL1A2	Collagen, Type I, Alpha 2	-5.4	43.5	0.00022359
CCL2	**Chemokine (C-C Motif) Ligand 2**	**-5.4**	**42.5**	**0.000340768**
LOC100134	N/A	-5.3	40.6	0.000224357
COL6A3	Collagen, Type VI, Alpha 3	-5.3	39.2	0.00014335
PLAU	Plasminogen Activator, Urokinase	-5.3	39.1	0.000190415
MT1E	Metallothionein 1E	-5.2	36.2	0.000896331
ACTA2	Actin, Alpha 2, Smooth Muscle, Aorta	-5.1	35.3	0.00014335
TNFRSF11B	Tumor Necrosis Factor Receptor Superfamily, Member 11b	-5.1	35.1	0.000194125
CXCL1	**C-X-C Motif Chemokine 1**	**-5.0**	**32.6**	**0.00014335**
CCND1	Cyclin D1	-5.0	31.9	0.000137683
CSF2	Colony Stimulating Factor 2 (Granulocyte-Macrophage)	-5.0	31.8	0.000281008
COL4A1	Collagen, Type IV, Alpha 1	-5.0	31.4	0.00016268
IL1B	**Interleukin 1, Beta**	**-4.9**	**29.6**	**0.00066248**
CALD1	Caldesmon 1	-4.9	29.0	0.00014335
MT1A	Metallothionein 1A	-4.8	28.8	0.000814687
CDH2	Cadherin 2, Type 1, N-Cadherin	-4.8	28.3	0.00014335
IFIT1	Interferon-Induced Protein With Tetratricopeptide Repeats 1	-4.8	26.9	0.001498876
LOC387882	N/A	-4.7	26.2	0.000362444
TPM1	Tropomyosin 1 (Alpha)	-4.7	25.5	0.00014335
RND3	Rho Family GTPase 3	-4.6	24.5	0.000137683
MFGE8	Milk Fat Globule-EGF Factor 8 Protein	-4.6	24.4	0.00016268
CTGF	Connective Tissue Growth Factor	-4.6	24.0	0.00016268
COL1A1	Collagen, Type I, Alpha 1	-4.6	23.7	0.000172355
TPM1	Tropomyosin 1 (Alpha)	-4.6	23.7	0.000185526
CDC20	Cell Division Cycle 20	-4.6	23.6	0.000198962
LUM	Lumican	-4.6	23.5	0.000190415
FSTL1	Follistatin-Like 1	-4.5	23.2	0.000160592
IGFBP5	Insulin-Like Growth Factor Binding Protein 5	-4.5	22.9	0.000190415
CYR61	Cysteine-Rich, Angiogenic Inducer, 61	-4.5	22.5	0.000306103
PLOD2	Procollagen-Lysine, 2-Oxoglutarate 5-Dioxygenase 2	-4.5	22.0	0.00016268
THY1	Thy-1 Cell Surface Antigen	-4.5	22.0	0.00014335
FSCN1	Fascin Actin-Bundling Protein 1	-4.5	21.9	0.000149587
GREM1	Gremlin 1, DAN Family BMP Antagonist	-4.5	21.9	0.00014335
COL6A3	Collagen, Type VI, Alpha 3	-4.4	21.0	0.000160592
FLNC	Filamin C, Gamma	-4.4	21.0	0.00014335
IGFBP5	Insulin-Like Growth Factor Binding Protein 5	-4.4	20.9	0.000205266
SPARC	Secreted Protein, Acidic, Cysteine-Rich (Osteonectin)	-4.4	20.5	0.00014335
FBLN1	Fibulin 1	-4.3	20.4	0.00014335
IER3	Immediate Early Response 3	-4.3	20.0	0.000281008

FHL2	Four And A Half LIM Domains 2	-4.3	20.0	0.00014335
IFITM3	Interferon Induced Transmembrane Protein 3	-4.3	19.8	0.000341991
MEG3	Maternally Expressed 3 (Non-Protein Coding)	-4.3	19.5	0.000471982
PTGS2	Prostaglandin-Endoperoxide Synthase 2 (Prostaglandin G/H Synthase And Cyclooxygenase)	-4.3	19.5	0.00014335
UBE2C	Ubiquitin-Conjugating Enzyme E2C	-4.3	19.4	0.00014335
COL6A1	Collagen, Type VI, Alpha 1	-4.3	19.3	0.000214013
FAT1	FAT Atypical Cadherin 1	-4.3	19.1	0.000198962
GAS6	Growth Arrest-Specific 6	-4.2	18.3	0.000211144
GAS6	Growth Arrest-Specific 6	-4.2	18.0	0.000190415
ACTN1	Actinin, Alpha 1	-4.2	17.8	0.000205266
COL5A2	Collagen, Type V, Alpha 2	-4.1	17.5	0.000308347
RAI14	Retinoic Acid Induced 14	-4.1	17.4	0.00014335
IGFBP7	Insulin-Like Growth Factor Binding Protein 7	-4.1	17.4	0.000190415
PLS3	Plastin 3	-4.1	17.3	0.00014335
RAGE	Advanced Glycosylation End Product-Specific Receptor	-4.1	17.1	0.00014335
UBE2C	Ubiquitin-Conjugating Enzyme E2C	-4.1	17.1	0.00014335
VEGFC	Vascular Endothelial Growth Factor C	-4.1	17.0	0.000216559
MMP3	Matrix Metallopeptidase 3	-4.1	16.6	0.000445667
AXL	AXL Receptor Tyrosine Kinase	-4.0	16.2	0.00014335
PRRX2	Paired Related Homeobox 2	-4.0	16.1	0.000186638
LOX	Lysyl Oxidase	-3.9	15.1	0.000160592
PRKCDBP	Protein Kinase C, Delta Binding Protein	-3.9	15.0	0.00014335
TOP2A	Topoisomerase (DNA) II Alpha 170kDa	-3.9	14.9	0.00014335
IL8	**Interleukin 8**	**-3.9**	**14.6**	**0.000211144**
IFIT3	Interferon-Induced Protein With Tetratricopeptide Repeats...	-3.8	14.0	0.001822449
DCN	Decorin	-3.8	13.9	0.00022957
FRMD6	FERM Domain Containing 6	-3.8	13.6	0.000190415
LOC441019		-3.8	13.5	0.000541679
AXL	AXL Receptor Tyrosine Kinase	-3.8	13.5	0.00014335
TAGLN	Transgelin	-3.7	13.4	0.000190415
ACTG2	Actin, Gamma 2, Smooth Muscle, Enteric	-3.7	13.4	0.008566589
DKK1	Dickkopf WNT Signalling Pathway Inhibitor 1	-3.7	13.2	0.00014335
CLDN11	Claudin 11	-3.7	12.9	0.001197107
OXTR	Oxytocin Receptor	-3.7	12.7	0.000205266
TAGLN	Transgelin	-3.7	12.6	0.000665922
COL5A1	Collagen, Type V, Alpha 1	-3.7	12.6	0.00016268
FERMT2	Fermitin Family Member 2	-3.6	12.4	0.000163358
LOC493869	N/A	-3.6	12.4	0.000160592
TMEM166	N/A	-3.6	12.4	0.00014335
ASPM	Asp (Abnormal Spindle) Homolog, Microcephaly Associated...	-3.6	12.1	0.00014335
CD248	CD248 Molecule, Endosialin	-3.6	12.0	0.000608343
NT5E	5'-Nucleotidase, Ecto (CD73)	-3.5	11.7	0.00014335
ANTXR1	Anthrax Toxin Receptor 1	-3.5	11.7	0.000225323
SLC7A2	Solute Carrier Family 7	-3.5	11.7	0.000151974
TNC	Tenascin C	-3.5	11.6	0.000190415
STC2	Stanniocalcin 2	-3.5	11.6	0.000691301
LPAR1	Lysophosphatidic Acid Receptor 1	-3.5	11.5	0.000217914

b) Upregulated in CLL cells following Co-culture with CM				
TargetID	**Name**	**logFC**	**FC**	**adj.P.Val**
CCL3L3	Chemokine (C-C Motif) Ligand 3-Like 3	-4.2	18.5	0.176974619
CCL3	Chemokine (C-C Motif) Ligand 3	-4.1	17.2	0.163888118
IL1B	Interleukin 1, Beta	-3.9	14.8	0.218139199
LOC72883	N/A	-3.8	14.3	0.078351774
CCL3L1	Chemokine (C-C Motif) Ligand 3-Like 1	-3.8	13.9	0.216237789
IL6	Interleukin 6	-3.8	13.7	0.176974619
CCL3L1	Chemokine (C-C Motif) Ligand 3-Like 1	-3.5	11.6	0.163888118
CCL4L1	Chemokine (C-C Motif) Ligand 4-Like 1	-3.5	11.6	0.11667252
CXCL5	Chemokine (C-X-C Motif) Ligand 5	-3.5	11.6	0.204174082
CCL4L2	Chemokine (C-C Motif) Ligand 4-Like 2	-3.4	10.8	0.11667252
CCL3L1	Chemokine (C-C Motif) Ligand 3-Like 1	-3.4	10.3	0.078351774
IL1A	Interleukin 1, Alpha	-3.4	10.2	0.305060157
PTGS2	Prostaglandin-Endoperoxide Synthase 2	-3.3	10.1	0.21968549
CCL2	Chemokine (C-C Motif) Ligand 2	-3.2	9.2	0.413667399
TNF	Tumor Necrosis Factor	-3.0	8.1	0.216237789
IL1RN	Interleukin 1 Receptor Antagonist	-2.8	7.0	0.219121207
IL24	Interleukin 24	-2.7	6.7	0.11667252
CXCL1	Chemokine (C-X-C Motif) Ligand 1	-2.5	5.6	0.439667846
CXCL2	Chemokine (C-X-C Motif) Ligand 2	-2.3	5.1	0.11667252
IL1RN	IL1RN	-2.3	4.9	0.422328015
IER3	Immediate Early Response 3	-2.2	4.7	0.123139593
IL8	Interleukin 8	-2.1	4.2	0.218139199
PTGS2	Prostaglandin-Endoperoxide Synthase 2	-2.0	4.0	0.234400825
IL8	Interleukin 8	-1.8	3.5	0.248900178
CXCL5	Chemokine (C-X-C Motif) Ligand 5	-1.8	3.5	0.452447979
SOD2	Superoxide Dismutase 2	-1.6	3.1	0.505547634
CTSL1	Cathepsin L	-1.6	3.0	0.504532297
CTSL1	Cathepsin L	-1.6	3.0	0.45156067
PPBP	Pro-Platelet Basic Protein (Chemokine (C-X-C Motif) Ligand 7)	-1.6	3.0	0.505547634
SOD2	Superoxide Dismutase 2	-1.5	2.9	0.305060157
SLC25A24	Solute Carrier Family 25 (Mitochondrial Carrier; Phosphate Carrier), Member 24	-1.5	2.9	0.305060157
RIN2	Ras And Rab Interactor 2	-1.4	2.7	0.505547634
NLRP3	NLR Family, Pyrin Domain Containing 3	-1.4	2.6	0.218139199
IL24	Interleukin 24	-1.3	2.5	0.234400825
LOC728830	N/A	-1.3	2.4	0.218139199
IL24	Interleukin 24	-1.2	2.3	0.218139199
NLRP3	NLR Family, Pyrin Domain Containing 3	-1.2	2.3	0.413667399
NFKBIZ	Nuclear Factor Of Kappa Light Polypeptide Gene Enhancer In B-Cells Inhibitor, Zeta	-1.1	2.2	0.504532297
MIR302C	MicroRNA 302c	-1.0	2.0	0.248900178
ID2	Inhibitor Of DNA Binding 2, Dominant Negative Helix-Loop-Helix Protein	-1.0	2.0	0.218139199
MAFF	V-Maf Avian Musculoaponeurotic Fibrosarcoma Oncogene Homolog F	-1.0	2.0	0.496602727
CYP4B1	Cytochrome P450, Family 4, Subfamily B, Polypeptide 1	-0.9	1.9	0.305060157
CD40	CD40 Molecule, TNF Receptor Superfamily Member 5	-0.9	1.8	0.472787243
PLAUR	Plasminogen Activator, Urokinase Receptor	-0.9	1.8	0.439667846
BST2	Bone Marrow Stromal Cell Antigen 2	-0.8	1.7	0.472787243
TPM2	Tropomyosin 2 (Beta)	-0.8	1.7	0.452447979
LOC10012968	N/A	-0.8	1.7	0.305388832
ID2	Inhibitor Of DNA Binding 2, Dominant Negative Helix-Loop-Helix Protein	-0.8	1.7	0.305060157
GNLY	Granulysin	-0.7	1.7	0.413667399
TPM2	Tropomyosin 2 (Beta)	-0.7	1.7	0.395948545
SREBF1	Sterol Regulatory Element Binding Transcription Factor 1	-0.6	1.5	0.45156067
TICAM1	Toll-Like Receptor Adaptor Molecule 1	-0.6	1.5	0.486772469

HDAC9	Histone Deacetylase 9	-0.6	1.5	0.412740023
CRKRS	Cyclin-Dependent Kinase 12	-0.6	1.5	0.472787243
CASZ1	Castor Zinc Finger 1	-0.6	1.5	0.482905463
TAP1	Transporter 1, ATP-Binding Cassette, Sub-Family B	-0.5	1.4	0.505547634
AXIN1	Axin 1	0.4	0.7	0.504532297
GFOD1	Glucose-Fructose Oxidoreductase Domain Containing 1	0.5	0.7	0.49180744
BSCL2	Berardinelli-Seip Congenital Lipodystrophy 2 (Seipin)	0.5	0.7	0.486772469
SMAD6	SMAD Family Member 6	0.5	0.7	0.504532297
HS.559665	N/A	0.5	0.7	0.504532297
FYTTD1	Forty-Two-Three Domain Containing 1	0.5	0.7	0.504532297
FKSG30	N/A	0.5	0.7	0.45156067
NQO1	NAD(P)H Dehydrogenase, Quinone 1	0.5	0.7	0.440952698
AIF1	Allograft Inflammatory Factor 1	0.6	0.7	0.504532297
TRAPPC2L	Trafficking Protein Particle Complex 2-Like	0.6	0.7	0.398548586
NMT2	N-Myristoyltransferase 2	0.6	0.7	0.422328015
FAM167A	Family With Sequence Similarity 167, Member A	0.6	0.7	0.486772469
FAM62B	Extended Synaptotagmin-Like Protein 2	0.6	0.7	0.452447979
KIAA0226	N/A	0.6	0.6	0.472787243
C8ORF13	Family With Sequence Similarity 167, Member A	0.6	0.6	0.422328015
DIRC2	Disrupted In Renal Carcinoma 2	0.6	0.6	0.319181181
C5AR1	Complement Component 5a Receptor 1	0.7	0.6	0.305060157
AVPI1	Arginine Vasopressin-Induced 1	0.7	0.6	0.334152532
GPR162	G Protein-Coupled Receptor 162	0.7	0.6	0.486772469
ZNF10	Zinc Finger Protein 10	0.7	0.6	0.439667846
FBXO10	F-Box Protein 10	0.7	0.6	0.504532297
SIDT1	SID1 Transmembrane Family, Member 1	0.7	0.6	0.452447979
C14ORF173	Inverted Formin, FH2 And WH2 Domain Containing	0.7	0.6	0.422328015
TP53I13	Tumor Protein P53 Inducible Protein 13	0.7	0.6	0.45156067
MCM6	Minichromosome Maintenance Complex Component 6	0.7	0.6	0.292135196
VIL2	Ezrin	0.8	0.6	0.486772469
HMGB2	High Mobility Group Box 2	0.8	0.6	0.413667399
DUSP6	Dual Specificity Phosphatase 6	0.8	0.6	0.469803305
ST3GAL5	ST3 Beta-Galactoside Alpha-2,3-Sialyltransferase 5	0.8	0.6	0.486772469
VCAN	Versican	0.8	0.6	0.486772469
NMT2	N-Myristoyltransferase 2	0.9	0.5	0.305060157
CD36	CD36 Molecule (Thrombospondin Receptor)	1.0	0.5	0.413667399
TSC22D3	TSC22 Domain Family, Member 3	1.0	0.5	0.305060157
HMGB2	High Mobility Group Box 2	1.0	0.5	0.441364846
LOC10012955	N/A	1.1	0.5	0.441364846
KIAA1683	N/A	1.2	0.4	0.218139199
FCN1	Ficolin	1.2	0.4	0.45156067
TGFBI	Transforming Growth Factor, Beta-Induced	1.3	0.4	0.218139199
OLR1	Oxidized Low Density Lipoprotein (Lectin-Like) Receptor 1	1.5	0.4	0.234400825
FUCA1	Fucosidase, Alpha-L- 1, Tissue	1.5	0.4	0.334152532
CSF1R	Colony Stimulating Factor 1 Receptor	1.6	0.3	0.495173033
LYZ	Lysozyme	1.7	0.3	0.505547634
TSC22D3	TSC22 Domain Family, Member 3	1.8	0.3	0.504532297
RGS2	Regulator Of G-Protein Signalling 2	2.7	0.2	0.422328015

GSEA additional data

Additional data for GSEA comparison of CLL cells cultured alone and CLL cells cultured with HFFF2-CM using the C2-curated gene set from the Msig database. Included are tables for top 20 gene sets with the greatest positive and negative normalized enrichment score (NES). Those with a positive ES are enriched in the first phenotype, CLL cells cultured alone, those with a negative ES are enriched in the second phenotype, CLL cells cultured with HFFF2-CM. There is also the snapshot images for the listed gene setsCLL versus CM tables

CLL vs CM, Ranked Gene list, Negative ES

NAME	SIZE	ES	NES	NOM p-val	FDR q-val	FWER p-val	RANK AT MAX	LEADING EDGE
REACTOME_CHEMOKINE_RECEPTORS_BIND_CHEMOKINES	55	-0.8322597	-3.0467155	0	0	0	210	tags=29%, list=1%, signal=29%
REACTOME_DESTABILIZATION_OF_MRNA_BY_AUF1_HNRNP_D0	52	-0.8277568	-2.8966653	0	0	0	2851	tags=69%, list=8%, signal=75%
REACTOME_ACTIVATION_OF_NF_KAPPAB_IN_B_CELLS	63	-0.7886971	-2.887905	0	0	0	2851	tags=63%, list=8%, signal=69%
REACTOME_SCF_BETA_TRCP_MEDIATED_DEGRADATION_OF_EMI1	50	-0.8061496	-2.875088	0	0	0	4231	tags=74%, list=12%, signal=84%
KEGG_PROTEASOME	46	-0.8499774	-2.8638568	0	0	0	3263	tags=76%, list=9%, signal=84%
REACTOME_CYCLIN_E_ASSOCIATED_EVENTS_DURING_G1_S_TRANSITION_	64	-0.75637954	-2.8435693	0	0	0	4231	tags=64%, list=12%, signal=73%
REACTOME_CDK_MEDIATED_PHOSPHORYLATION_AND_REMOVAL_OF_CDC6	47	-0.82320267	-2.8085501	0	0	0	4231	tags=79%, list=12%, signal=90%
REACTOME_P53_DEPENDENT_G1_DNA_DAMAGE_RESPONSE	55	-0.7787897	-2.7881062	0	0	0	4231	tags=69%, list=12%, signal=79%
BIOCARTA_PROTEASOME_PATHWAY	28	-0.8883512	-2.785973	0	0	0	2851	tags=86%, list=8%, signal=93%
PID_IL23_PATHWAY	37	-0.85942686	-2.7825677	0	0	0	831	tags=38%, list=2%, signal=39%
REACTOME_SCFSKP2_MEDIATED_DEGRADATION_OF_P27_P21	55	-0.7820684	-2.7817516	0	0	0	4231	tags=71%, list=12%, signal=81%
REACTOME_VIF_MEDIATED_DEGRADATION_OF_APOBEC3G	51	-0.80474985	-2.7678246	0	0	0	4231	tags=76%, list=12%, signal=87%
REACTOME_P53_INDEPENDENT_G1_S_DNA_DAMAGE_CHECKPOINT	50	-0.7831037	-2.7669878	0	0	0	4231	tags=72%, list=12%, signal=82%
REACTOME_AUTODEGRADATION_OF_THE_E3_UBIQUITIN_LIGASE_COP1	49	-0.8036358	-2.7323136	0	0	0	4231	tags=73%, list=12%, signal=84%
KEGG_CYTOKINE_CYTOKINE_RECEPTOR_INTERACTION	265	-0.60265017	-2.7166264	0	0	0	2086	tags=17%, list=6%, signal=18%
REACTOME_ER_PHAGOSOME_PATHWAY	59	-0.7472505	-2.7140596	0	0	0	2851	tags=64%, list=8%, signal=70%
REACTOME_CDT1_ASSOCIATION_WITH_THE_CDC6_ORC_ORIGIN_COMPLEX	49	-0.79569286	-2.6918182	0	0	0	4231	tags=73%, list=12%, signal=84%
REACTOME_CROSS_PRESENTATION_OF_SOLUBLE_EXOGENOUS_ANTIGENS_ENDOSOMES	48	-0.8121457	-2.6899989	0	0	0	3263	tags=69%, list=9%, signal=76%
REACTOME_REGULATION_OF_ORNITHINE_DECARBOXYLASE_ODC	49	-0.76412696	-2.6880827	0	0	0	3263	tags=67%, list=9%, signal=74%
KEGG_NOD_LIKE_RECEPTOR_SIGNALING_PATHWAY	59	-0.72989064	-2.6487284	0	0	0	1892	tags=37%, list=5%, signal=39%
REACTOME_REGULATION_OF_MRNA_STABILITY_BY_PROTEINS_THAT_BIND_AU_RICH_ELEMENTS	83	-0.6850985	-2.6159563	0	0	0	4231	tags=61%, list=12%, signal=70%

REACTOME_DOWNSTREAM_SIGNALING_EVENTS_OF_B_CELL_RECEPTOR_BCR	94	-0.66159797	-2.5699317	0	0	0	2851	tags=47%, list=8%, signal=51%
KEGG_CHEMOKINE_SIGNALING_PATHWAY	188	-0.58877486	-2.5391095	0	0	0	2118	tags=19%, list=6%, signal=20%
BIOCARTA_INFLAM_PATHWAY	29	-0.7963812	-2.5243828	0	0	0	1821	tags=38%, list=5%, signal=40%
REACTOME_CYTOKINE_SIGNALING_IN_IMMUNE_SYSTEM	264	-0.5590043	-2.4555438	0	0	0	2754	tags=33%, list=8%, signal=35%
REACTOME_APC_C_CDC20_MEDIATED_DEGRADATION_OF_MITOTIC_PROTEINS	69	-0.67294693	-2.4521437	0	0	0	4344	tags=61%, list=13%, signal=69%
REACTOME_INTERFERON_SIGNALING	157	-0.5932395	-2.4395423	0	0	0	2632	tags=38%, list=8%, signal=40%
PID_IL27_PATHWAY	26	-0.8198586	-2.4298565	0	0	0	1614	tags=42%, list=5%, signal=44%
REACTOME_APC_C_CDH1_MEDIATED_DEGRADATION_OF_CDC20_AND_OTHER_APC_C_CDH1_TARGETED_PROTEINS_IN_LATE_MITOSIS_EARLY_G1	69	-0.66432476	-2.4206471	0	0	0	4344	tags=59%, list=13%, signal=68%
REACTOME_PEPTIDE_LIGAND_BINDING_RECEPTORS	186	-0.57698506	-2.4138412	0	0	0	210	tags=9%, list=1%, signal=9%
REACTOME_AUTODEGRADATION_OF_CDH1_BY_CDH1_APC_C	61	-0.6669593	-2.4050257	0	0	0	4344	tags=62%, list=13%, signal=71%
REACTOME_FORMATION_OF_TUBULIN_FOLDING_INTERMEDIATES_BY_CCT_TRIC	20	-0.83808523	-2.3986204	0	5.97E-05	0.001	2274	tags=60%, list=7%, signal=64%
BIOCARTA_CYTOKINE_PATHWAY	21	-0.8237618	-2.3832054	0	5.79E-05	0.001	1821	tags=48%, list=5%, signal=50%
REACTOME_INTERFERON_ALPHA_BETA_SIGNALING	63	-0.6632899	-2.3813791	0	5.62E-05	0.001	1237	tags=38%, list=4%, signal=39%
REACTOME_REGULATION_OF_MITOTIC_CELL_CYCLE	81	-0.6281353	-2.3718631	0	5.46E-05	0.001	4344	tags=54%, list=13%, signal=62%
REACTOME_ANTIGEN_PROCESSING_CROSS_PRESENTATION	74	-0.6343631	-2.3669467	0	5.31E-05	0.001	2851	tags=53%, list=8%, signal=57%
NABA_SECRETED_FACTORS	334	-0.525286	-2.3574023	0	5.17E-05	0.001	2539	tags=13%, list=7%, signal=14%
REACTOME_REGULATION_OF_APOPTOSIS	57	-0.67891943	-2.3504105	0	5.03E-05	0.001	4231	tags=65%, list=12%, signal=74%
KEGG_SPLICEOSOME	114	-0.5784973	-2.3440263	0	1.02E-04	0.002	3205	tags=43%, list=9%, signal=47%
BIOCARTA_IL1R_PATHWAY	32	-0.7377493	-2.3430128	0	9.97E-05	0.002	2522	tags=50%, list=7%, signal=54%
REACTOME_HOST_INTERACTIONS_OF_HIV_FACTORS	127	-0.5789987	-2.3371623	0	1.44E-04	0.003	3263	tags=46%, list=9%, signal=50%
PID_MYC_ACTIV_PATHWAY	79	-0.62125045	-2.3231318	0	1.86E-04	0.004	2927	tags=43%, list=8%, signal=47%
REACTOME_SIGNALING_BY_WNT	64	-0.6532218	-2.2962308	0	2.76E-04	0.006	4231	tags=61%, list=12%, signal=69%
REACTOME_MRNA_SPLICING	99	-0.580511	-2.2951279	0	2.70E-	0.006	3568	tags=46%, list=10%,

					04			signal=52%
BIOCARTA_ERYTH_PATHWAY	15	-0.8609921	-2.28123	0	3.06E-04	0.007	13	tags=20%, list=0%, signal=20%
BIOCARTA_IL17_PATHWAY	15	-0.8321547	-2.2669628	0	3.78E-04	0.009	1265	tags=20%, list=4%, signal=21%
REACTOME_ANTIVIRAL_MECHANISM_BY_IFN_STIMULATED_GENES	65	-0.6141908	-2.2668707	0	3.70E-04	0.009	2578	tags=42%, list=7%, signal=45%
REACTOME_ASSEMBLY_OF_THE_PRE_REPLICATIVE_COMPLEX	58	-0.61201996	-2.2513947	0	4.05E-04	0.01	2851	tags=57%, list=8%, signal=62%
KEGG_GRAFT_VERSUS_HOST_DISEASE	42	-0.66562015	-2.2423692	0	5.52E-04	0.014	2695	tags=31%, list=8%, signal=34%
REACTOME_CYTOSOLIC_TRNA_AMINOACYLATION	23	-0.76014525	-2.2364786	0	6.11E-04	0.016	4260	tags=74%, list=12%, signal=84%

CLL vs CM, Ranked Gene list Positive ES

NAME	SIZE	ES	NES	NOM p-val	FDR q-val	FWER p-val	RANK AT MAX	LEADING EDGE
REACTOME_RNA_POL_I_PROMOTER_OPENING	59	0.6480464	1.9293168	0	0.02058614	0.028	5818	tags=47%, list=17%, signal=57%
REACTOME_DNA_STRAND_ELONGATION	29	0.6924409	1.8861182	0	0.021683782	0.058	4656	tags=59%, list=13%, signal=68%
KEGG_VALINE_LEUCINE_AND_ISOLEUCINE_DEGRADATION	44	0.64978534	1.8725266	0.001302083	0.01715681	0.068	4103	tags=50%, list=12%, signal=57%
REACTOME_GENERIC_TRANSCRIPTION_PATHWAY	345	0.52795213	1.8396139	0	0.0267135	0.136	5067	tags=34%, list=15%, signal=40%
KEGG_GLYCOSYLPHOSPHATIDYLINOSITOL_GPI_ANCHOR_BIOSYNTHESIS	25	0.7032496	1.8176003	0	0.032113645	0.195	3195	tags=52%, list=9%, signal=57%
REACTOME_ACTIVATION_OF_THE_PRE_REPLICATIVE_COMPLEX	24	0.7048559	1.8086503	0	0.031296793	0.224	4430	tags=50%, list=13%, signal=57%
KEGG_OTHER_GLYCAN_DEGRADATION	15	0.7761934	1.7878118	0	0.039239112	0.313	1548	tags=40%, list=4%, signal=42%
REACTOME_AMYLOIDS	80	0.5759954	1.7822443	0	0.037833214	0.339	5820	tags=39%, list=17%, signal=46%
REACTOME_PACKAGING_OF_TELOMERE_ENDS	48	0.6154465	1.77313	0	0.03975207	0.392	6380	tags=48%, list=18%, signal=59%
BIOCARTA_TGFB_PATHWAY	18	0.72595716	1.7681148	0.002812941	0.03967168	0.418	5532	tags=56%, list=16%, signal=66%
REACTOME_GLUTATHIONE_CONJUGATION	23	0.68232816	1.7643951	0.002743484	0.039089262	0.436	1986	tags=35%, list=6%, signal=37%
PID_NECTIN_PATHWAY	30	0.66147906	1.7573645	0	0.040118482	0.472	6311	tags=53%, list=18%, signal=65%
KEGG_GLYCOSPHINGOLIPID_BIOSYNTHESIS_GANGLIO_SERIES	15	0.74965405	1.726261	0.002886003	0.061528347	0.65	4461	tags=47%, list=13%, signal=54%
PID_S1P_S1P2_PATHWAY	24	0.6582497	1.702791	0.001342282	0.08135174	0.768	5198	tags=42%, list=15%, signal=49%
KEGG_LYSOSOME	121	0.5210808	1.6929958	0	0.08800834	0.814	3245	tags=28%, list=9%, signal=31%
REACTOME_ACTIVATION_OF_ATR_IN_RESPONSE_TO_REPLICATION_STRESS	31	0.6297361	1.6928954	0.002673797	0.08264778	0.814	4656	tags=35%, list=13%, signal=41%
REACTOME_MEIOTIC_RECOMBINATION	83	0.5387143	1.6794792	0.001149425	0.09346256	0.871	7151	tags=46%, list=21%, signal=58%
REACTOME_DEPOSITION_OF_NEW_CENPA_CONTAINING_NUCLEOSOMES_AT_THE_CENTROMERE	61	0.5615829	1.6654005	0	0.10937314	0.922	5818	tags=43%, list=17%, signal=51%
REACTOME_SEMA4D_INDUCED_CELL_MIGRATION_AND_GROWTH_CONE_COLLAPSE	24	0.6412189	1.6601421	0.008230452	0.11159968	0.936	6096	tags=50%, list=18%, signal=61%
PID_WNT_NONCANONICAL_PATHWAY	30	0.6298824	1.6584425	0.002604167	0.10892995	0.943	7519	tags=53%, list=22%, signal=68%

REACTOME_SYNTHESIS_OF_GLYCOSYLPHOSPHATIDYLINOSITOL_GPI	17	0.69079393	1.6454663	0.0121 13055	0.12159366	0.966	3177	tags=47%, list=9%, signal=52%
REACTOME_G2_M_CHECKPOINTS	37	0.5927138	1.6363263	0.0051 94805	0.1313577	0.978	4656	tags=32%, list=13%, signal=37%
KEGG_DNA_REPLICATION	36	0.59825647	1.628617	0.0091 02731	0.13899226	0.988	4685	tags=50%, list=14%, signal=58%
REACTOME_RECRUITMENT_OF_MITOTIC_CENTROSOME_PROTEINS_AND_COMPLEXES	58	0.5440548	1.6205022	0.0036 80982	0.14924616	0.994	4379	tags=41%, list=13%, signal=47%
KEGG_PHOSPHATIDYLINOSITOL_SIGNALING_SYSTEM	76	0.5242632	1.6193335	0	0.14560954	0.994	7091	tags=36%, list=20%, signal=45%
KEGG_BUTANOATE_METABOLISM	34	0.5870797	1.6050903	0.0013 08901	0.16532372	0.997	4103	tags=35%, list=12%, signal=40%
KEGG_METABOLISM_OF_XENOBIOTICS_BY_CYTOCHROME_P450	70	0.52309203	1.5934019	0.0036 10108	0.18364264	0.999	3993	tags=21%, list=12%, signal=24%
REACTOME_LOSS_OF_NLP_FROM_MITOTIC_CENTROSOMES	51	0.54194474	1.5928605	0.0037 03704	0.17823592	0.999	4379	tags=43%, list=13%, signal=49%
BIOCARTA_GPCR_PATHWAY	34	0.5861991	1.58433	0.0079 36508	0.18981856	0.999	3907	tags=35%, list=11%, signal=40%
REACTOME_GLYCOGEN_BREAKDOWN_GLYCOGENOLYSIS	17	0.6603037	1.5774666	0.0131 19534	0.19939147	0.999	4163	tags=41%, list=12%, signal=47%
REACTOME_SIGNALING_BY_RHO_GTPASES	107	0.49422935	1.5769717	0.0011 40251	0.19386177	0.999	6455	tags=34%, list=19%, signal=41%
REACTOME_BRANCHED_CHAIN_AMINO_ACID_CATABOLISM	17	0.66222864	1.5722885	0.0187 05036	0.19796714	1	3798	tags=59%, list=11%, signal=66%
PID_RHOA_PATHWAY	44	0.5493669	1.5668409	0.0101 78117	0.20490722	1	6096	tags=43%, list=18%, signal=52%
REACTOME_TELOMERE_MAINTENANCE	74	0.50601053	1.563119	0.0096 15385	0.20712653	1	5818	tags=43%, list=17%, signal=52%
BIOCARTA_HDAC_PATHWAY	28	0.5996712	1.5602328	0.0188 93387	0.20768905	1	5523	tags=43%, list=16%, signal=51%
KEGG_INOSITOL_PHOSPHATE_METABOLISM	54	0.51979095	1.5560983	0.0112 6408	0.21074721	1	6833	tags=37%, list=20%, signal=46%
REACTOME_DAG_AND_IP3_SIGNALING	31	0.5717687	1.5523164	0.0091 26467	0.21440199	1	3279	tags=26%, list=9%, signal=28%
PID_AR_NONGENOMIC_PATHWAY	31	0.5847443	1.5506974	0.0131 75231	0.21224909	1	5794	tags=39%, list=17%, signal=46%
REACTOME_NRAGE_SIGNALS_DEATH_THROUGH_JNK	43	0.5454308	1.550464	0.0065 27415	0.20750183	1	4212	tags=28%, list=12%, signal=32%
BIOCARTA_FCER1_PATHWAY	38	0.55919886	1.5479268	0.0077 31959	0.207987	1	5523	tags=39%, list=16%, signal=47%
PID_ARF6_TRAFFICKING_PATHWAY	49	0.53465813	1.5469373	0.0075 37689	0.20537154	1	4388	tags=29%, list=13%, signal=33%
KEGG_DRUG_METABOLISM_CYTOCHROME_P450	72	0.5049168	1.5454742	0.0096 03841	0.20371601	1	3141	tags=18%, list=9%, signal=20%
REACTOME_CELL_DEATH_SIGNALLING_VIA_NRAGE_NRIF_AND_NADE	59	0.52220136	1.5452288	0.0107	0.19952622	1	4466	tags=25%, list=13%,

				91367				signal=29%
BIOCARTA_BCR_PATHWAY	34	0.566078	1.5440661	0.0256 06468	0.19762224	1	4212	tags=32%, list=12%, signal=37%
KEGG_LEUKOCYTE_TRANSENDOTHELIAL_MIGRATION	114	0.47325563	1.5253983	0.0033 93665	0.2365976	1	6462	tags=34%, list=19%, signal=42%
PID_RHOA_REG_PATHWAY	44	0.52727354	1.5139326	0.0174 3462	0.2596046	1	5217	tags=32%, list=15%, signal=37%
REACTOME_MEIOTIC_SYNAPSIS	72	0.49431774	1.5135179	0.0143 71257	0.25521028	1	5818	tags=36%, list=17%, signal=43%
REACTOME_MEIOSIS	112	0.47104016	1.5131121	0.0056 62514	0.2507419	1	5818	tags=36%, list=17%, signal=43%
PID_P38_ALPHA_BETA_PATHWAY	30	0.56237924	1.5071862	0.0305 73249	0.2606671	1	7108	tags=43%, list=20%, signal=54%
SA_B_CELL_RECEPTOR_COMPLEXES	24	0.5957047	1.5062298	0.0280 11205	0.25817788	1	4903	tags=38%, list=14%, signal=44%

Table: Snapshot of enrichment results

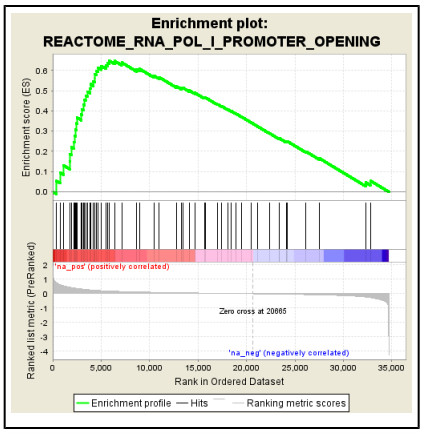

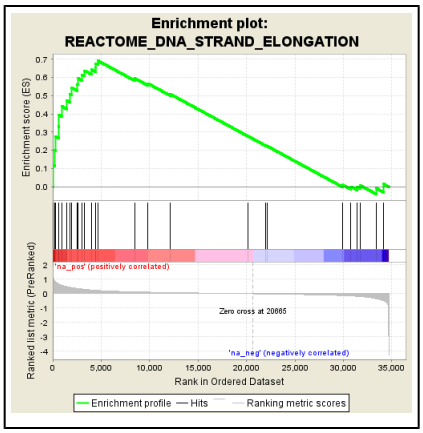

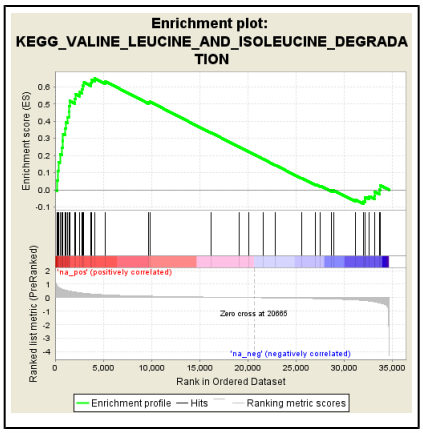

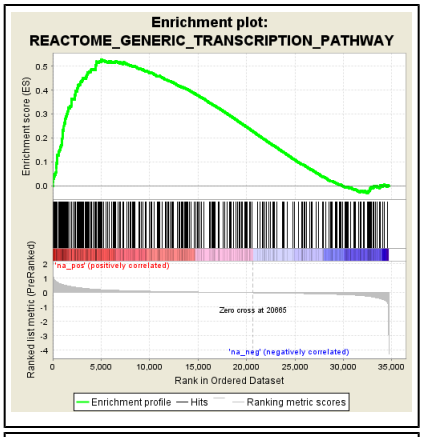

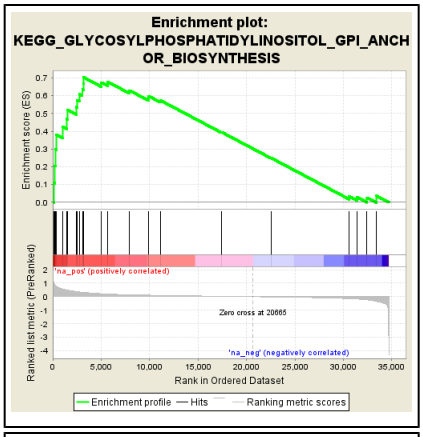

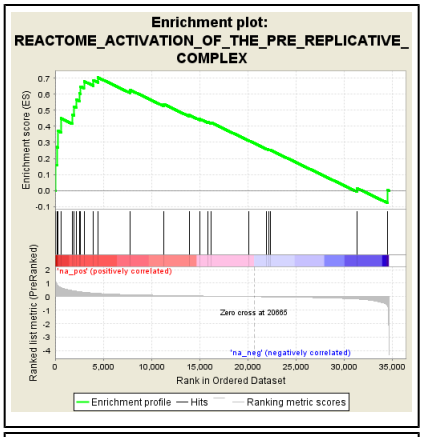

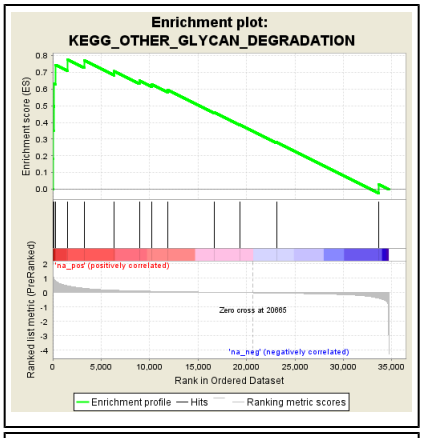

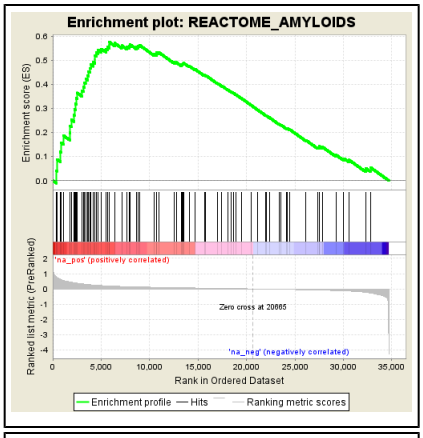

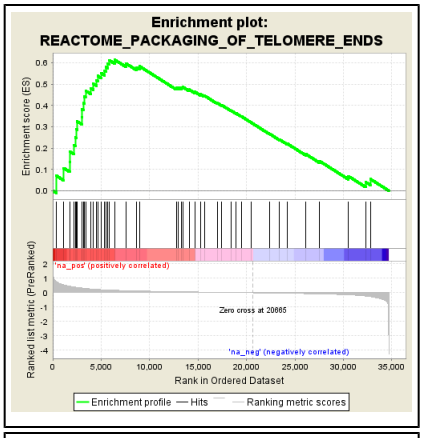

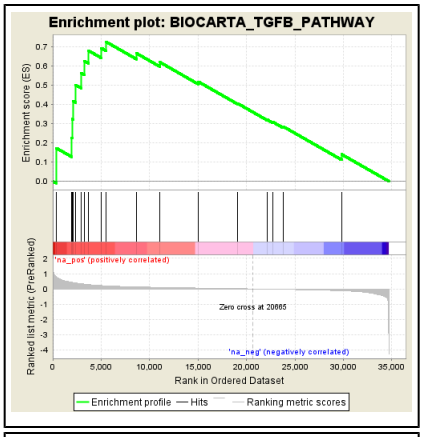

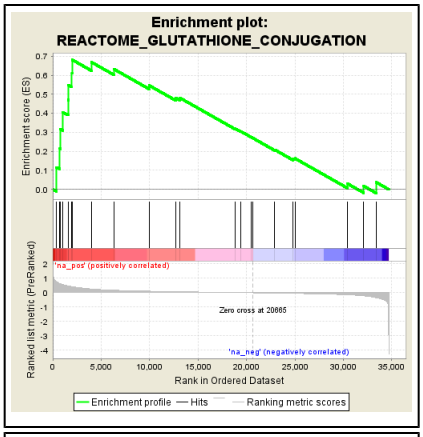

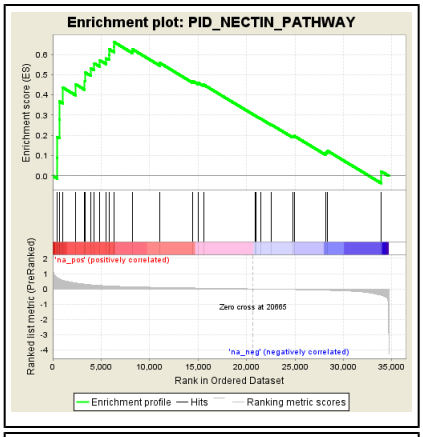

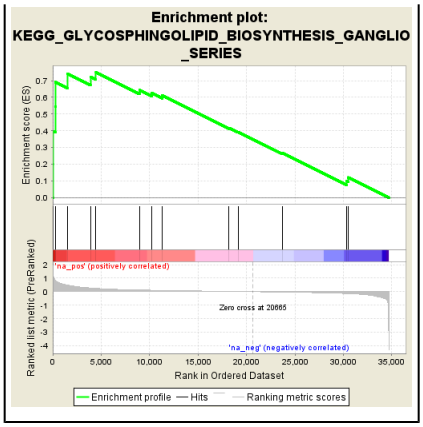
Enrichment plot:
KEGG_GLYCOSPHINGOLIPID_BIOSYNTHESIS_GANGLIO_SERIES
Enrichment score (ES)
Ranked list metric (PreRanked)
'na_pos' (positively correlated)
Zero cross at 20665
'na_neg' (negatively correlated)
Rank in Ordered Dataset
Enrichment profile
Hits
Ranking metric scores

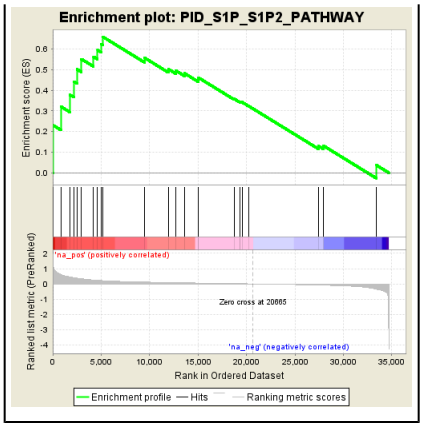
Enrichment plot: PID_S1P_S1P2_PATHWAY
Enrichment score (ES)
Ranked list metric (PreRanked)
'na_pos' (positively correlated)
Zero cross at 20665
'na_neg' (negatively correlated)
Rank in Ordered Dataset
Enrichment profile
Hits
Ranking metric scores

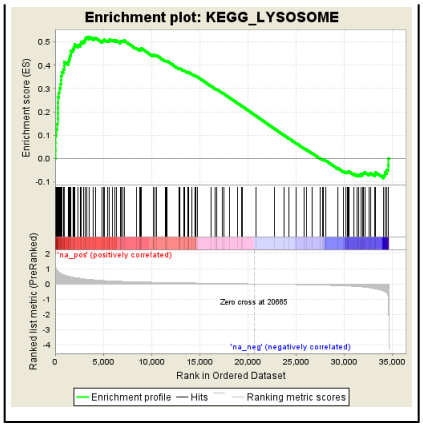
Enrichment plot: KEGG_LYSOSOME
Enrichment score (ES)
Ranked list metric (PreRanked)
'na_pos' (positively correlated)
Zero cross at 20665
'na_neg' (negatively correlated)
Rank in Ordered Dataset
Enrichment profile
Hits
Ranking metric scores

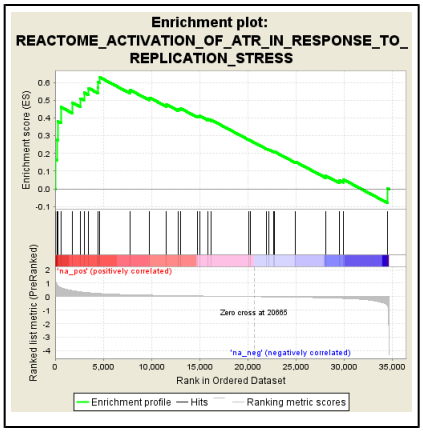
Enrichment plot:
REACTOME_ACTIVATION_OF_ATR_IN_RESPONSE_TO_REPLICATION_STRESS
Enrichment score (ES)
Ranked list metric (PreRanked)
'na_pos' (positively correlated)
Zero cross at 20665
'na_neg' (negatively correlated)
Rank in Ordered Dataset
Enrichment profile
Hits
Ranking metric scores

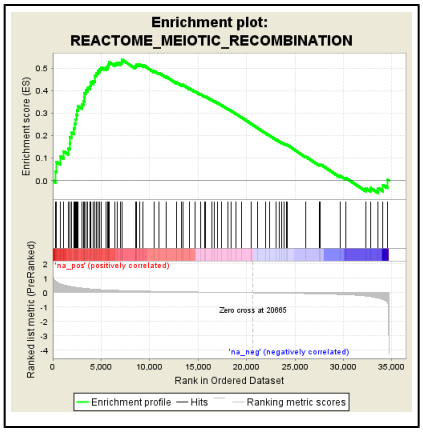
Enrichment plot:
REACTOME_MEIOTIC_RECOMBINATION
Enrichment score (ES)
Ranked list metric (PreRanked)
'na_pos' (positively correlated)
Zero cross at 20665
'na_neg' (negatively correlated)
Rank in Ordered Dataset
Enrichment profile
Hits
Ranking metric scores

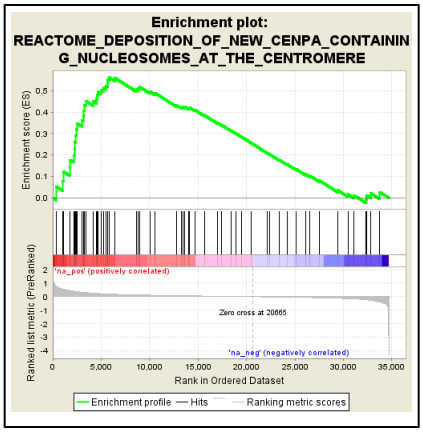
Enrichment plot:
REACTOME_DEPOSITION_OF_NEW_CENPA_CONTAINING_NUCLEOSOMES_AT_THE_CENTROMERE
Enrichment score (ES)
Ranked list metric (PreRanked)
'na_pos' (positively correlated)
Zero cross at 20665
'na_neg' (negatively correlated)
Rank in Ordered Dataset
Enrichment profile
Hits
Ranking metric scores

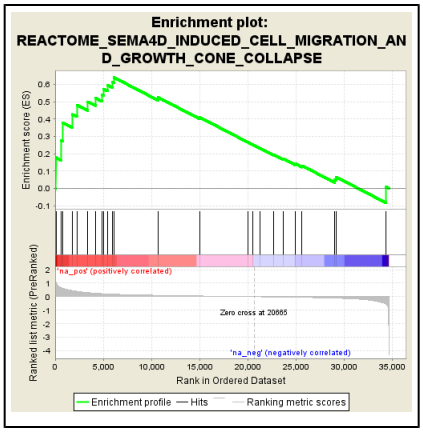
Enrichment plot:
REACTOME_SEMA4D_INDUCED_CELL_MIGRATION_AND_GROWTH_CONE_COLLAPSE
Enrichment score (ES)
Ranked list metric (PreRanked)
'na_pos' (positively correlated)
Zero cross at 20665
'na_neg' (negatively correlated)
Rank in Ordered Dataset
Enrichment profile
Hits
Ranking metric scores

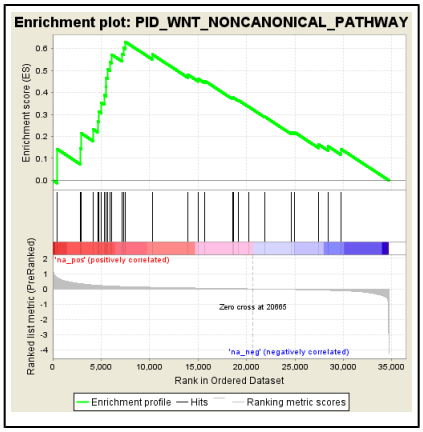
Enrichment plot: PID_WNT_NONCANONICAL_PATHWAY
Enrichment score (ES)
Ranked list metric (PreRanked)
'na_pos' (positively correlated)
Zero cross at 20665
'na_neg' (negatively correlated)
Rank in Ordered Dataset
Enrichment profile
Hits
Ranking metric scores

Table: Snapshot of enrichment results

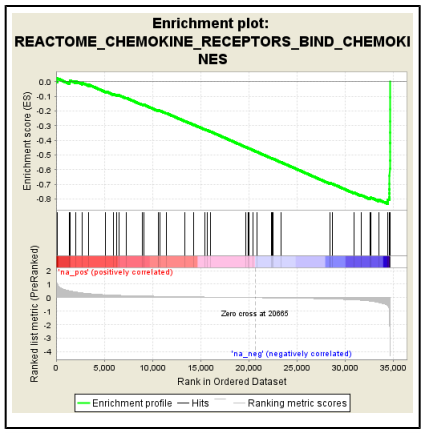

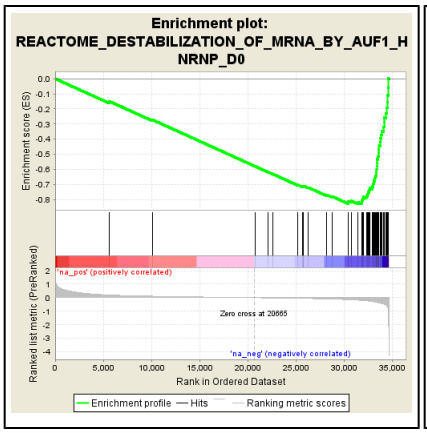

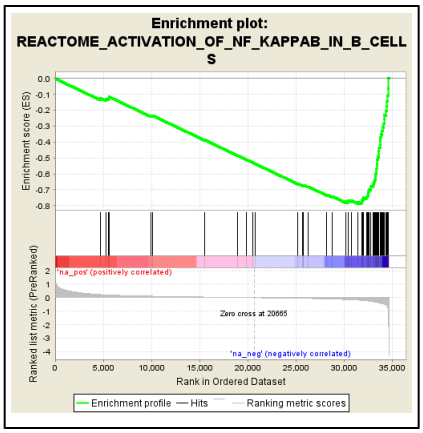

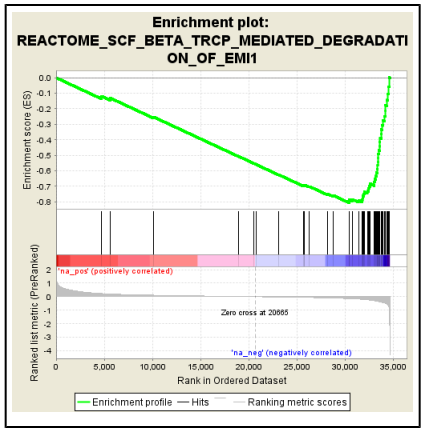

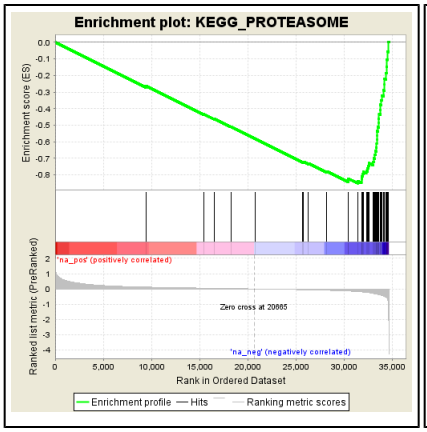

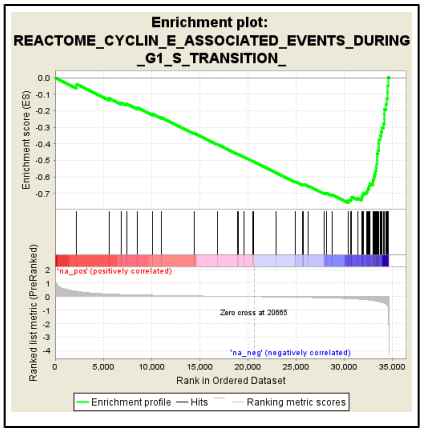

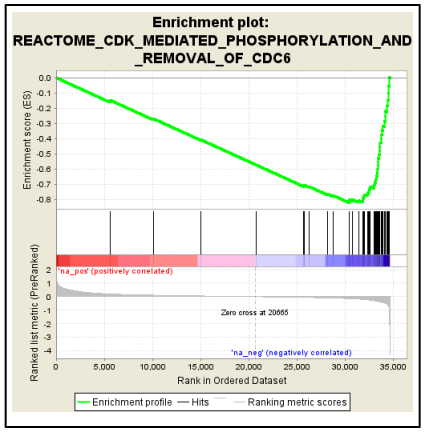

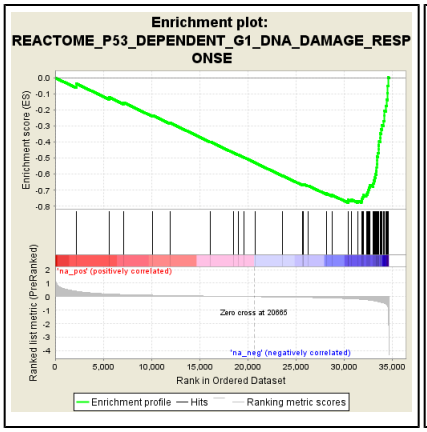

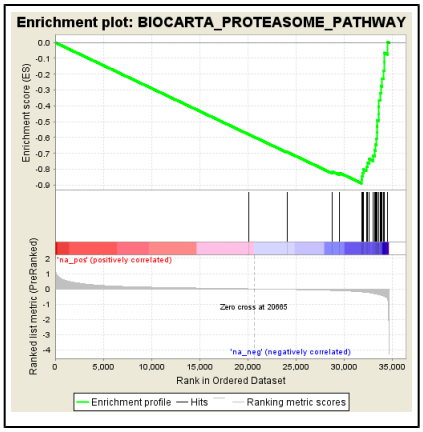

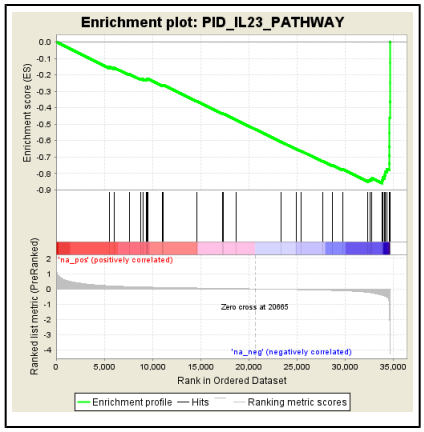

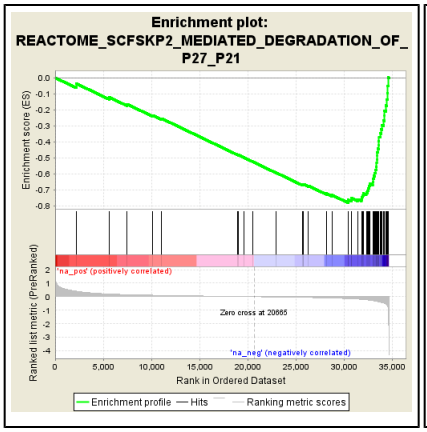

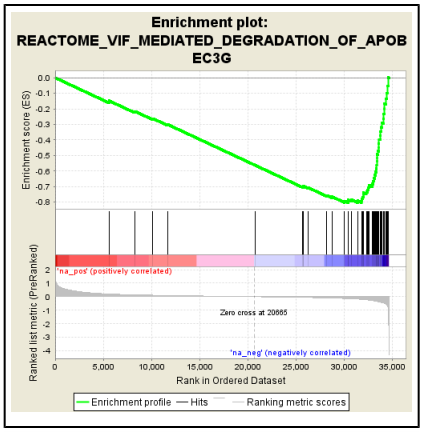

Enrichment plot: REACTOME_P53_INDEPENDENT_G1_S_DNA_DAMAGE_CHECKPOINT

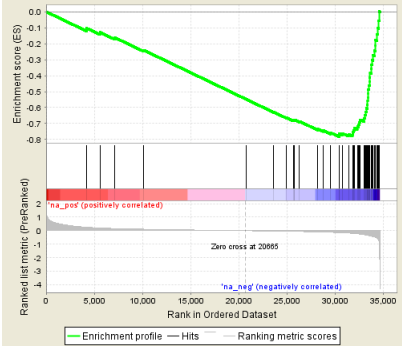

Enrichment plot: REACTOME_AUTODEGRADATION_OF_THE_E3_UBIQUITIN_LIGASE_COP1

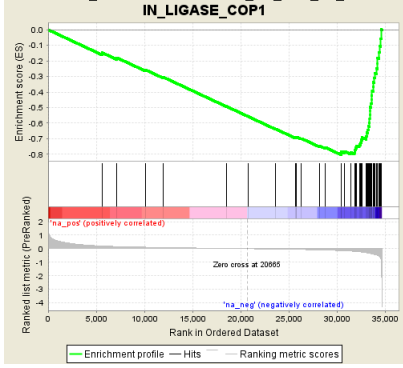

Enrichment plot: KEGG_CYTOKINE_CYTOKINE_RECEPTOR_INTERACTION

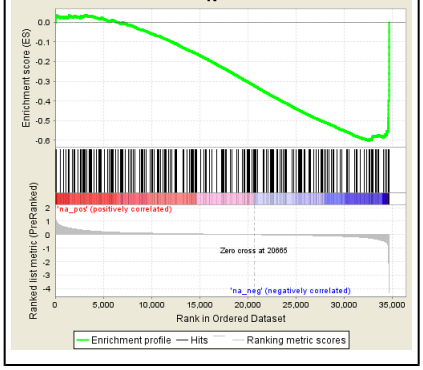

Enrichment plot: REACTOME_ER_PHAGOSOME_PATHWAY

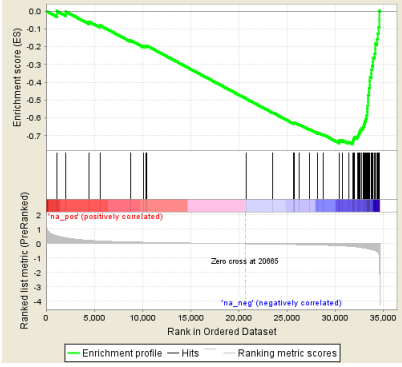

Enrichment plot: REACTOME_CDT1_ASSOCIATION_WITH_THE_CDC6_ORC_ORIGIN_COMPLEX

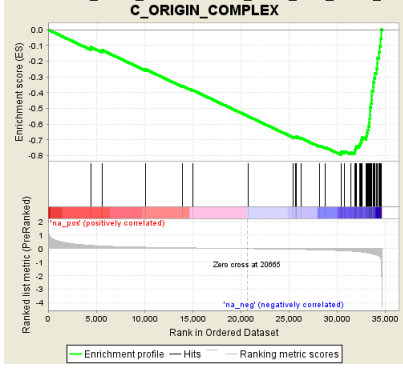

Enrichment plot: REACTOME_CROSS_PRESENTATION_OF_SOLUBLE_EXOGENOUS_ANTIGENS_ENDOSOMES

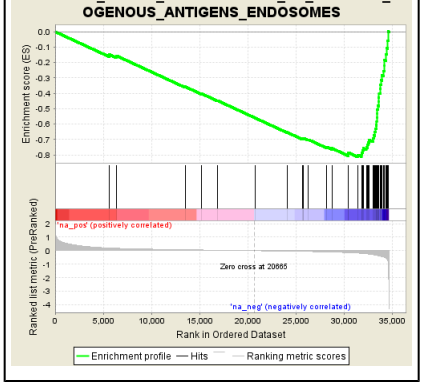

Enrichment plot: REACTOME_REGULATION_OF_ORNITHINE_DECARBOXYLASE_ODC

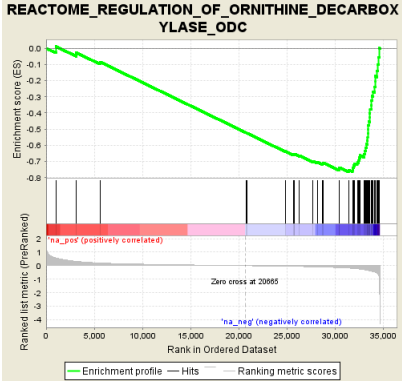

Enrichment plot: KEGG_NOD_LIKE_RECEPTOR_SIGNALING_PATHWAY

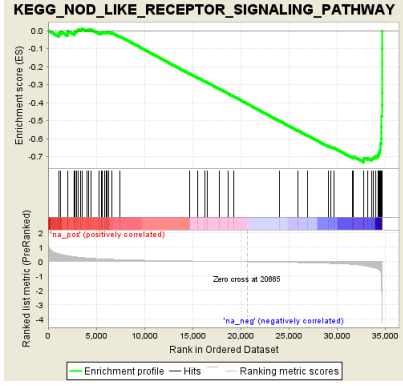

Table: Snapshot of enrichment results

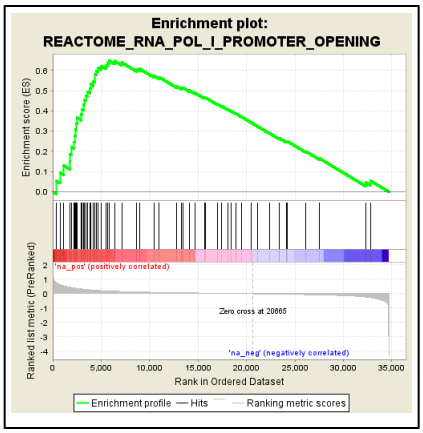

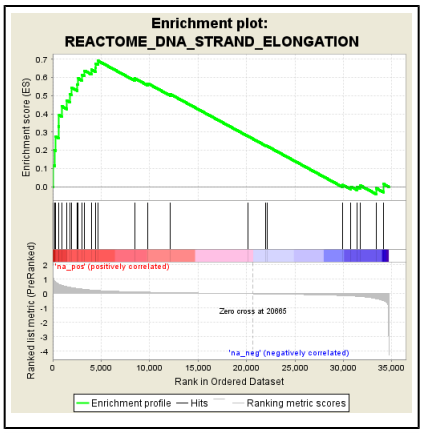

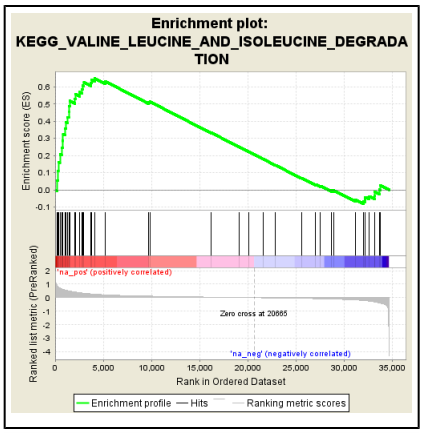

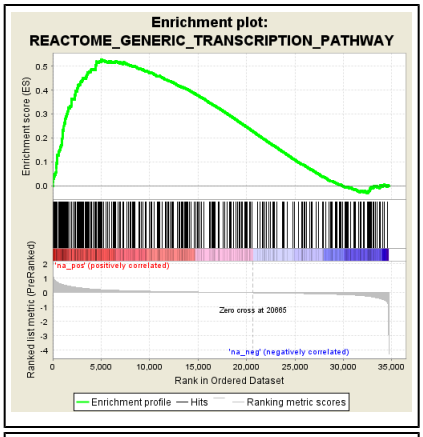

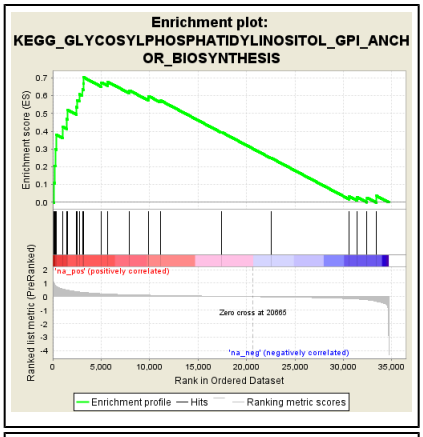

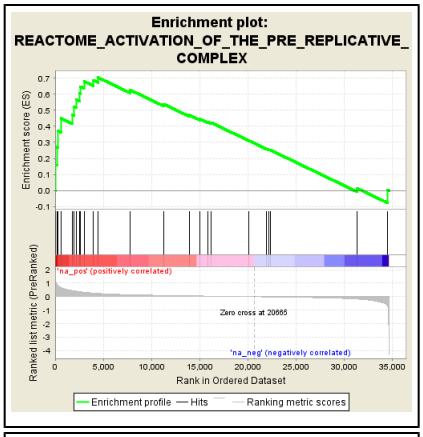

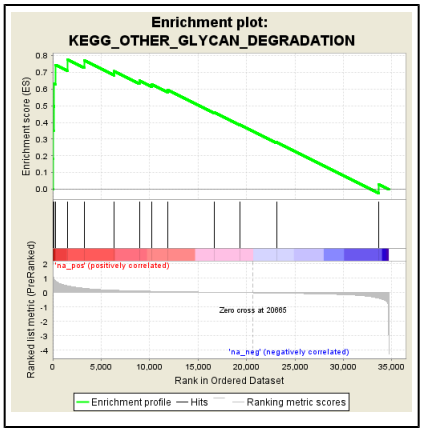

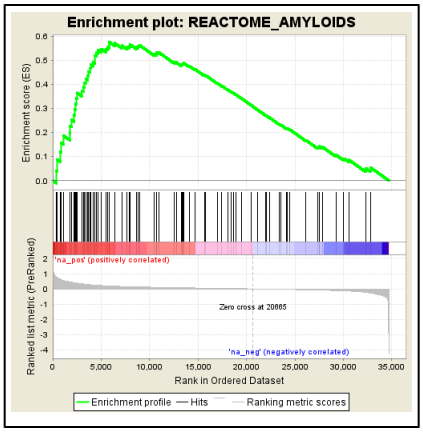

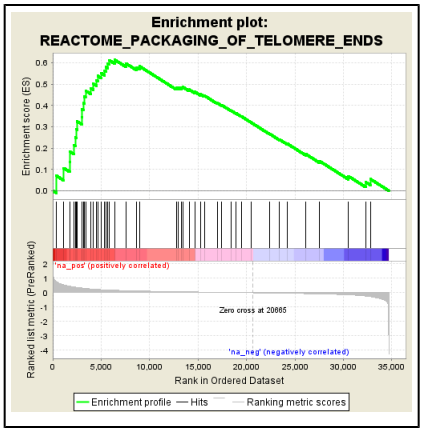

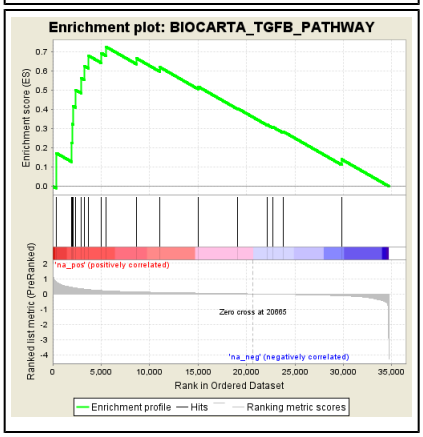

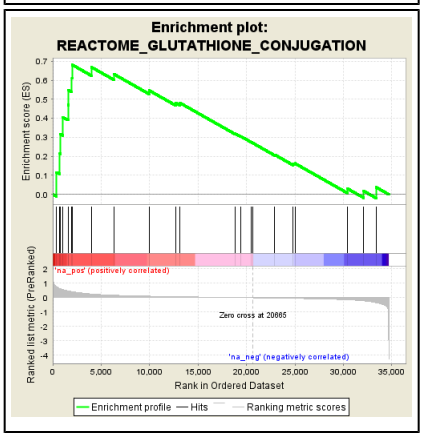

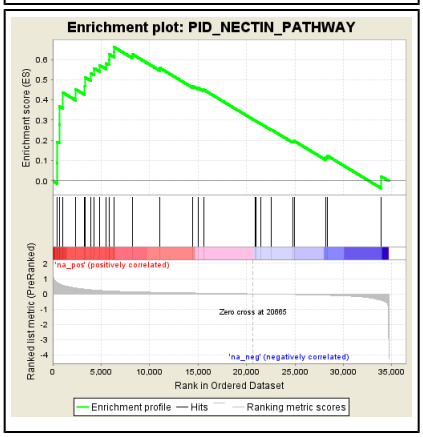

Enrichment plot: KEGG_GLYCOSPHINGOLIPID_BIOSYNTHESIS_GANGLIO_SERIES

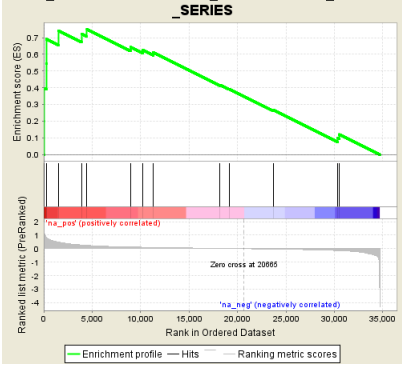

Enrichment plot: PID_S1P_S1P2_PATHWAY

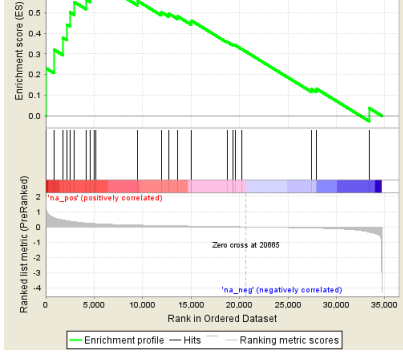

Enrichment plot: KEGG_LYSOSOME

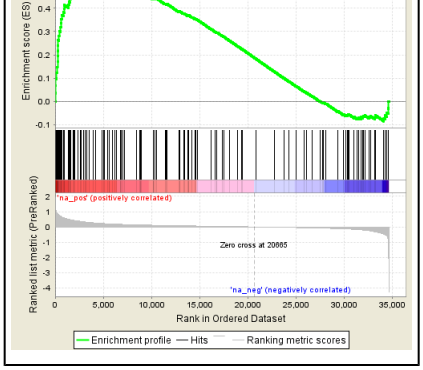

Enrichment plot: REACTOME_ACTIVATION_OF_ATR_IN_RESPONSE_TO_REPLICATION_STRESS

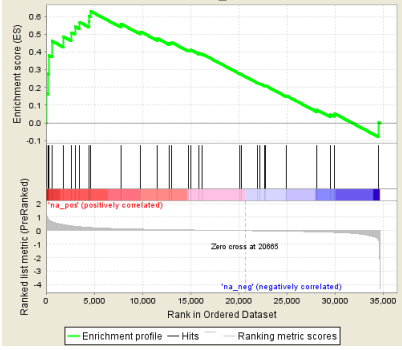

Enrichment plot: REACTOME_MEIOTIC_RECOMBINATION

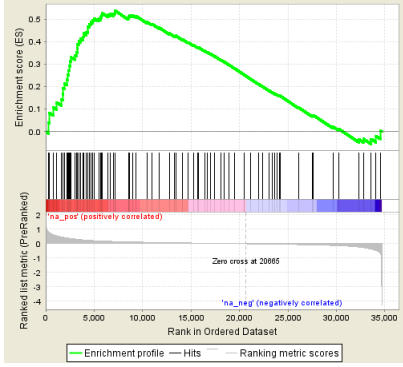

Enrichment plot: REACTOME_DEPOSITION_OF_NEW_CENPA_CONTAINING_NUCLEOSOMES_AT_THE_CENTROMERE

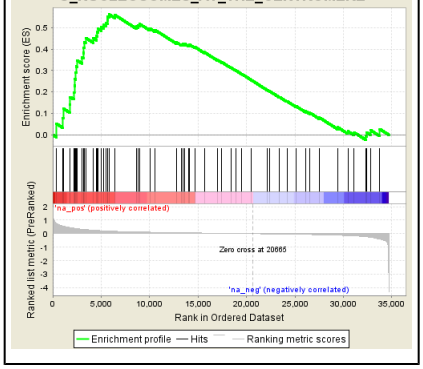

Enrichment plot: REACTOME_SEMA4D_INDUCED_CELL_MIGRATION_AND_GROWTH_CONE_COLLAPSE

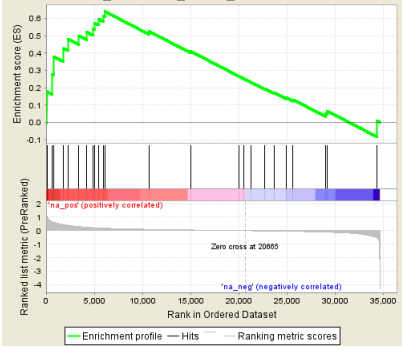

Enrichment plot: PID_WNT_NONCANONICAL_PATHWAY

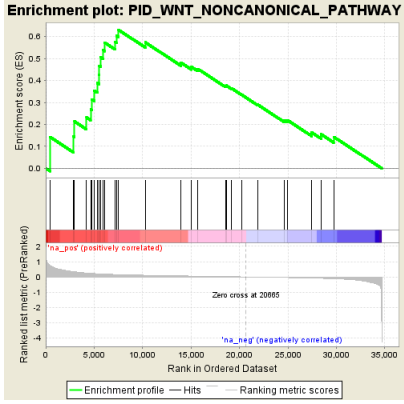

Table: Snapshot of enrichment results

Enrichment plot: REACTOME_CHEMOKINE_RECEPTORS_BIND_CHEMOKINES

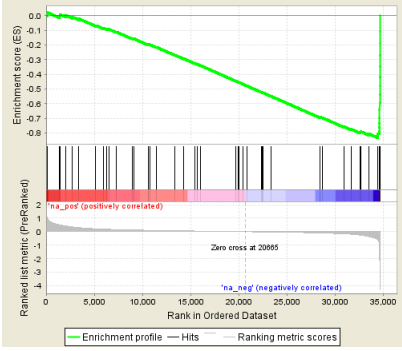

Enrichment plot: REACTOME_DESTABILIZATION_OF_MRNA_BY_AUF1_HNRNP_D0

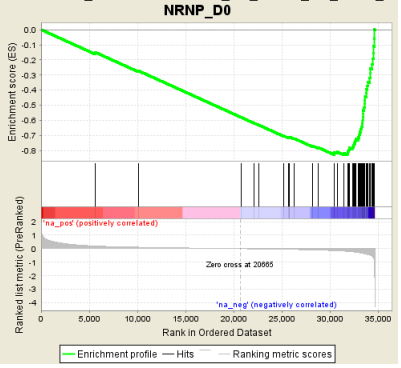

Enrichment plot: REACTOME_ACTIVATION_OF_NF_KAPPAB_IN_B_CELLS

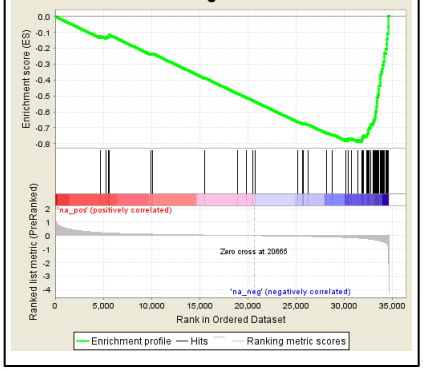

Enrichment plot: REACTOME_SCF_BETA_TRCP_MEDIATED_DEGRADATION_OF_EMI1

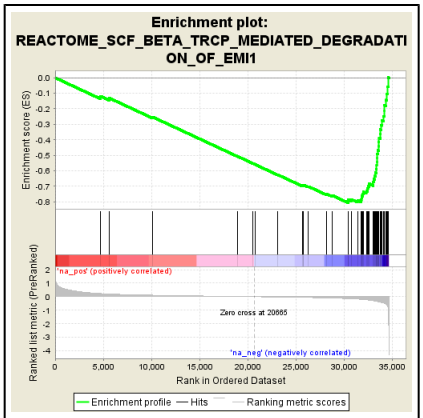

Enrichment plot: KEGG_PROTEASOME

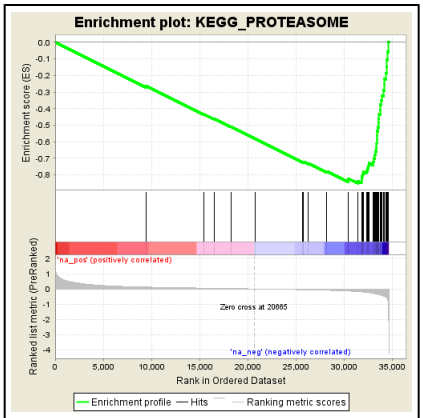

Enrichment plot: REACTOME_CYCLIN_E_ASSOCIATED_EVENTS_DURING_G1_S_TRANSITION_

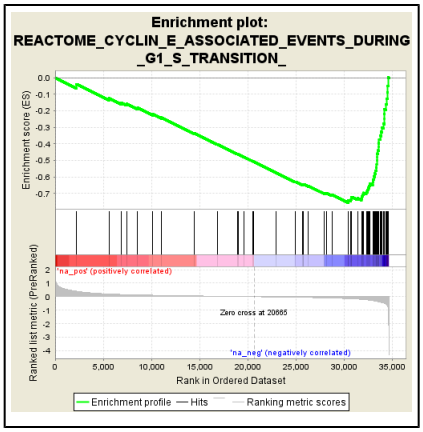

Enrichment plot: REACTOME_CDK_MEDIATED_PHOSPHORYLATION_AND_REMOVAL_OF_CDC6

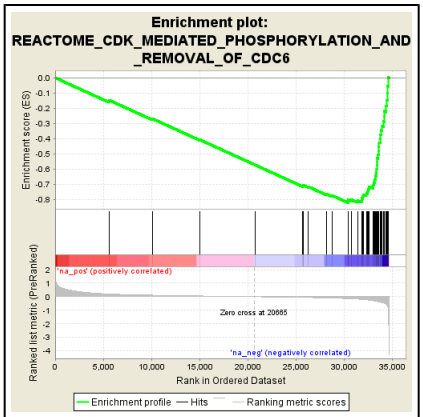

Enrichment plot: REACTOME_P53_DEPENDENT_G1_DNA_DAMAGE_RESPONSE

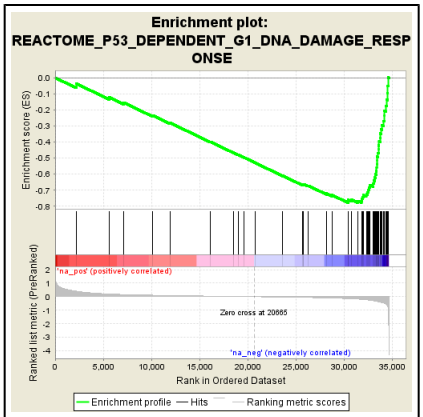

Enrichment plot: BIOCARTA_PROTEASOME_PATHWAY

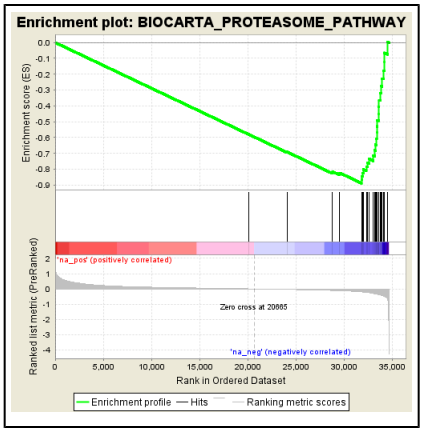

Enrichment plot: PID_IL23_PATHWAY

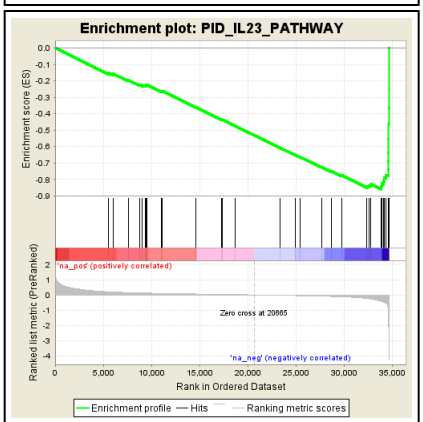

Enrichment plot: REACTOME_SCFSKP2_MEDIATED_DEGRADATION_OF_P27_P21

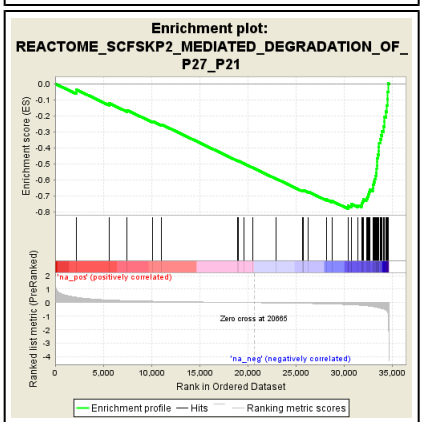

Enrichment plot: REACTOME_VIF_MEDIATED_DEGRADATION_OF_APOBEC3G

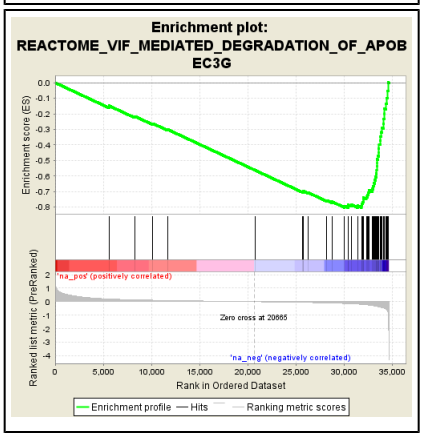

Enrichment plot: REACTOME_P53_INDEPENDENT_G1_S_DNA_DAMAGE_CHECKPOINT

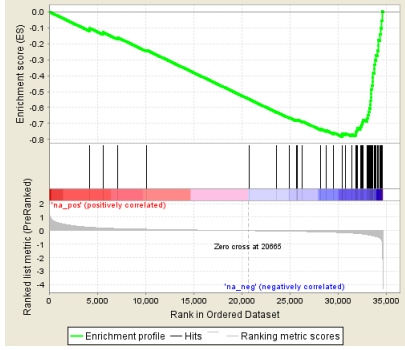

Enrichment plot: REACTOME_AUTODEGRADATION_OF_THE_E3_UBIQUITIN_LIGASE_COP1

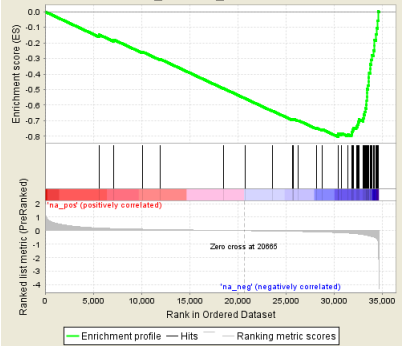

Enrichment plot: KEGG_CYTOKINE_CYTOKINE_RECEPTOR_INTERACTION

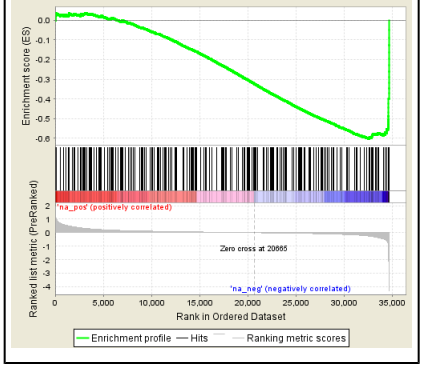

Enrichment plot: REACTOME_ER_PHAGOSOME_PATHWAY

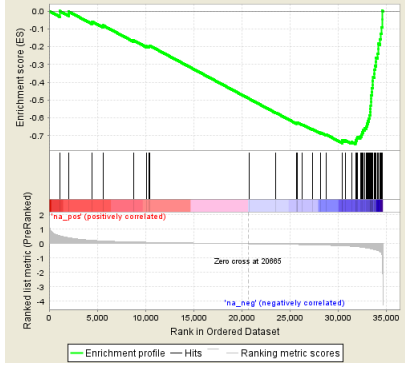

Enrichment plot: REACTOME_CDT1_ASSOCIATION_WITH_THE_CDC6_ORC_ORIGIN_COMPLEX

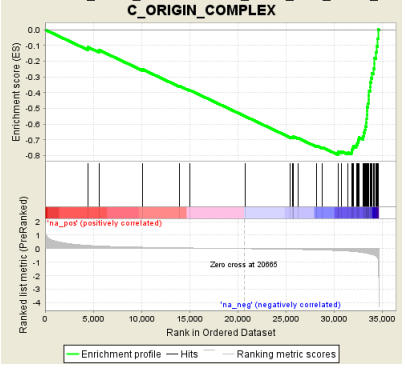

Enrichment plot: REACTOME_CROSS_PRESENTATION_OF_SOLUBLE_EXOGENOUS_ANTIGENS_ENDOSOMES

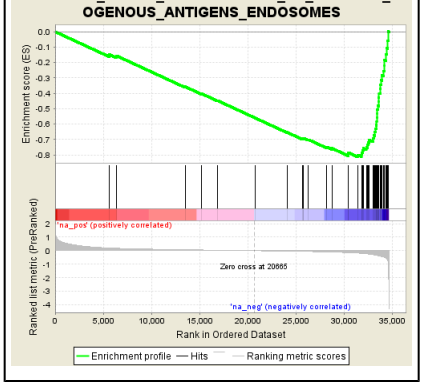

Enrichment plot: REACTOME_REGULATION_OF_ORNITHINE_DECARBOXYLASE_ODC

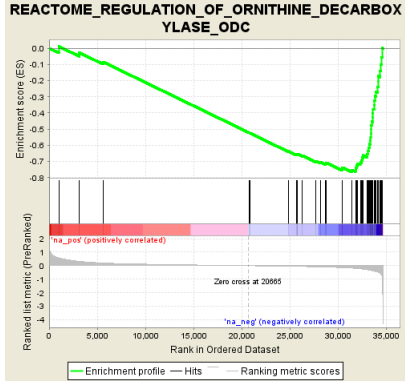

Enrichment plot: KEGG_NOD_LIKE_RECEPTOR_SIGNALING_PATHWAY